Linear structural mechanics

Lecture notes

POLITECNICO
MILANO 1863

Author: Dario FILA

Acronyms

DOFs	Degrees Of Freedom
PVW	Principle of Virtual Work
PCVW	Principle of Complementary Virtual Work
CL	Constitutive Law
CPT	Classical Plate Theory
MPT	Mindlin Plate Theory
CLT	Classical Lamination Theory
TSS	Transverse Shear Stress
DSV	De Saint Venant
CG	Center of Gravity
SC	Shear Center
UD	Uni-Directional
FE	Finite Element
FEA	Finite Element Analysis
FEM	Finite Element Method

Abstract

This document is a collection of notes taken during my master's degree in aeronautical engineering. It is not a book, a guide, or anything of the sort, just personal notes that I decided to write in a Word document.

The purpose of this document is to reorganize material provided by various professors and books in a way that prioritizes my personal understanding. I did not write this because I believe I can explain these concepts better than the sources mentioned, but because the way I have structured the sentences and explained the concepts is what best suits my own comprehension.

To anyone who comes into possession of this document, please keep in mind that these are essentially personal notes. As such, there may be errors—either conceptual or formal. If you notice any mistakes, I kindly encourage you to email me at: dario.fila@mail.polimi.it so they can be corrected.

I hope this document proves useful to anyone who reads it.

Table of Contents

1. CONTINUUM MECHANICS 1

1.1. STRESS AND STRAIN 1
1.1.1. The concept of stress 1
1.1.2. Cauchy Stress theorem 2
1.1.3. Strain 4
1.2. CONSTITUTIVE EQUATIONS 6
1.2.1. Elasticity 6
1.2.2. Hyperelasticity 6
1.2.3. Isotropic materials 8
1.2.3.1. Axial stress state 10
1.2.3.2. Beam stress state 10
1.2.3.3. Plane stress state 11
1.2.3.4. Plane strain state 12
1.3. COMPATIBILITY EQUATIONS 13
1.4. EQUILIBRIUM EQUATIONS 14
1.4.1. Conservation of linear momentum 14
1.4.2. Conservation of angular momentum 15
1.4.3. Symmetry of the stress tensor 16
1.5. VARIATIONAL FORMS 18
1.5.1. Principle of virtual work 18
1.5.1.1. PVW from strong form 18
1.5.1.2. Strong form from PVW 20
1.5.2. Principle of complementary virtual work 21
1.5.2.1. PCVW from compatibility 21
1.5.2.2. Compatibility from PCVW 22
1.5.3. Minimum potential energy principle 23
1.5.4. Menabrea's theorem 24
1.5.5. Hamilton's principle 25

2. BEAMS 28

2.1. DE SAINT VENANT SOLUTION 29
2.1.1. De Saint Venant principle 29
2.1.2. Semi-inverse solution 31
2.1.3. DSV beam governing equations 32
2.1.4. DSV solution for axial stress 33
2.1.4.1. DSV solution for pure axial load 36
2.1.4.2. DSV solution for pure bending 37
2.1.5. DSV solution for torsion 41
2.1.5.1. Governing equations 41
2.1.5.2. Solution 42
2.1.5.3. Meaning of warping 44
2.1.5.4. Evaluation of the torsional constant *J* 45
2.1.5.5. Strain and complementary strain energies 46
2.1.6. Shear stresses of thin-walled sections 47
2.1.6.1. Fluid analogy 47
2.1.6.2. Open profiles 49
2.1.6.3. Closed profiles 51
2.1.7. Energetic formulations 54
2.1.7.1. Strain energy 54
2.1.7.2. Variational formulation (PCVW) 56
2.1.8. Summary of the DSV solution 58
2.1.8.1. Governing equations 58
2.1.8.2. DSV solution for total axial stress 59
2.1.8.3. Pure axial load 60
2.1.8.4. Pure bending 60
2.1.8.5. DSV solution for torsion 62
2.1.8.6. Thin walled sections 62

2.1.8.7. Strain end complementary strain energies 63
2.2. KINEMATIC BEAM FORMULATIONS 64
2.2.1. Timoshenko beam model 65
2.2.1.1. Generalized coordinates 65
2.2.1.2. Generalized strains 66
2.2.1.3. Shear deformability 66
2.2.1.4. Generalized stresses 67
2.2.1.5. Generalized forces 68
2.2.1.6. Equilibrium conditions (loads) 69
2.2.1.7. Constitutive law 71
2.2.1.8. Equilibrium conditions (displacements) 73
2.2.1.9. Shear stress correction 73
2.2.1.10. Boundary conditions 74
2.2.1.11. Strain inconsistency 76
2.2.2. Euler-Bernoulli beam model 77
2.2.2.1. Generalized coordinates 77
2.2.2.2. Generalized strains 78
2.2.2.3. Generalized stresses 79
2.2.2.4. Generalized forces 81
2.2.2.5. Equilibrium conditions via PVW (loads) 82
2.2.2.6. Equilibrium equations via infinitesimal element 83
2.2.2.7. Constitutive law 84
2.2.2.8. Equilibrium conditions (displacements) 86
2.2.2.9. Torsion 87
2.2.2.10. Dynamic equilibrium equations 90
2.2.2.11. Boundary conditions 91
2.2.2.12. Variational form 94

3. PLATES 98

3.1. CLASSICAL PLATE THEORY 98
3.1.1. Generalized coordinates 99
3.1.2. Generalized strains 99
3.1.3. Generalized stresses 100
3.1.4. Transverse shear stresses 102
3.1.5. Equilibrium equations 102
3.1.5.1. Internal actions form 103
3.1.5.2. Displacement form 104
3.1.6. Variational formulation 106
3.2. MINDLIN PLATE THEORY 106
3.2.1. Generalized coordinates 107
3.2.2. Generalized strains 108
3.2.3. Shear strains and stresses 108
3.2.4. Cylindrical bending 109
3.2.5. Variational form 110
3.3. CLASSICAL LAMINATION THEORY 111
3.3.1. Generalized coordinates 112
3.3.2. Generalized strains 112
3.3.3. Constitutive law 113
3.3.4. Generalized stresses 115
3.3.5. Hygrothermal effects 116
3.3.6. Direct and inverse approaches 117

4. AEROSPACE STRUCTURES 121

4.1. INTRODUCTION TO AEROSTRUCTURES 122
4.2. SEMI-MONOCOQUE BEAM MODEL 125
4.2.1. Shear flow equation 126
4.2.2. Model assumptions 127
4.2.3. Solution procedure – general aspects 130
4.2.3.1. Evaluation of inertia moments 130
4.2.3.2. Evaluation of the stresses 130

4.2.3.3. Number of equations ... 131
4.2.4. Solution procedure for open sections ... 131
4.2.4.1. Shear stresses ... 131
4.2.4.2. Shear center ... 132
4.2.5. Solution procedure for single-cell closed section ... 134
4.2.5.1. Shear stresses ... 134
4.2.5.2. Shear center ... 134
4.2.6. Solution procedure for multi-cell closed section ... 136
4.2.6.1. Shear stress ... 136
4.2.6.2. Shear center ... 136
4.2.7. Evaluation of section properties ... 137
4.2.7.1. Axial and bending stiffnesses ... 137
4.2.7.2. Torsional stiffness ... 137
4.2.7.3. Shear stiffness ... 138
4.3. RIBS AND FRAMES ... 140
4.3.1. Functions ... 140
4.3.1.1. Shape ... 140
4.3.1.2. Load introduction ... 140
4.3.1.3. Improving buckling behavior ... 142
4.3.2. Analysis of ribs and frames ... 143
4.3.3. Symmetries ... 144
4.4. JUNCTIONS ... 148
4.4.1. Welded joints ... 148
4.4.1.1. Groove-butt welded joints ... 148
4.4.1.2. Fillet welds ... 150
4.4.2. Bolted joints ... 150

5. RITZ AND GALERKIN METHODS ... 157

5.1. RITZ METHOD ... 158
5.1.1. Approximation ... 158
5.1.2. Convergence ... 160
5.1.3. Features ... 161
5.2. GALERKIN METHOD ... 162
5.2.1. Collocation ... 162
5.2.2. Bubnov-Galerkin ... 163
5.2.3. Modified Bubnov-Galerkin ... 163
5.3. TRIAL FUNCTIONS FOR BEAMS ... 164
5.3.1. Cantilever beam ... 164
5.3.2. Fixed and simply supported beam ... 165
5.3.3. Simply supported beam ... 165
5.3.4. Clamped-clamped beam ... 166

6. FINITE ELEMENT METHOD ... 169

6.1. INTRODUCTION ... 170
6.1.1. Review of displacement based approach ... 170
6.1.2. The finite element procedure ... 174
6.1.3. Element vs global POV ... 177
6.2. SHAPE FUNCTIONS ... 178
6.2.1. Generalized coordinate elements ... 180
6.2.1.1. Example: linear triangular element ... 180
6.2.1.2. Example: linear square element ... 181
6.2.1.3. Example: Euler-Bernoulli linear beam element ... 182
6.2.2. Lagrange interpolation formula ... 182
6.3. ISOPARAMETRIC FORMULATION AND NUMERICAL INTEGRATION ... 184
6.3.1. Isoparametric elements ... 184
6.3.2. Numerical integration ... 185
6.3.3. Stress recovery ... 187
6.3.1. Full and reduced integration ... 187
6.3.2. Example: bar element ... 188

6.4. BASIC FE AND THEIR BEHAVIOR 189
6.4.1. Linear 2D triangular elements (CST) 189
6.4.2. Linear and quadratic 2D square elements (Q4 – Q8) 190
6.4.3. Plate and shell elements 191
6.4.3.1. Plate elements 192
6.4.3.2. Shell elements 194
6.5. MESHING 197
6.6. CONVERGENCE 200
6.6.1. Definition of convergence 200
6.6.2. Criteria for monotonic convergence 200
6.6.3. Properties of FE solution 201
6.6.4. Rate of convergence 202
6.7. CONSTRAINTS AND INTERACTIONS 204
6.7.1. Transformation matrices 204
6.7.2. Multi-point constraints and rigid bodies 204
6.7.3. Lagrange multiplier method 205
6.7.4. Penalty method 206
6.7.5. Overview of constraints in Abaqus 206

7. STRENGTH BASED CRITERIA 209

7.1. STATIC CRITERIA 212
7.1.1. Galileo-Rankine 212
7.1.2. Guest-Tresca and Von Mises 212
7.1.3. Drucker-Prager 213
7.1.4. Statistical approach for brittle materials 214
7.2. FATIGUE CRITERIA 216
7.2.1. Uniaxial fatigue 217
7.2.1.1. Whooler curve 217
7.2.1.2. Haigh diagram 220
7.2.2. Multiaxial fatigue 221
7.2.2.1. Gough-Poullard criterion 222
7.2.2.2. Sines criterion 224

8. FRACTURE MECHANICS 227

8.1. CRACK STRENGTH 228
8.1.1. Irwin empirical approach 228
8.1.2. Griffith/energy approach 231
8.1.3. Equivalence between K and energy approach 233
8.2. FATIGUE CRACK GROWTH 234
8.3. NON-DESTRUCTIVE EVALUATION (NDE) 235

9. COMPOSITE MATERIALS 237

9.1. COMPOSITE DAMAGE 238
9.1.1. Intralaminar damage 238
9.1.1.1. Transverse matrix cracking 238
9.1.1.2. Fiber tensile failure 240
9.1.1.3. Fiber compressive failure 241
9.1.2. Delaminations 242
9.1.2.1. Causes of delaminations 242
9.1.2.2. Characterization tests 245
9.2. STRENGTH BASED CRITERIA (ORTHOTROPY) 250
9.2.1. Allowables 251
9.2.1.1. Lamina level 251
9.2.1.2. Laminate level 251
9.2.2. Stress field 253
9.2.2.1. Out of plane stress components 253
9.2.2.2. Hygrothermal effects 253
9.3. STRENGTH CRITERIA 254

9.3.1. Maximum stress and strain *256*
9.3.2. Tsai-Hill criterion *258*
9.3.2 Hoffmann criterion *259*
9.3.3. Tsai-Wu criterion *261*
9.3.4. Hashin-Rotem criterion *262*
9.3.5. Delamination onset criteria *263*
9.3.6. Comparison of lamina-level criteria *263*
9.3.7. Laminate level *264*
9.4. BUILDING BLOCK APPROACH 265
9.4.3. Application of building block approach *268*
9.4.3.1. Group A - material property development 268
9.4.3.2. Group B - design value development 268
9.4.3.3. Group C - analysis verification 269

10. APPENDIX 272

10.1. DATA ANALYSIS 272
10.1.1. Statistical descriptive quantities *272*
10.1.1.1. Sample mean, median and mode 272
10.1.1.2. Sample variance and standard deviation 273
10.1.1.3. Sample percentiles 273
10.1.2. Chebyshev's inequality *274*
10.1.3. Elements of probability *276*
10.1.3.1. Random variables 277
10.1.3.2. Conditional reliability 278
10.1.3.3. Hazard rate 279
10.1.4. Normal distributions *281*
10.1.5. Weibull distribution *284*
10.1.6. Estimators *286*
10.1.7. Other statistical distributions *288*
10.1.7.1. Histogram 288
10.1.7.2. Scatter diagrams 288
10.2. DSV SOLUTION FOR SHEAR – EXAMPLES 291
10.2.1. Open sections *291*
10.2.1.1. Example 1 291
10.2.1.2. Example 2 292
10.2.1.3. Example 3 292
10.2.2. Closed sections *293*
10.2.2.1. Example 4 293
10.3. SYMMETRY IN BEAMS - EXAMPLES 295
10.3.1. Example 1 ..... *295*
10.3.2. Example 2 ..... *296*
10.4. RITZ METHOD 297
10.4.1. Example 1 ..... *297*
10.4.2. Example 2 ..... *299*
10.4.2.1. Solution with one polynomial term 301
10.4.2.2. Solution using two polynomial terms 301
10.4.2.3. Solution using three polynomial terms 302
10.4.3. Example 3 ..... *303*

REFERENCES 306

1. Continuum mechanics

1.1. Stress and strain

1.1.1. The concept of stress

We begin this section by clarifying the meaning of stress, which is something more profound than the common idea of "force per unit area". Clearly, stress is a force per unit area from a dimensional standpoint. However, the idea of stress is associated with the exchange of internal forces. An insightful description is available from the Feynman lectures on physics, and is reported below for the sake of completeness:

"Consider a block of some elastic material – say a block of jello. If we make a cut through the block, the material on each side of the cut will, in general, get displaced by the internal forces. Before the cut was made, there must have been forces between the two parts of the block that kept the material in place. We can define the stresses in terms of these forces."

The discussion that follows is based on the idea of a Cauchy continuum: a continuum whose infinitesimal elements are capable of internally exchanging forces but not moments per unit volume/surface. Such model holds for several continuums, but it is important to point out that considering Cauchy continuums is a modelling assumption. A continuum that is able to also exchange moments per unit volume/surface is called a polar continuum. Thus, for a Cauchy continuum we'll have that:

$$\lim_{\Delta v \to 0} \frac{\Delta \underline{M}}{\Delta v} = 0 \qquad \lim_{\Delta v \to 0} \frac{\Delta \underline{F}}{\Delta v} = \underline{b} \qquad \text{Volume loads}$$

$$\lim_{\Delta a \to 0} \frac{\Delta \underline{M}}{\Delta a} = 0 \qquad \lim_{\Delta a \to 0} \frac{\Delta \underline{F}}{\Delta a} = \underline{t} \qquad \text{Surface loads}$$

In order to study the internal exchange of forces, i.e. the stresses, consider a body which is virtually cut. We define the infinitesimal resultant of internal forces $d\mathbf{f}$ acting on an element of the virtual (internal) surface dS as the product between the Cauchy traction or stress vector $\boldsymbol{t}$ and dS. Note that $\boldsymbol{t}$ may not be parallel to $\boldsymbol{n}$.

$$d\underline{f} = \underline{t} ds \qquad \text{where} \quad \underline{t} = \underline{t}(\underline{x}, t, \underline{n}) \tag{1.1}$$

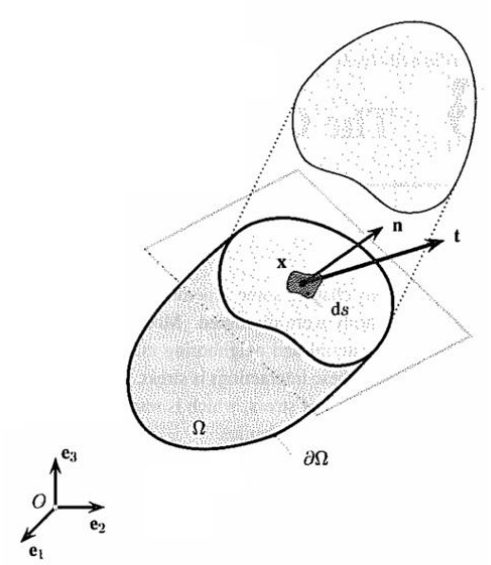

Figure 1.1: Traction vector $\boldsymbol{t}$ acting on an infinitesimal element internal surface with outward normal.

1.1.2. Cauchy Stress theorem

There exists a unique second order tensor $\boldsymbol{\sigma}$ so that:

$$\underline{t} = \underline{\sigma}(\underline{x}, t) \cdot \underline{n} \qquad \text{or} \qquad t_a = \sigma_{ab} n_b \tag{1.2}$$

Where $\boldsymbol{\sigma}$ is the Cauchy stress tensor. Cauchy's stress theorem, also known as Cauchy's law or equation, is one of the most important axioms of continuum mechanics. Basically, it states that if the traction vector $\boldsymbol{t}$ depends on the outwards normal $\boldsymbol{n}$, then it must be linear with $\boldsymbol{n}$.

In order to prove this theorem, consider Cauchy's tetrahedron, depicted in Figure 1.2, for which $\boldsymbol{n}$ is the normal to the oblique face, while ds_i are the surfaces of normal $\boldsymbol{e_i}$. The loads acting on Cauchy's tetrahedron are the forces $\boldsymbol{t}(\boldsymbol{e}_i)dS_i$, where $\boldsymbol{t}(\boldsymbol{e}_i)$ is the traction vector acting on the face of normal $\boldsymbol{e}_i$, the force $\boldsymbol{t}(\boldsymbol{n})dS$ where $\boldsymbol{t}(\boldsymbol{n})$ is the traction vector acting on the face of arbitrary orientation/normal $\boldsymbol{n}$, and the body forces $\boldsymbol{b}dV$. Note that, as it has already been established, $\boldsymbol{t}(-\boldsymbol{e_i})$ is not necessarily parallel to the face normal $\boldsymbol{e_i}$. The equilibrium of the tetrahedron can be imposed in terms of forces as follows:

$$\underline{t}(\underline{n})ds + \sum_{i=1}^{3} \underline{t}(-\underline{e}_i)ds_i + \underline{f}dv = 0$$

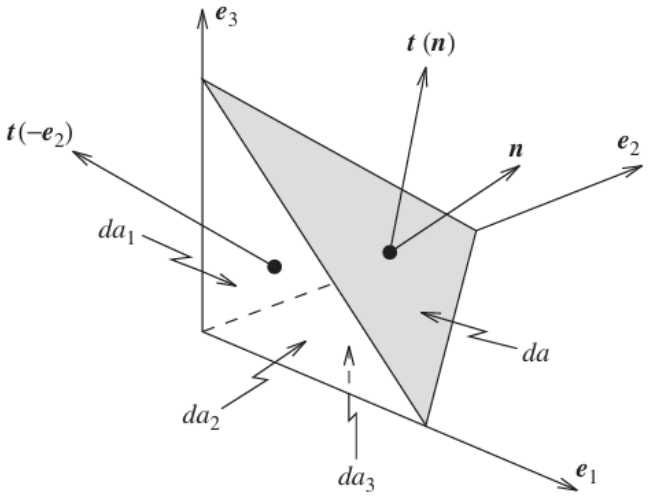

Figure 1.2: Cauchy tetrahedron.

From Newton's third law of action and reaction it must be that $\boldsymbol{t}(-\boldsymbol{e}_i) = -\boldsymbol{t}(\boldsymbol{e}_i) = -\boldsymbol{t}_i$. Moreover, the surface ds_i of the face of normal $\boldsymbol{e}_i$ can be expressed in terms of the surface ds of the face of normal $\boldsymbol{n}$ simply as $ds_i = \boldsymbol{e}_i \cdot \boldsymbol{n} ds$ (the projection of ds onto ds_i). Using these two relations we can rewrite the equilibrium as follows:

$$\underline{t}(\underline{n}) - \sum_{i=1}^{3} \underline{t}_i(\underline{e}_i \cdot \underline{n}) + \underline{f}\frac{dv}{ds} = 0 \quad \xrightarrow{dv/ds \to 0} \quad \underline{t} = \sum_{i=1}^{3} \underline{t}_i(\underline{e}_i \cdot \underline{n})$$

Where we divided the whole equation by ds and then used that $dv \propto dl^3$ goes to zero faster than $ds \propto dl^2$ as $dl \to 0$. We can further elaborate the previous expression as follows:

$$\underline{t}(\underline{n}) = \sum_{i=1}^{3} \underline{t}_i(\underline{e}_i \cdot \underline{n}) = \sum_{i=1}^{3} (\underline{t}_i \otimes \underline{e}_i) \cdot \underline{n} = \underline{\sigma} \cdot \underline{n}$$

$$\underline{t}(\underline{n}) = \underline{\sigma} \cdot \underline{n} \tag{1.3}$$

Where we introduced the ***Cauchy stress tensor*** $\boldsymbol{\sigma}$, a second order tensor that provides the traction vector $\boldsymbol{t}$ acting on a surface of generic orientation when given the outward normal $\boldsymbol{n}$ of such surface as an input. In order to obtain the traction vector $\boldsymbol{t}_i = \boldsymbol{t}(\boldsymbol{e}_i)$ acting on the surface of normal $\boldsymbol{e}_i$, we simply write:

$$\underline{t}_i = \underline{t}(\underline{e}_i) = \sum_{j}^{3} \sigma_{ji}\underline{e}_j \quad \rightarrow \quad \begin{cases} \underline{t}(\underline{e}_1) = \sigma_{11}\underline{e}_1 + \sigma_{21}\underline{e}_2 + \sigma_{31}\underline{e}_3 \\ \underline{t}(\underline{e}_2) = \sigma_{12}\underline{e}_1 + \sigma_{22}\underline{e}_2 + \sigma_{32}\underline{e}_3 \\ \underline{t}(\underline{e}_3) = \sigma_{13}\underline{e}_1 + \sigma_{23}\underline{e}_2 + \sigma_{33}\underline{e}_3 \end{cases} \tag{1.4}$$

Some ***properties*** of $\boldsymbol{\sigma}$ are:

- Index convention: for the generic entry σ_{ij}, the first index i represents the direction of the stress component while the second index j represents the direction of the normal of the

face on which the stress component acts upon. Note, however, that it is common in the engineering community to reverse such convention.

- Tensor components physical meaning: the extra-diagonal terms $i \neq j$ represent shear stresses, related to changes of shape, while diagonal terms $i = j$ represent normal stresses, related to changes in volume.
- Symmetric tensor: implying that $\sigma_{ij} = \sigma_{ji}$, which will be proven in section 1.4.

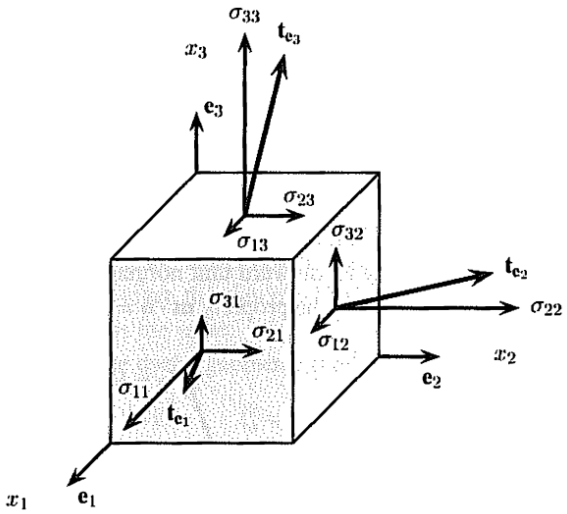

Figure 1.3: stress components.

1.1.3. Strain

The ***Green- Lagrange strain tensor*** $\boldsymbol{\varepsilon}$ can be defined in a similar way to the stress tensor.

$$\underline{\underline{\varepsilon}} = \begin{bmatrix} \varepsilon_{xx} & \varepsilon_{xy} & \varepsilon_{xz} \\ \varepsilon_{yx} & \varepsilon_{yy} & \varepsilon_{yz} \\ \varepsilon_{zx} & \varepsilon_{zy} & \varepsilon_{zz} \end{bmatrix} \quad \text{where} \quad [\varepsilon_{ij}] = [-] \tag{1.5}$$

This tensor is symmetric, of the second order, and has normal and shear components as well. Normal strain components ε_{ii} represent change in volume, while shear strain components ε_{ij} represent change in shape. Such components are also non-dimensional. Strain components can be expressed as a function of displacements $\boldsymbol{u}$ via the following kinematic law:

$$\varepsilon_{ij} = \frac{1}{2}\left(\nabla \underline{u} + \nabla \underline{u}^T + \nabla \underline{u} \nabla \underline{u}^T\right) = \frac{1}{2}\left(u_{i/j} + u_{j/i} + u_{k/i} u_{k/j}\right) \tag{1.6}$$

Note that we will indicate the displacements as $\boldsymbol{u} = \{u_1, u_2, u_3\} = \{u, v, w\}$. A couple of examples of the full expression of strain components are the following:

$$\varepsilon_{xx} = \frac{1}{2}\left(\frac{\partial u}{\partial x} + \frac{\partial u}{\partial x} + \frac{\partial u}{\partial x}\frac{\partial u}{\partial x} + \frac{\partial v}{\partial x}\frac{\partial v}{\partial x} + \frac{\partial w}{\partial x}\frac{\partial w}{\partial x}\right)$$

$$\varepsilon_{xy} = \frac{1}{2}\left(\frac{\partial u}{\partial y} + \frac{\partial v}{\partial x} + \frac{\partial u}{\partial x}\frac{\partial u}{\partial y} + \frac{\partial v}{\partial x}\frac{\partial v}{\partial y} + \frac{\partial w}{\partial x}\frac{\partial w}{\partial y}\right)$$

Starting from equation ((1.6), we can obtain the small strain tensor assuming displacements and rotations to be small. The small strain tensor is expressed as follows:

$$\varepsilon_{ij} = \frac{1}{2}\left(\nabla \underline{u} + \nabla \underline{u}^{T}\right) = \frac{1}{2}\left(u_{i/j} + u_{j/i}\right) \tag{1.7}$$

1.2. Constitutive equations

Constitutive equations, or constitutive laws (CL), relate stresses $\boldsymbol{\sigma}$ to strains $\boldsymbol{\varepsilon}$. We'll assume that the stress state in a point is a function of the strain only in the same point, this takes the name of ***axiom of locality***. Intuitively, constitutive law are a function of the material considered. Thus, we now present different models that will be used through the course.

1.2.1. Elasticity

A material is said to be elastic if its deformation under loading is completely reversible. This simply means that the loading and unloading phases are directed along the same path. For a space application, this type of response can be attributed to the foam core of a sandwich panel. The constitutive law will be generally expressed as:

$$\begin{cases} \underline{\underline{\sigma}} = \underline{\underline{\sigma}}\left(\underline{\underline{\varepsilon}}\right) & \text{or} \quad \sigma_{ik} = \sigma_{ik}(\varepsilon_{ik}) \\ \underline{\underline{\varepsilon}} = \underline{\underline{\varepsilon}}\left(\underline{\underline{\sigma}}\right) & \text{or} \quad \varepsilon_{ik} = \varepsilon_{ik}(\sigma_{ik}) \end{cases} \tag{1.8}$$

Here, the top equation, $\boldsymbol{\sigma} = \boldsymbol{\sigma}(\boldsymbol{\varepsilon})$, is what we typically refer to as the constitutive equation, while the bottom equation $\boldsymbol{\varepsilon} = \boldsymbol{\varepsilon}(\boldsymbol{\sigma})$ is the inverse constitutive law.

If a material is linear-elastic, its constitutive law is the well-known ***Hooke's law***, which relates the stress and strain tensor via the fourth-order ***elasticity tensor*** $\mathbb{C}$, and the strains to stresses via the inverse of the elasticity tensor $\boldsymbol{S} = \mathbb{C}^{-1}$:

$$\begin{cases} \underline{\underline{\sigma}} = \underline{\underline{\underline{\underline{\mathbb{C}}}}} : \underline{\underline{\varepsilon}} & \text{or} \quad \sigma_{ij} = \mathbb{C}_{ijkl}\varepsilon_{kl} \quad \text{and thus} \quad \mathbb{C}_{ijkl} = \partial\sigma_{ij}/\partial\varepsilon_{kl} \\ \underline{\underline{\varepsilon}} = \underline{\underline{\underline{\underline{S}}}} : \underline{\underline{\sigma}} & \text{or} \quad \varepsilon_{ij} = S_{ijkl}\sigma_{kl} \quad \text{and thus} \quad S_{ijkl} = \partial\varepsilon_{ij}/\partial\sigma_{kl} \end{cases} \tag{1.9}$$

Here $\{i, j, k, l\} = \{x, y, z\}$ or equivalently $\{1,2,3\}$. The elasticity tensor, and its inverse, present some symmetries that reduce their number of independent entries. At this stage, its symmetries are only those implied by the symmetries of the stress and strain tensors, called minor symmetries. They bring down the number of unknown entries of $\mathbb{C}$ and $\boldsymbol{S}$ to 36.

$$\begin{cases} \sigma_{ij} = \sigma_{ji} & \rightarrow \begin{cases} \mathbb{C}_{ijkl} = \mathbb{C}_{jikl} \\ S_{ijkl} = S_{jikl} \end{cases} \\ \varepsilon_{kl} = \varepsilon_{lk} & \rightarrow \begin{cases} \mathbb{C}_{ijkl} = \mathbb{C}_{ijlk} \\ S_{ijkl} = S_{ijlk} \end{cases} \end{cases}$$

1.2.2. Hyperelasticity

A material is said to be hyperelastic if the stress and strain tensors can be obtained from potential functions. More precisely, we define the ***strain energy density*** $u(\boldsymbol{\varepsilon})$ and ***complementary strain energy density*** $u^*(\boldsymbol{\sigma})$ as:

$$\begin{cases} \underline{\underline{\sigma}} = \dfrac{\partial u}{\partial \underline{\underline{\varepsilon}}} = u_{/\underline{\underline{\varepsilon}}} & \text{or} \quad \sigma_{ij} = u_{/\varepsilon_{ij}} \quad \text{and so} \quad du = \underline{\underline{\sigma}} : d\underline{\underline{\varepsilon}} \\ \underline{\underline{\varepsilon}} = \dfrac{\partial u^*}{\partial \underline{\underline{\sigma}}} = u^*_{/\underline{\underline{\sigma}}} & \text{or} \quad \varepsilon_{ij} = u^*_{/\sigma_{ij}} \quad \text{and so} \quad du^* = \underline{\underline{\varepsilon}} : d\underline{\underline{\sigma}} \end{cases} \tag{1.10}$$

Here $[u] = [u^*] = J/m^3 = Nm/m^3$, so the total strain and complementary strain energies U and U^* can be obtained as the volume integral of the densities over the body's volume:

$$\begin{cases} U = \int_V u \, dV = \int_V \underline{\underline{\sigma}} : d\underline{\underline{\varepsilon}} \\ U^* = \int_V u^* dV = \int_V \underline{\underline{\varepsilon}} : d\underline{\underline{\sigma}} \end{cases} \tag{1.11}$$

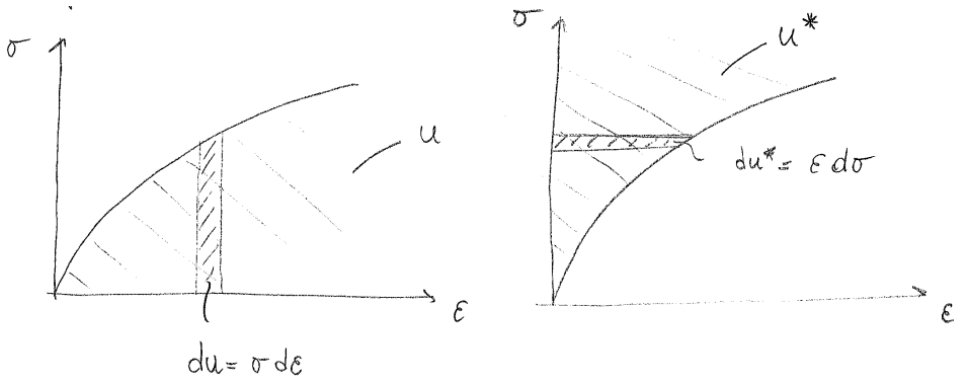

Figure 1.4: left) strain energy; right) complementary strain energy.

The response of hyperelastic materials is ***path independent***, meaning that it only depend on their initial and final state of the deformation process. This is easily demonstrated by computing the ***deformation work density*** w_D and the ***complementary deformation work density*** w_D^* associated to a generic 1D deformation process:

$$\begin{cases} w_D = \int_{\varepsilon_1}^{\varepsilon_2} \sigma(\varepsilon) d\varepsilon = \int_{\varepsilon_1}^{\varepsilon_2} u_{/\varepsilon} d\varepsilon = u(\varepsilon_2) - u(\varepsilon_1) \\ w_D^* = \int_{\sigma_1}^{\sigma_2} \varepsilon(\sigma) d\sigma = \int_{\sigma_1}^{\sigma_2} u_{/\sigma}^* d\sigma = u^*(\sigma_2) - u^*(\sigma_1) \end{cases} \tag{1.12}$$

Observation. We'll always assume that the initial state of the loading process is the reference configuration of the body, and thus $\varepsilon_1 = \sigma_1 = 0$. Under this assumption, the ***strain energy densities*** $\boldsymbol{u, u^*}$ ***coincide with the deformation work densities*** $\boldsymbol{w_D, w_D^*}$.

If the material is linear-hyperelastic, then its constitutive law can be expressed using Hooke's law as per equation (1.9). The linear constitutive equation paired with the existence of the strain energy densities u and u^* has some important ***implications***:

- The strain energy densities u and u^* can be obtained as follows:

$$\begin{cases} u = w_D = \int_0^{\underline{\underline{\varepsilon}}_1} du = \int_0^{\underline{\underline{\varepsilon}}_1} \underline{\underline{\sigma}} : d\underline{\underline{\varepsilon}} = \frac{1}{2} \underline{\underline{\sigma}} : \underline{\underline{\varepsilon}} = \frac{1}{2} \underline{\underline{\varepsilon}} : \underline{\underline{\mathbb{C}}} : \underline{\underline{\varepsilon}} \\ u^* = w_D^* = \int_0^{\underline{\underline{\sigma}}_1} du^* = \int_0^{\underline{\underline{\sigma}}_1} \underline{\underline{\varepsilon}} : d\underline{\underline{\sigma}} = \frac{1}{2} \underline{\underline{\sigma}} : \underline{\underline{\varepsilon}} = \frac{1}{2} \underline{\underline{\sigma}} : \underline{\underline{\underline{\underline{S}}}} : \underline{\underline{\sigma}} \end{cases} \tag{1.13}$$

  Consequently, the total strain and complementary strain energies stored in a continuous body during a loading process can be computed as the integrals of u and u^*, respectively:

$$\begin{cases} U = W_D = \int_V u\, dV = \frac{1}{2}\int_V \underline{\underline{\sigma}} : \underline{\underline{\varepsilon}}\, dV = \frac{1}{2}\int_V \underline{\underline{\varepsilon}} : \underline{\underline{\mathbb{C}}} : \underline{\underline{\varepsilon}}\, dV \\ U^* = W_D^* = \int_V u^* dV = \frac{1}{2}\int_V \underline{\underline{\sigma}} : \underline{\underline{\varepsilon}}\, dV = \frac{1}{2}\int_V \underline{\underline{\sigma}} : \underline{\underline{\underline{\underline{S}}}} : \underline{\underline{\sigma}}\, dV \end{cases} \tag{1.14}$$

- The elasticity tensor $\mathbb{C}$ and its inverse $\boldsymbol{S}$ can be computed as the second derivatives of u and u^* with respect to $\boldsymbol{\varepsilon}$ and $\boldsymbol{\sigma}$ twice, respectively.

$$\begin{cases} \mathbb{C}_{ijkl} = \dfrac{\partial \sigma_{ij}}{\partial \varepsilon_{kl}} = \dfrac{\partial^2 u}{\partial \varepsilon_{ij}\partial \varepsilon_{kl}} \\ S_{ijkl} = \dfrac{\partial \varepsilon_{ij}}{\partial \sigma_{kl}} = \dfrac{\partial^2 u^*}{\partial \sigma_{ij}\partial \sigma_{kl}} \end{cases} \tag{1.15}$$

- The formulation of $\mathbb{C}$ and $\boldsymbol{S}$ in (1.15) allows us to identify the major symmetry of these tensors, which brings down the total number of their independent components to 21.

$$\begin{cases} \mathbb{C}_{ijkl} = \dfrac{\partial^2 u}{\partial \varepsilon_{ij}\partial \varepsilon_{kl}} = \dfrac{\partial^2 u}{\partial \varepsilon_{kl}\partial \varepsilon_{ij}} \quad \rightarrow \quad \mathbb{C}_{ijkl} = \mathbb{C}_{klij} \\ S_{ijkl} = \dfrac{\partial^2 u^*}{\partial \sigma_{ij}\partial \sigma_{kl}} = \dfrac{\partial^2 u^*}{\partial \sigma_{kl}\partial \sigma_{ij}} \quad \rightarrow \quad S_{ijkl} = S_{klij} \end{cases}$$

1.2.3. Isotropic materials

Some additional considerations about the independent components of $\mathbb{C}$ can be made. For linear-hyperelastic-homogeneous materials the components of $\mathbb{C}$ and $\boldsymbol{S}$ are constant thorough the whole continuous body, they do not depend on the specific point considered. For linear-hyperelastic-homogeneous-isotropic materials the elasticity tensor has only two independent components, ***Young's modulus E*** and ***Poisson's ratio ν***. When discussing metals, we'll always refer to this type of CL, which reads:

$$\begin{cases} \tau_{ij} = \lambda \delta_{ij} \varepsilon_{kk} + 2\mu \varepsilon_{ij} \\ \varepsilon_{ij} = \dfrac{1+\nu}{E}\tau_{ij} - \dfrac{\nu}{E}\tau_{kk}\delta_{ij} \end{cases} \tag{1.16}$$

Where δ_{ij} is the Kronecker delta, a mathematical operator that is 1 if $j = i$, 0 otherwise. Moreover, μ and λ are the ***Lamé constants***, defined as follows:

$$\mu = G = \frac{E}{2(1+\nu)} \qquad \lambda = \frac{E\nu}{(1+\nu)(1-2\nu)} \tag{1.17}$$

Using the Lamé constants, the constitutive laws in equation (1.16) in full form would be:

$$\begin{Bmatrix}\sigma_{xx}\\ \sigma_{yy}\\ \sigma_{zz}\\ \tau_{yz}\\ \tau_{xz}\\ \tau_{xy}\end{Bmatrix} = \frac{E}{(1+\nu)(1-2\nu)}\begin{bmatrix}\begin{bmatrix}1-\nu & \nu & \nu\\ \nu & 1-\nu & \nu\\ \nu & \nu & 1-\nu\end{bmatrix} & [0]\\ [0] & \frac{1-2\nu}{\nu}\begin{bmatrix}1 & 0 & 0\\ 0 & 1 & 0\\ 0 & 0 & 1\end{bmatrix}\end{bmatrix}\begin{Bmatrix}\varepsilon_{xx}\\ \varepsilon_{yy}\\ \varepsilon_{zz}\\ \gamma_{yz}\\ \gamma_{xz}\\ \gamma_{xy}\end{Bmatrix}$$

$$\begin{Bmatrix}\varepsilon_{xx}\\ \varepsilon_{yy}\\ \varepsilon_{zz}\\ \gamma_{yz}\\ \gamma_{xz}\\ \gamma_{xy}\end{Bmatrix} = \frac{1}{E}\begin{bmatrix}\begin{bmatrix}1 & -\nu & -\nu\\ -\nu & 1 & -\nu\\ -\nu & -\nu & 1\end{bmatrix} & [0]\\ [0] & 2(1+\nu)\begin{bmatrix}1 & 0 & 0\\ 0 & 1 & 0\\ 0 & 0 & 1\end{bmatrix}\end{bmatrix}\begin{Bmatrix}\sigma_{xx}\\ \sigma_{yy}\\ \sigma_{zz}\\ \tau_{yz}\\ \tau_{xz}\\ \tau_{xy}\end{Bmatrix} \tag{1.18}$$

Observation. For an isotropic material normal and shear stresses are completely decoupled. Moreover, when we discuss linear-elastic materials in the following chapters of this document, we will always imply linear, hyperelastic, homogeneous and isotropic materials.

Note that, in the constitutive equations above, the stress and strains tensors have been expressed as vectors rather than second order tensors. This is called ***Kelvin-Voigt notation***, and it is often used because it makes very convenient handling equations in structural mechanics. Essentially, given the symmetry of $\boldsymbol{\sigma}, \boldsymbol{\varepsilon}, \mathbb{C}$ and $\boldsymbol{S}$, we can stack their independent components into vectors and matrices. The way we perform this is according to what is depicted in Figure 1.5. It is important to remember that even if these quantities are represented as vectors and matrices, their tensorial nature must be considered when handling them. For example, rotating the stress tensor, even if written in Voigt notation, implies rotating a second order tensor, not a vector. This highlight the fact the matrices and vectors are not tensor, they are a useful way to represent tensors, but the two are different things. For this reason, vectors and matrices in Voigt notation may be represented with the symbols $\{\cdot\}$ and $[\cdot]$, respectively. We'll in general indicate them with the underbars as if they were tensors. Thus, the CL of a linear-hyperelastic material can be written as follows:

$$\begin{cases} u = \frac{1}{2}\underline{\underline{\sigma}} : \underline{\underline{\varepsilon}} = \frac{1}{2}\underline{\underline{\varepsilon}} : \underline{\underline{\underline{\underline{\mathbb{C}}}}} : \underline{\underline{\varepsilon}} \quad \rightarrow \quad u = \frac{1}{2}\{\sigma\}^T\{\varepsilon\} = \frac{1}{2}\{\varepsilon\}^T[\mathbb{C}]\{\varepsilon\} \\ u^* = \frac{1}{2}\underline{\underline{\sigma}} : \underline{\underline{\varepsilon}} = \frac{1}{2}\underline{\underline{\sigma}} : \underline{\underline{\underline{\underline{S}}}} : \underline{\underline{\sigma}} \quad \rightarrow \quad u^* = \frac{1}{2}\{\sigma\}^T\{\varepsilon\} = \frac{1}{2}\{\sigma\}^T[S]\{\sigma\} \end{cases} \tag{1.19}$$

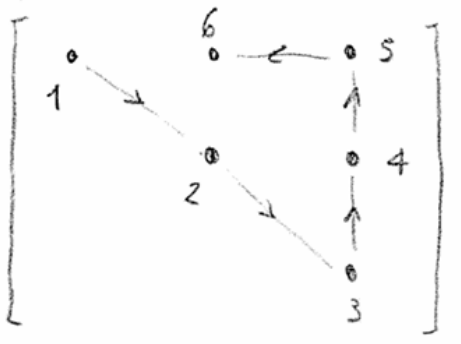

Figure 1.5: stress tensor in Voigt notation.

1.2.3.1. Axial stress state

This type of stress state is typical of rods, which are beam-like structural elements that can only transmit axial loads. Assuming that the rod axis is the z-axis, ***all stresses but σ_{zz} are null***. Thus, the CL will read:

$$\begin{Bmatrix} \varepsilon_{xx} \\ \varepsilon_{yy} \\ \varepsilon_{zz} \\ \gamma_{xy} \\ \gamma_{yz} \\ \gamma_{zx} \end{Bmatrix} = \frac{1}{E} \begin{bmatrix} \begin{bmatrix} 1 & -\nu & -\nu \\ -\nu & 1 & -\nu \\ -\nu & -\nu & 1 \end{bmatrix} & [0] \\ [0] & 2(1+\nu) \begin{bmatrix} 1 & 0 & 0 \\ 0 & 1 & 0 \\ 0 & 0 & 1 \end{bmatrix} \end{bmatrix} \begin{Bmatrix} 0 \\ 0 \\ \sigma_{zz} \\ 0 \\ 0 \\ 0 \end{Bmatrix}$$

Because shear and normal stresses are decoupled, and because all shear stresses are null, all shear strains are null as well. However, ***not all normal strains are null***. In fact, explicitly writing the non-null terms of the CL, it is clear that the normal strains in the plane of the cross section, ε_{xx} and ε_{yy}, are not null. More precisely, as the rod elongates the cross section shrinks due to the Poisson's effect, as shown in Figure 1.6.

$$\begin{cases} \varepsilon_{xx} = -\nu \dfrac{\sigma_{zz}}{E} \\ \varepsilon_{yy} = -\nu \dfrac{\sigma_{zz}}{E} \\ \varepsilon_{zz} = \dfrac{\sigma_{zz}}{E} \end{cases} \tag{1.20}$$

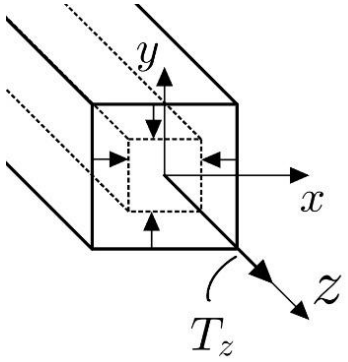

Figure 1.6: displacements of a rod subject to axial loading.

1.2.3.2. Beam stress state

A beam, differently from rods, will generally be subject to shear loads as well as axial loads. Beams will be discussed in depth in Chapter 2, nonetheless, we report here only what's necessary to discuss the constitutive law of beams. The reference frame is the same of rods. The very ***basic assumption*** of beam theory is that the stress components σ_{xx}, σ_{yy} and τ_{xy} are all null. Consequently, the only non-null stress components will be the ones acting on the cross sectional plane σ_{zz}, τ_{zx} and τ_{zy}. Under this assumption, the CL of equation (1.18) reduces to:

$$\begin{Bmatrix} \varepsilon_{xx} \\ \varepsilon_{yy} \\ \varepsilon_{zz} \\ \gamma_{yz} \\ \gamma_{xz} \\ \gamma_{xy} \end{Bmatrix} = \frac{1}{E} \begin{bmatrix} \begin{bmatrix} 1 & -\nu & -\nu \\ -\nu & 1 & -\nu \\ -\nu & -\nu & 1 \end{bmatrix} & [0] \\ [0] & 2(1+\nu) \begin{bmatrix} 1 & 0 & 0 \\ 0 & 1 & 0 \\ 0 & 0 & 1 \end{bmatrix} \end{bmatrix} \begin{Bmatrix} 0 \\ 0 \\ \sigma_{zz} \\ \tau_{yz} \\ \tau_{xz} \\ 0 \end{Bmatrix}$$

Thus, additionally to the strain components in equation (1.20), characterizing the purely axial stress state of rods, beams also present non-null shear strains γ_{zx}, γ_{zy}:

$$\begin{cases} \varepsilon_{xx} = -\dfrac{\nu\sigma_{zz}}{E} \\ \varepsilon_{yy} = -\dfrac{\nu\sigma_{zz}}{E} \\ \varepsilon_{zz} = \dfrac{\sigma_{zz}}{E} \end{cases} \qquad \begin{cases} \gamma_{xy} = 0 \\ \gamma_{yz} = \dfrac{\tau_{yz}}{G} \\ \gamma_{xz} = \dfrac{\tau_{xz}}{G} \end{cases} \tag{1.21}$$

In beams, axial stresses can be generated by axial loads as well as by bending moments. This affects the expression of the normal axial stress σ_{zz} and the strain and displacement fields. More precisely, the axial stress will be computed as:

$$\sigma_{zz} = \begin{cases} \dfrac{T_z}{A}, & \text{pure axial load} \\ \dfrac{M_x}{I_{xx}} y, & \text{pure bending load} \end{cases}$$

The beam deformation in the case of pure axial load is the one presented in Figure 1.6, while the one due to pure bending loading is depicted in Figure 1.7. Notice that, for pure bending, since all shear strains are null, the beam cross sections remain normal to the beam axis during bending.

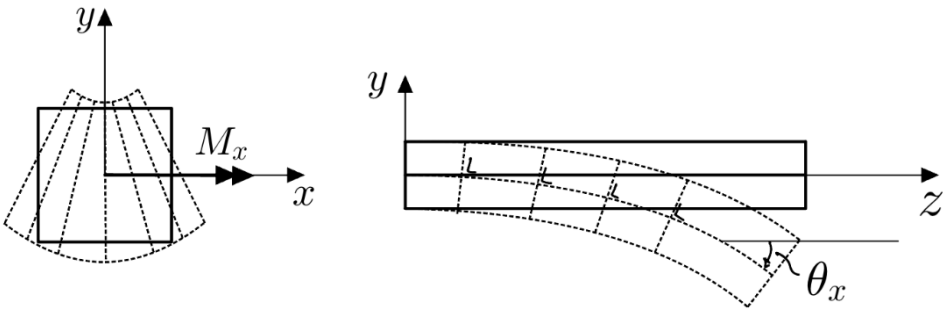

Figure 1.7: deformation of a beam's cross section (left) and axis (right) due to a pure bending moment M_x.

1.2.3.3. Plane stress state

Plates are discussed in detail in Chapter 3, we report here only what needed to discuss the CL. The typical reference frame for plates is with the x-y-axes as the in-plane coordinates, and the z-axis as the out-of-plane coordinate, as in the figure below.

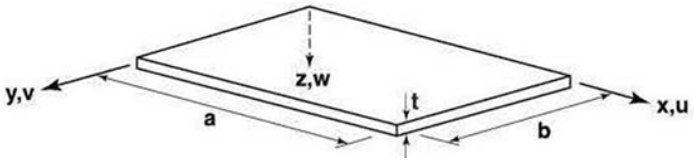

Figure 1.8: plate with reference frame.

A plane state of stress implies that all the out-of-plane stresses σ_{zz}, τ_{xz} and τ_{yz} are null. This, however, does not imply that the out-of-plane normal strain ε_{zz} is null. This stress state is typical

of many aeronautical components, such as panels in the semi-monocoque scheme. Under this assumption, the CL of equation (1.18) reduces to:

$$\begin{Bmatrix}\varepsilon_{xx}\\ \varepsilon_{yy}\\ \gamma_{xy}\end{Bmatrix}=\frac{1}{E}\begin{bmatrix}1 & -\nu & 0\\ -\nu & 1 & 0\\ 0 & 0 & 2(1+\nu)\end{bmatrix}\begin{Bmatrix}\sigma_{xx}\\ \sigma_{yy}\\ \tau_{xy}\end{Bmatrix}$$
$$\begin{Bmatrix}\sigma_{xx}\\ \sigma_{yy}\\ \tau_{xy}\end{Bmatrix}=\frac{E}{1-\nu^2}\begin{bmatrix}1 & \nu & 0\\ \nu & 1 & 0\\ 0 & 0 & \frac{1-\nu}{2}\end{bmatrix}\begin{Bmatrix}\varepsilon_{xx}\\ \varepsilon_{yy}\\ \gamma_{xy}\end{Bmatrix} \tag{1.22}$$

1.2.3.4. Plane strain state

This CL implies that the out-of-plane strain ε_{zz} is null, while the corresponding stress component σ_{zz} is not null. This condition is typical of beams constrained at their ends, not free to deform along the axial coordinate, or gaskets. The CL will be:

$$\begin{Bmatrix}\sigma_{xx}\\ \sigma_{yy}\\ \sigma_{zz}\end{Bmatrix}=\frac{E}{(1+\nu)(1-2\nu)}\begin{bmatrix}1-\nu & \nu & \nu\\ \nu & 1-\nu & \nu\\ \nu & \nu & 1-\nu\end{bmatrix}\begin{Bmatrix}\varepsilon_{xx}\\ \varepsilon_{yy}\\ 0\end{Bmatrix}$$
$$\begin{Bmatrix}\varepsilon_{xx}\\ \varepsilon_{yy}\\ 0\end{Bmatrix}=\frac{1}{E}\begin{bmatrix}1 & -\nu & -\nu\\ -\nu & 1 & -\nu\\ -\nu & -\nu & 1\end{bmatrix}\begin{Bmatrix}\sigma_{xx}\\ \sigma_{yy}\\ \sigma_{zz}\end{Bmatrix} \tag{1.23}$$

Here, the last equation of the CL in the form $\boldsymbol{\varepsilon}=\boldsymbol{\varepsilon}(\boldsymbol{\sigma})$ simply states that the out-of-plane stress component is not independent, but it is determined as $\sigma_{zz}=\nu\left(\sigma_{xx}+\sigma_{yy}\right)$.

1.3. Compatibility equations

Compatibility equations express a simple idea: the displacement field is required to respect some conditions in order to be "compatible". In short, compatibility equations express relations between the terms ε_{ij} to guarantee the compatibility of the resulting strain field. The condition to be fulfilled to guarantee compatibility is the following:

$$\underline{\underline{\varepsilon}} = \frac{1}{2}\left(\nabla\underline{u} + \nabla\underline{u}^T\right) \quad \text{or} \quad \underline{\underline{\varepsilon}} - \frac{1}{2}\left(\nabla\underline{u} + \nabla\underline{u}^T\right) = 0$$

Where, sometimes, the second form is preferred in order to clarify that it is an equation and not a definition. Often, the compatibility condition is imposed in a strong manner and does not need to be imposed. In many other cases, the De Saint Venant problem is an example, the strains are part of the problem unknowns. In such cases, the deformation field must satisfy the compatibility conditions in order to make it sure that the solution, both in terms of displacements and strains, is compatible.

To derive the compatibility equations, we begin with the strain components associated to the x-y plane. According to the definition provided by the small strain tensor $\boldsymbol{\varepsilon}$, and taking the derivatives of these strains as below, we may define the first compatibility equation:

$$\begin{cases} \varepsilon_{xx} = u_{/x} \\ \varepsilon_{yy} = v_{/y} \\ \gamma_{xy} = u_{/y} + v_{/x} \end{cases} \rightarrow \begin{cases} \varepsilon_{xx/yy} = u_{/xyy} \\ \varepsilon_{yy/xx} = v_{/yxx} \\ \gamma_{xy/xy} = u_{/xyy} + v_{/xxy} \end{cases} \rightarrow \quad \varepsilon_{xx/yy} + \varepsilon_{yy/xx} - \gamma_{xy/xy} = 0$$

Consider now the three shearing strains along with ε_{xx}, by applying a similar process we obtain a second compatibility equation:

$$\begin{cases} \gamma_{xy} = u_{/y} + v_{/x} \\ \gamma_{yz} = v_{/z} + w_{/y} \\ \gamma_{zx} = w_{/x} + u_{/z} \\ \varepsilon_{xx} = u_{/x} \end{cases} \rightarrow \begin{cases} \gamma_{xy/xz} = u_{/xyz} + v_{/xxz} \\ \gamma_{yz/xx} = v_{/xxz} + w_{/xxy} \\ \gamma_{zx/xy} = w_{/xxy} + u_{/xyz} \\ \varepsilon_{xx/yz} = u_{/xyz} \end{cases} \rightarrow \gamma_{xy/xz} + \gamma_{zx/xy} - \gamma_{yz/xx} - 2\varepsilon_{xx/yz} = 0$$

Starting from the two equations here derived, we may obtain the remaining compatibility equations by cycling the indices $x \rightarrow y \rightarrow z$ in a closed loop. This yields the following equations:

$$\begin{cases} \varepsilon_{xx/yy} + \varepsilon_{yy/xx} - \gamma_{xy/xy} = 0 \\ \varepsilon_{yy/zz} + \varepsilon_{zz/yy} - \gamma_{yz/yz} = 0 \\ \varepsilon_{zz/xx} + \varepsilon_{xx/zz} - \gamma_{zx/zx} = 0 \\ \gamma_{xy/xz} + \gamma_{zx/xy} - \gamma_{yz/xx} - 2\varepsilon_{xx/yz} = 0 \\ \gamma_{yz/yx} + \gamma_{xy/yz} - \gamma_{zx/yy} - 2\varepsilon_{yy/zx} = 0 \\ \gamma_{zx/zy} + \gamma_{yz/zx} - \gamma_{xy/zz} - 2\varepsilon_{zz/xy} = 0 \end{cases} \tag{1.24}$$

In elasticity it is useful sometimes to solve problems using compatibility equations rather than imposing that $\varepsilon_{ij} = 1/2\left(u_{i/j} + u_{j/i}\right)$, which invokes both strains and displacements components.

1.4. Equilibrium equations

1.4.1. Conservation of linear momentum

Continuum body approach. The conservation of linear momentum is simply Newtons second law, and it states that the time derivative of the linear momentum $m\mathbf{v}$, is equal to the externally applied forces $\boldsymbol{f}(t)$.

$$\frac{D}{Dt}(m\underline{v}) = \underline{f}(t) \tag{1.25}$$

To adapt this equation to continuous bodies, we can rewrite the mass in terms of density and the total force in terms of body forces $\boldsymbol{b}$ and traction forces $\boldsymbol{t}$. By doing so we obtain:

$$\frac{D}{Dt}\int_v \rho\underline{v}(\underline{x},t)dv = \int_v \underline{b}\, dv + \int_s \underline{t}\, ds$$

The time derivative of the left hand side simply yields:

$$\frac{D}{Dt}\int_v \rho\underline{v}(\underline{x},t)dv = \int_v \rho\underline{a}(\underline{x},t)dv$$

The right hand side of the equilibrium equation is rewritten using the definition of stress tensor $\boldsymbol{\sigma}$ and then using the divergence theorem.

$$\int_v \underline{b}dv + \int_s \underline{t}ds = \int_v \underline{b}dv + \int_s \underline{\underline{\sigma}}\cdot\underline{n}ds = \int_v \underline{b}dv + \int_v \nabla\cdot\underline{\underline{\sigma}}dv$$

The linear momentum conservation equation is then:

$$\rho_0\underline{a} = \underline{b} + \nabla\cdot\underline{\underline{\sigma}} \tag{1.26}$$

Infinitesimal element approach. An alternative approach to the linear momentum equilibrium equation is to impose this equilibrium condition on the stresses acting on an infinitesimal element of the elastic continuous body [1]. Assume the infinitesimal element shown in Figure 1.9 to have dimensions $d\boldsymbol{x} = \{dx, dy, dz\}^T$. In general, stresses on opposite faces of such element are not equal, but they still must satisfy equilibrium accounting for body forces $\boldsymbol{b} = \{b_x, b_y, b_z\}^T$ as well, not shown in the figure. Some additional ***observations***:

- Surface forces acting on the boundary of the body, although contributing to the production of the internal stress system, do not directly feature in the equilibrium equations.
- Note that the ***notation of the stresses*** in Figure 1.9 is opposite to the one previously defined, i.e. the first index identifies the normal of the face, while the second represents the stress direction.
- In this case we neglect inertial forces.

Consider the equilibrium of the element along the x-axis:

$$\left(\sigma_x + \frac{\partial \sigma_x}{\partial x}dx - \sigma_x\right)dydz + \left(\tau_{yx} + \frac{\partial \tau_{yx}}{\partial y}dy - \tau_{yx}\right)dxdz + \left(\tau_{zx} + \frac{\partial \tau_{zx}}{\partial z}dz - \tau_{zx}\right)dxdy + b_x dxdydz = 0$$

$$\frac{\partial \sigma_x}{\partial x} + \frac{\partial \tau_{yx}}{\partial y} + \frac{\partial \tau_{zx}}{\partial z} + b_x = 0$$

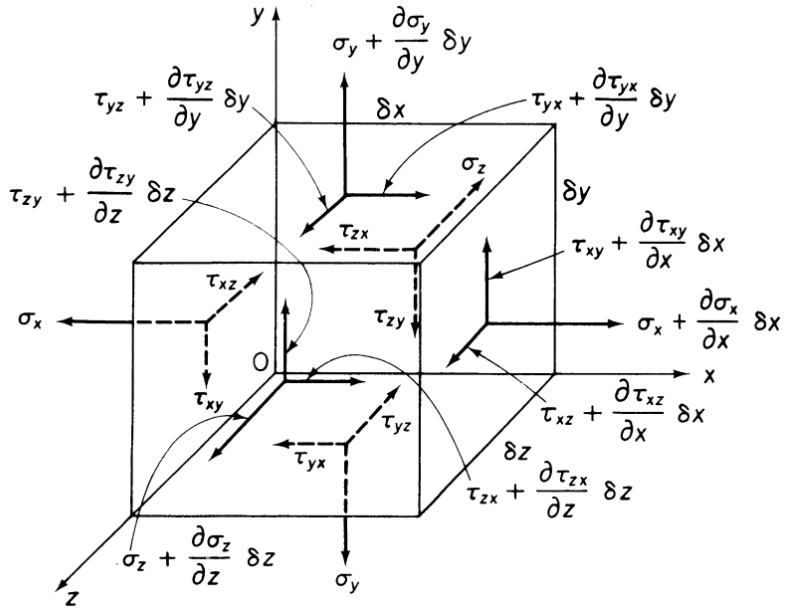

Figure 1.9: stresses acting on a point of the elastic body.

Analogous equations to the one just obtained can be written along the y-z-axes, resulting in a system of three equations representing equilibrium. Exploiting the symmetry of the stress tensor, which will be proven in section 1.4.3, it's clear that the system of equation (1.27) is completely equivalent to (the static case of) the system in equation (1.26).

$$\begin{cases} \frac{\partial \sigma_{xx}}{\partial x} + \frac{\partial \tau_{xy}}{\partial y} + \frac{\partial \tau_{xz}}{\partial z} + b_x = 0 \\ \frac{\partial \tau_{yx}}{\partial x} + \frac{\partial \sigma_{yy}}{\partial y} + \frac{\partial \tau_{yz}}{\partial z} + b_y = 0 \\ \frac{\partial \tau_{zx}}{\partial x} + \frac{\partial \tau_{zy}}{\partial y} + \frac{\partial \sigma_{zz}}{\partial z} + b_z = 0 \end{cases} \quad \rightarrow \quad \sigma_{ij/j} + b_i = 0 \quad \rightarrow \quad \nabla \cdot \underline{\underline{\sigma}} + \underline{b} = \underline{0} \tag{1.27}$$

1.4.2. Conservation of angular momentum

The conservation of angular momentum relates the external moments $\boldsymbol{M}$, the position $\boldsymbol{x}$ and velocity $\mathbf{v}$ of the particle in a spatial frame as follows:

$$\frac{D}{Dt}\left(\underline{x} \times m\underline{v}\right) = \underline{M}(t) \tag{1.28}$$

To adapt this equation to a 3D continuum we express the mass m in terms of density ρ, and the external moments vector $\boldsymbol{M}$ in terms of body forces $\boldsymbol{b}$, body moments $\boldsymbol{m}$, surface forces $\boldsymbol{t}$ and surface moments $\boldsymbol{c}$.

$$\frac{D}{Dt}\int_v \underline{x}\times\rho\underline{v}\,dv = \int_v (\underline{x}\times\underline{b}+\underline{m})dv + \int_s (\underline{x}\times\underline{t}+\underline{c})ds$$

Recall that a Cauchy continuum cannot exchange moments per unit volume and/or surface, thus $\boldsymbol{m}=\boldsymbol{c}=\mathbf{0}$. Thus, the conservation of angular momentum for a Cauchy continuum reads:

$$\frac{D}{Dt}\int_v \underline{x}\times\rho\underline{v}\,dv = \int_v \underline{x}\times\underline{b}\,dv + \int_s \underline{x}\times\underline{t}\,ds$$

The time derivative on the left hand side simply yields:

$$\frac{D}{Dt}\int_v \underline{x}\times\rho\underline{v}\,dv = \int_v \frac{D\underline{x}}{Dt}\times\rho\underline{v} + \underline{x}\times\rho\frac{D\underline{v}}{Dt}dv = \int_v \underline{v}\times\rho\underline{v} + \underline{x}\times\rho\underline{a}\,dv = \int_v \underline{x}\times\rho\underline{a}\,dv$$

Where we used that $\mathbf{v}\times\mathbf{v}=\mathbf{0}$. The right hand side of the equation does not need rewriting. Thus, the angular momentum equilibrium equation is the following:

$$\int_v \underline{x}\times\rho\underline{a}\,dv = \int_v \underline{x}\times\underline{b}dv + \int_s \underline{x}\times\underline{t}ds \tag{1.29}$$

Observation. For this conservation principle we do not present the case of continuous body approach and infinitesimal element approach. This is because the latter directly leads to the symmetry of $\boldsymbol{\sigma}$, which is the only reason we introduced this equilibrium equation to begin with.

1.4.3. Symmetry of the stress tensor

Continuous body approach. Equation ((1.29) can be used to prove the symmetry of the Cauchy stress tensor $\boldsymbol{\sigma}$. We start by expressing the spatial traction vector $\boldsymbol{t}$ in terms of the Cauchy stress tensor $\boldsymbol{\sigma}$:

$$\int_s \underline{x}\times\underline{t}ds = \int_s \underline{x}\times\left(\underline{\sigma}\cdot\underline{n}\right)ds$$

We now want to rewrite this integral in the form of $\int_s(\cdot)\cdot\boldsymbol{n}\,ds$ to then apply the divergence theorem to obtain a volume integral. To this end, recall that $\boldsymbol{a}\times\boldsymbol{b}=\varepsilon_{ijk}a_jb_k$, where ε_{ijk} is the ***permutation operator***, which can assume three values:

- $\varepsilon_{ijk}=+1$ if the indices increase until the limit is reached and then they start over.
- $\varepsilon_{ijk}=-1$ if the indices are not increasing but there are no doubles.
- $\varepsilon_{ijk}=0$ if the indices have one double, i.e. 212 or 311.

$$\int_s \underline{x}\times\left(\underline{\sigma}\cdot\underline{n}\right)ds = \int_s \varepsilon_{ijk}x_j\sigma_{kr}n_r ds$$

We now apply the divergence theorem, yielding:

$$\int_v \varepsilon_{ijk}\left(x_j\sigma_{kr}\right)_{/r}dv = \int_v \varepsilon_{ijk}\left(x_{j/r}\sigma_{kr}+x_j\sigma_{kr/r}\right)dv \xrightarrow{x_{j/r}=\delta_{jr}} \int_v \varepsilon_{ijk}\left(\sigma_{kj}+x_j\sigma_{kr/r}\right)dv$$

Where we used that $x_{i/r} = 1$ if $r = i$, 0 otherwise. Thus, the integral can be written as follows:

$$\int_v \varepsilon_{ijk}\left(\sigma_{kj} + x_j \sigma_{kr/r}\right) dv = \int_v \varepsilon_{ijk}\sigma_{kj} + \underline{x} \times \nabla \cdot \underline{\underline{\sigma}} dv$$

Using this result, we can rewrite the balance of angular momentum as follows:

$$\int_v \underline{x} \times \rho \underline{a} dv = \int_v \underline{x} \times \underline{b} dv + \int_v \underline{x} \times \nabla \cdot \underline{\underline{\sigma}} dv + \int_v \varepsilon_{ijk}\sigma_{ji} dv$$

Since the equation must hold true for any volume v, we may write:

$$\underline{x} \times \left(\rho \underline{a} - \underline{b} - \nabla \cdot \underline{\underline{\sigma}}\right) = \varepsilon_{ijk}\sigma_{ji}$$

Recall the linear momentum balance equation ((1.26), according to which the left hand side of the above equation is null. We remain with:

$$\varepsilon_{ijk}\sigma_{kj} = 0$$

This last equation corresponds to a system of three scalar equations, for $i = 1,2,3$. Given the interpretation of the permutation operator, such equations prove the symmetry of the Cauchy stress tensor.

$$\begin{cases} \varepsilon_{123}\sigma_{32} + \varepsilon_{132}\sigma_{23} = 0 \\ \varepsilon_{213}\sigma_{31} + \varepsilon_{231}\sigma_{13} = 0 \\ \varepsilon_{312}\sigma_{21} + \varepsilon_{321}\sigma_{12} = 0 \end{cases} \rightarrow \begin{cases} +\sigma_{32} - \sigma_{23} = 0 \\ -\sigma_{31} + \sigma_{13} = 0 \\ +\sigma_{21} - \sigma_{12} = 0 \end{cases} \rightarrow \underline{\underline{\sigma}} = \underline{\underline{\sigma}}^T \tag{1.30}$$

Infinitesimal element approach. As previously mentioned, in this case writing the angular momentum equilibrium equation directly leads to the symmetry of the stress tensor. With respect to Figure 1.9, we take moments about an axis through the center of the element and parallel to the z-axis. Thus, the only terms contributing to the moment equilibrium are those related to τ_{xy} and τ_{yx}. In this case the differentiation between the two matters because of the arms of the respective stress components, which are different. Rotational equilibrium reads:

$$\left(\tau_{xy} + \frac{\partial \tau_{xy}}{\partial x} dx + \tau_{xy}\right) dydz \cdot \frac{dx}{2} - \left(\tau_{yx} + \frac{\partial \tau_{yx}}{\partial y} dy + \tau_{yx}\right) dxdz \cdot \frac{dy}{2} = 0$$

$$\frac{1}{2}\left(2\tau_{xy} + \frac{\partial \tau_{xy}}{\partial x} dx\right) - \frac{1}{2}\left(2\tau_{yx} + \frac{\partial \tau_{yx}}{\partial y} dy\right) = 0$$

For an infinitesimal element $\{dx, dy\} \rightarrow 0$, and thus the equation simplifies to $\tau_{xy} = \tau_{yx}$. Writing the same equations along the x-y-axes we obtain similar relations, proving that $\boldsymbol{\sigma} = \boldsymbol{\sigma}^T$.

$$\begin{cases} \tau_{xy} = \tau_{yx} \\ \tau_{yz} = \tau_{zy} \\ \tau_{zx} = \tau_{xz} \end{cases} \rightarrow \underline{\underline{\sigma}} = \underline{\underline{\sigma}}^T \tag{1.31}$$

1.5. Variational forms

The solution of the elastic problem, or structural problem, requires that both equilibrium and compatibility are fulfilled. Both sets of equations have been derived in the previous sections. When the solution is obtained by solving the PDEs, i.e. the indefinite equilibrium equations, it is said that the problem is formulated in a ***strong form***. Another approach consists in solving the problem in a ***weak form***. This latter approach is the more common one in structural mechanics, for various reasons (numerical implementation is relatively easy, the requirements on the regularity of the solution are relaxed and more). Among the class of weak form formulations, a special set is given by the ***variational principles***, such as:

- PVW and Minimum Potential energy: they impose equilibrium while compatibility is assumed to be satisfied a priori. The unknown field is the displacement field $\boldsymbol{u}$, making these displacement-based approaches.
- CPVW and Menabrea's theorem: they impose compatibility while equilibrium is satisfied a priori. In this case the unknown field is the force/load field $\boldsymbol{t}$, making these force-based approaches.

Observation. Despite the mentioned variational principles requiring either compatibility or equilibrium to be satisfied a priori, there exist more advanced variational principles for which this is not a prerequisite to solve to structural problem. We call these class ***mixed approaches***, and they are not subject of this section, we'll focus on the previously mentioned principle.

1.5.1. Principle of virtual work

1.5.1.1. PVW from strong form

In order to obtain the weak form one must start from the strong form of equilibrium, i.e. the equilibrium and compatibility conditions:

$$\begin{cases} \underline{b} + \nabla \cdot \underline{\underline{\sigma}} = \underline{0} & \text{in } V \\ \underline{\underline{\varepsilon}} - \frac{1}{2}\left(\nabla \underline{u} + \nabla \underline{u}^T\right) = \underline{\underline{0}} & \text{in } V \\ \underline{t} - \underline{\hat{t}} = \underline{0} & \text{on } S_F \\ \underline{u} - \underline{\hat{u}} = \underline{0} & \text{on } S_u \end{cases} \tag{1.32}$$

Where $\boldsymbol{b}$ is the body force, $\hat{\boldsymbol{t}}$ is the prescribed surface force on the surface S_F, and $\hat{\boldsymbol{u}}$ is the prescribed displacement on the surface S_u. The surfaces S_u and S_F are the portions of the external surface of the body of volume V where loads and displacements are prescribed, respectively. They must be such that their intersection is null, i.e. $S_F \cap S_u = 0$, and their union must form the complete surface of the body, i.e. $S = S_u \cup S_F$. Note that a point that is not constrained belongs to S_F even when the prescribed load is zero. An unloaded portion of the body is a portion of S_F where the load is zero.

Observation. The equations of the strong form are written in the general form $\mathrm{f}(\boldsymbol{x}) = \boldsymbol{0}$ rather than the form $\boldsymbol{\varepsilon} = 1/2(\nabla\delta\boldsymbol{u} + \nabla\delta\boldsymbol{u}^T)$, taking the compatibility equation as an example. This is to highlight that these are not to be interpreted as definitions in this context, but as conditions (of compatibility and equilibrium) to be satisfied in order to find a proper solution to the structural problem.

As previously mentioned, we assume that the compatibility conditions on S_u and in V are satisfied a priori. In order to obtain the weak form, consider a virtual displacement field $\delta\boldsymbol{u}$ such that it's

continuous in V, arbitrary, and it satisfies the compatibility condition $\delta\boldsymbol{u} = \mathbf{0}$ on S_u. Using such virtual displacement we may write:

$$\int_V \delta\underline{u} \cdot \left(\nabla \cdot \underline{\underline{\sigma}} + \underline{b}\right) dV - \int_V \delta\underline{u} \cdot \left(\underline{t} - \underline{\hat{t}}\right) dS = 0 \qquad \forall \delta\underline{u} : \delta\underline{u} = \underline{0} \text{ on } S_u$$

Because the integrals above are of the form $\int \delta\boldsymbol{u}(\dots) = 0$ and $\delta\boldsymbol{u}$ is arbitrary, it must be true that $(\dots) = 0$ for any $\delta\boldsymbol{u}$. In other words, we are enforcing equilibrium to always be verified, in the volume via the linear momentum equilibrium equation and on the external surface of the body via the natural BC. The first term of the volume integral may be rewritten using index notation:

$$\begin{aligned}\int_V \delta\underline{u} \cdot \nabla \cdot \underline{\underline{\sigma}} dV &= \int_V \delta u_i \sigma_{ij/j} dV = \int_V \left[\left(\delta u_i \sigma_{ij}\right)_{/j} - \delta u_{i/j}\, \sigma_{ij}\right] dV \\ &= \int_V \left[\nabla \cdot \left(\delta\underline{u} \cdot \underline{\underline{\sigma}}\right) - \nabla\delta\underline{u} : \underline{\underline{\sigma}}\right] dV\end{aligned}$$

Applying the divergence theorem to the first volume integral and using $S = S_F + S_u$ yields:

$$\int_V \nabla \cdot \left(\delta\underline{u} \cdot \underline{\underline{\sigma}}\right) dV = \int_S \delta\underline{u} \cdot \underline{\underline{\sigma}} \cdot \underline{n}\, dS = \underbrace{\int_{S_u} \delta\underline{u} \cdot \underline{\underline{\sigma}} \cdot \underline{n}\, dS}_{\delta\underline{u}=\underline{0} \text{ on } S_u} + \int_{S_F} \delta\underline{u} \cdot \underline{\underline{\sigma}} \cdot \underline{n}\, dS = \int_{S_F} \delta\underline{u} \cdot \underline{t} dS$$

Where we used that $\boldsymbol{\sigma} \cdot \boldsymbol{n} = \boldsymbol{t}$ and we enforced the compatibility of the virtual displacement field on the constrained portion of the external surface of the body, i.e. $\delta\boldsymbol{u} = \mathbf{0}$ on S_u. We now focus on the term $\nabla\delta\boldsymbol{u} : \boldsymbol{\sigma}$, exploiting the symmetry of the stress tensor $\boldsymbol{\sigma} = \boldsymbol{\sigma}^{\boldsymbol{T}}$ it follows that $\boldsymbol{\sigma}$: sym$(\cdot) = \boldsymbol{\sigma}$: $(\cdot)$. Applying this at the case at hand yields:

$$\nabla\delta\underline{u} : \underline{\underline{\sigma}} = \text{sym}\left(\nabla\delta\underline{u}\right) : \underline{\underline{\sigma}} = \frac{1}{2}\left(\nabla\delta\underline{u} + \nabla\delta\underline{u}^T\right) : \underline{\underline{\sigma}} = \delta\underline{\underline{\varepsilon}} : \underline{\underline{\sigma}}$$

Where the fact that $\delta\boldsymbol{\varepsilon} = 1/2(\nabla\delta\boldsymbol{u} + \nabla\delta\boldsymbol{u}^T)$ is satisfied because compatibility is granted a priori. Substituting what we found into the original equation, we obtain the following:

$$\int_{S_F} \delta\underline{u} \cdot \underline{t} dS - \int_V \delta\underline{\underline{\varepsilon}} : \underline{\underline{\sigma}}\, dV + \int_V \delta\underline{u} \cdot \underline{b}\, dV - \int_V \delta\underline{u} \cdot \left(\underline{t} - \underline{\hat{t}}\right) dS = 0 \qquad \forall \delta\underline{u} : \delta\underline{u} = \underline{0} \text{ on } S_u$$

Reorganizing and simplifying the above equation yields the ***Principle of Virtual Work (PVW)***, which states that if a structure is in equilibrium, then the internal virtual work δW_D must be equal to the external virtual work δW_e.

$$\underbrace{\int_V \delta\underline{\underline{\varepsilon}} : \underline{\underline{\sigma}}\, dV}_{\delta W_D} = \underbrace{\int_V \delta\underline{u} \cdot \underline{b}\, dV + \int_{S_F} \delta\underline{u} \cdot \underline{\hat{t}}\, dS}_{\delta W_e} \qquad \forall \delta\underline{u} : \delta\underline{u} = \underline{0} \text{ on } S_u \tag{1.33}$$

Some ***important observations*** can be made:

- The PVW is one scalar equation containing all the information of the strong form, which is a system of equations containing PDEs.
- Enforcing equilibrium via the weak form, i.e. the PVW, implies that its solution satisfies both the equilibrium equation in V and the equilibrium condition on S_F.

- Because no reference is made about any type of CL in the PVW formulation, the PVW holds true for any continuum body. We will see that this is not true for the total potential energy principle and Menabrea's theorem.

1.5.1.2. Strong form from PVW

Clearly, the reverse process can be performed, and the equilibrium conditions can be obtained starting from the PVW. Staring from equation (1.33), the virtual strain energy density δu can be rewritten as follows:

$$\delta u = \delta\underline{\underline{\varepsilon}} : \underline{\underline{\sigma}} = \frac{1}{2}\left(\nabla\delta\underline{u} + \nabla\delta\underline{u}^T\right) : \underline{\underline{\sigma}} = \mathrm{sym}\left(\nabla\delta\underline{u}\right) : \underline{\underline{\sigma}} = \nabla\delta\underline{u} : \underline{\underline{\sigma}}$$

Where we used the symmetry of the stress tensor and the fact that compatibility is granted a priori. Thus, the internal virtual work is rewritten as follows:

$$\delta W_D = \int_V \delta\underline{\underline{\varepsilon}} : \underline{\underline{\sigma}}\, dV = \int_V \nabla\delta\underline{u} : \underline{\underline{\sigma}}\, dV \qquad \forall\delta\underline{u} : \delta\underline{u} = \underline{0} \text{ on } S_u$$

Using index notation we can rewrite the internal virtual work as follows:

$$\delta W_D = \int_V \delta u_{i/k}\sigma_{ik} dV = \int_V \left[(\delta u_i\sigma_{ik})_{/k} - \delta u_i\sigma_{ik/k}\right] dV = \int_V \left[\nabla\cdot\left(\delta\underline{u}\cdot\underline{\underline{\sigma}}\right) - \delta\underline{u}\cdot\nabla\cdot\underline{\underline{\sigma}}\right] dV$$

The first part of this integral can be rewritten as follows:

$$\int_V \nabla\cdot\left(\delta\underline{u}\cdot\underline{\underline{\sigma}}\right) dV = \int_{S_F} \delta\underline{u}\cdot\underline{\underline{\sigma}}\cdot\underline{n}\, dS = \int_{S_F} \delta\underline{u}\cdot\underline{t}\, dS$$

Where we used the divergence theorem and then $\boldsymbol{\sigma}\cdot\boldsymbol{n} = \boldsymbol{t}$. Thus, the PVW can be written as follows:

$$\int_V \delta\underline{u}\cdot\left(\underline{b} + \nabla\cdot\underline{\underline{\sigma}}\right) dV + \int_{S_F} \delta\underline{u}\cdot\left(\hat{\underline{t}} - \underline{t}\right) dS \qquad \forall\delta\underline{u} : \delta\underline{u} = \underline{0} \text{ on } S_u$$

If this equation is verified for any $\delta\boldsymbol{u}$ and compatibility is satisfied a priori, then it must also be true that:

$$\begin{cases} \underline{b} + \nabla\cdot\underline{\underline{\sigma}} = \underline{0} & \text{in } V \\ \underline{\underline{\varepsilon}} - \frac{1}{2}\left(\nabla\underline{u} + \nabla\underline{u}^T\right) = \underline{\underline{0}} & \text{in } V \\ \underline{t} - \hat{\underline{t}} = \underline{0} & \text{on } S_F \\ \underline{u} - \hat{\underline{u}} = \underline{0} & \text{on } S_u \end{cases}$$

1.5.2. Principle of complementary virtual work

1.5.2.1. PCVW from compatibility

Again, in order to obtain the weak form one must start from the strong form:

$$\begin{cases} \underline{b} + \nabla \cdot \underline{\underline{\sigma}} = \underline{0} & \text{in } V \\ \underline{\underline{\varepsilon}} - \frac{1}{2}\left(\nabla \underline{u} + \nabla \underline{u}^T\right) = \underline{\underline{0}} & \text{in } V \\ \underline{t} - \underline{\hat{t}} = \underline{0} & \text{on } S_F \\ \underline{u} - \underline{\hat{u}} = \underline{0} & \text{on } S_u \end{cases}$$

In this case we assume that equilibrium conditions in V and S_F are satisfied a priori, and we must find the solution of the structural problem, in terms of forces, that satisfies compatibility. Thus, consider the virtual fields $\delta\boldsymbol{\sigma}$ and $\delta\boldsymbol{b}$ such that they are arbitrary, continuous in V and respect the equilibrium conditions. Then, the compatibility conditions can be reformulated as follows:

$$\int_V \delta\underline{\underline{\sigma}} : \left[\underline{\underline{\varepsilon}} - \frac{1}{2}\left(\nabla \underline{u} + \nabla \underline{u}^T\right)\right] dV + \int_{S_u} \delta\underline{t} \cdot \left(\underline{u} - \underline{\hat{u}}\right) dS = 0$$

$$\forall \delta\underline{\underline{\sigma}} \text{ and } \delta\underline{b} : \begin{cases} \nabla \cdot \delta\underline{\underline{\sigma}} + \delta\underline{b} = \underline{0} & \text{in } V \\ \delta\underline{\underline{\sigma}} \cdot \underline{n} = \delta\underline{t} = \delta\underline{\hat{t}} & \text{on } S_F \end{cases}$$

We elaborate the volume integral by exploiting the symmetry of the stress tensor $\delta\boldsymbol{\sigma} : (\cdot) = \delta\boldsymbol{\sigma} : \mathrm{sym}(\cdot)$, which yields:

$$\int_V -\delta\underline{\underline{\sigma}} : \frac{1}{2}\left(\nabla \underline{u} + \nabla \underline{u}^T\right) dV = \int_V -\delta\underline{\underline{\sigma}} : \mathrm{sym}\left(\nabla \underline{u}\right) dV = \int_V -\delta\underline{\underline{\sigma}} : \nabla \underline{u}\, dV$$

Now using index notation:

$$\begin{aligned} \int_V -\delta\underline{\underline{\sigma}} : \nabla \underline{u} dV &= \int_V -\delta\sigma_{ij} u_{i/j} dV = \int_V \delta\sigma_{ij/j} u_i - \left(\delta\sigma_{ij} u_i\right)_{/j} dV \\ &= \int_V \left[\underline{u} \cdot \nabla \cdot \delta\underline{\underline{\sigma}} - \nabla \cdot \left(\underline{u} \cdot \delta\underline{\underline{\sigma}}\right)\right] dV \end{aligned}$$

The first part of the volume integral is rewritten by enforcing the equilibrium condition $\nabla \cdot \delta\boldsymbol{\sigma} + \delta\boldsymbol{b} = \mathbf{0}$, yielding:

$$\int_V \underline{u} \cdot \nabla \cdot \delta\underline{\underline{\sigma}}\, dV = -\int_V \underline{u} \cdot \delta\underline{b}\, dV$$

The second part of the volume integral obtained can be rewritten using the divergence theorem and then enforcing the equilibrium condition $\delta\boldsymbol{\sigma} \cdot \boldsymbol{n} = \delta\hat{\boldsymbol{t}}$ on S_F. This yields:

$$\begin{aligned} \int_V -\nabla \cdot \left(\underline{u} \cdot \delta\underline{\underline{\sigma}}\right) dV &= -\int_S \underline{u} \cdot \delta\underline{\underline{\sigma}} \cdot \underline{n}\, dS = -\int_{S_u + S_F} \underline{u} \cdot \delta\underline{\underline{\sigma}} \cdot \underline{n}\, dS_u \\ &= -\int_{S_u} \underline{u} \cdot \delta\underline{t}\, dS - \int_{S_F} \underline{u} \cdot \delta\underline{\hat{t}}\, dS_F \end{aligned}$$

Using the results obtained, the variational statement can be rewritten as follows:

$$\int_V \left(\delta\underline{\underline{\sigma}} : \underline{\underline{\varepsilon}} - \delta\underline{b}\cdot\underline{u}\right) dV - \int_{S_u} \underline{u}\cdot\delta\underline{t}\, dS + \int_{S_F} \underline{u}\cdot\delta\hat{\underline{t}}\, dS + \int_{S_u} \delta\underline{t}\left(\underline{u} - \hat{\underline{u}}\right) dS = 0$$

Simplifying and rearranging the above equation allows us to define the ***Principle of Complementary Virtual Work (PCVW)***: if a system is in equilibrium, the complementary internal virtual work δW_D^* is equal to the complementary external virtual work δW_e^*:

$$\underbrace{\int_V \delta\underline{\underline{\sigma}} : \underline{\underline{\varepsilon}}\, dV}_{\delta W_D^*} = \underbrace{\int_V \delta\underline{b}\cdot\underline{u}\, dV + \int_{S_F} \delta\hat{\underline{t}}\cdot\underline{u}\, dS + \int_{S_u} \delta\underline{t}\cdot\hat{\underline{u}}\, dS}_{\delta W_e^*} \tag{1.34}$$

$$\forall \delta\underline{\underline{\sigma}} \text{ and } \delta\underline{b} : \begin{cases} \nabla\cdot\delta\underline{\underline{\sigma}} + \delta\underline{b} = \underline{0} & \text{in } V \\ \delta\underline{\underline{\sigma}}\cdot\underline{n} = \delta\underline{t} = \delta\hat{\underline{t}} & \text{on } S_F \end{cases}$$

1.5.2.2. Compatibility from PCVW

As for the PVW, the compatibility conditions can be obtained starting from the PCVW. To account for the fact that the variations $\delta\boldsymbol{\sigma}$ and $\delta\boldsymbol{t}$ are in equilibrium, the variational statement can be modified by introducing those conditions via the ***Lagrange multipliers*** $\boldsymbol{\lambda}, \boldsymbol{\mu}$:

$$\delta W_D^* = \delta W_e^* - \int_V \underline{\lambda}\cdot\left(\nabla\cdot\delta\underline{\underline{\sigma}} + \delta\underline{b}\right) dV + \int_{S_F} \underline{\mu}\cdot(\delta t - \delta\hat{t}) dS$$

$$\forall \delta\underline{\underline{\sigma}} : \begin{cases} \nabla\cdot\delta\underline{\underline{\sigma}} + \delta\underline{b} = \underline{0} & \text{in } V \\ \delta\underline{\underline{\sigma}}\cdot\underline{n} = \delta\underline{t} = \delta\hat{\underline{t}} & \text{on } S_F \end{cases}$$

It is clear that the expression of the PCVW is unchanged if $\nabla\cdot\delta\boldsymbol{\sigma} + \delta\boldsymbol{b} = \boldsymbol{0}$ and $\delta\boldsymbol{t} = \delta\hat{\boldsymbol{t}}$. In order to obtain the compatibility equation from this equation, rearrange the contribution multiplying $\boldsymbol{\lambda}$:

$$\int_V \underline{\lambda}\cdot\left(\nabla\cdot\delta\underline{\underline{\sigma}} + \delta\underline{b}\right) dV = \int_V \left(\lambda_i\delta\sigma_{ij/j} + \lambda_i\delta b_i\right) dV = \int_V \left(\left(\lambda_i\delta\sigma_{ij}\right)_{/j} - \lambda_{i/j}\delta\sigma_{ij} + \lambda_i\delta b_i\right) dV$$
$$= \int_V \left(\left(\lambda_i\delta\sigma_{ij}\right)_{/j} - \frac{1}{2}\left(\lambda_{i/j} + \lambda_{j/i}\right)\delta\sigma_{ij} + \lambda_i\delta b_i\right) dV$$

Switch back to vector notation, apply the divergence theorem, and split the surface integral in the integrals over S_u and S_F:

$$\int_V \left(\nabla\cdot\left(\underline{\lambda}\cdot\delta\underline{\underline{\sigma}}\right) - \delta\underline{\underline{\sigma}} : \frac{1}{2}\left(\nabla\underline{\lambda} + \nabla\underline{\lambda}^T\right) + \delta\underline{b}\cdot\underline{\lambda}\right) dV$$
$$= \int_S \underline{\lambda}\cdot\delta\underline{\underline{\sigma}}\cdot\underline{n}\, dS - \int_V \left(\delta\underline{\underline{\sigma}} : \frac{1}{2}\left(\nabla\underline{\lambda} + \nabla\underline{\lambda}^T\right) - \delta\underline{b}\cdot\underline{\lambda}\right) dV$$
$$= \int_S \delta\underline{t}\cdot\underline{\lambda}\, dS - \int_V \left(\delta\underline{\underline{\sigma}} : \frac{1}{2}\left(\nabla\underline{\lambda} + \nabla\underline{\lambda}^T\right) - \delta\underline{b}\cdot\underline{\lambda}\right) dV$$
$$= \int_{S_u} \delta\underline{t}\cdot\underline{\lambda}\, dS + \int_{S_F} \delta\underline{t}\cdot\underline{\lambda}\, dS\, dS - \int_V \left(\delta\underline{\underline{\sigma}} : \frac{1}{2}\left(\nabla\underline{\lambda} + \nabla\underline{\lambda}^T\right) - \delta\underline{b}\cdot\underline{\lambda}\right) dV$$

Thus, the PCVW augmented by the Lagrange multipliers reads:

$$\underbrace{\int_V \delta\underline{\underline{\sigma}} : \underline{\underline{\varepsilon}}\, dV}_{\delta W_D^*} = \underbrace{\int_V \delta\underline{b}\cdot\underline{u}\, dV + \int_{S_F} \delta\underline{\hat{t}}\cdot\underline{u}\, dS + \int_{S_u} \delta\underline{t}\cdot\underline{\hat{u}}\, dS}_{\delta W_e^*} - \int_{S_u} \delta\underline{t}\cdot\underline{\lambda}\, dS\, dS - \int_{S_F} \delta\underline{t}\cdot\underline{\lambda}\, dS +$$
$$+ \int_V \left(\delta\underline{\underline{\sigma}} : \frac{1}{2}\left(\nabla\underline{\lambda} + \nabla\underline{\lambda}^T\right) - \delta\underline{b}\cdot\underline{\lambda}\right) dV + \int_{S_F} \underline{\mu}\cdot(\delta t - \delta\hat{t}) dS$$

$$\forall\delta\underline{\underline{\sigma}} : \begin{cases} \nabla\cdot\delta\underline{\underline{\sigma}} + \delta\underline{b} = \underline{0} & \text{in } V \\ \delta\underline{\underline{\sigma}}\cdot\underline{n} = \delta\underline{t} = \delta\underline{\hat{t}} & \text{on } S_F \end{cases}$$

Then, from the scalar equation of the augmented PCVW, we obtain the following set of equations:

$$\begin{cases} \underline{\underline{\varepsilon}} = \frac{1}{2}\left(\nabla\underline{\lambda} + \nabla\underline{\lambda}^T\right) & \text{in } V \quad (1) \\ \underline{u} = \underline{\lambda} & \text{in } V \quad (2) \\ \underline{u} = \underline{\mu} & \text{on } S_F \quad (3) \\ \underline{\hat{u}} = \underline{\lambda} & \text{on } S_u \quad (4) \\ \underline{\lambda} = \underline{\mu} & \text{on } S_F \quad (5) \end{cases}$$

From equations (2) and (4) it is clear that the Lagrangian multiplier $\boldsymbol{\lambda}$ is the displacement field $\boldsymbol{u}$. Thus, the equations can be expressed by replacing $\boldsymbol{\lambda}$ with $\boldsymbol{u}$, yielding the compatibility equations:

$$\begin{cases} \underline{\underline{\varepsilon}} = \frac{1}{2}\left(\nabla\underline{u} + \nabla\underline{u}^T\right) & \text{in } V \\ \underline{u} = \underline{\hat{u}} & \text{on } S_u \end{cases}$$

1.5.3. Minimum potential energy principle

The minimum potential energy principle is essentially the energetic counterpart of the PVW. It has been stated that the PVW holds true irrespective of the type of material considered, i.e. for any constitutive law. To define the Minimum Potential energy principle, ***we must introduce the CL of an hyperelastic material***. Consider now the PVW:

$$\delta W_D = \delta W_e \quad \rightarrow \quad \int_V \delta\underline{\underline{\varepsilon}} : \underline{\underline{\sigma}}\, dV = \int_V \delta\underline{u}\cdot\underline{b}\, dV + \int_{S_F} \delta\underline{u}\cdot\underline{\hat{t}}\, dS$$

For hyperelastic materials it has been found that the stress can be obtained from a potential strain energy $\boldsymbol{\sigma} = U_{/\boldsymbol{\varepsilon}}$. By substitution into the internal virtual work δW_D we obtain:

$$\delta W_D = \int_V \delta\underline{\underline{\varepsilon}} : \underline{\underline{\sigma}}\, dV = \int_V \delta\underline{\underline{\varepsilon}} : u_{\backslash\delta\underline{\underline{\varepsilon}}}\, dV = \int_V \delta u dV = \delta U$$

Where u is the complementary strain energy density, and δu is the virtual counterpart. It follows that the equilibrium condition expressed by the PVW can be rewritten in terms of potential energies as follows:

$$\delta W_D - \delta W_e = 0 \quad \rightarrow \quad \delta U + \delta V = 0 \tag{1.35}$$

Where U is the strain energy of an hyperelastic material and V is the potential of external loads, essentially minus the external virtual work. Equation (1.35) states that equilibrium is achieved when the total potential energy $\Pi = U + V$ is at its minimum, i.e. when it's first variation is null $\delta\Pi = 0$. Thus, the equilibrium condition can be stated as:

$$\delta\Pi = \delta U + \delta V = 0 \tag{1.36}$$

1.5.4. Menabrea's theorem

Similarly to the minimum potential energy principle and the PVW, Menabrea's theorem is the energy counterpart of the PCVW. Thus, once again we must introduce the constitutive law of an hyperelastic material. The PCVW, and by extension Menabrea's theorem, is a force-based formulation of equilibrium, meaning that it relies on the complementary strain energy U^*, from which the strains can be recovered as $\boldsymbol{\varepsilon} = U_{/\boldsymbol{\sigma}}$.

$$\delta W_D^* = \delta W_e^* \quad \rightarrow \quad \int_V \underline{\underline{\varepsilon}} : \delta\underline{\underline{\sigma}}\, dV = \int_V \delta\underline{b} \cdot \underline{u}\, dV + \int_{S_F} \delta\underline{\hat{t}} \cdot \underline{u}\, dS + \int_{S_u} \delta\underline{t} \cdot \underline{\hat{u}}\, dS$$

Rewriting the complementary virtual internal energy δW_D^* using the CL of an hyperelastic material $\boldsymbol{\varepsilon} = U^*_{/\boldsymbol{\sigma}}$ yields:

$$\delta W_D^* = \int_V \underline{\underline{\varepsilon}} : \delta\underline{\underline{\sigma}}\, dV = \int_V u^*_{\backslash\delta\underline{\underline{\sigma}}} : \delta\underline{\underline{\sigma}}\, dV = \int_V \delta u^* dV = \delta U^*$$

Where u^* is the complementary strain energy density, and δu^* is the virtual counterpart. Naturally, we arrive at the same formulation of the minimum total potential energy principle, but in terms of complementary energies. The equilibrium condition in energetic terms reads:

$$\delta W_D^* = \delta W_e^* \quad \rightarrow \quad \delta U^* + \delta V^* = \delta\Pi^* = 0 \tag{1.37}$$

Where δU^* is the virtual complementary strain energy, δV is minus the complementary virtual external work δW_e^*, and $\delta\Pi^*$ is the virtual total complementary energy. In this case, equilibrium is reached when $\delta\Pi^* = 0$.

1.5.5. Hamilton's principle

Consider the displacement field $\boldsymbol{u} = \boldsymbol{u}(\boldsymbol{x}, t)$ and consider a virtual displacement field $\delta\boldsymbol{u}$ such that:

$$\begin{cases} \delta\underline{u}(\underline{x}, t) = 0 & \text{on } S_u \ \forall t \\ \delta\underline{u}(\underline{x}, t_1) = \delta\underline{u}(\underline{x}, t_2) = 0 & \text{in } V \ \forall \underline{x} \end{cases}$$

The first condition is identical to the compatibility requirement of the PVW. The second condition states that the perturbated configuration at $t = t_1$ and at $t = t_2$ is equal to the actual configuration, i.e. $\boldsymbol{u} + \delta\boldsymbol{u} = \boldsymbol{u}$. Consider now the PVW, accounting for the inertial terms:

$$\int_V \delta\underline{\underline{\varepsilon}} : \underline{\underline{\sigma}}\, dV = \int_V \delta\underline{u} \cdot \underline{b}\, dV + \int_{S_F} \delta\underline{u} \cdot \hat{\underline{t}}\, dS - \int_V \delta\underline{u} \cdot \rho\ddot{\underline{u}} dV$$

Integrate now the whole PVW equation from t_1 to t_2:

$$\int_{t_1}^{t_2} \left\{ \int_V \delta\underline{\underline{\varepsilon}} : \underline{\underline{\sigma}}\, dV \right\} dt = \int_{t_1}^{t_2} \left\{ \int_V \delta\underline{u} \cdot \underline{b}\, dV + \int_{S_F} \delta\underline{u} \cdot \hat{\underline{t}}\, dS - \int_V \delta\underline{u} \cdot \rho\ddot{\underline{u}} dV \right\} dt$$

The last term can be integrated by parts as follows:

$$\begin{aligned} \int_{t_1}^{t_2} \left\{ \int_V \delta\underline{u} \cdot \rho\ddot{\underline{u}} dV \right\} dt &= \int_{t_1}^{t_2} \left\{ \int_V \frac{D}{Dt}(\delta\underline{u} \cdot \dot{\underline{u}}\rho) dV \right\} dt - \int_{t_1}^{t_2} \left\{ \int_V (\,\delta\dot{\underline{u}} \cdot \dot{\underline{u}}\rho) dV \right\} dt \\ &= \underbrace{\int_V \delta\underline{u} \cdot \dot{\underline{u}}\rho\, dV \Big|_{t_1}^{t_2}}_{\delta\underline{u}(t_1)=\delta\underline{u}(t_2)=0} - \int_{t_1}^{t_2} \left\{ \int_V (\,\delta\dot{\underline{u}} \cdot \dot{\underline{u}}\rho) dV \right\} dt = - \int_{t_1}^{t_2} \left\{ \int_V (\,\delta\dot{\underline{u}} \cdot \dot{\underline{u}}\rho) dV \right\} dt \end{aligned}$$

By substitution in the PVW we obtain:

$$\int_{t_1}^{t_2} \left\{ \int_V \delta\underline{\underline{\varepsilon}} : \underline{\underline{\sigma}}\, dV - \int_V \delta\underline{u} \cdot \underline{b}\, dV - \int_{S_F} \delta\underline{u} \cdot \hat{\underline{t}}\, dS - \int_V (\,\delta\dot{\underline{u}} \cdot \dot{\underline{u}}\rho) dV \right\} dt = 0$$

In such equation we can identify the strain energy U and external potential energy V, already introduced in the total potential energy principle. The additional term is the kinetic energy K, defined as follows:

$$K = \int_V (\,\delta\dot{\underline{u}} \cdot \dot{\underline{u}}\rho) dV$$

Thus, we obtain ***Hamilton's principle***:

$$\int_{t_1}^{t_2} (\delta U + \delta V - \delta K) dt = \int_{t_1}^{t_2} \delta L\, dt = 0 \tag{1.38}$$

2. Beams

A ***beam*** is a structural component that has one dimension significantly larger than the other two and which can be obtained by rigidly translating the cross section along an axis, called the beam axis. In this chapter we present a set of structural theories aiming at providing closed form solution for structural analysis of beams. The general form of the structural problem for any structure is the one in equation (1.32), hereby reported:

$$\begin{cases} \underline{b} + \nabla \cdot \underline{\underline{\sigma}} = \underline{0} & \text{in } V \\ \underline{\underline{\varepsilon}} - \frac{1}{2}\left(\nabla \underline{u} + \nabla \underline{u}^T\right) = \underline{\underline{0}} & \text{in } V \\ \underline{t} - \underline{\hat{t}} = \underline{0} & \text{on } S_F \\ \underline{u} - \underline{\hat{u}} = \underline{0} & \text{on } S_u \end{cases}$$

These set of equations impose equilibrium and compatibility through the volume of the body (first two equations), and on the body's boundary via the natural and essential BCs, the third and fourth equations respectively. However, solving this set of equations results to be quite complicated, since it involves a set of PDEs. It will be shown that, in general, the ***key idea of structural theories*** is to simplify the structural problem by identifying global quantities over a region of the structure. We refer to such global quantities as ***generalized parameters***. We will see that this approach applies to both types of beam theories that are presented here: the De Saint Venant (DSV) solution and the kinematic beam models. The beam solution derived with the framework of the DSV beam theory provides a fundamental background in structural analysis. In fact, it provides an exact solution for the axial stress σ_{zz}, while solutions for shear stresses are obtained by introducing approximations. The DSV solution is obtained by taking an initial guess of the stress field and verifying afterwards if it satisfies the equilibrium and compatibility conditions. The kinematic models instead make initial assumptions about how the beam will deform, this is called the ***kinematic law*** of the beam. Then, one can compute the strains, stresses and equilibrium conditions afterwards. Note that kinematic law is not a guess solution that we verify afterwards, as with the DSV approach. Naturally, considering global quantities introduces a ***certain degree of approximation***. However, such approximations allow us to obtain useful closed form solutions that allow us to understand which are the quantities that affect the phenomena we are interested in studying and how.

2.1. De Saint Venant solution

2.1.1. De Saint Venant principle

Consider a beam with constant cross section along its beam axis, which is assumed to be straight. Assume that the beam reference system is taken so that the beam axis is the z-axis, and the x-y-axes identify the cross section plane.

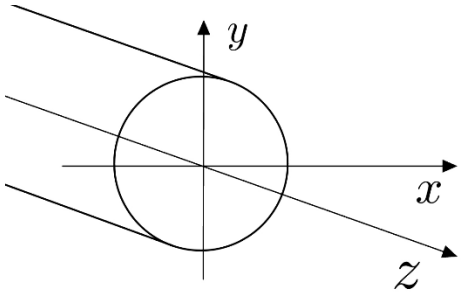

Figure 2.1: beam reference system.

Assume that the beam is subject to an arbitrary loading condition. In general, in the region where the loads are applied, the stress distribution on a beam section will be composed of a term representing the mean stress $\bar{\sigma}(x,y)$ and one representing the local effects due to load application $\sigma_L(x,y)$. Thus:

$$\sigma_{\text{tot}}(x,y) = \bar{\sigma}(x,y) + \sigma_L(x,y) \tag{2.1}$$

The ***DSV principle*** states that the stress distribution $\sigma_{\text{tot}}(x,y)$ on a beam section is not affected by the local effects $\sigma_L(x,y)$ if it's computed at a distance of the maximum size of the section from the load application region. In other words, the local effects σ_L decay rapidly and become negligible as we move away from the load application region, as depicted in the example below. For this reason, the DSV solutions are also referred to as ***central solutions***.

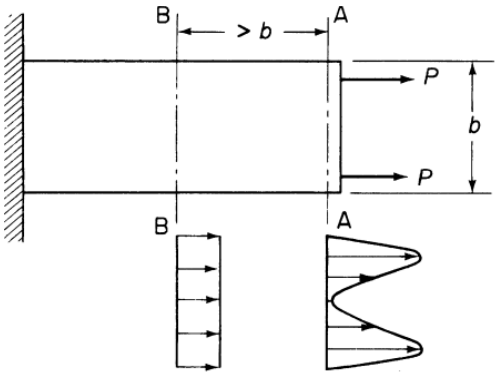

Figure 2.2: local effects due to load application on the internal stress distribution of a beam section.

As a direct consequence of the DSV principle, for sections sufficiently far from the load application region, ***equilibrium can be imposed in terms of internal actions***. Internal actions are stress resultants computed by integrating the stresses acting on a beam cross section over the area of the section, and they are defined as below. Thus, ***internal actions are the generalized stress parameters***. The internal actions are positive if going in the direction of the respective axis, as depicted in Figure 2.3.

$$\begin{cases} T_x = \int_A \sigma_{xz} dA \\ T_y = \int_A \sigma_{yz} dA \\ T_z = \int_A \sigma_{zz} dA \end{cases} \qquad \begin{cases} M_x = \int_A \sigma_{zz} y dA \\ M_y = \int_A -\sigma_{zz} x dA \\ M_z = \int_A (\sigma_{yz} x - \sigma_{xz} y) dA \end{cases} \tag{2.2}$$

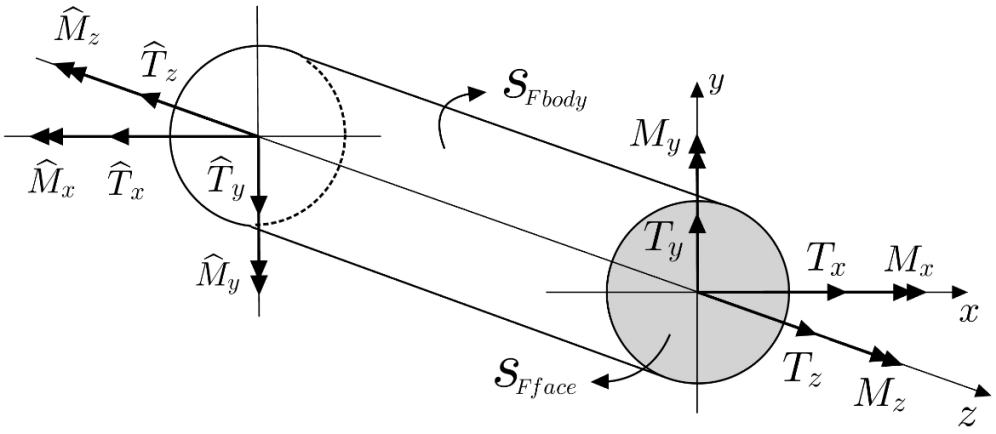

Figure 2.3: loads and reaction forces on a beam.

Having defined the internal actions, we can gain more insight on why imposing equilibrium in terms of internal actions is not adequate near load application regions. Simply stated, the local stress distribution is self-equilibrating, meaning that its resultant is null $T_L = 0$. This implies that local stress effects only "reshape" the stress distribution, but do not change its magnitude.

$$T_z = \int_A \sigma_{tot} dA = \int_A (\bar{\sigma} + \sigma_L) dA = \bar{T}_z + T_{zL} = \bar{T}_z \quad \text{since} \quad T_{zL} = \int_A \sigma_L dA = 0$$

Therefore, multiple stress distributions can produce the same internal actions, and equilibrium of resultants alone is not sufficient to uniquely determine the stress field since they are not able to account for self-equilibrating local effects. Consequently, in order to uniquely determine the stress distribution near the load application region, equilibrium must be enforced pointwise through Cauchy's equation (1.32).

Observation. It has been stated that the DSV principle is introduced to simplify structural problem, and that it allows to impose equilibrium in terms of internal actions far away from load application regions. It follows that internal action equilibrium must simplify the structural problem, but why? Because equilibrium in terms of internal actions is simply a set of force equilibrium relations, not a set of PDEs ($\boldsymbol{\nabla} \cdot \boldsymbol{\sigma} = \mathbf{0}$).

$$\begin{cases} T_x = \hat{T}_x \\ T_y = \hat{T}_y \\ T_z = \hat{T}_z \end{cases} \qquad \begin{cases} M_x = \widehat{M}_x + z T_y \\ M_y = \widehat{M}_y - z T_x \\ M_z = \widehat{M}_z \end{cases} \tag{2.3}$$

A closed form solution is now required to actually retrieve the stresses if the internal actions are known. Once this relations are known, then one can determine the internal actions (1), retrieve the stresses (2) and eventually verify if the beam yields or not. Then, the strains can be retrieved from the CL (3), and finally the displacement field can be retrieved as well (4).

2.1.2. Semi-inverse solution

The starting point of the structural problem is the strong form of equation (1.32). In order to simplify this set of equations we ***assume*** that:

- The cross section of the beam is constant along its axis, which is assumed to be straight.
- Reference system is taken to be centroidal and principal, so that $S_x = S_y = I_{xy} = 0$.
- Material is isotropic, linear-elastic and homogeneous, so that the CL is that of (1.16).
- DSV principle: loads and constraints are applied at the ends of the beam, so that its lateral surface is unloaded and unconstrained and we look for a central solution.

Searching for a central solution allows us to "split" the natural BC, or Cauchy condition. More precisely, on the external lateral surface of the beam S_{Fbody} we impose the natural BC in its differential form $\boldsymbol{\sigma} \cdot \boldsymbol{n} - \hat{\boldsymbol{t}} = \boldsymbol{0}$. Since S_{Fbody} is unloaded and unconstrained $\hat{\boldsymbol{t}} = \boldsymbol{0} \rightarrow \boldsymbol{\sigma} \cdot \boldsymbol{n} = \boldsymbol{0}$. On the beam sections S_{Fface} we apply the Cauchy condition via the internal actions. Both these surfaces are highlighted in Figure 2.3. Thus, starting from (1.32), under the assumptions mentioned above, the structural problem for a beam can be formulated as follows:

$$\begin{cases} \nabla \cdot \underline{\underline{\sigma}} = \underline{0} & \text{in } V \\ \text{Compatibility eq. ns} & \text{in } V \\ \underline{\underline{\sigma}} \cdot \underline{n} = \underline{0} & \text{on } S_{Fbody} \\ \text{Internal actions} & \text{on } S_{Fface} \end{cases} \tag{2.4}$$

Moreover, instead of enforcing compatibility in the form of $\boldsymbol{\varepsilon} - 1/2(\nabla \boldsymbol{u} + \nabla \boldsymbol{u}^T) = \boldsymbol{0}$, we enforce it via the compatibility equations (1.24). We present in this section the ***semi-inverse approach***. That is, instead of obtaining a solution starting from (2.4), an ***initial guess solution*** is proposed. Then, it is checked ex-post if such guess solution satisfies the set of governing equations in (2.4). The guess solution is taken as:

$$\sigma_{xx} = \sigma_{yy} = \sigma_{xy} = 0 \tag{2.5}$$

Using such guess solution (which is the exact one, spoiler), we now simplify the structural problem identified by the set of equations in (2.4).

Observation. Using the DSV principle as here presented implies that the material is isotropic and homogeneous. If this is not the case, as for composite materials, the stress state will be 3D in order to restore compatibility, and so $\sigma_{xx} \neq 0, \sigma_{yy} \neq 0$ and $\sigma_{xy} \neq 0$. An example is presented in the figure below, where a component σ_{xx} will have to develop in order to grant a compatible deformation field. We point out that for beam of nonhomogeneous materials, such as composites, the DSV solution can still be obtained, but the approach to be used is different from the semi-inverse strategy here illustrated.

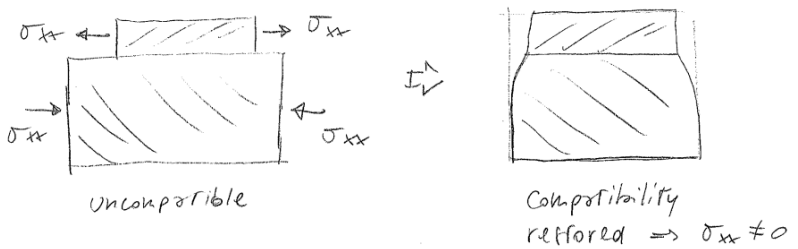

Figure 2.4: 3D stress state for compatibility enforcement on a nonhomogeneous beam.

2.1.3. DSV beam governing equations

According to the guess solution, the equilibrium equations simplify as follows:

$$\nabla \cdot \underline{\underline{\sigma}} = \begin{cases} \sigma_{xx/x} + \tau_{xy/y} + \tau_{xz/z} = 0 \\ \tau_{yx/x} + \sigma_{yy/y} + \tau_{yz/z} = 0 \\ \tau_{zx/x} + \tau_{zy/y} + \sigma_{zz/z} = 0 \end{cases} \rightarrow \begin{cases} \tau_{xz/z} = 0 \\ \tau_{yz/z} = 0 \\ \tau_{zx/x} + \tau_{zy/y} + \sigma_{zz/z} = 0 \end{cases}$$

The first two equations imply that the shear stresses τ_{xz} and τ_{yz} are not a function of the axial coordinate z. The last equation, coupled with the first two, implies that σ_{zz} can be up to linear in the axial coordinate z. Recall the constitutive law for an isotropic, linear-elastic homogeneous material of equation (1.18), hereby reported:

$$\begin{Bmatrix} \varepsilon_{xx} \\ \varepsilon_{yy} \\ \varepsilon_{zz} \\ \gamma_{xy} \\ \gamma_{yz} \\ \gamma_{zx} \end{Bmatrix} = \frac{1}{E} \begin{bmatrix} \begin{bmatrix} 1 & -\nu & -\nu \\ -\nu & 1 & -\nu \\ -\nu & -\nu & 1 \end{bmatrix} & [0] \\ [0] & 2(1+\nu) \begin{bmatrix} 1 & 0 & 0 \\ 0 & 1 & 0 \\ 0 & 0 & 1 \end{bmatrix} \end{bmatrix} \begin{Bmatrix} \sigma_{xx} \\ \sigma_{yy} \\ \sigma_{zz} \\ \tau_{xy} \\ \tau_{yz} \\ \tau_{zx} \end{Bmatrix}$$

According to the guess solution $\sigma_{xx} = \sigma_{yy} = \sigma_{xy} = 0$, and so the CL provides with:

$$\begin{cases} \varepsilon_{xx} = -\dfrac{\nu \sigma_{zz}}{E} \\ \varepsilon_{yy} = -\dfrac{\nu \sigma_{zz}}{E} \\ \varepsilon_{zz} = \dfrac{\sigma_{zz}}{E} \end{cases} \qquad \begin{cases} \gamma_{xy} = 0 \\ \gamma_{yz} = \dfrac{\tau_{yz}}{G} \\ \gamma_{xz} = \dfrac{\tau_{xz}}{G} \end{cases} \tag{2.6}$$

Note that, in general, the cross section of the beam actually changes shape since some shear strains components are not null. In section 1.3 the compatibility equations were found to be:

$$\begin{cases} \varepsilon_{xx/yy} + \varepsilon_{yy/xx} - \gamma_{xy/xy} = 0 \\ \varepsilon_{yy/zz} + \varepsilon_{zz/yy} - \gamma_{yz/yz} = 0 \\ \varepsilon_{zz/xx} + \varepsilon_{xx/zz} - \gamma_{zx/zx} = 0 \\ \gamma_{xy/xz} + \gamma_{zx/xy} - \gamma_{yz/xx} - 2\varepsilon_{xx/yz} = 0 \\ \gamma_{yz/yx} + \gamma_{xy/yz} - \gamma_{zx/yy} - 2\varepsilon_{yy/zx} = 0 \\ \gamma_{zx/zy} + \gamma_{yz/zx} - \gamma_{xy/zz} - 2\varepsilon_{zz/xy} = 0 \end{cases}$$

From the CL we known that $\gamma_{xy} = 0$. Adding the equilibrium equations to the CL we that the derivatives of $\gamma_{xz} = \sigma_{xz}/G$ and $\gamma_{yz} = \sigma_{yz}/G$ with respect to z are null. The same applies to $\varepsilon_{xx}, \varepsilon_{yy}$ and ε_{zz}, all functions of σ_{zz}, which derived twice with respect to z is null. Thus, the compatibility equations reduce to:

$$\begin{cases} \varepsilon_{xx/yy} + \varepsilon_{yy/xx} = 0 \\ \varepsilon_{zz/yy} = 0 \\ \varepsilon_{zz/xx} = 0 \\ \gamma_{zx/xy} - \gamma_{yz/xx} - 2\varepsilon_{xx/yz} = 0 \\ \gamma_{yz/yx} - \gamma_{zx/yy} - 2\varepsilon_{yy/zx} = 0 \\ \varepsilon_{zz/xy} = 0 \end{cases}$$

Expressing the strains in terms of stresses via the CL and rearranging yields:

$$\begin{cases} \sigma_{zz/yy} = 0 \\ \sigma_{zz/xx} = 0 \\ -\bar{\nu}\sigma_{zz/yz} = \tau_{zx/xy} - \tau_{yz/xx} \\ -\bar{\nu}\sigma_{zz/xz} = \tau_{zy/xy} - \tau_{xz/yy} \\ \sigma_{zz/xy} = 0 \end{cases} \quad \text{where} \quad \bar{\nu} = \frac{2E}{\nu G}$$

Thus, the general form of the governing equations for a beam according to the DSV assumptions are the following:

$$\begin{cases} \begin{cases} \tau_{xz/z} = \tau_{yz/z} = 0 \\ \tau_{zx/x} + \tau_{zy/y} + \sigma_{zz/z} = 0 \end{cases} & \text{in } V \\ \begin{cases} \sigma_{zz/yy} = \sigma_{zz/xx} = \sigma_{zz/xy} = 0 \\ -\bar{\nu}\sigma_{zz/yz} = \tau_{zx/xy} - \tau_{yz/xx} \\ -\bar{\nu}\sigma_{zz/xz} = \tau_{zy/xy} - \tau_{xz/yy} \end{cases} & \text{in } V \\ \underline{\underline{\sigma}} \cdot \underline{n} = 0 & \text{on } S_{F_{body}} \\ \text{Internal actions} & \text{on } S_{F_{face}} \end{cases} \tag{2.7}$$

In the following sections, when investigating the axial solution we will only select and consider the relevant equations for axial equilibrium and compatibility. The same will be done for the shear solution. We remind that the ***goal*** is to obtain a closed form solution that allows us to determine the stresses starting from the internal actions, because the internal actions are very easy to determine.

2.1.4. DSV solution for axial stress

We start by writing only the relevant equations of the structural problem as formulated in equation (2.7) for the axial stress:

$$\begin{cases} \tau_{zx/x} + \tau_{zy/y} + \sigma_{zz/z} = 0 & \text{in } V \\ \sigma_{zz/yy} = \sigma_{zz/xx} = \sigma_{zz/xy} = 0 & \text{in } V \\ \underline{\underline{\sigma}} \cdot \underline{n} = 0 & \text{on } S_{F_{body}} \\ \begin{cases} T_z = \int_A \sigma_{zz} dA \\ M_x = \int_A \sigma_{zz} y dA \\ M_y = -\int_A \sigma_{zz} x dA \end{cases} & \text{on } S_{F_{face}} \end{cases} \tag{2.8}$$

These equations are the starting point to obtain the axial solution. Let us investigate the Cauchy condition first $\boldsymbol{\sigma} \cdot \boldsymbol{n} = \boldsymbol{0}$. In this expression $\boldsymbol{n}$ is the normal to the external surface of the beam, which fully expressed reads $\boldsymbol{n} = n_x \boldsymbol{e}_x + n_y \boldsymbol{e}_y$. Thus, the relevant stress components of $\boldsymbol{\sigma}$ are the only non-null components that act along the same axes $\boldsymbol{e}_x, \boldsymbol{e}_y$, i.e. the shear strains. For this reason, we replace in the Cauchy condition the stress tensor with the ***shear vector*** $\boldsymbol{\tau}$, defined as follows:

$$\underline{\tau} = \tau_{xz}\underline{e}_x + \tau_{yz}\underline{e}_y \tag{2.9}$$

By updating the Cauchy condition with the shear vector, it is easy to observe that such BC imposes the shear vector $\boldsymbol{\tau}$ to be tangent to the external surface of the beam $S_{F_{body}}$ in its every point.

$$\underline{\underline{\sigma}} \cdot \underline{n} = \underline{0} \quad \rightarrow \quad \underline{\tau} \cdot \underline{n} = \underline{0} \quad \rightarrow \quad \underline{\tau} \perp \underline{n} \text{ on } S_{F_{body}}$$

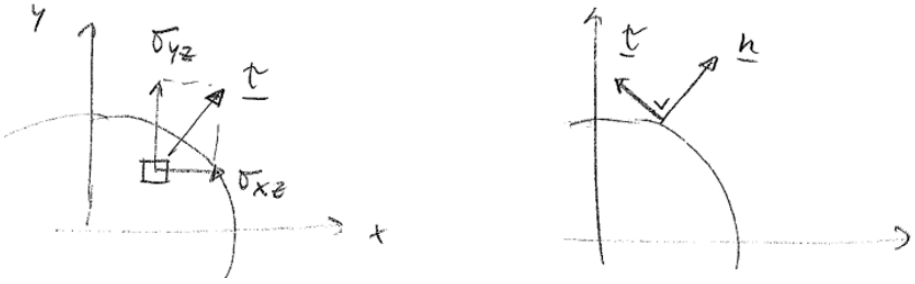

Figure 2.5: stress vector on beam external surface.

We now integrate the axial equilibrium equation over the cross section:

$$\int_A \left(\tau_{zx/x} + \tau_{zy/y} + \sigma_{zz/z}\right) dA = \int_A \left(\nabla \cdot \underline{\tau} + \sigma_{zz/z}\right) dA = \underbrace{\oint_{\partial A} \underline{\tau} \cdot \underline{n} ds}_{0} + \int_A \sigma_{zz/z} dA = 0$$

Consider now the following results:

$$\begin{cases} \sigma_{zz/yy} = \sigma_{zz/xx} = \sigma_{zz/xy} = 0 & \text{from compatibility} \\ \int_A \sigma_{zz/z} dA = 0 & \text{from equilibirum} \end{cases}$$

It follows that σ_{zz} is expressed in the following general form:

$$\sigma_{zz} = A_0 + A_1 x + A_2 y + (A_3 x + A_4 y) z \tag{2.10}$$

Note that $\sigma_{zz/z} = A_3 x + A_4 y$ but its integral in dA is still null if the coordinate system is taken as centroidal, which is one of the assumptions. We now determine the exact expression of the coefficients of equation (2.10) using the internal actions definition and equilibrium equations in terms of internal actions (2.3). According to the definition of the internal actions we'll write:

$$T_z = \int_A \sigma_{zz} dA = A_0 A$$

$$M_x = \int_A \sigma_{zz} y dA = \int_A (A_0 + A_1 x + A_2 y + (A_3 x + A_4 y) z) y dA = \int_A (A_2 y^2 + A_4 y^2 z) dA$$
$$= I_{xx}(A_2 + z A_4)$$

$$M_y = -\int_A \sigma_{zz} x dA = -\int_A (A_0 + A_1 x + A_2 y + (A_3 x + A_4 y) z) x dA = -\int_A (A_1 x^2 + A_3 x^2 z) dA$$
$$= -I_{yy}(A_1 + z A_3)$$

From the equilibrium equations in terms of stress resultants (2.3), we obtain the equations below on the left. Then, equating the constant and linear parts of each equation yields the expression of the coefficients A_i:

$$\begin{cases} T_z = \text{const} = A_0 A \\ M_x = \widehat{M}_x + z T_y = I_{xx}(A_2 + z A_4) \\ M_y = \widehat{M}_y - z T_x = -I_{yy}(A_1 + z A_3) \end{cases} \quad \rightarrow \quad \begin{cases} A_0 = T_z / A \\ A_2 = \widehat{M}_x / I_{xx} \\ A_4 = T_y / I_{xx} \\ A_1 = -\widehat{M}_y / I_{yy} \\ A_3 = T_x / I_{yy} \end{cases}$$

By substitution in general expression of σ_{zz} (2.10) we obtain:

$$\sigma_{zz} = \frac{T_z}{A} - \frac{\widehat{M}_y}{I_{yy}} x + \frac{\widehat{M}_x}{I_{xx}} y + \left(\frac{T_x}{I_{yy}} x + \frac{T_y}{I_{xx}} y \right) z = \frac{T_z}{A} - \frac{\widehat{M}_y + z T_x}{I_{yy}} x + \frac{\widehat{M}_x + z T_y}{I_{xx}} y$$

Invoking once again the equilibrium equations in terms of internal actions (2.3) yields the following expression of the axial stress in a beam in terms of the internal actions:

$$\boxed{\sigma_{zz} = \frac{T_z}{A} - \frac{M_y}{I_{yy}} x + \frac{M_x}{I_{xx}} y} \tag{2.11}$$

A series of important ***observations*** must be made:

- This is the exact solution: in fact it satisfies the equilibrium and compatibility related to axial equilibrium, and at the same time the essential BC and the relevant internal action definitions have been used to obtain the equation.
- Linearity: this result implies that axial stress is linear with the internal actions. Thus, if the if the loads are magnified by a factor λ, then so are the stresses.
- Stress does not depend on the elastic properties of the beam's material. That's because the internal actions equilibrate the externally applied loads (they are natural BCs applied to the beam cross section!) and they are statically equivalent to the internal state of stress in the beam. Thus, the internal stresses only depend on the applied loads. The difference between two beams made of different materials subject to the same loads will show in the deformations.
- Decoupling: we can consider separately the contribution coming from a pure axial force T_z and those coming from bending moments M_x, M_y. For this reason we will investigate the solution in the two cases separately.

2.1.4.1. DSV solution for pure axial load

Consider the case in which only an axial force is applied to the beam. Then, according to the general axial solution (2.11), the ***axial stress*** reduces to what is written below. It is clear that σ_{zz} is constant along the beam axis and uniformly distributed on the beam cross section, as depicted in Figure 2.6 – right.

$$\sigma_{zz} = \frac{T_z}{A} \tag{2.12}$$

The ***strain field*** is the same of that of a rod, i.e. a beam-like structural element that is subject to purely axial load. In section 1.2 the CL of such elements has been found to be characterized by non-null normal strains, while all shear strains are null. Consequently, a beam subject to pure traction does not distort in this loading scenario.

$$\underline{\varepsilon} = \begin{cases} \varepsilon_{xx} = -\dfrac{\nu\sigma_{zz}}{E} = -\nu\dfrac{T_z}{EA} \\ \varepsilon_{yy} = -\dfrac{\nu\sigma_{zz}}{E} = -\nu\dfrac{T_z}{EA} \\ \varepsilon_{zz} = \dfrac{\sigma_{zz}}{E} = \dfrac{T_z}{EA} \\ \gamma_{xy} = \gamma_{yz} = \gamma_{xz} = 0 \end{cases} \tag{2.13}$$

It follows that the quantities in energy conjugacy for a pure axial load are the axial strain ε_{zz} and the axial internal action T_z. To retrieve the ***displacement field*** we simply apply the small strain tensor definition (1.7) and integrate the strains. This process yields:

$$\underline{u} = \begin{cases} u = -\nu\dfrac{T_z}{EA}x \\ v = -\nu\dfrac{T_z}{EA}y \\ w = \dfrac{T_z}{EA}z \end{cases} \tag{2.14}$$

This solution implies that if a positive axial load T_z is applied to the beam, then it elongates axially in a linear manner $w \propto z$, while it shrinks linearly in the cross section due to Poisson's effect, as $u \propto -x$ and $v \propto -y$. A graphical representation of this displacement field is presented in Figure 2.6 – left. If the axial load is compressive, then the beam cross section will expand while the beam shrinks axially.

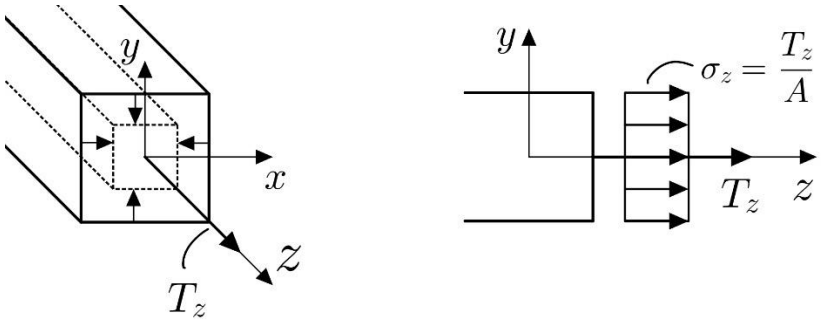

Figure 2.6: displacement of a beam's cross section subject to pure traction (left) and relative stress state (right) according to the DSV solution.

We now investigate the ***strain energy*** due to a pure axial load $U^{(a)}$. It has been stated that for beams it is convenient to express the stresses on the cross sections in terms of internal actions, since these can be obtained from simple force-equilibrium relations. The same reasoning carries on for strain energy, using internal actions simplifies the process of solving the structural problem via PVW and PCVW. The strain energy for pure axial load $U^{(a)}$ can be expressed as follows:

$$U^{(a)} = \frac{1}{2}\int_V \varepsilon_{zz}\sigma_{zz}dV = \frac{1}{2}\int_V \varepsilon_{zz}\frac{T_z}{A}dV = \frac{1}{2}\int_l \varepsilon_{zz}T_z dz$$

Here, the strain ε_{zz} and the internal actions T_z represent the ***generalized parameters***. More precisely, the generalized stress parameter is T_z and the generalized strain parameter is ε_{zz}. Generalized parameters are global quantities that are used to enforce global equilibrium (and compatibility). In fact, recall that an internal action is a stress resultant of the cross section, thus in this sense it is a global quantity. We will see that generalized parameters will be extensively used in kinematic beam models (section 2.2).

In a displacement-based approach to solve the structural problem, the quantities in $U^{(a)}$ must be all expressed in terms of generalized strains to produce a proper strain energy $U = U(\boldsymbol{\varepsilon})$. In a force-based approach we need to express the strain energy in terms of generalized stresses to produce a proper complementary strain energy $U^* = U^*(\boldsymbol{\sigma})$. In order to do this, we need a ***generalized CL*** that links generalized stresses to generalized strains, in this case ε_{zz} and T_z. Naturally, this generalized CL is closely related to the "local CL", i.e. that of equation (2.6). For the case at hand, the generalized CL is immediately obtained from (2.13) as follows:

$$T_z = EA\varepsilon_{zz} = EAw_{0\backslash z} \tag{2.15}$$

Using such relation, the strain energies are obtained as:

$$\begin{cases} U^{*(a)} = \frac{1}{2}\int_l T_z\frac{T_z}{EA}dz \\ U^{(a)} = \frac{1}{2}\int_l \varepsilon_{zz}^2 EAdz = \frac{1}{2}\int_l w_{\backslash z}^2 EAdz \end{cases} \tag{2.16}$$

2.1.4.2. DSV solution for pure bending

Consider the case for which a pure bending moment about the x-axis is applied at the beam ends, what follows can naturally be extended to a pure moment about the y-axis. In such case, the ***axial stress*** reads:

$$\sigma_{zz} = \frac{M_x}{I_{xx}}y \tag{2.17}$$

In general, σ_{zz} is constant along the x-axis and linear in the y-axis, producing the well-known "butterfly" distribution presented in.. However, recall that the bending internal actions reads $M_x = \widehat{M}_x - zT_y$, and thus ***two scenarios*** can be identified:

- Pure bending moment $T_y = 0$: then the internal action reads $M_x = \widehat{M}_x$ and it's constant along the beam axis (z), as in Figure 2.7 – left.

- Shear-induced bending moment $T_y \neq 0$: in this case the internal action grows linearly with z due to effect of the shear load, as in Figure 2.7 – right.

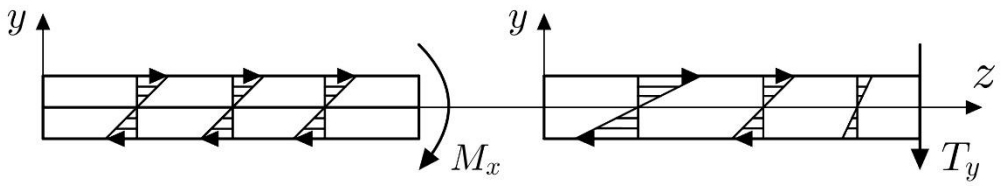

Figure 2.7: stress distribution for a beam subject to pure bending (left) and concentrated shear load (right).

The ***strain field*** has the general expression of the one for a purely axial load, however the normal stress σ_{zz} will have a different formulation. More precisely, the strains due to a bending moment can be computed starting from (1.8) as follows:

$$\underline{\varepsilon} = \begin{cases} \varepsilon_{xx} = -\dfrac{\nu\sigma_{zz}}{E} = -\nu\dfrac{M_x}{EI_{xx}}y \\ \varepsilon_{yy} = -\dfrac{\nu\sigma_{zz}}{E} = -\nu\dfrac{M_x}{EI_{xx}}y \\ \varepsilon_{zz} = \dfrac{\sigma_{zz}}{E} = \dfrac{M_x}{EI_{xx}}y \\ \gamma_{ij} = 0 \end{cases}$$

Observation. It is important to notice that, according to the DSV solution, a beam subject to pure bending has null shear strains. This implies that the ***beam cross sections remain normal to beam axis during bending***, as $\gamma_{xz} = \gamma_{yz} = 0$. This consideration will be the basis for formulating the beam problem from a kinematic point of view. That is, this is the basic assumption of the Euler-Bernoulli beam model (section 2.2.2).

The ***displacement field*** is obtained by integrating the strains:

$$\underline{u} = \begin{cases} u = -\nu\dfrac{M_x}{EI_{xx}}xy + f_u(y,z) \\ v = -\nu\dfrac{M_x}{EI_{xx}}\dfrac{y^2}{2} + f_v(x,z) \\ w = \dfrac{M_x}{EI_{xx}}yz + f_w(x,y) \end{cases}$$

Where the functions f_u, f_v and f_w represent constant terms that are byproducts of the integration. Taking f_u as an example, the constant term will not be a function of the integration variable x, but it can be a function of the other two variables y, z. Thus, this is "constant term" with respect to x only. The same applies to f_v and f_w. The ***physical meaning*** of this terms is to represent the contribution to the displacement field of the shear strains, in fact we determine such constant terms using the shear strains. More precisely, we assume that $f_u = f_w = 0$, and we solve for f_v:

$$\begin{cases} \gamma_{yx} = u_{\backslash y} + v_{\backslash x} = -\nu \dfrac{M_x}{EI_{xx}} x + f_{v\backslash x} = 0 \\ \gamma_{yz} = w_{\backslash y} + v_{\backslash z} = \dfrac{M_x}{EI_{xx}} z + f_{v\backslash z} = 0 \end{cases} \quad \rightarrow \quad f_v = \nu \frac{M_x}{EI_{xx}} \frac{x^2}{2} - \frac{M_x}{EI_{xx}} \frac{z^2}{2}$$

Where $\gamma_{yz} = \gamma_{xy} = 0$ since the only non-null stress is σ_{zz}, and from the CL (2.6) it follows that they must be null. By substitution, we obtain the following displacement field:

$$\underline{u} = \begin{cases} u = -\nu \dfrac{M_x}{EI_{xx}} xy \\ v = -\dfrac{M_x}{2EI_{xx}} \left(z^2 + \nu(y^2 - x^2)\right) \\ w = \dfrac{M_x}{EI_{xx}} yz \end{cases} \tag{2.18}$$

From the displacement field above, ***two separate displacement fields can be identified***, that of the beam axis and that of the generic beam section separately. More precisely:

- Cross section: the displacement of the cross section is given by the u and v at a fixed z coordinate. From the expressions of u and v reported in equation (2.18), it's clear that the vertical displacement v of the cross section is quadratic in x and y, while the horizontal displacement u is linear in the same coordinates. As a result, the cross section will deform as depicted in Figure 2.8 – left.
- Beam axis: the beam axis is identified by setting $x = y = 0$, which yields the following displacement field:

$$\underline{u}^{(axis)} \begin{cases} u = 0 \\ v = -\dfrac{M_x}{2EI_{xx}} z^2 \\ w = 0 \end{cases}$$

The only non-null component is the vertical displacement v, the derivatives of which have important physical meanings. The first derivative of v with respect to z is the ***beam rotation*** θ_{xx}. The second derivative of v with respect to z is the ***beam curvature*** k_{xx}.

$$\begin{cases} \theta_{xx} = -v_{\backslash z} = \dfrac{M_x}{EI_{xx}} z \\ k_{xx} = -v_{\backslash zz} = \dfrac{M_x}{EI_{xx}} \end{cases} \tag{2.19}$$

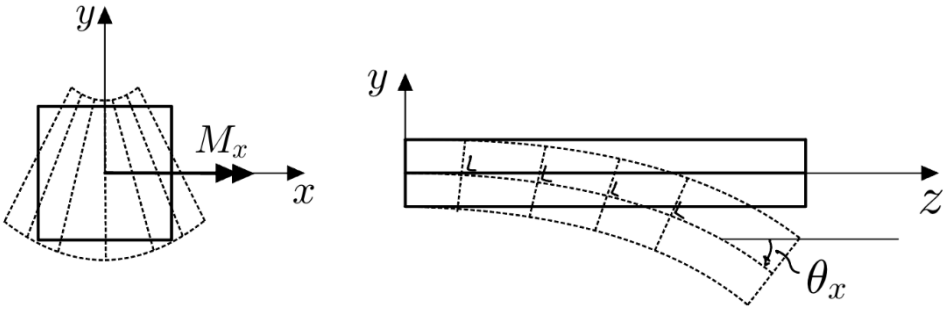

Figure 2.8: deformation of a beam's cross section (left) and axis (right) due to a pure bending moment M_x.

We now investigate the ***bending strain energy*** $U^{(b)}$ generated by a pure bending load. Consider first the case in which only a moment M_x is applied. The strain energy reads:

$$U^{(b)} = \frac{1}{2}\int_V \varepsilon_{zz}\sigma_{zz}dV = \frac{1}{2}\int_V \frac{\sigma_{zz}^2}{E}dV = \frac{1}{2}\int_V \frac{1}{E}\left(\frac{M_x}{I_{xx}}y\right)^2 dV$$

Recall that $I_{xx} = \int_A y^2\, dA$, and so:

$$U^{(b)} = \frac{1}{2}\int_l \frac{1}{E}\frac{M_x^2}{I_{xx}}dz$$

Using the definition of curvature $k_x = M_x/EI_{xx}$ we obtain that the ***generalized stresses*** are the bending internal actions M_x and M_y, while the ***generalized strains*** are the respective curvatures k_y and k_x:

$$U^{(b)} = \frac{1}{2}\int_l \left(M_x k_{xx} + M_y k_{yy}\right)dz \tag{2.20}$$

Once again we want to obtain a proper bending strain energy $U^{(b)}$ and a proper complementary bending strain energy $U^{*(b)}$. In order to do this we need a generalized CL that relates generalized stresses and strains. Such CL is provided by the definition of the curvature:

$$\begin{cases} M_x = EI_{xx}k_x = -EI_{xx}v_{\backslash zz} \\ M_y = EI_{yy}k_y = +EI_{yy}u_{\backslash zz} \end{cases} \tag{2.21}$$

Thus, the strain and complementary strain bending energies are immediately obtained as follows:

$$\begin{cases} U^{*(b)} = \frac{1}{2}\int_l \left(M_x\frac{M_x}{EI_{xx}} + M_y\frac{M_y}{EI_{yy}}\right)dz \\ U^{(b)} = \frac{1}{2}\int_l \left(EI_{xx}k_{xx}^2 + EI_{yy}k_{yy}^2\right)dz = \frac{1}{2}\int_l \left(EI_{xx}v_{\backslash zz}^2 + EI_{yy}u_{\backslash zz}^2\right)dz \end{cases} \tag{2.22}$$

2.1.5. DSV solution for torsion

The DSV solution for axial stress σ_{zz} shows that a closed form solution can be found calculating the direct stress. However, for aerospace structures it is of paramount importance to be able to quantify shear tresses and torsional stiffness as well. For example, structural design is often shaped by aeroelastic phenomena, such as wing divergence. If such phenomena are not properly accounted for by means of requirements on the torsional stiffness of the wing, it would result in catastrophic failure of the aircraft. More generally, evaluation of shear stresses is needed in order to verify whether a structure will yield or fail.

Overall, the problem of the evaluation of the shear stresses is a complex one and closed-form solutions can be hardly found. The ***goal*** of this section is to provide a closed-form solution that allows us to compute the shear stresses starting from the internal torsional action M_t or M_z. In other words, we want to be able to compute the shear stresses if a moment M_t is applied. We will tackle this problem in two phases. In section 2.1.5 we discuss the solution procedure for the torsional problem of a beam under the DSV hypotheses. It will be shown that the solution of the governing equations allows us to determine the warping of the generic beam cross section. From this quantity we can then retrieve the stresses, torsional stiffness and the displacement field. However, determining the warping function $\Psi(x, y)$ can be quite hard. Thus, we reformulate the problem in terms of stresses. In section 2.1.6 we discuss ***approximate*** solutions for thin-walled structures that allow us to derive closed form solutions of the stresses, and thus whole torsional problem.

2.1.5.1. Governing equations

The semi-inverse approach can be formulated for the torsional problem starting from the general guess solution (2.5), and adding the condition $\sigma_{zz} = 0$. Thus, the guess solution for a beam subject to pure torsion is the following:

$$\sigma_{zz} = \sigma_{xx} = \sigma_{yy} = \sigma_{xy} = 0 \tag{2.23}$$

According to this updated guess solution, the governing equations can be obtained by updating the general governing equations (2.7). If $\sigma_{zz} = 0$, then the equilibrium equations reduce to:

$$\begin{cases} \tau_{xz/z} = 0 \\ \tau_{yz/z} = 0 \\ \tau_{zx/x} + \tau_{zy/y} = \nabla \cdot \underline{\tau} = 0 \end{cases}$$

Observation. Recall that the first two equations state that the cross section shear stresses are not a function of the axial coordinate z. This means that the third equation must be verified in each cross section of the beam $S_{F_{face}}$ in order to be verified across its whole volume V.

The compatibility equations reduce to:

$$\begin{cases} \sigma_{zz/yy} = \sigma_{zz/xx} = \sigma_{zz/xy} = \sigma_{zz} = 0 \\ \tau_{zx/xy} - \tau_{yz/xx} = 0 \\ \tau_{zy/xy} - \tau_{xz/yy} = 0 \end{cases}$$

The last two equations can be reorganized for convenience as follows:

$$\begin{cases} \tau_{zx/xy} - \tau_{yz/xx} = \left(\tau_{zx/y} - \tau_{yz/x}\right)_{/x} = 0 \\ \tau_{zy/xy} - \tau_{xz/yy} = \left(\tau_{zy/x} - \tau_{xz/y}\right)_{/y} = 0 \end{cases} \quad \rightarrow \quad \tau_{zy/x} - \tau_{xz/y} = C$$

Where C is a constant. The only relevant internal action to consider is the torsional moment, i.e.

$$M_z = M_t = \int_A \left(-\sigma_{xz} y + \sigma_{yz} x\right) dA$$

Thus, the governing equations for the DSV solution for torsion are the following:

$$\boxed{\begin{cases} \tau_{zx/x} + \tau_{zy/y} = \nabla \cdot \underline{\tau} = 0 & \text{in } V \\ \tau_{zy/x} - \tau_{xz/y} = C & \text{in } V \\ \underline{\tau} \cdot \underline{n} = 0 & \text{on } S_{F_{body}} \\ M_t = \int_A \left(-\tau_{xz} y + \tau_{yz} x\right) dA & \text{on } S_{F_{face}} \end{cases}} \tag{2.24}$$

2.1.5.2. Solution

The guess solution reads $\sigma_{zz} = \sigma_{xx} = \sigma_{yy} = \sigma_{xy} = 0$. Consequently, from the CL of equation (2.6) it follows that $\varepsilon_{xx} = \varepsilon_{yy} = \varepsilon_{zz} = \gamma_{xy} = 0$ and the only nonnull strain components are γ_{xz} and γ_{yz}. From the null components we can conclude that:

$$\begin{cases} \varepsilon_{xx} = u_{\backslash x} = 0 & \rightarrow \quad u = u(y,z) \\ \varepsilon_{yy} = v_{\backslash y} = 0 & \rightarrow \quad v = v(x,z) \\ \varepsilon_{zz} = w_{\backslash z} = 0 & \rightarrow \quad w = w(x,y) \end{cases}$$

Consider now the rotation $\theta(z)$ of the cross section, presented in Figure 2.9 and defined as:

$$\theta(z) = z\theta' = z\theta_{\backslash z} \tag{2.25}$$

Where $\boldsymbol{\theta'}$ ***is the torsion***, constant along the z-axis. Using this quantity, we may express the displacements of the points of the beam section as follows:

$$\begin{cases} u = u(y,z) = -y\theta = -yz\theta' \\ v = v(x,z) = x\theta = xz\theta' \\ w(x,y) = \theta'\Psi(x,y) \end{cases} \tag{2.26}$$

Where $\boldsymbol{\Psi(x,y)}$ ***is the warping function***, the physical meaning of this quantity will be discussed in section (2.1.5.3). For now it is sufficient to specify that within the context of the DSV solution the beam is free to warp, i.e. warping is not prevented by the BCs. Note that since the displacement components respect the dependencies imposed by the CL and strain definition (u is not a function of x, v not of y and w not of z), this displacement field agrees with the guess solution.

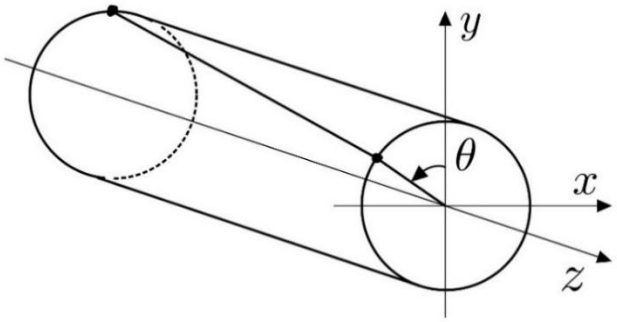

Figure 2.9: torsional rotation on a beam.

Using the displacement formulation of equation (2.26) we can rewrite the governing equations in (2.24). We start from the equilibrium equation, the shear stresses can be rewritten as:

$$\begin{cases}\tau_{xz} = G\gamma_{xz} = G\left(w_{\backslash x} + u_{\backslash z}\right) = G\left(\theta'\Psi_{\backslash x} - y\theta'\right) = G\theta'\left(\Psi_{\backslash x} - y\right)\\ \tau_{yz} = G\gamma_{yz} = G\left(w_{\backslash y} + v_{\backslash z}\right) = G\left(\theta'\Psi_{\backslash y} + x\theta'\right) = G\theta'\left(\Psi_{\backslash y} + x\right)\end{cases}$$

And thus the equilibrium equation becomes:

$$\tau_{zx/x} + \tau_{zy/y} = G\theta'\left(\Psi_{\backslash xx} + \Psi_{\backslash yy}\right) = 0$$

The compatibility equation can be rewritten as:

$$\tau_{zy\backslash x} - \tau_{xz\backslash y} = G\theta'\left(\Psi_{\backslash xy} + 1\right) - G\theta'\left(\Psi_{\backslash xy} - 1\right) = 2G\theta' = C$$

The natural BC is rewritten as follows:

$$\underline{\tau}\cdot\underline{n} = \tau_{xz}n_x + \tau_{yz}n_y = G\theta'\left(\Psi_{\backslash x} - y\right)n_x + G\theta'\left(\Psi_{\backslash y} + x\right)n_y = 0 \quad \rightarrow \quad \Psi_{\backslash n} = yn_x - xn_y$$

The internal torsional action M_t will then be expressed as follows:

$$M_t = \int_A \left(-\tau_{xz}y + \tau_{yz}x\right)dA = G\theta' \int_A \left(-\Psi_{\backslash x}y + y^2\right) + \left(\Psi_{\backslash y}x + x^2\right)dA = GJ\theta'$$

Where ***GJ is the torsional stiffness***, and ***J is the torsional constant*** (a second area moment) that can be defined as follows:

$$J = \int_A \left(y^2 - \Psi_{\backslash x}y\right) + \left(x^2 + \Psi_{\backslash y}x\right)dA \tag{2.27}$$

Observation. Note that ***J is not the polar moment of inertia J_p***. This is due to the contribution of the warping $\Psi(x, y)$. In the particular case of null warping $\Psi = 0$ then $J = J_p$. We will discuss in the next section of how this condition also corresponds to the case of a circular cross section, for which one may in fact recall that $J = J_p$. However, in general $J \leq J_p$.

Thus, the updated governing equations can be rewritten in terms of the warp function and torsion as:

$$\boxed{\begin{cases} G\theta'\left(\Psi_{\backslash xx} + \Psi_{\backslash yy}\right) = 0 & \text{in } V \\ 2G\theta' = C & \text{in } V \\ \Psi_{\backslash n} = yn_x - xn_y & \text{on } S_{F\,body} \\ M_t = GJ\theta' & \text{on } S_{F\,face} \end{cases}} \tag{2.28}$$

The problem represented by the set of equations above is a well-posed Neuman problem, meaning that a solution can be found and the initial guess was correct. The solution of system (2.28) is the warping function $\Psi(x, y)$, from which we can retrieve the shear stresses τ_{xz} and τ_{yz} and the torsional constant J. Once these are known, we can determine the internal torsional action M_t via its definition in (2.24). At this point, we can determine the torsion from the internal action equivalence $\theta' = M_t/GJ$. Finally, knowing the torsion and the warping function, the displacement field $\boldsymbol{u}$ can be retrieved from (2.26).

Observation. Note that the compatibility equation is superfluous here, as it states that the product $2G\theta'$ is a constant. From the internal action equivalence one can easily observe that $C = 2M_t/J$.

2.1.5.3. Meaning of warping

It is interesting to investigate what is the physical meaning of warping. Consider the expression of the shear stresses that we obtained in the previous section:

$$\begin{cases} \tau_{xz} = G\theta'\left(\Psi_{\backslash x} - y\right) \\ \tau_{yz} = G\theta'\left(\Psi_{\backslash y} + x\right) \end{cases}$$

Now assume that the section does not warp $\Psi = 0$, so that the shear stresses simply reduce to:

$$\begin{cases} \tau_{xz} = -G\theta' y = -ky \\ \tau_{yz} = +G\theta' x = +kx \end{cases}$$

Where k is constant because G and θ' are both constant. Then, according to the sketch in Figure 2.10, the shear stresses at a generic point P along the cross section boundary can be expressed as follows:

$$\begin{cases} y = d\sin\theta \\ x = d\cos\theta \end{cases} \quad \rightarrow \quad \begin{cases} \tau_{xz} = -ky = -kd\sin\theta \\ \tau_{yz} = +kx = +kd\cos\theta \end{cases}$$

Where $d = |\overline{OP}|$. This implies that $\boldsymbol{\tau}$ is always normal to $\overline{OP}$, and so if $\overline{OP}$ is not parallel to the normal $\boldsymbol{n}$ of the cross section in point P, then $\boldsymbol{\tau} \cdot \boldsymbol{n} \neq \boldsymbol{0}$ and the Cauchy condition is violated. It is easy to observe from Figure 2.10 that, for a cross section of generic shape, $\overline{OP}$ is not parallel to the normal $\boldsymbol{n}$, and thus the Cauchy condition is always violated if warping is not considered. The particular case in which $\overline{OP} \parallel \boldsymbol{n}$ and thus warping is not needed is the case of circular cross section. In this case, the normal to the section in every point of its boundary reads $\overline{OP} = \boldsymbol{n} = \cos\theta\,\boldsymbol{e}_1 + \sin\theta\,\boldsymbol{e}_2$, and thus the Cauchy condition is respected:

$$\begin{aligned} \underline{\tau} \cdot \underline{n} &= \left(\tau_{xz}\underline{e}_1 + \tau_{yz}\underline{e}_2\right) \cdot \left(\cos\theta\,\underline{e}_1 + \sin\theta\,\underline{e}_2\right) \\ &= \left(-kd\sin\theta\,\underline{e}_1 + kd\cos\theta\,\underline{e}_2\right) \cdot \left(\cos\theta\,\underline{e}_1 + \sin\theta\,\underline{e}_2\right) \\ &= kd(-\sin\theta\cos\theta + \sin\theta\cos\theta) = 0 \end{aligned}$$

Recall that the circular section case is also the case for which $J = J_P$. Thus, we can conclude that the ***physical meaning of warping*** is to restore the Cauchy equilibrium $\boldsymbol{\tau} \cdot \boldsymbol{n} = \mathbf{0}$ for a cross section of generic shape on its boundary.

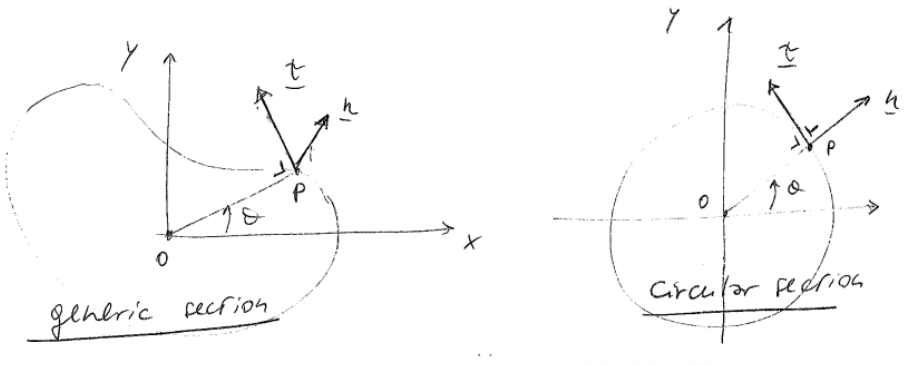

Figure 2.10: shear stresses acting on a generic (left) and circular (right) beam cross section boundary.

2.1.5.4. Evaluation of the torsional constant J

It was found from the solution of the torsional problem of a beam under the DSV hypotheses that:

$$J = \int_A \left(y^2 - \Psi_{\backslash x} y\right) + \left(x^2 + \Psi_{\backslash y} x\right) dA = \int_A \left(x^2 + y^2 + \Psi_{\backslash y} x - \Psi_{\backslash x} y\right) dA$$

Thus, the evaluation of J requires the knowledge of the warping function $\Psi(x, y)$, which can be obtained by solving the torsional problem (2.28). We now reformulate J in a convenient way, starting from:

$$\int_A \left(\Psi_{\backslash y} x - \Psi_{\backslash x} y\right) dA = \int_A \left((\Psi x)_{\backslash y} - (\Psi y)_{\backslash x}\right) dA = \int_{\partial A} \left(\Psi x n_y - \Psi y n_x\right) d\Gamma$$
$$= \int_{\partial A} \Psi \left(x n_y - y n_x\right) d\Gamma$$

Recall now from (2.28) that $\Psi_{\backslash n} = y n_x - x n_y$, and so by substitution we obtain:

$$\int_{\partial A} \Psi \left(x n_y - y n_x\right) d\Gamma = -\int_{\partial A} \Psi \Psi_{\backslash n} d\Gamma = -\int_{\partial A} \Psi \nabla \Psi \cdot \underline{n} d\Gamma$$

Applying now the divergence theorem yields:

$$-\int_{\partial A} \Psi \nabla \Psi \cdot \underline{n} d\Gamma = -\int_A \nabla \cdot (\Psi \nabla \Psi) dA = -\int_A \left[\left(\Psi \Psi_{\backslash x}\right)_{\backslash x} + \left(\Psi \Psi_{\backslash y}\right)_{\backslash y}\right] dA$$
$$= -\int_A \left[\Psi_{\backslash x}^2 + \Psi \Psi_{\backslash xx} + \Psi_{\backslash y}^2 + \Psi \Psi_{\backslash yy}\right] dA =$$
$$= -\int_A \left[\Psi_{\backslash x}^2 + \Psi_{\backslash y}^2 + \Psi \left(\Psi_{\backslash xx} + \Psi_{\backslash yy}\right)\right] dA = -\int_A \left(\Psi_{\backslash x}^2 + \Psi_{\backslash y}^2\right) dA$$

Where we used that $\Psi_{\backslash xx} + \Psi_{\backslash yy} = 0$ from (2.28). Thus, we obtained that:

$$\int_A (\Psi_{\backslash y} x - \Psi_{\backslash x} y) dA = -\int_A (\Psi_{\backslash x}^2 + \Psi_{\backslash y}^2) dA$$

Plug this result in the expression of J:

$$\begin{aligned} J &= \int_A (x^2 + y^2 + \Psi_{\backslash y} x - \Psi_{\backslash x} y) dA \\ &= \int_A (x^2 + y^2 + \Psi_{\backslash y} x - \Psi_{\backslash x} y) dA + \int_A \underbrace{(\Psi_{\backslash y} x - \Psi_{\backslash x} y + \Psi_{\backslash x}^2 + \Psi_{\backslash y}^2)}_{=0} dA \\ &= \int_A (x^2 + y^2 + 2\Psi_{\backslash y} x - 2\Psi_{\backslash x} y + \Psi_{\backslash x}^2 + \Psi_{\backslash y}^2) dA \\ &= \int_A \left[(\Psi_{\backslash y} + x)^2 + (\Psi_{\backslash x} - y)^2 \right] dA \end{aligned}$$

Now recall that the shear stresses have been found to be:

$$\begin{cases} \tau_{xz} = G\theta'(\Psi_{\backslash x} - y) \\ \tau_{yz} = G\theta'(\Psi_{\backslash y} + x) \end{cases} \quad \rightarrow \quad J = (G\theta')^2 \int_A (\tau_{yz}^2 + \tau_{xz}^2) dA$$

But $M_t = GJ\theta'$ and so $(G\theta')^2 = (M_t/J)^2$, by substitution we (finally) obtain the expression of J reported below. This formulation of the inertia J (naturally equivalent to (2.27)), is such that in order to determine the torsional constant J we only require the shear stresses, and not the warping Ψ. A way to estimate the shear stresses has yet to be provided, and it will be the topic of section 2.1.6.

$$J = \frac{M_t^2}{\int_A (\tau_{yz}^2 + \tau_{xz}^2) dA} \tag{2.29}$$

2.1.5.5. Strain and complementary strain energies

The strain energy due to shear loads $U^{(s)}$ can be written as follows:

$$U^{(s)} = \int_V (\gamma_{zx}\tau_{zx} + \gamma_{zy}\tau_{zy}) dV = \frac{1}{2}\int_V \frac{1}{G}(\tau_{xz}^2 + \tau_{yz}^2) dV$$

The shear stresses can be rewritten using (2.29), yielding:

$$U^{(s)} = \frac{1}{2}\int_V \frac{1}{G}(\tau_{xz}^2 + \tau_{yz}^2) dV = \frac{1}{2}\int_l M_z \frac{M_z}{GJ} dz$$

The equation reported above is actually the shear complementary strain energy $U^{*(s)}$ since it is expressed in terms of generalized stresses, and thus $U^* = U^*(\boldsymbol{\sigma})$. In this case the generalized stress parameter is the torsional internal action M_z. In order to obtain a proper strain energy we need to express every term in the above equation in terms of generalized strain, which in this case is the torsion θ'. To do this we require a ***generalized CL***, linking generalized stresses and strains. Such CL is provided by the last equation of (2.28), which reads:

$$M_z = GJ\theta' \tag{2.30}$$

If follows that the shear strain energy can be expressed as follows:

$$U^{(s)} = \frac{1}{2}\int_l \theta' M_z dz$$

Then, using the generalized CL we can obtain a proper shear strain energy that is fully a function of the strains $U^{(s)} = U^{(s)}(\boldsymbol{\varepsilon})$, or a complementary shear strain energy that is fully a function of generalized stresses $U^{*(s)} = U^{*(s)}(\boldsymbol{\sigma})$. This yields:

$$\begin{cases} U^{*(s)} = \frac{1}{2}\int_l M_z \frac{M_z}{GJ} dz \\ U^{(s)} = \frac{1}{2}\int_l GJ\theta'^2 dz \end{cases} \tag{2.31}$$

2.1.6. Shear stresses of thin-walled sections

In most cases, typical aerospace structures are characterized by thin-walled sections, meaning that thickness is small in relation to the dimensions of the section. In these cases, the shear stresses can be determined by introducing proper ***approximations*** related to the small thickness. We'll analyze open and closed cross sections. The set of governing equations is that of the torsional problem of a DSV beam (2.24), reported here:

$$\begin{cases} \tau_{zx\backslash x} + \tau_{zy\backslash y} = \nabla \cdot \underline{\tau} = 0 & \text{in } V \\ \tau_{zy\backslash x} - \tau_{xz\backslash y} = 2G\theta' & \text{in } V \\ \underline{\tau} \cdot \underline{n} = 0 & \text{on } S_{F_{body}} \\ M_t = GJ\theta' & \text{on } S_{F_{face}} \end{cases}$$

2.1.6.1. Fluid analogy

The analogy between the flow of shear stresses in a beam section with the motion of a fluid allows us to qualitatively understand how the shear flows in the section of a beam. By replacing the shear vector $\boldsymbol{\tau}$ with the velocity vector $\mathbf{v}$ in the equilibrium conditions of the system above, we obtain the equations describing the mass balance and the tangency condition for an incompressible fluid.

$$\begin{cases} \nabla \cdot \underline{\tau} = 0 & \text{in } S_{F_{face}} \\ \underline{\tau} \cdot \underline{n} = 0 & \text{on } S_{F_{body}} \end{cases} \quad \rightarrow \quad \begin{cases} \nabla \cdot \underline{\mathrm{v}} = 0 & \text{in } A \\ \underline{\mathrm{v}} \cdot \underline{n} = 0 & \text{on } \Gamma \end{cases}$$

Here, we replaced the beam section area with the generic area A, and the beam lateral surface with the boundary Γ. Consider now the three examples in Figure 2.11:

- Case 1 (left): the torsional moment M_z is the internal action, so the shear stresses should satisfy equivalence with M_t (but not the overall equilibrium!). If the shear stresses must respect the tangency condition, then their direction is easily obtained.
- Case 2 (center): the flow does not need to reverse its direction along the thickness to satisfy the tangency condition, it simply circulates inside the loop.

- Case 3 (right): similarly to case 1, the presence of the cut requires the shear flow to reverse direction along the thickness in proximity of the cut in order to satisfy the tangency condition.

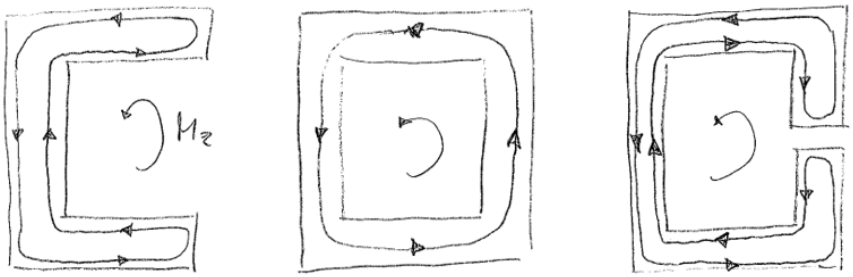

Figure 2.11: beam cross sections.

Thus, if a section is open the shear flow will reverse its direction through the thickness. This implies that the arm d between the shear flows is very small (Figure 2.12 – left). Consequently, in order to satisfy the equivalence of the above equation, the magnitude of the shear stresses will have to be high. On the contrary, closed sections develop shear stresses that are characterized by relatively long arms (Figure 2.12 – right). As a consequence, in order to satisfy the equivalence between the shear stress distribution and the internal action M_t, the shear stresses magnitude will be lower than for an open cross section. We can ***summarize these observations*** as follows:

- Open-section → higher stresses → higher deformation → lower torsional stiffness!
- Close-section → lower stresses → lower deformation → higher torsional stiffness!

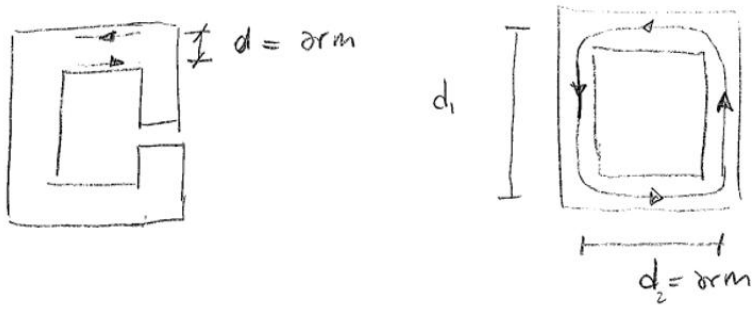

Figure 2.12: shear flows arm for an open (left) and closed (right) beam cross section.

From a mathematical standpoint, the previous observations can be formalized as follows. We integrate the shear flow equilibrium equation over an arbitrary portion of the section A', depicted in Figure 2.13 – left. This yields:

$$\int_{A'} \nabla \cdot \underline{\tau} dA = \oint_{\Gamma} \underline{\tau} \cdot \underline{n} d\Gamma = \phi = 0$$

Where we define ϕ as the net flow of the shear stresses outflowing from the boundary Γ of A'. It is possible to split the boundary of A in two components, one that does not intersect the cross section Γ_1 and one that does Γ_2. Naturally, no shear flow is crossing Γ_1, and thus:

$$\oint_{\Gamma} \underline{\tau} \cdot \underline{n} d\Gamma = \oint_{\Gamma_1} \underline{\tau} \cdot \underline{n} d\Gamma_1 + \oint_{\Gamma_2} \underline{\tau} \cdot \underline{n} d\Gamma_2 = \oint_{\Gamma_2} \underline{\tau} \cdot \underline{n} d\Gamma_2 = \phi_2 = 0$$

It follows that, for $\phi_2 = 0$ to be verified, part of the shear stresses must be directed in one direction, and another part in the opposite direction, as depicted in Figure 2.12. If a closed cross

section is considered (Figure 2.13 – right), then it is easy to conclude that the shear flow entering from Γ_2 must be equal to that exiting from Γ_3.

$$\oint_{\Gamma} \underline{\tau} \cdot \underline{n} d\Gamma = \underbrace{\oint_{\Gamma_1} \underline{\tau} \cdot \underline{n} d\Gamma_1}_{=0} + \oint_{\Gamma_2} \underline{\tau} \cdot \underline{n} d\Gamma_2 + \oint_{\Gamma_3} \underline{\tau} \cdot \underline{n} d\Gamma_3 = 0 \quad \rightarrow \quad \phi_2 = -\phi_3$$

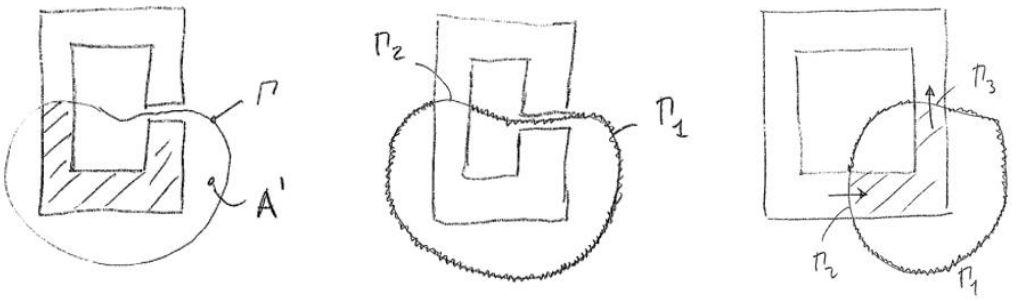

Figure 2.13: left) surface A' and boundary Γ; center) boundaries Γ_1 and Γ_2; right) closed section flows.

2.1.6.2. Open profiles

Consider the open profile presented in Figure 2.14, i.e. a narrow strip subject to a torsional moment M_z. A series of open profile sections can be approximated as an assembly of this basic geometry. For this reason, we base our discussion on this basic element. A qualitative analysis reveals that the shear stresses will be directed as depicted below. It is clear that $\sigma_{yz} \approx 0$ in most of the section apart from the external portions, where the shear flow is directed along the thickness to reverse it direction.

Figure 2.14: strip subject to torsional moment and relative shear flow.

Assuming that $\sigma_{yz} = 0$. the governing equations of equilibrium and compatibility become:

$$\begin{cases} \tau_{zx\backslash x} = 0 \\ -\tau_{xz\backslash y} = 2M_t/J \end{cases}$$

From previous discussion we know that τ_{xz} is not a function of z, from the equilibrium equation above we can conclude that it is also not a function of y. Thus, we expect τ_{xz} to be of the form:

$$\tau_{xz} = Ay$$

Where A is a constant. Apply this to the compatibility equation and we obtain:

$$-\tau_{xz\backslash y} = A = \frac{2M_t}{J} \quad \rightarrow \quad A = -\frac{2M_t}{J}$$

Thus, the approximate solution for shear stress τ_{xz} results to be ***linear along the thickness*** $\boldsymbol{y}$:

$$\tau_{xz} = -\frac{2M_t}{J}y \tag{2.32}$$

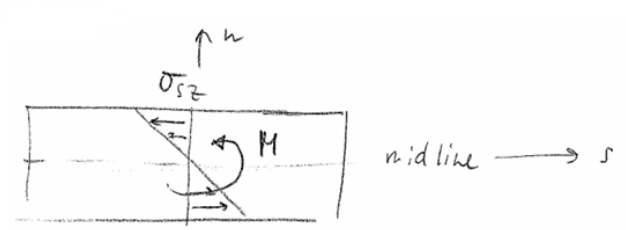

Figure 2.15: linear shear stress distribution on a thin walled beam due to a torsional moment.

The value of J can be easily computed by substitution of this expression of τ_{xz} and $\tau_{yz} = 0$ into equation (2.29). this yields:

$$J = \frac{M_t^2}{\int_A(\tau_{yz}^2 + \tau_{xz}^2)dA} = \frac{M_t^2}{\int_A\left(\frac{2M_t}{J}y\right)^2 dA} = \frac{J^2}{\int_A 4y^2 dA} \quad \rightarrow \quad J = \int_A 4y^2 dA \tag{2.33}$$

Naturally, the exact expression of the inertia J depends on the cross section geometry. In general, we'll differentiate between sections with constant thickness or variable thickness (the latter case could be useful for approximating a wing with this model). The strip presented in Figure 2.14 has constant thickness, and thus we can simply write:

$$J = \int_A 4y^2 dA = \int_{-a/2}^{+a/2}\int_{-b/2}^{+b/2} 4y^2 dydx = \int_{-a/2}^{+a/2}\frac{b^3}{3}dx = \frac{1}{3}ab^3$$

If the thickness is not constant $b = b(x)$, we'll write:

$$J = \int_{-b/2}^{+b/2}\frac{b^3(x)}{3}dx$$

As mentioned at the beginning of this section, it's possible to model numerous open sections of generic shapes as assemblies of narrow strips. We denote n_i the normal axis of the i-th strip, normal to shear flow direction and running along the strip thickness b_i. With s_i we denote the tangent axis of the i-th strip, tangent to the shear flow direction and running along its width a_i. An example is reported in Figure 2.16. Then, for each strip we may write:

$$\begin{cases}\tau_{nz} = 0 \\ \tau_{sz} = -\dfrac{2M_t}{J}n\end{cases} \quad \text{and} \quad J = \begin{cases}\displaystyle\int_{-b/2}^{+b/2}\frac{b^3(x)}{3}dx, & b = b(x) \\ \dfrac{1}{3}ab^3, & b = \text{const}\end{cases}$$

Some applicative examples for computing shear stresses, torsional stiffness and rotation due to an applied torsional moment M_t to open sections are presented in the appendix (section 10.2).

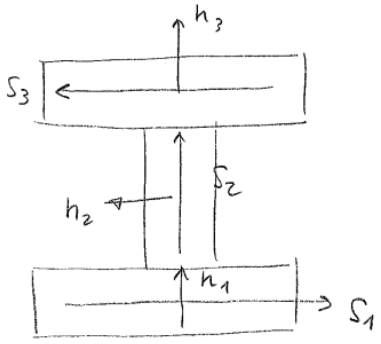

Figure 2.16: "I" beam decomposed in an assembly of strips.

Observation. It is interesting to evaluate the resultant over the strip in Figure 2.14 associated to the solution here derived, equations (2.32) and (2.33). The strip has constant thickness, and thus $J = ab/3$. Then, by definition:

$$M_t = \int_A \left(-\tau_{xz} y + \tau_{yz} x\right) dA = \int_A -\tau_{xz} y dA = \int_{-a/2}^{+a/2} \int_{-b/2}^{+b/2} \frac{2M_t}{J} y^2 dy dx = \frac{2M_t}{J} \frac{a}{3} \left(y^3\right)_{-b/2}^{+b/2}$$
$$= \frac{2M_t}{J} \frac{a}{3} \frac{b^3}{4} = 2M_t \frac{ab^3}{12J} = 2M_t \frac{ab^3}{12} \frac{3}{ab^3} = \frac{M_t}{2}$$

The equation is not identically satisfied, i.e. the equivalence between the shear stresses and the internal torsional action is not respected. Why? Because we assumed $\sigma_{yz} = 0$. Although this term has really low modulus, it's multiplied by a long arm, and thus it provides an important contribution to M_t, but we are neglecting it.

2.1.6.3. Closed profiles

It was found with the hydraulic analogy that the shear flows in a closed thin-walled section are generally lower in modulus than for an open section, considering the same torsional moment applied M_t. This is due to the fact that the arms of the shear stresses are much higher for closed sections, implying that to satisfy the internal action equivalence (2.24) the shear stresses modulus must be lower. For thin-walled sections, it can be reasonably ***assumed that τ_{sz} is constant along the thickness*** (or along n) ***and parallel to the midline***. Naturally, the smaller the thickness of the section the more valid is this assumption. Note that this is in contrast to what has been found for open cross sections, for which τ_{sz} has been found to be linear in n.

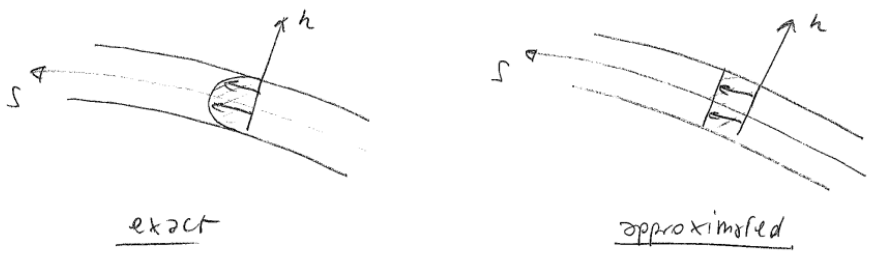

Figure 2.17: exact (left) and approximated (right) shear flow distribution in a thin-walled section.

This assumption simplifies the derivation of a closed-form solution for shear stress of thin-walled sections. Recall the equilibrium condition:

$$\nabla \cdot \underline{\tau} = 0 \quad \rightarrow \quad \int_{A'} \nabla \cdot \underline{\tau} dA' = \oint_{\Gamma} \underline{\tau} \cdot \underline{n} d\Gamma = \phi = 0$$

Also recall that the contour integral can be split by identifying the parts of the contour that intersect the section Γ_2 and Γ_3, and the part that does not Γ_1. Intuitively $\oint_{\Gamma_1}(\dots)d\Gamma_1 = 0$, and so we remain with:

$$\oint_{\Gamma_2} \underline{\tau} \cdot \underline{n} d\Gamma_2 + \oint_{\Gamma_3} \underline{\tau} \cdot \underline{n} d\Gamma_3 = \phi_2 + \phi_3 = 0$$

If the shear stresses τ_{sz} are constant through the normal axis n (the thickness), then they only depend on the tangent axis coordinates S, i.e. $\tau_{sz} = \tau_{sz}(S)$. As a consequence, the contour integral components of the boundaries $\Gamma_{2,3}$ that cut through the section thickness simply yield:

$$\begin{cases} \phi_2 = \oint_{\Gamma_2} \underline{\tau} \cdot \underline{n} d\Gamma_2 = \int_{-\frac{t_2}{2}}^{+\frac{t_2}{2}} \tau_{sz}(S_0) dn = \tau_{sz}(S_0) t_2 = q_{in} \\ \phi_3 = \oint_{\Gamma_3} \underline{\tau} \cdot \underline{n} d\Gamma_3 = \int_{-\frac{t_3}{2}}^{+\frac{t_3}{2}} -\tau_{sz}(S_1) dn = -\tau_{sz}(S_1) t_3 = -q_{out} \end{cases}$$

$$\phi_2 + \phi_3 = q_{in} - q_{out} = 0$$

Where we defined the ***shear flows*** $\boldsymbol{q_i}$ $[N/mm]$ entering and exiting the boundary A' as q_{in} and q_{out}, respectively. Note that the signs multiplying the shear flows are due to the convention of the normal versor characterizing the surface A'. In our case, we assumed the normal $\boldsymbol{n}$ to be positive if entering A', thus according to Figure 2.18 – right, the positive term is q_{in}. Is it easy to observe that if the sign convention is reversed, the result would be the same.

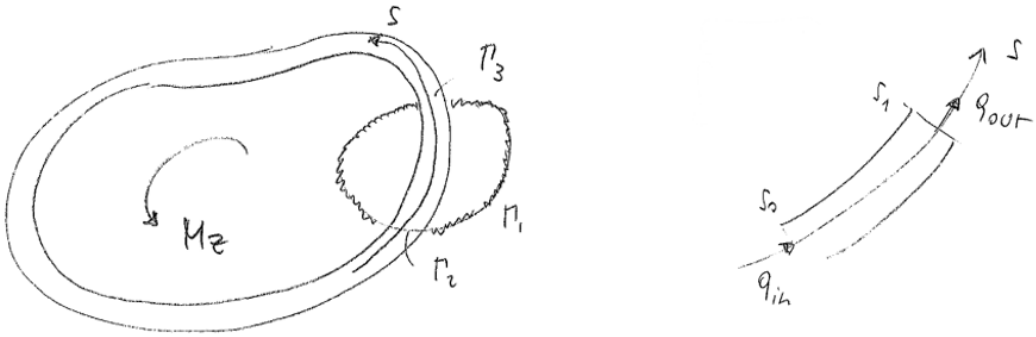

Figure 2.18: left) contour of A'; right) shear flows flowing through A'.

Observation. It is important to point out the physical meaning of the condition $q_{in} = q_{out}$. This simply means that ***the shear flow q is constant along the shear axis S of the section***. The shear stresses and the thickness may not be constant along S, but the shear flow q must be.

The relation between the shear flow and the torsional moment M_z can be obtained by imposing the equivalence between the two. Being the shear stress τ_{sz} constant through the section thickens, and acting along its midline, we represent the section through its midline. Consider a generic pole O and the shear flow acting on a generic point of the section midline, tangent to such point (Figure

2.19 – left). Then, the torsional moment due to a portion of the section midline ds can be expressed as follows:

$$dM_z = qds \cdot r(s) = qr(s)ds$$

Where $r(s)$ is the arm between q and the pole O, in general a function of the shear axis s. The total moment will then be the integral of dM over the shear axis s, yielding:

$$M_z = \oint_\Gamma qr(s)ds = \oint_\Gamma qr(s)ds = q\oint_\Gamma r(s)ds$$

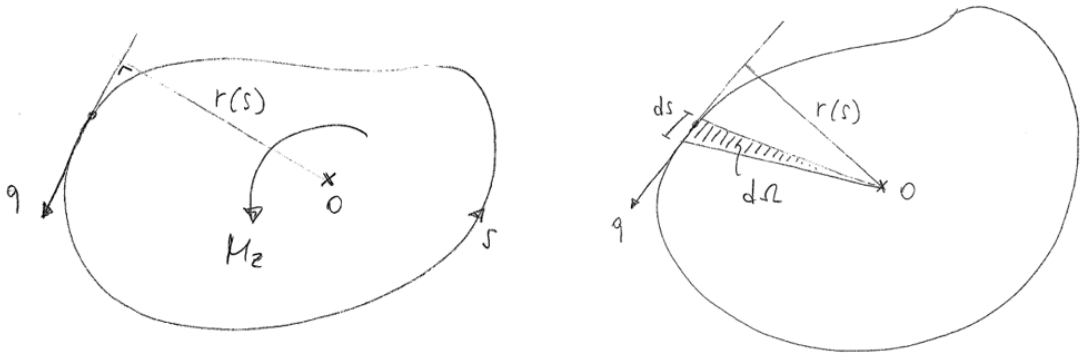

Figure 2.19: closed cross section of a beam represented through its midline.

The above integral can be evaluated by inspecting its graphical representation, presented in Figure 2.19 – right. The area of the triangle $d\Omega$ is given by $r(s)ds/2$, thus:

$$2d\Omega = r(s)ds \quad \rightarrow \quad \oint_\Gamma r(s)ds = \oint_\Gamma 2d\Omega = 2\Omega$$

Where Ω is the area of the cross section. using the above relation, we obtain ***Bredt formula***, relating shear flow to the internal torsional action acting on the beam cross section:

$$M_z = 2\Omega q \tag{2.34}$$

The torsional inertia J can be evaluated as:

$$J = \frac{M_t^2}{\int_A(\tau_{yz}^2 + \tau_{xz}^2)dA} = \frac{M_t^2}{\int_A \tau_{sz}^2 dA} = \frac{M_t^2}{\int_t \oint_\Gamma \left(\frac{q}{t(s)}\right)^2 d\Gamma dt} = \frac{M_t^2}{\int_t \oint_\Gamma \left(\frac{M_t/2\Omega}{t(s)}\right)^2 d\Gamma dt} = \frac{4\Omega^2}{\oint_\Gamma \frac{1}{t(s)} d\Gamma}$$

$$J = \frac{4\Omega^2}{\oint_\Gamma \frac{1}{t(s)} d\Gamma} \tag{2.35}$$

An applicative example is presented in the appendix (section 10.2). Such example compares the torsional stiffness of two cross sections of identical geometry. However, in one case the section is closed, and in the other it has a cut that makes it an open section.

2.1.7. Energetic formulations

2.1.7.1. Strain energy

The DSV solution allows us to express the strain energy U and the complementary strain energy U^* as a function of the internal actions. Recall from section 1.2 that the strain energy density u and the complementary strain energy density u^* can be expressed as follows:

$$\begin{cases} u = u\left(\underline{\underline{\varepsilon}}\right) = \frac{1}{2}\underline{\underline{\sigma}}\left(\underline{\underline{\varepsilon}}\right) : \underline{\underline{\varepsilon}} \\ u^* = u^*\left(\underline{\underline{\sigma}}\right) = \frac{1}{2}\underline{\underline{\sigma}} : \underline{\underline{\varepsilon}}\left(\underline{\underline{\sigma}}\right) \end{cases}$$

Where u^* is used in force-based approaches to impose compatibility (via Menabrea's theorem), while u is used in displacement-based approaches to impose equilibrium (via Minimum potential energy principle). Also recall that in the linear case $u = u^*$.

It has been found that expressing the strain energies in terms of internal actions leads to the identification of generalized parameters. These are global quantities that impose equilibrium and compatibility at a global level. Generalized stresses are the internal actions $T_z, M_x M_y, M_z$, stress resultants over the cross section, thus in fact global quantities. The generalized strains are found by identifying those quantities that are in energy conjugacy with the generalized stresses. It has been found that the generalized strains are $\varepsilon_{zz}, k_x, k_y, \theta'$. Thus, we'll write:

$$U = \frac{1}{2}\int_l \left(T_z\varepsilon_{zz} + M_x k_x + M_y k_y + M_z\theta'\right)dz$$

We now introduce the components related to the pure shear actions τ_{zx} and τ_{zy} as well. The generalized stresses will be the internal actions T_x and T_y, respectively. Recall that such internal actions are stress resultants, therefore approximate solutions for the shear stresses are needed to quantify them. The respective generalized strains can be formalized as being γ_{0zx} and γ_{0zy}. Thus, the ***general form of the strain energy*** is as follows:

$$U = \frac{1}{2}\int_l \left(T_z\varepsilon_{zz} + T_x\gamma_{0zx} + T_y\gamma_{0zy} + M_x k_x + M_y k_y + M_z\theta'\right)dz \tag{2.36}$$

Observation. Here, the contributions coming from the shear internal actions must be taken with respect to a reference system that is centered in the shear center of the section. The shear center is the point of the beam section where an applied shear load does not generate a torsional moment. This concept is better discussed in section 4.2. Note however that shear center and barycenter of the section (needed for principal axes) may not coincide.

In order to obtain a proper strain energy, all the terms inside the above equation must be expressed in terms of generalized strains, so that $U = U(\boldsymbol{\varepsilon})$. Similarly, to obtain a proper complementary strain energy all the terms must be expressed in terms of generalized stresses, so that $U^* = U^*(\boldsymbol{\sigma})$. To obtain either formulation a generalized CL is needed, i.e. a CL that relates generalized stresses to generalized strains. Such generalized CL for axial, bending and torsion has been found to be:

$$\begin{Bmatrix} T_z \\ M_x \\ M_y \\ M_z \end{Bmatrix} = \begin{bmatrix} EA & 0 & & \\ 0 & EI_{xx} & \underline{\underline{0}} & \\ & & EI_{yy} & 0 \\ & \underline{\underline{0}} & 0 & GJ \end{bmatrix} \begin{Bmatrix} \varepsilon_{zz} \\ k_x \\ k_y \\ \theta' \end{Bmatrix} = \begin{bmatrix} EA & 0 & & \\ 0 & EI_{xx} & \underline{\underline{0}} & \\ & & EI_{yy} & 0 \\ & \underline{\underline{0}} & 0 & GJ \end{bmatrix} \begin{Bmatrix} w_{\backslash z} \\ -v_{\backslash zz} \\ -u_{\backslash zz} \\ \theta' \end{Bmatrix}$$

Similar relations can be found for the shear stresses terms, i.e. the shear internal actions are related to the generalized strains via shear stiffnesses GA^*. More precisely:

$$\begin{cases} T_x = GA_x^* \gamma_{0zx} \\ T_y = GA_x^* \gamma_{0zy} \end{cases} \tag{2.37}$$

Here the stiffness is represented as GA^* because it is not the product between G and A, even for isotropic, homogeneous beams. However, it illustrates that the shear stiffness depends on the shear modulus G and an area related quantity A^*, making GA^* dimensionally a force. Thus, accounting for the shear CL of (2.37), the full CL of a DSV beam reads:

$$\begin{Bmatrix} T_x \\ T_y \\ T_z \\ M_x \\ M_y \\ M_z \end{Bmatrix} = \begin{bmatrix} GA_x^* & 0 & 0 & & & \\ 0 & GA_y^* & 0 & & \underline{\underline{0}} & \\ 0 & 0 & EA & & & \\ & & & EI_{xx} & 0 & 0 \\ & \underline{\underline{0}} & & 0 & EI_{yy} & 0 \\ & & & 0 & 0 & GJ \end{bmatrix} \begin{Bmatrix} \gamma_{0zx} \\ \gamma_{0zy} \\ \varepsilon_{zz} \\ k_x \\ k_y \\ \theta' \end{Bmatrix} \tag{2.38}$$

Using such relations, the strain energies are obtained as:

$$\begin{cases} U^* = \frac{1}{2}\int_l \left(T_x \frac{T_x}{GA_x^*} + T_y \frac{T_y}{GA_y^*} + T_z \frac{T_z}{EA} + M_x \frac{M_x}{EI_{xx}} + M_y \frac{M_y}{EI_{yy}} + M_z \frac{M_z}{GJ} \right) dz \\ U = \frac{1}{2}\int_l \left(\gamma_{0zx}^2 GA_x^* + \gamma_{0zy}^2 GA_y^* + \varepsilon_{zz}^2 EA + k_x^2 EI_{xx} + k_y^2 EI_{yy} + \theta'^2 GJ \right) dz \end{cases} \tag{2.39}$$

When using approximation methods it is useful to express the strain energy in terms of displacements derivatives. This is because the mentioned approximation methods usually provide an approximation of the displacement field. Thus, we will write:

$$U = \frac{1}{2}\int_l \left(w_{\backslash z}^2 EA + v_{\backslash zz}^2 EI_{xx} + u_{\backslash zz}^2 EI_{yy} + \theta'^2 GJ \right) dz \tag{2.40}$$

Effect of shear deformability. The strain energy of the pure shear loads contributions have been considered for completeness. However, it is easy to prove that their contribution to the total strain energy is often negligible for beams. Intuitively, a beam subject to a shear load will be way more compliant in bending than in transverse shear deformation. This simply means that the beam will tend to bend more than to deform its cross section due to shear. To quantify the effect of shear deformability in beams, consider the simple example of Figure 2.20. The section properties, internal actions and resulting shear and bending strain energies of such beam will be:

$$\begin{cases} J = \frac{1}{12}a^4 \\ A^* = \frac{5}{6}a^2 \end{cases} \qquad \begin{cases} T_y = -F \\ M_x = -Fz \end{cases}$$

$$\begin{cases} U^{\text{shear}} = \frac{1}{2}\int_l T_y \frac{T_y}{GA^*} dz = \frac{1}{2}\frac{F^2 l}{GA^*} \\ U^{\text{bending}} = \frac{1}{2}\int_l M_x \frac{M_x}{EI} dz = \frac{1}{2}\frac{F^2 l^3}{3EI} \end{cases}$$

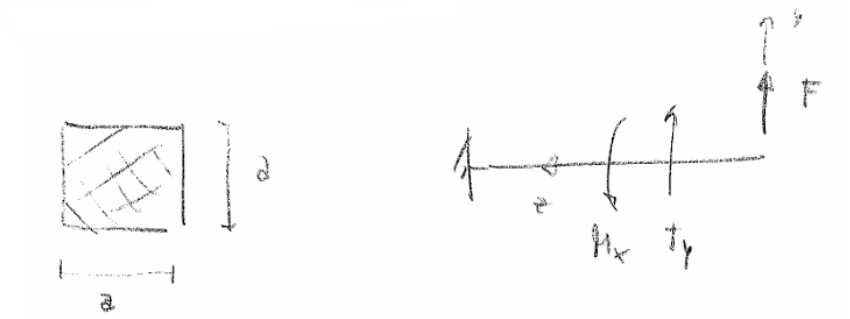

Figure 2.20: compact square-section beam.

It is interesting to investigate the ratio between the shear and bending strain energies. More precisely, such ratio is proportional to the inverse of the square of the ***slenderness ratio λ*** of a beam, as defined below. Here we assumed that G is of the same order of E, and A^* of that of A.

$$\frac{U^{\text{shear}}}{U^{\text{bending}}} = \frac{\frac{1}{2}\frac{F^2 l}{GA^*}}{\frac{F^2 l^3}{3EI}} = 3\frac{EI}{GA^* l^2} \propto \lambda^{-2} \qquad \text{where} \quad \lambda = \sqrt{\frac{Al^2}{I}} \tag{2.41}$$

This result implies that for slender compact beams $\lambda^{\uparrow}$ the strain energy due to bending is much higher than to that due to shear. We will see that this is generally not true for thin-walled beams (see section **Error! Reference source not found.**). This result is again due to the fact that a slender beam is much more compliant in bending than in shear. Assuming that the cross section dimension is $a = 100mm$, the length of the beam is $l = 1m$, and that $E \approx 2G$, the ratio of the strain energies shows that the shear component is less than 1% of the bending strain energy.

$$\frac{U^{\text{shear}}}{U^{\text{bending}}} = \frac{3}{5} \cdot 10^{-2} = \frac{3}{500} < 1\%$$

Thus, the ***shear strain energy can often be neglected for beams with more than acceptable error***.

2.1.7.2. Variational formulation (PCVW)

The DSV solution for beams can be coupled with the variational tools developed in section 1.5 and applied to beams, or system of beams, in order to (1) compute displacement and rotations in parts of the structure, and (2) solve statically undetermined systems. These two problems are solved in the context of force-based approaches, i.e. PCVW and Menabrea's theorem. Note that force-based approaches are useful to analytically solve simple problem. However, as the number of DOFs increases, it is generally simpler to use displacement-based approaches, as the numerical implementation is substantially easier. For linear-hyperelastic materials, the use of the PCVW or Menabrea's theorem is interchangeable. In fact, they impose equilibrium as follows:

$$\begin{cases} \delta W_D^* - \delta W_e^* = 0 \\ \delta U^* + \delta V^* = 0 \end{cases}$$

Where the virtual complementary strain energy δU^* can be obtained from the complementary virtual internal work δW_D^* by introducing the CL of an hyper elastic material:

$$\delta W_D^* = \int_V \underline{\underline{\varepsilon}} : \delta\underline{\underline{\sigma}}\, dV = \int_V U_{\backslash\underline{\underline{\sigma}}} : \delta\underline{\underline{\sigma}}\, dV = \int_V \delta u^* dV = \delta U^*$$

Thus, the two approaches yield the same result. The variational forms of equilibrium for a DSV beam is then easily obtained from the formulations of the strain energy as reported in equation (2.39). The displacement-based variational form of equilibrium, for imposing equilibrium and obtained via PVW and minimum potential energy principle, reads $\delta W_D = \delta W_e$, explicitly written:

$$\begin{aligned}\int_l \big(&\delta\gamma_{0zx} GA_x^* \gamma_{0zx} + \delta\gamma_{0zy} GA_y^* \gamma_{0zy} + \delta\varepsilon_{zz} EA\varepsilon_{zz} + \delta k_x EI_{xx} k_x + \delta k_y EI_{yy} k_y \\ &+ \delta\theta' GJ\theta'\big)dx = F_i \delta\hat{u}_i + M_j \delta\hat{\theta}_j + \hat{F}_r \delta u_r + \hat{M}_s \delta\theta_s\end{aligned} \tag{2.42}$$

Where we only considered concentrated external forces and moments in the external virtual work. The force-based variational form of equilibrium, for imposing compatibility and obtained via PCVW and Menabrea's theorem, reads $\delta W_D^* = \delta W_e^*$, explicitly written:

$$\begin{aligned}\int_l \left(\delta T_x \frac{T_x}{GA_x^*} + \delta T_y \frac{T_y}{GA_y^*} + \delta T_z \frac{T_z}{EA} + \delta M_y \frac{M_y}{EI_{yy}} + \delta M_z \frac{M_z}{EI_{zz}}\right) dx \\ = \delta F_i \hat{u}_i + \delta M_j \hat{\theta}_j + \delta \hat{F}_r u_r + \delta \hat{M}_s \theta_s\end{aligned} \tag{2.43}$$

2.1.8. Summary of the DSV solution

2.1.8.1. Governing equations

The structural problem in its most general form can be formulated as follows:

$$\begin{cases} \underline{b} + \nabla \cdot \underline{\underline{\sigma}} = 0 & \text{in } V \\ \underline{\underline{\varepsilon}} - \frac{1}{2}\left(\nabla \underline{u} + \nabla \underline{u}^T\right) = 0 & \text{in } V \\ \underline{t} - \hat{\underline{t}} = \underline{0} & \text{on } S_F \\ \underline{u} - \hat{\underline{u}} = \underline{0} & \text{on } S_u \end{cases}$$

A simplified problem with closed form solutions can be formulated via the DSV principle and hypotheses, which are:

- The cross section of the beam is constant along its axis, which is assumed to be straight.
- Material is isotropic, elastic and homogeneous, so that the CL will be that of (1.16).
- Loads and constraints are applied at the ends of the beam, so that its lateral surface is unloaded and unconstrained.

Under the assumptions mentioned above, the structural problem for a beam can be formulated as follows:

$$\begin{cases} \nabla \cdot \underline{\underline{\sigma}} = 0 & \text{in } V \\ \text{Compatibility eq. ns} & \text{in } V \\ \underline{\underline{\sigma}} \cdot \underline{n} = 0 & \text{on } S_{Fbody} \\ \text{Internal actions} & \text{on } S_{Fface} \end{cases}$$

Where we used compatibility equations instead of the compatibility conditions. The natural BCs on the beam cross sections S_{Fface} are expressed in terms of internal actions, which are stress resultants over the beam cross section, defined as follows:

$$\begin{cases} T_x = \int_A \sigma_{xz} dA \\ T_y = \int_A \sigma_{yz} dA \\ T_z = \int_A \sigma_{zz} dA \end{cases} \qquad \begin{cases} M_x = \int_A \sigma_{zz} y dA \\ M_y = \int_A -\sigma_{zz} x dA \\ M_z = \int_A \left(\sigma_{yz} x - \sigma_{xz} y\right) dA \end{cases}$$

In the solution procedure a CL will be needed, for a 3D isotropic, homogeneous, linear-elastic material the CL reads:

$$\begin{Bmatrix} \varepsilon_{xx} \\ \varepsilon_{yy} \\ \varepsilon_{zz} \\ \gamma_{xy} \\ \gamma_{yz} \\ \gamma_{zx} \end{Bmatrix} = \frac{1}{E} \begin{bmatrix} \begin{bmatrix} 1 & -\nu & -\nu \\ -\nu & 1 & -\nu \\ -\nu & -\nu & 1 \end{bmatrix} & [0] \\ [0] & 2(1+\nu) \begin{bmatrix} 1 & 0 & 0 \\ 0 & 1 & 0 \\ 0 & 0 & 1 \end{bmatrix} \end{bmatrix} \begin{Bmatrix} \sigma_{xx} \\ \sigma_{yy} \\ \sigma_{zz} \\ \tau_{xy} \\ \tau_{yz} \\ \tau_{zx} \end{Bmatrix}$$

According to the semi-inverse solution procedure, the guess solution is taken as:

$$\sigma_{xx} = \sigma_{yy} = \sigma_{xy} = 0$$

According to this guess solution, the governing equations can be expressed as reported below. Starting from these equations, we want to determine closed-form solutions that relate stresses to internal actions. This greatly simplifies the evaluation of the stresses and, in general, the structural problem for beams, because internal actions can be obtained from simple force equilibrium relations.

$$\begin{cases} \begin{cases} \tau_{xz/z} = \tau_{yz/z} = 0 \\ \tau_{zx/x} + \tau_{zy/y} + \sigma_{zz/z} = 0 \end{cases} & \text{in } V \\ \begin{cases} \sigma_{zz/yy} = \sigma_{zz/xx} = \sigma_{zz/xy} = 0 \\ -\bar{\nu}\sigma_{zz/yz} = \tau_{zx/xy} - \tau_{yz/xx} \\ -\bar{\nu}\sigma_{zz/xz} = \tau_{zy/xy} - \tau_{xz/yy} \end{cases} & \text{in } V \\ \underline{\underline{\sigma}} \cdot \underline{n} = 0 & \text{on } S_{F_{body}} \\ \text{Internal actions} & \text{on } S_{F_{face}} \end{cases}$$

The CL also simplifies to:

$$\begin{Bmatrix} \varepsilon_{xx} \\ \varepsilon_{yy} \\ \varepsilon_{zz} \\ \gamma_{xy} \\ \gamma_{yz} \\ \gamma_{zx} \end{Bmatrix} = \frac{1}{E} \begin{bmatrix} \begin{bmatrix} 1 & -\nu & -\nu \\ -\nu & 1 & -\nu \\ -\nu & -\nu & 1 \end{bmatrix} & [0] \\ [0] & 2(1+\nu)\begin{bmatrix} 1 & 0 & 0 \\ 0 & 1 & 0 \\ 0 & 0 & 1 \end{bmatrix} \end{bmatrix} \begin{Bmatrix} 0 \\ 0 \\ \sigma_{zz} \\ 0 \\ \tau_{yz} \\ \tau_{zx} \end{Bmatrix}$$

Explicitly writing each term yields:

$$\begin{cases} \varepsilon_{xx} = -\nu\dfrac{\sigma_{zz}}{E} \\ \varepsilon_{yy} = -\nu\dfrac{\sigma_{zz}}{E} \\ \varepsilon_{zz} = \dfrac{\sigma_{zz}}{E} \end{cases} \qquad \begin{cases} \gamma_{xy} = 0 \\ \gamma_{yz} = \dfrac{\tau_{yz}}{G} \\ \gamma_{xz} = \dfrac{\tau_{xz}}{G} \end{cases}$$

2.1.8.2. DSV solution for total axial stress

We start by writing only the relevant equations of the system above, which are:

$$\begin{cases} \tau_{zx/x} + \tau_{zy/y} + \sigma_{zz/z} = 0 & \text{in } V \\ \sigma_{zz/yy} = \sigma_{zz/xx} = \sigma_{zz/xy} = 0 & \text{in } V \\ \underline{\underline{\sigma}} \cdot \underline{n} = 0 & \text{on } S_{F_{body}} \\ \begin{cases} T_z = \displaystyle\int_A \sigma_{zz} dA \\ M_x = \displaystyle\int_A \sigma_{zz} y dA \\ M_y = -\displaystyle\int_A \sigma_{zz} x dA \end{cases} & \text{on } S_{F_{face}} \end{cases}$$

Solving this problem leads to the following equation of the axial stress, which is an exact solution to the set of equations reported above:

$$\boxed{\sigma_{zz} = \frac{T_z}{A} - \frac{M_y}{I_{yy}}x + \frac{M_x}{I_{xx}}y}$$

The axial and bending terms are decoupled, and thus they can be studied separately.

2.1.8.3. Pure axial load

For a pure axial load the axial stress is simply:

$$\sigma_{zz} = \frac{T_z}{A}$$

The strains can be recovered by applying the CL for an isotropic, homogeneous, linear-elastic material subject to an axial stress state $(\sigma_{xx} = \sigma_{yy} = \sigma_{xy} = 0)$. This yields:

$$\underline{\varepsilon} = \begin{cases} \varepsilon_{xx} = -\dfrac{\nu\sigma_{zz}}{E} = -\nu\dfrac{T_z}{EA} \\ \varepsilon_{yy} = -\dfrac{\nu\sigma_{zz}}{E} = -\nu\dfrac{T_z}{EA} \\ \varepsilon_{zz} = \dfrac{\sigma_{zz}}{E} = \dfrac{T_z}{EA} \\ \gamma_{xy} = \gamma_{yz} = \gamma_{xz} = 0 \end{cases}$$

The displacement field can be retrieved via the definition of the small strain tensor, thus by integration of the strain components. This yields:

$$\underline{u} = \begin{cases} u = -\nu\dfrac{T_z}{EA}x \\ v = -\nu\dfrac{T_z}{EA}y \\ w = \dfrac{T_z}{EA}z \end{cases}$$

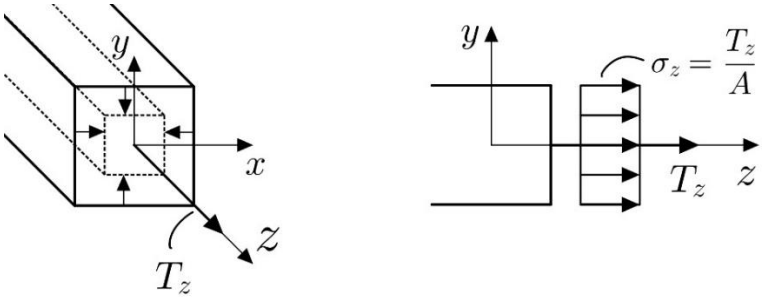

2.1.8.4. Pure bending

For a pure bending load about the x-axis the stress is the following, uniform along the x-axis and linear along the y-axis. If the bending moment is produced by a shear load, then σ_{zz} is also linear along the z-axis.

$$\sigma_{zz} = \frac{M_x}{I_{xx}} y$$

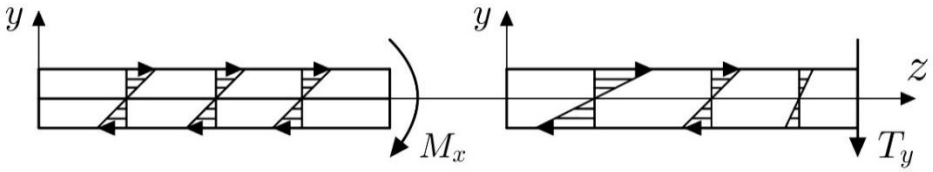

The strains can once again be recovered from the CL of a DSV beam, yielding:

$$\underline{\varepsilon} = \begin{cases} \varepsilon_{xx} = -\dfrac{\nu\sigma_{zz}}{E} = -\nu\dfrac{M_x}{EI_{xx}} y \\ \varepsilon_{yy} = -\dfrac{\nu\sigma_{zz}}{E} = -\nu\dfrac{M_x}{EI_{xx}} y \\ \varepsilon_{zz} = \dfrac{\sigma_{zz}}{E} = \dfrac{M_x}{EI_{xx}} y \\ \gamma_{ij} = 0 \end{cases}$$

The displacement field is once again obtain by integrating the strains:

$$\underline{u} = \begin{cases} u = -\nu\dfrac{M_x}{EI_{xx}} xy \\ v = -\dfrac{M_x}{2EI_{xx}}\left(z^2 + \nu(y^2 - x^2)\right) \\ w = \dfrac{M_x}{EI_{xx}} yz \end{cases}$$

Two separate displacement fields can be identified, on is about the cross sections of the beam, the second is about the beam axis. Both are presented in the figure below. From the displacements of the beam axis we can define the rotation and curvature of the beam axis.

$$\underline{u}^{(axis)} = \begin{cases} u = 0 \\ v = -\dfrac{M_x}{2EI_{xx}} z^2 \\ w = 0 \end{cases} \quad \rightarrow \quad \begin{cases} \theta_x = -v_{\backslash z} = \dfrac{M_x}{EI_{xx}} z \\ k_x = -v_{\backslash zz} = \dfrac{M_x}{EI_{xx}} \end{cases}$$

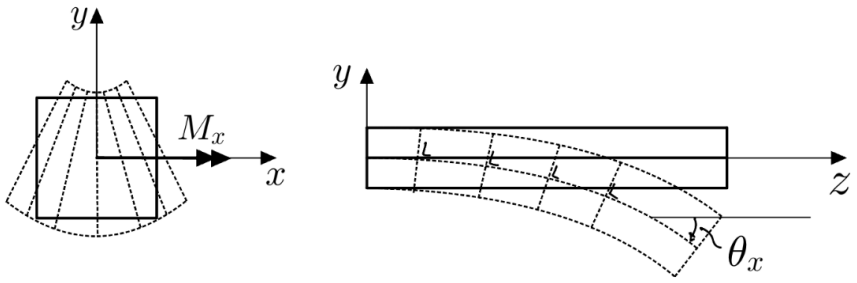

2.1.8.5. DSV solution for torsion

The guess solution for a beam subject to pure torsion is the following:

$$\sigma_{zz} = \sigma_{xx} = \sigma_{yy} = \sigma_{xy} = 0$$

The governing equations simplify further from the case of the axial stress, and they result to be:

$$\begin{cases} \tau_{zx/x} + \tau_{zy/y} = \nabla \cdot \underline{\tau} = 0 & \text{in } V \\ \tau_{zy/x} - \tau_{xz/y} = C & \text{in } V \\ \underline{\tau} \cdot \underline{n} = 0 & \text{on } S_{F_{body}} \\ M_t = \int_A (-\tau_{xz} y + \tau_{yz} x) dA & \text{on } S_{F_{face}} \end{cases}$$

According to these governing equations, the displacement field can be assumed to be:

$$\begin{cases} u = u(y,z) = -y\theta = -y\theta' z \\ v = v(x,z) = x\theta = x\theta' z \\ w(x,y) = \theta' \Psi(x,y) \end{cases}$$

Where θ is the rotation, θ' is the torsion and $\Psi(x,y)$ is the warping. The governing equations can then be rewritten as follows:

$$\begin{cases} G\theta' (\Psi_{\backslash xx} + \Psi_{\backslash yy}) = 0 & \text{in } V \\ 2G\theta' = C & \text{in } V \\ \Psi_{\backslash n} = y n_x - x n_y & \text{on } S_{F_{body}} \\ M_t = GJ\theta' & \text{on } S_{F_{face}} \end{cases}$$

Where J is the torsional constant, defined as follows:

$$J = \int_A (y^2 - \Psi_{\backslash x} y) + (x^2 + \Psi_{\backslash y} x) dA$$

The set of equations reported above can be solver for the warping Ψ. However, this can be hard, and it is preferred to reformulate the problem in terms of stresses. So we express the torsional constant as follows:

$$J = \frac{M_t^2}{\int_A (\tau_{yz}^2 + \tau_{xz}^2) dA}$$

2.1.8.6. Thin walled sections

To obtain a closed form equation that relates the torsional moment M_t and the shear stresses τ_{xz}, τ_{yz} we must introduce some assumptions. We consider specifically thin-walled structures, as these are typical in the aerospace field. We distinguish between:

- Open cross sections: we can consider most open sections as an assembly of strips. For each of these strips we can identify s as the axis tangent to the shear flow, while n is the axis normal to shear flow. The strip is assumed to have a width (dimension running along

s) that is way bigger than its thickness (dimension along n). Thus we assume $\tau_{nz} = 0$, and we obtain:

$$\begin{cases} \tau_{nz} = 0 \\ \tau_{sz} = -\dfrac{2M_t}{J} n \end{cases} \quad \text{and} \quad J = \begin{cases} \displaystyle\int_{-s/2}^{+s/2} \frac{n^3(x)}{3} ds\,, & n = n(x) \\ \dfrac{1}{3} s n^3, & n = \text{const} \end{cases}$$

- Closed cross sections: we assume the shear stress τ_{sz} to be constant along the thickness. Then, by introducing the shear flow $q = \tau_{sz} \cdot t$, constant along the s-axis. The relation between q and M_t is provided by Bradt formula, which is then used to determine the torsional constant.

$$\begin{cases} M_z = 2\Omega q \\ J = \dfrac{4\Omega^2}{\oint_\Gamma \dfrac{1}{t(s)} d\Gamma} \end{cases}$$

2.1.8.7. Strain end complementary strain energies

2.2. Kinematic beam formulations

The beam solution derived with the framework of the DSV beam theory provides a fundamental background in structural analysis. In fact, it shows how structural theories aim at simplifying the structural problem by identifying global quantities over a region of the structure. The shear flows, an average quantity $q = \int \tau_{sz} dt$, were indeed assumed constant along the thickness and then used as unknowns of the problem solution.

Despite the usefulness of the DSV solution, it is intuitive to formulate the beam problem from a different perspective, i.e. starting from the kinematics of the beam. The ***key idea of kinematic models*** is to be able to retrieve the displacement field in the whole structural element, the beam, if the displacements of an element of lower dimensionality is known, the beam axis. This is possible if kinematic assumptions are formulated, which allow to identify the generalized coordinates $\boldsymbol{u}_0$. From the generalized coordinates we will obtain the generalized strains $\boldsymbol{\varepsilon}_0, \boldsymbol{k}$ via the small strain tensor definition, or in other words the compatibility condition. Then, generalized stresses $\boldsymbol{N}, \boldsymbol{M}$ and generalized external forces $\hat{\boldsymbol{n}}$ can be retrieved from the internal and external virtual energies, respectively. Applying the PVW will then yield all of the equilibrium conditions: equilibrium equations and BCs, both natural and essential.

$$\text{3D} \xrightarrow{\text{kinematic assumptions}} \text{1D: } \underline{u}_0 \xrightarrow{\text{compatibility condition}} \begin{cases} \underline{\varepsilon}_0 \\ \underline{k} \end{cases} \rightarrow \begin{cases} \delta W_D \rightarrow \underline{N}, \underline{M} \\ \delta W_e \rightarrow \underline{\hat{n}} \end{cases} \xrightarrow{\text{PVW}} \begin{matrix} \text{equilibirum} \\ \text{equations + BCs} \end{matrix}$$

It is important to point out that kinematic beam theories must not be considered as separate or independent from the DSV solution. In fact, both approaches are based on generalized quantities that impose global but not local equilibrium, and thus both are approximative to some degree. In fact, we'll see that multiple inconsistencies can be pointed out in the kinematic approach. However, despite being approximative, ***kinematic formulations are advantageous for many reasons***: ease of numerical implementation, ease of extension to nonlinear problems, and easily applicable to more complex structural elements, such as plates and shells.

For consistency with the vast majority of the literature dealing with kinematic formulations, the ***sign convention*** used here considers the x-axis as the beam axis, while the y-z-axes describe the plane of the beam section. Thus, the internal actions and the solution for axial stress read:

$$\begin{cases} M_x = \int_A (\tau_{zx} y - \tau_{yx} z) dA \\ M_y = \int_A \sigma_{xx} z dA \\ M_z = \int_A -\sigma_{xx} y dA \end{cases} \rightarrow \quad \sigma_{xx} = \frac{T_x}{A} + \frac{M_y}{I_{yy}} z - \frac{M_z}{I_{zz}} y$$

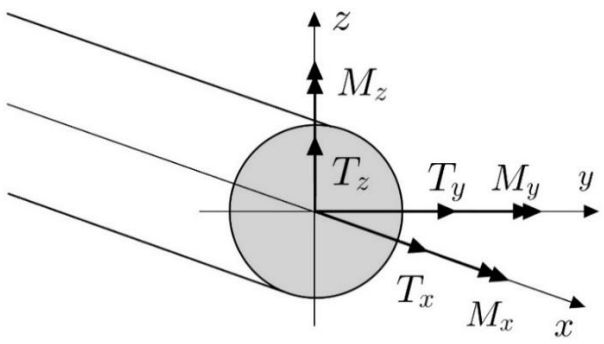

Figure 2.21: internal action convention for kinematic beam model.

2.2.1. Timoshenko beam model

2.2.1.1. Generalized coordinates

For simplicity, consider a planar beam, that is a beam that can only bend in the plane of the paper. The discussion ahead can be extended to the case of a 3D beam. The kinematic model proposed by Timoshenko ***assumes*** that the sections normal to the beam axis remain straight during deformation (1) but not necessarily normal to the beam axis during bending (2). Condition (2) is referred to as ***normality condition***, and it has important consequences that we'll discuss shortly. Under these assumptions, the displacement field of the points on the beam cross section are not a function of the position on the section. Thus, the displacement field can be ***approximated*** via global quantities:

$$\begin{cases} u(x,z) = u_0(x) + z\varphi_x(x) \\ w(x) = w_0(x) \end{cases} \tag{2.44}$$

Observation. This displacement field is not an initial guess that we will verify post-ex, as we did for the DSV solution. This is a (good) approximation!

Here the index "0" denotes the quantities that are related to the beam axis displacement. Thus, $u_0(x)$ is the axial displacement of the beam axis, while $w_0(x)$ is its vertical displacement, caused by a bending action (shear or pure moment). Notice that the bending action induces an axial displacement as well, which can be approximated as $z \tan \varphi_x \approx z\varphi_x$, where $\varphi_x(x)$ is the rotation of the generic cross section (Figure 2.22). For the Timoshenko beam model, the ***generalized coordinates*** are:

$$\underline{u}_0 = \begin{Bmatrix} u_0(x) \\ w_0(x) \\ \varphi_x(x) \end{Bmatrix} \tag{2.45}$$

These alone do not quantify the actual displacement of a point of the beam, but a combination of them does. If all the generalized coordinates are known, then the displacements of all the points of the beam are known as well. This kinematic description allows us to approximate the displacement field of the whole beam by referring to the displacements of the beam axis, i.e. the generalized coordinates.

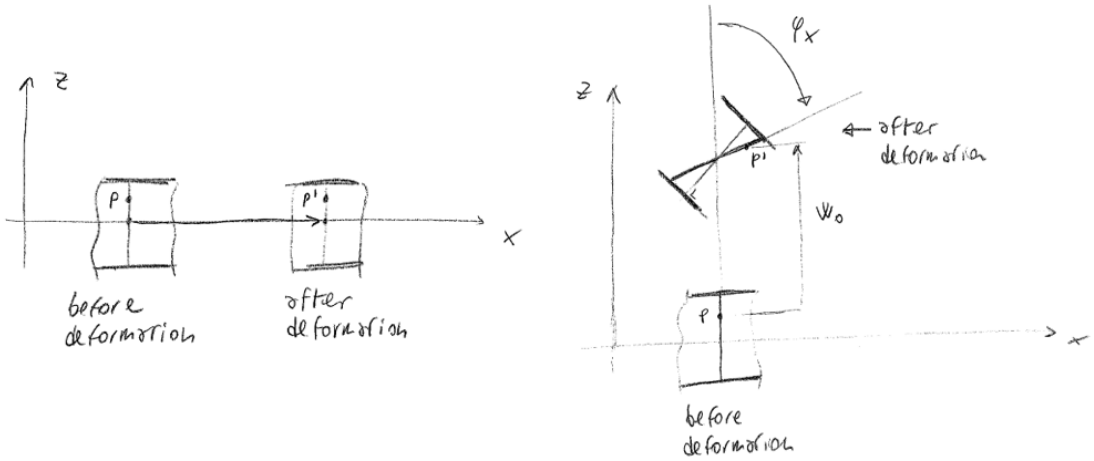

Figure 2.22: left) axial displacement; right) vertical displacement with bending-induced rotation.

2.2.1.2. Generalized strains

Having determined the displacement field of the whole beam, we can retrieve the strains via the definition of the small strain tensor $\boldsymbol{\varepsilon}$ of equation (1.7). This yields:

$$\begin{cases} \varepsilon_{xx}(x,z) = u(x,z)_{\backslash x} = u_{0\backslash x}(x) + z\varphi_{x\backslash x}(x) \\ \gamma_{zx}(x) = w_{\backslash x}(x) + u_{\backslash z}(x,z) = w_{0\backslash x}(x) + \varphi_x(x) \\ \varepsilon_{zz}(x) = w_{\backslash z}(x) = 0 \end{cases}$$

Such strains can be conveniently rewritten to identify the ***generalized strains***: membranal strains $\boldsymbol{\varepsilon}_0$ and flexural strains $\boldsymbol{k}$. The entries of the flexural strains $\boldsymbol{k}$ are derivatives of rotations, i.e. curvatures. A structural element develops curvatures only if a bending action, i.e. a flexion, is present, hence the name. Thus, the strain field in terms of the generalized strains reads:

$$\underline{\varepsilon} = \underline{\varepsilon}_0 + z\underline{k} \tag{2.46}$$

$$\underline{\varepsilon}_0 = \begin{Bmatrix} \varepsilon_{0xx} = u_{0\backslash x} \\ \gamma_{0zx} = w_{0\backslash x} + \varphi_x \end{Bmatrix} \qquad \underline{k} = \begin{Bmatrix} k_{xx} = \varphi_{x\backslash x} \\ 0 \end{Bmatrix} \tag{2.47}$$

Observation. Is that of equation (2.46) a compatible strain field? Yes, because the generalized strains have been determined by explicitly imposing the compatibility of strains, i.e. the definition of the small strain tensor $\boldsymbol{\varepsilon} = (\nabla\boldsymbol{u} + \nabla\boldsymbol{u}^T)/2$ or equivalently $\boldsymbol{\varepsilon} - (\nabla\boldsymbol{u} + \nabla\boldsymbol{u}^T)/2 = 0$ (as its reported in the formulation of the structural problem (1.32)).

2.2.1.3. Shear deformability

Place special attention to the shear strain γ_{zx}, which has been found to be:

$$\gamma_{zx} = \gamma_{zx0} = w_{0\backslash x} + \varphi_x$$

Here φ_x has been defined as the total rotation of the generic beam cross section, depicted in Figure 2.22, and which can be expressed as follows:

$$\varphi_x = -w_{0\backslash x} + \theta$$

The Timoshenko model does not enforce the normality condition, meaning that the beam cross sections do not remain normal to the beam axis during bending. Physically, this implies that the sections rotate more than if they remained normal to the beam axis during bending. In other words, the ***Timoshenko model accounts for shear deformability***. Analytically, this additional rotation is represented by $\Delta\varphi$, which makes the shear strain γ_{zx} non-null:

$$\gamma_{zx} = \gamma_{zx0} = w_{0\backslash x} + \varphi_x = w_{0\backslash x} - w_{0\backslash x} + \theta = \theta$$

In the next section we'll discuss the Euler Bernoulli beam model. Such model enforces the normality condition, meaning that it is assumed that beam cross sections remain normal to its axis during bending. Physically, the normality condition implies no shear deformability. Analytically, this translated in $\Delta\varphi = 0$, which in turn implies no shear stress.

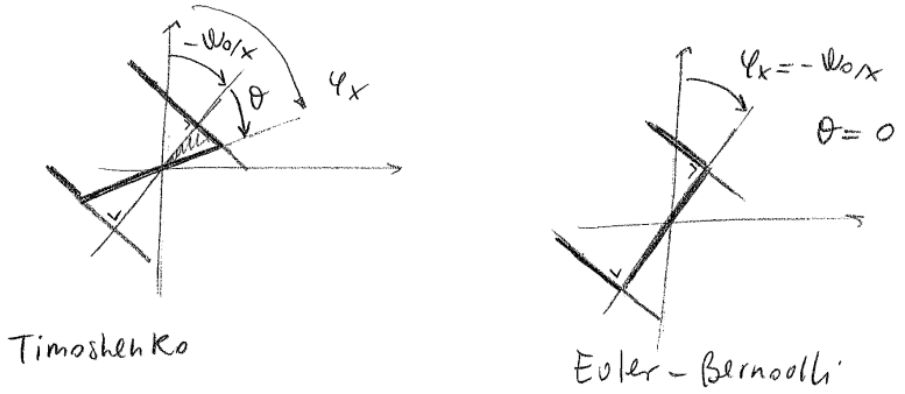

Figure 2.23: beam cross section rotation according to Timoshenko (left) and Euler-Bernoulli (right).

We (will) have two models, one accounts for shear deformability, and the other does not. When do we use one and when the other? In general, every beam has a degree of shear deformability, and so $\gamma_{zx} \neq 0$ in general. However, for thin beams this contribution can be safely neglected, while it must be accounted for in thick beams. This is easy to accept if we investigate the axial stress:

$$\varepsilon_{xx}(x,z) = u(x,z)_{\backslash x} = u_{0\backslash x}(x) + z\varphi_{x\backslash x}(x)$$

Here, the flexural contribution is proportional to z, however if the beam is thin then z should be quite small. Thus, the approximation of $\varphi \approx -w_{0\backslash x}$ introduces very little error. Intuitively, the approximation error of neglecting shear deformability increases as z does, i.e. as the beam gets thicker. Thus, summarizing:

- Thin beams → Euler-Bernoulli.
- Thick beams → Timoshenko.

2.2.1.4. Generalized stresses

Starting from the kinematic assumptions we determined the generalized coordinates $\boldsymbol{u}_0(x)$. Then, applying the definition of the small strain tensor we defined the generalized strains $\boldsymbol{\varepsilon}_0$ and $\boldsymbol{k}$. We now obtain the generalized stress measures by identifying those quantities that are in energy conjugacy with the generalized strain measures. In other words, we apply the PVW:

$$\delta W_D = \int_V \delta\underline{\underline{\varepsilon}} : \underline{\underline{\sigma}} dV = \int_V (\delta\varepsilon_{xx}\sigma_{xx} + \delta\varepsilon_{zz}\sigma_{zz} + \delta\gamma_{zx}\tau_{zx})dV$$

Recalling that $\varepsilon_{zz} = 0$, we remain with:

$$\delta W_D = \int_V (\delta\varepsilon_{xx}\sigma_{xx} + \delta\gamma_{zx}\tau_{zx})dV$$

Expressing the strains in terms of the generalized strains via equation (2.46), we obtain:

$$\delta W_D = \int_V [\delta(\varepsilon_{0xx} + zk_{xx})\sigma_{xx} + \delta\gamma_{0zx}\tau_{zx}]dV = \int_V [\delta\varepsilon_{0xx}\sigma_{xx} + \delta k_{xx}z\sigma_{xx} + \delta\gamma_{0zx}\tau_{zx}]dV$$

Recall now that the generalized strains are a function of the generalized coordinates $u_0(x), w_0(x)$ and $\varphi_x(x)$, which are not a function of the section coordinates A. Thus, we rewrite the integral as follows:

$$\delta W_D = \int_l \left(\delta\varepsilon_{0xx} \cdot \int_A \sigma_{xx} dA \right) dx + \int_l \left(\delta k_{xx} \cdot \int_A z\sigma_{xx} dA \right) dx + \int_l \left(\delta\gamma_{0zx} \cdot \int_A \tau_{zx} dA \right) dx$$
$$= \int_l (\delta\varepsilon_{0xx} \cdot N_x) dx + \int_l (\delta k_{xx} \cdot M_y) dx + \int_l (\delta\gamma_{0zx} \cdot Q_z) dx$$

Thus, we conclude that the ***generalized stress measures are the internal actions***, because these are the quantities in energy conjugacy with the generalized strains.

$$\underline{N} = \begin{Bmatrix} N_x = \int_A \sigma_{xx} dA \\ Q_z = \int_A \tau_{zx} dA \end{Bmatrix} \qquad \underline{M} = \begin{Bmatrix} 0 \\ M_y = \int_A z\sigma_{xx} dA \end{Bmatrix} \tag{2.48}$$

The internal virtual work δW_D can then be rewritten in terms of generalized strain and stresses, yielding:

$$\delta W_D = \int_l (\delta\varepsilon_{0xx} \cdot N_x + \delta k_{xx} \cdot M_y + \delta\gamma_{0zx} \cdot Q_z) dx = \int_l (\delta\underline{\varepsilon}_0^T \cdot \underline{N} + \delta\underline{k}^T \cdot \underline{M}) dx \tag{2.49}$$

2.2.1.5. Generalized forces

The generalized forces can be obtained as those external forces that work with the generalized coordinates to produce an external virtual work δW_e. Consider the presence of the volume forces F_x and F_z, then the external virtual work δW_e reads:

$$\delta W_e = \int_V (\delta u F_x + \delta w F_z) dV = \int_V (\delta u_0 F_x + \delta\varphi_x z F_x + \delta w_0 F_z) dV$$
$$= \int_l \left(\delta u_0 \int_A F_x dA + \delta\varphi_x \int_A z F_x dA + \delta w_0 \int_A F_z dA \right) dx =$$
$$= \int_l (\delta u_0 \cdot \hat{n}_x + \delta\varphi_x \cdot \hat{m}_y + \delta w_0 \cdot \hat{n}_z) dx$$

We obtain that the ***generalized force measures are the forces per unit length acting on the beam axis***.

$$\underline{\hat{n}} = \begin{Bmatrix} \hat{n}_x = \int_A F_x dA \\ \hat{n}_z = \int_A F_z dA \\ \hat{m}_y = \int_A z F_x dA \end{Bmatrix} \tag{2.50}$$

The external virtual work can then be rewritten in terms of generalized coordinates and force parameters:

$$\delta W_e = \int_l \left(\delta u_0 \cdot \hat{n}_x + \delta\varphi_x \cdot \hat{m}_y + \delta w_0 \cdot \hat{n}_z\right) dx = \int_l \left(\delta \underline{u}_0^T \cdot \underline{\hat{n}}\right) dx \tag{2.51}$$

2.2.1.6. Equilibrium conditions (loads)

Weak form approach. It is now possible to derive the equilibrium conditions for the Timoshenko beam. In order to do so, we present first the weak form approach. The external virtual work δW_e is obtained by the product of the first variation of the generalized coordinates $\delta \boldsymbol{u}_0$ and the generalized forces $\hat{\boldsymbol{n}}$. In addition to $\hat{\boldsymbol{n}}$, we also consider any possible concentrated load at the ends of the beam. Thus, we'll write:

$$\begin{aligned}\delta W_e &= \int_l \left(\delta \underline{u}_0^T \cdot \underline{\hat{n}}\right) dx + \text{concentrated loads} \\ &= \int_l \left(\delta u_0 \hat{n}_x + \delta\varphi_x \hat{m}_y + \delta w_0 \hat{n}_z\right) dx + \delta u_0(0)\hat{N}_0 + \delta w_0(0)\hat{Q}_0 + \delta\varphi_x(0)\hat{M}_0 \\ &+ \delta u_0(l)\hat{N}_l + \delta w_0(l)\hat{Q}_l + \delta\varphi_x(l)\hat{M}_l\end{aligned}$$

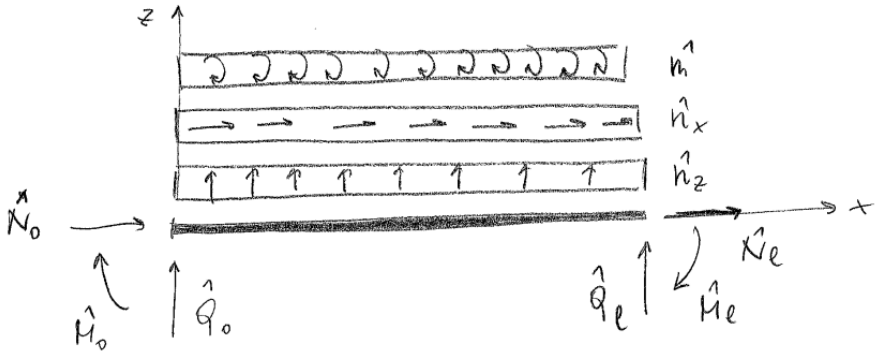

Figure 2.24: external loads acting on the beam axis.

The internal virtual work δW_D can be expressed as the product of the first variation of the generalized strains $\delta\boldsymbol{\varepsilon}_0, \delta\boldsymbol{k}$ and the generalized stresses $\boldsymbol{N}, \boldsymbol{M}$. This yields:

$$\begin{aligned}\delta W_D &= \int_l \left(\delta \underline{\varepsilon}_0^T \cdot \underline{N} + \delta \underline{k}^T \cdot \underline{M}\right) dx = \int_l \left(\delta\varepsilon_{0xx} \cdot N_x + \delta k_{xx} \cdot M_y + \delta\gamma_{0zx} \cdot Q_z\right) dx \\ &= \int_l \left(\delta u_{0\backslash x} N_x + \delta\varphi_{x\backslash x} M_y + \delta\left(w_{0\backslash x} + \varphi_x\right) Q_z\right) dx\end{aligned}$$

In order to obtain the equilibrium equations from the PWV, we need to express both virtual works in terms of virtual displacements $\delta \boldsymbol{u}_0$, to then invoke the arbitrariness of such quantities and identify the equations. The internal virtual work is expressed in terms of virtual generalized strains, from which the virtual displacements can be obtained integrating by parts. Recalling that:

$$\left(\delta u_0 N_x\right)_{\backslash x} = \delta u_{0\backslash x} N_x + \delta u_0 N_{x\backslash x} \quad \rightarrow \quad \delta u_{0\backslash x} N_x = \left(\delta u_0 N_x\right)_{\backslash x} - \delta u_0 N_{x\backslash x}$$

Applying this to all the terms of δW_D yields:

$$\delta W_D = -\int_l \left(\delta u_0 N_{x\backslash x} + \delta\varphi_x M_{y\backslash x} + \delta w_0 Q_{z\backslash x} - \delta\varphi_x Q_z\right) dx + \left(\delta u_0 N_x + \delta\varphi_x M_y + \delta w_0 Q_z\right)\Big|_0^l$$

The PVW can then be rewritten as follows:

$$\int_l \left[\delta u_0\left(N_{x\backslash x}+\hat{n}_x\right)+\delta w_0\left(Q_{z\backslash x}+\hat{n}_z\right)+\delta\varphi_x\left(M_{y\backslash x}-Q_z+\hat{m}_y\right)\right]dx+$$
$$-\delta u_0(l)\left[N_x(l)-\hat{N}_l\right]+\delta u_0(0)\left[N_x(0)+\hat{N}_0\right]+$$
$$-\delta\varphi_x(l)\left[M_y(l)-\hat{M}_l\right]+\delta\varphi_x(0)\left[M_x(0)+\hat{M}_0\right]+$$
$$-\delta w_0(l)\left[Q_z(l)-\hat{Q}_l\right]+\delta w_0(0)\left[Q_z(0)+\hat{Q}_0\right]=0$$

Due to the arbitrariness of the virtual displacements, ***we are able to retrieve from the PVW single scalar equation all the equilibrium conditions***, i.e. the equilibrium equations, natural and essential BCs.

$$\begin{cases} N_{x\backslash x}+\hat{n}_x=0 \\ Q_{z\backslash x}+\hat{n}_z=0 \\ M_{y\backslash x}-Q_z+\hat{m}_y=0 \end{cases} \quad \text{in } x\in[0,l] \quad \begin{cases} N_x(0)=-\hat{N}_0 & \text{or} & \delta u(0)=0 \\ N_x(l)=+\hat{N}_l & \text{or} & \delta u(l)=0 \\ M_y(0)=-\hat{M}_0 & \text{or} & \delta\varphi(0)=0 \\ M_y(l)=+\hat{M}_l & \text{or} & \delta\varphi(l)=0 \\ Q_z(0)=-\hat{Q}_0 & \text{or} & \delta w(0)=0 \\ Q_z(l)=+\hat{Q}_l & \text{or} & \delta w(l)=0 \end{cases} \tag{2.52}$$

Infinitesimal element approach. It is easier to obtain the equilibrium equations of the beam by considering an infinitesimal beam element (Figure 2.25). From simple equilibrium considerations we obtain:

$$\begin{cases} N_x+dN_x+\hat{n}_x dx-N_x=0 \\ Q_z+dQ_z+\hat{n}_z dx-Q_z=0 \\ M_y+dM_y+\hat{m}_x dx-Q_z dx-M_y=0 \end{cases} \rightarrow \begin{cases} N_{x\backslash x}+\hat{n}_x=0 \\ Q_{z\backslash x}+\hat{n}_z=0 \\ M_{y\backslash x}-Q_z+\hat{m}_y=0 \end{cases}$$

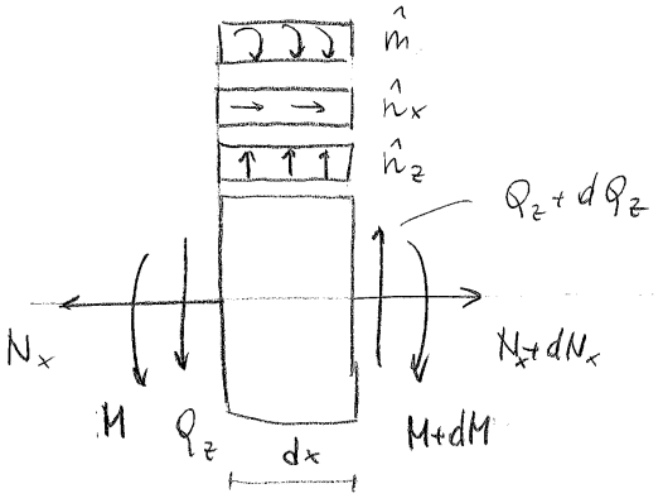

Figure 2.25: infinitesimal beam element.

Observations. Some ***important observations*** must be made about the equilibrium conditions (equilibrium equations, essential and natural BCs) of equation (2.52):

- They have been determined from a single scalar equation, that of the PVW. This shows the utility of the PVW.
- Recall that the PVW imposes equilibrium but requires compatibility to be satisfied a priori. We already mentioned in section 2.2.1.2 that this condition is satisfied, as the

generalized strains that enter the PVW have been determined by explicitly imposing the compatibility of strains, i.e. $\boldsymbol{\varepsilon} = (\nabla \boldsymbol{u} + \nabla \boldsymbol{u}^T)/2$.

- ***The equilibrium conditions depend on the kinematic model***. in deriving the equilibrium conditions, we enforced the kinematic assumptions of the Timoshenko model. More precisely, the PVW has been expressed in terms of generalized quantities, which depend on the kinematic model of Timoshenko. If a different kinematic model is used, such as the Euler-Bernoulli model, then the equilibrium conditions will also be different.
- The axial and bending equilibrium are fully decoupled, and thus they are often treated separately for convenience.
- They ***define the equilibrium requirements at global level because global/generalized quantities are used***. Since all kinematic model are based on the definition of generalized quantities, it follows that this is an ***intrinsic property of all kinematic models***. In other words, the equilibrium equations here obtained imply global, but not local, satisfaction of the 3D equilibrium equations. In fact, the equilibrium equations of equation (2.52) are written in terms of internal actions $\boldsymbol{N}$ and forces per unit length $\hat{\boldsymbol{n}}$. Both of these terms are obtained by integrating quantities across the beam cross section. Thus, as for the DSV solution, the internal actions and generalized forces are not able to uniquely identify the precise stress field producing a sectional resultant (review 2.1.1). We show the example presented when discussing the limitations of the DSV solution, which apply to this case as well. In this example the internal action produced by the load distributions in section A-A is the same of the one produced by the load distributions in B-B. The same applies to generalized forces.

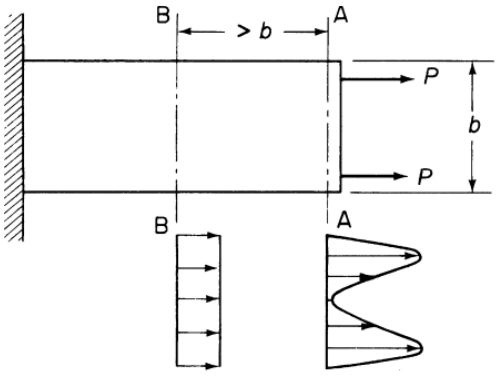

Figure 2.26: local effects due to load application on the internal stress distribution of a beam section.

2.2.1.7. Constitutive law

The equilibrium conditions have been derived independently from the constitutive law. The CL establishes a relation between stresses and strains, and thus between generalized stresses and generalized strains. The choice of the CL for kinematic models is based on the same kind of assumptions of the kinematic law. That is, we approximated the displacements of every point of the beam with a kinematic law that only considers the beam axis displacements and rotations. In the same way, we assume that the stress state is an axial one. The CL then reads:

$$\underline{\sigma} = \underline{\underline{D}} \cdot \underline{\varepsilon} = \underline{\underline{D}} \cdot \left(\underline{\varepsilon}_0 + z\underline{k}\right) \tag{2.53}$$

Writing the full form of the above system yields:

$$\begin{Bmatrix}\sigma_{xx}\\ \tau_{zx}\end{Bmatrix} = \begin{bmatrix}E & 0\\ 0 & G\end{bmatrix}\begin{Bmatrix}\varepsilon_{xx}\\ \gamma_{zx}\end{Bmatrix} = \begin{bmatrix}E & 0\\ 0 & G\end{bmatrix}\left(\begin{Bmatrix}\varepsilon_{0xx}\\ \gamma_{0zx}\end{Bmatrix} + z\begin{Bmatrix}k_{xx}\\ 0\end{Bmatrix}\right) = \begin{bmatrix}E & 0\\ 0 & G\end{bmatrix}\left(\begin{Bmatrix}u_{0\backslash x}\\ w_{0\backslash x} + \varphi_x\end{Bmatrix} + z\begin{Bmatrix}\varphi_{x\backslash x}\\ 0\end{Bmatrix}\right)$$

Recall now the expression of the generalized stresses:

$$N_x = \int_A \sigma_{xx} dA = \int_A E\varepsilon_{xx} dA = \int_A E\left(u_{0\backslash x} + z\varphi_{x\backslash x}\right) dA = \int_A E u_{0\backslash x} dA + \underbrace{\int_A Ez\varphi_{x\backslash x} dA}_{=0 \text{ principal axes}}$$

$$= \int_A E u_{0\backslash x} dA = EA u_{0\backslash x} = EA\varepsilon_{0xx}$$

$$M_y = \int_A z\sigma_{xx} dA = \int_A zE\varepsilon_{xx} dA = \int_A E\left(zu_{0\backslash x} + z^2\varphi_{x\backslash x}\right) dA = \underbrace{\int_A Ezu_{0\backslash x} dA}_{=0 \text{ principal axes}} + \int_A Ez^2\varphi_{x\backslash x} dA$$

$$= \int_A Ez^2\varphi_{x\backslash x} dA = EI\varphi_{x\backslash x} = EIk_{xx}$$

$$Q_z = \int_A \tau_{zx} dA = \int_A G\gamma_{0zx} dA = \int_A G\left(w_{0\backslash x} + \varphi_x\right) dA = GA\left(w_{0\backslash x} + \varphi_x\right) = GA\gamma_{0zx}$$

Thus, we can define a generalized CL as for the DSV solutions that relates generalized strains to generalized stresses:

$$\begin{Bmatrix} N_x \\ M_y \\ Q_z \end{Bmatrix} = \begin{bmatrix} EA & 0 & 0 \\ 0 & EI & 0 \\ 0 & 0 & GA \end{bmatrix} \begin{Bmatrix} \varepsilon_{0xx} \\ k_{xx} \\ \gamma_{0zx} \end{Bmatrix} = \begin{bmatrix} EA & 0 & 0 \\ 0 & EI & 0 \\ 0 & 0 & GA \end{bmatrix} \begin{Bmatrix} u_{0\backslash x} \\ \varphi_{x\backslash x} \\ w_{0\backslash x} + \varphi_x \end{Bmatrix} \tag{2.54}$$

This is not yet CL adopted for a Timoshenko beam. To understand why, we compare the strain energies for a Timoshenko beam U^{Tim} and that provided by the DSV solution U^{DSV}.

$$\begin{cases} U^{\text{Tim}} = \delta W_D = \dfrac{1}{2}\displaystyle\int_l \left(N_x \frac{N_x}{EA} + Q_z \frac{Q_z}{GA} + M_y \frac{M_y}{EI}\right) dA \\ U^{DSV} = \delta W_D = \dfrac{1}{2}\displaystyle\int_l \left(N_x \frac{N_x}{EA} + Q_z \frac{Q_z}{GA^*} + M_y \frac{M_y}{EI}\right) dA \end{cases}$$

It can be seen that the two models provide a consistent formulation of the strain energy. This is an indicator of the fact that the Timoshenko model, despite being approximative, provides a good estimation of the exact solution (DSV). However, one difference can be spotted between U^{Tim} and U^{DSV}: the shear stiffness term is different. Since $GA > GA^*$, the ***Timoshenko model overestimates the shear stiffness of the beam***. For this reason, the term GA is often corrected to GA^* to provide the beam with additional shear deformability, in accordance with the DSV result. Thus, the Timoshenko beam CL is the following:

$$\begin{Bmatrix} N_x \\ M_y \\ Q_z \end{Bmatrix} = \begin{bmatrix} EA & 0 & 0 \\ 0 & EI & 0 \\ 0 & 0 & GA^* \end{bmatrix} \begin{Bmatrix} \varepsilon_{0xx} \\ k_{xx} \\ \gamma_{0zx} \end{Bmatrix} \tag{2.55}$$

Observation. The correction of the shear stiffness represents a link between the (exact) DSV solution and the Timoshenko model. Thus, ***the kinematic model has not to be interpreted as an independent approach from the DSV result***.

2.2.1.8. Equilibrium conditions (displacements)

In the previous section the CL has been defined, introducing a link between stresses $\boldsymbol{\sigma}$ and strains $\boldsymbol{\varepsilon}$, and between generalized stresses $\boldsymbol{N}$ and generalized strains $\boldsymbol{u}_0$. The CL also allows us to express the equilibrium conditions in terms of displacement derivatives. This is desirable in a displacement-based formulation of the elastic problem. By substitution of equation (2.55) in (2.52) we obtain:

$$\begin{cases} N_{x\backslash x} + \hat{n}_x = 0 \\ Q_{z\backslash x} + \hat{n}_z = 0 \\ M_{y\backslash x} - Q_z + \hat{m}_y = 0 \end{cases} \quad \rightarrow \quad \begin{cases} \left(EAu_{0\backslash x}\right)_{\backslash x} + \hat{n}_x = 0 \\ \left[GA^*\left(w_{0\backslash x} + \varphi_x\right)\right]_{\backslash x} + \hat{n}_z = 0 \\ \left(EI\varphi_{x\backslash x}\right)_{\backslash x} - GA^*\left(w_{0\backslash x} + \varphi_x\right) + \hat{m}_y = 0 \end{cases}$$

If the section is constant along the beam axis, then the equilibrium equations of a Timoshenko beam can be expressed in terms of three ordinary differential equations and three unknown functions, the generalized displacements $\boldsymbol{u}_0$.

$$\begin{cases} EAu_{0\backslash xx} + \hat{n}_x = 0 \\ GA^*\left(w_{0\backslash xx} + \varphi_{x\backslash x}\right) + \hat{n}_z = 0 \\ EI\varphi_{x\backslash xx} - GA^*\left(w_{0\backslash x} + \varphi_x\right) + \hat{m}_y = 0 \end{cases} \quad \text{in } x \in [0, l] \tag{2.56}$$

$$\text{BCs:} \quad \begin{cases} EAu_{0\backslash x} = \mp\hat{N}_x & \text{or} \quad \delta u_0 = 0 \quad \text{in} \quad x = 0, l \\ EI\varphi_{x\backslash x} = \mp\hat{M}_y & \text{or} \quad \delta\varphi_x = 0 \quad \text{in} \quad x = 0, l \\ GA^*\left(\varphi_{x\backslash x} + w_{0\backslash xx}\right) = \mp\hat{Q}_z & \text{or} \quad \delta w_0 = 0 \quad \text{in} \quad x = 0, l \end{cases}$$

Solving the equilibrium equations in displacement form provides with the generalized coordinates $\boldsymbol{u}_0$. Once these are known, the displacement field of the whole beam can be retrieved via the kinematic law of equation (2.44). Knowing $\boldsymbol{u}_0$, the strains are also available from equations (2.46) and (2.47). Then, using the CL we may also retrieve the stresses from equation (2.53) and the internal actions from equation (2.55).

Observation. Recall that the BCs on the left of (2.56) are the natural boundary conditions. They express equilibrium at the boundaries of the structural element, the beam in this case, with external loads. The derivatives of the unknown functions appear in the formulation of natural BCs, for this reason they are sometimes denoted as ***Neumann-type boundary conditions***. The BCs on the right of (2.56) are the essential BCs, geometric type of conditions that involve the generalized displacements, but not their derivatives. For this reason they are sometimes referred to as ***Dirichlet-type boundary conditions***.

2.2.1.9. Shear stress correction

It is interesting to investigate the distribution of the stresses provided by equation (2.53), reported here:

$$\underline{\sigma} = \underline{\underline{D}} \cdot \left(\underline{\varepsilon}_0 + z\underline{k}\right) \quad \rightarrow \quad \begin{Bmatrix} \sigma_{xx} \\ \tau_{zx} \end{Bmatrix} = \begin{bmatrix} E & 0 \\ 0 & G \end{bmatrix} \left(\begin{Bmatrix} \varepsilon_{0xx} \\ \gamma_{0zx} \end{Bmatrix} + z \begin{Bmatrix} k_{xx} \\ 0 \end{Bmatrix} \right)$$

It is clear that the axial stress is characterized by a constant part, the axial contribution, and a linear part in z, due to bending. This is consistent with what has been found with the DSV solution.

The shear stress, on the other hand, is constant through the thickness, which is not consistent with the Jourawski solution, which states that the transverse shear stresses should be quadratic in z. We then conclude that ***the Timoshenko model accurately predicts axial stresses but provides a raw approximation of the shear stress***. This is not surprising as the axial strain energy of the Timoshenko model is consistent with the one of the DSV solution, while the transverse shear strain energy needed a correction to recover the DSV solution. Moreover, the correction is applied to the strain energy, meaning that shear deformability is properly accounted for at global level. At a local level the shear stress is not corrected, which translates to an approximated constant distribution of the exact quadratic one.

It follows that an alternative way of determining the shear stress is needed. A typical approach consists in evaluating the shear stress by direct integration of the following 3D equilibrium equation:

$$\sigma_{xx\backslash x} + \tau_{xz\backslash z} = 0 \quad \rightarrow \quad \tau_{xz\backslash z} = -\sigma_{xx\backslash x}$$

Consider now a generic point along the beam axis $x = \bar{x}$, integration through the thickness of the previous equation yields:

$$\tau_{xz}(\bar{x}, z) = -\int_{-t/2}^{z} \sigma_{xx\backslash x}(\bar{x}, \zeta) d\zeta$$

Where ζ is a dummy coordinate, parallel to the z-axis, that goes from $-t/2$ to z. Recall now that:

$$\sigma_{xx} = E\left(u_{0\backslash x} + z\varphi_{x\backslash x}\right) \quad \rightarrow \quad \sigma_{xx\backslash x} = E\left(u_{0\backslash xx} + z\varphi_{x\backslash xx}\right)$$

And so the integral yields a shear stress distribution that is quadratic across the thickness, which is the expected behavior.

$$\begin{aligned} \tau_{xz}(\bar{x}, z) &= -E \int_{-\frac{t}{2}}^{z} \left(u_{0\backslash xx} + \zeta\varphi_{x\backslash xx}\right) d\zeta \\ &= -E\left[u_{0\backslash xx}\left(z + \frac{t}{2}\right) + \varphi_{x\backslash xx}\left(\frac{z^2}{2} - \frac{t^2}{8}\right)\right] \end{aligned} \tag{2.57}$$

2.2.1.10. Boundary conditions

A few remarks have been made about boundary conditions through this section, we repeat them here for convenience:

- The set of BCs has been automatically derived from the PVW along with the equilibrium conditions, from one simple scalar equation.
- If the kinematic assumptions change so do the BCs.
- Dirichlet BCs are the geometric ones, on generalized displacements, Neumann BCs are the natural BCs, expressing equilibrium with external forces on the body's boundary. They involve the generalized coordinates derivatives and are called Neumann BCs.

The ***definition of the BCs depends on the set of the constraints applied at the beam ends***. In general, constraints like rollers and sliders prevent the beam to move in a certain way. Thus, they require geometric BCs, i.e. the ones on displacements and rotations. Instead, if an external load is applied to the boundary of the body, which for a beam can only be at the beam ends (DSV

assumptions), then an internal force must develop in the body to balance the external force. It follows that in this case natural BCs are required. In regard to beams, three prevalent scenarios can be identified:

- Free constraint: the beam is not prevented to move in any way, thus no essential BCs are needed, only natural ones.
- Simply supported: the only geometric condition is $w_0 = 0$ at both ends of the beam, the applied moments have to be balanced by natural BCs.
- Clamped: all the DOFs of the beam are locked, thus only geometric BCs have to be placed at both ends of the beam $u_0 = w_0 = \varphi_x = 0$, there is no need for natural BCs.

We present some examples below, discussing axial, bending and torsional equilibrium separately since these are all decoupled problems.

Axial equilibrium

Free – Free	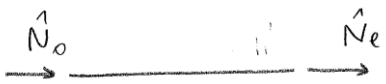	$\begin{cases} EAu_{0\backslash x}(0) = -\hat{N}_0 \\ EAu_{0\backslash x}(l) = +\hat{N}_l \end{cases}$
Clamp – Free	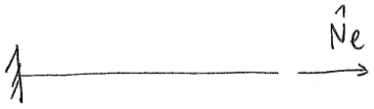	$\begin{cases} u_0(0) = 0 \\ EAu_{0\backslash x}(l) = +\hat{N}_l \end{cases}$
Clamp – Clamp	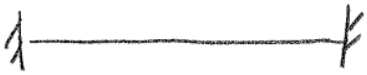	$\begin{cases} u_0(0) = 0 \\ u_0(l) = 0 \end{cases}$

Bending equilibrium

Free – Free		$\begin{cases} GA^*\left(\varphi_x(0) + w_{0\backslash x}(0)\right) = -\hat{Q}_0 \\ GA^*\left(\varphi_x(l) + w_{0\backslash x}(l)\right) = +\hat{Q}_l \\ EI\varphi_{x\backslash x}(0) = -\hat{M}_0 \\ EI\varphi_{x\backslash x}(l) = +\hat{M}_l \end{cases}$
SS – SS		$\begin{cases} w_0(0) = 0 \\ w_0(l) = 0 \\ EI\varphi_{x\backslash x}(0) = -\hat{M}_0 \\ EI\varphi_{x\backslash x}(l) = +\hat{M}_l \end{cases}$
Clamp – SS		$\begin{cases} w_0(0) = 0 \\ \varphi_x(0) = 0 \\ w_0(l) = 0 \\ EI\varphi_{x\backslash x}(l) = +\hat{M}_l \end{cases}$
Clamp – Clamp		$\begin{cases} w_0(0) = 0 \\ \varphi_x(0) = 0 \\ w_0(l) = 0 \\ \varphi_x(l) = 0 \end{cases}$

2.2.1.11. Strain inconsistency

According to the kinematic assumptions of the Timoshenko model, the strain component $\varepsilon_{zz} = 0$ since the displacement along the z-axis is not a function of the z-coordinate, $w = w(x)$. However, this is inconsistent with the assumption of axial stress state. To clarify this point, recall the CL for a 3D linear-elastic, isotropic and homogeneous body (1.18):

$$\begin{Bmatrix} \varepsilon_{xx} \\ \varepsilon_{yy} \\ \varepsilon_{zz} \\ \gamma_{xy} \\ \gamma_{yz} \\ \gamma_{zx} \end{Bmatrix} = \frac{1}{E} \begin{bmatrix} \begin{bmatrix} 1 & -\nu & -\nu \\ -\nu & 1 & -\nu \\ -\nu & -\nu & 1 \end{bmatrix} & [0] \\ [0] & 2(1+\nu) \begin{bmatrix} 1 & 0 & 0 \\ 0 & 1 & 0 \\ 0 & 0 & 1 \end{bmatrix} \end{bmatrix} \begin{Bmatrix} \sigma_{xx} \\ \sigma_{yy} \\ \sigma_{zz} \\ \tau_{xy} \\ \tau_{yz} \\ \tau_{zx} \end{Bmatrix}$$

According to the DSV solution, to which we refer because it is the exact one for axial stress, it must be that $\sigma_{zz} = \sigma_{yy} = \sigma_{zy} = 0$. Under such assumptions, the CL for a 3D beam reduces to:

$$\begin{Bmatrix} \sigma_{xx} \\ \tau_{yx} \\ \tau_{zx} \end{Bmatrix} = \begin{bmatrix} E & 0 & 0 \\ 0 & G & 0 \\ 0 & 0 & G \end{bmatrix} \begin{Bmatrix} \varepsilon_{xx} \\ \gamma_{yx} \\ \gamma_{zx} \end{Bmatrix}$$

From the CL of a 3D body, it's clear that the strain component ε_{zz} should be different from zero if either σ_{xx}, σ_{yy} or σ_{zz} are different from zero. For an axial stress state we should have that:

$$\varepsilon_{zz} = -\frac{\nu}{E}\sigma_{xx} \neq 0$$

Thus, the inconsistency lies in the fact that ***the kinematic law provides with*** $\varepsilon_{zz} = 0$ ***while the CL requires*** $\varepsilon_{zz} \neq 0$. This inconsistency does not alter the value of the strain energy since in any case the stress component $\sigma_{zz} = 0$, and thus $\varepsilon_{zz}\sigma_{zz} = 0$ in any case.

2.2.2. Euler-Bernoulli beam model

2.2.2.1. Generalized coordinates

The Euler-Bernoulli beam model is a kinematic model that allows us to perform structural analysis on slender structural elements, beams. Kinematic models start from a set of kinematic assumptions to introduce global/generalized quantities that simplify the solution of the structural problem. One set of such generalized quantities are the generalized stresses, commonly known as internal actions. These are simply stress resultants over the beam cross section, and they will be used in formulating equilibrium conditions. Internal actions are defined as follows:

$$\begin{cases} N = \int_A \sigma_{xx} dA \\ Q_y = \int_A \tau_{yx} dA \\ Q_z = \int_A \tau_{zx} dA \end{cases} \qquad \begin{cases} M_x = \int_A (\tau_{zx} y - \tau_{yx} z) dA \\ M_y = \int_A z \sigma_{xx} dA \\ M_z = \int_A -y \sigma_{xx} dA \end{cases} \tag{2.58}$$

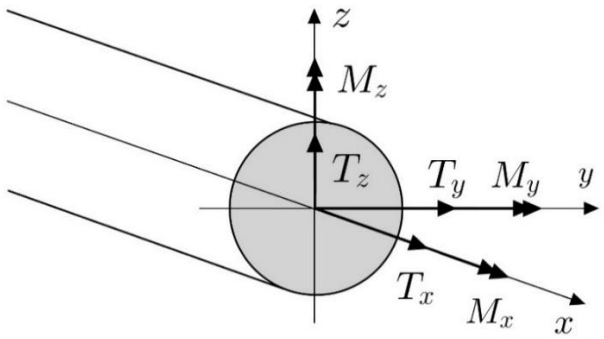

Figure 2.27: internal action convention for kinematic beam models.

The Euler-Bernoulli model formulation starts from the ***kinematic assumptions***, which require the beam cross sections to (1) remain undeformed and (2) normal to beam axis during flexion (normality condition). According to these assumptions, the displacement of the points lying on the beam cross section is not a function of their position on the cross section. As a consequence, the displacement field can be expressed in terms of the displacements of the beam axis:

$$\begin{cases} u(x,z) = u_0(x) - y\varphi_z(x) + z\varphi_y(x) \\ v(x) = v_0(x) \\ w(x) = w_0(x) \end{cases}$$

Where the index "0" identifies the quantities related to the beam axis. The rotation angle about the y-axis φ_y and that about the z-axis φ_z can be determined from geometric considerations. With respect to Figure 2.28, the generic point P of the beam cross section will displace of w_0, while a point Q infinitesimally close to P will displace of $w_0 + dw$. The same applies to bending in the $y - x$ plane. Then, if we remain in the field of small displacements, we obtain:

$$\begin{cases} dl \cdot \cos(-\varphi_y) = dx \\ dl \cdot \sin(-\varphi_y) = dw_0 \end{cases} \quad \rightarrow \quad \tan(-\varphi_y) \approx -\varphi_y = w_{0\backslash x}$$

$$\begin{cases} dl \cdot \cos(+\varphi_z) = dx \\ dl \cdot \sin(+\varphi_z) = dv_0 \end{cases} \quad \rightarrow \quad \tan(+\varphi_z) \approx +\varphi_z = v_{0\backslash x}$$

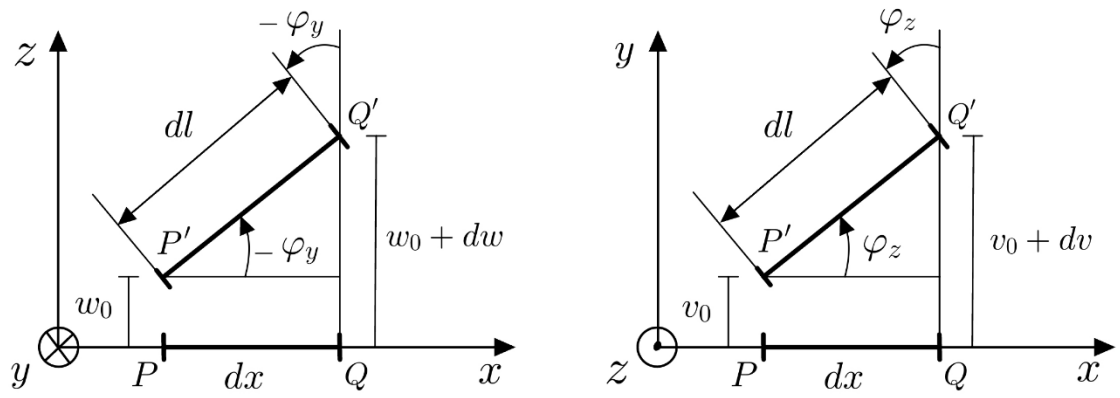

Figure 2.28: beam element rotation about the y-axis (left) and the z-axis (right).

Thus, under the assumptions of the Euler-Bernoulli model, the displacement field of every point of the beam (the kinematic model) can be ***approximated*** as follows:

$$\underline{u} = \begin{cases} u(x,y,z) = u_0(x) - yv_{0\backslash x}(x) - zw_{0\backslash x}(x) \\ v(x) = v_0(x) \\ w(x) = w_0(x) \end{cases} \tag{2.59}$$

Thus, the ***generalized coordinates*** of the Euler-Bernoulli beam model are the displacements of the beam axis, all a function of the axial coordinate x. These are quantities that express the displacement field in a global sense, i.e. over the entire cross section, which is assumed to displace without deformation.

$$\underline{u}_0(x) = \begin{Bmatrix} u_0(x) \\ v_0(x) \\ w_0(x) \end{Bmatrix} \tag{2.60}$$

2.2.2.2. Generalized strains

The generalized strains are obtained by applying the definition of the small strain tensor, which automatically provides a compatible displacement field. This will allow us to obtain the equilibrium conditions by directly applying the PVW. Expressing the displacements according to the kinematic model of equation (2.60) yields:

$$\begin{cases} \varepsilon_{xx} = u_{\backslash x} = u_{0\backslash x} - yv_{0\backslash xx} - zw_{0\backslash xx} \\ \varepsilon_{yy} = v_{\backslash y} = 0 \\ \varepsilon_{zz} = w_{\backslash z} = 0 \end{cases} \qquad \begin{cases} \gamma_{xy} = v_{\backslash x} + u_{\backslash y} = v_{0\backslash x} - v_{0\backslash x} = 0 \\ \gamma_{yz} = w_{\backslash y} + v_{\backslash z} = 0 + 0 = 0 \\ \gamma_{zx} = w_{\backslash x} + u_{\backslash z} = w_{0\backslash x} - w_{0\backslash x} = 0 \end{cases}$$

The only non-null strain component is the axial strain ε_{xx} from which we can identify two types of generalized strains: membranal and flexural strains. Membranal strains ε_{0xx} quantify the strain of the beam axis, hence the index "0", while flexural strains k_y, k_x quantify strains induced by flexion.

$$\varepsilon_{xx} = \varepsilon_{0xx} + yk_z + zk_y \tag{2.61}$$

Since flexural strains are essentially curvatures, they are named after the axis of bending. Simply put, a bending moment about the y-axis will generate a curvature about the same axis, thus we write $M_y \rightarrow k_y = -w_{0\backslash xx}$. The same for the z-axis $M_z \rightarrow k_z$. Another way of seeing this, a moment M_y will generate displacements about the z-axis, and so k_y will be linked to w, in the same way M_z will displace the beam along the y-axis, and so k_z will be linked to v. Thus, the ***generalized strains*** are simply:

$$\underline{\varepsilon}_0 = \{\varepsilon_{0xx} = u_{0\backslash x}\} \qquad \underline{k} = \begin{Bmatrix} k_z = -v_{0\backslash xx} \\ k_y = -w_{0\backslash xx} \end{Bmatrix} \tag{2.62}$$

Observation. From the kinematic field described above, it is easy to observe that the shear strains are all null $\gamma_{zx} = \gamma_{yx} = 0$. This implies that the ***Euler-Bernoulli beam model does not account for shear deformability***, and it is a direct consequence of the normality condition. This characteristic of the Euler-Bernoulli model gives us insight into when it is acceptable to adopt such model. In short, shear deformability is always present to some degree, but it can be neglected for thin beams. For thick beams neglecting shear deformability introduces too much error, thus the Timoshenko model must be used.

2.2.2.3. Generalized stresses

The generalized stresses are those quantities in energy conjugacy with the generalized strains. Thus, we investigate the internal virtual work δW_D to determine them. Considering the only non-null strain component ε_{xx}, we'll write:

$$\begin{aligned} \delta W_D = \int_V \delta\varepsilon_{xx}\sigma_{xx}dV &= \int_V \delta(\varepsilon_{0xx} + zk_y + yk_z)\sigma_{xx}dV \\ &= \int_l \left(\delta\varepsilon_{0xx}\int_A \sigma_{xx}\,dA + \delta k_y \int_A z\sigma_{xx}dA + \delta k_z \int_A y\sigma_{xx}dA\right)dx \\ &= \int_l (\delta\varepsilon_{0xx}N_x + \delta k_y M_y - \delta k_z M_z)dx \end{aligned}$$

Thus, the ***generalized stresses*** are the internal actions.

$$\underline{N} = \left\{N_x = \int_A \sigma_{xx}dA\right\} \qquad \underline{M} = \begin{Bmatrix} M_z = \int_A -y\sigma_{xx}dA \\ M_y = \int_A z\sigma_{xx}dA \end{Bmatrix} \tag{2.63}$$

Using this definition of the generalized stress parameters, and the previously obtained generalized strains, we can express the ***internal virtual work fully in terms of generalized parameters***:

$$\begin{aligned} \delta W_D = \int_V \delta\varepsilon_{xx}\sigma_{xx}dV &= \int_l (\delta\underline{\varepsilon}_0^T \cdot \underline{N} + \delta\underline{k}^T \cdot \underline{M})dx = \int_l (\delta\varepsilon_{0xx}N_x + \delta k_y M_y - \delta k_z M_z)dx \\ &= \int_l (\delta u_{0\backslash x}N_x - \delta w_{0\backslash xx}M_y + \delta v_{0\backslash xx}M_z)dx \end{aligned}$$

In order to use the PVW to obtain the equilibrium condition for this model (section 2.2.2.5), we need to express both δW_D and δW_e in terms of virtual generalized displacements $\delta\boldsymbol{u}_0$. Then, once equilibrium has been imposed as $\delta W_D = \delta W_e$, we can retrieve all the equilibrium conditions at once. In order to express δW_D in terms of virtual generalized displacements $\delta\boldsymbol{u}_0$, we need to

integrate by parts the axial strain $\delta\varepsilon_{0xx}$ once, and the curvatures k_y, k_z twice. We start from the axial term:

$$(\delta u_0 N_x)_{\backslash x} = \delta u_{0\backslash x} N_x + \delta u_0 N_{x\backslash x} \quad \rightarrow \quad \delta u_{0\backslash x} N_x = (\delta u_0 N_x)_{\backslash x} - \delta u_0 N_{x\backslash x}$$

By substitution:

$$\int_l (\delta u_{0\backslash x} N_x) dx = -\int_l (\delta u_0 N_{x\backslash x}) dx + (\delta u_0 N_x)_0^l$$

The curvature about the y-axis k_y can be integrated by parts twice as follows:

$$\begin{cases} (\delta w_{0\backslash x} M_y)_{\backslash x} = \delta w_{0\backslash xx} M_y + \delta w_{0\backslash x} M_{y\backslash x} \quad \rightarrow \quad \delta w_{0\backslash xx} M_y = (\delta w_{0\backslash x} M_y)_{\backslash x} - \delta w_{0\backslash x} M_{y\backslash x} \\ (\delta w_0 M_{y\backslash x})_{\backslash x} = \delta w_{0\backslash x} M_{y\backslash x} + \delta w_0 M_{y\backslash xx} \quad \rightarrow \quad \delta w_{0\backslash x} M_{y\backslash x} = (\delta w_0 M_{y\backslash x})_{\backslash x} - \delta w_0 M_{y\backslash xx} \end{cases}$$

By substitution:

$$\begin{aligned} \int_l (-\delta w_{0\backslash xx} M_y) dx &= \int_l (\delta w_{0\backslash x} M_{y\backslash x}) dx - (\delta w_{0\backslash x} M_y)_0^l \\ &= -\int_l (\delta w_0 M_{y\backslash xx}) dx + (\delta w_0 M_{y\backslash x} - \delta w_{0\backslash x} M_y)_0^l \end{aligned}$$

Repeating the same process for the curvature about the z-axis k_z yields:

$$\begin{cases} (\delta v_{0\backslash x} M_z)_{\backslash x} = \delta v_{0\backslash xx} M_z + \delta v_{0\backslash x} M_{z\backslash x} \quad \rightarrow \quad \delta v_{0\backslash xx} M_z = (\delta v_{0\backslash x} M_z)_{\backslash x} - \delta v_{0\backslash x} M_{z\backslash x} \\ (\delta v_0 M_{z\backslash x})_{\backslash x} = \delta v_{0\backslash x} M_{z\backslash x} + \delta v_0 M_{z\backslash xx} \quad \rightarrow \quad \delta v_{0\backslash x} M_{z\backslash x} = (\delta v_0 M_{z\backslash x})_{\backslash x} - \delta v_0 M_{z\backslash xx} \end{cases}$$

$$\begin{aligned} \int_l (\delta v_{0\backslash xx} M_z) dx &= -\int_l (\delta v_{0\backslash x} M_{z\backslash x}) dx + (\delta v_{0\backslash x} M_z)_0^l \\ &= \int_l (\delta v_0 M_{z\backslash xx}) dx + (\delta v_{0\backslash x} M_z - \delta v_0 M_{z\backslash x})_0^l \end{aligned}$$

Thus, the internal virtual work δW_D expressed in terms of virtual generalized coordinates $\delta \boldsymbol{u}_0$ reads:

$$\begin{aligned} \delta W_D = -\int_l & (\delta u_0 N_{x\backslash x} + \delta w_0 M_{y\backslash xx} - \delta v_0 M_{z\backslash xx}) dx \\ & + (\delta u_0 N_x + \delta w_0 M_{y\backslash x} - \delta w_{0\backslash x} M_y + \delta v_{0\backslash x} M_z - \delta v_0 M_{z\backslash x})_0^l \\ & = -\int_l (\delta u_0 N_{x\backslash x} + \delta w_0 M_{y\backslash xx} - \delta v_0 M_{z\backslash xx}) dx + \delta u_0(l) N_x(l) \\ & - \delta u_0(0) N_x(0) + \delta w_0(l) M_{y\backslash x}(l) - \delta w_0(0) M_{y\backslash x}(0) \\ & - \delta w_{0\backslash x}(l) M_y(l) + \delta w_{0\backslash x}(0) M_y(0) + \delta v_{0\backslash x}(l) M_z(l) \\ & - \delta v_{0\backslash x}(0) M_z(0) - \delta v_0(l) M_{z\backslash x}(l) + \delta v_0(0) M_{z\backslash x}(0) \end{aligned} \tag{2.64}$$

2.2.2.4. Generalized forces

The generalized forces are the quantities in energy-conjugacy with generalized displacement, so that their product produces a proper external virtual work δW_e. The generalized forces can be obtained starting from expressing the virtual external work due to the volume forces F_x, F_y, F_z. In this case we'll write:

$$\delta W_e = \int_V (\delta u F_x + \delta v F_y + \delta w F_z) dV = \int_V [\delta(u_0 - y v_{0\backslash x} - z w_{0\backslash x}) F_x + \delta v_0 F_y + \delta w_0 F_z] dV$$

$$= \int_V (\delta u_0 F_x - y \delta v_{0\backslash x} F_x - z \delta w_{0\backslash x} F_x + \delta v_0 F_y + \delta w_0 F_z) dV =$$

$$= \int_l \left(\delta u_0 \int_A F_x dA - \delta v_{0\backslash x} \int_A y F_x dA - \delta w_{0\backslash x} \int_A z F_x dA + \delta v_0 \int_A F_y dA + \delta w_0 \int_A F_z dA \right) dx$$

$$= \int_l (\delta u_0 \hat{n}_x - \delta v_{0\backslash x} \hat{m}_z - \delta w_{0\backslash x} \hat{m}_y + \delta v_0 \hat{n}_y + \delta w_0 \hat{n}_z) dx$$

The proper formulation of an external virtual work is the one expressed in terms of virtual displacements. In order to obtain this, the terms $\hat{m}_y$ and $\hat{m}_z$ must be integrated by parts, yielding:

$$(\delta w_0 \hat{m}_y)_{\backslash x} = \delta w_{0\backslash x} \hat{m}_y + \delta w_0 \hat{m}_{y\backslash x} \quad \rightarrow \quad \delta w_{0\backslash x} \hat{m}_y = (\delta w_0 \hat{m}_y)_{\backslash x} - \delta w_0 \hat{m}_{y\backslash x}$$

$$(\delta v_0 \hat{m}_z)_{\backslash x} = \delta v_{0\backslash x} \hat{m}_z + \delta v_0 \hat{m}_{z\backslash x} \quad \rightarrow \quad \delta v_{0\backslash x} \hat{m}_z = (\delta v_0 \hat{m}_z)_{\backslash x} - \delta v_0 \hat{m}_{z\backslash x}$$

Observation. This result implies that, for an Euler-Bernoulli beam, the externally applied distributed moments $\hat{m}_y$ and $\hat{m}_z$ are not generalized forces. The immediate reason is that they are not in energy conjugacy with the generalized displacements (definition of a generalized force). The deeper reason is the kinematic field of an Euler-Bernoulli beam: in order to enforce the normality condition, the rotations φ_y and φ_z are not independent. Rather, they are axial derivatives of the generalized coordinates. For this reason, in order to obtain proper work conjugates, one has to integrate by parts. This shows that the work conjugates to the generalized displacements are the axial derivatives of the distributed moments $\hat{m}_{y\backslash x}$ and $\hat{m}_{z\backslash x}$. We will see in the next section that, for an Euler-Bernoulli beam, the axial derivatives of the moments are the shear loads. Thus, one can interpret the ***shear internal action as the reaction force that enforces the normality condition***.

For simplicity, we assume that the moments per unit span $\hat{m}_y$ and $\hat{m}_z$ are uniformly distributed, so that the respective contributions in the external virtual work is null. This is easily shown as follows:

$$\int_l (-\delta w_{0\backslash x} \hat{m}_y) dx = -(\delta w_0 \hat{m}_y)_0^l + \int_l (\delta w_0 \hat{m}_{y\backslash x}) dx = 0 + 0 = 0$$

$$\int_l (-\delta v_{0\backslash x} \hat{m}_z) dx = -(\delta v_0 \hat{m}_z)_0^l + \int_0^l (\delta v_0 \hat{m}_{z\backslash x}) dx = 0 + 0 = 0$$

Thus, the virtual external energy due to (uniformly) distributed loads can be expressed as follows:

$$\delta W_e = \int_0^l (\delta \underline{u}_0^T \cdot \underline{\hat{n}}) dx = \int_l (\delta u_0 \hat{n}_x + \delta v_0 \hat{n}_y + \delta w_0 \hat{n}_z) dx$$

Consequently, one set of generalized forces are the distributed loads per unit length $\hat{\boldsymbol{n}}$.

$$\underline{\hat{n}} = \begin{Bmatrix} \hat{n}_x \\ \hat{n}_y \\ \hat{n}_z \end{Bmatrix} \tag{2.65}$$

In order to retrieve the equilibrium conditions from the PVW, we must also consider the virtual work generated by the concentrated loads applied at the beam ends. These are not to be confused with internal actions, which are generalized stress parameters, and are thus denoted by the "hat" operator $\widehat{N}, \widehat{Q}, \widehat{M}$. For such concentrated loads, the external virtual work reads:

$$\begin{aligned} \delta W_e = &\left(\delta u_0 \widehat{N}_x + \delta v_0 \widehat{Q}_y + \delta w_0 \widehat{Q}_z - \delta v_{0\backslash x} \widehat{M}_z - \delta w_{0\backslash x} \widehat{M}_y\right)_0^l \\ &= \delta u_0(0)\widehat{N}_{x0} + \delta u_0(l)\widehat{N}_{xl} + \delta v_0(0)\widehat{Q}_{y0} + \delta v_0(l)\widehat{Q}_{yl} + \delta w_0(0)\widehat{Q}_{z0} \\ &+ \delta w_0(l)\widehat{Q}_{zl} - \delta v_{0\backslash x}(0)\widehat{M}_{z0} - \delta v_{0\backslash x}(l)\widehat{M}_{zl} - \delta w_{0\backslash x}(0)\widehat{M}_{y0} - \delta w_{0\backslash x}(l)\widehat{M}_{yl} \end{aligned}$$

The total external virtual work in terms of generalized forces and concentrated loads can then be expressed as follows:

$$\begin{aligned} \delta W_e = &\int_0^l \left(\delta \underline{u}_0^T \cdot \underline{\hat{n}}\right) dx + \left(\delta u_0 \widehat{N}_x + \delta v_0 \widehat{Q}_y + \delta w_0 \widehat{Q}_z - \delta v_{0\backslash x} \widehat{M}_z - \delta w_{0\backslash x} \widehat{M}_y\right)_0^l \\ &= \int_l \left(\delta u_0 \hat{n}_x + \delta v_0 \hat{n}_y + \delta w_0 \hat{n}_z\right) dx + \delta u_0(0)\widehat{N}_{x0} + \delta u_0(l)\widehat{N}_{xl} \\ &+ \delta v_0(0)\widehat{Q}_{y0} + \delta v_0(l)\widehat{Q}_{yl} + \delta w_0(0)\widehat{Q}_{z0} + \delta w_0(l)\widehat{Q}_{zl} \\ &- \delta v_{0\backslash x}(0)\widehat{M}_{z0} - \delta v_{0\backslash x}(l)\widehat{M}_{zl} - \delta w_{0\backslash x}(0)\widehat{M}_{y0} - \delta w_{0\backslash x}(l)\widehat{M}_{yl} \end{aligned} \tag{2.66}$$

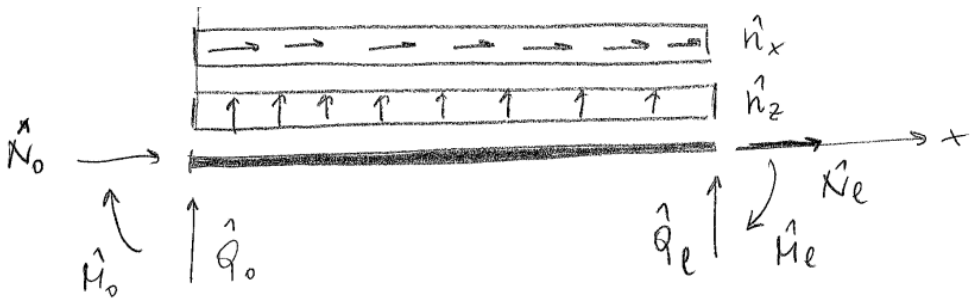

Figure 2.29: external loads acting on the beam axis in the $x - z$ plane.

2.2.2.5. Equilibrium conditions via PVW (loads)

The equilibrium conditions (equilibrium equations, essential and natural BCs) can all be obtained by applying the PVW. Thus, we impose that $\delta W_D - \delta W_e = 0$ for any $\delta \boldsymbol{u}_0$ that respects the BCs, and as long as compatibility is already satisfied (which it is). Using the expression of δW_D of equation (2.64) and that of δW_e of equation (2.66), we obtain the following equation:

$$\begin{aligned} 0 = -\int_l &\left[\delta u_0\left(N_{x\backslash x} - \hat{n}_x\right) - \delta v_0\left(M_{z\backslash xx} - \hat{n}_y\right) + \delta w_0\left(M_{y\backslash xx} + \hat{n}_z\right)\right] dx \\ &-\delta u_0(l)\left[N_x(l) - \widehat{N}_{xl}\right] + \delta u_0(0)\left[N_x(0) + \widehat{N}_{x0}\right] \\ &-\delta v_0(l)\left[M_{z\backslash x}(l) - \widehat{Q}_{yl}\right] + \delta v_0(0)\left[M_{z\backslash x}(0) - \widehat{Q}_{y0}\right] \end{aligned}$$

$$
\begin{aligned}
&+\delta w_0(l)\left[M_{y\backslash x}(l)-\hat{Q}_{zl}\right]-\delta w_0(0)\left[M_{y\backslash x}(0)+\hat{Q}_{z0}\right]\\
&+\delta v_{0\backslash x}(l)\left[M_z(l)-\hat{M}_{zl}\right]-\delta v_{0\backslash x}(0)\left[M_z(0)+\hat{M}_{z0}\right]\\
&-\delta w_{0\backslash x}(l)\left[M_y(l)-\hat{M}_{yl}\right]+\delta w_{0\backslash x}(0)\left[M_y(0)+\hat{M}_{y0}\right]
\end{aligned}
$$

Thus, the ***equilibrium conditions in terms of loads*** are found to be the following:

$$
\begin{cases} N_{x\backslash x}+\hat{n}_x=0\\ M_{y\backslash xx}+\hat{n}_z=0\\ M_{z\backslash xx}-\hat{n}_y=0 \end{cases}
\quad \text{in } x\in[0,l] \quad
\begin{cases}
N_x(0)=-\hat{N}_{x0} & \text{or} & \delta u_0(0)=0\\
N_x(l)=+\hat{N}_{xl} & \text{or} & \delta u_0(l)=0\\
M_{z\backslash x}(0)=+\hat{Q}_{y0} & \text{or} & \delta v_0(0)=0\\
M_{z\backslash x}(l)=+\hat{Q}_{yl} & \text{or} & \delta v_0(l)=0\\
M_{y\backslash x}(0)=-\hat{Q}_{z0} & \text{or} & \delta w_0(0)=0\\
M_{y\backslash x}(l)=+\hat{Q}_{zl} & \text{or} & \delta w_0(l)=0\\
M_z(0)=-\hat{M}_{z0} & \text{or} & \delta v_{0\backslash x}(0)=0\\
M_z(l)=+\hat{M}_{zl} & \text{or} & \delta v_{0\backslash x}(l)=0\\
M_y(0)=-\hat{M}_{y0} & \text{or} & \delta w_{0\backslash x}(0)=0\\
M_y(l)=+\hat{M}_{yl} & \text{or} & \delta w_{0\backslash x}(l)=0
\end{cases}
\tag{2.67}
$$

On the left we report the equilibrium equations, the first expresses axial equilibrium, while the other two express bending equilibrium (the first about the y-axis and the second about the z-axis). On the right are reported the boundary conditions, first the natural ones and after the essential ones. From the natural BCs we can notice that ***the derivative of a bending moment is a shear force***. This will be also proved fairly easily when we derive such equations from the equilibrium of an infinitesimal element.

2.2.2.6. Equilibrium equations via infinitesimal element

The use of the Principle of Virtual Work (PVW) to impose equilibrium is extremely powerful, as it allows one to derive the complete set of equilibrium conditions, including both the governing differential equations and the associated boundary conditions. However, this approach can be rather laborious. For this reason, a more direct method is often introduced: by enforcing equilibrium on an infinitesimal beam element, the governing differential equations can be obtained in a much simpler way. It must be emphasized, however, that ***this local equilibrium approach does not yield the full set of equilibrium conditions***, as it does not provide the boundary conditions, which are instead naturally obtained through the PVW formulation.

We start by deriving the axial equilibrium equation. Considering the scheme in Figure 2.30, axial equilibrium reads:

$$
N_x+dN_x-N_x+\hat{n}_x dx=0 \quad \rightarrow \quad N_{x\backslash x}+\hat{n}_x=0
$$

We now obtain the bending equilibrium about the y-axis, with respect to the scheme in Figure 2.31 we'll write:

$$
\begin{cases} Q_z+dQ_z-Q_z+\hat{n}_z dx=0\\ M_y+dM_y-M_y+\hat{m}_y dx-Q_z dx+\hat{n}_z dx\dfrac{dx}{2}=0 \end{cases}
\quad \rightarrow \quad
\begin{cases} Q_{z\backslash x}+\hat{n}_z=0\\ M_{y\backslash x}+\hat{m}_y-Q_z=0 \end{cases}
$$

Where the moments due to shear loads in the second equation were taken with respect to P. Where we neglected the term $\hat{n}_z dx^2/2$ because it is a higher order infinitesimal with respect to the others. By differentiating the second equation with respect to x once more, and using the first one, we obtain:

$$M_{y\backslash xx} + \hat{m}_{y\backslash x} + \hat{n}_z = 0$$

Assuming that $\hat{m}_y$ is uniformly distributed along the x-axis, as we did in section 2.2.2.4, we obtain the same equilibrium equation of the system in (2.64):

$$M_{y\backslash xx} + \hat{n}_z = 0$$

Repeating the same reasoning for the bending equilibrium about the z-axis coupled with shear equilibrium along the y-axis, we obtain the third equilibrium equation of the system in (2.64):

$$\begin{cases} Q_y + dQ_y - Q_y + \hat{n}_y dx = 0 \\ -M_z - dM_z + M_z - \hat{m}_z dx - Q_y dx + \hat{n}_y dx \dfrac{dx}{2} = 0 \end{cases} \rightarrow \begin{cases} Q_{y\backslash x} + \hat{n}_y = 0 \\ -M_{z\backslash x} - \hat{m}_z - Q_y = 0 \end{cases}$$

Differentiating the second equation and substituting the first one, and assuming $\hat{m}_z$ to be constant along the x-axis yields:

$$M_{z\backslash xx} - \hat{n}_y = 0$$

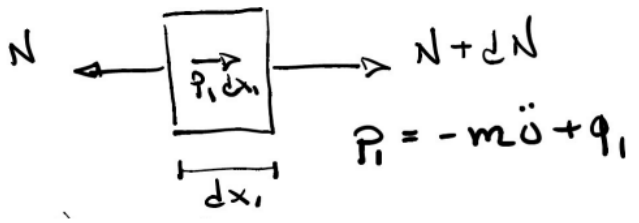

Figure 2.30: infinitesimal beam element subject to axial loads.

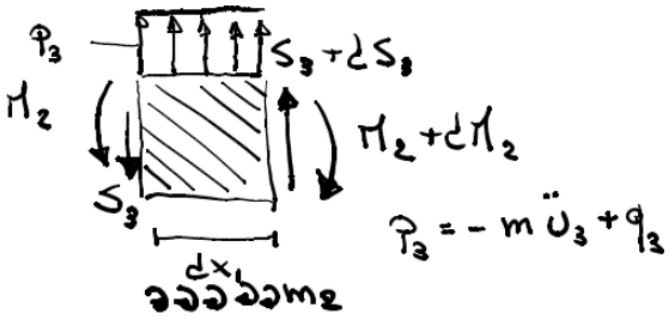

Figure 2.31: infinitesimal beam element subject to bending and shear loads in the x-z plane (top) and the x-y plane (bottom).

2.2.2.7. Constitutive law

The CL establishes the relation between stresses and strains. In the framework of a kinematic model such as this one, the CL can be used to express the generalized stresses $\boldsymbol{N}, \boldsymbol{M}$ in terms of generalized strains $\boldsymbol{\varepsilon}_0$ and $\boldsymbol{k}$. For kinematic model the CL is suggested by the approximation used

to model the kinematic field of the beam. This simply means that, due to the assumed displacement field, the only non-null strain component is the axial strain. Thus, it is intuitive to assume an ***axial stress state***:

$$\sigma_{xx} = E\varepsilon_{xx} = E\left(\varepsilon_{0xx} + yk_z + zk_y\right) \tag{2.68}$$

We initially do not assume the reference system to be either centroidal or principal. Recall that the DSV solution makes these assumptions, thus if we want to use the DSV solution for evaluating stresses, this must be verified. Thus, the generalized stresses can be expressed as follows:

$$N_x = \int_A \sigma_{xx} dA = \int_A E\left(\varepsilon_{0xx} + yk_z + zk_y\right) dA = \int_A E\varepsilon_{0xx} dA + \int_A Eyk_z dA + \int_A Ezk_y dA$$
$$= EA\varepsilon_{0xx} + ES_z k_z + ES_y k_y = EAu_{0\backslash x} - ES_z w_{0\backslash xx} - ES_y v_{0\backslash xx}$$

$$M_y = \int_A z\sigma_{xx} dA = \int_A zE\left(\varepsilon_{0xx} + yk_z + zk_y\right) dA = \int_A zE\varepsilon_{0xx} dA + \int_A Ezyk_z dA + \int_A Ez^2 k_y dA$$
$$= ES_y\varepsilon_{0xx} + EI_{yz}k_z + EI_{yy}k_y = ES_z u_{0\backslash x} - EI_{yz}v_{0\backslash xx} - EI_{yy}w_{0\backslash xx}$$

$$M_z = \int_A -y\sigma_{xx} dA = \int_A -yE\left(\varepsilon_{0xx} + yk_z + zk_y\right) dA$$
$$= \int_A -yE\varepsilon_{0xx} dA - \int_A Ey^2 k_z dA - \int_A Eyzk_y dA$$
$$= -ES_z\varepsilon_{0xx} - EI_{zz}k_z - EI_{zy}k_y = -ES_z u_{0\backslash x} + EI_{zz}w_{0\backslash xx} + EI_{yz}v_{0\backslash xx}$$

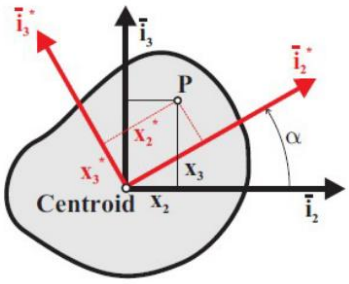

Figure 2.32: beam centroidal but not principal reference system.

Thus, the most general form of the generalized CL linking generalized stresses and generalized strains is obtained as follows:

$$\begin{Bmatrix} N_x \\ M_y \\ M_z \end{Bmatrix} = \begin{bmatrix} EA & ES_z & -ES_y \\ ES_y & EI_{yy} & -EI_{yz} \\ -ES_z & -EI_{zy} & EI_{zz} \end{bmatrix} \begin{Bmatrix} \varepsilon_{0xx} \\ k_y \\ -k_z \end{Bmatrix} = \begin{bmatrix} EA & ES_z & -ES_y \\ ES_y & EI_{yy} & -EI_{yz} \\ -ES_z & -EI_{zy} & EI_{zz} \end{bmatrix} \begin{Bmatrix} u_{0\backslash x} \\ -w_{0\backslash xx} \\ v_{0\backslash xx} \end{Bmatrix} \tag{2.69}$$

However, if the reference system is taken to be centroidal, then the static moments are null $S_y = S_z = 0$. This ***decouples the axial problem/equilibrium from the bending ones***. If the reference system is also principal, then the mixed inertia moment is null as well $I_{zy} = 0$, ***decoupling the two bending equations/problems as well***. If the reference system is not principal, the rotation angle about the x-axis that renders the system principal is:

$$\tan\alpha = \frac{2I_{zy}}{I_{yy} - I_{zz}}$$

Where the angle α is the angle between the principal axis, represented in black in Figure 2.32, and the generic one, represented in red. Consequently, if the reference system is both centroidal and principal, the CL simplifies to:

$$\begin{Bmatrix} N_x \\ M_y \\ M_z \end{Bmatrix} = \begin{bmatrix} EA & 0 & 0 \\ 0 & EI_{yy} & 0 \\ 0 & 0 & EI_{zz} \end{bmatrix} \begin{Bmatrix} \varepsilon_{0xx} \\ k_y \\ -k_z \end{Bmatrix} = \begin{bmatrix} EA & 0 & 0 \\ 0 & EI_{yy} & 0 \\ 0 & 0 & EI_{zz} \end{bmatrix} \begin{Bmatrix} u_{0\backslash x} \\ -w_{0\backslash xx} \\ v_{0\backslash xx} \end{Bmatrix} \tag{2.70}$$

Observation. The CL does not provide an expression for the shear forces $\hat{Q}_y$ and $\hat{Q}_z$. This does not mean that they are null, in fact they can be retrieved as the derivatives of the bending moments. Thus, the shear forces are generally different than zero although they do not appear in the CL.

2.2.2.8. Equilibrium conditions (displacements)

Having introduced the CL we can now express the equilibrium conditions in terms of generalized strains as well. Being these displacements derivatives, this for of the equilibrium conditions is advantageous when displacement-based approaches are used to solve the structural problem. By simple substitution of the expression of the internal actions $\boldsymbol{N}, \boldsymbol{M}$ of equation (2.70) into the equilibrium conditions of equation (2.67) we obtain:

$$\begin{cases} EAu_{0\backslash xx} + \hat{n}_x = 0 \\ \left(EIw_{0\backslash xx}\right)_{\backslash xx} - \hat{n}_z = 0 \\ \left(EIv_{0\backslash xx}\right)_{\backslash xx} - \hat{n}_y = 0 \end{cases} \quad \text{in } x \in [0, l]$$

$$\text{BCs:} \begin{cases} EAu_{0\backslash x}(0) = -\hat{N}_{x0} & \text{or} & \delta u_0(0) = 0 \\ EAu_{0\backslash x}(l) = +\hat{N}_{xl} & \text{or} & \delta u_0(l) = 0 \\ \left(EI_{zz}v_{0\backslash xx}\right)_{\backslash x}(0) = +\hat{Q}_{y0} & \text{or} & \delta v_0(0) = 0 \\ \left(EI_{zz}v_{0\backslash xx}\right)_{\backslash x}(l) = +\hat{Q}_{yl} & \text{or} & \delta v_0(l) = 0 \\ \left(EI_{yy}w_{0\backslash xx}\right)_{\backslash x}(0) = +\hat{Q}_{z0} & \text{or} & \delta w_0(0) = 0 \\ \left(EI_{yy}w_{0\backslash xx}\right)_{\backslash x}(l) = -\hat{Q}_{zl} & \text{or} & \delta w_0(l) = 0 \\ EI_{zz}v_{0\backslash xx}(0) = -\hat{M}_{z0} & \text{or} & \delta v_{0\backslash x}(0) = 0 \\ EI_{zz}v_{0\backslash xx}(l) = +\hat{M}_{zl} & \text{or} & \delta v_{0\backslash x}(l) = 0 \\ EI_{yy}w_{0\backslash xx}(0) = +\hat{M}_{y0} & \text{or} & \delta w_{0\backslash x}(0) = 0 \\ EI_{yy}w_{0\backslash xx}(l) = -\hat{M}_{yl} & \text{or} & \delta w_{0\backslash x}(l) = 0 \end{cases} \tag{2.71}$$

If the section is constant along the beam axis, then the equilibrium equations of an Euler-Bernoulli beam can be expressed in terms of three ordinary differential equations and three unknown functions, the generalized displacements $\boldsymbol{u}_0$.

$$\begin{cases} EAu_{0\backslash xx} + \hat{n}_x = 0 \\ EIw_{0\backslash xxxx} - \hat{n}_z = 0 \\ EIv_{0\backslash xxxx} - \hat{n}_y = 0 \end{cases} \quad \text{in } x \in [0, l] \tag{2.72}$$

$$\text{BCs:}\quad \begin{cases} EAu_{0\backslash x}(0) = -\hat{N}_{x0} & \text{or} \quad \delta u_0(0) = 0 \\ EAu_{0\backslash x}(l) = +\hat{N}_{xl} & \text{or} \quad \delta u_0(l) = 0 \\ EI_{zz}v_{0\backslash xxx}(0) = +\hat{Q}_{y0} & \text{or} \quad \delta v_0(0) = 0 \\ EI_{zz}v_{0\backslash xxx}(l) = +\hat{Q}_{yl} & \text{or} \quad \delta v_0(l) = 0 \\ EI_{yy}w_{0\backslash xxx}(0) = +\hat{Q}_{z0} & \text{or} \quad \delta w_0(0) = 0 \\ EI_{yy}w_{0\backslash xxx}(l) = -\hat{Q}_{zl} & \text{or} \quad \delta w_0(l) = 0 \\ EI_{zz}v_{0\backslash xx}(0) = -\hat{M}_{z0} & \text{or} \quad \delta v_{0\backslash x}(0) = 0 \\ EI_{zz}v_{0\backslash xx}(l) = +\hat{M}_{zl} & \text{or} \quad \delta v_{0\backslash x}(l) = 0 \\ EI_{yy}w_{0\backslash xx}(0) = +\hat{M}_{y0} & \text{or} \quad \delta w_{0\backslash x}(0) = 0 \\ EI_{yy}w_{0\backslash xx}(l) = -\hat{M}_{yl} & \text{or} \quad \delta w_{0\backslash x}(l) = 0 \end{cases}$$

2.2.2.9. Torsion

It can be observed that no information is provided by the Euler-Bernoulli beam model about the torsional response of the beam. The torsional equilibrium equation in terms of loads can be easily derived by imposing torsional equilibrium on an infinitesimal beam element. Considering the scheme in **Error! Reference source not found.**, imposing equilibrium yields:

$$M_x + dM_x - M_x + \hat{m}_x dx = 0 \quad \rightarrow \quad M_{x\backslash x} + \hat{m}_x = 0 \tag{2.73}$$

Here, the distributed torsional moment $\hat{m}_x$ can be interpreted as the ***generalized force parameter for torsion***. Thus, the equilibrium equations in terms of loads of an Euler-Bernoulli beam read:

$$\begin{cases} N_{x\backslash x} + \hat{n}_x = 0 \\ M_{y\backslash xx} + \hat{n}_z = 0 \\ M_{z\backslash xx} - \hat{n}_y = 0 \\ M_{x\backslash x} + \hat{m}_x = 0 \end{cases} \tag{2.74}$$

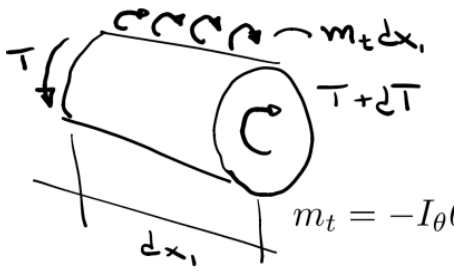

Figure 2.33: infinitesimal beam element subject to torsional loads.

In order to include the CL for torsion, we need to recall the DSV solution. We will provide an initial guess solution of the stress field. We'll use such guess to approximate the kinematic model in torsion of the beam, similarly to kinematic models. From the kinematic model we'll retrieve strains, stresses, and finally the torsional internal action. This will provide with the CL for torsion of a beam. The DSV guess solution for shear is the following:

$$\sigma_{zz} = \sigma_{xx} = \sigma_{yy} = \tau_{zy} = 0$$

Thus, all normal stresses are null, as well as the shear stress that does not lie on the beam cross section. According to this ***assumed*** stress field, the displacement field can be expressed as follows:

$$\begin{cases} u(y,z) = \theta'\Psi(y,z) \\ v(x,z) = -z\theta = -zx\theta' \\ w(y,z) = +y\theta = +yx\theta' \end{cases}$$

Where Ψ is the warping function, θ is the beam cross section rotation, which can be interpreted as ***generalized coordinates for torsion***. The section rotation can be expressed as $\theta = x\theta'$, where $\theta' = \theta_{\backslash x}$ is the torsion, constant along the beam axis. ***Assuming that the beam has a circular cross section*** render the warping is null $\Psi = 0$. Thus, the displacement field reads:

$$\begin{cases} u(y,z) = 0 \\ v(x,z) = -zx\theta' \\ w(y,z) = +yx\theta' \end{cases}$$

According to this displacement field and the definition of the small strain tensor **Error! Reference source not found.**, the only non-null strain components are the sectional shear strains. We can compute such strains by applying **Error! Reference source not found.**, recall that every time we compute strains this way, compatibility is automatically satisfied. This yields:

$$\begin{cases} \gamma_{yx} = v_{\backslash x} + u_{\backslash y} = -z\theta' \\ \gamma_{zx} = w_{\backslash x} + u_{\backslash z} = y\theta' \end{cases}$$

Thus, the torsion θ' can be interpreted as a ***generalized strain for torsion***. Now the stresses can be recovered by applying the CL for an isotropic, homogeneous, linear-elastic material **Error! Reference source not found.**:

$$\begin{cases} \tau_{yx} = G\gamma_{yx} = -z\theta' G \\ \tau_{zx} = G\gamma_{zx} = y\theta' G \end{cases}$$

We now use this result in the definition of the torsional internal action M_x of equation (2.58):

$$M_x = \int_A (\tau_{zx} y - \tau_{yx} z) dA = \int_A G(y^2 + z^2)\theta' dA = GJ\theta' \tag{2.75}$$

This torsional moment can be interpreted as the ***generalized stress for torsion***. Thus, the full CL for an Euler-Bernoulli beam with circular cross section and a reference system that is centroidal and principal reads:

$$\begin{Bmatrix} N_x \\ M_y \\ M_z \\ M_x \end{Bmatrix} = \begin{bmatrix} EA & 0 & 0 & 0 \\ 0 & EI_{yy} & 0 & 0 \\ 0 & 0 & EI_{zz} & 0 \\ 0 & 0 & 0 & GJ \end{bmatrix} \begin{Bmatrix} \varepsilon_{0xx} \\ k_y \\ -k_z \\ \theta_{\backslash x} \end{Bmatrix} = \begin{bmatrix} EA & 0 & 0 & 0 \\ 0 & EI_{yy} & 0 & 0 \\ 0 & 0 & EI_{zz} & 0 \\ 0 & 0 & 0 & GJ \end{bmatrix} \begin{Bmatrix} u_{0\backslash x} \\ -w_{0\backslash xx} \\ v_{0\backslash xx} \\ \theta_{\backslash x} \end{Bmatrix} \tag{2.76}$$

Observation. It is important to point out that the CL obtained for torsion is valid only for beams with circular cross section. If this is not satisfied, then warping Ψ is not null, and other

approximative solution must be adopted. Moreover, it is easy to notice that the axial, bending and torsional equilibrium ***problems are all decoupled***.

As previously stated, the BCs are not provided by this approach of obtaining the equilibrium equations. However, having now introduced the CL for torsion, we identified the torsion as the generalized strain parameter for M_x. Thus, for torsion it is easy to accept that the BCs should be as follows:

$$\begin{cases} M_x(0) = -\widehat{M}_{x0} & \text{or} \quad \delta\theta_x(0) = 0 \\ M_x(l) = +\widehat{M}_{xl} & \text{or} \quad \delta\theta_x(l) = 0 \end{cases}$$

Then, the axial, bending and torsional equilibrium conditions for an Euler-Bernoulli beam result to be four PDEs and twelve BCs, either natural or essential, and they read:

$$\begin{cases} N_{x\backslash x} + \hat{n}_x = 0 \\ M_{y\backslash xx} + \hat{n}_z = 0 \\ M_{z\backslash xx} - \hat{n}_y = 0 \\ M_{x\backslash x} + \hat{m}_x = 0 \end{cases} \quad \text{in } x \in [0, l] \quad \begin{cases} N_x(0) = -\widehat{N}_{x0} & \text{or} & \delta u_0(0) = 0 \\ N_x(l) = +\widehat{N}_{xl} & \text{or} & \delta u_0(l) = 0 \\ M_{z\backslash x}(0) = +\hat{Q}_{y0} & \text{or} & \delta v_0(0) = 0 \\ M_{z\backslash x}(l) = -\hat{Q}_{yl} & \text{or} & \delta v_0(l) = 0 \\ M_{y\backslash x}(0) = -\hat{Q}_{z0} & \text{or} & \delta w_0(0) = 0 \\ M_{y\backslash x}(l) = +\hat{Q}_{zl} & \text{or} & \delta w_0(l) = 0 \\ M_z(0) = +\widehat{M}_{z0} & \text{or} & \delta v_{0\backslash x}(0) = 0 \\ M_z(l) = -\widehat{M}_{zl} & \text{or} & \delta v_{0\backslash x}(l) = 0 \\ M_y(0) = -\widehat{M}_{y0} & \text{or} & \delta w_{0\backslash x}(0) = 0 \\ M_y(l) = +\widehat{M}_{yl} & \text{or} & \delta w_{0\backslash x}(l) = 0 \\ M_x(0) = -\widehat{M}_{x0} & \text{or} & \delta\theta_x(0) = 0 \\ M_x(l) = +\widehat{M}_{xl} & \text{or} & \delta\theta_x(l) = 0 \end{cases} \tag{2.77}$$

Using this extended CL of equation (2.76), the equilibrium conditions can be expressed in terms of generalized strains, yielding:

$$\begin{cases} EAu_{0\backslash xx} + \hat{n}_x = 0 \\ \left(EIw_{0\backslash xx}\right)_{\backslash xx} - \hat{n}_z = 0 \\ \left(EIv_{0\backslash xx}\right)_{\backslash xx} - \hat{n}_y = 0 \\ \left(GJ\theta_{\backslash x}\right)_{\backslash x} + \hat{m}_x = 0 \end{cases} \quad \text{in } x \in [0, l] \tag{2.78}$$

$$\text{BCs:}\quad \begin{cases} EAu_{0\backslash x}(0) = -\hat{N}_{x0} & \text{or} \quad \delta u_0(0) = 0 \\ EAu_{0\backslash x}(l) = +\hat{N}_{xl} & \text{or} \quad \delta u_0(l) = 0 \\ \left(EI_{zz}v_{0\backslash xx}\right)_{\backslash x}(0) = +\hat{Q}_{y0} & \text{or} \quad \delta v_0(0) = 0 \\ \left(EI_{zz}v_{0\backslash xx}\right)_{\backslash x}(l) = +\hat{Q}_{yl} & \text{or} \quad \delta v_0(l) = 0 \\ \left(EI_{yy}w_{0\backslash xx}\right)_{\backslash x}(0) = +\hat{Q}_{z0} & \text{or} \quad \delta w_0(0) = 0 \\ \left(EI_{yy}w_{0\backslash xx}\right)_{\backslash x}(l) = -\hat{Q}_{zl} & \text{or} \quad \delta w_0(l) = 0 \\ EI_{zz}v_{0\backslash xx}(0) = -\hat{M}_{z0} & \text{or} \quad \delta v_{0\backslash x}(0) = 0 \\ EI_{zz}v_{0\backslash xx}(l) = +\hat{M}_{zl} & \text{or} \quad \delta v_{0\backslash x}(l) = 0 \\ EI_{yy}w_{0\backslash xx}(0) = +\hat{M}_{y0} & \text{or} \quad \delta w_{0\backslash x}(0) = 0 \\ EI_{yy}w_{0\backslash xx}(l) = -\hat{M}_{yl} & \text{or} \quad \delta w_{0\backslash x}(l) = 0 \\ GJ\theta_{\backslash x}(0) = -\hat{M}_{x0} & \text{or} \quad \delta\theta_x(0) = 0 \\ GJ\theta_{\backslash x}(l) = +\hat{M}_{xl} & \text{or} \quad \delta\theta_x(l) = 0 \end{cases}$$

If the section has constant geometry and material properties along the beam axis, then the equilibrium equations simplify to:

$$\begin{cases} EAu_{0\backslash xx} + \hat{n}_x = 0 \\ EIw_{0\backslash xxxx} - \hat{n}_z = 0 \\ EIv_{0\backslash xxxx} - \hat{n}_y = 0 \\ GJ\theta_{\backslash xx} + \hat{m}_x = 0 \end{cases} \quad \text{in } x \in [0, l]$$

$$\text{BCs:}\quad \begin{cases} EAu_{0\backslash x}(0) = -\hat{N}_{x0} & \text{or} \quad \delta u_0(0) = 0 \\ EAu_{0\backslash x}(l) = +\hat{N}_{xl} & \text{or} \quad \delta u_0(l) = 0 \\ EI_{zz}v_{0\backslash xxx}(0) = +\hat{Q}_{y0} & \text{or} \quad \delta v_0(0) = 0 \\ EI_{zz}v_{0\backslash xxx}(l) = +\hat{Q}_{yl} & \text{or} \quad \delta v_0(l) = 0 \\ EI_{yy}w_{0\backslash xxx}(0) = +\hat{Q}_{z0} & \text{or} \quad \delta w_0(0) = 0 \\ EI_{yy}w_{0\backslash xxx}(l) = -\hat{Q}_{zl} & \text{or} \quad \delta w_0(l) = 0 \\ EI_{zz}v_{0\backslash xx}(0) = -\hat{M}_{z0} & \text{or} \quad \delta v_{0\backslash x}(0) = 0 \\ EI_{zz}v_{0\backslash xx}(l) = +\hat{M}_{zl} & \text{or} \quad \delta v_{0\backslash x}(l) = 0 \\ EI_{yy}w_{0\backslash xx}(0) = +\hat{M}_{y0} & \text{or} \quad \delta w_{0\backslash x}(0) = 0 \\ EI_{yy}w_{0\backslash xx}(l) = -\hat{M}_{yl} & \text{or} \quad \delta w_{0\backslash x}(l) = 0 \\ GJ\theta_{\backslash x}(0) = +\hat{M}_{x0} & \text{or} \quad \delta\theta_x(0) = 0 \\ GJ\theta_{\backslash x}(l) = -\hat{M}_{xl} & \text{or} \quad \delta\theta_x(l) = 0 \end{cases} \tag{2.79}$$

2.2.2.10. Dynamic equilibrium equations

The dynamic equilibrium equations can be very easily obtained from the ones in equations (2.78) and (2.79). In short, we can interpret the generalized forces $\hat{\boldsymbol{n}}$ as composed by a static component and an inertial one. Thus, we'll write:

$$\underline{\hat{n}} = \begin{Bmatrix} \hat{n}_x \\ \hat{n}_y \\ \hat{n}_z \\ \hat{m}_x \end{Bmatrix} \quad \rightarrow \quad \underline{\hat{n}} = \begin{Bmatrix} \hat{n}_x - m\ddot{u} \\ \hat{n}_y - m\ddot{v} \\ \hat{n}_z - m\ddot{w} \\ \hat{m}_x - I_\theta \ddot{\theta} \end{Bmatrix} \tag{2.80}$$

Where I_θ is the polar mass moment of inertia with respect to the centroid of the section. According to these expressions of the generalized forces, the equilibrium equations in terms of loads can be expressed as follows:

$$\begin{cases} N_{x\backslash x} + \hat{n}_x - m\ddot{u} = 0 \\ M_{y\backslash xx} + \hat{n}_z - m\ddot{w} = 0 \\ M_{z\backslash xx} - \hat{n}_y + m\ddot{v} = 0 \\ M_{x\backslash x} + \hat{m}_x - I_\theta \ddot{\theta} = 0 \end{cases} \quad \text{in } x \in [0, l] \quad + \quad \begin{cases} 12 \text{ BCs} \\ 8 \text{ ICs} \end{cases} \tag{2.81}$$

Naturally, in order to uniquely identify the dynamic structural problem, ***initial conditions (ICs) must be provided***. More precisely, two ICs per equation are needed, since these are all second order ODEs. The same equations can be expressed in terms of generalized stains by invoking the CL (2.70):

$$\begin{cases} EAu_{0\backslash xx} + \hat{n}_x - m\ddot{u} = 0 \\ \left(EIw_{0\backslash xx}\right)_{\backslash xx} - \hat{n}_z + m\ddot{w} = 0 \\ \left(EIv_{0\backslash xx}\right)_{\backslash xx} - \hat{n}_y + m\ddot{v} = 0 \\ \left(GJ\theta_{\backslash x}\right)_{\backslash x} + \hat{m}_x - I_\theta \ddot{\theta} = 0 \end{cases} \quad \text{in } x \in [0, l] \quad + \quad \begin{cases} 12 \text{ BCs} \\ 8 \text{ ICs} \end{cases} \tag{2.82}$$

If the beam has constant properties along its axis, then we obtain:

$$\begin{cases} EAu_{0\backslash xx} + \hat{n}_x - m\ddot{u} = 0 \\ EIw_{0\backslash xxxx} - \hat{n}_z + m\ddot{w} = 0 \\ EIv_{0\backslash xxxx} - \hat{n}_y + m\ddot{v} = 0 \\ GJ\theta_{\backslash xx} + \hat{m}_x - I_\theta \ddot{\theta} = 0 \end{cases} \quad \text{in } x \in [0, l] \quad + \quad \begin{cases} 12 \text{ BCs} \\ 8 \text{ ICs} \end{cases} \tag{2.83}$$

2.2.2.11. Boundary conditions

In the previous sections we derived the equilibrium conditions for an Euler-Bernoulli beam subject to axial, bending and torsional loads. Such equilibrium conditions are the equilibrium equations and the BCs. The latter were introduced as natural and geometric for every possible load case at both the beam ends. Thus, a criterion to understand which to choose must be established.

Intuitively, ***the choice of which type of BCs to use depends on the type of constraints***. Recall that essential BCs express which DOFs of the continuous body are constrained and how, while natural BCs express force equilibrium at the body's boundary. Thus, if the body is prevented to move somehow on a region of its outer boundary, usually denoted as S_u (see section **Error! Reference source not found.**), then an essential BCs must be considered. On the other hand, if an external load is applied to the body on a portion of its surface, usually denoted as S_F, then a natural BCs will be required. If neither a geometric restraint nor a load is applied to the body's external boundary, then it is assumed that a load of magnitude zero is applied. In the context of beam theory, both S_u and S_F represent the beam cross section at the beam ends.

We report some examples below by separately discussing axial, bending and torsional equilibrium separately, since these are decoupled problems. In general, the types of constraints and relative BCs are the following:

- Free: only natural BCs since no geometric restriction is placed on the beam.
- Clamped: only essential BCs are required since the beam is fully constrained.
- Simply supported: essential BCs are placed on vertical displacement, while natural BCs are required for balancing bending moments.

Axial equilibrium

Free – Free		$\begin{cases} EAu_{0\backslash x}(0) = -\hat{N}_{x0} \\ EAu_{0\backslash x}(l) = +\hat{N}_{xl} \end{cases}$
Clamp – Free	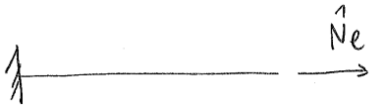	$\begin{cases} u_0(0) = 0 \\ EAu_{0\backslash x}(l) = +\hat{N}_{xl} \end{cases}$
Clamp – Clamp		$\begin{cases} u_0(0) = 0 \\ u_0(l) = 0 \end{cases}$

Bending equilibrium about the y-axis, so $x - z$ plane

Free – Free		$\begin{cases} EI_{yy}w_{0\backslash xxx}(0) = +\hat{Q}_{z0} \\ EI_{yy}w_{0\backslash xxx}(l) = -\hat{Q}_{zl} \\ EI_{yy}w_{0\backslash xx}(0) = +\hat{M}_{y0} \\ EI_{yy}w_{0\backslash xx}(l) = -\hat{M}_{yl} \end{cases}$
SS – SS		$\begin{cases} w_0(0) = 0 \\ w_0(l) = 0 \\ EI_{yy}w_{0\backslash xx}(0) = +\hat{M}_{y0} \\ EI_{yy}w_{0\backslash xx}(l) = -\hat{M}_{yl} \end{cases}$
Clamp – SS		$\begin{cases} w_0(0) = 0 \\ w_{0\backslash x}(0) = 0 \\ w_0(l) = 0 \\ EI_{yy}w_{0\backslash xx}(l) = +\hat{M}_{yl} \end{cases}$
Clamp – Clamp		$\begin{cases} w_0(0) = 0 \\ w_{0\backslash x}(0) = 0 \\ w_0(l) = 0 \\ w_{0\backslash x}(l) = 0 \end{cases}$
Clamp – Free	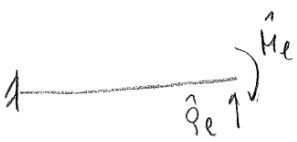	$\begin{cases} w_0(0) = 0 \\ w_{0\backslash x}(0) = 0 \\ EI_{yy}w_{0\backslash xxx}(l) = -\hat{Q}_{zl} \\ EI_{yy}w_{0\backslash xx}(l) = -\hat{M}_{yl} \end{cases}$

In the examples written above, writing the essential BCs is trivial, and natural BCs can be retrieved from the various equations presented in this chapter However, remembering them by heart is impractical, thus we show a methodology that one can use to derive them on the spot. Take the following problem, the first one of the above ones:

No geometric constraints are present, thus only natural BCs are required. The internal actions must develop at the boundaries of the beam to balance the applied loads. Internal actions are always taken in the positive direction of the respective axis. First, we isolate the sections on which the external forces are applied. Then, considering those sections, we also represent the internal actions, which for the section at the beam end $x = l$ implies that the direction of the internal actions is reversed (Figure 2.35). Then, force equilibrium is applied between the internal actions and the external loads, yielding:

$$\begin{cases} Q_z(0) + \hat{Q}_{z0} = 0 \\ Q_z(l) - \hat{Q}_{zl} = 0 \\ M_y(0) + \hat{M}_{y0} = 0 \\ M_y(l) - \hat{M}_{yl} = 0 \end{cases}$$

Since $Q_z = M_{y\backslash x}$ and from the CL $M_y = -EI_{yy}w_{0\backslash xx}$, we obtain the same set of BCs presented previously:

$$\begin{cases} M_{y\backslash x}(0) + \hat{Q}_{z0} = 0 \\ M_{y\backslash x}(l) - \hat{Q}_{zl} = 0 \\ M_y(0) + \hat{M}_{y0} = 0 \\ M_y(l) - \hat{M}_{yl} = 0 \end{cases} \rightarrow \begin{cases} -EI_{yy}w_{0\backslash xxx}(0) + \hat{Q}_{z0} = 0 \\ -EI_{yy}w_{0\backslash xxx}(l) - \hat{Q}_{zl} = 0 \\ -EI_{yy}w_{0\backslash xx}(0) + \hat{M}_{y0} = 0 \\ -EI_{yy}w_{0\backslash xx}(l) - \hat{M}_{yl} = 0 \end{cases} \rightarrow \begin{cases} EI_{yy}w_{0\backslash xxx}(0) = +\hat{Q}_{z0} \\ EI_{yy}w_{0\backslash xxx}(l) = -\hat{Q}_{zl} \\ EI_{yy}w_{0\backslash xx}(0) = +\hat{M}_{y0} \\ EI_{yy}w_{0\backslash xx}(l) = -\hat{M}_{yl} \end{cases}$$

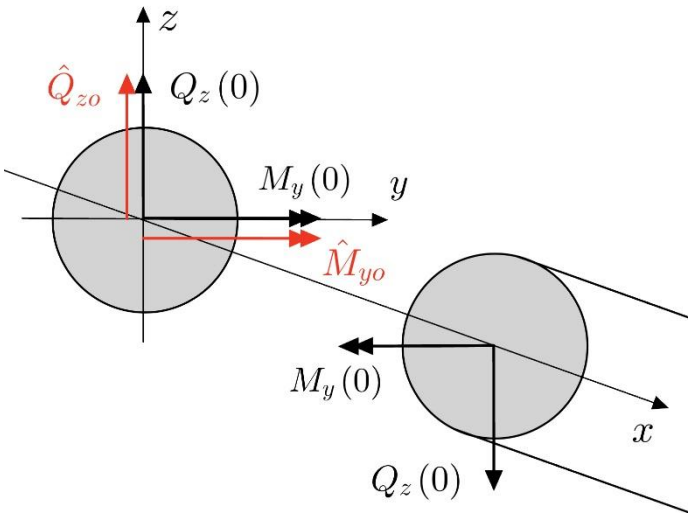

Figure 2.34: internal actions and applied loads at the left side of the beam $x = 0$.

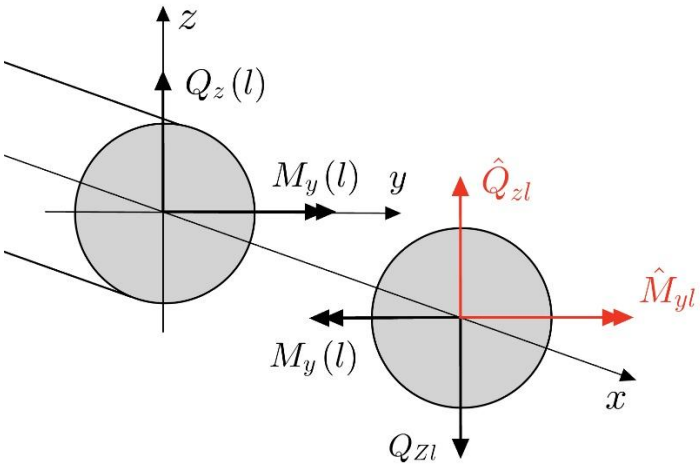

Figure 2.35: internal actions and applied loads at the right side of the beam $x = l$.

2.2.2.12. Variational form

The variational form of equilibrium, i.e. the PVW, has already been obtained during the definition of the model. We report here the formulation of the internal virtual work, both in terms of internal actions, for force-based approaches, and in terms of generalized strains, for displacement based-approaches. The internal virtual work in generally expressed as follows:

$$\delta W_D = \int_V \left(\delta \underline{\underline{\varepsilon}} : \underline{\underline{\sigma}}\right) dV = \int_V \left(\varepsilon_{ij}\sigma_{ij}\right) dV$$

For a kinematic model such as the Euler-Bernoulli one, the PVW can be expressed in terms of generalized quantities. Thus, the internal virtual work, instead of the strain and stress tensors, will be expressed in terms of generalized strains and generalized stresses. The generalized strains and stresses that have been found to be in energy conjugacy are the following:

$$\begin{cases} \varepsilon_{0xx} = u_{0\backslash x} & \rightarrow \quad N_x = \int_A \sigma_{xx} dA \\ k_y = -w_{0\backslash xx} & \rightarrow \quad M_y = \int_A z\sigma_{xx} dA \\ k_z = -v_{0\backslash xx} & \rightarrow \quad M_z = \int_A -y\sigma_{xx} dA \\ \theta' = \theta_{\backslash x} & \rightarrow \quad M_x = \int_A \left(\tau_{zx} y - \tau_{yx} z\right) dA \end{cases}$$

Thus, the general form of the PVW for an Euler-Bernoulli beam reads:

$$\delta W_D = \int_l \left(\delta\varepsilon_{0xx} N_x + \delta k_y M_y + \delta k_z M_z + \delta\theta_{\backslash x} M_x\right) dx$$

Using the CL (2.76), we can express the internal virtual work either fully in terms of generalized strains or stresses. The CL reads:

$$\begin{Bmatrix} N_x \\ M_y \\ M_z \\ M_x \end{Bmatrix} = \begin{bmatrix} EA & 0 & 0 & 0 \\ 0 & EI_{yy} & 0 & 0 \\ 0 & 0 & EI_{zz} & 0 \\ 0 & 0 & 0 & GJ \end{bmatrix} \begin{Bmatrix} \varepsilon_{0xx} \\ k_y \\ -k_z \\ \theta_{\backslash x} \end{Bmatrix}$$

The displacement-based form reads:

$$\begin{aligned} \delta W_D &= \int_l \left(\delta\varepsilon_{0xx} EA \varepsilon_{0xx} + \delta k_y M_y k_y + \delta k_z M_z k_z + \delta\theta_{\backslash x} M_x \theta_{\backslash x}\right) dx \\ &= \int_l \left(\delta u_{0\backslash x} EA u_{0\backslash x} + \delta w_{0\backslash xx} M_y w_{0\backslash xx} + \delta v_{0\backslash xx} M_z v_{0\backslash xx} + \delta\theta_{\backslash x} M_x \theta_{\backslash x}\right) dx \end{aligned}$$

Using the CL the other way around yields the force-based approach internal virtual work:

$$\delta W_D = \int_l \left(\delta N_x \frac{N_x}{EA} + \delta M_y \frac{M_y}{EI_{yy}} - \delta M_z \frac{M_z}{EI_{zz}} + \delta M_x \frac{M_x}{GJ}\right) dx$$

Thus, the internal virtual work of an Euler-Bernoulli beam can generally be expressed as follows:

$$\begin{aligned} \delta W_D &= \int_l \left(\delta\varepsilon_{0xx} N_x + \delta k_y M_y + \delta k_z M_z + \delta\theta_{\backslash x} M_x\right) dx = \\ &= \int_l \left(\delta\varepsilon_{0xx} EA \varepsilon_{0xx} + \delta k_y M_y k_y + \delta k_z M_z k_z + \delta\theta_{\backslash x} M_x \theta_{\backslash x}\right) dx = \\ &= \int_l \left(\delta u_{0\backslash x} EA u_{0\backslash x} + \delta w_{0\backslash xx} M_y w_{0\backslash xx} + \delta v_{0\backslash xx} M_z v_{0\backslash xx} + \delta\theta_{\backslash x} M_x \theta_{\backslash x}\right) dx = \\ &= \int_l \left(\delta N_x \frac{N_x}{EA} + \delta M_y \frac{M_y}{EI_{yy}} - \delta M_z \frac{M_z}{EI_{zz}} + \delta M_x \frac{M_x}{GJ}\right) dx \end{aligned} \tag{2.84}$$

3. Plates

A ***plate*** is a structural element that has one dimension much smaller than the other two ($t/ab \approx 1/20$). For plates, the general reference system is the following: x and y axes represent the in-plane coordinates, z-axis represents the out-of-plane coordinate. The reference system and the geometrical quantities are reported in Figure 3.1.

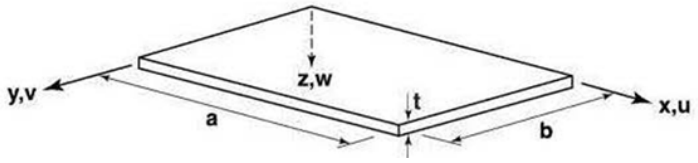

Figure 3.1: plate reference system.

3.1. Classical plate theory

Classical plate theory (CPT) is a ***kinematic model*** that describes the displacement field in the whole plate based only on the displacement of the midplane. CPT is based on the following ***assumptions***:

- Small displacements and rotations: described by the small strain tensor $\boldsymbol{\varepsilon}$ (1.7).
- Constitutive law: as is typical for kinematic models, the constitutive law is provided by the same type of approximation used for the kinematic law. It has been stated that kinematic plate theories describe the displacement in the plate based on the displacement of its midplane. The same kind of consideration is then used to obtain the CL, resulting in a plane stress state. Such CL has been introduced in section 1.2.3.3 for ***isotropic materials***, and it reads $\boldsymbol{\sigma} = \boldsymbol{Q\varepsilon}$, or in expanded form:

$$\begin{Bmatrix} \sigma_{xx} \\ \sigma_{yy} \\ \tau_{xy} \end{Bmatrix} = \frac{E}{1-\nu^2} \begin{bmatrix} 1 & \nu & 0 \\ \nu & 1 & 0 \\ 0 & 0 & \dfrac{1-\nu}{2} \end{bmatrix} \begin{Bmatrix} \varepsilon_{xx} \\ \varepsilon_{yy} \\ \gamma_{xy} \end{Bmatrix} \tag{3.1}$$

- Kirchhoff hypotheses: these are hypotheses on which the kinematic law is based upon. Kirchhoff hypotheses assume that during a bending action of the plate (1) its midplane is

not deformed and (2) its cross sections remain normal to midplane and undeformed. The latter is sometimes referred to as ***normality condition***.

3.1.1. Generalized coordinates

Kirchhoff hypotheses lead to the following kinematic law for a so-called Kirchhoff plate:

$$\begin{cases} u(x_0, y_0, z) = u_0(x_0, y_0) + z\theta_x = u_0(x_0, y_0) - zw_{0/x} \\ v(x_0, y_0, z) = v_0(x_0, y_0) + z\theta_y = v_0(x_0, y_0) - zw_{0/y} \\ w(x_0, y_0, z) \approx w_0(x_0, y_0) \end{cases} \tag{3.2}$$

Here, the quantities denoted with the index 0 are related to the midplane of the plate. Thus, $\boldsymbol{x}_0 = \{x_0, y_0\}$ are the in-plane coordinates of the midplane of the plate, while $\boldsymbol{u}_0 = \{u_0, v_0, w_0\}$ are the its displacement components. Similarly to the case of the Euler-Bernoulli beam, discussed in section 2.2.1, the normality condition allows to express the cross-section rotations θ_x and θ_y as first derivatives of the transverse displacement of the midplane w_0, as depicted in Figure 3.2. Moreover, it is important to remark that, as it's typical of kinematic models, the kinematic law allows to describe the displacement of the whole continuous 3D body, in this case the plate, based only on the displacements of an element of lower dimensionality, in this case the 2D midplane.

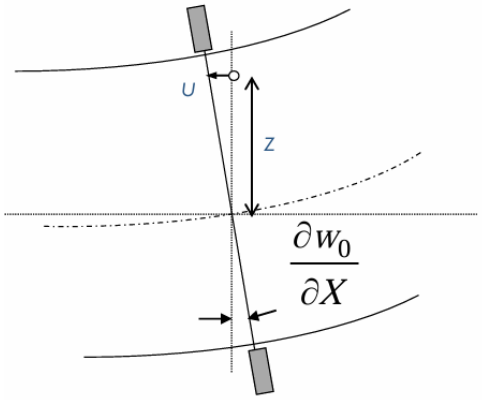

Figure 3.2: midplane rotation contribution to displacement.

It follows from the kinematic law (3.2) that the generalized coordinates $\boldsymbol{u}_0$ of this model are the displacements components of the midplane:

$$\underline{u}_0(x_0, y_0) = \begin{Bmatrix} u_0(x_0, y_0) \\ v_0(x_0, y_0) \\ w_0(x_0, y_0) \end{Bmatrix} \tag{3.3}$$

3.1.2. Generalized strains

A compatible strain field is automatically obtained if we derive the strain components, starting from the displacement field of (3.2), using the small strain tensor definition of equation (1.7). This yields:

$$\begin{cases} \varepsilon_{xx} = u_{/x} = u_{0/x} - zw_{/xx} = \varepsilon_{0xx} + zk_{xx} \\ \varepsilon_{yy} = v_{/y} = v_{0/y} - zw_{/yy} = \varepsilon_{0yy} + zk_{yy} \\ \varepsilon_{xy} = \frac{1}{2}(u_{/y} + v_{/x}) = \frac{1}{2}(u_{0/y} + v_{0/x}) - zw_{/xy} = \varepsilon_{0xy} + zk_{xy} \end{cases}$$

All other strain components are null. Thus, similarly to the Euler-Bernoulli beam model (section 2.2.2), ***the Kirchhoff plate model does not account for shear deformability*** since $\gamma_{xz} = \gamma_{yz} = 0$. As for the EB beam model, this is a direct consequence of the normality condition. The strain field inside the plate can be expressed as the sum of two contributions. Membranal strains $\boldsymbol{\varepsilon_s}$ represent the strains associated to in-plane deformation of the midplane, while flexural strains $\boldsymbol{k}$ represent the strains induced by bending actions. In fact, the entries of the flexural strains are curvatures, which due to the normality condition can be expressed as second derivatives of the transverse displacement of the midplane w_0. The strain field can then be expressed in compact form as follows:

$$\underline{\varepsilon}(x_0, y_0, z) = \underline{\varepsilon}_0(x_0, y_0) + z\underline{k}(x_0, y_0) \tag{3.4}$$

Thus, the ***generalized strains*** of the Kirchhoff plate model are the membranal and flexural strains:

$$\underline{\varepsilon}_0(x_0, y_0) = \begin{cases} \varepsilon_{0xx} = u_{0/x} \\ \varepsilon_{0yy} = v_{0/y} \\ \varepsilon_{0xy} = \dfrac{1}{2}\left(u_{0/y} + v_{0/x}\right) \end{cases} \qquad \underline{k}(x_0, y_0) \begin{cases} k_{xx} = -w_{0\backslash xx} \\ k_{yy} = -w_{0\backslash yy} \\ k_{xy} = -w_{0\backslash xy} \end{cases} \tag{3.5}$$

3.1.3. Generalized stresses

The generalized stresses are those quantities that are in energy conjugacy with the generalized strains. Thus, in order to define the generalized stresses one must write the internal virtual work and elaborate the expression in order to write it in terms of the generalized strains and stresses. This leads to the definition of the ***generalized stresses as the internal actions***, which are depicted in Figure 3.3. In this section we skip the procedure and present the results only. The internal actions are obtained by integrating the stress components through the thickness, assuming that the mid plane is at $z_0 = 0$. According to a plane-stress CL and the generalized strains of equation (3.4), the stresses can be expressed as follows:

$$\underline{\sigma} = \underline{\underline{Q}}\,\underline{\varepsilon} = \underline{\underline{Q}}\left(\underline{\varepsilon}_s + z\underline{k}\right) \tag{3.6}$$

Integration through the thickness provides with:

$$\begin{cases} \underline{N} = \displaystyle\int_{-\frac{t}{2}}^{\frac{t}{2}} \underline{\sigma} dz = \underline{\underline{Q}} \int_{-\frac{t}{2}}^{\frac{t}{2}} \left(\underline{\varepsilon}_0 + z\underline{k}\right) dz = \underline{\underline{Q}} t \underline{\varepsilon}_0 = \underline{\underline{A}}\underline{\varepsilon}_0 \\ \underline{M} = \displaystyle\int_{-\frac{t}{2}}^{\frac{t}{2}} \underline{\sigma} z dz = \underline{\underline{Q}} \int_{-\frac{t}{2}}^{\frac{t}{2}} \left(\underline{\varepsilon}_0 + z\underline{k}\right) z dz = \underline{\underline{Q}} \frac{t^3}{12} \underline{k} = \underline{\underline{D}}\underline{k} \end{cases} \tag{3.7}$$

Here $\boldsymbol{N} = \{N_x, N_y, N_{xy}\}$ are the in-plane forces per until length $[N/m]$ acting on the midplane of the plate, while $\boldsymbol{M} = \{M_x, M_y, M_{xy}\}$ are the moments per unit length $[Nm/m]$ acting about the midplane of the plate. These sets of loads, i.e. the generalized stresses of this model, are defined as follows:

$$N_{xx} = \int_{-\frac{t}{2}}^{\frac{t}{2}} \tau_{xx} dz \qquad M_{xx} = \int_{-\frac{t}{2}}^{\frac{t}{2}} \tau_{xx} z dz$$
$$N_{yy} = \int_{-\frac{t}{2}}^{\frac{t}{2}} \tau_{yy} dz \qquad M_{yy} = \int_{-\frac{t}{2}}^{\frac{t}{2}} \tau_{yy} z dz \qquad Q_x = \int_{-\frac{t}{2}}^{\frac{t}{2}} \tau_{zx} dz \qquad (3.8)$$
$$N_{xy} = \int_{-\frac{t}{2}}^{\frac{t}{2}} \tau_{xy} dz \qquad M_{xy} = \int_{-\frac{t}{2}}^{\frac{t}{2}} \tau_{xy} z dz \qquad Q_y = \int_{-\frac{t}{2}}^{\frac{t}{2}} \tau_{zy} dz$$

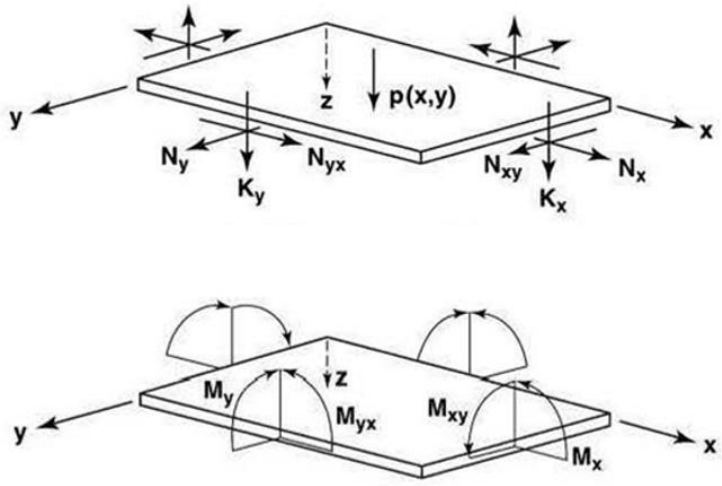

Figure 3.3: forces (top) and moments (bottom) per unit length acting on and about the plate's midplane.

In equations (3.7) we introduced the ***membranal stiffness matrix A***, which relates membranal strains $\boldsymbol{\varepsilon}_0$ to in-plane forces per unit length $\boldsymbol{N}$, while the ***flexural stiffness matrix D*** related flexural strains $\boldsymbol{k}$ to the moments per unit length acting on the midplane $\boldsymbol{M}$. Such matrices are defined as follows:

$$\begin{cases} \underline{\underline{A}} = t\underline{\underline{Q}} = t\dfrac{E}{1-\nu^2}\begin{bmatrix} 1 & \nu & 0 \\ \nu & 1 & 0 \\ 0 & 0 & \dfrac{1-\nu}{2} \end{bmatrix} = A\begin{bmatrix} 1 & \nu & 0 \\ \nu & 1 & 0 \\ 0 & 0 & \dfrac{1-\nu}{2} \end{bmatrix} \\ \underline{\underline{D}} = \dfrac{t^3}{12}\underline{\underline{Q}} = \dfrac{t^3}{12}\dfrac{E}{1-\nu^2}\begin{bmatrix} 1 & \nu & 0 \\ \nu & 1 & 0 \\ 0 & 0 & \dfrac{1-\nu}{2} \end{bmatrix} = D\begin{bmatrix} 1 & \nu & 0 \\ \nu & 1 & 0 \\ 0 & 0 & \dfrac{1-\nu}{2} \end{bmatrix} \end{cases} \qquad (3.9)$$

Where we introduced the ***membranal stiffness*** A and ***bending stiffness*** D of the plate, defined as follows:

$$\begin{cases} A = t\dfrac{E}{(1-\nu^2)} \\ D = \dfrac{t^3}{12}\dfrac{E}{(1-\nu^2)} \end{cases} \qquad (3.10)$$

Typically, the CL is written by defining the two by two ABD matrix, where matrix $\boldsymbol{B}$ is the one in entries (2,1) and (1,2). Intuitively, because matrix $\boldsymbol{B}$ sits in the extra-diagonal entries, it relates membranal loads $\boldsymbol{N}$ to bending displacement $\boldsymbol{k}$, or curvatures, and it also relates moments $\boldsymbol{M}$ to

purely membranal strains $\boldsymbol{\varepsilon}_0$. ***For an isotropic plate matrix B is always null, implying that membranal and flexural actions are always decoupled***. Thus, the CL of an isotropic Kirchhoff plate is the following:

$$\begin{Bmatrix} \underline{N} \\ \underline{M} \end{Bmatrix} = \begin{bmatrix} \underline{\underline{A}} & \underline{\underline{0}} \\ \underline{\underline{0}} & \underline{\underline{D}} \end{bmatrix} \begin{Bmatrix} \underline{\varepsilon_0} \\ \underline{k} \end{Bmatrix} \tag{3.11}$$

Or in compact form:

$$\underline{F} = \underline{\underline{K}}\, \underline{\varepsilon} \tag{3.12}$$

3.1.4. Transverse shear stresses

From the solution of plate equilibrium, which in a displacement-based approach is $w(x_0, y_0)$, it's possible to recover the transverse shear forces per unit length $\boldsymbol{Q}$ or $\boldsymbol{K}$ in Figure 3.3. From such generalized stresses, the actual transverse shear stresses τ_{xz} and τ_{yz} can be recovered. In order to do so, first integrate of the moment equilibrium equations through the plate thickness to obtain $Q_i = Q_i(M_{ij})$, then apply the plane stress CL to express $M_{ij} = M_{ij}(w_{/ij})$. At this point a theory is required to evaluate how Q_x and Q_y are distributed.

$$\begin{cases} Q_x = M_{yy/x} + M_{xy/y} \\ Q_y = M_{xx/y} + M_{xy/x} \end{cases} \quad \text{where} \quad \begin{cases} M_{xx} = -D\left(w_{/xx} + \nu w_{/yy}\right) \\ M_{yy} = -D\left(w_{/yy} + \nu w_{/xx}\right) \\ M_{xy} = -D(1-\nu) w_{/xy} \end{cases}$$

Then, the strains are computed simply as $\tau_{iz} = Q_i/t$. It must be pointed out that this is a way to recover the transverse generalized stresses, however their definition is that of equation (3.8). In fact, having assumed that the plate is subject to a plane-stress state implies by definition that $\tau_{xz} = \tau_{yz} = 0$. It follows that being able to recover such stress components represents an ***inconsistency in the formulation of the model***. This can be explained by considering that the shear stiffness of a thin plate is much higher than its bending stiffness, but it is not null. Thus, although τ_{xz} and τ_{yz} are negligible, and thus we do neglect them, this is an approximation and they are not actually zero. Moreover, in order to guarantee equilibrium, it can be proven that the transverse generalized stresses $\boldsymbol{Q}$ must be null on the top and bottom surfaces of the plate.

3.1.5. Equilibrium equations

In this section we want to obtain the most general formulation of the equilibrium equations for a Kirchhoff plate. In order to do so, we start from the linear momentum equilibrium equation (1.26) in the static case and neglecting body forces $\boldsymbol{a} = \boldsymbol{b} = \boldsymbol{0}$. Such equation reads:

$$\sigma_{ij/j} = 0 \quad \rightarrow \quad \begin{cases} \sigma_{xx/x} + \tau_{xy/y} + \tau_{xz/z} = 0 \\ \tau_{yx/x} + \sigma_{yy/y} + \tau_{yz/z} = 0 \\ \tau_{zx/x} + \tau_{zy/y} + \sigma_{zz/z} = 0 \end{cases}$$

Consider the generic plate subject to the forces and stresses depicted in Figure 3.3. We'll refer to the distributed pressure acting on the plate upper surface as q instead of p. Integration through

the thickness of these equilibrium equations leads to them being expressed as a function of the internal actions $\boldsymbol{N}, \boldsymbol{M}$ and $\boldsymbol{Q}$.

3.1.5.1. Internal actions form

In this section we obtain the equilibrium equations in terms of the internal actions, generalized stresses, of a Kirchhoff plate.

Membranal internal actions. We directly integrate the three equations above:

$$\int_{-\frac{t}{2}}^{\frac{t}{2}}(\sigma_{xx/x}+\tau_{xy/y}+\tau_{xz/z})dz=\int_{-\frac{t}{2}}^{\frac{t}{2}}\sigma_{xx/x}dz+\int_{-\frac{t}{2}}^{\frac{t}{2}}\tau_{xy/y}dz+\int_{-\frac{t}{2}}^{\frac{t}{2}}\tau_{xz/z}dz=$$
$$=N_{xx/x}+N_{xy/y}+0=0$$

$$\int_{-\frac{t}{2}}^{\frac{t}{2}}(\tau_{yx/x}+\sigma_{yy/y}+\tau_{yz/z})dz=\int_{-\frac{t}{2}}^{\frac{t}{2}}\tau_{yx/x}dz+\int_{-\frac{t}{2}}^{\frac{t}{2}}\sigma_{yy/y}dz+\int_{-\frac{t}{2}}^{\frac{t}{2}}\tau_{yz/z}dz=$$
$$=N_{yx/x}+N_{yy/y}+0=0$$

$$\int_{-\frac{t}{2}}^{\frac{t}{2}}(\tau_{zx/x}+\tau_{zy/y}+\sigma_{zz/z})dz=\int_{-\frac{t}{2}}^{\frac{t}{2}}\tau_{zx/x}dz+\int_{-\frac{t}{2}}^{\frac{t}{2}}\tau_{zy/y}dz+\int_{-\frac{t}{2}}^{\frac{t}{2}}\sigma_{zz/z}dz=$$
$$=Q_{x/x}+Q_{y/y}+q=0$$

Note that in these integrals we switched the derivation/integration order to obtain the force resultants. Taking as an example the first integral of the first equation, we simply write:

$$\int_{-\frac{t}{2}}^{\frac{t}{2}}\tau_{xx/x}dz=\frac{\partial}{\partial x}\int_{-\frac{t}{2}}^{\frac{t}{2}}\tau_{xx}dz=\frac{\partial}{\partial x}N_{xx}=N_{xx/x}$$

And the same approach has been used for many of the integrals hereby computed. Place special attention to the last integrals of the first two equilibrium equation. These integrals yields zero because τ_{xz} and τ_{yz} must be null at the top and bottom surfaces of the plate. Thus:

$$\int_{-\frac{t}{2}}^{\frac{t}{2}}\tau_{xz/z}dz=\tau_{xz}|_{-\frac{h}{2}}^{+\frac{h}{2}}=0-0=0 \qquad \int_{-\frac{t}{2}}^{\frac{t}{2}}\tau_{yz/z}dz=\tau_{yz}|_{-\frac{h}{2}}^{+\frac{h}{2}}=0-0=0$$

Lastly, the last integral of the last equilibrium equation yields the surface load acting on the top surface of the plate. This integral is computed as follows:

$$\int_{-\frac{t}{2}}^{\frac{t}{2}}\tau_{zz/z}dz=\tau_{zz}|_{-\frac{h}{2}}^{+\frac{h}{2}}=q-0=q$$

Internal moments. We multiply the equilibrium equations by z and then perform the integrals:

$$\int_{-\frac{t}{2}}^{\frac{t}{2}}(\tau_{xx/x}+\tau_{xy/y}+\tau_{xz/z})zdz=\cdots=M_{xx/x}+M_{xy/y}-Q_x=0$$

$$\int_{-\frac{t}{2}}^{\frac{t}{2}}(\tau_{yx/x}+\tau_{yy/y}+\tau_{yz/z})zdz=\cdots=M_{yx/x}+M_{yy/y}-Q_y=0$$

$$\int_{-\frac{t}{2}}^{\frac{t}{2}}(\tau_{zx/x}+\tau_{zy/y}+\tau_{zz/z})zdz=\cdots=Q_{x/x}+Q_{y/y}+q=0$$

Note that in these last three equations, Q_x and Q_y are obtained integrating by parts as follows:

$$(\tau_{xz}\cdot z)_{/z}=\tau_{xz/z}\cdot z+\tau_{xz}\quad\rightarrow\quad\tau_{xz/z}\cdot z=(\tau_{xz}\cdot z)_{/z}-\tau_{xz}$$

$$\int_{-\frac{t}{2}}^{\frac{t}{2}}\tau_{xz/z}\cdot zdz=\int_{-\frac{t}{2}}^{\frac{t}{2}}((\tau_{xz}\cdot z)_{/z}-\tau_{xz})dz=(\tau_{xz}\cdot z)|_{-\frac{h}{2}}^{+\frac{h}{2}}-Q_x=0-Q_x=-Q_x$$

Substituting the first two moment equilibrium equations into the last force equilibrium equation yields:

$$\begin{aligned}Q_{x/x}+Q_{y/y}+q&=M_{xx/xx}+M_{xy/yx}+M_{yx/xy}+M_{yy/yy}+q\\&=M_{xx/xx}+2M_{xy/yx}+M_{yy/yy}+q=0\end{aligned}$$

Thus, the ***equilibrium equations in terms of stress resultants*** can be expressed as follows:

$$\begin{cases}N_{xx/x}+N_{xy/y}=0\\N_{yx/x}+N_{yy/y}=0\\M_{xx/xx}+2M_{xy/yx}+M_{yy/yy}+q=0\end{cases}\tag{3.13}$$

3.1.5.2. Displacement form

If the solution of the structural problem is sought via a displacement-based approach, as it's typical for numerical implementation (FEM) or buckling analysis, the above equations must be expressed in terms of the displacements components. Here, we focus only on the out-of-plane equilibrium equation, since this is the relevant one in buckling analysis. Thus, we first express the moments via the constitutive law (3.1), then we invoke the kinematic law (3.2) to obtain the displacement formulation. Note that still no buckling related simplification has been made.

$$M_{xx} = \int_{-\frac{t}{2}}^{+\frac{t}{2}} \tau_{xx} z dz = \int_{-\frac{t}{2}}^{+\frac{t}{2}} \frac{E}{1-\nu^2}\left(\varepsilon_{xx} + \nu\varepsilon_{yy}\right) z dz =$$

$$= \int_{-\frac{t}{2}}^{+\frac{t}{2}} \frac{E}{1-\nu^2}\left(u_{s/x} - z w_{/xx} + \nu v_{s/y} - \nu z w_{/yy}\right) z dz =$$

$$= -\frac{E}{1-\nu^2}\int_{-\frac{t}{2}}^{+\frac{t}{2}} z^2\left(w_{/xx} + \nu w_{/yy}\right) dz = -\frac{E}{1-\nu^2}\frac{t^3}{12}\left(w_{/xx} + \nu w_{/yy}\right) =$$

$$= -D\left(w_{/xx} + \nu w_{/yy}\right)$$

$$M_{yy} = \int_{-\frac{t}{2}}^{+\frac{t}{2}} \tau_{yy} z dz = \int_{-\frac{t}{2}}^{+\frac{t}{2}} \frac{E}{1-\nu^2}\left(\varepsilon_{yy} + \nu\varepsilon_{xx}\right) z dz =$$

$$= \int_{-\frac{t}{2}}^{+\frac{t}{2}} \frac{E}{1-\nu^2}\left(v_{s/y} - z w_{/yy} + \nu u_{s/x} - \nu z w_{/xx}\right) z dz =$$

$$= -\frac{E}{1-\nu^2}\int_{-\frac{t}{2}}^{+\frac{t}{2}} z^2\left(w_{/yy} + \nu w_{/xx}\right) dz = -\frac{E}{1-\nu^2}\frac{t^3}{12}\left(w_{/yy} + \nu w_{/xx}\right) =$$

$$= -D\left(w_{/yy} + \nu w_{/xx}\right)$$

$$M_{xy} = \int_{-\frac{t}{2}}^{+\frac{t}{2}} \tau_{xy} z dz = \int_{-\frac{t}{2}}^{+\frac{t}{2}} \frac{E}{1+\nu}\varepsilon_{xy} z dz = \int_{-\frac{t}{2}}^{+\frac{t}{2}} \frac{E}{1+\nu}\left[\frac{1}{2}\left(u_{s/y} + v_{s/x}\right) - z w_{/xy}\right] z dz =$$

$$= -\frac{E}{1-\nu^2}(1-\nu)\int_{-\frac{t}{2}}^{+\frac{t}{2}} z^2 w_{/xy} dz = -\frac{E}{1-\nu^2}\frac{t^3}{12}(1-\nu) w_{/xy}$$

$$= -(1-\nu) D w_{/xy}$$

Substitution in the out of plane equilibrium equation yields the generic out of plane equilibrium equation of a classic plate in terms of displacements:

$$M_{xx/xx} + 2M_{xy/yx} + M_{yy/yy} + q$$

$$= -D\left(w_{/xxxx} + \nu w_{/yyxx}\right) - 2(1-\nu) D w_{/xxyy} - D\left(w_{/yyyy} + \nu w_{/xxyy}\right) + q$$

$$= -D\left(w_{/xxyy} + 2w_{/xxyy} + w_{/yyyy}\right) + q$$

$$\nabla^4 w = w_{/xxxx} + 2w_{/xxyy} + w_{/yyyy} = \frac{q}{D} \tag{3.14}$$

The ***most general form of the equilibrium equations for a classic plate*** then becomes:

$$\boxed{\begin{cases} N_{xx/x} + N_{xy/y} = 0 \\ N_{yx/x} + N_{yy/y} = 0 \\ \nabla^4 w = q/D \end{cases}} \tag{3.15}$$

3.1.6. Variational formulation

We present in this section a very generic variational formulation of a Kirchhoff plate, which will be used in section 6.4 in order to discuss plate and shell elements. Let Ω be the area of the plate midplane and Γ_0 its boundary, the internal virtual work δW_D can be expressed as follows:

$$\delta W_D = \int_V \delta\underline{\underline{\varepsilon}} : \underline{\underline{\sigma}} dV = \int_\Omega \left(\delta\underline{\varepsilon}_0^T \underline{N} + \delta\underline{k}^T \underline{M}\right) d\Omega = \int_\Omega \left(\delta\underline{\varepsilon}_0^T \underline{\underline{A}}\, \underline{\varepsilon}_0 + \delta\underline{k}^T \underline{\underline{D}}\, \underline{k}\right) d\Omega \tag{3.16}$$

In order to define the external virtual work δW_e the external loads must be defined. With respect to Figure 3.4, let p be external pressure applied to the midplane surface Ω. Let $\hat{Q}_n$ be the externally applied transverse shear load per unit length applied to the plate's boundary Γ_σ. Let $\hat{N}_n$ and $\hat{N}_s$ be in plane normal and shear loads per unit length, respectively, applied to the plate's boundary Γ_σ. Let $\hat{M}_n$ and $\hat{M}_s$ be externally applied normal and shear moments per unit length, respectively, applied to the plate's boundary Γ_σ. Then, the virtual external work δW_e can be expressed as follows:

$$\delta W_e = \int_\Omega p\delta w \, d\Omega + \int_{\Gamma_\sigma} \left[\delta u_{0n}\hat{N}_n + \delta u_{0s}\hat{N}_s + \delta w_0 \hat{Q}_n + \delta\theta_n \hat{M}_n + \delta\theta_s \hat{M}_s\right] d\Gamma_\sigma \tag{3.17}$$

Here, u_{0n} and u_{0s} are the in-plane normal and shear displacement components that are in energy conjugacy with $\hat{N}_n$ and $\hat{N}_s$, respectively. The same consideration applies to w_0, θ_n and θ_s. Denoting the imposed displacements with the bar symbol, for example $\bar{u}$, the essential BCs of the problem will then be:

$$\begin{cases} u_{0n} = \bar{u}_{0n} \\ u_{0s} = \bar{u}_{0s} \\ w_0 = \bar{w}_0 \\ \theta_n = \bar{\theta}_n \\ \theta_s = \bar{\theta}_s \end{cases} \quad \text{on } \Gamma_\sigma \tag{3.18}$$

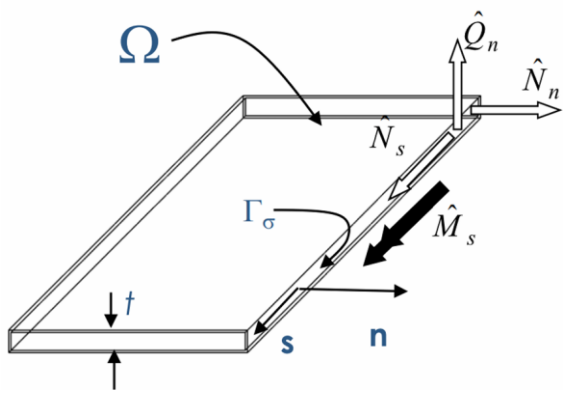

Figure 3.4: Loads acting on a plate.

3.2. Mindlin plate theory

The Mindlin plate theory (MPT) is another kinematic plate theory. The difference between MPT and CPT is of kinematic nature, and it affect the generalized coordinates, the generalized strains and the transverse shear stress resultants $\boldsymbol{Q}$. For this reason, we only discuss these aspects, as the rest of the formulation of the Mindlin plate model is identical to the Kirchhoff plate model.

The ***fundamental difference*** between the CPT and the MPT is that the latter does not enforce the normality condition during bending. This implies that the cross sections of the plate do not remain normal the midplane during bending. More precisely, the cross sections of a Mindlin plate rotate more than those of a Kirchhoff plate. We will discuss in the section dedicated to the generalized strains of this model that this additional rotation is due to the shear strains γ_{xz} and γ_{yz}. A graphical representation of the deformation process of a Mindlin plate cross section during bending is presented in Figure 3.5.

It will be discussed in the next sections that this kinematic behavior of the Mindlin plate implies that its curvatures are not second derivatives of the transverse displacement w. Rather, they are first derivatives of the cross section rotations θ_x and θ_y, which are now independent DOFs from w_0. The ***numerical implications*** of this are that Mindlin shell elements, discussed in section 6.4, require C^0 continuity of the interpolating functions of the generalized coordinates in a finite element procedure. Contrarily, shell elements based on CPT, which are never actually used, would require C^1 continuous interpolating functions of the generalized coordinates due to the curvatures being second derivatives of w_0.

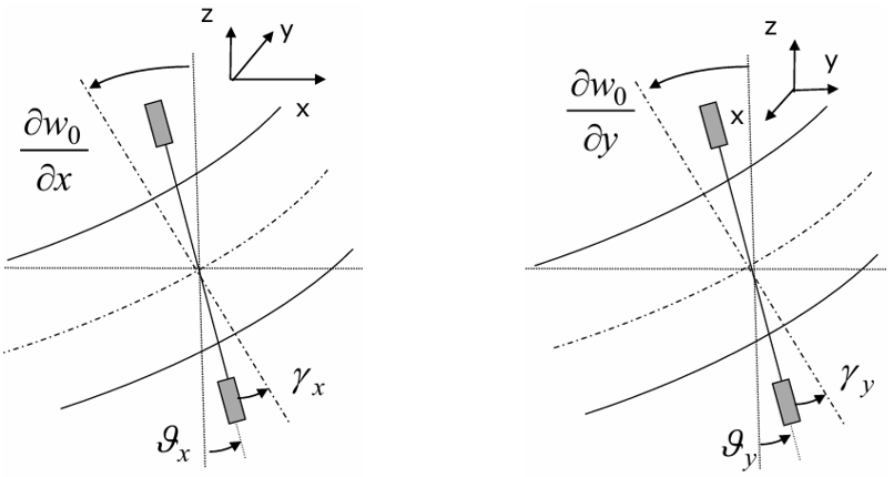

Figure 3.5: rotation of the cross sections of a Mindlin plate in the z-x plane (left) and z-y plane (right).

3.2.1. Generalized coordinates

The kinematic law of a Mindlin plate is very similar to that of a Kirchhoff plate. For a Mindlin plate we want again to identify those quantities related to the midplane that allow us to describe the displacement field in the whole plate. The difference with respect to CPT is that the rotations of the cross sections of the plate cannot be approximated as transverse displacements derivatives, i.e.

$$\begin{cases} \theta_x = -w_{\backslash x} \\ \theta_y \neq -w_{\backslash y} \end{cases}$$

The kinematic law of a Mindlin plate is obtained as follows:

$$\begin{cases} u(x_0, y_0, z) = u_0(x_0, y_0) - z\theta_x \\ v(x_0, y_0, z) = v_0(x_0, y_0) - z\theta_y \\ w(x_0, y_0, z) \approx w_0(x_0, y_0) \end{cases} \tag{3.19}$$

Thus, the generalized coordinates of a Mindlin plate are five, against the three of the Kirchhoff plate (3.3), and they read:

$$\underline{u}_0(x_0, y_0) = \begin{Bmatrix} u_0(x_0, y_0) \\ v_0(x_0, y_0) \\ w_0(x_0, y_0) \end{Bmatrix} \quad \text{and} \quad \underline{\theta}(x_0, y_0) = \begin{Bmatrix} \theta_x(x_0, y_0) \\ \theta_y(x_0, y_0) \end{Bmatrix} \tag{3.20}$$

3.2.2. Generalized strains

The generalized strains are obtained by applying the definition of the small strain tensor (1.7) to the displacement field of a Mindlin plate (3.19). This leads to:

$$\begin{cases} \varepsilon_{xx} = u_{/x} = u_{0/x} - z\theta_{x\backslash x} = \varepsilon_{0xx} + zk_{xx} \\ \varepsilon_{yy} = v_{/y} = v_{0/y} - z\theta_{y\backslash y} = \varepsilon_{0yy} + zk_{yy} \\ \varepsilon_{xy} = \frac{1}{2}\left(u_{/y} + v_{/x}\right) = \frac{1}{2}\left(u_{0/y} + v_{0/x}\right) - z\left(\theta_{x/y} + \theta_{y/x}\right) = \varepsilon_{0xy} + zk_{xy} \end{cases}$$

Transverse shear strains will be discussed in the next section. Similarly to what has been outlined for a Kirchhoff plate, we can identify membranal strains $\boldsymbol{\varepsilon}_0$ and flexural strains $\boldsymbol{k}$. Membranal strains have the exact same formulation to those of a Kirchhoff plate, while flexural strains are different. This is due to the fat that curvatures are no longer obtained as second derivatives of w, but as derivatives of the generic rotations θ_x and θ_y. The strain field can then be expressed in compact form as

$$\underline{\varepsilon}(x_0, y_0, z) = \underline{\varepsilon}_0(x_0, y_0) + z\underline{k}(x_0, y_0) \tag{3.21}$$

and the generalized strains of the Mindlin plate are:

$$\underline{\varepsilon}_0(x_0, y_0) = \begin{cases} \varepsilon_{0xx} = u_{0/x} \\ \varepsilon_{0yy} = v_{0/y} \\ \varepsilon_{0xy} = \frac{1}{2}\left(u_{0/y} + v_{0/x}\right) \end{cases}$$

$$\underline{k}(x_0, y_0) = \begin{cases} k_{xx} = -\theta_{x/x} \\ k_{yy} = -\theta_{y/y} \\ k_{xy} = -\theta_{x/y} - \theta_{y/x} \end{cases} \tag{3.22}$$

3.2.3. Shear strains and stresses

In the previous section we limited the discussion only to the generalized strains. For this reason, we only discussed the in-plane strain components $\varepsilon_{xx}, \varepsilon_{yy}$ and ε_{xy}. Identifying the membranal and flexural strain components leads to the identification of the curvatures as derivatives of the rotation angles θ_x and θ_y. It has been stated that these angles are not the second derivatives of the transverse displacement w due to the effect of shear strains. Here, we compute the shear strains γ_{xz} and γ_{yz} starting from the kinematic law of the Mindlin plate (3.19) in order to outline such aspect of this model. The shear strains are obtained as follows:

$$\begin{cases}\gamma_{xz} = w_{/x} + u_{/z} = w_{0/x} + (u_0 - z\theta_x)_{/z} = w_{0/x} - \theta_x \\ \gamma_{yz} = w_{/y} + v_{/z} = w_{0/y} + (v_0 - z\theta_y)_{/z} = w_{0/y} - \theta_y\end{cases}$$

And thus the cross section's rotations are obtained as

$$\begin{cases}-\theta_x = \gamma_{xz} - w_{0/x} \\ -\theta_y = \gamma_{yz} - w_{0/y}\end{cases}$$

Clearly, if the plate's shear deformability can be neglected, and thus $\gamma_{xz} = \gamma_{yz} = 0$, the cross section rotations revert back to what is provided by the Kirchhoff plate model. From the above formulation of the shear strains we can easily recover the corresponding shear stresses. According to the CL of an isotropic continuum body (1.18), the shear stresses are obtain as

$$\begin{cases}\tau_{xz} = G\gamma_{xz} = G(w_{0/x} - \theta_x) \\ \tau_{yz} = G\gamma_{yz} = G(w_{0/y} - \theta_y)\end{cases} \tag{3.23}$$

Then, the transverse shear stress resultants $\boldsymbol{Q}$ are obtained via integration through the thickness of the shear stresses. This yields:

$$\begin{cases}Q_x = \int_{-\frac{t}{2}}^{\frac{t}{2}} \tau_{xz} dz = t\tau_{xz} = tG\gamma_{xz} \\ Q_y = \int_{-\frac{t}{2}}^{\frac{t}{2}} \tau_{yz} dz = t\tau_{yz} = tG\gamma_{yz}\end{cases} \tag{3.24}$$

3.2.4. Cylindrical bending

Notice from the expression of the transverse shear stresses of equation (3.23) that they are constant with the thickness coordinate z. The reader should recall from previous courses that the correct transverse shear stress distribution is parabolic with the maximum value at the mid plane $z = 0$ while being null at the top and bottom plate surfaces $z = \pm t/2$.

In order to obtain a solution similar to the one just described, we employ the cylindrical bending correction. It is imagined to wrap the plate around a cylinder, so that the geometric properties of the plate are constant along the cylinder axis y. It is also assumed that the stresses are constant along the y-axis. The equilibrium along the x-axis reads:

$$dy \int_{-\frac{t}{2}}^{z} \sigma_{xx} dz + dxdy\tau_{xz}(z) = 0 \quad \rightarrow \quad \tau_{xz}(z) = -\frac{d}{dx}\int_{-\frac{t}{2}}^{z} \sigma_{xx} dz$$

Assuming the plate behaves like a beam and that σ_{xx} is only due to bending action, we'll write:

$$\tau_{xz}(z) = -\frac{d}{dx}\int_{-\frac{t}{2}}^{z} \frac{M_y}{I_{yy}} z dz = -\frac{d}{dx}\int_{-\frac{t}{2}}^{z} \frac{M_y}{\frac{t^3}{12}} z dz = -\frac{dM_y}{dx}\frac{12}{t^3}\int_{-\frac{t}{2}}^{z} z dz = -Q_x \frac{12}{t^3}\left(\frac{z^2}{2} - \frac{t^2}{8}\right)$$

$$\tau_{xz}(z) = Q_x \frac{3}{2t}\left[1 - \left(\frac{2z}{t}\right)^2\right] \tag{3.25}$$

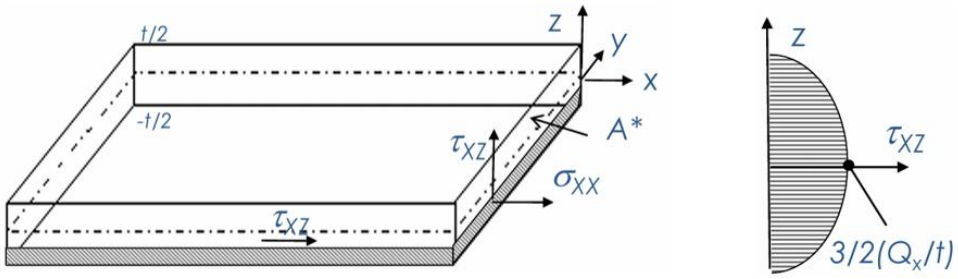

Figure 3.6: cylindrical bending configuration (left) and transverse shear stress distribution (right).

We now introduce a ***shear correction factor*** K_s that quantifies the difference between the constant distribution and the corrected one. Such parameter is obtained by comparing the strain energy associated to the transverse shear stress provided by the Mindlin plate U^M and that provided by the cylindrical bending correction U^{CB}. The two strain energies are obtained as

$$\begin{cases} U^{CB} = \frac{1}{2}\int_{-\frac{t}{2}}^{\frac{t}{2}} \gamma_{xz}\tau_{xz}dz = \frac{1}{2}\int_{-\frac{t}{2}}^{\frac{t}{2}} \frac{\tau_{xz}^2}{G}dz = \frac{1}{2G}\int_{-\frac{t}{2}}^{\frac{t}{2}} \left\{Q_x \frac{3}{2t}\left[1 - \left(\frac{2z}{t}\right)^2\right]\right\}^2 dz = \frac{3}{5}\frac{Q_x^2}{Gt} \\ U^{M} = \frac{1}{2}\int_{-\frac{t}{2}}^{\frac{t}{2}} \gamma_{xz}\tau_{xz}dz = \frac{1}{2}\int_{-\frac{t}{2}}^{\frac{t}{2}} \frac{\tau_{xz}^2}{G}dz = \frac{1}{2}\frac{Q_x^2}{Gt} \end{cases}$$

The ratio of the two provides with the following expression of the shear correction factor:

$$K_s = \frac{U^{CB}}{U^M} = \frac{5}{6} \tag{3.26}$$

3.2.5. Variational form

The internal virtual work is similar to that of CPT, the only difference is that the shear strains γ_{xz} and γ_{yz} are not null. Thus, an additional term in the internal virtual work δW_D associated to such strain components must be considered. The virtual internal work will therefore be:

$$\begin{aligned} \delta W_D &= \int_\Omega \left(\delta\underline{\varepsilon}_0^T \underline{N} + \delta\underline{k}^T \underline{M} + \delta\underline{\gamma}^T \underline{Q}\right) d\Omega \\ &= \int_\Omega \left(\delta\underline{\varepsilon}_0^T \underline{\underline{A}}\, \underline{\varepsilon}_0 + \delta\underline{k}^T \underline{\underline{D}}\, \underline{k} + \delta\underline{\gamma}^T \underline{\underline{D}}^{TSS} \underline{\gamma}\right) d\Omega \end{aligned} \tag{3.27}$$

Where we introduced the ***transverse shear stiffness matrix*** $\boldsymbol{D}^{TSS}$, obtained by correcting the transverse shear stiffness of the plate $Gt\boldsymbol{I}$, where $\boldsymbol{I} \in \mathbb{R}^{2\times 2}$, by the shear correction factor K_s:

$$\underline{\underline{D}}^{TSS} = GtK_s\underline{\underline{I}} \tag{3.28}$$

Here the shear stiffness of the plate $Gt\boldsymbol{I}$ has been obtained simply as that quantity that relates the generalized shear strains γ_{xz} and γ_{yz} to the generalized shear stresses Q_x and Q_y. According to

equations (3.24), which precisely expresses such relations, the transverse shear stiffness is the one reported above.

3.3. Classical lamination theory

Classical lamination theory (CLT) is the analytical model ***used for composite plate analysis***. Composite materials will be discussed in detail in Chapter 9, in this section we only discuss composite plates. Composite plates are made of 2 or more ***plies*** or ***laminae***, i.e. the composite material layers or sheets, stacked on top of each other to form the plate. The number of plies and the sequence of their orientation angles θ defines the ***layup sequence*** or lamination sequence or ply stack. Being a composite plate made of multiple plies, each with its own orientation, two reference systems can be identified. We define the ***global axes*** $\boldsymbol{X} = \{X, Y, Z\}$ the laminate or plate coordinates, such that usually the X-axis runs parallel to the long edge of the plate, the Y-axis is orthogonal to the X-axis but still in-plane, and the Z-axis is the out-of-plane axis. We define the local reference frame of the i-th ply as the ***material axes*** $\boldsymbol{x}_i = \{x_i, y_i, z_i\}$, such that the x-axis is in the direction of the fibers, the y-axis is the in-plane coordinate orthogonal to the x-axis, and the z-axis again the out of plane coordinate. Note that the material and global frames have coincident out of plane coordinate, i.e. $z = Z$. To rotate vectors form material to global axes we use the rotation matrix $\boldsymbol{T}$, which for a generic ply rotated of θ with respect to global axes is defined as follows:

$$\underline{\underline{T}} = \begin{bmatrix} \cos^2\theta & \sin^2\theta & 2\sin\theta\cos\theta \\ \sin^2\theta & \cos^2\theta & -2\sin\theta\cos\theta \\ -\sin\theta\cos\theta & \sin\theta\cos\theta & \cos^2\theta - \sin^2\theta \end{bmatrix} \tag{3.29}$$

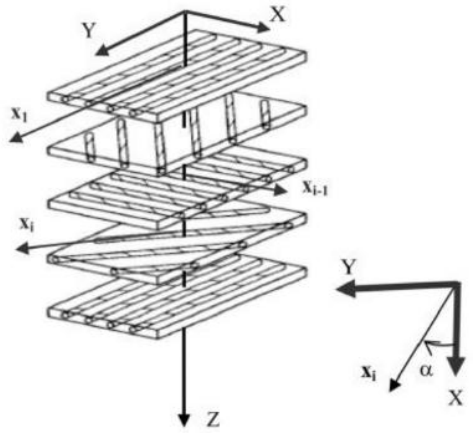

Figure 3.7: Representation of material and global axes.

Because a composite plate is made of many plies, each of different material and oriented differently, it follows that even if the strain is continuous across the plate thickness, the stress is not. This is essentially due to the fact that each ply has a different stiffness, either membranal or flexural, when the same composite plate is loaded with a given load.

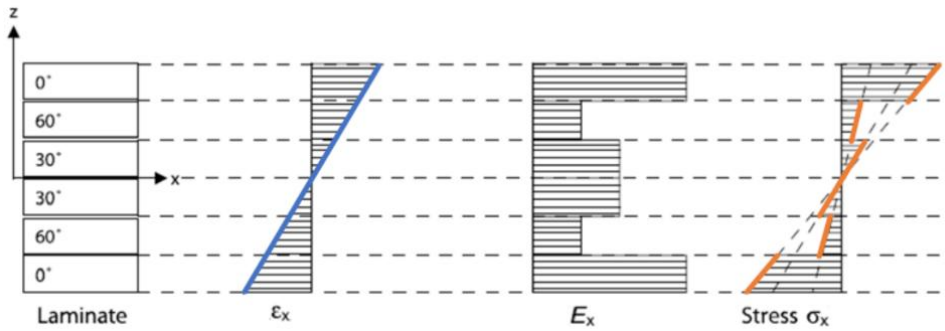

Figure 3.8: stress/strain distribution for composite materials.

3.3.1. Generalized coordinates

In classical lamination theory it is assumed that each ply behaves as a Mindlin plate, thus ***CLT builds on MPT***. Thus, the kinematic hypotheses are the same and so is the kinematic law of this model:

$$\begin{cases} u(x_0, y_0, z) = u_0(x_0, y_0) - z\theta_x \\ v(x_0, y_0, z) = v_0(x_0, y_0) - z\theta_y \\ w(x_0, y_0, z) \approx w_0(x_0, y_0) \end{cases} \tag{3.30}$$

Thus, the generalized coordinates of a composite plate are the same five of a Mindlin plate, and they read:

$$\underline{u}_0(x_0, y_0) = \begin{Bmatrix} u_0(x_0, y_0) \\ v_0(x_0, y_0) \\ w_0(x_0, y_0) \end{Bmatrix} \quad \text{and} \quad \underline{\theta}(x_0, y_0) = \begin{Bmatrix} \theta_x(x_0, y_0) \\ \theta_y(x_0, y_0) \end{Bmatrix} \tag{3.31}$$

Because CLT builds upon MPT, a ***key limitation*** of such model can already be pointed out. Since MPT is unable to provide an accurate distribution of transverse shear stresses, the same applies to CLT. It will be discussed in Chapter 9 that transverse shear stresses promote delaminations, which are the most severe type of damage in composite materials. Thus, evaluation of such stress components is of paramount importance for composite design, and the inability of such model to accurately predict transverse shear stresses is a big limitation that has to be compensated for numerically or experimentally.

3.3.2. Generalized strains

Naturally, the generalized strains of a composite plate according to CLT are the same as those of a Mindlin plate, and they read:

$$\underline{\varepsilon}_0(x_0, y_0) = \begin{cases} \varepsilon_{0xx} = u_{0/x} \\ \varepsilon_{0yy} = v_{0/y} \\ \varepsilon_{0xy} = \frac{1}{2}(u_{0/y} + v_{0/x}) \end{cases} \tag{3.32}$$

$$\underline{k}(x_0, y_0) = \begin{cases} k_{xx} = -\theta_{x/x} \\ k_{yy} = -\theta_{y/y} \\ k_{xy} = -\theta_{x/y} - \theta_{y/x} \end{cases}$$

Where $\boldsymbol{\varepsilon}_0$ are membranal strains and $\boldsymbol{k}$ flexural strains. The strain field can then be expressed in compact form as follows:

$$\underline{\varepsilon}(x_0, y_0, z) = \underline{\varepsilon_0}(x_0, y_0) + z\underline{k}(x_0, y_0) \tag{3.33}$$

Note that in the above equation the generalized strains $\boldsymbol{\varepsilon}_0$ and $\boldsymbol{k}$ are those of the whole composite plate, not those of a single lamina or ply.

3.3.3. Constitutive law

The key difference between isotropic Mindlin plates and composite plates intuitively lies in the constitutive law. Because CLT is based on a kinematic model, it is a kinematic model itself. Moreover, recall that in such models the CL is obtained by applying the same kind of assumptions that drive the definition of the kinematic law. Thus, the thin composite plate is assumed to be in a plane stress state, which for an orthotropic lamina is described as:

$$\underline{\sigma} = \underline{\underline{Q}}\,\underline{\varepsilon} \tag{3.34}$$

Or in expanded form:

$$\begin{Bmatrix} \sigma_{xx} \\ \sigma_{yy} \\ \tau_{xy} \end{Bmatrix} = \begin{bmatrix} \dfrac{E_x}{1-\nu_{xy}\nu_{yx}} & \dfrac{\nu_{xy}E_y}{1-\nu_{xy}\nu_{yx}} & 0 \\ \dfrac{\nu_{yx}E_x}{1-\nu_{xy}\nu_{yx}} & \dfrac{E_y}{1-\nu_{xy}\nu_{yx}} & 0 \\ 0 & 0 & G_{xy} \end{bmatrix} \begin{Bmatrix} \varepsilon_{xx} \\ \varepsilon_{yy} \\ \gamma_{xy} \end{Bmatrix} \tag{3.35}$$

Or inversely in compact form:

$$\underline{\varepsilon} = \underline{\underline{Q}}^{-1}\underline{\sigma} = \underline{\underline{S}}\,\underline{\sigma} \tag{3.36}$$

Or in expanded form:

$$\begin{Bmatrix} \varepsilon_{xx} \\ \varepsilon_{yy} \\ \gamma_{xy} \end{Bmatrix} = \begin{bmatrix} \dfrac{1}{E_x} & -\dfrac{\nu_{xy}}{E_y} & 0 \\ -\dfrac{\nu_{yx}}{E_x} & \dfrac{1}{E_y} & 0 \\ 0 & 0 & \dfrac{1}{G_{xy}} \end{bmatrix} \begin{Bmatrix} \sigma_{xx} \\ \sigma_{yy} \\ \tau_{xy} \end{Bmatrix} \tag{3.37}$$

Where the stiffness and compliance matrices are identified by four independent material-related constants, which are $E_x, E_y, \nu_{xy}, G_{xy}$. It must be pointed out that the Poisson's ratios ν_{xy} and ν_{yx} are not independent quantities, rather they are related as follows:

$$\frac{E_x}{\nu_{xy}} = \frac{E_y}{\nu_{yx}} \tag{3.38}$$

The constitutive law as written in equations (3.35) and (3.37) is expressed in material coordinates, i.e. the local ply reference frame. For the generic ply oriented at the generic angle θ with respect to global frame, the CL can be expressed in global coordinates by simply applying the rotation matrix $\boldsymbol{T}$ as defined in equation (3.35) to both the stress $\boldsymbol{\sigma}$ and the strain $\boldsymbol{\varepsilon}$ vectors. More precisely, for stresses we'll write:

$$\begin{Bmatrix}\sigma_{xx}\\ \sigma_{yy}\\ \tau_{xy}\end{Bmatrix} = \underline{\underline{T}}\begin{Bmatrix}\sigma_{XX}\\ \sigma_{YY}\\ \tau_{XY}\end{Bmatrix} \quad \rightarrow \quad \begin{Bmatrix}\sigma_{XX}\\ \sigma_{YY}\\ \tau_{XY}\end{Bmatrix} = \underline{\underline{T}}^{-1}\begin{Bmatrix}\sigma_{xx}\\ \sigma_{yy}\\ \tau_{xy}\end{Bmatrix} \tag{3.39}$$

Strains must be rotated more carefully, since the conversion between engineering shear strain γ_{XY} and physical shear strain $\varepsilon_{XY} = 1/2\gamma_{XY}$ must be considered. The conversion between these two strains is carried out via a matrix $\boldsymbol{R}$ defined as follows:

$$\underline{\underline{R}} = \begin{bmatrix}1 & 0 & 0\\ 0 & 1 & 0\\ 0 & 0 & 2\end{bmatrix} \tag{3.40}$$

So that

$$\begin{Bmatrix}\varepsilon_{xx}\\ \varepsilon_{yy}\\ \varepsilon_{xy}\end{Bmatrix} = \underline{\underline{R}}\begin{Bmatrix}\varepsilon_{xx}\\ \varepsilon_{yy}\\ \gamma_{xy}\end{Bmatrix}$$

Thus, rotation of the strain vector from local to global frame, and conversion from physical to engineering shear strain are carried out as follows:

$$\begin{Bmatrix}\varepsilon_{xx}\\ \varepsilon_{yy}\\ \varepsilon_{xy}\end{Bmatrix} = \underline{\underline{R}}\,\underline{\underline{T}}\,\underline{\underline{R}}^{-1}\begin{Bmatrix}\varepsilon_{XX}\\ \varepsilon_{YY}\\ \gamma_{XY}\end{Bmatrix} = \underline{\underline{T}}^{-T}\begin{Bmatrix}\varepsilon_{XX}\\ \varepsilon_{YY}\\ \gamma_{XY}\end{Bmatrix} \tag{3.41}$$

Where we first applied $\boldsymbol{R}^{-1}$ to obtain the physical shear strain ε_{xy}, then we rotate from global to local coordinate vie the rotation matrix $\boldsymbol{T}$, then we re-applied $\boldsymbol{R}$ in order to revert to engineering shear strain γ_{xy}. Thus, the CL can be expressed in global axes as follows:

$$\begin{Bmatrix}\sigma_{XX}\\ \sigma_{YY}\\ \tau_{XY}\end{Bmatrix} = \underline{\underline{T}}^{-1}\begin{Bmatrix}\sigma_{xx}\\ \sigma_{yy}\\ \tau_{xy}\end{Bmatrix} = \underline{\underline{T}}^{-1}\underline{\underline{Q}}\begin{Bmatrix}\varepsilon_{xx}\\ \varepsilon_{yy}\\ \varepsilon_{xy}\end{Bmatrix} = \underline{\underline{T}}^{-1}\underline{\underline{Q}}\,\underline{\underline{T}}^{-T}\begin{Bmatrix}\varepsilon_{XX}\\ \varepsilon_{YY}\\ \gamma_{XY}\end{Bmatrix} = \underline{\underline{\bar{Q}}}\begin{Bmatrix}\varepsilon_{XX}\\ \varepsilon_{YY}\\ \gamma_{XY}\end{Bmatrix}$$

Where we introduced the global ***rotated stiffness matrix*** $\bar{\boldsymbol{Q}}$, defined as follows:

$$\underline{\underline{\bar{Q}}} = \underline{\underline{T}}^{-1}\underline{\underline{Q}}\,\underline{\underline{T}}^{-T} \tag{3.42}$$

Thus, the constitutive law of the composite plate in global frame can be expressed in terms of the generalized strains of the CLT model as follows:

$$\underline{\sigma} = \underline{\underline{\bar{Q}}}\,\underline{\varepsilon} = \underline{\underline{\bar{Q}}}\left(\underline{\varepsilon}_0 + z\underline{k}\right) \tag{3.43}$$

3.3.4. Generalized stresses

Once again, the generalized stresses are the same as those of the Mindlin plate, i.e. internal actions or stress resultant. The difference with respect to the Mindlin plate is due to the nature of the material, which now is orthotropic rather than isotropic. For this reason, the stress resultants are defined slightly differently.

Let N be number of plies composing the plate, let the thickness of the i-th ply be defined by the thickness coordinates z_{i-1} and z_i. The forces per unit thickness $\boldsymbol{N} = \{N_{xx}, N_{yy}, N_{xy}\}$ acting on the midplane of the plate, and the moments per unit thickness $\boldsymbol{M} = \{M_{xx}, M_{yy}, M_{xy}\}$ acting about the midplane of the plate are obtained as follows:

$$\underline{N} = \int_{-t/2}^{t/2} \underline{\sigma} dz = \sum_i^N \int_{z_{i-1}}^{z_i} \underline{\sigma} dz = \sum_i^N \int_{z_{i-1}}^{z_i} \underline{\underline{\bar{Q}}}\left(\underline{\varepsilon}_0 + z\underline{k}\right) dz = \sum_i^N \left[\int_{z_{i-1}}^{z_i} \underline{\underline{\bar{Q}}}\,\underline{\varepsilon}_0 dz + \int_{z_{i-1}}^{z_i} \underline{\underline{\bar{Q}}}\, z\underline{k} dz \right]$$
$$= \underline{\underline{A}}\,\underline{\varepsilon}_0 + \underline{\underline{B}}\,\underline{k}$$

$$\underline{M} = \int_{-t/2}^{t/2} \underline{\sigma} z dz = \sum_i^N \int_{z_{i-1}}^{z_i} \underline{\sigma} z dz = \sum_i^N \int_{z_{i-1}}^{z_i} \underline{\underline{\bar{Q}}} z\left(\underline{\varepsilon}_0 + z\underline{k}\right) dz = \sum_i^N \left[\int_{z_{i-1}}^{z_i} \underline{\underline{\bar{Q}}} z\,\underline{\varepsilon}_0 dz + \int_{z_{i-1}}^{z_i} \underline{\underline{\bar{Q}}} z^2 \underline{k} dz \right]$$
$$= \underline{\underline{B}}\,\underline{\varepsilon}_0 + \underline{\underline{D}}\,\underline{k}$$

Thus, the generalized constitutive law for an orthotropic plate can be expressed as usual via the ABD matrix, yielding:

$$\begin{Bmatrix} \underline{N} \\ \underline{M} \end{Bmatrix} = \begin{bmatrix} \underline{\underline{A}} & \underline{\underline{B}} \\ \underline{\underline{B}} & \underline{\underline{D}} \end{bmatrix} \begin{Bmatrix} \underline{\varepsilon}_0 \\ \underline{k} \end{Bmatrix} \tag{3.44}$$

Or in compact form:

$$\underline{F} = \underline{\underline{K}}\,\underline{\varepsilon} \tag{3.45}$$

It is immediately clear that, contrarily to isotropic plates, ***for composite plates the B stiffness matrix is not null***. Physically, this implies that membranal actions are not decoupled from flexural actions, and vice versa. The entries of the stiffness matrices ***A***, ***B*** and ***D*** are obtained as follows:

$$\begin{cases} A_{hk} = \sum_i^N (\bar{Q}_{hk})_i (Z_i - Z_{i-1}) \\ B_{hk} = \frac{1}{2} \sum_i^N (\bar{Q}_{hk})_i \left(Z_i^2 - Z_{i-1}^2\right) \\ D_{hk} = \frac{1}{3} \sum_i^N (\bar{Q}_{hk})_i \left(Z_i^3 - Z_{i-1}^3\right) \end{cases} \tag{3.46}$$

Let us now discuss some ***important configurations*** for composite plates:

- Symmetrical laminate → decouples in-plane and bending actions → $\boldsymbol{B} = 0$: for each ply with angle θ there is another one with the same angle θ in a symmetrical position with respect to the middle axis of the laminate.
- Anti-symmetrical laminate → decouples bending and torsion → $D_{13} = D_{23} = 0$: for each ply with angle θ there is another one with the opposite angle $-\theta$ in a symmetrical position with respect to the middle axis of the laminate.
- Balanced laminate → decouples axial and shear action → $A_{13} = A_{23} = 0$: for each ply with angle θ there is another with opposite angle $-\theta$ in any position inside the laminate.

Symmetry and asymmetry are incompatible, unless we consider (1) only unidirectional UD laminae at [0] and [90], or fabric FB laminae at [45] as [+45] and [-45] plies are identical in this case. Symmetric laminates are preferred to anti-symmetric ones because those are distorted by cooling process due to extension-bending coupling.

3.3.5. Hygrothermal effects

With classical lamination theory it is possible to model hygrothermal effects. It will be discussed in Chapter 9 that such effects, related to humidity and thermal expansion, are of great importance in composite design.

Let $\boldsymbol{\alpha}$ be the vector of coefficients of thermal expansion defined in material axes and let ΔT be the temperature variation. The strain induced by thermal expansion can be expressed as follows:

$$\underline{\varepsilon}^{th} = \Delta T \begin{Bmatrix} \alpha_x \\ \alpha_y \\ 0 \end{Bmatrix} \tag{3.47}$$

Similarly, let $\boldsymbol{\beta}$ be the vector of swelling coefficients and let c be the relative mass increment coefficient. Thus, the hygric-induced strains in material axes are obtained as

$$\underline{\varepsilon}^{hygro} = c \begin{Bmatrix} \beta_{xx} \\ \beta_{yy} \\ 0 \end{Bmatrix} \tag{3.48}$$

Note that shear deformation due to hygrothermal effects is null because orthotropic materials have 3 mutually orthogonal planes of symmetry, so the shear strains cancel out. The total strain experienced by the composite plate can then be expressed as the sum of the mechanical, the thermal and the hygric strain components, yielding:

$$\underline{\varepsilon}^{tot} = \underline{\varepsilon}^{mech} + \underline{\varepsilon}^{th} + \underline{\varepsilon}^{hygro} \tag{3.49}$$

Where $\boldsymbol{\varepsilon}^{mech} = \{\varepsilon_{xx}, \varepsilon_{yy}, \gamma_{xy}\}$. The stresses on the plate can be computed starting from the strains via the CL. However, the CL is only able to relate mechanical-induced stresses to mechanical-induced strains. Thus, the mechanical stresses will be:

$$\underline{\sigma}^{mech} = \underline{\underline{Q}}\,\underline{\varepsilon}^{mech} = \underline{\underline{Q}}\left(\underline{\varepsilon}^{tot} - \underline{\varepsilon}^{th} - \underline{\varepsilon}^{hygro}\right) = \underline{\sigma}^{tot} + \underline{\sigma}^{th} + \underline{\sigma}^{hygro}$$

Rotation of the hygrothermal stresses from material to global axes is carried out via the rotation matrix $\boldsymbol{T}$ associated to the generic ply, yielding:

$$\begin{cases} \underline{\sigma}^{th} = \begin{Bmatrix} \sigma_{XX} \\ \sigma_{YY} \\ \tau_{XY} \end{Bmatrix}^{th} = \underline{\underline{T}}^{-1} \left(-\underline{\underline{Q}} \Delta T \begin{Bmatrix} \alpha_x \\ \alpha_y \\ 0 \end{Bmatrix} \right) = -\underline{\underline{\bar{Q}}} \Delta T \begin{Bmatrix} \alpha_x \\ \alpha_y \\ 0 \end{Bmatrix} \\ \underline{\sigma}^{hygro} = \begin{Bmatrix} \sigma_{XX} \\ \sigma_{YY} \\ \tau_{XY} \end{Bmatrix}^{hygro} = \underline{\underline{T}}^{-1} \left(-\underline{\underline{Q}} c \begin{Bmatrix} \beta_{xx} \\ \beta_{yy} \\ 0 \end{Bmatrix} \right) = -\underline{\underline{\bar{Q}}} c \begin{Bmatrix} \beta_{xx} \\ \beta_{yy} \\ 0 \end{Bmatrix} \end{cases}$$

Where we defined the equivalent stiffness matrix as $\bar{\boldsymbol{Q}} = \boldsymbol{T^{-1}Q}$. Hygrothermal stress resultants are obtained by integration through the thickness of the hygrothermal stresses. This yields:

$$\begin{cases} \underline{N}^{th} = \int_{-\frac{t}{2}}^{+\frac{t}{2}} \underline{\sigma}^{th} dz = -\sum_{i}^{N} \underline{\sigma}_i^{th} (z_i - z_{i-1}) \\ \underline{M}^{th} = \int_{-\frac{t}{2}}^{+\frac{t}{2}} \underline{\sigma}^{th} z dz = -\frac{1}{2} \sum_{i}^{N} \underline{\sigma}_i^{th} \left(z_i^2 - z_{i-1}^2 \right) \end{cases}$$

$$\begin{cases} \underline{N}^{hygro} = \int_{-\frac{t}{2}}^{+\frac{t}{2}} \underline{\sigma}^{hygro} dz = -\sum_{i}^{N} \underline{\sigma}_i^{hygro} (z_i - z_{i-1}) \\ \underline{M}^{hygro} = \int_{-\frac{t}{2}}^{+\frac{t}{2}} \underline{\sigma}^{hygro} z dz = -\frac{1}{2} \sum_{i}^{N} \underline{\sigma}_i^{hygro} \left(z_i^2 - z_{i-1}^2 \right) \end{cases}$$

Such hygrothermal components will then be added to the CL:

$$\begin{Bmatrix} \underline{N} - \underline{N}^{th} - \underline{N}^{hygro} \\ \underline{M} - \underline{M}^{th} - \underline{M}^{hygro} \end{Bmatrix} = \begin{bmatrix} \underline{\underline{A}} & \underline{\underline{B}} \\ \underline{\underline{B}} & \underline{\underline{D}} \end{bmatrix} \begin{Bmatrix} \underline{\varepsilon}_0 \\ \underline{k} \end{Bmatrix} \tag{3.50}$$

Or in compact form:

$$\underline{F} - \underline{F}^{th} - \underline{F}^{hygro} = \underline{\underline{K}}\, \underline{\varepsilon} \tag{3.51}$$

3.3.6. Direct and inverse approaches

Classical lamination theory can be implemented in two ways: direct procedure and inverse procedure. The ***direct procedure*** is the following:

- Inputs: the mechanical properties of each ply $E_x, E_y, G_{xy}, \nu_{xy}$, their thickness t_i and their orientation angle θ_i.
- Compute the stiffness matrix of each $\boldsymbol{Q}_i$ ply in its local material frame via the CL (3.35):

$$\underline{\underline{Q_i}} = \begin{bmatrix} \frac{E_x}{1 - \nu_{xy}\nu_{yx}} & \frac{\nu_{xy} E_y}{1 - \nu_{xy}\nu_{yx}} & 0 \\ \frac{\nu_{yx} E_x}{1 - \nu_{xy}\nu_{yx}} & \frac{E_y}{1 - \nu_{xy}\nu_{yx}} & 0 \\ 0 & 0 & G_{xy} \end{bmatrix}$$

- Rotate the stiffness matrix of each ply $\boldsymbol{Q}_i$ to global frame $\bar{\boldsymbol{Q}}_i$ via equation (3.42):

$$\underline{\underline{\bar{Q}_i}} = \underline{\underline{T_i}}^{-1}\underline{\underline{Q_i}}\,\underline{\underline{T_i}}^{-T}$$

- Compute and assembly of the laminate sub-matrices $\boldsymbol{A}, \boldsymbol{B}, \boldsymbol{D}$ via equations (3.46).
- Output: the ABD matrix of the composite plate, or equivalently is stiffness matrix $\boldsymbol{K}$.

The ***inverse procedure*** is the following:

- Inputs: the ABD matrix and the loads $\boldsymbol{N}$ and $\boldsymbol{M}$.
- Compute the generalized strains $\boldsymbol{\varepsilon}$ in global axes inverting equation (3.45):

$$\underline{\varepsilon} = \underline{\underline{K}}^{-1}\underline{F}$$

- Compute the strain state in each ply in global axes as

$$\underline{\varepsilon_i} = \underline{\varepsilon_0} + z_i\underline{k}$$

- Rotate the strains in each ply in material axes via equation (3.41):

$$\begin{Bmatrix}\varepsilon_{xx}\\ \varepsilon_{yy}\\ \varepsilon_{xy}\end{Bmatrix}_i = \underline{\underline{T_i}}^{-T}\begin{Bmatrix}\varepsilon_{XX}\\ \varepsilon_{YY}\\ \gamma_{XY}\end{Bmatrix}_i$$

- Compute the stresses in each ply in material axes via the CL (3.34):

$$\underline{\sigma}_i = \underline{\underline{Q_i}}\,\underline{\varepsilon_i}$$

- Output: the stress state in each ply in material frame, and if required in global frame by applying equation (3.39):

$$\begin{Bmatrix}\sigma_{XX}\\ \sigma_{YY}\\ \tau_{XY}\end{Bmatrix}_i = \underline{\underline{T_i}}^{-1}\begin{Bmatrix}\sigma_{xx}\\ \sigma_{yy}\\ \tau_{xy}\end{Bmatrix}_i$$

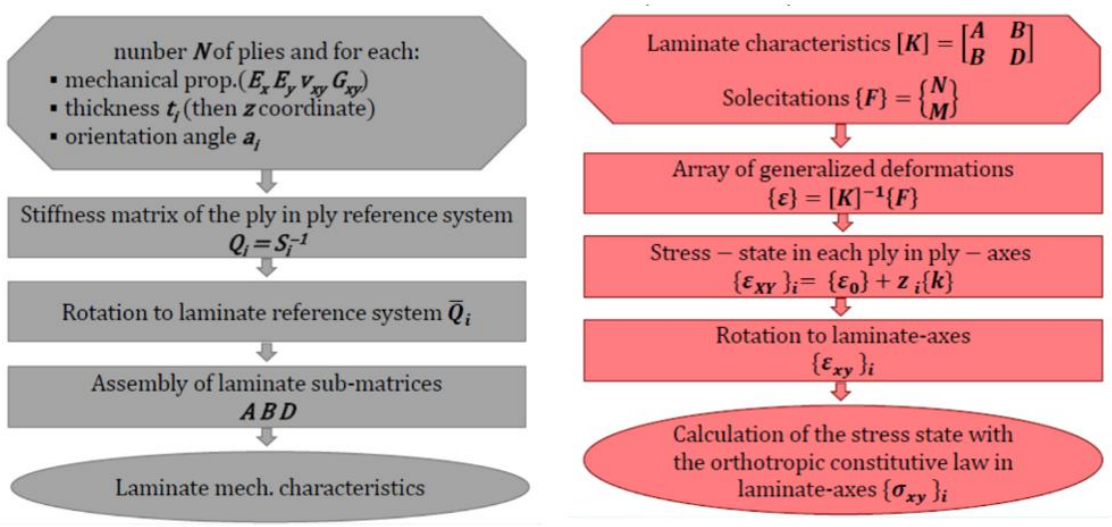
nunber N of plies and for each:
▪ mechanical prop.($E_x E_y \nu_{xy} G_{xy}$)
▪ thickness t_i (then z coordinate)
▪ orientation angle a_i
Stiffness matrix of the ply in ply reference system
$Q_i = S_i^{-1}$
Rotation to laminate reference system $\bar{Q}_i$
Assembly of laminate sub-matrices
$A\,B\,D$
Laminate mech. characteristics
Laminate characteristics $[K] = \begin{bmatrix} A & B \\ B & D \end{bmatrix}$
Solecitations $\{F\} = \begin{Bmatrix} N \\ M \end{Bmatrix}$
Array of generalized deformations
$\{\varepsilon\} = [K]^{-1}\{F\}$
Stress – state in each ply in ply – axes
$\{\varepsilon_{XY}\}_i = \{\varepsilon_0\} + z_i\{k\}$
Rotation to laminate-axes
$\{\varepsilon_{xy}\}_i$
Calculation of the stress state with the orthotropic constitutive law in laminate-axes $\{\sigma_{xy}\}_i$

Figure 3.9: direct (left) and inverse (right) approaches for CLT implementation.

4. Aerospace structures

The design of any engineering system, such as aerospace structures, is a complex endeavor made of a sequence of phases, represented in Figure 4.1. The design process starts from the requirements and specifications of the project. These are maximum speed, maximum altitude, cruise speed, payload, military or civil applications and of which kind and so on. For what concerns structural design, particularly important is the ***evaluation of the loads*** acting on the structure. In general, the loads can be of different nature: aerodynamic, inertial, due to the propulsion system, induced by a differential pressure between the inside and outside of the structure and so on. For the scopes of this course the ***loads will always assumed to be known*** and available from previous analyses. Once requirements and specifications are known, a conceptual design can be formulated, such as the overall configuration of the aircraft. After the conceptual design follows the preliminary design phase, characterized by a lot of uncertainty about the specific characteristics of the aircraft structural components, which are continuously iterated upon during this phase. A typical source of uncertainty during this phase would be the shape/configuration of some components. Thus, in order to test many possible designs, simplified models that usually have closed form analytical solutions are employed in this phase. Such models are easy to understand and implement but provide insight into the role played by the design variables in the systems general behavior, the structure in our case.

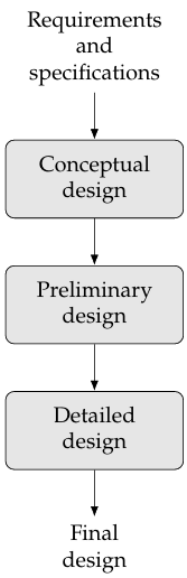

Figure 4.1: design process.

The ***goal*** of this section is to introduce simplified structural theories for aerospace structures in particular. In general, for such structures ***beam and plate models are widely used to perform preliminary design***. For example, preliminary modal analyses are carried out on the so-called stick models, which approximate the whole aircraft as an assembly of beams (Figure 4.2). The initial beam model scheme can be imagined as isostatic (statically determined), since this choice allows to study the design of various parts of the structure independently from one another. In fact, if an isostatic scheme is adopted, the internal actions are readily available from the applied loads. Again, note that this is not a suboptimal strategy, but an engineering approach to begin a lengthy and complex design process.

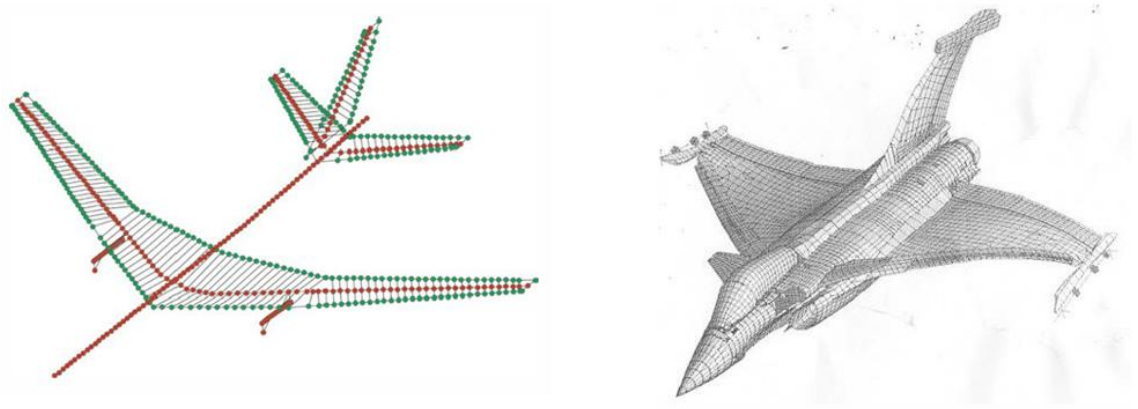

Figure 4.2: aircraft stick model.

4.1. Introduction to aerostructures

The basic functions of an aircraft's structure are to transmit and resist the applied loads and to provide an aerodynamic shape and to protect passengers, payload, systems, and the like from the environmental conditions encountered in flight. These requirements, in most aircraft, result in thin-shell structures where the outer surface or skin of the shell is usually supported by longitudinal stiffening members and transverse frames to enable it to resist bending, compressive, and torsional loads without buckling (a type of structural instability phenomena) [1] – chapter 12.2. The early aeronautical beams where characterized by spars (or longerons), longitudinal elements carrying bending and axial forces, ribs and frames, transverse elements transmitting shear forces, and a fabric cover that enveloped the rest of the structure but carried no load.

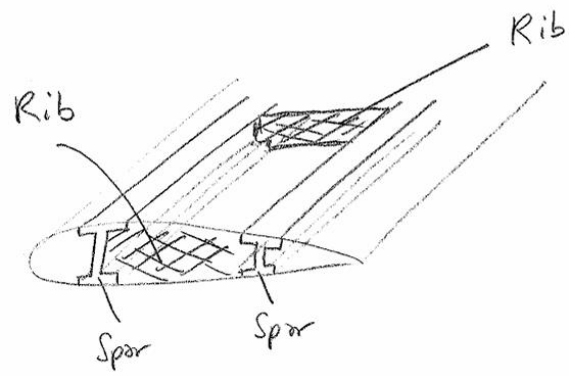

Figure 4.3: typical configuration of an early aeronautical structure.

For the early, low speed vehicles, this configuration was adequate. However, the increasing performance of aircrafts, and thus increasing speed, led to a shift of paradigm of the structural configuration. In particular, higher speed generate higher torsional loads, and thus higher torsional stiffness is required from the structures. Moreover, covers must also be stiffer in order to guarantee the desired aerodynamic shape and provide the expected aerodynamic behavior. These considerations bring us to the currently adopted structural configurations for aerostructures, i.e. the previously mentioned thin-shell structures. Such structures are known as ***semi-monocoque***, while thin shells that rely entirely on their skins for their capacity to resist loads are referred to as ***monocoque***. Moreover, boxed configurations are usually employed as they are more efficient layouts in terms of weight and torsional stiffness.

Figure 4.4: boxed wig section with longitudinal stiffening elements and stressed skin.

The exact structure depends on the part of the aircraft considered, e.g. wing, fuselage, tail etc. However, no matter how complex the internal structural arrangement, the different components perform the same kind of function. The ***components of a stressed skin construction*** (semi-monocoque) are the skin, frames and ribs, spars and stringers. The ***load distribution*** in these components is as follows: resistance to shear and torsional loads is supplied by shear stresses developed in the skin and spar webs, while axial and bending loads are reacted by the combined action of skin and stringers.

We go over the function of a thin-walled structure components one by one. The primary function of the ***wing skin*** is to form an impermeable surface for supporting the aerodynamic pressure distribution from which the wing generates lift. These aerodynamic forces are transmitted in turn to the ribs and stringers by the skin through plate and membrane action. The ***shape of the wing's cross-section*** is governed by aerodynamics and clearly must be maintained for all combinations of load; this is one of the functions of the ***ribs***. Moreover, ribs distribute concentrated loads into the structure and redistribute stress around discontinuities. Ribs increase the column buckling stress of the longitudinal stiffeners by providing end restraint and establishing their column length (Figure 4.5); in a similar manner, they increase the plate buckling stress of the skin panels. The dimensions of ribs are governed by their spanwise position in the wing and by the loads they are required to support. In the outer portions of the wing, where the cross-section may be relatively small if the wing is tapered and the loads are light, ribs act primarily as formers for the airfoil shape. A light structure is sufficient for this purpose, whereas at sections closer to the wing root, where the ribs are required to absorb and transmit large concentrated applied loads, such as those from the undercarriage, engine thrust, and fuselage attachment point reactions, a much more rugged construction is necessary. Between these two extremes are ribs that support hinge reactions from ailerons, flaps, and other control surfaces, plus the many internal loads from fuel, armament, and systems installations.

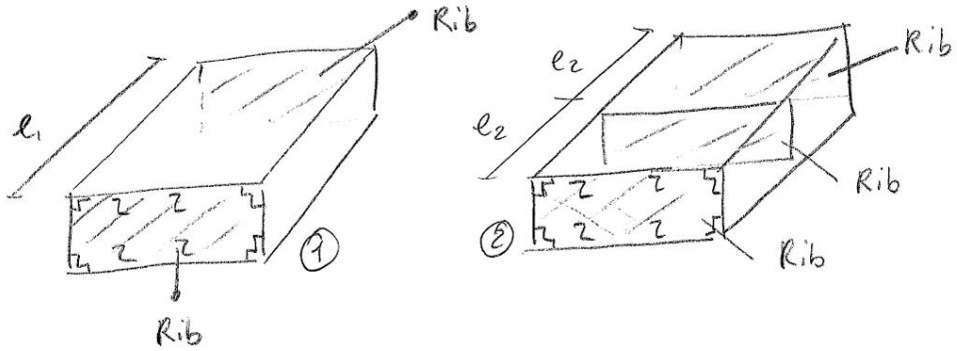

Figure 4.5: ribs.

Although the thin skin is efficient for resisting shear and tensile loads, it buckles under relatively low compressive loads. Rather than increase the skin thickness and suffer a consequent weight penalty, ***stringers*** are attached to the skin and ribs, thereby dividing the skin into small panels and increasing the buckling and failing stresses. This stabilizing action of the stringers on the skin is, in fact, reciprocated to some extent although the effect normal to the surface of the skin is minimal. Stringers rely chiefly on rib attachments for preventing column action in this direction. We noted in the previous paragraph the combined action of stringers and skin in resisting axial and bending loads. Stringers can be of different shapes, as depicted in the figure below.

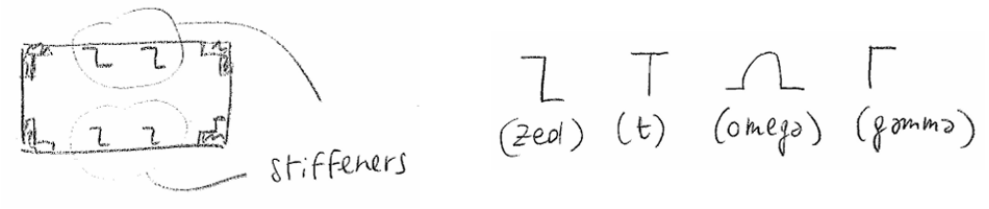

Figure 4.6: stringer typical cross section shapes.

Spar webs develop shear stresses to resist shear and torsional loads, aiding the skin. They also perform a secondary but significant function in stabilizing, with the skin, the spar flanges, or caps, which are therefore capable of supporting large compressive loads from axial and bending effects.

Observation. While the majority of these remarks have been directed towards wing structures, they apply to all the aerodynamic surfaces, namely, wings, horizontal and vertical tails.

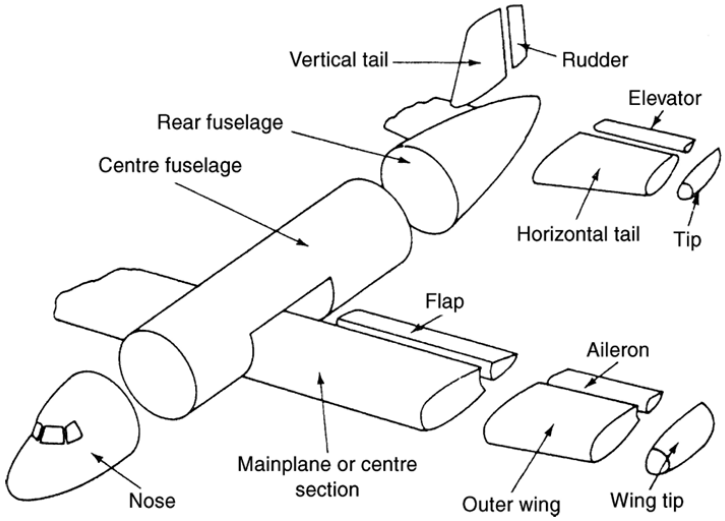

Figure 4.7: typical sub-assembly breakdown.

As a conclusive remark, aerostructures are highly efficient structures. Weight is the most crucial aspect. In many cases, the wing boxes depicted in the previous figures are just one example, the configuration is characterized by reduced thickness (of the order of a few millimeters), and for this reason they are referred to as ***thin-walled structures***. For such type of structures, two aspect become relevant:

- Shear stress and deformability: they dominate the structure's response and thus cannot be neglected as for structures with compact sections.
- Buckling: the reduced thickness coupled with loading conditions that promote buckling makes buckling behavior an aspect of crucial importance.

4.2. Semi-monocoque beam model

In the previous section it has been stated that the typical aerostructure is a thin-walled structure, or semi-monocoque structure, in which the skin carries shear and axial loads while the stiffening longitudinal elements mainly carry bending and axial loads, helping with buckling as well. The ***goal*** of this section is obtain approximate closed-form solutions for torsion and shear of these types of structures. More precisely, from now on we will refer to the semi-monocoque model as the modelling approach that can be used to model aerostructural beams, and not the aerostructure configuration per se (which is a thin-walled structure). ***The semi-monocoque scheme directly builds on the DSV solution***. Recall from section 2.1 that the DSV solution for beams provides the exact axial stress σ_{zz} (section 2.1.4). Such solution can be applied to any beam irrespective to the specific cross section shape. Contrarily, the evaluation of the shear stress components τ_{xz} and τ_{yz} is a more complex task. The fluid analogy provided qualitative insight into how the shear stresses flow for single cell closed sections and for opened beam profiles (section 2.1.6). Then, approximate solutions have been found for torsion of the previously mentioned cases. In this section, we will introduce a series of assumptions, based on the thin-walled configuration typical of aerostructures, and that are the basis of the semi-monocoque model, that will allow us to find closed-form approximate analytical solutions for shear stresses due to internal shear and torsional actions. Naturally, we'll use the same reference system of the DSV solution. That is, the z-axis is the bam axis, x-y-axes define the plane of the beam cross-section, as depicted in the figure below. We report here the definition of the internal actions (2.2) and their equilibrium relations (2.3) according to this reference system. Moreover, according to the DSV solution, natural BCs are imposed point-wise for the external surface of the beam S_{Fbody}, i.e. via Cauchy condition $\boldsymbol{\tau} \cdot \boldsymbol{n} = \boldsymbol{0}$, while they are imposed in terms of internal actions on the beam cross sections S_{Fface}.

$$\begin{cases} T_x = \int_A \sigma_{xz} dA \\ T_y = \int_A \sigma_{yz} dA \\ T_z = \int_A \sigma_{zz} dA \end{cases} \qquad \begin{cases} M_x = \int_A \sigma_{zz} y dA \\ M_y = \int_A -\sigma_{zz} x dA \\ M_z = \int_A (\sigma_{yz} x - \sigma_{xz} y) dA \end{cases} \tag{4.1}$$

$$\begin{cases} T_x = \hat{T}_x \\ T_y = \hat{T}_y \\ T_z = \hat{T}_z \end{cases} \qquad \begin{cases} M_x = \hat{M}_x + z T_y \\ M_y = \hat{M}_y - z T_x \\ M_z = \hat{M}_z \end{cases} \tag{4.2}$$

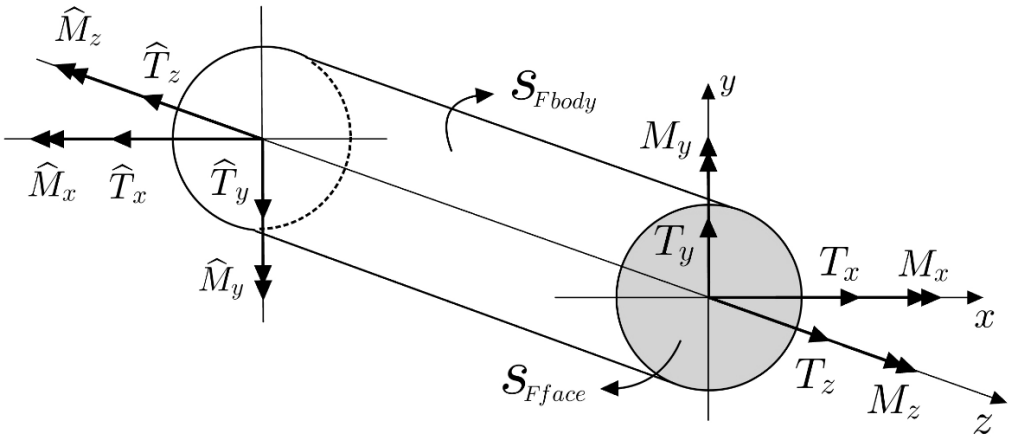

Figure 4.8: loads and reaction forces on a beam.

4.2.1. Shear flow equation

Consider the generic thin-walled beam section, subject to internal forces T_x, T_y and M_z. A strategy to obtain the shear stresses starts from the equilibrium conditions:

$$\begin{cases} \begin{cases} \tau_{xz/z} = 0 \\ \tau_{yz/z} = 0 \\ \tau_{zx/x} + \tau_{zy/y} + \sigma_{zz/z} = 0 \end{cases} & \text{in } V \\ \underline{\tau} \cdot \underline{n} = \underline{0} & \text{in } V \\ \begin{cases} T_y = \int_A \tau_{yz} dA \\ T_x = \int_A \tau_{xz} dA \\ M_z = \int_A (\tau_{yz} x - \tau_{xz} y) dA \end{cases} & \text{on } S_{Fface} \end{cases} \tag{4.3}$$

The equilibrium equations along the x-y-axes in the first system of (4.3), i.e. the first two, simply state that the shear flows are not a function of the axial coordinate z. The ***shear flow equation is an alternative form of the axial equilibrium equation***, i.e. the one along the z-axis. Such equilibrium equation can be rewritten as follows:

$$\tau_{zx/x} + \tau_{zy/y} + \sigma_{zz/z} = \nabla \cdot \underline{\tau} + \sigma_{zz/z} = 0$$

$$\nabla \cdot \underline{\tau} = -\sigma_{zz/z} \tag{4.4}$$

From this equation, the shear flow q can be obtained by simply integrating the left hand side over an arbitrary portion A' of the beam cross sectional area A, and applying the divergence theorem. This yields:

$$\int_{A'} \nabla \cdot \underline{\tau} \, dA' = \int_{\partial A'} (\underline{\tau} \cdot \underline{n}) \partial A' = q \tag{4.5}$$

Recall that the shear flow q is assumed to act along the midline of the section, and the shear stress τ is assumed to be constant along the thickness of the beam section (Figure 4.9). The right hand side of (4.4) can be expressed in two equivalent ways. The first one is obtained by integrating $-\sigma_{zz\backslash z}$ over A' and reversing the order of integration and differentiation. This yields:

$$q = -\int_{A'} \sigma_{zz\backslash z} dA' = -\frac{\partial}{\partial z} \int_{A'} \sigma_{zz} dA' = -T'_{z\backslash z}$$

$$q = -T'_{z\backslash z} \tag{4.6}$$

Where T'_z is the stress resultant of σ_{zz} over the area A'. This form of the shear flow equation highlights the fact that the shear flows q are obtained from an axial equilibrium equation. The operative form of the shear flow equation is obtained by using the DSV solution for σ_{zz}:

$$q = -\int_{A'}\left[\frac{\partial}{\partial z}\left(\frac{T_z}{A} + \frac{M_x}{I_{xx}}y - \frac{M_y}{I_{yy}}x\right)\right]dA'$$

The beam properties A, I_{xx} and I_{yy} are constant along its axis because of the DSV assumptions, the beam is assumed to be a 2D section extruded along a straight axis. By using the internal actions equilibrium relations of equation (4.2) and applying the derivative with respect to z, we obtain:

$$q = \int_{A'}\left(-\frac{T_y}{I_{xx}}y - \frac{T_x}{I_{yy}}x\right)dA' = -\frac{T_y}{I_{xx}}S'_y - \frac{T_x}{I_{yy}}S'_x$$

$$q = -T_y\frac{S'_x}{I_{xx}} - T_x\frac{S'_y}{I_{yy}} \tag{4.7}$$

Figure 4.9: exact (left) and approximated (right) shear flow distribution in a thin-walled section.

Observation. Because we did not consider the compatibility equations, the shear flow as obtained here does respect the equilibrium conditions but not necessarily the compatibility conditions.

4.2.2. Model assumptions

We discuss in this section the application of the shear flow equation to aerostructures. This discussion is based on the DSV solution for shear stress presented in section 2.1.6. Aerostructures can be modelled via the semi-monocoque model, which is based on the ***fundamental assumption that the panels of the structure are thin***. Consider an "I" beam with an applied shear load T_y. We assume that the web is thin in relation to the typical dimensions of the section. The direction of the shear flows, depicted in Figure 4.10 – left, can be traced according to the fluid analogy. It is clear that the web is the main actor in carrying shear flow, while the two flanges provide the dominant bending stiffness contribution of the section.

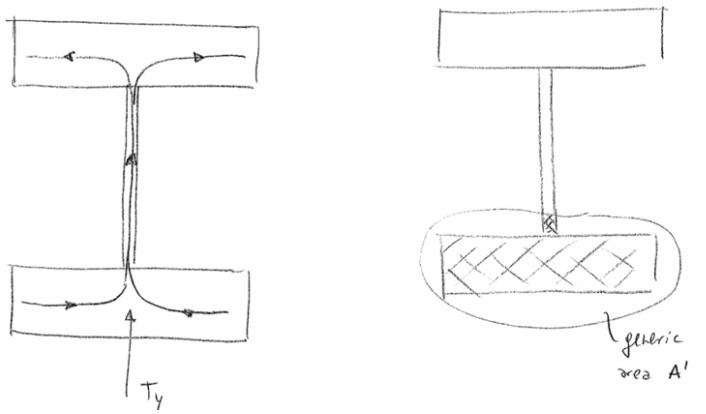

Figure 4.10: left) shear flow fluid analogy; right) arbitrary area A'.

The shear flow can then be evaluated by means of equation (4.7) for the area A' depicted in Figure 4.10 – right, and it yields:

$$q = -T_y \frac{S'_x}{I_{xx}} \quad \text{where} \quad S'_x = \int_{A'} y dA' = S_x^{(flange)} + \int_{-\frac{h}{2}}^{y} \eta t d\eta = S_x^{(flange)} + \frac{t}{2}\left(y^2 - \frac{h^2}{4}\right)$$

It follows that the static moment S'_x is composed of a constant term and one that is quadratic in y (Figure 4.11). However, as is typical in aerostructures, the thickness of the web is very low. This allows us to neglect the parabolic contribution to the static moment, which is then ***assumed*** to be constant along the web. As a consequence, we can model the web of the I section as a line with no associated area, capable of transferring shear forces only, but not capable of changing their intensity. It is also ***assumed*** that the flanges, or stringers in an aerostructure, have small sectional area with respect to the dimensions of the section. This assumption allows to model the stringers as two lumped areas in the location of their barycenter, i.e. at $\pm h/2$ on the y-axis (Figure 4.11).

According to this model, because webs do not have an associated area while stringers are modelled as lumped areas, the static moments, and thus the shear flows, will change only if the arbitrary portion A' is expanded enough to contain new stringers. For example, the outflowing shear flow from A_1 in Figure 4.11 will be the same as that outflowing from A_2 since the static moments associated to both areas are also the same.

Thus, assuming panels are thin allows to assume that the shear flow is constant in the panels, because the variation of static moment, and thus of shear flow, for a thin panel is negligible. This implies that there can be no change of shear flow unless we "cross" a stringer. The thicker the panels, the stronger the approximation introduced by this assumption. It's responsibility of the designer to verify the adequacy of this model.

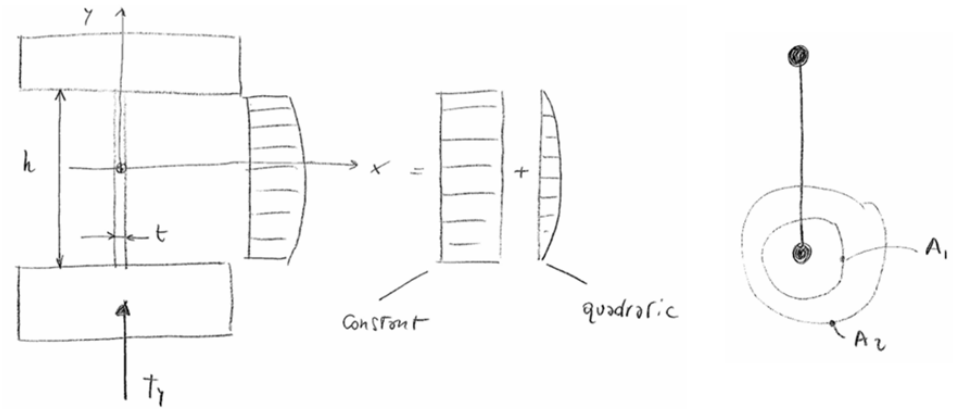

Figure 4.11: quadratic and constant contributions to shear flow in the web.

Some important ***remarks on the semi-monocoque scheme***:

- Ribs and frames are assumed to be infinitely stiff in the in-plane direction, while they are considered highly compliant in the out-of-plane direction. This is due to the fact that when a rib is loaded in-plane, its response is dominated by its membrane stiffness. Generally speaking, the membrane stiffness of a plate is much higher than its bending stiffness, which instead dominates the out-of-plane behavior.
- Load distribution: having lumped areas in stringers, it follows that shear loads are carried by panels, while axial loads are carried by stringers.
- The lumped areas are comprehensive of the panel and stringer areas. It can be useful, however, to know that the model can be refined by defining some additional lumped areas that model only the panel contributions, as in the example below.

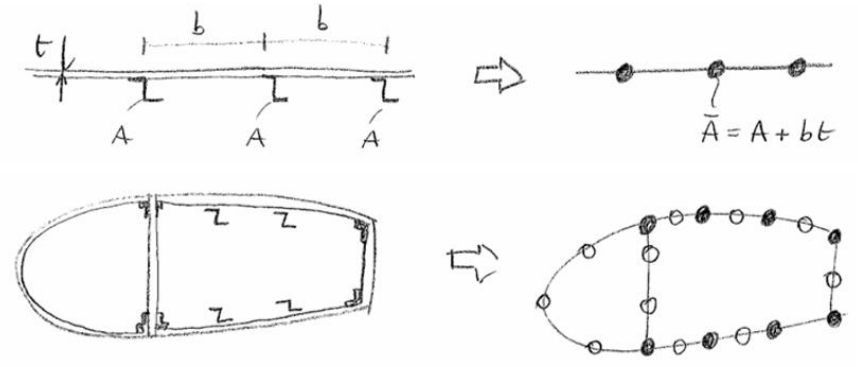

Figure 4.12: top) basic semi-monocoque area lumping; bottom) refined lumping process.

- Panels (open thin-walled sections) cannot react to torsional loads: recall from section 2.1.6.2 that for thin walled sections the shear stress distribution due to a torsional moment is linear in the thickness direction. In the context of the semi-monocoque approximation the shear flow, referred to the midline, will be zero, as the integral of the linear shear distribution is null. Being the shear flow equivalent to the shear internal actions, this result implies that panels in a semi-monocoque model cannot react to torsional loads.

$$q = \int_t \tau_{sz}(n)dn = 0$$

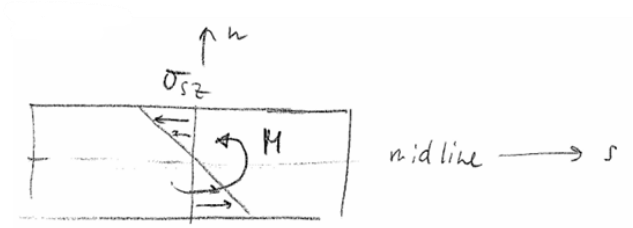

Figure 4.13: linear shear stress distribution on a thin walled beam due to a torsional moment.

- When the stringer area is lumped, it should be paid attention to not artificially increase the bending stiffness of the section. Take the example in , the contribution of the stringer to the second moment of inertia is:

$$I_{xx} = I_{xx}^{(local)} + Ad_1^2$$

Where the first term is he moment of inertia of the stringer local axes. When the stringer is lumped, its contribution to the moment of inertia becomes $I_{xx} = Ad_2^2$. This lumping process tends to increase the bending stiffness as $d_2 > d_1$ and so $Ad_2^2 > Ad_1^2$. For this reason, the lumped area of the stringer would be better approximated by imposing:

$$A^{lumped} d_2^2 = Ad_1^2 \quad \rightarrow \quad A^{lumped} = A\frac{d_1^2}{d_2^2}$$

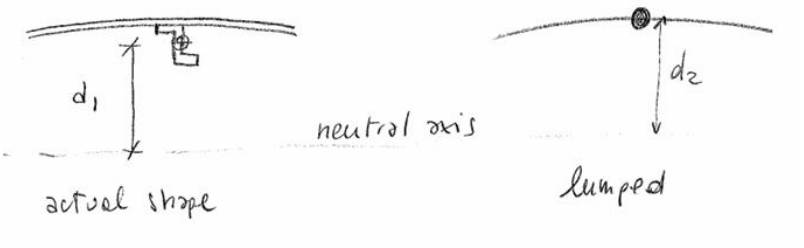

Figure 4.14: lumping process of a stringer.

4.2.3. Solution procedure – general aspects

4.2.3.1. Evaluation of inertia moments

The solution of the shear stresses developed on a beam cross section is found via the semi-monocoque scheme by discretization of the section into lumped areas and then applying the shear flow equation (4.7). To evaluate the shear flow equation one needs to compute the first and second inertia moments of a section. Since the shear flow equation has been derived starting from the DSV solution, which assumes principal and centroidal reference frame, one has to compute the inertia moments with respect to such axes. The principal axes are often available from symmetry considerations, as in the examples of **Error! Reference source not found.**. Whenever the section does not display any kind of symmetry, the principal axes can be determined as follows. First we consider a generic system $\bar{x}, \bar{y}$ and evaluate the position of the centroid of the section as follows:

$$\begin{cases} x_{CG} = \dfrac{\sum A_i \bar{x}_i}{\sum A_i} \\ y_{CG} = \dfrac{\sum A_i \bar{y}_i}{\sum A_i} \end{cases}$$

Then we determine the area moment of inertia of the section with respect to a reference system $\tilde{x}, \tilde{y}$ with origin in the centroid x_{CG}, y_{CG}. This allows us to evaluate the angle α, defined as follows:

$$\begin{cases} I_{\tilde{x}\tilde{x}} = \sum A_i \tilde{y}_i^2 \\ I_{\tilde{y}\tilde{y}} = \sum A_i \tilde{x}_i^2 \\ I_{\tilde{x}\tilde{y}} = \sum A_i \tilde{x}_i \tilde{y}_i \end{cases} \quad \rightarrow \quad \alpha = \frac{1}{2}\operatorname{atan}\left(\frac{2I_{\tilde{x}\tilde{y}}}{I_{\tilde{y}\tilde{y}} - I_{\tilde{x}\tilde{x}}}\right)$$

If such angle is different from zero, we obtain the principal axes by rotate the reference system $\tilde{x}, \tilde{y}$ by this angle:

$$\begin{cases} x = +\cos\alpha\, \tilde{x} + \sin\alpha\, \tilde{y} \\ y = -\sin\alpha\, \tilde{x} + \cos\alpha\, \tilde{y} \end{cases}$$

4.2.3.2. Evaluation of the stresses

The axial stresses developing on the i-th stringer can be obtained according to the DSV solution for axial stress:

$$\sigma_{zzi} = \frac{T}{A} + \frac{M_x}{I_{xx}} y_i - \frac{M_y}{I_{yy}} x_i$$

Where A, I_{xx} and I_{yy} are referred to the whole cross section, while y_i and x_i identify the stringer location with respect to the principal axes. The shear stresses are obtained using the shear flow equations:

$$q = -T_y \frac{S'_x}{I_{xx}} - T_x \frac{S'_y}{I_{yy}} = -T_{z\backslash z}$$

Then, based on the DSV shear solution, we assume that the shear stress is constant along the thickness-wise direction and that the shear flow acts on the midline of the thickness. Thus, shear stresses are recovered simply as $\tau = q/t$. Thus, once the shear flows are known, so are the sear stresses.

4.2.3.3. Number of equations

The number of equations and the overall solution procedure depends on the type of section. In general, we can classify semi-monocoque approximations of beam sections in three categories: open sections, closed single-cell sections, and closed multi-cell sections. We indicate the number of stringers with n, the number of panels with m and the number of cells as $N = m - n + 1$.

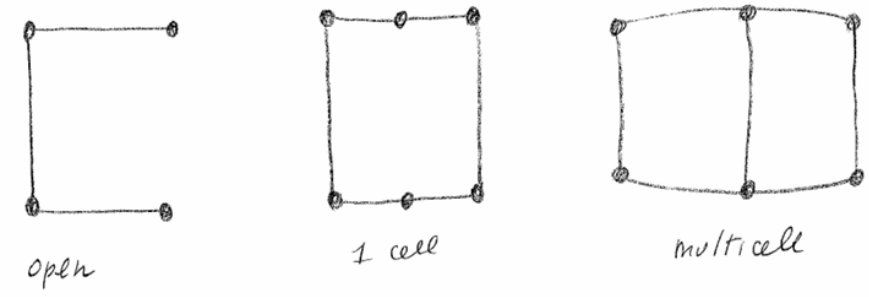

Figure 4.15: types of semi-monocoque beam sections.

When solving a section it is possible to write $n - 1$ linearly independent shear flow equations. However, the number of unknown shear flows is equal to the number of panels m. It follows that we need $m - (n - 1) = m - n + 1 = N$ additional equations, same as the number of cells. The additional equation is provided by Bredt formula (2.34) applied to the semi-monocoque section:

$$M_z = 2 \sum_i \Omega_i q_i \tag{4.8}$$

4.2.4. Solution procedure for open sections

4.2.4.1. Shear stresses

Consider as an example the C-section subject to internal forces T_x and T_y depicted in Figure 4.16. The number or panels is $m = 3$, thus we have three unknown shear flows to determine. The number of independent shear flow equations that we can write is equal to the number of stringers minus one, i.e. $n - 1 = 3$. Thus, we can solve the shear problem only using the shear flow equations:

$$\begin{cases} q_1 = -T_x \dfrac{S'_{y1}}{I_{yy}} - T_y \dfrac{S'_{x1}}{I_{xx}} \\ q_2 = -T_x \dfrac{S'_{y2}}{I_{yy}} - T_y \dfrac{S'_{x2}}{I_{xx}} \\ q_3 = -T_x \dfrac{S'_{y3}}{I_{yy}} - T_y \dfrac{S'_{x3}}{I_{xx}} \end{cases}$$

However, a clear relationships can be established between the static moments of the arbitrary areas A_1, A_2 and A_3. More precisely:

$$\begin{cases} S'_{y1} = S_{y1} \\ S'_{x1} = S_{x1} \end{cases} \qquad \begin{cases} S'_{y2} = S_{y1} + S_{y2} \\ S'_{x2} = S_{x1} + S_{x2} \end{cases} \qquad \begin{cases} S'_{y3} = S_{y1} + S_{y2} + S_{y3} \\ S'_{x3} = S_{x1} + S_{x2} + S_{x3} \end{cases}$$

According to these relations, we obtain the solution simply as:

$$\begin{cases} q_1 = -T_x \dfrac{S_{y1}}{I_{yy}} - T_y \dfrac{S_{x1}}{I_{xx}} \\ q_2 = -T_x \dfrac{S_{y1} + S_{y2}}{I_{yy}} - T_y \dfrac{S_{x1} + S_{x2}}{I_{xx}} \\ q_3 = -T_x \dfrac{S_{y1} + S_{y2} + S_{y3}}{I_{yy}} - T_y \dfrac{S_{x1} + S_{x2} + S_{x3}}{I_{xx}} \end{cases}$$

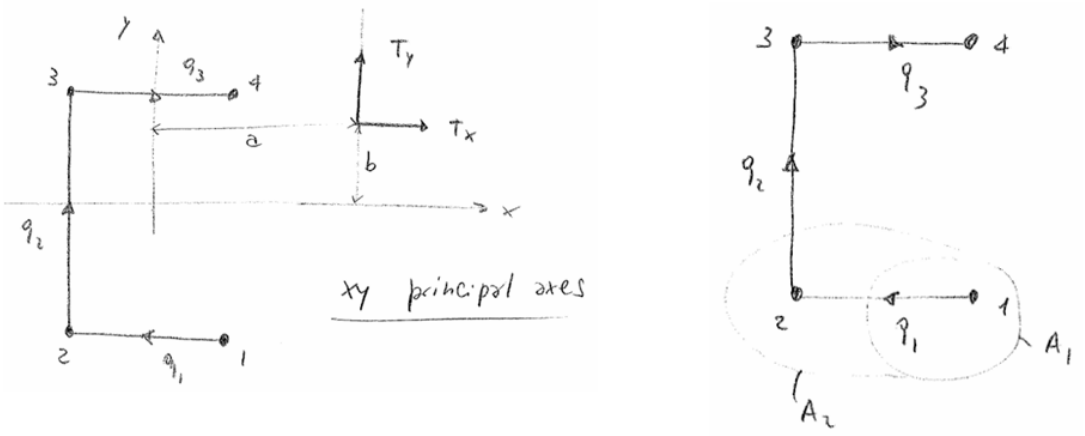

Figure 4.16: left) C-section with semi-monocoque scheme, right) shear flows.

4.2.4.2. Shear center

Following the determination of shear flows, and thus shear stresses, we can determine another important property of a section: its ***shear center***. Recall that the shear center is the point at which a shear load does not generate torsional moments on the section. For the same section of Figure 4.16, to determine the shear center we impose that the shear flows q_i are generated purely by shear loads T_x, T_y applied to an initially arbitrary location $\{a, b\}$ (Figure 4.17). To do so, we use the equivalence of internal torsional action and shear flows (Bredt's formula) applied to a semi-monocoque section:

$$M_z = 2\sum_i \Omega_i q_i \quad \rightarrow \quad T_x a - T_y b = 2q_1\Omega_1 + 2q_2\Omega_2 + 2q_3\Omega_3$$

The previous equation can be rewritten using the expression of the shear flows previously derived:

$$T_x a - T_y b = 2\sum_i \Omega_i q_i = 2\sum_i \Omega_i \left(-T_x \frac{S'_{yi}}{I_{yy}} - T_y \frac{S'_{xi}}{I_{xx}}\right) = -\frac{2T_x}{I_{yy}}\sum_i \Omega_i S'_{yi} - \frac{2T_y}{I_{xx}}\sum_i \Omega_i S'_{xi}$$

$$T_y\left(a - \frac{2}{I_{xx}}\sum_i \Omega_i S'_{xi}\right) = T_x\left(b - \frac{2}{I_{yy}}\sum_i \Omega_i S'_{yi}\right)$$

$$T_y(a - x_{SC}) = T_x(b - y_{SC})$$

$$b - y_{SC} = \frac{T_y}{T_x}(a - x_{SC})$$

Thus, the location of the shear center can be determined as follows, it is easy to notice that for an homogeneous section it is only a geometric property of the cross section (because it depends only on static moments and area moments):

$$\begin{cases} x_{SC} = \dfrac{2}{I_{xx}}\displaystyle\sum_i \Omega_i S'_{xi} \\ y_{SC} = \dfrac{2}{I_{yy}}\displaystyle\sum_i \Omega_i S'_{yi} \end{cases} \tag{4.9}$$

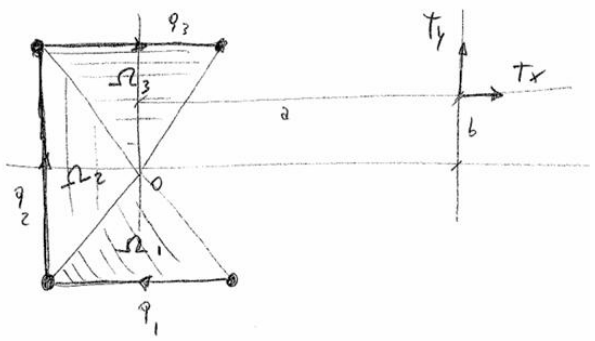

Figure 4.17: C semi-monocoque section.

Observation. To determine both the shear flows and the shear center, there are subjective choices that can greatly simplify the problem. For example, a proper choice of the areas A'_i can greatly simplify the evaluation of the shear flows. Moreover, symmetry considerations can help in reducing the number of shear flows evaluations required. In the example of Figure 4.16, it is clear that if the area of the bottom right stringer is equal to that of the top right one, i.e. $A_1 = A_4$, then the shear flow q_1 exiting A_1 is the same as q_3 entering A_4. When determining the shear center, or in general when using the moment equivalence relation, one can choose the pole about which to measure the moments so to have some of the Ω_i being null. For example, in Figure 4.17 we could have placed the pole "O" in the bottom left stringer, which makes $\Omega_1 = \Omega_2 = 0$. This simplifies the moment equivalence equation.

4.2.5. Solution procedure for single-cell closed section

A closed section with one cell is characterized by m panels, and thus m unknown shear flows, $n-1$ independent shear flow equations (number of stringers) and 1 equivalence condition between shear flows and the internal moment. Thus, single celled close sections are a statically determined scheme. In fact, the solution can be found using equilibrium conditions only, i.e. the shear flow equations (axial equilibrium). Compatibility does not need to be enforced, as for statically determined beam problems.

4.2.5.1. Shear stresses

The evaluation of the shear stresses for an open cross section is the following:

- It is imagined to "open" one arbitrary panel of the cross section. Then, in all panels but the open one, it is imagined the presence of $n-1$ ***dummy shear flows*** $\boldsymbol{q_i'}$, which can be obtained by applying $n-1$ times the shear flow equation (4.7). Moreover, a ***circulating flow*** $\boldsymbol{q^*}$ is imagined to flow in all the panels of the closed cell.
- The value of the circulating flow is obtained by imposing the equivalence condition to internal moments with respect to any arbitrary point P:
- The additional equation needed to evaluate the circulating flux q^* is provided by the moment equivalence equation with respect to any arbitrary point P. Assuming that the internal actions are T_y, T_x and M_z, we'll write:

$$M_t + T_y x_P + T_x x_P = \sum_i (2\Omega_i q_i') + 2q^* \Omega_{cell}$$

- Once the circulating flux q^* has been determined, the actual shear fluxes acting on the section's panels are obtained by the algebraic sum of the dummy fluxes q_i' and q^*. For each panel, if the two fluxes have the same direction, then we write $q_i = q_i' + q^*$, otherwise $q_i = q_i' - q^*$.
- Stresses are retrieved by assuming that they are constant across the thickness of the panels, and thus $\tau_i = q_i / t_i$.

4.2.5.2. Shear center

The evaluation of the shear center for single celled closed sections relies on determining the torsion of the section θ' and imposing it to be zero. The point for which this condition is satisfied is the shear center. The evaluation of the torsion is also needed for (1) solving sections with more than one cell, and (2) evaluating the torsional stiffness $GJ = M_z/\theta'$ of a section, discussed in section 4.2.7.

The evaluation of the torsion θ' is conducted applying the PCVW, the shear flows are assumed to be known. Considering a two celled closed section, for generality, the real and dummy systems are obtained as follows:

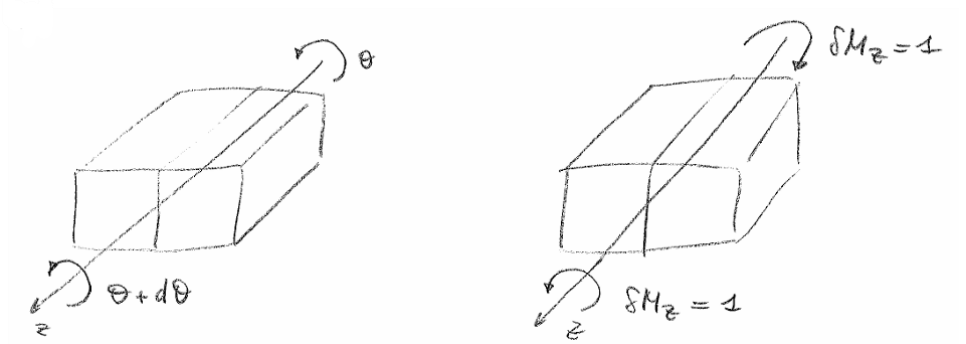

Figure 4.18: left) real system for torsion; right) dummy system for torsion of a semi-monocoque section.

The external virtual works can be written as follows:

$$\delta W_e^* = \delta M_z(\theta + d\theta) - \delta M_z\theta = \delta M_z d\theta = d\theta$$

Where we set $\delta M_z = 1$ due to the arbitrariness of the virtual internal actions. The internal virtual work for one closed cell of m panels can be written as follows:

$$\delta W_D^* = \sum_m \int_{V_m} \delta\tau_m \gamma_m dV_m = \sum_m \int_{V_m} \frac{\delta q_m}{t_m} \gamma_m dV_m$$

Using the equivalence between shear flows and internal torsional action we obtain:

$$\delta W_D^* = \sum_m \int_{V_m} \frac{\delta q_m}{t_m} \gamma_m dV_m = \sum_m \int_{V_m} \frac{1}{t_m} \frac{1}{2\Omega_{cell}} \gamma_m dV_m$$

Here we used again that $\delta M_z = 1$. Recall now the CL for shear stresses $\gamma = \tau/G$. Moreover, for thin-walled beams the shear stress is assumed to be constant through the thickness, and thus $\gamma = q/tG$. By substitution we obtain:

$$\delta W_D^* = \sum_m \int_{V_m} \frac{1}{t_m} \frac{1}{2\Omega_{cell}} \gamma_m dV_m = \sum_m \frac{1}{2\Omega_{cell} t_m^2 G} \int_{V_m} q_m dV_m$$

The infinitesimal volume of a panel of a thin-walled beam can be expressed as $dV_m = t_m l_m dz$. Here, l_m and t_m are the length and thickness of the m-th panel, respectively, and are assumed to be constant in z. Thus, the integration variable and bounds reduce to $dz \in [0, l]$, where l is the length of the beam. The internal virtual work can be rewritten as follows:

$$\delta W_D^* = \sum_m \frac{1}{2\Omega_{cell} t_m^2 G} \int_{V_m} q_m dV_m = \frac{1}{2\Omega_{cell} G} \sum_m \int_l q_m \frac{l_m}{t_m} dz$$

Imposing equilibrium $\delta W_D^* = \delta W_e^*$ leads to the following expression for estimating the torsion θ' of a semi-monocoque beam:

$$\theta' = \frac{d\theta}{dz} \approx \frac{1}{2\Omega_{cell} G} \sum_m q_m \frac{l_m}{t_m} \tag{4.10}$$

Then, the shar center is found by imposing null torsion $\theta' = 0$, implying null rotation of the cross section, and solving for x_{sc} leads to the identification of the shear center.

Observation. Notice that it has been specified the evaluation of the torsion via equation (4.10) is an approximation of the actual torsion. In fact, this is easy to accept because equation (4.10) is based on the semi-monocoque model, an approximative model.

4.2.6. Solution procedure for multi-cell closed section

Consider the case of a section characterized by $N > 1$ cells. This implies that we have more panels m than independent shear flow equations $n - 1$ plus 1 equivalence condition. The problem is thus statically indetermined, and the number of independent equations to impose is:

$$m - (n - 1 + 1) = m - n \quad \xrightarrow{N = n - m + 1} \quad m - n = N - 1$$

Thus, we need $N - 1$ additional equations, which are provided by compatibility conditions placed on the torsion of the cells of the section $\theta_1' = \theta_2' = \cdots = \theta_N'$.

4.2.6.1. Shear stress

The procedure to evaluate the shear stresses of a multi-celled closed section is summarized as follows:

- Cut one panel per cell.
- Evaluate the flows q_i' using the shear flow equation.
- Impose the moment equivalence equation about the arbitrary point P, in this case we'll also have N circulating fluxes:

$$M_z + T_y x_P + T_x y_P = \sum_i 2\Omega_i q_i' + \sum_N 2\Omega_N q_N^*$$

- Impose $N - 1$ compatibility conditions about the torsion θ' of the section, which can be estimated via equation (4.10). Note that here one has to consider for each cell only the shear fluxes flowing through the panels of such cell. This implies that the circulating fluxes of adjacent cells q_{Nj}^* must also be considered when evaluating θ_i for $i \neq j$.

$$\theta_1' = \theta_2' = \cdots = \theta_N'$$

- Solve the system of equations for the N circulating fluxes q_N^* and retrieve the actual fluxes q_i. Then shear stresses are obtained as $\tau_i = q_i / t_i$.

4.2.6.2. Shear center

The evaluation of the shear center is straightforward because essentially the steps required for the evaluation of the shear stresses need to be repeated, with one additional condition $\theta' = 0$. The difference lies in the fact that the shear forces T_x and T_y are usually chosen to be of unitary value. The left-hand-side of the moment equivalence equation will provide with:

$$T_y x_{sc} + T_x y_{sc}$$

The additional condition that is placed on the torsional compatibility equations will be $\theta' = 0$. The solution of the resulting system of equations will provide with x_{sc} and y_{sc}.

4.2.7. Evaluation of section properties

The section properties of a semi-monocoque beam need to be evaluated as part of the modellization process. They might then be needed for further analysis, such as with FE beam models, for which such properties must naturally be provided.

4.2.7.1. Axial and bending stiffnesses

These are easily computed as follows:

$$\begin{cases} EA = E\sum_i^n A_i \\ EI_{xx} = E\sum_i^n A_i y_i^2 = E\sum_i^n I_{xx_i} \\ EI_{yy} = E\sum_i^n A_i x_i^2 = E\sum_i^n I_{yy_i} \end{cases} \tag{4.11}$$

4.2.7.2. Torsional stiffness

In general, the torsional stiffness of a semi-monocoque section can be computed using the torsional CL:

$$M_z = GJ\theta' \quad \rightarrow \quad GJ = \frac{M_z}{\theta'}$$

Where M_z is an ***arbitrary*** torsional moment, i.e. we can choose $M_z = 1$, and the torsion θ' can be estimated as follows:

$$\theta' = \frac{1}{2\Omega G}\sum q_i \frac{l_i}{t_i}$$

Note that for open cross section this yields $GJ = 0$, while for single celled closed sections we may also compute the torsional stiffness via equation (2.35) for the torsional constant, introduced in section 2.1.6.3 and reported here:

$$J = \frac{4\Omega^2}{\oint_\Gamma \frac{1}{t(s)} d\Gamma}$$

4.2.7.3. Shear stiffness

The evaluation of the shear stiffness of a section is ***extremely relevant for thin walled beams***, such as the ones that are modelled with the semi monocoque model. Contrarily, as mentioned in section 2.1.7, this is not the case for slender compact beams. The reason lies in the fact that for thin-walled beams the strain energy contribution due to shear loads in not negligible, while for compact beams it is. To clarify this point, consider the slender beam presented in Figure 4.19, characterized by a concentrated shear load at its tip and a squared cross section. The internal actions through such beams are:

$$\begin{cases} T_y = -F \\ M_x = -Fz \end{cases}$$

Thus, the strain energies associated to shear U^S and bending U^B of such beam with a compact section are:

$$\begin{cases} U^S = \int_0^l \frac{T_y^2}{GA_y^*} dz = \frac{1}{2}\frac{Fl^2}{GA_y^*} \\ U^B = \int_0^l \frac{Mx^2}{EI_{xx}} dz = \frac{1}{2}\frac{F^2 l^3}{3EI_{xx}} \end{cases}$$

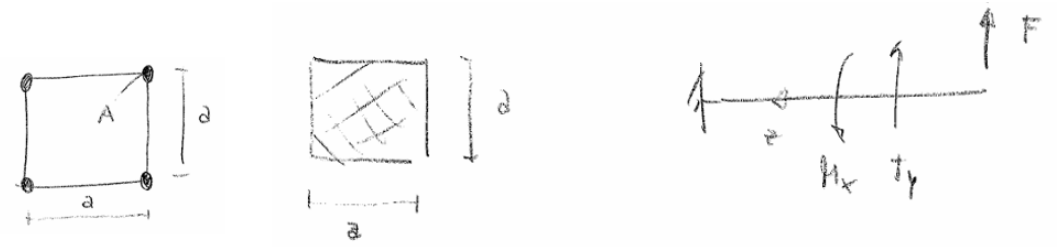

Figure 4.19: compact square-section beam.

Assuming that $E \approx 2G$, $l = 1\text{m}$ and $a = 0.1\text{m}$, the energy associated to shear is less than 1% of that associated to bending:

$$\frac{U^S}{U^B} = \frac{\frac{1}{2}\frac{F^2 l}{GA^*}}{\frac{1}{2}\frac{F^2 l^3}{3EI}} = 3\frac{EI}{GA^* l^2} = \frac{3}{5}\frac{a^2}{l^2} = \frac{3}{500}$$

Consider now the thin-walled model of the same beam section presented in Figure 4.19. The geometric properties of such section are assumed to be:

$$A = \frac{1}{12}a^2 \qquad t = \frac{1}{120}a^2 \qquad I = 4A\left(\frac{a}{2}\right)^2 = Aa^2 = \frac{1}{12}a^4$$

In order to compute the shear stiffness of such section ,we need to estimate the portion of its cross sectional area that contributes to shear stiffness A^*. The procedure will be illustrated afterwards, and it leads to equation (4.12), from which we obtain $A^* = 2at$. Assuming again that $E \approx 2G$, $l = 1\text{m}$ and $a = 0.1\text{m}$, according to the semi-monocoque model the energy associated to shear is about 30% of that associated to bending:

$$\frac{U^S}{U^B} = 3\frac{EI}{GA^* l^2} \approx \frac{6}{l^2}\frac{a^4}{12}\frac{1}{2at} = \frac{1}{4}\frac{a^3}{l^2 t} = \frac{1}{4}\frac{a^3}{l^2}\frac{120}{a} = 30\frac{a^2}{l^2} = 0.3$$

It follows that ***for thin-walled beams the shear strain contribution is not negligible because shear deformability is high***, in other words the beam is not as stiff in shear as a compact beam.

A strategy to estimate the shear stiffness GA^* is then required. The evaluation of the shear stiffnesses GA_x^* and GA_y^* requires the ability to solve the section of a semi-monocoque beam when shear forces T_x and T_y are applied to the shear center of the section. Then, the shear stiffnesses are obtained via an energy equivalence of the internal complementary virtual work δW_D^* of the compact and thin-walled beams. To clarify the procedure, consider an arbitrary T_x passing through the shear center of the section. The expression of δW_D^* used here is slightly different from the one used to obtain the torsion. More precisely, we do not use the equivalence between torsional moment and shear strains, since it is assumed that the shear strain energy is due to shear loads passing through the shear center, and thus no torsion is considered. The complementary internal virtual work δW_D^* of a cell made of m panels for a thin-walled beam will be:

$$\delta W_D^* = \sum_m \int_{V_m} \delta\tau_m \gamma_m dV_m = \sum_m \int_{V_m} \frac{\delta\tau_m \tau_m}{G} dV_m$$

Recalling that for a thin-walled beam the shear stress is assumed to be constant across its thickness $\tau = q/t$, the above equation can be rewritten as follows:

$$\delta W_D^* = \sum_m \int_{V_m} \frac{\delta q_m q_m}{G t_m^2} dV_m$$

The volume of the panels of a thin-walled beam can be expressed as $dV_m = l_m t_m dz$, where dz goes from 0 to the beam length l and we assume the panels to have constant geometry along the bam axis z. By substitution we obtain:

$$\delta W_D^* = \sum_m \int_l \delta q_m \frac{q_m}{G t_m^2} l_m t_m dz = \sum_m \int_l \delta q_m \frac{l_m}{G t_m} q_m dz$$

The complementary internal virtual work δW_D^* of a compact beam will be:

$$\delta W_D^* = \int_l \frac{\delta T_x T_x}{GA_x^*} dz$$

Equating the two expressions of δW_D^* leads to the shear stiffness GA_x^* to be:

$$GA_x^* = \frac{\delta T_x T_x}{\sum_m \delta q_m \frac{l_m}{G t_m} q_m} \tag{4.12}$$

4.3. Ribs and frames

Ribs and frames are essential components in a thin-walled structure for the reasons discussed in section 4.1. The difference between ribs and frames is that the former are used in wings, while the latter (also referred to as rings) are used in fuselages or cylindrical shells of launchers.

4.3.1. Functions

4.3.1.1. Shape

The presence of transverse stiffening elements, modelled as infinitely stiff in the in-plane direction, ensures that the shape of the cross section is maintained despite the action of the aerodynamic loads. This is crucial for preserving aerodynamic performance.

Figure 4.20: aerodynamic shape preserved by ribs (left) and deformed due to the absence of ribs (right).

Not that this condition, i.e. the rigid rotation of the section of the wing, a thin-walled beam, is consistent with the solution for torsion obtained from the DSV beam theory. Moreover, the presence of ribs ensures that the shape of the section is preserved even when the DSV are not respected, such as the case of a distributed load, such as the aerodynamic loads.

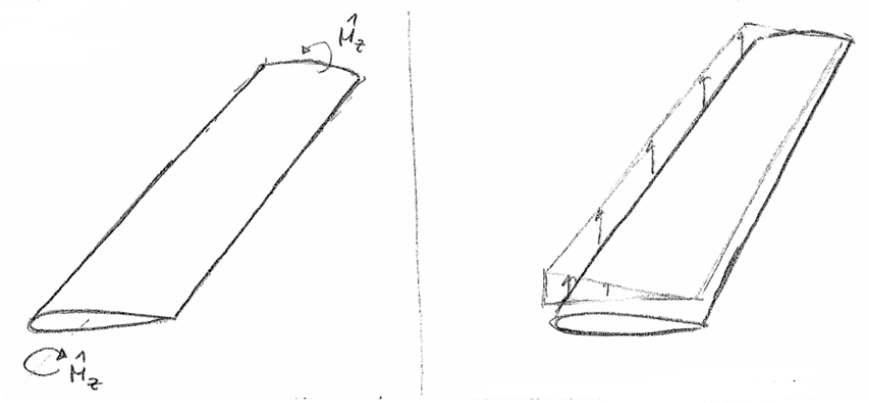

Figure 4.21: left) loads in accordance with DSV solution; right) distributed loads.

4.3.1.2. Load introduction

This is a direct consequence of their role in maintaining the wing shape. For thin-walled sections, the load introduction has to be associated with a locally in-plane stiffer region, i.e. a rib/frame, in order to preserve the section shape. In general, the choice of the location of a number of ribs is dictated by the design itself. In particular, ribs will be placed in correspondence of those points where ***concentrated loads*** need to be introduced, such as in correspondence of engines, junction between wing and fuselage, openings, actuators (Figure 4.22 – left). Naturally, ***distributed aerodynamic loads*** must also be introduced in the structure. In order to guarantee proper load introduction of such loads, additional ribs to those needed for concentrated loads will be placed along the wing to achieve a distribution which is approximately homogeneous (Figure 4.22 – right).

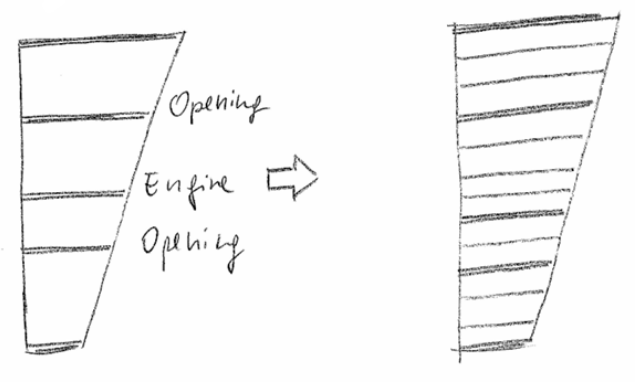

Figure 4.22: ribs placement along a wing.

Moreover, the presence of ribs along the wing has the added benefit of providing support for the cover panels in terms of bending-induced displacements. In this sense, it is worth highlighting the ratio between the chord c of the wing and the pitch of the ribs b, i.e. the distance between two consecutive ribs along the wing. As a simplified model, it can be assumed that the portion of the panel from rib to rib is a simply supported plate as depicted in Figure 4.23 – left. An exact solution for this problem can be easily found, and it can be shown that the maximum bending displacement due to pressure load in terms of the aspect ratio $r = c/p$ is the one in Figure 4.23 right. It should be noted that plate bending is a local phenomenon, which is therefore not captured by the DSV beam model, on which the semi monocoque-model builds upon.

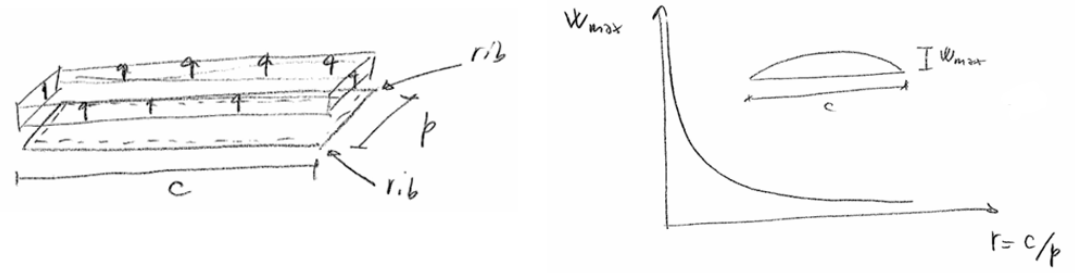

Figure 4.23: left) idealization of the cover panel between two consecutive ribs; right) bending displacement of the panel due to aerodynamic loads in terms of aspect ratio $r = c/p$.

The distributed loads acting on the panels are transferred to the rest of the structure by ribs and spars. Spars are another type of transverse stiffening element perpendicular to ribs (Figure 4.24 – left) which also support panels. More precisely, if $r = c/p = 1$ then ribs and spars introduce the load in equal measure. However, is more typical that $r = c/p \gg 1$ for which the ribs introduce most of the load. This scenario leads to the scheme represented in Figure 4.25.

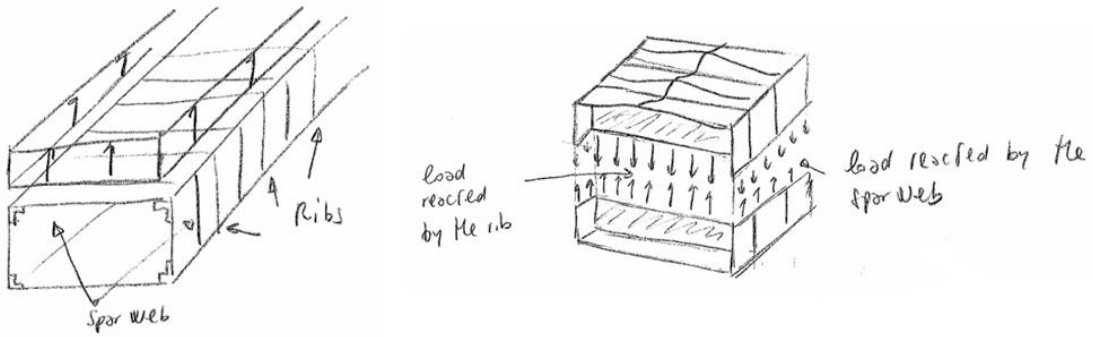

Figure 4.24: left) web spars and ribs; right) reaction loads on ribs and spars.

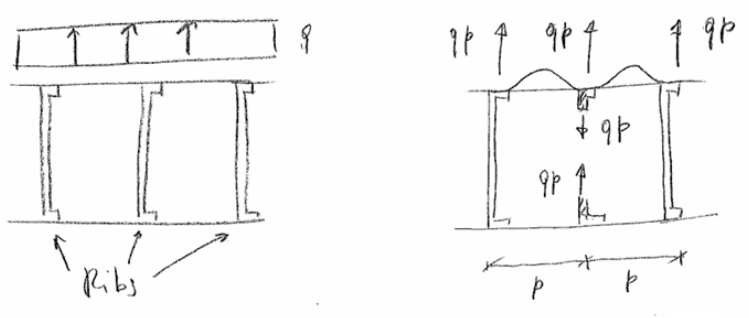

Figure 4.25: distributed aerodynamic load introduced entirely by the ribs and related local plate/panel bending.

In the context of the semi-monocoque scheme, it is then assumed that all loads are introduced by ribs. The concentrated loads are effectively applied to ribs, while the ones distributed on panels are condensed to a set of statically equivalent loads applied to ribs. As previously discussed, this has the effect of filtering out the local effects of plate bending, while preserving the global behavior of the structure. Accordingly, the internal forces will be characterized by the following behavior:

- Shear T_x, T_y piecewise constant.
- Bending moments M_x, M_y piecewise linear.
- Torsion M_z piecewise constant.

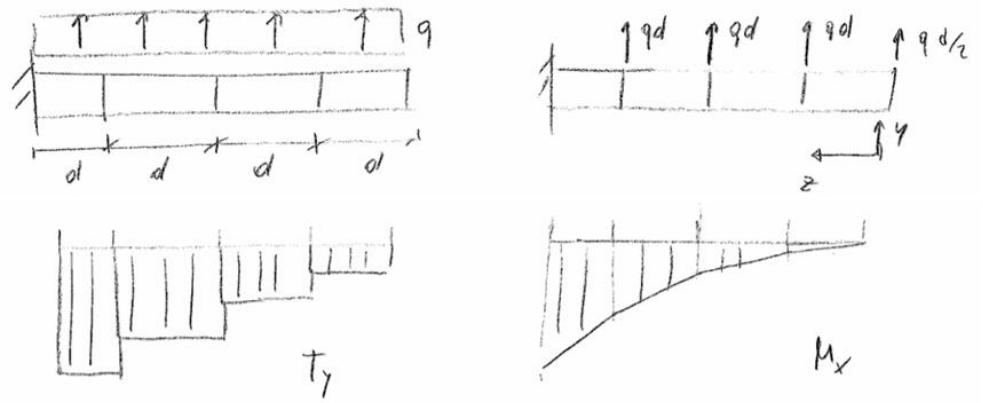

Figure 4.26: types of load distribution for a semi-monocoque wing with loads introduced only by ribs.

4.3.1.3. Improving buckling behavior

Buckling is a type of structural instability phenomenon, thus it is in general preferred to avoid it. As a first approximation we can assume that the stringer in between two consecutive ribs would buckle according to the Euler's buckling load:

$$P_{cr} = EI\frac{\pi^2}{\lambda^2}$$

Where λ is the half wave-length of the buckled configuration. The value of this parameter depends on how the stringer is constrained against the ribs. Assuming the stringer to be pinned to the ribs, then $\lambda = d$, where d is the pitch. Thus, in order to increase the buckling load one has to reduce d, which in practical terms means to introduce another rib.

$$EI\frac{\pi^2}{d_1^2} < EI\frac{\pi^2}{d_2^2} \quad \text{if} \quad d_1 > d_2$$

4.3.2. Analysis of ribs and frames

The analysis of ribs and frames is carried out by evaluating the section where the rib or frame is attached to the skin. This is because the two parts are connected with junctions and so there is an exchange of shear flows along the junction lines. This is the mechanism with which the ribs and frames introduce the load in the rest of the structure.

The ***analysis procedure of ribs*** is carried out in the following steps:

- First we consider the section where the rib is attached, and we obtain its semi-monocoque model.

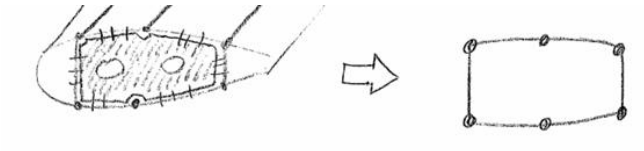

Figure 4.27: semi-monocoque model of a rib.

- We apply the loads acting on the rib and determine the equivalent shear flows that equilibrate them. This means that after determining the shear flows due to the externally applied load, we reverse their direction, because they must equilibrate such loads. Note that the external loads can be determined based on the jumps in the internal actions diagrams, as we assume that the loads are introduced by the ribs only. Alternatively, the loads can be given as input to the structural analysis phase.

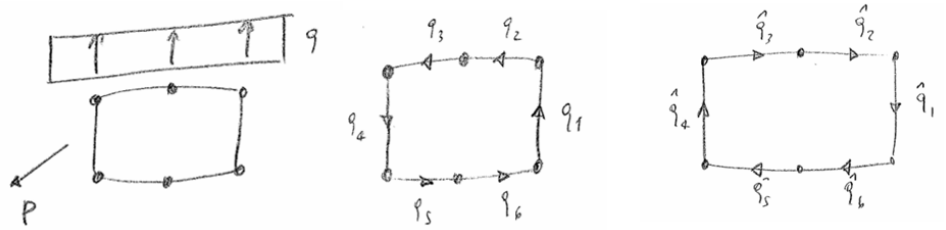

Figure 4.28: shear flows on a rib.

- A beam model can be adopted for preliminary analysis of the rib. In this phase we consider both the externally applied loads and the shear flows equilibrating them. More precisely, $\hat{m}$ and $\hat{n}$ are the distributed loads obtained from the shear flows, while F_A and F_B are the force resultants along the webs.

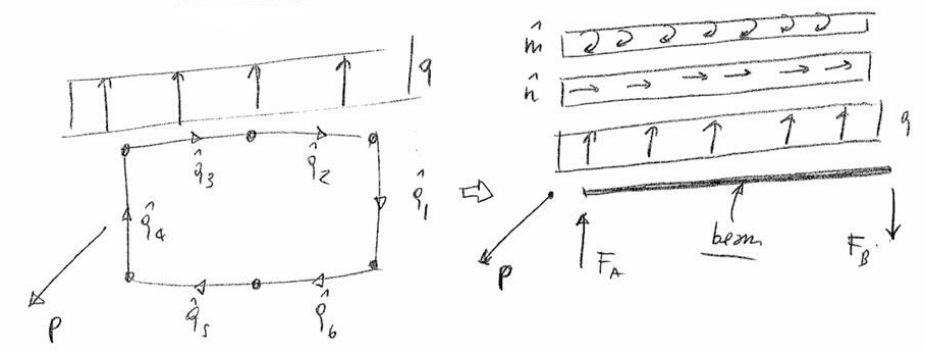

Figure 4.29: beam model of a rib.

- Once the beam model of the rib and all the applied loads are obtained, stress evaluation can be carried out.

For what concerns frames, the analysis procedure is analogous to the one outlined for ribs. In fact, the two structural elements serve the same role, however ribs are those present in wing-like structures, while frames are those in cylindrical shells structures, such as the fuselage. Thus the ***analysis procedure of frames*** can be defined as follows:

- Obtain the semi-monocoque model of the frame section.
- Compute the shear flows generated by the externally applied loads.
- Reverse the direction of such shear flows to obtain those that equilibrate the applied loads.
- Solve for the internal actions resulting of the self-equilibrating loads of the previous step.

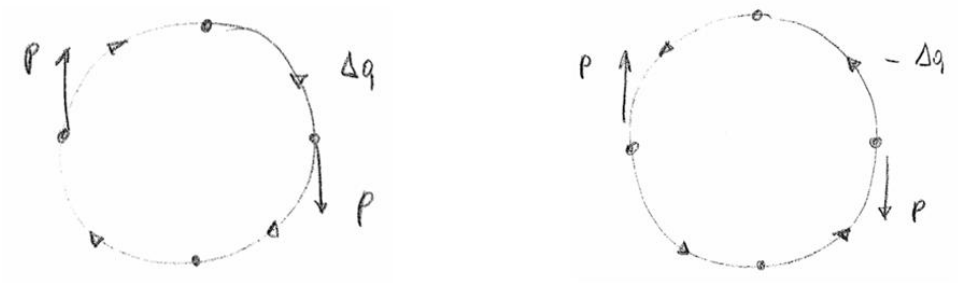

Figure 4.30: shear flows generated by external loads (left) and that equilibrate the external loads (right).

4.3.3. Symmetries

When symmetry can be applied, one can analyze only part of the structure instead of the entire entity. This is useful as it generally simplifies the problem solution from an analytical point of view, and numerically it reduces drastically the computational time required for FEA of complex numerical models.

The symmetry of a structure is determined by ***three key factors***: geometry (1), material and stiffness (2), and boundary conditions (3). If all three conditions meet the symmetry requirements, then we can simplify the problem since:

- Symmetric loading → symmetric response.
- Anti-symmetric loading → anti-symmetric response.

A common case is given by ***plane symmetries***, which are characterized by one or more axis about which the structure can be rotated of 180° without changing its geometry and BCs. For example, in the case of ribs, a rotation of 180° as the one in the figure below does not alter the rib geometry,

i.e. after the rotation, the rib configuration is as before the rotation. The same applies for the beam in the figure, for which BCs must also be considered (the rib is self-equilibrating).

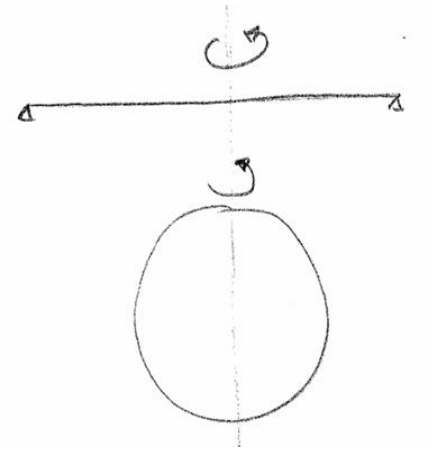

Figure 4.31: symmetry axis of a beam (top) and of a rib (bottom).

A typical example of the use of symmetries in aerostructures is with frames, which in a plane analysis are three times statically indetermined systems. Such problem could be simplified by exploiting the symmetry of the structure, which allows rewrite the applied loads in a symmetric $\hat{P}$ and an anti-symmetric $\tilde{P}$ contribution.

$$\begin{cases} \hat{P} = \dfrac{P_A + P_B}{2} \\ \tilde{P} = \dfrac{P_A - P_B}{2} \end{cases}$$

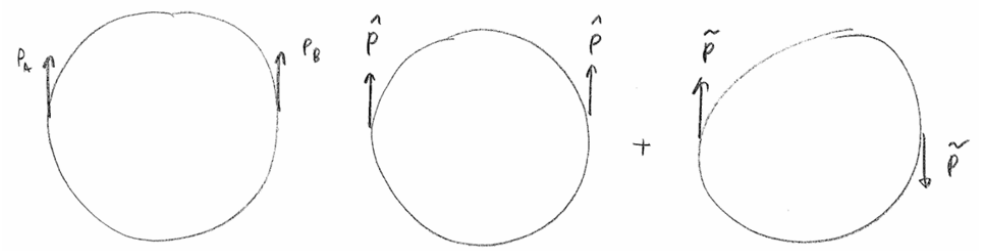

Figure 4.32: loaded frame with symmetric load decomposition.

The advantage is that the originally complex problem is simplified in two problems that are easier to solve. The symmetric system is two times statically indetermined, while the anti-symmetric one only one time. The symmetry and anti-symmetry conditions are as follows:

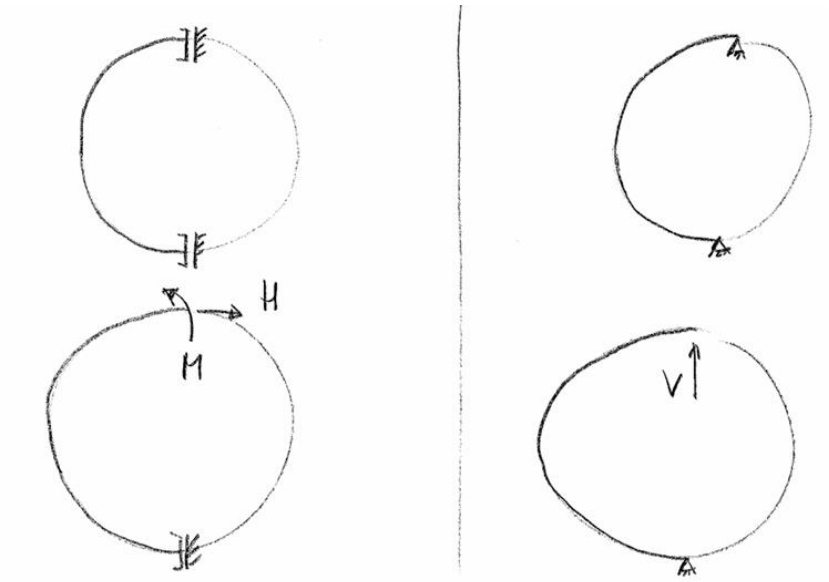

Figure 4.33: left) symmetry conditions, right) anti-symmetry conditions.

In the case of 3D beams the generic point is characterized by three displacement components $\boldsymbol{u} = \{u, v, w\}$ and three rotation components $\boldsymbol{\theta} = \{\theta_x, \theta_y, \theta_z\}$. Similarly, the internal exchange of forces is carried out via internal actions in the form of three forces $\boldsymbol{T} = \{T_x, T_y, T_z\}$ and three moments $\boldsymbol{M} = \{M_x, M_y, M_z\}$.

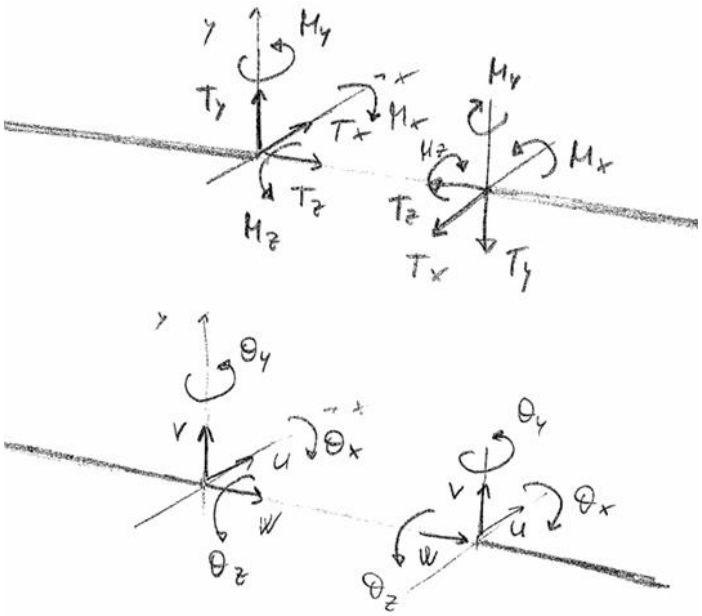

Figure 4.34: top) internal forces and moments; bottom) internal displacements and rotations.

In this case, the symmetry conditions are more easily understood starting from the displacements and rotations. Then, a reaction force or moment exists for any component set to zero. Some applicative examples of symmetry in beams are discussed in the appendix (section 10.3).

$$\text{symmetric: } \begin{cases} u \neq 0 \rightarrow T_x = 0 \\ v \neq 0 \rightarrow T_y = 0 \\ w = 0 \rightarrow T_z \neq 0 \\ \theta_x = 0 \rightarrow M_x \neq 0 \\ \theta_y = 0 \rightarrow M_y \neq 0 \\ \theta_z \neq 0 \rightarrow M_z = 0 \end{cases} \qquad \text{anti} - \text{symmetric: } \begin{cases} u = 0 \rightarrow T_x \neq 0 \\ v = 0 \rightarrow T_y \neq 0 \\ w \neq 0 \rightarrow T_z = 0 \\ \theta_x \neq 0 \rightarrow M_x = 0 \\ \theta_y \neq 0 \rightarrow M_y = 0 \\ \theta_z = 0 \rightarrow M_z \neq 0 \end{cases}$$

Figure 4.35: left) symmetric equivalent BCs; right) anti-symmetric equivalent BCs.

Observation. It is important to carefully evaluate the application of symmetry considerations when dealing with non-linear phenomena. Buckling, which is one of such phenomena, is such that even if geometry, material/stiffness and BCs are all symmetric, the buckling response of a structural element is not. Thus, studying buckling under symmetry considerations may lead to artificially "hiding" some buckling modes.

4.4. Junctions

Joints play a fundamental role in aeronautical structures, as they ensure the transfer of loads between structural elements while maintaining overall integrity and safety. Among the various joining methods, bolted and welded joints are the most widely employed. Bolted joints offer flexibility since they can be easily assembled, disassembled, and used to connect dissimilar materials. However, they require larger space, increase structural weight, and may loosen under vibration. Welded joints, on the other hand, provide lightweight and compact solutions that are not prone to loosening, but they are permanent, demand skilled workmanship, and can create critical sites for fatigue crack initiation.

4.4.1. Welded joints

The reference technical standard for welded joints are the UNI EN 1993 part 1-8 and the CNR 10011. The latter suggest ***reducing the multiaxial stress state in the weld to an equivalent stress*** $\boldsymbol{\sigma_{id}}$ and compare it to material strength. However, such equivalent stress is not obtained via the cartesian stress components. Due to the relatively complex stress state in the welded region, the following stress components are defined:

- $\sigma_\perp$ = normal stress to the longitudinal cross section of the weld, acts normal to weld direction.
- $\sigma_\parallel$ = normal stress to the normal cross section of the weld, acts parallel to weld direction.
- $\tau_\perp$ = shear stress acting normal to weld direction.
- $\tau_\parallel$ = shear stress acting parallel to weld direction.

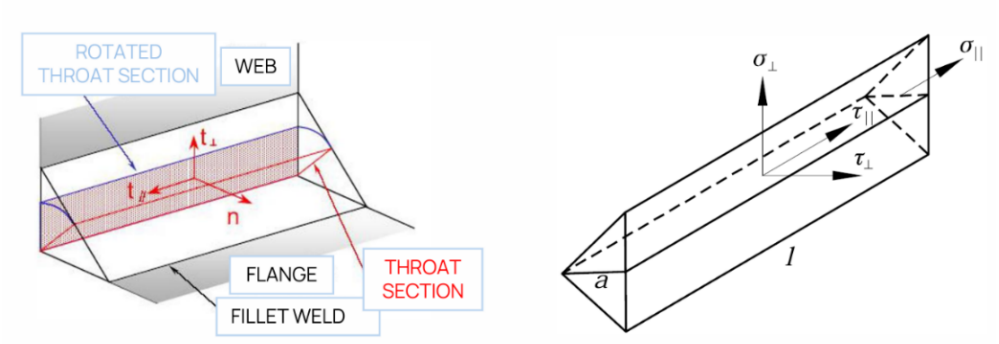

Figure 4.36: examples of groove-butt and fillet welds.

Using these stress component, it's possible to compute the ***equivalent uniaxial stress*** $\boldsymbol{\sigma_{id}}$ via the Von Mises stress for a plane stress state as follows:

$$\sigma_{id} = \sqrt{\sigma_\perp^2 + \sigma_\parallel^2 + \sigma_\perp \sigma_\parallel + 3\tau_\parallel^2} \tag{4.13}$$

4.4.1.1. Groove-butt welded joints

A groove weld is a weld made in a groove between two members, while a butt weld is a performed between two elements approximately in the same plane. Thus, a butt weld is not necessarily a groove weld, and vice versa. Typical groove butt welds are presented in Figure 4.37, along with the characteristic dimensions to be used in welded joints assessment.

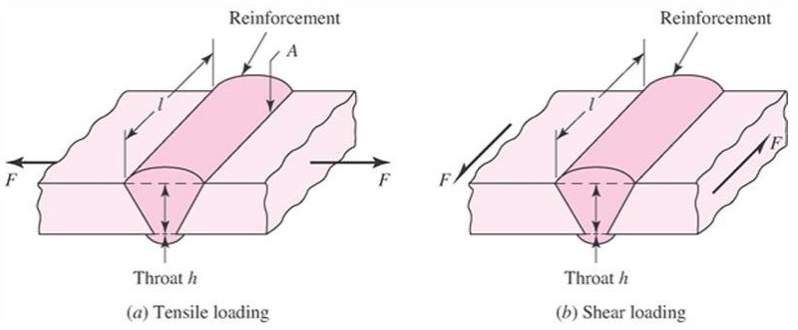

Figure 4.37: groove butt welds.

Such parameter is to be compared to some sort of ***allowable***, two approaches exist:

- Limit state: different effects are combined in order to provide a more refined estimation of the load acting on the weld. The parameter obtained is called *design resistance of the material* f_d. It's generally noticeably lower than the material allowable used in the other approach, thus *more conservative*.
- Allowable stress: the comparison is carried out using the material allowable itself, thus it's a *less conservative* approach than the previous one.

Limit state		
Material	f_d N/mm²	
	$t \leq 40$	$t > 40$
Fe 360	235	210
Fe 430	275	250
Fe 510	355	315
t = thickness in *mm*		

Allowable stress		
Material	σ_{adm} N/mm²	
	$t \leq 40$	$t > 40$
Fe 360	160	140
Fe 430	190	170
Fe 510	240	210
t = thickness in *mm*		

Table 4.1: allowables for welded joints assessment.

It's important to point out the effect of thickness: thicker plates statistically have more defects in them, thus allowables must be tighter for such plates. A second crucial aspect is the level of precision in the manufacturing and inspection processes applied to the welds. Based on these, we distinguish between I class, stricter controls, and II class, less strict controls. Clearly, for II class joints allowables will be lower to compensate for less than optimal control procedures.

(Limit state)	
Joint	$\sigma_{id} \leq$
I class	f_d
II class	0,85 f_d
f_d = Design resistance of material	

(Allowable stress)	
Joint	$\sigma_{id} \leq$
I class	σ_{adm}
II class	0,85 σ_{adm}
σ_{adm} = Allowable stress of material	

Table 4.2: allowables for I and II class welded joints.

Thus, the assessment for a groove-butt welded joint can be carried out as follows:

$$\begin{cases} \sigma_{id} \leq k\sigma_{adm} & \text{for allowable stress} \\ \sigma_{id} \leq k f_d & \text{for limit state} \end{cases} \quad \text{where} \quad \begin{cases} k = 1 & \text{for I class weld} \\ k = 0.85 & \text{for II class weld} \end{cases} \tag{4.14}$$

4.4.1.2. Fillet welds

For fillet weld the throat section a has great significance in the definition of the stresses. The throat is defined as the height of the biggest triangle inscribable in the weld. The throat section is the reference taken to define the stresses previously introduced. However, in fillet joints assessment it's common practice to rotate the throat section on one of its sides to facilitate the assessment. This has two consequences, we basically revert back to the stress definitions given previously (1), and the $\sigma_{\parallel}$ is always negligible for these joints.

This leads to the following implementation of the ***fillet joint assessment***:

1) If all the three stress components are present ($\tau_{||}$, $\sigma_{\perp}$, $\tau_{\perp}$), the following limits must be respected:

$$\sqrt{\tau_{\perp}^2 + \sigma_{\perp}^2 + \tau_{||}^2} \leq \begin{cases} 0.85\ \sigma_{adm} & \text{for steel Fe 360} \\ 0.70\ \sigma_{adm} & \text{for steel Fe 430 and Fe 510} \end{cases}$$

$$|\tau_{\perp}| + |\sigma_{\perp}| \leq \begin{cases} \sigma_{adm} & \text{for steel Fe 360} \\ 0.85\ \sigma_{adm} & \text{for steel Fe 430 and Fe 510} \end{cases}$$

2) If only $\sigma_{\perp}$ and $\tau_{\perp}$ are present, it is sufficient to verify [2] and the following two limits as well:

$$|\tau_{\perp}| \leq \begin{cases} 0.85\ \sigma_{adm} & \text{for steel Fe 360} \\ 0.70\ \sigma_{adm} & \text{for steel Fe 430 and Fe 510} \end{cases}$$

$$|\sigma_{\perp}| \leq \begin{cases} 0.85\ \sigma_{adm} & \text{for steel Fe 360} \\ 0.70\ \sigma_{adm} & \text{for steel Fe 430 and Fe 510} \end{cases}$$

3) If either $\tau_{||}$ and $\tau_{\perp}$ or $\sigma_{\perp}$ and $\tau_{||}$ are present, it is sufficient to verify [1].

4) If one of the three stress components is present (either $\tau_{||}$, $\sigma_{\perp}$ or $\tau_{\perp}$), it is sufficient to verify the following:

$$|\tau_{\perp}|, |\sigma_{\perp}|, |\tau_{||}| \leq \begin{cases} 0.85\ \sigma_{adm} & \text{for steel Fe 360} \\ 0.70\ \sigma_{adm} & \text{for steel Fe 430 and Fe 510} \end{cases}$$

4.4.2. Bolted joints

Bolts are widely used in many engineering applications; thus they have been standardized to a high degree. Their strength and allowables are tabulated with respect to the ***class*** of the bolt. The class is a pair of numbers that identifies yielding and maximum strength as follows:

$$AB \quad \rightarrow \quad \begin{cases} \sigma_y = A \cdot B \cdot 10MPa \\ \sigma_{UTS} = A \cdot 100MPa \end{cases}$$

Tensione ammissibile					
Classe vite	f_t (UTS) N/mm²	f_y ($R_{p0,2}$) N/mm²	$f_{k,N}$ N/mm²	$\sigma_{b,adm}$ N/mm²	$\tau_{b,adm}$ N/mm²
4.6	400	240	240	160	113
5.6	500	300	300	200	141
6.6	600	360	360	240	170
8.8	800	640	560	373	264
10.9	1 000	900	700	467	330
12.9	1 200	1080	840	560	396

$f_{k,N}$ è assunto pari al minore dei due valori $f_{k,N} = 0,7\ f_t$, $f_{k,N} = f_y$ essendo f_t ed f_y le tensioni di rottura e di snervamento secondo UNI 3740.

$\sigma_{b,adm}$, $\tau_{b,adm}$ tensioni ammissibili a trazione ed a taglio.

Figure 4.38: bolt admissible as a function of bolt class.

Another standardized quantity is the ***mean diameter*** of bolts with threaded regions of triangular profile. According to UNI-4535-64, the following tables are to be taken as reference.

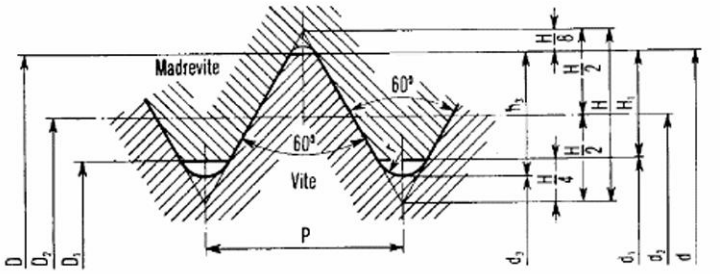

d = diameter of external thread
D = diameter of internal thread

Figure 4.39: bolt thread cross section.

Nominal diameter (major diameter)			Pitch	Mean diameter	Minimum diameter (external thread)		Minimum diameter (internal thread)	Depth	Height	Fillet radius	Tensile area (A_{res})	Minimum area
Colonna 1	Colonna 2	Colonna 3	P	$d_2 = D_2$	d_3	d_1	D_1	h_3	H_1	r	mm²	mm²
10			1,5	9,026	8,160	8,376	8,376	0,920	0,812	0,217	58,0	52,3
		11	1,5	10,026	9,160	9,376	9,376	0,920	0,812	0,217	72,3	65,9
12			1,75	10,863	9,853	10,106	10,106	1,074	0,947	0,253	84,3	76,2
	14		2	12,701	11,546	11,835	11,835	1,227	1,083	0,289	115	105
16			2	14,701	13,546	13,835	13,835	1,227	1,083	0,289	157	144
	18		2,5	16,376	14,933	15,294	15,294	1,534	1,353	0,361	192	175
20			2,5	18,376	16,933	17,294	17,294	1,534	1,353	0,361	245	225
	22		2,5	20,376	18,933	19,294	19,294	1,534	1,353	0,361	303	282
24			3	22,051	20,319	20,752	20,752	1,840	1,624	0,433	353	324
	27		3	25,051	23,319	23,752	23,752	1,840	1,624	0,433	459	427

Figure 4.40: bolt geometrical quantities as a function of nominal diameter.

The advantages and disadvantages of bolted joints have already been discussed. By regulation EN 1993-1-8 (2005), bolted joints are classified into:

- Nominally pinned: capable of transmitting internal forces without developing significant moments, thus rotations must be accepted under loading conditions.
- Semi-rigid.
- Rigid: rotational stiffness is sufficiently high to justify an analysis based on full continuity.

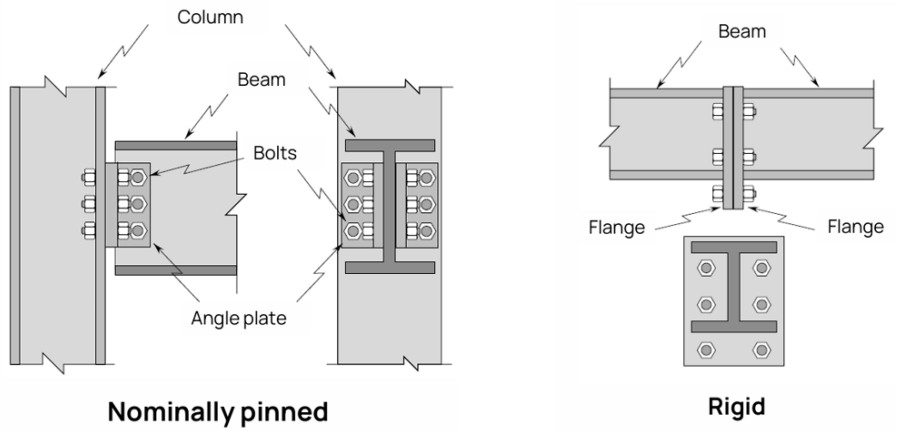

Figure 4.41: bolted joints.

In is depicted the ***behavior of the joint*** as a function of the in-plane force transmitted from the plates:

1. The joint works purely through friction, no shear contribution. The axial load normal to the contact plane generates friction between the bolt, the nut and the plate surfaces in between.
2. As soon as $F_t = F_{\text{fr}}$ the joint slips and the lateral surface of the bolt comes into contact with the surface of the holes in the plates. The load is carried by the bolt, not anymore by friction.
3. As the shear load V_b increases so does the slip Δl through a linear elastic law.
4. Yielding strength of the material is reached, and plastic deformation occurs.

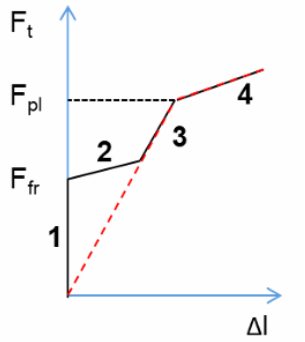

Figure 4.42: bolted joint behavior.

To ***assess*** whether joint work through friction or not, the following formula must be used:

$$F_b < \frac{F_{\text{fr}}}{1.25} \quad \text{where} \quad \begin{cases} F_{\text{fr}} = f \cdot n_f \cdot V_0 \\ V_0 = 0.8 \cdot f_{k,N} \cdot A_{res} \end{cases} \tag{4.15}$$

Where V_0 is the preload, f is the static friction coefficient, n_f is the number of plate interfaces (for two plates there will be one interface, so $n_f = 1$), $f_{k,N}$ is tabulated and A_{res} is computed using the diameters in the tables of Figure 4.40:

$$A_{res} = \frac{\pi}{4}(D_2^2 - D_1^2)$$

Furthermore, the required torque to generate V_0 can be approximately computed as follows:

$$M_t \approx 0.2 \cdot V_0 \cdot d$$

Where d is the nominal diameter. Such torque has two components: one winning the friction between the bolt and the nut M'' and one that wins the friction between nut and plate surface M'.

$$\begin{cases} M' = \frac{3}{8}M = \frac{3}{8}0.2 \cdot V_0 \cdot d \\ M'' = \frac{5}{8}M = \frac{5}{8}0.2 \cdot V_0 \cdot d \end{cases}$$

Once the bolts start carrying the load, three ***failure modes*** can occur, regulations (UNI EN 1993-1-8 and CNR 10011) impose how to perform the assessment for all three:

- Shear failure: the bolt itself fails, the assessment is carried out by verifying that the stress acting on the bolt is lower than the allowable. A distinction is made with regard to whether the contact between plates and bolts occurs at the shank or the thread of the bolt.

$$\begin{cases} \tau = \dfrac{F}{n_f \cdot n_b \cdot A_{nom}} \leq \tau_{adm} & \text{shank contact} \\ \tau = \dfrac{F}{n_f \cdot n_b \cdot A_{res}} \leq \tau_{adm} & \text{thread contact} \end{cases} \tag{4.16}$$

  Where n_f is the number of plate interfaces, n_b is the number of bolts, A_{nom} is the area of the bolt computed using the nominal diameter, while A_{res} is already been introduced.

- Bearing failure: the plate undergoes plastic deformation in the region surrounding the hole. Thus, assessment is carried out by comparing the reference pressure p_{ref} of such region to the reference stress σ_{ref}.

$$p_{rif} = \frac{F}{t \cdot d} \leq \sigma_{ref} \tag{4.17}$$

  The reference stress σ_{ref} is a function of the ratio between the mean diameter of the bolt d and distance between the center of the hole and the closest edge of the plate a. Possible σ_{ref} values are reported in the following table:

Ratio	$\boldsymbol{\sigma_{ref}}$
$\frac{a}{d} \geq 3$	$2.5\sigma_{adm}$
$3 \geq \frac{a}{d} \geq 2$	$2\sigma_{adm}$
$2 \geq \frac{a}{d} \geq 1.5$	$1.4\sigma_{adm}$
$1.5 \geq \frac{a}{d} \geq 1$	σ_{adm}

Table 4.3: σ_{ref} as a function of the ratio a/d.

- Tensile failure: the plate tears across its cross section. Thus, the assessment is carried out by ensuring that the stress acting on the plate cross section is lower than the plate allowable.

$$\sigma = \frac{F}{t(h-d)} \leq \sigma_{adm} \tag{4.18}$$

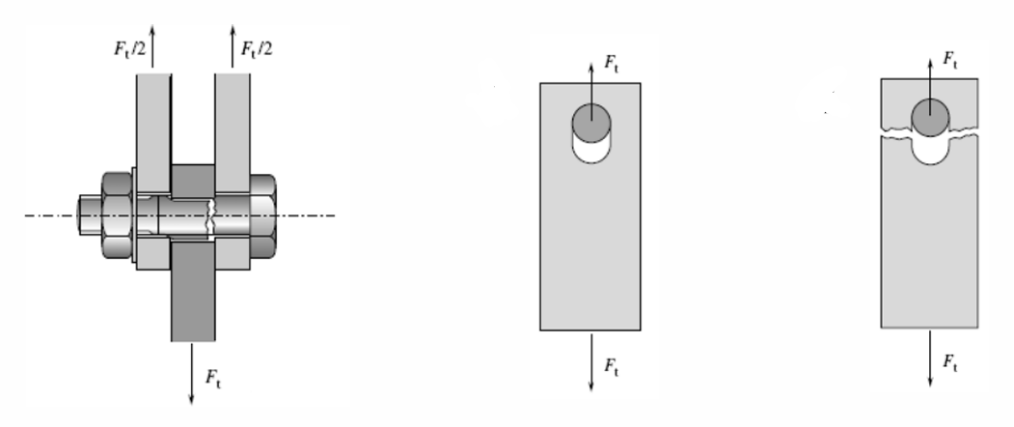

Figure 4.43: left) shear failure; center) bearing failure; right) tear failure.

5. Ritz and Galerkin methods

These method are ***approximating techniques*** that are based on the variational formulation of the structural problem, for the Ritz method, and on the strong form for the Galerkin method. We consider only the displacement-based formulation of the structural problem, i.e. $\Pi = \Pi(\boldsymbol{u})$. Consequently, the Ritz and Galerkin methods will be used to approximate the stationarity or equilibrium condition $\delta\Pi = 0$ or $\delta W_D = \delta W_e$. Naturally, such methods can also be applied to force-based formulations. The ***key idea*** of these methods is to transform the structural problem from a differential one (PDEs stem from the condition $\delta\Pi = 0$) into an algebraic one (linear system of equations), with clear advantages in terms of simplicity of the solution procedure. The transformation is carried out by approximating the unknown functions, $\boldsymbol{u}$ in this case, as a linear combination of functions, called ***trial functions***, each multiplied by an unknown scalar amplitude or ***weight***. The scalar amplitudes then become the unknown of the problem. Consider the differential problem which is governed by the equation:

$$Au = f \tag{5.1}$$

Where A is the differential operator, u is the unknown function, and f is the forcing term. Assume now that the weak form of such differential problem can be expressed as follows:

$$I(u) = \frac{1}{2}B(u,u) - l(u) \tag{5.2}$$

Where $I(u)$ is the functional, $B(\cdot,\cdot)$ is a bilinear operator (quadratic in u) and $l(u)$ is a linear operator. In the context of the structural problem, the functional $I(u)$ can be seen as the total potential energy Π, while the differential problem of equation (5.1) is the Euler-Lagrange equation associated with such functional. An applicative example of such notation is provided in Figure

5.1, depicting a truss with axial stiffness EA and a distributed axial load. The strong and weak forms of such problem would be:

$$\begin{cases} \begin{cases} EAu_{\backslash xx} + \hat{n} = 0 \\ u(0) = 0 \\ EAu_{\backslash x}(l) = 0 \end{cases}, & \text{strong form} \\ \Pi = \frac{1}{2}\int_l EAu_{\backslash x}^2 dx - \int_l u\hat{n}dx\,, & \text{weak form} \end{cases}$$

According to the notation introduced, we can identify the following terms:

$$\begin{cases} A = EA(\cdot)_{\backslash xx} \\ f = -\hat{n} \end{cases} \quad \text{and} \quad \begin{cases} B(\cdot,\cdot) = \frac{1}{2}\int_l EA(\cdot)_{\backslash x}(\cdot)_{\backslash x} dx \\ l(\cdot) = \int_l (\cdot)\hat{n}dx \end{cases}$$

Figure 5.1: axially loaded truss.

5.1. Ritz method

5.1.1. Approximation

In the context of the structural problem, the Ritz method approximates the displacement field u as follows:

$$\tilde{u}(x) = \sum_{i=1}^{N} \left(c_i \phi_i(x) + \phi_0(x)\right) \tag{5.3}$$

Where $\phi(x)$ and $\phi_0(x)$ are the chosen trial functions, thus also known, and c_i are the unknown amplitudes/weights to be determined via the PVW. Note that such approximation of the displacement field $\tilde{u}$ can be interpreted as an additional kinematic assumption that is overlaid to those of the kinematic model itself. Indeed, the choice of the trial function is an aprioristic assumption of the expected behavior of the displacement field. The trial functions $\phi(x)$ and $\phi_0(x)$ must fulfill the following ***requirements***:

- Compatible with the essential BCs but not necessarily the natural ones. Recall that the solution of the PVW automatically satisfies the natural BCs, but not the essential ones. When the BCs are not homogeneous, i.e. displacements are prescribed in the general form $u = \hat{u}$ on S_u, the trial functions will ideally be such that $\phi_i = 0$ and $\phi_0 = \hat{u}$ on S_u. If the BCs are homogeneous and thus no displacement is prescribed, then $\phi_0 = 0$.
- Continuous and differentiable up to the maximum order n of derivative required by the functional: the trial function should then be at least of order C^{n-1}.
- Complete and linearly independent: to clarify the requirement of completeness, consider a polynomial function of the type $\tilde{u} = c_0 + c_1 x + \cdots + c_n x^n$. This is a complete set of polynomial functions. If we were to remove the quadratic term, the approximation of $\tilde{u}$ will never be able to properly approach/describe a quadratic solution. Thus, the

completeness of the set could be interpreted as the ability of the approximate functions to describe any arbitrary curve. It must be pointed out that ***the requirement of completeness is crucial to guarantee the energetic/global convergence of the method***. In some cases, the trial functions could be capable of describing any function but not the potential function Π. Being the total potential energy a global quantity and the ultimate object of the approximation, via the equilibrium condition $\delta\Pi = 0$, completeness must be intended energetically. The difference with respect to local convergence is discussed in the next section.

In general, the higher the number of terms in the approximation and the closer the approximated solution will be to the exact one. Moreover, the ***most commonly used trial functions are the polynomial and the trigonometric type***. However, some important remarks must be pointed out about both these choices:

- Polynomials: they allow the fulfillment of the essential BCs in an easy way. However they suffer from a major disadvantage: the number of trial function that can be used is limited to $N \approx 10$ for numerical reasons. More precisely, the ill-conditioning of the stiffness matrix $\boldsymbol{K}$ becomes more severe as the number of polynomial trial functions increases. A much better choice are ***orthogonal polynomials***, such as those suggested by Legendre, Chebyshev and Jacobi, which avoid the problem just mentioned. In addition, they offer good convergence properties, and the accuracy of the solution is much higher than that of simple polynomial trial functions.
- Trigonometric: they generally perform worse than orthogonal polynomials, however they provide a series of advantages and are thus frequently used. Trigonometric functions are C^{∞} differentiable. Sometimes the exact solution of the problem is of trigonometric type (e.g. the Navier solution for plates). For some sets of BCs, typically simply-supported edges or hinges, the sine-type trial function identically satisfies the essential and the natural BCs. Lastly, trigonometric functions are orthogonal, preventing ill-conditioning of the stiffness matrix and granting good convergence properties.

Observation. While the three previous requirements are often cited in the majority of textbooks, it is worth emphasizing that a ***fourth condition*** would, in principle, need to be added: the trial function should satisfy, in addition to the essential BCs, also the complementary BCs. The complementary conditions specify that:

- The generalized displacement energetically conjugated with the prescribed generalized force on S_F is different from zero.
- The generalized force energetically conjugated with the prescribed generalized displacements on S_u is different from zero.

The idea is simple, and it can be clarified by means of an example. Consider again the rod depicted in Figure 5.1, the stationary condition on the total potential energy of such structural element is:

$$\delta\Pi = \int_l \delta u_{\backslash x} EA u_{\backslash x} dx - \int_l \delta u \hat{n} dx = \int_l \delta u \left(EA u_{\backslash xx} + \hat{n}\right) dx + \delta u EA u_{\backslash x}\Big|_0^l = 0$$

Similarly to the procedure outlined for the kinematic beam models in section 2.2, from the variational form we can retrieve the equilibrium equations and the BCs. In this case we obtain:

$$\begin{cases} EAu_{\backslash xx} + \hat{n} = 0 & \\ EAu_{\backslash x}(0) = 0 & \text{or} \quad \delta u(0) = 0 \\ EAu_{\backslash x}(l) = 0 & \text{or} \quad \delta u(l) = 0 \end{cases}$$

For the problem at hand, we select the essential BC $u(0) = 0$ at $x = 0$, because a geometric constraint is placed there, and $EAu_{\backslash x}(l) = 0$. The complementary BCs will then be:

$$\begin{cases} EAu_{\backslash x}(0) \neq 0 \\ u(l) \neq 0 \end{cases}$$

Thus, the complementary conditions state that the displacement u cannot be null at $x = l$, because at this location the displacement is unknown, and thus its value cannot be specified a priori. Similarly, the reaction force $EAu_{\backslash x}(0)$ at the clamp cannot be zero, because the clamped condition requires a non-null reaction force at this location. Based on such considerations, it is clear that the approximation

$$\tilde{u}(x) = c_1 \sin\left(\frac{\pi x}{l}\right)$$

Does not respect the complementary BC $u(l) \neq 0$.

The ***solution procedure*** to the structural problem using the Ritz method can be summarized as:

- Substitute the Ritz approximation of the displacement field $\tilde{u}$ (equation (5.3)) into the variational form of equilibrium:

$$I(u) \approx I(\tilde{u}) = \frac{1}{2} B(\tilde{u}, \tilde{u}) - l(\tilde{u})$$

- Impose the stationarity of the approximated functional:

$$\delta I(\tilde{u}) = \frac{\partial I}{\partial c_1} \delta c_1 + \cdots + \frac{\partial I}{\partial c_N} \delta c_N = \frac{\partial I}{\partial c_i} \delta c_i$$

- The stationarity condition is then reduced to N algebraic equations to be solved:

$$\frac{\partial I}{\partial c_i} = 0 \qquad i = 1, \ldots, N$$

5.1.2. Convergence

The method of Ritz achieves ***monotonic convergence of the total potential energy*** Π, meaning that as the number of trial functions is increased, the value of Π approaches the right one as follows:

$$\Pi \geq \Pi^2 \geq \Pi^3 \geq \cdots \geq \Pi^N \geq \Pi^{\text{exact}}$$

This property is easy to accept by recalling that the solution of the weak form is associated to the condition $\delta\Pi = 0$, corresponding to the minimum value of Π. This implies that the stiffness of the model is progressively reduced as the number of DOFs is increased. The total potential energy then provides a global measure of the stiffness and, as previously mentioned, the convergence of the total potential energy is global, not local. A model with few DOFs is globally stiffer than a model with more DOF, and thus the displacements will globally be smaller for the first with

respect to the second. Even so, locally the inverse is possible. It is then necessary to distinguish between the two measures of convergence:

$$\begin{cases} \lim_{N\to\infty} \|e_N^u\|_\infty & \text{where} \quad e_N^u = \max_{\underline{x}\in\Omega} |u - \tilde{u}_N|^2, & \text{local measure} \\ \lim_{N\to\infty} \|e_N^u\|_{L^2} & \text{where} \quad e_N^u = \sqrt{\int_\Omega (u - \tilde{u}_N)^2 d\Omega}, & \text{global measure} \end{cases} \tag{5.4}$$

The local measure guarantees that the maximum difference between the approximate solution and the exact one gets smaller as N increases. ***Local convergence is guaranteed if and only if the solution is continuous up to $n-1$ times***, where n is the highest order of derivative appearing in Π. In structural mechanics, this is usually verified for the displacement field, which is always a continuous function. Thus, displacements converge uniformly. On the contrary, the stresses may be discontinuous functions. Thus, convergence of the generalized stresses is of the global type but not local. Moreover, when derivatives of the approximated displacement field are considered, like for stresses and strains, the convergence rate is slower.

In order to understand how many Ritz terms N to consider, a ***convergence study*** should be carried out. In general, the number of terms is dependent on the kind of analysis and the goal of the analysis itself. For a static analysis aimed at the evaluation of the stress distribution, one possibility would be to check the natural BCs and set a tolerance value to consider as a stopping criterion over the number of functions N. Another possibility would be to monitor the stress in some spots of interest check the convergence as N increases. In the case of free-vibrations or buckling analysis, the response of interest is a global quantity, the natural frequencies or the buckling load, respectively. Thus, the convergence of the solution should be checked with respect to how much these values change with increasing terms of the Ritz approximation N.

5.1.3. Features

A series of important considerations can be made about the stiffness matrix $\boldsymbol{K}$:

- Consider the stiffness matrix $\boldsymbol{K}$ of the system $\boldsymbol{Kc} = \boldsymbol{f}$ obtained using two trial functions.

$$\underline{\underline{K}} = \begin{bmatrix} K_{11} & K_{12} \\ K_{21} & K_{22} \end{bmatrix}$$

  Increasing the number of trial functions to four leads to a stiffness matrix of dimensions 4×4, whose first 2×2 coefficients are the same coefficients of the previous stiffness matrix. Thus, when the number of DOFs is increased, it is not necessary to recompute all the terms of $\boldsymbol{K}$. A sub-potion of them can be obtained from the previous discretization obtained with less DOFs.
- Whenever possible, the adoption of orthogonal trial functions is a convenient choice. In this case, $B(\phi_i, \phi_j) = \delta_{ij}$, i.e. a Kronecker delta, a mathematical operator that is 1 when $i = j$ and 0 otherwise. This implies that the diagonal matrix is diagonal. This makes the numerical solution of the system $\boldsymbol{Kc} = \boldsymbol{f}$ much more efficient. Moreover, K can be stored as a sparse matrix with added benefits in terms of the amount of memory required to implement the method.
- In general, the stiffness matrix $\boldsymbol{K}$ is fully populated unless trial functions are orthogonal. Moreover, $\boldsymbol{K}$ is symmetric and semi-positive defined, so one could only compute the symmetric $N(N+1)/2$ terms instead of the full $N \times N$ entries.

The natural BCs are satisfied in a weak sense. As the number of DOFs increases, the approximated solution convergences to the exact one, which implies better satisfaction of the equilibrium equations as well as of the natural BCs.

Lastly, despite the method being highly efficient as accurate results can be obtained using few DOFs, it does have important ***drawbacks***, such as:

- The handling of the domains with complex shapes is not always easy. The method works well for simple geometries, such as circular, rectangular, plates and so on.
- When BCs are modified, the entries of the matrices $\boldsymbol{K, M,}$ ... must be re-computed, because the trial functions change. This is a major drawback comparing the Ritz method to the finite element method (FEM), discussed in chapter 6, where a change of the BCs does not imply re-computation of the cited matrices.

5.2. Galerkin method

The Galerkin method is based on the approximation of the unknown functions $\tilde{u}$ of equation (5.3). However, differently from the Ritz method, such approximation is ***applied to the strong form*** of equilibrium, i.e. (1.32), or more in general $Au = f$. By doing so, we can define a ***residual*** or ***error*** $\boldsymbol{R}$ as follows

$$Au = f \quad \rightarrow \quad Au - f = 0 \quad \overset{u \approx \tilde{u}}{\longrightarrow} \quad R = A\tilde{u} - f \neq 0$$

Where the residual is, in general, different from zero since $\tilde{u}$ is only an approximation of u. The method of Galerkin is based on the idea of setting to zero the weighted residual over the domain Ω. The residual is weighted against ***weight functions*** ψ_i, the form of which determines the specific type of Galerkin method. Thus:

$$\int_{\Omega} \psi_i R d\Omega = 0 \tag{5.5}$$

As previously mentioned, different choices of weight functions are possible, based on which we can identify different types of Galerkin methods.

5.2.1. Collocation

The collocation method corresponds to the case for which the weight functions are chosen to be Dirac's delta. Thus, we'll write:

$$\int_{\Omega} \psi_i R d\Omega = \int_{\Omega} \delta(\underline{x} - \underline{x_i}) R d\Omega = 0$$

This leads to a formulation where the weighted residuals are set to zero in a discrete number of points N in the domain Ω.

$$R_i = A\tilde{u}(\underline{x_i}) - f = 0 \quad \text{for } i = 1, \dots, N$$

5.2.2. Bubnov-Galerkin

The Bubnov-Galerkin method corresponds to the case in which the weight functions ψ_i are chosen to be equal to the trial functions ϕ_i used for approximating the unknown function u. Thus, the weighted integral reads:

$$\int_\Omega \phi_i R d\Omega = 0 \tag{5.6}$$

Expanding the integral leads to:

$$\begin{aligned}\int_\Omega \phi_i(A\tilde{u} - f)d\Omega &= \int_\Omega \phi_i \left[A\left(\sum_i^N c_i\phi_i + \phi_0\right) - f\right] d\Omega \\ &= \int_\Omega \phi_i \left(A\sum_i^N c_i\phi_i\right) d\Omega + \int_\Omega \phi_i(A\phi_0 - f) = 0\end{aligned}$$

The equation above represents a system of equations that can be expressed as follows:

$$\underline{\underline{K}}\,\underline{c} = \underline{f} \quad \text{where} \quad \begin{cases} K_{ij} = \int_\Omega \phi_i A\phi_j d\Omega \\ f_i = -\int_\Omega \phi_i(A\phi_0 - f)\, d\Omega \end{cases} \tag{5.7}$$

The ***requirements of the trial and weighting functions*** of the Galerkin method are the following:

- Continuous and differentiable up to the highest order of derivative appearing in the differential equations, which is usually higher than that appearing in the weak form.
- Complete: same as for the Ritz method.
- Compatible with both natural and essential BCs. In fact, no information about the natural BCs is contained in the approximated equations (5.7), contrary to the weak form approximated via the Ritz method.

5.2.3. Modified Bubnov-Galerkin

The requirement of compatibility of the trial functions may sometimes make determining their form quite difficult. In order to relax such requirement and recover the advantage of Ritz in the context of a strong form-based method, the Modified Galerkin method is introduced. Consider the problem in the form:

$$\begin{cases} Au = f, & \text{in } \Omega \quad (\text{equilibrium equations}) \\ u = \hat{u}, & \text{in } S_u \quad (\text{natural } BC) \\ Bu = \hat{f}, & \text{in } S_F \quad (\text{essential } BC) \end{cases}$$

The residual is constructed by accounting for a domain and a boundary-related contribution:

$$\begin{cases} R_\Omega = A\tilde{u} - f \\ R_F = B\tilde{u} - \hat{f} \end{cases}$$

And the weighted residual formulation is then:

$$\int_\Omega \phi_i R d\Omega = \int_\Omega \phi_i R_\Omega d\Omega + \int_{S_F} \phi_i R_F dS_F = \int_\Omega \phi_i (A\tilde{u} - f) d\Omega + \int_{S_F} \phi_i \left(B\tilde{u} - \hat{f}\right) dS_F$$

Recalling the approximation $\tilde{u}$ of equation (5.3):

$$\int_\Omega \phi_i \left[A\left(\sum_i^N c_i \phi_i(\underline{x}) + \phi_0(\underline{x}) \right) - f \right] d\Omega + \int_{S_F} \phi_i \left[B\left(\sum_i^N c_i \phi_i(\underline{x}) + \phi_0(\underline{x}) \right) - \hat{f} \right] dS_F$$

Once again, the above system of equations can be written in the form:

$$\underline{\underline{K}}\underline{c} = \underline{f} \quad \text{where} \quad \begin{cases} K_{ij} = \int_\Omega \phi_i A \phi_j d\Omega + \int_{S_F} \phi_i B \phi_j dS_F \\ f_i = -\int_\Omega \phi_i (A\phi_0 - f)\, d\Omega - \int_{S_F} \phi_i \left(B\phi_0 - \hat{f}\right) dS_F \end{cases} \tag{5.8}$$

Where the two contributions obtained by integrating over S_F are the ones associated with the natural BCs.

5.3. Trial functions for beams

Some applicative examples of the Ritz method are presented in the appendix (10.4). We discuss in this section some notable trial function formulations specifically for beams.

5.3.1. Cantilever beam

With respect to the scheme in Figure 5.2, we want to estimate the transverse displacement w. Taking a polynomial approximation with N terms, we'll write:

$$w = a_0 + a_1 x + a_2 x^2 + \cdots + a_N x^N$$

Applying the essential BCs yields:

$$\begin{cases} w(0) = 0 \\ w_{\backslash x}(0) = 0 \end{cases} \rightarrow \begin{cases} a_0 = 0 \\ a_1 = 0 \end{cases} \rightarrow \quad w = a_2 x^2 + \cdots + a_N x^N$$

Figure 5.2: cantilever beam.

It can be useful to express the trial functions in non-dimensional form as follows:

$$w = a_2 \frac{x^2}{l^2} + \cdots + a_N \frac{x^N}{l^N}$$

The shape functions are then:

$$\phi_i = \left(\frac{x}{l}\right)^i \qquad i = 2,..,N \tag{5.9}$$

5.3.2. Fixed and simply supported beam

Considering the scheme in Figure 5.3, we want to estimate the transverse displacement w with a polynomial approximation:

$$w = a_0 + a_1 x + a_2 x^2 + \cdots + a_N x^N$$

Applying the essential BCs yields:

$$\begin{cases} w(0) = 0 \\ w_{\backslash x}(0) = 0 \\ w(l) = 0 \end{cases} \rightarrow \begin{cases} a_0 = 0 \\ a_1 = 0 \\ a_2 l^2 + \cdots + a_n l^N = 0 \end{cases} \rightarrow \quad w = (-a_3 l - a_N l^{N-2})x^2 + \cdots + a_N x^N$$

Figure 5.3: fixed and simply supported beam.

Reorganizing the displacement approximation and expressing it in non-dimensional form yields:

$$w = a_3 \frac{x^2}{l^2}\left(\frac{x}{l} - 1\right) + a_4 \frac{x^2}{l^2}\left(\frac{x^2}{l^2} - 1\right) + \cdots$$

Generalizing:

$$\phi_i(x) = \frac{x^2}{l^2}\left[\left(\frac{x}{l}\right)^{i-2} - 1\right] \qquad i = 1, \ldots, N \tag{5.10}$$

5.3.3. Simply supported beam

The beam is represented in Figure 5.4, the essential BCs are $w(0) = w(l) = 0$. We can approximate the transverse displacement using either polynomials or trigonometric functions. Using polynomial trial functions yields:

$$w = a_0 + a_1 x + a_2 x^2 + \cdots + a_N x^N$$

Applying the BCs yields:

$$\begin{cases} w(0) = 0 \\ w(l) = 0 \end{cases} \rightarrow \begin{cases} a_0 = 0 \\ a_1 l + a_2 l^2 + \cdots a_N l^N = 0 \end{cases}$$

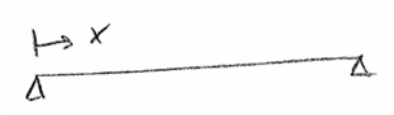

Figure 5.4: simply supported beam.

Rearranging the expression of the displacement yields:

$$w = (-a_2 l - a_3 l^2 - \cdots a_N l^{N-1})x + a_2 x^2 + \cdots a_N x^N = a_2(x^2 - lx) + a_3(x^3 - l^2 x) + \cdots$$

In non-dimensional form:

$$w = a_2\left(\frac{x^2}{l^2} - \frac{x}{l}\right) + a_3\left(\frac{x^3}{l^3} - \frac{x}{l}\right) + \cdots$$

Generalizing:

$$\phi_i(x) = \frac{x^i}{l^i} - \frac{x}{l} \qquad i = 2, .., N \tag{5.11}$$

The trigonometric approach can simply be formulated as below, which clearly satisfied the essential BCs:

$$\phi_i(x) = \sin\left(\frac{i\pi x}{l}\right) \qquad i = 1, \dots, N \tag{5.12}$$

5.3.4. Clamped-clamped beam

The boundary conditions are $w(0) = w_{\backslash x}(0) = w(l) = w_{\backslash x}(l) = 0$. We can again use both polynomial and trigonometric trial functions. The general formulation of the polynomial ones is a bit more involved than the previous cases, but it found with the same general procedure, i.e. applying the essential BCs. The result is the following:

$$\phi_i(x) = \left(\frac{x}{l}\right)^i - (i-2)\left(\frac{x}{l}\right)^3 + (i-3)\left(\frac{x}{l}\right)^2 \qquad i = 4, \dots, N \tag{5.13}$$

Once again, the trigonometric alternative is easier:

$$\phi_i(x) = 1 - \cos\frac{2i\pi x}{l} \qquad i = 1, \dots N \tag{5.14}$$

6. Finite element method

The finite-element method (FEM) is a key aspect in the design process of structural components, a schematization of which is reported in Figure 6.1. First, the structure is idealized with a mathematical model, i.e. the so-called governing equations accompanied by appropriate BCs and material assumptions and so on. Such governing equations are usually differential equations, either ordinary or partial. However, the mathematical model must be suited to the complexity of the phenomena described, and thus they might be simpler than ODEs or PDEs.

The mathematical model is then approximated with a numerical model via discretization of the space and time domains. In the case of structural analysis, this means that a finite element model of the structure under investigation is created. This process results in the approximation of the differential governing equations into a set of linear algebraic equations. The level of approximation introduced by the numerical model with respect to the analytical model, in the case of the FEM, depends on mesh density, choice of mesh elements, interpolation scheme etc. Clearly, it's generally desirable to reduce approximation error introduced by the numerical model. However, it is important to point out that such error can only be reduced to the point where its results perfectly represents those of the mathematical model. This is because the numerical model is intrinsically based on the mathematical model. The numerical model is then used to run a numerical analysis, the finite element analysis (FEA). the results of which verify the analytical results.

Once mathematical and numerical simulations have been carried out, interpretation of results is necessary to validate the results. Validation of results is needed to ensure adequate representation of the physical phenomenon by mathematical and numerical models. This is usually done via comparison with experimental data. If the validation is positive, the design process is completed. Otherwise, further refinement of either the mathematical model or the numerical model is needed.

Which model to refine depends on the observed fallacy: if the mathematical model adopted doesn't account for electromagnetic effects, but these phenomena produce non-negligible effects, the mathematical model needs to be changed, and consequently also the numerical one.

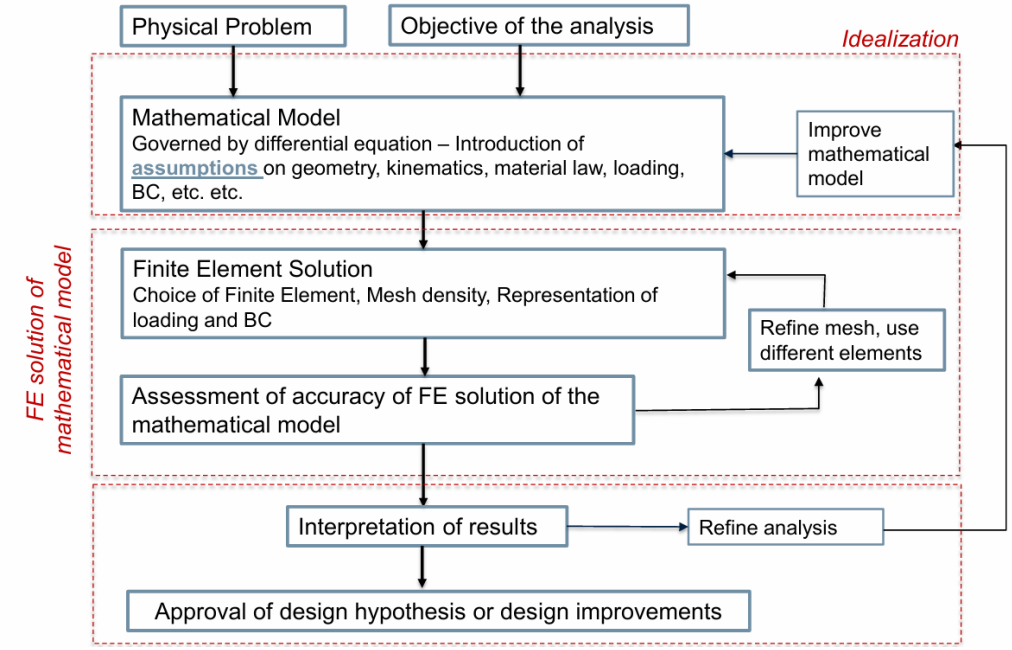
Physical Problem
Objective of the analysis
Idealization
Mathematical Model
Governed by differential equation – Introduction of assumptions on geometry, kinematics, material law, loading, BC, etc. etc.
Improve mathematical model
FE solution of mathematical model
Finite Element Solution
Choice of Finite Element, Mesh density, Representation of loading and BC
Refine mesh, use different elements
Assessment of accuracy of FE solution of the mathematical model
Interpretation of results
Refine analysis
Approval of design hypothesis or design improvements

Figure 6.1: schematization of the typical structural design process.

6.1. Introduction

6.1.1. Review of displacement based approach

In this section we will illustrate the application of the variational approach to the frame structure of beams depicted in Figure 6.2. This example serves to illustrate the general steps that are required to obtain the FE solution of a structure's numerical model. It is ***assumed*** that:

- Material properties of each beam are known.
- Geometry of each beam (length and cross section shape) is known.
- Planar case: the structure is allowed to displace only in the x-y plane.
- External loads are concentrated forces applied at the beam junctions.

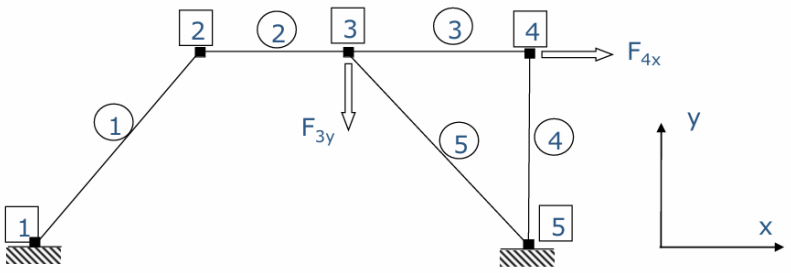

Figure 6.2: statically indetermined beam structure.

For the problem at hand, planar beam structure, each node will have 3 DOFs $\boldsymbol{u}_i = \{u_{ix}, u_{iy}, u_{i\theta}\}$, so that if N is the number of nodes, the total number of DOFs will be $n = 3xN$. The solution procedure of such problem requires the definition of multiple ***types of displacements***:

- $\bar{\boldsymbol{u}}_j \in \mathbb{R}^{6\times1}$: vector of local nodal displacements of the j-th beam in local frame.
- $\boldsymbol{u}_j \in \mathbb{R}^{6\times1}$: vector of local nodal displacements of the j-th beam in global frame.

- $\boldsymbol{U} \in \mathbb{R}^{n\times 1}$: vector of global nodal displacements of the whole structure in global frame.

$$\begin{cases} \underline{\bar{u}} = \{\bar{u}_{1x}\ \bar{u}_{1y}\ \bar{u}_{1\theta}\ \bar{u}_{2x}\ \bar{u}_{2y}\ \bar{u}_{2\theta}\}^T \\ \underline{u} = \{u_{1x}\ u_{1y}\ u_{1\theta}\ u_{2x}\ u_{2y}\ u_{2\theta}\}^T \\ \underline{U} = \{U_{1x}\ U_{1y}\ U_{1\theta}\ U_{2x}\ U_{2y}\ U_{2\theta}\ \dots\ U_{Nx}\ U_{Ny}\ U_{N\theta}\}^T \end{cases} \tag{6.1}$$

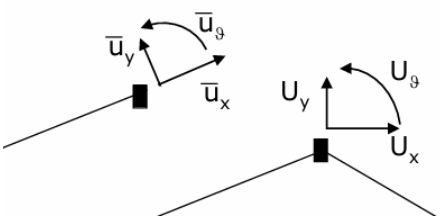

Figure 6.3: Representation of local and global DOFs.

The first step (1) in solving the problem at hand is to ***obtain the governing equations*** of the structure, which we'll see are in the form $\boldsymbol{Ku} = \boldsymbol{F}$. In order to do this, we first write the governing equation of each beam in local coordinates and using the local vector DOFs/nodal displacements $\bar{\boldsymbol{u}}_j$. Thus, for the j-th beam we'll write:

$$\underline{\bar{k}}_j \underline{\bar{u}}_j = \underline{\bar{F}}_j \tag{6.2}$$

Here, $\bar{\boldsymbol{k}}_j \in \mathbb{R}^{6\times 6}$ is the local stiffness matrix of the j-th beam related to its vector of local DOFs in local coordinates $\bar{\boldsymbol{u}}_j$. The entries of $\bar{\boldsymbol{k}}_j$ are known because the material and geometry of all beams are known. Starting from the above equation, the internal virtual work δW_D of the whole beam system can be expressed as the contribution of each beam:

$$\delta W_D = \sum_j^M \delta \underline{\bar{u}}_j^T \underline{\bar{k}}_j \underline{\bar{u}}_j \tag{6.3}$$

Where M is the number of beams. Here, all quantities are reported with the overbar, meaning that each term of the summatory is expressed in the local reference frame $\{\bar{\boldsymbol{x}}_j, \bar{\boldsymbol{y}}_j\}$ of the j-th beam. The displacements must be rotated into the global reference frame $\{\boldsymbol{x}, \boldsymbol{y}\}$ via a rotation matrix $\boldsymbol{T}_j \in \mathbb{R}^{6\times 6}$. Using such matrix we'll write:

$$\underline{\bar{u}}_j = \underline{T}_j \underline{u}_j \tag{6.4}$$

In order to define the rotation matrices $\boldsymbol{T}_j$, the angle θ_j between the local and global reference frames of every beam must be known. By substitution of equation (6.4) into equation (6.3), the internal virtual work in global coordinates can be expressed as follows:

$$\delta W_D = \sum_j^M \delta \underline{u}_j^T \underbrace{\underline{T}_j^T \underline{\bar{k}}_j \underline{T}_j}_{\underline{k}_j} \underline{u}_j = \sum_j^M \delta \underline{u}_j^T \underline{k}_j \underline{u}_j \tag{6.5}$$

The above formulation of the internal virtual energy is in global coordinates but still expressed using the local DOFs of each beam, which in this case are 6 per beam. The displacement vectors $\delta \boldsymbol{u}_j$ and $\boldsymbol{u}_j$ must then be rewritten so that they represent the contribution of each beam to the global finite element model. In order to clarify this concept, consider beam two of the structure in Figure 6.2. The vector of local DOFs expressed in global reference frame of such beam will be:

$$\underline{u}_3 = \{u_{2x}\ u_{2y}\ u_{2\theta}\ u_{3x}\ u_{3y}\ u_{3\theta}\}^T$$

Here, the horizontal displacement of node two, u_{2x}, in the first entry of the vector of local DOFs of beam three. However, the same displacement component will not be in the same position in the vector of global DOFs $\boldsymbol{U}$ of equation (6.1). More precisely, according to the convention we adopted in (6.1) for the displacement arrangement inside $\boldsymbol{U}$ (which is not the only possible one), u_{2x} will hold the fourth position in $\boldsymbol{U}$. Thus, the conversion of local DOFs into global DOFs can be analytically formalized via the assembly matrices $\boldsymbol{\Omega}_j \in \mathbb{R}^{6\times n}$. Such matrices are empty, but for some specific entries that hold value 1 that determine the conversion of the local DOF into a global DOF. Continuing with the previous example, to convert the local DOF u_{2x} into its global counterpart, the assembly matrix of the second beam $\boldsymbol{\Omega}_2$ will have a 1 in the first row-fourth column. In general, the conversion from local to global DOFs can be formalized as follows:

$$\underline{u}_j = \underline{\underline{\Omega}}_j \underline{U} \tag{6.6}$$

It must be pointed out that the assembly matrices $\boldsymbol{\Omega}_j$ are a formalization of the actual procedure that is carried out in FEA software, which make use of location arrays. By substitution of equation (6.6) into equation (6.5), the virtual internal energy can be expressed as follows:

$$\delta W_D = \sum_j^M \delta \underline{U}^T \underbrace{\underline{\underline{\Omega}}_j^T \underline{\underline{k}}_j \underline{\underline{\Omega}}_j}_{\underline{\underline{K}}_j} \underline{U} = \delta \underline{U}^T \sum_j^M \underline{\underline{K}}_j \underline{U} = \delta \underline{U}^T \underline{\underline{K}} \underline{U} \tag{6.7}$$

The external virtual work δW_e is simply expressed as follows:

$$\delta W_e = \delta \underline{U}^T \underline{F}_{ext} \tag{6.8}$$

By equating the internal virtual work δW_D as expressed in equation (6.7) to the external virtual work of equation (6.8), the governing equations of the structure is obtained as:

$$\underline{\underline{K}}\, \underline{U} = \underline{F}_{ext} \tag{6.9}$$

The second step (2) to solve the structural problem is to ***solve for displacements and reaction forces***. This process can be formalized as follows: we partition the displacements vector $\boldsymbol{U}$ and the vector of loads $\boldsymbol{F}$ in constrained and free portions. This procedure provides us with the two following systems of equations.

$$\begin{Bmatrix} \underline{U}_C \\ \underline{U}_F \end{Bmatrix} \begin{bmatrix} \underline{\underline{K}}_{CC} & \underline{\underline{K}}_{CF} \\ \underline{\underline{K}}_{FC} & \underline{\underline{K}}_{FF} \end{bmatrix} = \begin{Bmatrix} \underline{F}_C \\ \underline{F}_F \end{Bmatrix} \tag{6.10}$$

Here, everything is known but the displacements of the unconstrained nodes $\boldsymbol{U}_F$ and the reaction forces of the constrained nodes $\boldsymbol{F}_C$. In fact, $\boldsymbol{U}_C$ are the imposed (nodal) displacements, i.e. the essential BCs, and $\boldsymbol{F}_F$ are the externally applied loads. From the second of these system of equations we can determine $\boldsymbol{U}_F$ as follows:

$$\underline{U}_F = \underline{\underline{K}}_{FF}^{-1}\left(\underline{F}_F - \underline{\underline{K}}_{FC}\underline{U}_C\right) \tag{6.11}$$

Using this result, the reaction forces of the constrained nodes $\boldsymbol{F}_C$ can be determined from the first system of equations of (6.10):

$$\underline{F}_C = \underline{U}_C\underline{\underline{K}}_{CC} + \underline{U}_F\underline{\underline{K}}_{CF} \tag{6.12}$$

Once the displacements and reaction forces are known, the third and last step (3) is the so-called ***stress recovery*** procedure. Starting from the displacement in global frame and related to the whole structure $\boldsymbol{U}$, we can determine the forces in local coordinates acting on the j-th beam $\bar{\boldsymbol{F}}_j$.

$$\text{solve (6.10) for } \underline{U} \quad \overset{(6.6)}{\longrightarrow} \quad \underline{u}_j = \underline{\underline{\Omega}}_j\underline{U}_j \quad \overset{(6.4)}{\longrightarrow} \quad \underline{\bar{u}}_j = \underline{\underline{T}}_j\underline{u}_j \quad \overset{(6.2)}{\longrightarrow} \quad \underline{\bar{F}}_j = \underline{\underline{K}}_j\underline{\bar{u}}_j$$

Additionally, ***thermal effects*** (4) can be accounted for in this procedure. More precisely, the local displacements in local coordinates induced on the j-th beam by thermal expansion or contraction can be expressed as follows:

$$\underline{\bar{u}}_j^{th} = \Delta T\underline{\alpha}_j \quad \text{where} \quad \underline{\alpha} = \{\alpha \quad \alpha \quad \alpha \quad 0 \quad 0 \quad 0\}^T \tag{6.13}$$

Where we implicitly assumed the material to be isotropic, so that the shear components are null. Because the CL describes only mechanical effects, in order to account for thermal-induced displacements we must decouple mechanical and thermal effects in the CL. To do so, we simply write:

$$\underline{\bar{F}}_j = \underline{\underline{K}}_j\left(\underline{\bar{u}}_j^{tot} - \underline{\bar{u}}_j^{th}\right) = \underline{\underline{K}}_j\left(\underline{\bar{u}}_j^{tot} - \Delta T\underline{\alpha}_j\right) = \underline{\underline{K}}_j\underline{\bar{u}}_j^{tot} + \underline{\bar{F}}_j^{th} \tag{6.14}$$

Note that these thermal forces $\bar{\boldsymbol{F}}_j^{th}$ ***are generally fictitious*** unless the beam is properly constrained and not allowed to expand or contract. This implies that we must account for thermal induced reaction forces when computing the displacements as

$$\underline{\bar{F}}_j - \underline{\bar{F}}_j^{th} = \underline{\underline{K}}_j\underline{\bar{u}}_j^{tot} \tag{6.15}$$

However, we do not consider then during stress recovery, because they do not produce stresses.

6.1.2. The finite element procedure

Consider the continuous 3D body depicted in Figure 6.4. The essential BCs, i.e. imposed displacements, are applied to the constrained portion of its external surface S_u. The natural BCs, i.e. surface forces $\mathbf{f}^s = \{f_x^S, f_y^S, f_z^S\}$ are applied to the remaining portion of its external surface S_σ. External loads are composed by body forces $\mathbf{f}^B = \{f_x^B, f_y^B, f_z^B\}$ and a series of concentrated loads $\boldsymbol{R}_C^i = \{R_{Cx}^i, R_{Cy}^i, R_{Cz}^i\}$ acting on what will be the i-th node of the finite element (FE).

Observation. The body and surface loads $\mathbf{f}^b$ and $\mathbf{f}^s$ have been denoted as $\boldsymbol{b}$ and $\boldsymbol{t}$, respectively, in Chapter 1.

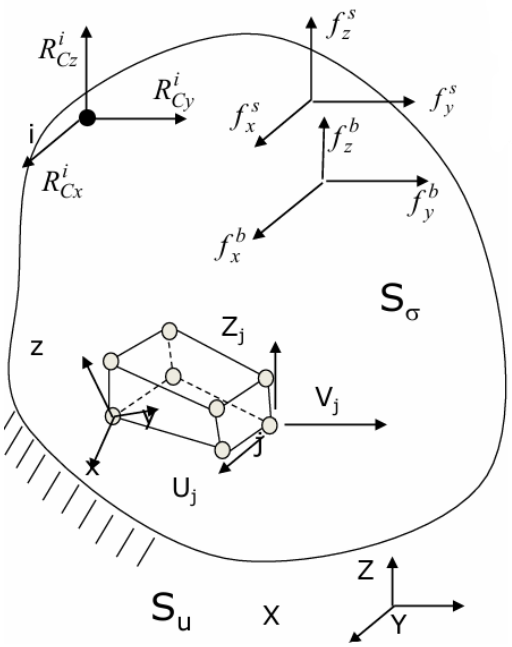

Figure 6.4: continuous 3D body with various types of forces applied and a finite element.

The ***key idea*** of the FEM is to approximate or discretize the continuous 3D body with a collection of smaller elements of (usually) much simpler geometry than the continuous body. Such elements are defined and connected to each other by their nodes, i.e. the circles of the representative FE in Figure 6.4. The FEM is usually applied to a displacement-based approach to the elastic/structural problem. Before the FE discretization, the unknowns of the problem are the displacements of each point of the continuous body, and thus the number of unknowns is infinite (because the body is characterized by an infinite number of points). Moreover, the governing equations to solve in order to determine the exact continuous displacement field are PDEs, which are notoriously difficult to solve, when this is even possible. In this context, the ***key advantages*** of the FE discretization of the original volume of the continuous body are that (1) it allows us to transform the unknowns of the problem into the nodal displacements of each FE. Intuitively, this results in a finite number of unknowns, directly related to the mesh (collection of FEs), over which we have direct control. Then, the displacement field inside each element is interpolated via shape functions (discussed in section 6.2) starting from the values of the nodal displacements of the same element. The second advantage (2) of the FE procedure is that the equations to solve in order to determine the nodal displacements are linear algebraic equations, notoriously easy to solve.

We now present the same steps discussed in the previous section that lead to the solution of a FE procedure applied to a generic continuous body. The first step (1) is to obtain the governing equations of the problem. It has been stated that the FEM is usually implemented with a displacement-based variational approach. This simply means that it is applied to the PVW, which for the body represented in Figure 6.4 reads:

$$\underbrace{\int_V \delta\underline{\varepsilon}^T \underline{\underline{D}}\, \underline{\varepsilon} dV}_{\delta W_D} = \underbrace{\int_V \delta\underline{U}^T\left(\underline{\mathrm{f}}^B - \rho\ddot{\underline{U}}\right)dV + \int_{S_F} \delta\underline{U}^T\, \underline{\mathrm{f}}^S dS + \sum_i^N \delta\underline{U}^{iT}\underline{R}_C^i}_{\delta W_e} \tag{6.16}$$

Where $\boldsymbol{D}$ is the elasticity tensor in Voigt notation (denoted as $\mathbb{C}$ in Chapter 1), N is the number of nodes of the FE mesh, and since each node has three displacement components, the number of DOFs is $n = 3N$. Notice that we accounted for inertial forces $\rho\ddot{\boldsymbol{U}}$ in the term of body forces. Moreover, here $\boldsymbol{U} \in \mathbb{R}^{3\times 1}$ is the vector of the continuous displacement field. In a FE procedure, such vector is discretized using nodal displacements and shape functions. More precisely, we define $\widehat{\boldsymbol{U}} \in \mathbb{R}^{n\times 1}$ as the vector of global DOFs expressed in global coordinates. The shape functions associated to the m-th FE are collected in the displacement interpolation matrix $\boldsymbol{H}^{(m)} \in \mathbb{R}^{3\times n}$. Thus, the displacement field inside the m-th element $\boldsymbol{u}^{(m)}$ is obtained as follows:

$$\underline{U}^{(m)} = \underline{\underline{H}}^{(m)}\, \underline{\widehat{U}}^{(m)} \tag{6.17}$$

In our discussion, we'll assume that $\widehat{\boldsymbol{U}}$ and $\boldsymbol{H}$ are organized as follows:

$$\begin{cases} \underline{U} = \{U\ \ V\ \ W\}^T & \in \mathbb{R}^{3\times 1} \\ \underline{\underline{H}} = \begin{bmatrix} \underline{N} \in \mathbb{R}^{1\times N} & \underline{0} \in \mathbb{R}^{1\times N} & \underline{0} \in \mathbb{R}^{1\times N} \\ \underline{0} \in \mathbb{R}^{1\times N} & \underline{N} \in \mathbb{R}^{1\times N} & \underline{0} \in \mathbb{R}^{1\times N} \\ \underline{0} \in \mathbb{R}^{1\times N} & \underline{0} \in \mathbb{R}^{1\times N} & \underline{N} \in \mathbb{R}^{1\times N} \end{bmatrix} & \in \mathbb{R}^{3\times n} \\ \underline{\widehat{U}} = \{U_1 \dots U_N\ \ V_1 \dots V_N\ \ W_1 \dots W_N\}^T & \in \mathbb{R}^{n\times 1} \end{cases} \tag{6.18}$$

Note that the entries of $\boldsymbol{H}$, i.e. the shape functions, are not denoted as h_i but with N_i. The difference between the global $\widehat{\boldsymbol{U}}, \boldsymbol{H}$ and those related to the m-th finite element $\widehat{\boldsymbol{U}}^{(m)}, \boldsymbol{H}^{(m)}$ is that the second ones only have a few non-null entries, i.e. those related to the m-th element. Using (6.17) and (6.18), the extern virtual work in equation (6.16) can be rewritten as follows:

$$\delta W_e = \sum_m \left(\delta\underline{\widehat{U}}^T \underbrace{\int_V \underline{\underline{H}}^{(m)T} \underline{\mathrm{f}}^{B(m)} dV^{(m)}}_{\underline{R}_B} + \delta\underline{\widehat{U}}^T \underbrace{\int_{S_1 \dots S_q} \underline{\underline{H}}^{S(m)T}\, \underline{\mathrm{f}}^{S(m)} dS}_{\underline{R}_S} \right) + \delta\underline{\widehat{U}}^T \underline{R}_C$$

$$\delta W_e = \delta\underline{\widehat{U}}^T\left(\underline{R}_B + \underline{R}_S + \underline{R}_C\right) = \delta\underline{\widehat{U}}^T \underline{F}$$

Where, the inertial term in the body forces has been moved to the virtual internal work. Here, $S_1 .. S_q$ are the faces of the FEs that are actually subject to the surface forces, and similarly $\boldsymbol{H}^{S(m)}$ is the displacement interpolation matrix related to the corresponding elements. Note that the application of the FE procedure to a continuous body results in the load vectors $\boldsymbol{R}_B$ and $\boldsymbol{R}_S$, while $\boldsymbol{R}_C$ was already present. These vectors represent the ***projections of the body and surface forces on the nodes of the FE model*** (due to the $\boldsymbol{H}$ matrices), to which all m elements contribute.

The internal virtual work can be approximated via the strain interpolation matrix $\boldsymbol{B}^{(m)} \in \mathbb{R}^{6\times n}$ of the m-th element. Such matrix is obtained by applying a differentiation matrix $\boldsymbol{\partial} \in \mathbb{R}^{6\times 3}$ to the displacement interpolation matrix $\boldsymbol{H}^{(m)}$. Thus, the strain field inside the m-th element will be approximated as follows:

$$\underline{\varepsilon}^{(m)} = \underline{\partial u}^{(m)} = \underline{\underline{\partial H}}^{(m)} \underline{\hat{U}} = \underline{\underline{B}}^{(m)} \underline{\hat{U}} \tag{6.19}$$

Where:

$$\underline{\underline{\partial}} = \begin{bmatrix} \partial(\cdot)/\partial x & 0 & 0 \\ 0 & \partial(\cdot)/\partial y & 0 \\ 0 & 0 & \partial(\cdot)/\partial z \\ \partial(\cdot)/\partial y & \partial(\cdot)/\partial x & 0 \\ 0 & \partial(\cdot)/\partial z & \partial(\cdot)/\partial y \\ \partial(\cdot)/\partial z & 0 & \partial(\cdot)/\partial x \end{bmatrix} \in \mathbb{R}^{6\times 3} \tag{6.20}$$

Observation. It is important to notice that the procedure just discussed implies that the strains are interpolated using nodal displacements, and thus the same shape functions used for displacement interpolation. No additional set of shape functions must be defined.

Using equation (6.19) to approximate the internal virtual work δW_D in equation (6.16) yields:

$$\delta W_D = \delta \underline{\hat{U}}^T \left[\sum_m \int_V \underline{\underline{H}}^{(m)T} \rho \underline{\underline{H}}^{(m)} dV \right] \underline{\ddot{\hat{U}}} + \delta \underline{\hat{U}}^T \left[\sum_m \int_V \underline{\underline{B}}^{(m)T} \underline{\underline{DB}}^{(m)} dV \right] \underline{\hat{U}} = \delta \underline{\hat{U}}^T \underline{\underline{M}} \underline{\ddot{\hat{U}}} + \delta \underline{\hat{U}}^T \underline{\underline{K}} \underline{\hat{U}}$$

Here, the discretization of the FEM leads to the definition of the stiffness matrix $\boldsymbol{K} \in \mathbb{R}^{n\times n}$ and of the mass matrix $\boldsymbol{M} \in \mathbb{R}^{n\times n}$, similarly to the example discussed in the previous section. Similarly to the external virtual work, in this case as well the terms $\boldsymbol{K\hat{U}}$ and $\boldsymbol{M\ddot{U}}$ are the ***projection onto the element nodes of the internal reaction forces and inertial forces***, respectively.

The final formulation of the FE approximation of the PVW applied to a continuous body is provided in the form of n (number of nodes) ODEs since we accounted for inertias as well. In the static case we obtain a system of n linear equations.

$$\begin{aligned} &\sum_m \int_V \underline{\underline{H}}^{(m)T} \rho \underline{\underline{H}}^{(m)} dV \, \underline{\ddot{\hat{U}}} + \sum_m \int_V \underline{\underline{B}}^{(m)T} \underline{\underline{DB}}^{(m)} dV \, \underline{\hat{U}} \\ &\qquad = \sum_m \left(\int_V \underline{\underline{H}}^{(m)T} \underline{\mathfrak{f}}^{B(m)} dV^{(m)} + \int_{S_1 \dots S_q} \underline{\underline{H}}^{S(m)T} \underline{\mathfrak{f}}^{S(m)} dS \right) + \underline{R_C} \end{aligned} \tag{6.21}$$

Or equivalently:

$$\underline{\underline{M}} \underline{\ddot{\hat{U}}} + \underline{\underline{K}} \underline{\hat{U}} = \underline{F} \tag{6.22}$$

The second step (2) in the FE procedure is the solution of the governing equations. This is again formalized by identifying the constrained and free portions of $\boldsymbol{\ddot{\hat{U}}}, \boldsymbol{\hat{U}}$ and $\boldsymbol{F}$, which results in the same kind of split for $\boldsymbol{K}$ and $\boldsymbol{M}$. This procedure leads to the following two systems of equations:

$$\begin{bmatrix} \underline{\underline{M}}_{CC} & \underline{\underline{M}}_{CF} \\ \underline{\underline{M}}_{FC} & \underline{\underline{M}}_{FF} \end{bmatrix} \begin{Bmatrix} \underline{\ddot{\hat{U}}}_C \\ \underline{\ddot{\hat{U}}}_F \end{Bmatrix} + \begin{bmatrix} \underline{\underline{K}}_{CC} & \underline{\underline{K}}_{CF} \\ \underline{\underline{K}}_{FC} & \underline{\underline{K}}_{FF} \end{bmatrix} \begin{Bmatrix} \underline{\hat{U}}_C \\ \underline{\hat{U}}_F \end{Bmatrix} = \begin{Bmatrix} \underline{F}_C \\ \underline{F}_F \end{Bmatrix} \tag{6.23}$$

From the second system the unconstrained nodal displacements and the respective acceleration $\widehat{\boldsymbol{U}}_F, \ddot{\boldsymbol{U}}_F$ can be computed and then used to compute the forces $\boldsymbol{F}_C$ acting on the constrained nodes from the second system. Because $\boldsymbol{F}_C$ represents the total forces acting on the constrained nodes, to isolate the reaction forces $\boldsymbol{R}_c$ we need to subtract the body and surface forces $\boldsymbol{R}_B, \boldsymbol{R}_S$ from $\boldsymbol{F}_C$:

$$\underline{R}_C = \underline{F}_F - \underline{R}_B - \underline{R}_S \tag{6.24}$$

From the solution of the FE procedure discussed above, two fundamental ***properties of the FE solution*** can be deduced:

- Nodal point equilibrium: it has been found that the virtual internal work δW_D represents the projection onto the FEs nodes of the internal reaction and inertial forces. Similarly, the external virtual work has been found to be the projection onto the FEs nodes of the externally applied loads. Thus, the equilibrium condition/governing equation of the FE procedure, i.e. $\delta W_D = \delta W_e$, simply states that the nodes of the mesh are in equilibrium under the action of external loads $\boldsymbol{F}$.
- Element equilibrium: each element is in equilibrium under the action of the external forces $\boldsymbol{F}^{(m)}$. This condition is automatically verified if the interpolating functions in the $\boldsymbol{H}$ matrix are able to represent rigid body motions, to which null deformation are associated. If the cited condition is verified, then for the generic m-th element the following equilibrium equation can be written:

$$\delta \underline{U}^{(m)^T} \underline{F}^{(m)} = \delta \underline{U}^{(m)^T} \int_{V^{(m)}} \underline{\underline{B}}^{(m)^T} \underline{\underline{D}} \underline{\underline{B}}^{(m)} dV = \int_{V^{(m)}} \left(\underline{\underline{B}}^{(m)} \delta \underline{U}^{(m)} \right)^T \underline{\sigma} dV = 0$$

6.1.3. Element vs global POV

The discussion in section 6.1.2 has been carried out by considering the vector of global DOFs $\boldsymbol{U}$. This global approach does not represent the actual procedure that is carried out in a FE code, it was however discussed because it's suited for mathematical derivation and interpretation of the FE solution procedure. Practical implementation of FE procedure is similar to the one discussed in 6.1.1 for the beam structure. Initially, the $\boldsymbol{K}, \boldsymbol{M}$ and $\boldsymbol{F}$ are computed at local level and for each element.

Thus, for the m-th element we'll identify the vector of local nodal displacements in local coordinates $\widehat{\boldsymbol{u}}^{(m)}$. Then, using the displacement and strain interpolation matrices of the m-th element $\boldsymbol{H}^{(m)}$ and $\boldsymbol{B}^{(m)}$, we can define the vectors of displacement and strain fields inside the m-th element in local coordinates $\boldsymbol{u}^{(m)}$ and $\boldsymbol{\varepsilon}^{(m)}$, respectively.

$$\begin{cases} \underline{u}^{(m)} = \underline{\underline{H}}^{(m)} \underline{\hat{u}}^{(m)} \\ \underline{\varepsilon}^{(m)} = \underline{\underline{B}}^{(m)} \underline{\hat{u}}^{(m)} \end{cases} \quad \text{where} \quad \begin{cases} \underline{u}^{(m)} \in \mathbb{R}^{3\times 1} \\ \underline{\underline{H}}^{(m)} \in \mathbb{R}^{3\times n^{(m)}} \\ \underline{\varepsilon}^{(m)} \in \mathbb{R}^{6\times 1} \\ \underline{\underline{B}}^{(m)} \in \mathbb{R}^{6\times n^{(m)}} \\ \underline{\hat{u}}^{(m)} \in \mathbb{R}^{1\times n^{(m)}} \end{cases}$$

Here, $n^{(m)}$ is the number of DOFs associated to the nodes of the m-th element. Thus, for an element with 6 nodes, each with 3 DOFs, we'll have that $n^{(m)} = 6 \times 3 = 18$ nodal DOFs. Once

these quantities are known, the local stiffness and mass matrices in local coordinates $\boldsymbol{K}^{(m)}$ and $\boldsymbol{M}^{(m)}$, as well as the projection onto the nodes of the m-th element in local coordinates of the externally applied body and surface forces, i.e. $\boldsymbol{R}_B^{(m)}$ and $\boldsymbol{R}_S^{(m)}$ can be obtained as follows:

$$\begin{cases} \underline{\underline{K}}^{(m)} = \int_{V^{(m)}} \underline{\underline{B}}^{(m)T} \underline{\underline{D}}^{(m)} \underline{\underline{B}}^{(m)} dV^{(m)} \in \mathbb{R}^{n^{(m)} \times n^{(m)}} \\ \underline{\underline{M}}^{(m)} = \int_{V^{(m)}} \underline{\underline{H}}^{(m)T} \rho \underline{\underline{H}}^{(m)} dV^{(m)} \quad \in \mathbb{R}^{n^{(m)} \times n^{(m)}} \\ \underline{R}_B^{(m)} = \int_{V^{(m)}} \underline{\underline{H}}^{(m)T} \underline{\mathrm{f}}_B dV^{(m)} \quad \in \mathbb{R}^{n^{(m)} \times 1} \\ \underline{R}_S^{(m)} = \int_{S_1^{(m)} \dots S_q^{(m)}} \underline{\underline{H}}^{(m)T} \underline{\mathrm{f}}_S dS_F^{(m)} \quad \in \mathbb{R}^{n^{(m)} \times 1} \end{cases} \tag{6.25}$$

Before assembly, the contribution of every element must be expressed in the same global frame. To achieve this, the vector of local nodal displacements in local coordinates of the m-th element $\hat{\boldsymbol{u}}^{(m)}$ as well as the displacement and strain interpolation matrices $\boldsymbol{H}^{(m)}$ and $\boldsymbol{B}^{(m)}$ must be rotated via a rotation matrix $\boldsymbol{T}^{(m)}$:

$$\begin{cases} \underline{\tilde{u}}^{(m)} = \underline{\underline{T}}^{(m)} \underline{\hat{u}}^{(m)} \\ \underline{\underline{H}}^{(m)} = \underline{\underline{\tilde{H}}}^{(m)} \underline{\underline{T}}^{(m)} \\ \underline{\underline{B}}^{(m)} = \underline{\underline{\tilde{B}}}^{(m)} \underline{\underline{T}}^{(m)} \end{cases} \quad \text{where} \quad \underline{\underline{T}}^{(m)} \in \mathbb{R}^{n^{(m)} \times n^{(m)}} \tag{6.26}$$

Using such relations, we'll express $\boldsymbol{K}, \boldsymbol{M}, \boldsymbol{R}_B$ and $\boldsymbol{R}_S$ in global coordinates as follows:

$$\begin{cases} \underline{\underline{K}}^{(m)} = \int_{V^{(m)}} \underline{\underline{T}}^{(m)T} \underline{\underline{\tilde{B}}}^{(m)T} \underline{\underline{D}}^{(m)} \underline{\underline{B}}^{(m)} \underline{\underline{T}}^{(m)} dV^{(m)} \in \mathbb{R}^{n^{(m)} \times n^{(m)}} \\ \underline{\underline{M}}^{(m)} = \int_{V^{(m)}} \underline{\underline{T}}^{(m)T} \underline{\underline{H}}^{(m)T} \rho \underline{\underline{H}}^{(m)} \underline{\underline{T}}^{(m)} dV^{(m)} \quad \in \mathbb{R}^{n^{(m)} \times n^{(m)}} \\ \underline{R}_B^{(m)} = \int_{V^{(m)}} \underline{\underline{T}}^{(m)T} \underline{\underline{H}}^{(m)T} \underline{\mathrm{f}}_B dV^{(m)} \quad \in \mathbb{R}^{n^{(m)} \times 1} \\ \underline{R}_S^{(m)} = \int_{S_1^{(m)} \dots S_q^{(m)}} \underline{\underline{T}}^{(m)T} \underline{\underline{H}}^{(m)T} \underline{\mathrm{f}}_S dS_F^{(m)} \quad \in \mathbb{R}^{n^{(m)} \times 1} \end{cases} \tag{6.27}$$

As previously mentioned, the assembly procedure is executed by means of a ***location arrays***, which consists in a table of correspondence between the local and global ID of the DOF. We previously formalized this process in section 6.1.1 via the assembly matrices $\boldsymbol{\Omega}_j$.

6.2. Shape functions

Shape functions are used in order to approximate the displacement field inside the elements starting from the nodal values. They are contained in the displacement interpolation matrix $\boldsymbol{H}$, while their space derivatives are used to interpolate the strain field and are contained in the strain interpolation matrix $\boldsymbol{B}$. Shape functions are ***usually polynomials***, either linear or quadratic, due to the simplicity in handling such functions. For example, computing the derivatives required to fill the $\boldsymbol{B}$ matrix is extremely easy with polynomial shape functions. Shape functions must satisfy the following ***requirements***:

- They are defined at element level: meaning that they are zero-valued outside the element domain. This is possible thanks to the isoparametric formulation of FEs.
- There must be as many polynomial coefficients as there are nodal displacements: this simply means that $\boldsymbol{H}$ must have the same number of columns, n, as the rows of $\widehat{\boldsymbol{U}}$, n.
- The shape function N_i must be valued 1 only at node i and go to zero as it approaches the other nodes of the same element. The trend at which goes to zero depends on if the shape function is linear or quadratic.

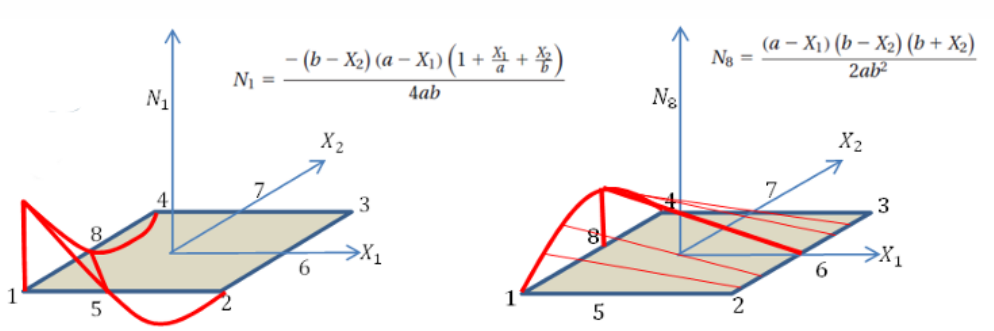

Figure 6.5: quadratic shape functions that are valued 1 at node i and go to 0 to all other nodes.

- The polynomials must be complete: meaning that it must contain the terms appearing in Pascal triangle (Figure 6.7). This ensures that the polynomial is:
  - ***Balanced*** in $x - y - z$ to ensure a compatible displacement field not only at element nodes but also along its boundaries. Sometimes incompatible elements are used, but in general compatibility is a requirement of shape functions.

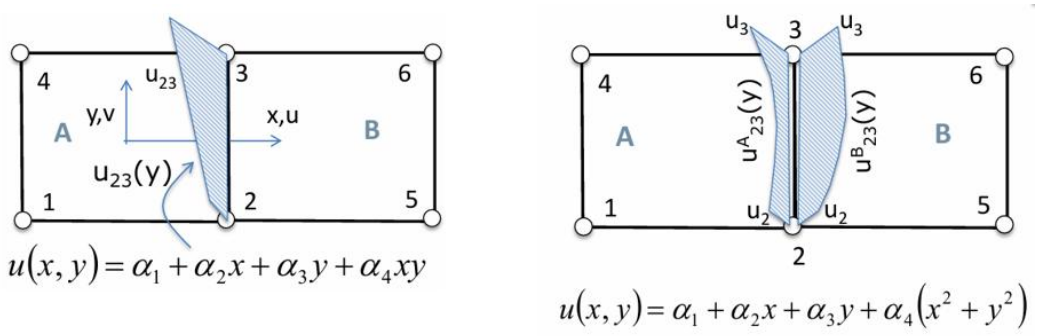

Figure 6.6: shape functions that lead to a compatible (left) and incompatible (right) FE along its edges.

  - ***Constant terms*** appear in the shape functions, corresponding to the row 0 of the Pascal triangle. The presence is of constant terms in the shape function formulation is of absolute importance as it allows the FEs to represent rigid body motions, which is a condition necessary to guarantee convergence of the FE procedure.

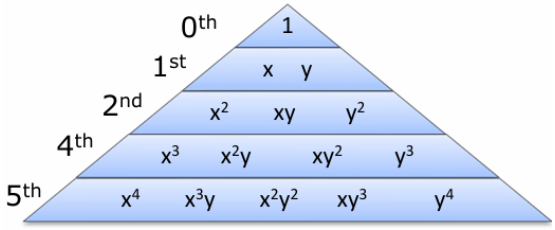

Figure 6.7: Pascal triangle.

6.2.1. Generalized coordinate elements

The shape functions can be obtained in many ways. Here, we discuss only two: the generalized coordinate element technique and the Lagrange interpolation formula. The former is discussed in this section, while the latter in the next section. The generalized coordinate element approach is discussed for ***didactic purpose only***, as it's not an efficient way to determine the shape functions for reasons that will be clear in short. We illustrate how this method works with three applicative examples.

6.2.1.1. Example: linear triangular element

Consider the 2D linear triangular element depicted in Figure 6.8. Being the element 2D, the only displacement components to consider are u and v. Moreover, since the element is linear and thus it has 3 nodes, the total number of DOFs to determine is $2 \times 3 = 6$. Because the two displacement components are completely decoupled, two decoupled polynomial interpolation functions are used. Because each displacement component is characterized by 3 unknown nodal displacements, each polynomial function has three unknown coefficients. Thus, the displacement field inside the FE will be approximated as follows:

$$\underline{u}(x,y) = \begin{cases} u(x,y) = \alpha_1 + \alpha_2 x + \alpha_3 y \\ v(x,y) = \beta_1 + \beta_2 x + \beta_3 y \end{cases} = \begin{bmatrix} 1 & x & y & 0 & 0 & 0 \\ 0 & 0 & 0 & 1 & x & y \end{bmatrix} \begin{Bmatrix} \alpha_1 \\ \alpha_2 \\ \alpha_3 \\ \beta_1 \\ \beta_2 \\ \beta_3 \end{Bmatrix} = \underline{\underline{\phi}}(x,y)\underline{\alpha}$$

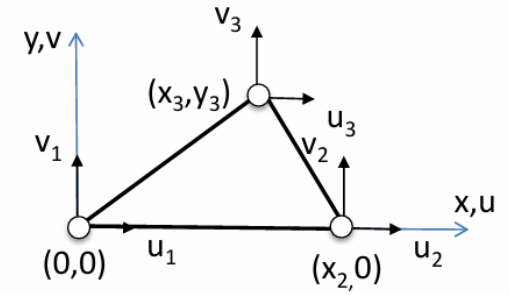

Figure 6.8: triangular element.

The linear relation between the vector of nodal displacements $\hat{\boldsymbol{u}}$ and the vector of polynomial coefficients $\boldsymbol{\alpha}$ will be expressed through the ***generalized coordinate matrix A***. Such matrix contains the nodal coordinates x_i, y_i of the element nodes in place of the generic x, y entries of matrix $\boldsymbol{\phi}$ and for every DOFs.

$$\underline{\hat{u}} = \underline{\underline{A}}\underline{\alpha} \quad \rightarrow \quad \begin{Bmatrix} u_1 \\ u_2 \\ u_3 \\ v_1 \\ v_2 \\ v_3 \end{Bmatrix} = \begin{matrix} \boldsymbol{\phi}_{(1,:)}(x = x_1, y = y_1) \\ \boldsymbol{\phi}_{(1,:)}(x = x_2, y = y_2) \\ \boldsymbol{\phi}_{(1,:)}(x = x_3, y = y_3) \\ \boldsymbol{\phi}_{(2,:)}(x = x_1, y = y_1) \\ \boldsymbol{\phi}_{(2,:)}(x = x_2, y = y_2) \\ \boldsymbol{\phi}_{(2,:)}(x = x_3, y = y_3) \end{matrix} \begin{bmatrix} 1 & 0 & 0 & & & \\ 1 & x_2 & 0 & & \underline{\underline{0}} & \\ 1 & x_3 & y_3 & & & \\ & & & 1 & 0 & 0 \\ & \underline{\underline{0}} & & 1 & x_2 & 0 \\ & & & 1 & x_3 & y_3 \end{bmatrix} \begin{Bmatrix} \alpha_1 \\ \alpha_2 \\ \alpha_3 \\ \beta_1 \\ \beta_2 \\ \beta_3 \end{Bmatrix}$$

Here, $\boldsymbol{\phi}_{(1,:)}$ and $\boldsymbol{\phi}_{(2,:)}$ means all the columns of the first and second rows of $\boldsymbol{\phi}$, respectively. The displacement interpolation matrix $\boldsymbol{H}$ can now be obtained via the $\boldsymbol{\phi}$ and $\boldsymbol{A}$ matrices as follows:

$$\begin{cases}\underline{\hat{u}} = \underline{\underline{A}}\,\underline{\alpha} \\ \underline{u} = \underline{\underline{\phi}}\,\underline{\alpha}\end{cases} \quad \rightarrow \quad \underline{u} = \underline{\underline{\phi}}\,\underline{\underline{A}}^{-1}\underline{\hat{u}} = \underline{\underline{H}}\,\underline{\hat{u}} \quad \rightarrow \quad \underline{\underline{H}} = \underline{\underline{\phi}}\,\underline{\underline{A}}^{-1} \tag{6.28}$$

6.2.1.2. Example: linear square element

Consider the 2D linear square element represented in Figure 6.9. We consider again two decoupled polynomial interpolation functions because the two displacements fields are decoupled as well. The element considered here has 4 nodes, thus each polynomial function will have 4 unknown coefficients.

$$\underline{u}(x,y) = \begin{cases} u(x.y) = \alpha_1 + \alpha_2 x + \alpha_3 y + \alpha_4 xy \\ v(x.y) = \beta_1 + \beta_2 x + \beta_3 y + \beta_4 xy \end{cases} = \begin{bmatrix} 1 & x & y & xy & 0 & 0 & 0 & 0 \\ 0 & 0 & 0 & 0 & 1 & x & y & xy \end{bmatrix} \begin{Bmatrix} \alpha_1 \\ \alpha_2 \\ \alpha_3 \\ \alpha_4 \\ \beta_1 \\ \beta_2 \\ \beta_3 \\ \beta_4 \end{Bmatrix} = \underline{\underline{\phi}}\,\underline{\alpha}$$

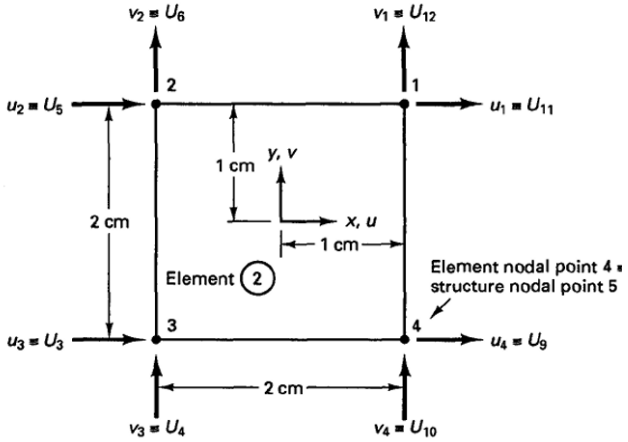

Figure 6.9: 2D square element.

The matrix of generalized nodal coordinates ***A*** is obtained as follows:

$$\underline{\hat{u}} = \underline{\underline{A}}\,\underline{\alpha} \quad \rightarrow \quad \begin{Bmatrix} u_1 \\ u_2 \\ u_3 \\ u_4 \\ v_1 \\ v_2 \\ v_3 \\ v_4 \end{Bmatrix} = \begin{bmatrix} 1 & 1 & 1 & 1 & & & & \\ 1 & -1 & 1 & -1 & & & \underline{0} & \\ 1 & -1 & -1 & 1 & & & & \\ 1 & 1 & -1 & -1 & & & & \\ & & & & 1 & 1 & 1 & 1 \\ & & \underline{0} & & 1 & -1 & 1 & -1 \\ & & & & 1 & -1 & -1 & 1 \\ & & & & 1 & 1 & -1 & -1 \end{bmatrix} \begin{Bmatrix} \alpha_1 \\ \alpha_2 \\ \alpha_3 \\ \alpha_4 \\ \beta_1 \\ \beta_2 \\ \beta_3 \\ \beta_4 \end{Bmatrix}$$

The matrix of the shape functions ***H*** can be found as follows:

$$\begin{cases}\underline{u} = \underline{\underline{\phi}}\,\underline{\alpha} \\ \underline{\hat{u}} = \underline{\underline{A}}\,\underline{\alpha}\end{cases} \quad \rightarrow \quad \underline{u} = \underline{\underline{\phi}}\,\underline{\underline{A}}^{-1}\underline{\hat{u}} = \underline{\underline{H}}\,\underline{\hat{u}}$$

$$\underline{\underline{\mathbf{H}}} = \frac{1}{4}\begin{bmatrix} (1+x)(1+y) & (1-x)(1+y) & (1-x)(1-y) & (1+x)(1-y) & 0 & 0 & 0 & 0 \\ 0 & 0 & 0 & 0 & (1+x)(1+y) & (1-x)(1+y) & (1-x)(1-y) & (1+x)(1-y) \end{bmatrix}$$

6.2.1.3. Example: Euler-Bernoulli linear beam element

Consider the Euler-Bernoulli linear beam element presented in Figure 6.10. For such element we want to approximate the vertical displacement field and the corresponding rotation. Being the beam an Euler-Bernoulli beam, the rotation of the cross section is obtained as a derivative of vertical displacements, i.e. $\theta_x = w_{\backslash x}$. Thus, we are required to interpolate the displacement field v as a C^1 field, meaning that both v and $v_{\backslash x}$ need to be continuous. In order to do so, ***Hermitian shape functions*** must be used, which indeed interpolate v and $\theta = v_{\backslash x}$ as continuous fields and obtain the shape functions of θ by a differentiation process. Because the two fields are coupled, we use one polynomial expression to obtain both. Because we have two nodes with two DOFs each, the polynomial will have 4 unknown coefficients in total. Thus, we'll write:

$$v(x) = \alpha_0 + \alpha_1 x + \alpha_2 x^2 + \alpha_3 x^3 = [1 \;\; x \;\; x^2 \;\; x^3]\begin{Bmatrix} \alpha_0 \\ \alpha_1 \\ \alpha_2 \\ \alpha_3 \end{Bmatrix} = \underline{\underline{\phi}}\,\underline{\alpha}$$

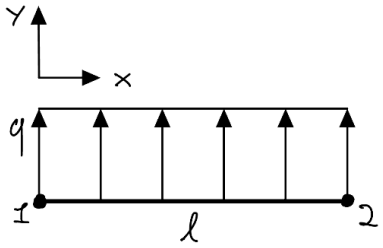

Figure 6.10: Euler-Bernoulli beam element.

The matrix of generalized nodal coordinates ***A*** will then be:

$$\underline{\hat{u}} = \underline{\underline{A}}\,\underline{\alpha} \quad \rightarrow \quad \begin{Bmatrix} v_1 \\ v_2 \\ \theta_1 \\ \theta_2 \end{Bmatrix} = \begin{matrix} \boldsymbol{\phi}(x=0) \\ \boldsymbol{\phi}(x=l) \\ \boldsymbol{\phi}_{\backslash x}(x=0) \\ \boldsymbol{\phi}_{\backslash x}(x=l) \end{matrix}\begin{bmatrix} 1 & 0 & 0 & 0 \\ 1 & l & l^2 & l^3 \\ 0 & 1 & 0 & 0 \\ 0 & 1 & 2l & 3l^2 \end{bmatrix}\begin{Bmatrix} \alpha_0 \\ \alpha_1 \\ \alpha_2 \\ \alpha_3 \end{Bmatrix}$$

The displacements interpolation matrix ***H*** is then found as before, where the first two shape functions interpolate v and the last two interpolate $\theta = v_{\backslash x}$.

$$\underline{\underline{H}} = \underline{\underline{\phi}}\,\underline{\underline{A}}^{-1} = \begin{bmatrix} \frac{2x^3}{27} - \frac{x^2}{3} + 1 & \frac{x^3}{9} - \frac{2x^2}{3} + x & -\frac{2x^3}{27} + \frac{x^2}{3} & \frac{x^3}{9} - \frac{x^2}{3} \end{bmatrix}$$

6.2.2. Lagrange interpolation formula

The second way to determine the shape functions is via the Lagrange interpolation formula. This is how we actually define the interpolation functions in the isoparametric elements (see section 6.3.1). The Lagrange interpolation formula is the following:

$$N_k = \frac{(x_1 - x)(x_2 - x) \dots [(x_k - x)] \dots (x_N - x)}{(x_1 - x_k)(x_2 - x_k) \dots (x_N - x_k)} \tag{6.29}$$

Such formula provides the interpolation function that is non-zero only at node k-th node. Note that in the formula below, the term in square bracket is omitted.

We now discuss an applicative example in which we determine the shape functions in $\boldsymbol{H}$ using the Lagrange interpolation formula. Consider the bilinear squared 2D element presented in Figure 6.11, characterized by a displacement field $\boldsymbol{u}(x, y)$ with the two in-plane components u, v. Thus, the displacement field FE approximation reads:

$$\underline{u}(x,y) = \underline{\underline{H}}(x,y)\underline{\hat{u}} \quad \text{where} \quad \begin{cases} \underline{u} \in \mathbb{R}^{2\times 1} \\ \underline{\underline{H}} \in \mathbb{R}^{2\times 8} \\ \underline{u} \in \mathbb{R}^{8\times 1} \end{cases}$$

We assume to use the same shape functions to interpolate both u and v. For this reason, it is sufficient to show the procedure for only one displacement component, and the shape functions are the same for the other component. Thus, the above approximation written in full form yields:

$$\begin{Bmatrix} u(x,y) \\ v(x,y) \end{Bmatrix} = \begin{bmatrix} N_1 & N_2 & N_3 & N_4 & 0 & 0 & 0 & 0 \\ 0 & 0 & 0 & 0 & N_1 & N_2 & N_3 & N_4 \end{bmatrix} \begin{Bmatrix} u_1 \\ \vdots \\ u_4 \\ v_1 \\ \vdots \\ v_4 \end{Bmatrix}$$

The shape functions are found in two steps. First, we interpolate the u displacement from nodes 1 and 3 to nodes 2 and 4, respectively. This yields:

$$u_{12}(x) = N_{x1}u_1 + N_{x2}u_2 = \frac{x_2 - x}{x_2 - x_1}u_1 + \frac{x_1 - x}{x_1 - x_2}u_2 = \frac{a - x}{2a}u_1 + \frac{a + x}{2a}u_2$$

$$u_{43}(x) = N_{x3}u_3 + N_{x4}u_4 = \frac{x_3 - x}{x_3 - x_4}u_4 + \frac{x_4 - x}{x_4 - x_3}u_3 = \frac{a - x}{2a}u_4 + \frac{a + x}{2a}u_3$$

Then, the interpolation of the u displacement field along the y-axis is carried out starting from $u_{12}(x)$ and $u_{34}(x)$. This yields:

$$u(x,y) = \frac{b - y}{2b}u_{12}(x) + \frac{b + y}{2b}u_{43}(x)$$

By substitution, we determine the shape functions N_i and matrix $\boldsymbol{H}$ as follows:

$$u(x,y) = \underbrace{\frac{a - x}{2a}\frac{b - y}{2b}}_{N_1}u_1 + \underbrace{\frac{a + x}{2a}\frac{b - y}{2b}}_{N_2}u_2 + \underbrace{\frac{a + x}{2a}\frac{b + y}{2b}}_{N_3}u_3 + \underbrace{\frac{a - x}{2a}\frac{b + y}{2b}}_{N_4}u_4$$

$$\underline{\underline{H}} = \begin{bmatrix} N_1 & N_2 & N_3 & N_4 & 0 & 0 & 0 & 0 \\ 0 & 0 & 0 & 0 & N_1 & N_2 & N_3 & N_4 \end{bmatrix}$$

Observation. The shape functions obtained with this approach are the same as the ones obtained with the generalized coordinate approach with $a = b = 1$. If the two approaches are equivalent, they should provide the same result.

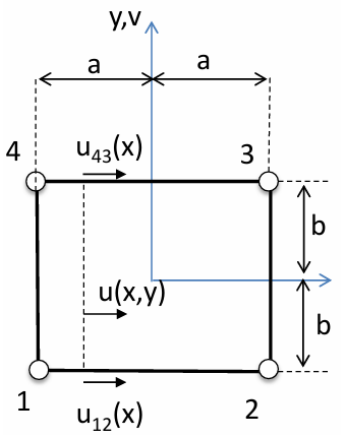

Figure 6.11: scheme of a bi-linear square FE.

6.3. Isoparametric formulation and numerical integration

6.3.1. Isoparametric elements

It has already been mentioned that in commercial FE software, the shape functions are defined at element level, and that this is possible due to the isoparametric formulation. The ***key idea*** of isoparametric formulation is that all elements existing in the physical domain $\boldsymbol{x} = (x, y, z)$ are mapped into extremely regular elements existing in the computational domain $\boldsymbol{\xi} = (\xi, \eta, \zeta)$. In an isoparametric formulation, the same shape functions used for interpolating the displacements are used to represent the element's geometry in the computational domain, not that this is not the only choice. Isoparametric mapping has two ***advantages***; both linked to the regular geometry of computational elements:

- The shape functions are defined in the computational domain $N^{\alpha}(\boldsymbol{\xi})$ using Lagrange interpolation formula: this way every element of any arbitrary geometry in the physical domain is mapped into the same extremely regular computational element using the same shape functions. In the computational domain the elements are cubes/squares/lines of dimensions ranging from -1 to 1.
- Numerical integration is carried out in the computational domain: the very regular geometry granted by isoparametric mapping greatly facilitates the process, more on this later.

The mapping process from the computational to the material/spatial domains is carried out via the ***Jacobian J***. In fact, such second order tensor is defined as follows:

$$\underline{\underline{J}} = \frac{d\underline{x}}{d\underline{\xi}} \quad \text{or} \quad J_{A\beta} = \frac{\partial x_A}{\partial \xi_\beta} \tag{6.30}$$

The finite element approximation of the Jacobian will be:

$$J_{A\beta} = \frac{\partial x_A}{\partial \xi_\beta} = x_{A/\beta} = \sum_\alpha (N^\alpha x_A^\alpha)_{/\beta} = \sum_\alpha N^\alpha_{/\beta} x_A^\alpha = \sum_\alpha \underline{x}^\alpha \otimes \nabla_\xi N^\alpha \tag{6.31}$$

Where $\nabla_\xi N^\alpha$ is the computational gradient of the shape functions N^α. Expressing such term in full form yields:

$$\nabla_\xi N^\alpha = \begin{Bmatrix} N^\alpha_{/\xi} \\ N^\alpha_{/\eta} \\ N^\alpha_{/\zeta} \end{Bmatrix} = \begin{Bmatrix} \dfrac{\partial N^\alpha}{\partial \xi} \\ \dfrac{\partial N^\alpha}{\partial \eta} \\ \dfrac{\partial N^\alpha}{\partial \zeta} \end{Bmatrix} \tag{6.32}$$

It is easy to notice from the definition of the Jacobian in (6.30) that the ***physical meaning*** of such operator is essentially to be a measure of the deformation that occurs to the FE during the mapping process from physical $\boldsymbol{x}$ to computational $\boldsymbol{\xi}$ domain. In fact, diagonal elements of $\boldsymbol{J}$ represent stretching of the finite element, while extra-diagonal terms represent change of shape/distortion. Starting from the definition of the Jacobian in (6.30), if the volume of the FE in the computational domain is $\Omega^{(m)}$, it can be proven that the following relation holds true:

$$\det \underline{\underline{J}} = \frac{dV}{d\Omega} \tag{6.33}$$

Using the above equation, the integrals appearing in the FE approximation of the PVW equation (6.21) can be computed as follows:

$$\int_{V^{(m)}} (\cdot) dV^{(m)} = \int_{\Omega^{(m)}} (\cdot) \det \underline{\underline{J}}\, d\Omega^{(m)} \tag{6.34}$$

Observation. From this formulation of the PVW integrals, one can notice that minimizing the integration error due to isoparametric mapping alone implies mathematically minimizing $\det \boldsymbol{J}$. Physically speaking, this means minimizing element distortion, which can be translated into generating a regular mesh, the more regular the better.

6.3.2. Numerical integration

Recall that the shape functions are defined in the computational domain, i.e. $N^\alpha = N^\alpha(\boldsymbol{\xi})$. However, the gradients appearing in the PVW are computed in the physical domain $\boldsymbol{x}$. In order to compute the physical gradients of the shape functions starting from the computational space, we apply the chain rule:

$$\nabla_\xi N^\alpha = \frac{\partial N^\alpha}{\partial \xi_\beta} = \frac{\partial N^\alpha}{\partial X_A} \frac{\partial X_A}{\partial \xi_\beta} = \nabla_0 N^\alpha \underline{\underline{J}} = \underline{\underline{J}}^T \nabla_0 N^\alpha$$

$$\nabla_0 N^\alpha = \underline{\underline{J}}^{-T} \nabla_\xi N^\alpha \tag{6.35}$$

Where $\nabla_0 N^\alpha$ is the physical gradient of the shape functions. However, this formulation of the physical gradient of the shape functions is still not refined enough. In fact, computing the

analytical expression of $\boldsymbol{J}$, and thus of $\boldsymbol{J}^{-T}$, can be extremely difficult. This problem is solved by numerical integration, which avoids the computation of the analytical expression of $\boldsymbol{J}$ altogether. Instead, numerical integration only requires the evaluation of the Jacobian at specific locations in the FE computational volume $\Omega^{(m)}$. Such points are called ***integration points*** (IPs), and their location depends on algorithm used for numerical integration, which we refer to as ***integration rule*** or ***integration scheme***. The most commonly used integration rule in FEA commercial code is the ***Gauss integration rule***. According to such approach, using N_{IP} integration points allows for an ***exact integration*** of polynomial functions of order $2N_{IP}-1$. Intuitively, higher order polynomials require more IPs to be (exactly) numerically integrated. The general expression of Gauss integration reads:

$$I=\int_V f(\underline{x})dV=\int_\Omega f\left(\underline{\xi}\right)\det\underline{\underline{J}}\left(\underline{\xi}\right)d\Omega\approx\sum_{\alpha=1}^{N_{IP}}f\left(\underline{\xi}_\alpha\right)\det\underline{\underline{J}}\left(\underline{\xi}_\alpha\right)\underline{w}_\alpha \tag{6.36}$$

Where $\boldsymbol{\xi}_\alpha$ are the coordinates of the Gauss' integration points, and $\boldsymbol{w}_\alpha$ are weights. The exact values of such quantities are reported in Table 6.1. We report below the formulation for the 1D, 2D and 3D cases:

$$I=\int_a^b f(x)\,dX=\int_{-1}^{+1}f(\xi)\det\left[\underline{\underline{J}}(\xi)\right]d\xi\approx\sum_{\alpha}^{N_{IP}}f(\xi_\alpha)\det\left[\underline{\underline{J}}(\xi_\alpha)\right]w_\alpha$$

$$I=\int_A f(x,y)dA=\int_{-1}^{+1}\int_{-1}^{+1}f(\xi,\eta)\det\left[\underline{\underline{J}}(\xi,\eta)\right]d\xi d\eta=$$
$$\approx\sum_{\alpha,\beta=1}^{N_{IP},N_{IP}}f\left(\xi_\alpha,\eta_\beta\right)\det\left[\underline{\underline{J}}\left(\xi_\alpha,\eta_\beta\right)\right]w_\alpha w_\beta$$

$$I=\int_V f(x,y,z)dV=\int_{-1}^{+1}\int_{-1}^{+1}\int_{-1}^{+1}f(\xi,\eta,\zeta)\det\left[\underline{\underline{J}}(\xi,\eta,\zeta)\right]d\xi d\eta d\zeta=$$
$$\approx\sum_{\alpha,\beta,\gamma=1}^{N_{IP},N_{IP},N_{IP}}f\left(\xi_\alpha,\eta_\beta,\zeta_\gamma\right)\det\left[\underline{\underline{J}}\left(\xi_\alpha,\eta_\beta,\zeta_\gamma\right)\right]w_\alpha w_\beta w_\gamma$$

N_{IP}	ξ_m	w_m
1	0	2
2	$-1/\sqrt{3}\quad+1/\sqrt{3}$	$1\quad1$
3	$-\sqrt{3/5}\quad0\quad+\sqrt{3/5}$	$5/9\quad8/9\quad5/9$

Table 6.1: Gauss integration scheme values.

Observation. It is clear by know that the Jacobian is needed twice if the isoparametric formulation is used: first in computing the physical gradients via $\boldsymbol{J}^{-T}$, and second to transform the integrals from V to Ω via $\det\boldsymbol{J}$.

6.3.3. Stress recovery

Once the FE solution has been obtained, i.e. once the nodal displacements $\widehat{\boldsymbol{U}}$ have been computed, one can retrieve the strain and stress fields. This procedure takes the name of ***stress recovery***, and it's carried out as follows. First, the strains are obtained from nodal displacements via the strain interpolation matrix $\boldsymbol{B}$, and the stresses are then recovered using the CL. Because the Jacobian is known only at the IPs, so is the $\boldsymbol{B}$ matrix, which requires the evaluation of the shape function physical derivatives to be computed. Consequently, strains and stresses are also known only at the IPs. In order to obtain a continuous contour, the following steps are implemented:

1. Use the shape functions to extrapolate such values to the element nodes.
2. At the common node between adjacent elements assign the average σ in order to smooth out discontinuities. This also makes it possible to detect on which nodes there are high discontinuities in stress values. In such region mesh refining is generally appropriate, although in some cases high stress gradients are to be expected (notches, force application regions, interface of 2 plies in composites etc.).
3. Use the shape functions used to interpolate the displacement field to interpolate the extrapolated nodal stress values and obtain a continuous contour.

6.3.1. Full and reduced integration

Intuitively, being numerical integration an approximative way to compute integrals, it could be a source of error in the FE process. In the previous sections, the Gauss integration rule that provides exact integration has been discussed. The term ***exact integration*** refers to an integration rule that introduces no error related to the numerical procedure.

In section 6.3.1 it has been discussed the physical meaning of the Jacobian, i.e. a measure of the distortion between the same physical and computational element. It's easy to accept, even qualitatively, that the more distorted the elements, the higher the order of integration needed for full integration. Thus, the term ***full integration*** is used to mean the integration that would be exact if the element geometry were not distorted. Examples of such integration schemes are provided in Figure 6.12.

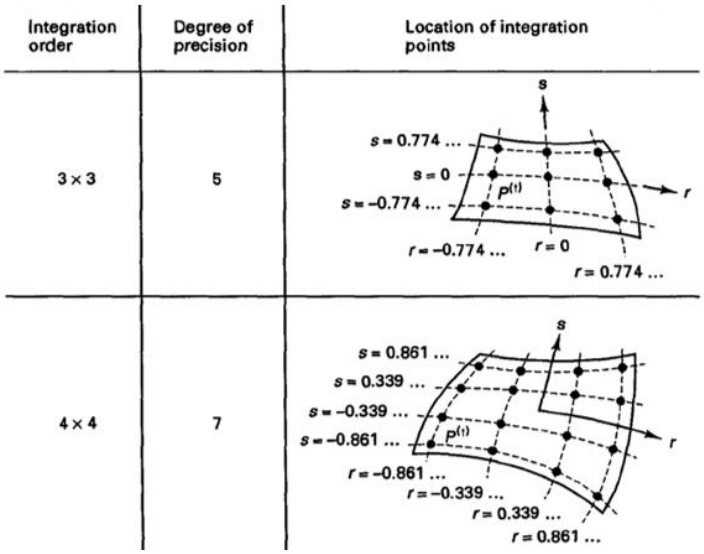

Figure 6.12: examples of full integration schemes.

To reduce computational cost, ***reduced integration*** could be adopted. That is, an integration scheme that uses less IPs than those needed for it to be exact/full. A second advantage of reduced integration is the ability to compensate for the over stiffness associated with compatible elements.

However, reduced integration has the ***critical problem*** of possibly introducing spurious zero-strain energy modes, as depicted in Figure 6.13 – right. Thus, reduced integration might not be able to correctly account for some deformation modes, to which null strain, and thus null stiffness, and thus null strain energy are associated in the PVW as a consequence.

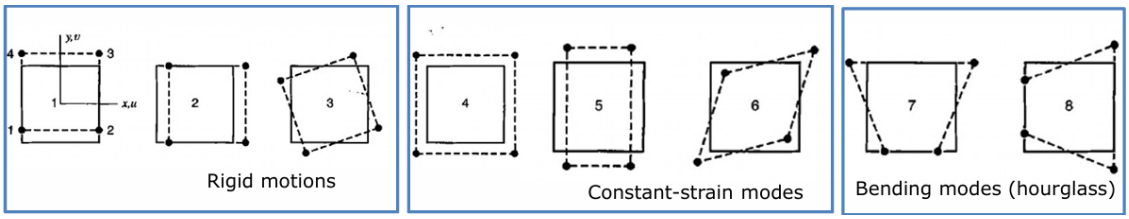

Figure 6.13: deformation modes of a 4 noded square element.

For example, deformation modes from 4 to 8 of a bilinear square element Q4 in Figure 6.13, can be correctly accounted for using full integration, and thus 4 IPs. Contrarily, reduced integration would use 1 IP placed in the center of such elements. For such an integration scheme, deformation modes 4 through 8 are not detectable. Modes 7 and 8, commonly referred to as ***hourglass mode***, are particularly insidious because they can be excited in adjacent elements and thus spread through the mesh. Spurious deformation modes with no associated strain energy that diffuse through the mesh are called ***communicable modes***. The hourglass mode is typical of square elements, and as previously mentioned, it is particularly dangerous with Q4 elements with reduced integration, because communicable. The same mode is, however, non-communicable in Q8 elements, i.e. squared elements with 8 nodes and thus quadratic formulation. Thus, Q8 elements are often used with reduced integration, which implies 2x2 Gauss rule. The hourglass mode in Q9 elements is instead communicable, thus Q8 are generally preferred to Q9.

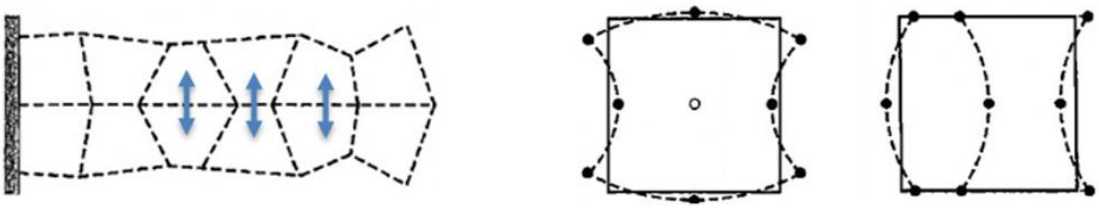

Figure 6.14: left) communicable hourglass Q4; right) non-communicable hourglass Q8 and communicable hourglass Q9.

6.3.2. Example: bar element

The global reference system is $\boldsymbol{x} = (x, y, z)$ with nodal points 1 and 2 having respectively coordinates x_1, x_2. A generic point inside the bar has coordinate x. We define the natural coordinate system as a monodimentional axis $-1 < \xi < 1$ (in the figure below denoted as r).

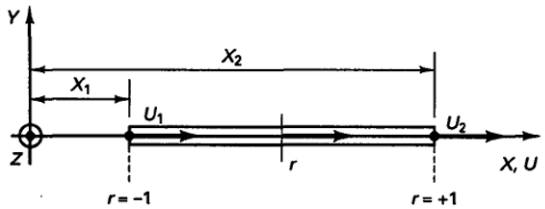

Figure 6.15: global and natural reference systems for a 1D FE.

We want to prove the effectiveness of the isoparametric elements by computing the stiffness matrix $\boldsymbol{K}$ of this element. Assuming constant beam elastic properties, we obtain:

$$\underline{\underline{K}} = \int_V \underline{\underline{B}}^T \underline{\underline{D}}\underline{\underline{B}} dV = AE \int_{x_1}^{x_2} \underline{\underline{B}}^T \underline{\underline{B}} dx$$

As previously mentioned, element geometry and displacements are mapped using the same shape functions $N_1(\xi)$ and $N_2(\xi)$. Also, such functions can be used for any generic 1D element of any length $x_2 - x_1$.

$$\begin{cases} x(\xi) = N_1(\xi)x_1 + N_2(\xi)x_2 = \frac{1}{2}(1-\xi)x_1 + \frac{1}{2}(1+\xi)x_2 \\ u(\xi) = N_1(\xi)u_1 + N_2(\xi)u_2 = \frac{1}{2}(1-\xi)u_1 + \frac{1}{2}(1+\xi)u_2 \end{cases} \tag{6.37}$$

To derive the strain we need to apply $\boldsymbol{D}$ to $\boldsymbol{H}$, in this monodimentional case it means we simply need to apply $\partial/\partial x$ by definition of strain. Following the chain rule, we obtain:

$$\varepsilon = \frac{du(\xi)}{dx} = \frac{du}{d\xi}\frac{d\xi}{dx} = \frac{u_2 - u_1}{2}\frac{2}{x_2 - x_1} = \frac{u_2 - u_1}{L} = \frac{1}{L}[1 \quad -1]\begin{Bmatrix} u_1 \\ u_2 \end{Bmatrix} \quad \rightarrow \quad \underline{\underline{B}} = \frac{1}{L}[1 \quad -1]$$

Now we need to express $dx = \mathrm{f}(d\xi)$ using the definition of the Jacobian, a mathematical operator representing distortion due to the mapping process. If $J^{\uparrow}$ there's high distortion, if $J \approx 1$ there's virtually no distortion.

$$J = \frac{dx}{d\xi} = \frac{L}{2} \quad \rightarrow \quad dx = \frac{L}{2}d\xi$$

The stiffness matrix is then computed as follows:

$$\underline{\underline{K}} = EA \int_{x_1}^{x_2} \underline{\underline{B}}^T \underline{\underline{B}} dx = \frac{EA}{L^2} \int_{-1}^{+1} \begin{bmatrix} 1 & -1 \\ -1 & 1 \end{bmatrix} \frac{L}{2} d\xi = \frac{EA}{L} \begin{bmatrix} 1 & -1 \\ -1 & 1 \end{bmatrix}$$

6.4. Basic FE and their behavior

6.4.1. Linear 2D triangular elements (CST)

These elements employ linear shape functions, as shown in the previous chapter. This implies that $[B]$ and thus $\underline{\varepsilon}$ are constant for these elements, for this reason these elements are commonly referred to as ***constant strain triangular elements CST***. This is generally a terrible result, because it means that we're not able to represent bending stresses accurately.

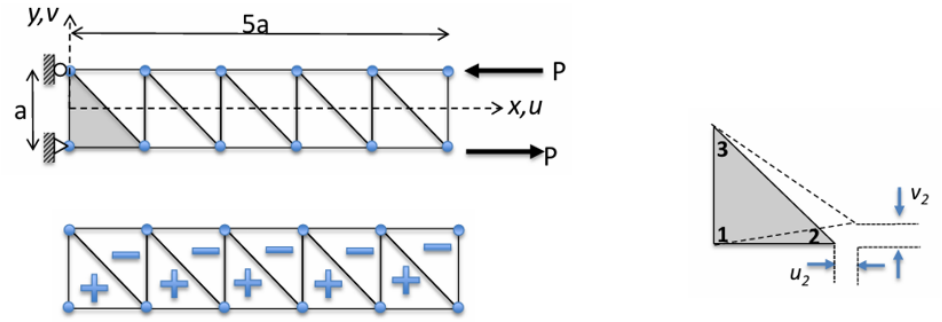

Figure 6.16: CST beam model.

Furthermore, we can see in Figure 6.16 that due to the fact that node 2 of the highlighted element is free to move, a spurious shear strain is generated. This shear component absorbs energy in the PVW formulation of the problem, which makes the model stiffer than it actually is[1] because we need more energy than it's really needed to achieve a given displacement of the beam. This phenomenon is called ***shear locking***.

6.4.2. Linear and quadratic 2D square elements (Q4 – Q8)

Linear square elements Q4, although better than CST, exhibit a ***significant shear locking in bending***. This is clear if we compare the strains of a real square physical element and the strains of a Q4 element:

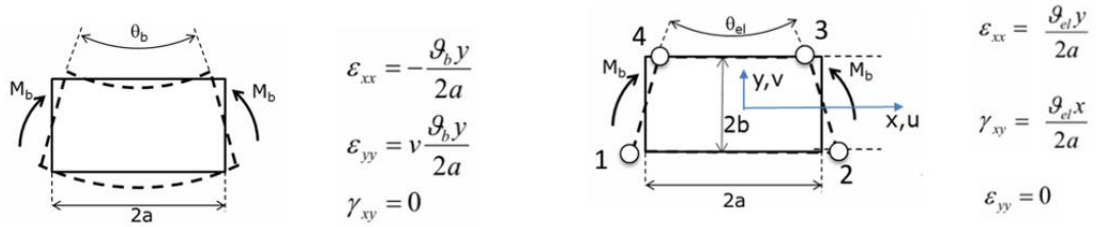

Figure 6.17: left) real strains; right) Q4 FE strains.

It can be proven that the ratio of the rotation of the FE and that of the real body element is inversely proportional to the square of the aspect ration a/b. This means that the higher this ratio is, the stiffer the element becomes with respect to real material behavior.

$$\frac{\theta_{el}}{\theta_b} = \frac{1-\nu^2}{1+\frac{1-\nu}{2}\left(\frac{a}{b}\right)^2}$$

To represent bending modes more accurately we can use square elements with 8 nodes - Q8. Such elements have three nodes on each edge, for a total of 8 nodes. This implies a quadratic interpolation formulas[2], which can better represent bending modes.

$$\underline{u}(x,y) = \begin{Bmatrix} u(x.y) = \alpha_1 + \alpha_2 x + \alpha_3 y + \alpha_4 xy + \alpha_5 x^2 + \alpha_6 y^2 + \alpha_7 x^2 y + \alpha_8 x y^2 \\ v(x.y) = \beta_1 + \beta_2 x + \beta_3 y + \beta_4 xy + \beta_5 x^2 + \beta_6 y^2 + \beta_7 x^2 y + \beta_8 x y^2 \end{Bmatrix}$$

[1] In general, FE models are always stiffer than their real counterparts due to the discretization of the domain.
[2] Note that these shape functions are not Lagrange polynomials because they are obtained by multiplying two polynomials.

A second way would be to use quadratic Q9 elements, which have an additional node in the center. Hence, an additional quadratic term x^2y^2 is added to the interpolation scheme. However, Q8 elements are generally preferred with respect to Q9 elements (see section 6.6.4).

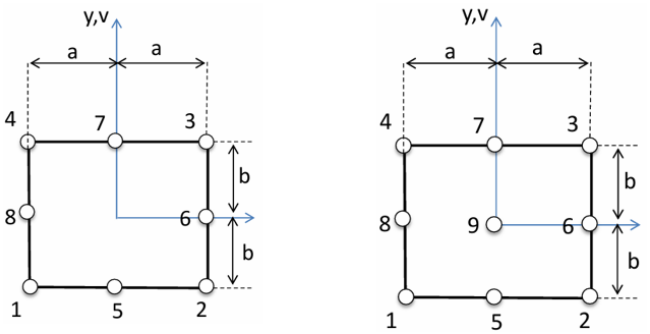

Figure 6.18: left) Q8 element; right) Q9 element.

A third way would be to use ***incompatible elements***: we relax the compatibility condition on element edges. As a result, such elements will have 8 nodal DOFs plus 4 additional DOFs related to the bending modes. Incompatible elements ***must be used with judgement***, as compatibility is a condition generally required for convergence of a FE code.

$$u(x,y)=\sum_{1}^{4} N_i u_i + \left(1-\left(\frac{x}{a}\right)^2\right)a_1 + \left(1-\left(\frac{y}{b}\right)^2\right)a_2$$

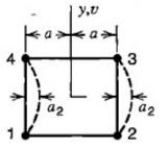

$$v(x,y)=\sum_{1}^{4} N_i v_i + \left(1-\left(\frac{x}{a}\right)^2\right)a_3 + \left(1-\left(\frac{y}{b}\right)^2\right)a_4$$

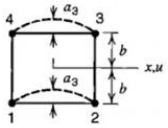

Incompatible elements represent gaps or overlaps that cannot exist in a physical continuum. Even so, they are able to represent constant strains and thus convergence can be achieved. Interestingly, such convergence is achieved from above, instead of from below like normal compatible elements. This happens because incompatible elements are more compliant than compatible elements.

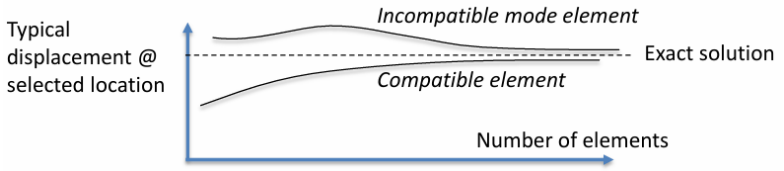

Figure 6.19: convergence of compatible and incompatible elements.

6.4.3. Plate and shell elements

Both plate and shell elements are based on MPT. The ***key difference*** is that in plate elements a transverse load does not generate membranal stress, while in shell elements they do. However, in practical applications such as tanks, development of in-plane stresses due to transversal loads is inevitable. For such reason, all 2D elements are shell elements.

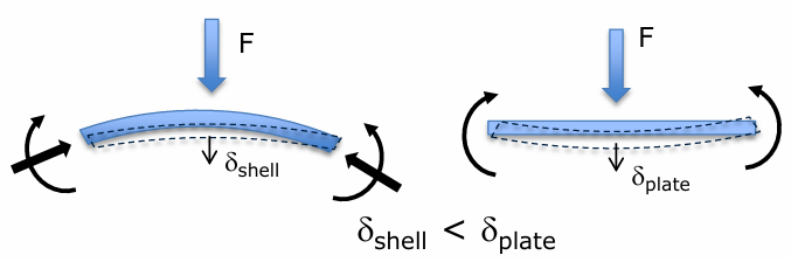

Figure 6.20: transverse displacement of plate and shell FEs due to transverse a load.

Note that the presence of additional membranal terms in shell elements makes them stiffer than plate elements, because then is an additional term, the membranal one, in δW_D that absorbs the δW_e. As a result, transverse displacement is lower in shells than plates.

$$\delta W_D = \int_\Omega \left(\delta \underline{\varepsilon}_0^T \underline{N} + \delta \underline{k}^T \underline{M} + \underline{\gamma}^T \underline{Q}\right) d\Omega = \int_\Omega \left(\delta \underline{\varepsilon}_0^T \underline{\underline{A}}\, \underline{\varepsilon}_0 + \delta \underline{k}^T \underline{\underline{D}}\, \underline{k} + \underline{\gamma}^T \underline{\underline{D}}^{TSS} \underline{\gamma}\right) d\Omega$$

$$\underline{\varepsilon}_0 = \begin{Bmatrix} \varepsilon_{0xx} \\ \varepsilon_{0yy} \\ \gamma_{0xy} \end{Bmatrix} = \begin{Bmatrix} \dfrac{\partial u_0}{\partial x} \\ \dfrac{\partial v_0}{\partial y} \\ \dfrac{\partial u_0}{\partial y} + \dfrac{\partial v_0}{\partial x} \end{Bmatrix} \qquad \underline{k} = \begin{Bmatrix} k_x \\ k_y \\ k_{xy} \end{Bmatrix} = \begin{Bmatrix} -\dfrac{\partial \theta_x}{\partial x} \\ -\dfrac{\partial \theta_y}{\partial y} \\ -\dfrac{\partial \theta_x}{\partial y} - \dfrac{\partial \theta_y}{\partial \mathrm{x}} \end{Bmatrix} \qquad \underline{\gamma} = \begin{Bmatrix} \gamma_{xz} \\ \gamma_{yz} \end{Bmatrix}$$

$$= \begin{Bmatrix} \dfrac{\partial w_0}{\partial x} - \theta_x \\ \dfrac{\partial w_0}{\partial y} - \theta_y \end{Bmatrix}$$

6.4.3.1. Plate elements

The virtual internal work δW_D for an isotropic Mindlin plate, neglecting membranal strain, can be expressed as follows:

$$\delta W_D = \int_\Omega \left(\delta \underline{k}^T \underline{M} + \underline{\gamma}^T \underline{Q}\right) d\Omega = \int_\Omega \left(\delta \underline{k}^T \underline{\underline{D}}\, \underline{k} + \underline{\gamma}^T \underline{\underline{D}}^{TSS} \underline{\gamma}\right) d\Omega$$

It's clear that FEM implementation of Mindlin plates is a C^0 problem, since only first derivatives appear in δW_D. For each node we have 3 DOFs (w, θ_x, θ_y), all of which will use same shape functions:

$$\underline{u} = \sum_i^N H_i [I]_{3x3} \underline{\hat{u}} \quad \rightarrow \quad \begin{Bmatrix} w \\ \theta_x \\ \theta_y \end{Bmatrix} = \sum_i^N \begin{bmatrix} H_i & 0 & 0 \\ 0 & H_i & 0 \\ 0 & 0 & H_i \end{bmatrix} \begin{Bmatrix} w_i \\ \theta_{xi} \\ \theta_{yi} \end{Bmatrix}$$

Where N = number of nodes. To compute $\underline{k}$ and $\underline{\gamma}$ we need to apply two separate $[D]$ matrices, which will lead to the definition of two separate $[B]$ and $[K]$ matrices. In particular:

$$\underline{k} = \underline{\underline{D}}^b \underline{u} = \sum_i^N \underbrace{\underline{\underline{D}}^b H_i [I]_{3x3}}_{[B]^b} \underline{\hat{u}} \quad \rightarrow \quad \begin{Bmatrix} -\frac{\partial \theta_x}{\partial x} \\ -\frac{\partial \theta_y}{\partial y} \\ -\frac{\partial \theta_x}{\partial y} - \frac{\partial \theta_y}{\partial x} \end{Bmatrix}$$

$$= \sum_i^N \begin{bmatrix} 0 & -\frac{\partial}{\partial x} & 0 \\ 0 & 0 & -\frac{\partial}{\partial y} \\ 0 & -\frac{\partial}{\partial y} & -\frac{\partial}{\partial x} \end{bmatrix} \begin{bmatrix} H_i & 0 & 0 \\ 0 & H_i & 0 \\ 0 & 0 & H_i \end{bmatrix} \begin{Bmatrix} w_i \\ \theta_{xi} \\ \theta_{yi} \end{Bmatrix}$$

$$\underline{\gamma} = \underline{\underline{D}}^{TSS} \underline{u} = \sum_i^N \underbrace{\underline{\underline{D}}^{TSS} H_i [I]_{3x3}}_{[B]^{TSS}} \underline{\hat{u}} \quad \rightarrow \quad \begin{Bmatrix} \frac{\partial w_0}{\partial x} - \theta_x \\ \frac{\partial w_0}{\partial y} - \theta_y \end{Bmatrix}$$

$$= \sum_i^N \begin{bmatrix} \frac{\partial}{\partial x} & -1 & 0 \\ \frac{\partial}{\partial y} & 0 & -1 \end{bmatrix} \begin{bmatrix} H_i & 0 & 0 \\ 0 & H_i & 0 \\ 0 & 0 & H_i \end{bmatrix} \begin{Bmatrix} w_i \\ \theta_{xi} \\ \theta_{yi} \end{Bmatrix}$$

Of course, using isoparametric elements, the computation of $\partial h_i / \partial x_i$ will be carried out via the Jacobian and numerical integration. More precisely:

$$\frac{\partial H_i}{\partial \underline{x}} = [J]^{-1} \frac{\partial H_i(\underline{r})}{\partial \underline{r}} \quad \rightarrow \quad \begin{Bmatrix} \frac{\partial h}{\partial x} \\ \frac{\partial h}{\partial y} \end{Bmatrix} = \begin{bmatrix} \frac{\partial r}{\partial x} & \frac{\partial s}{\partial x} \\ \frac{\partial r}{\partial y} & \frac{\partial s}{\partial y} \end{bmatrix} \begin{Bmatrix} \frac{\partial H_i(\underline{r})}{\partial r} \\ \frac{\partial H_i(\underline{r})}{\partial s} \end{Bmatrix}$$

The stiffness matrices will be defined as:

$$\underline{\underline{K}}^b = \int_{-1}^{+1} \int_{-1}^{+1} \underline{\underline{B}}^{b^T} \underline{\underline{D}}^b \underline{\underline{B}}^b \det J \, dr ds \qquad \underline{\underline{K}}^{TSS} = \int_{-1}^{+1} \int_{-1}^{+1} \underline{\underline{B}}^{TSS^T} \underline{\underline{D}}^{TSS} \underline{\underline{B}}^{TSS} \det J \, dr ds$$

Mindlin elements have a ***problem with shear locking related to TSS***. Recall that for Mindlin plates, $[D^B] \propto Gt^3$ while $[D^{TSS}] \propto Gt$, meaning that as $t^{\downarrow\downarrow}$ these elements will be way more compliant in bending than in transverse. In other words, with a natural BCs that favor bending, TSS should be negligible.

For Mindlin FE, this is not always the case, due to the fact that we use the same H_i for θ_x, θ_y and for w. This implies that inside the $\underline{\gamma}$ terms, we'll have polynomials of different orders. As a consequence, as $t \rightarrow 0$, these terms do not become negligible, and TSS develop in the FE. This is clearly visible in Figure 6.21.

The presence of these artificial TSS make Mindlin FE stiffer than those defined with the analytical solution. Moreover, due to the fact that as $t \rightarrow 0$ the TSSs should be smaller and smaller, but they're actually not, means that this shear locking phenomenon is more severe the thinner the plate.

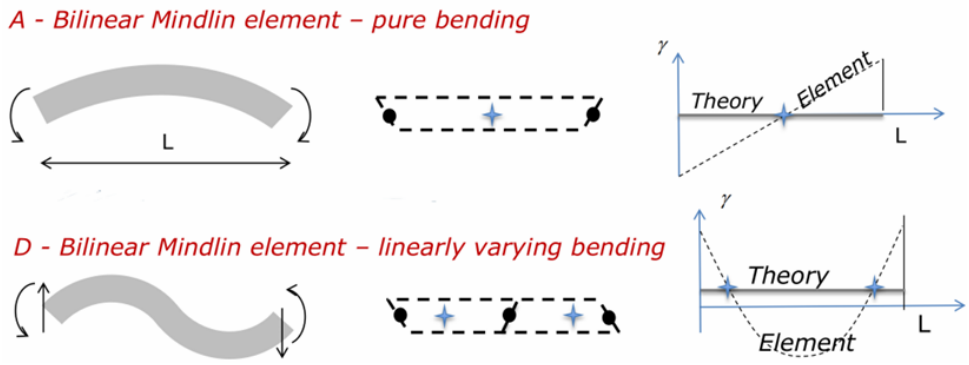

Figure 6.21: comparison of TSS provided by Mindlin FE and MPT in different loading conditions.

A solution to this problem would be an appropriate choice of integration points on which to compute $[K^{TSS}]$.
In particular, with respect to Figure 6.21, we avoid this problem if the IP coincide with the points where the FE and analytical solutions are identical. However, if the ratio $L/t > 100$, this solution is not sufficient to mitigate shear locking effects, and we need to adopt other improvement strategies, such as:

- Appropriate modification of G through the element thickness.
- Use different polynomials for θ_x, θ_y and w: this could lead to incompatible elements.
- Discrete Mindlin elements: correct values of γ can be enforced in specific points.
- Other variational principles: the displacement approach could be mixed with the force approach.

6.4.3.2. Shell elements

The virtual internal work δW_D now also contains membranal terms, as in Equation **Error! Reference source not found.**.

$$\delta W_D = \int_\Omega \left(\delta \underline{\varepsilon}_0^T \underline{N} + \delta \underline{k}^T \underline{M} + \underline{\gamma}^T \underline{Q}\right) d\Omega = \int_\Omega \left(\delta \underline{\varepsilon}_0^T \underline{\underline{A}}\, \underline{\varepsilon}_0 + \delta \underline{k}^T \underline{\underline{D}}\, \underline{k} + \underline{\gamma}^T \underline{\underline{D}}^{TSS} \underline{\gamma}\right) d\Omega$$

In this case, due to the membranal contribution, each node has 5 DOFs $(u_0, v_0, w_0, \theta_x, \theta_y)$, and a new stiffness matrix arises:

$$\underline{\underline{K}}^M = \int_{-1}^{+1} \int_{-1}^{+1} \underline{\underline{B}}^{M^T} \underline{\underline{D}}^M \underline{\underline{B}}^M \det J \, dr ds$$

Shell elements are generally curved. This is because in real 3D components, such as a tank, the points on the 2D mid-surface are generally not on the same plane. Thus, an algorithm is necessary to project such points on the same plane. Furthermore, flat elements have high membranal stiffness and low bending behavior, which tends to exclude bending from the response (bending locking).

The definition of curved shell elements is based on the isoparametric approach of mapping a solid FE. More precisely:

1. A solid element is defined in $\underline{r}(r, s, t)$, with $t \ll r, s$:
2. Each pair of nodes on the top and bottom surfaces is constrained so they have the same displacement of a line that connects them. This way we enforce the Mindlin hypothesis "cross sections remain plane in bending".

3. Top and bottom elements are eliminated in favor of midplane nodes, to which are assigned the same rotations of the lines connecting the original nodes.

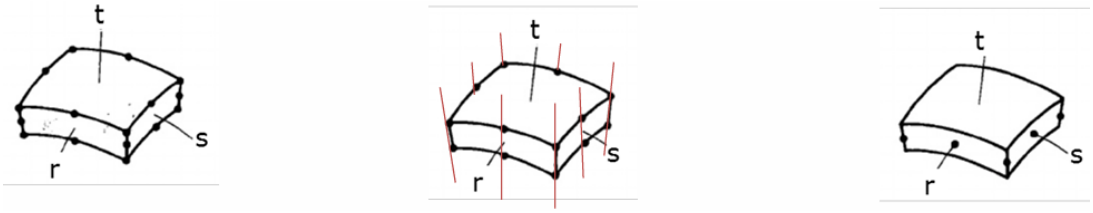

Figure 6.22: steps for defining the nodes of a shell element.

The mapping of the solid element in $\underline{r}$ is done by means of interpolation functions $H_i(r,s)$. Referring to Figure 6.23, *(i, j, k)* are respectively the nodes on the mid, upper and lower surfaces. TH_i is the thickness of the solid along the i-th node. t is parametrized thickness coordinate, such that $-1 < t < 1$. The mapping of such points is carried out as follows:

$$\begin{Bmatrix} x \\ y \\ z \end{Bmatrix} = \sum_i^N H_i \left(\begin{Bmatrix} x_i \\ y_i \\ z_i \end{Bmatrix} + t \cdot \frac{TH_i}{2} \begin{Bmatrix} x_j - x_k \\ y_j - y_k \\ z_j - z_k \end{Bmatrix} \right) \tag{6.38}$$

We can define the in-plane tangent vectors of the i-th node as follows:

$$[\mu_i] = [\underline{V}_{2i} \quad \underline{V}_{3i}] = \begin{bmatrix} x_{2j} - x_{2k} & x_{3j} - x_{3k} \\ y_{2j} - y_{2k} & y_{3j} - y_{3k} \\ z_{2j} - z_{2k} & z_{3j} - z_{3k} \end{bmatrix} \tag{6.39}$$

The displacements are then computed as follows:

$$\begin{Bmatrix} u \\ v \\ w \end{Bmatrix} = \sum_i^N H_i \left(\begin{Bmatrix} u_i \\ v_i \\ w_i \end{Bmatrix} + t \cdot \frac{TH_i}{2} [\mu_i] \begin{Bmatrix} \alpha_i \\ \beta_i \end{Bmatrix} \right) \tag{6.40}$$

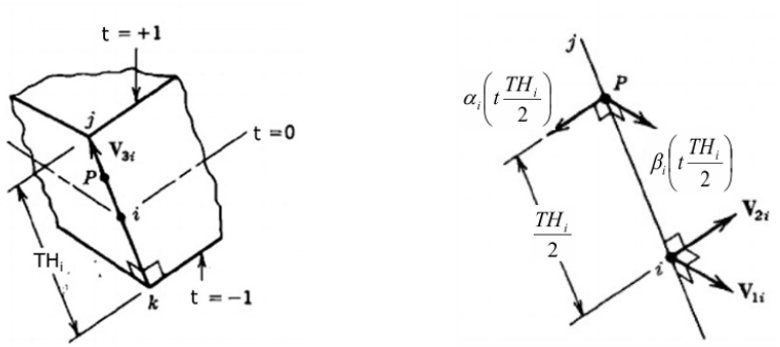

Figure 6.23: isoparametric thin solid element.

From these matrices, matrix $[B]$ can be obtained. Thus, via numerical integration, we can also obtain $[K]$.

$$\underline{\underline{K}} = \int_V \underline{\underline{B}}^T \underline{\underline{DB}} dxdydz = \int_V \underline{\underline{B}}^T \underline{\underline{DB}} \det J \, drdsdt$$

Generally, integration in the $r-s$ plane is performed using Gauss integration rule, while integration through the thickness follows Simpson rule (equidistant number of points specified by the user).

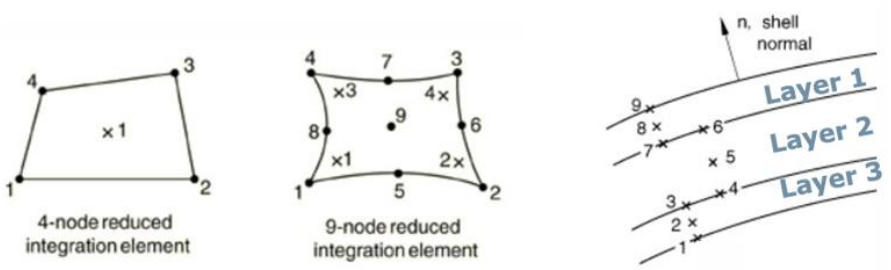

Figure 6.24: left) Gauss integration; right) Simpson integration.

6.5. Meshing

Meshing is the process by which the FEs and their connections are created, and a mesh is obtained. The creation of a mesh provides with the definition and numbering of the nodes and the elements themselves. This process is ***biggest bottleneck of FEA*** due to its high computational cost, which even surpasses that required to compute the solution. Because of this, the level of idealization of a structure, which in practical terms means the choice of the element types, becomes critical. More precisely, the level of idealization depends on the level of detail of the information we want to obtain from the simulation. For example, beam elements are enough to study the global behavior of a beam, but to study local effects (region of application of BCs, welded spots, joints etc.) we need shell or even solid elements.

Idealization	Comp. time	Model preparation
Beams	Small (few d.o.f's)	Geometry from scratch Meshing very simple Sections/orientation required
Plate/Shell (triangle or quadrilateral)	Medium	Mid-plane required Automatic meshing methods Thickness/material required
Solid (tetrahedral)	High	Geometry from CAD Automatic meshing methods
Solid (Hexahedral)	High	Geometry from CAD geometrical decomposition /manual sweep required

Table 6.2: FE choice and characteristics.

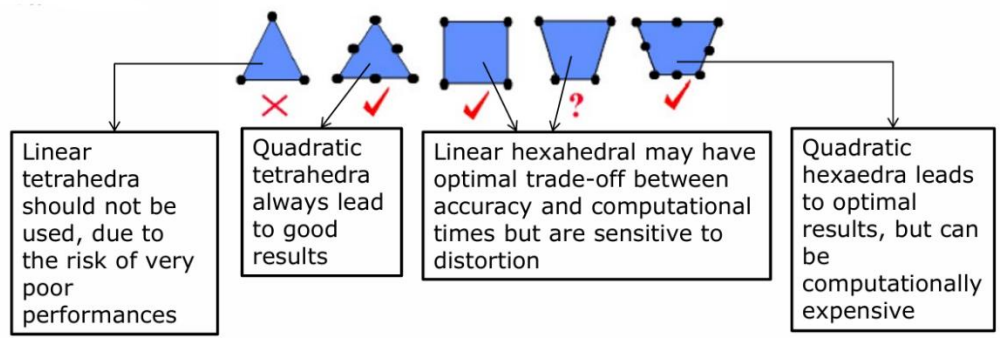
Linear tetrahedra should not be used, due to the risk of very poor performances
Quadratic tetrahedra always lead to good results
Linear hexahedral may have optimal trade-off between accuracy and computational times but are sensitive to distortion
Quadratic hexaedra leads to optimal results, but can be computationally expensive

Figure 6.25: performance comparison between different types of FEs.

In general, a mesh must satisfy the following ***requirements***:

- Discontinuities must be represented, both geometrical and material.
- BCs must be applicable as closely as possible to the actual physical case, often requiring ad hoc mesh refinement.
- The mesh must be conformal, i.e. continuity of edges and nodes at the boundaries of adjacent FEs must be guaranteed.
- FEs must not be excessively distorted or have a high aspect ratio: reducing mesh distortion is crucial for many reasons. First (1), it has been discussed in section 6.3.2 that distorted elements can increase the error of numerical integration via isoparametric mapping through the $\det \boldsymbol{J}$ term. Second (2), high aspect ratios, i.e. a measure of the distortion of an element, are often related to shear locking. Third (3), it will be discussed in the next section (6.6) that unrefined meshes in regions where high gradients are to be expected greatly reduce the convergence rate of the FE simulation. A typical example of such regions are those with sharp geometries. Here, an unrefined mesh will result in

distorted elements, which can be made more regular through mesh refinement. Meshes obtained from local element refinement are called ***graded meshes***, and they are extremely common. Meshes where all elements have uniform dimension h are called ***uniform meshes***, typical of a sub-set of the overall mesh of a component.

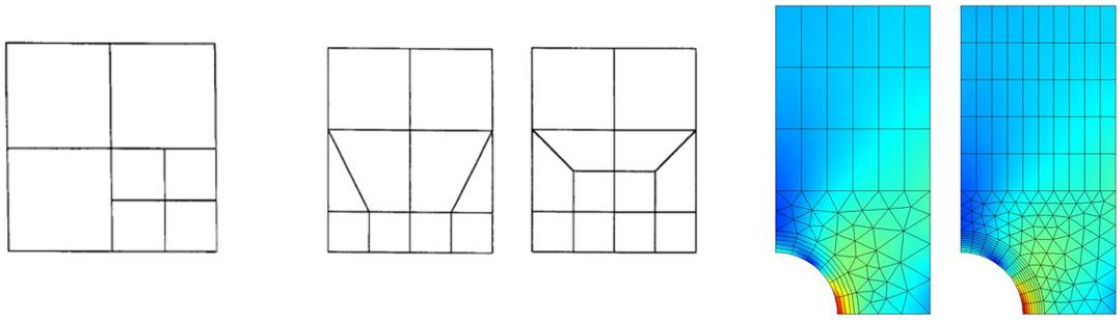

Figure 6.26: left) non-conforming and conforming meshes; right) graded mesh.

Observation. Some types of FEs can be obtained starting from other types of FEs, such as hexahedral FEs from tetrahedral FEs. Note that this is not usually done as the FEs generated using this strategy are often very distorted, resulting in poor mesh quality.

We briefly present now some of the most common ***automatic meshing techniques***, i.e. those that are implemented in commercial FEM software:

- ***Node first***: first, seeds are generated, which are simply markers on the geometric edges of the component to be meshed. Then, starting from the seeds, the internal nodes are generated according to some algorithm. For example, triangular elements are often generated using an algorithm called Delaunay triangulation. Quadrilateral mesh generation is more complex, it can be done from scratch or by conversion of a mesh of triangular FEs with subsequent smoothing, as depicted in Figure 6.27. Because the seed dimension or quantity is often user-specified, ***this is the practical way to perform local mesh refinement***. For this reason, seeds are not specific to one algorithm but are generally employed by all meshing techniques. Moreover, seeds can be placed on any edge of the component, even those artificially generated by the FEM analyst.

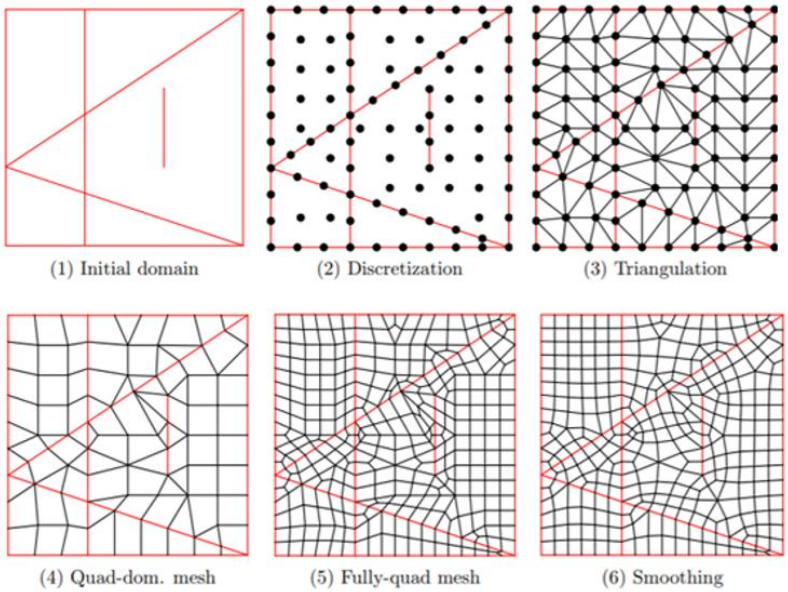

Figure 6.27: quad mesh generation algorithm.

A popular node-first algorithm used for mesh generation is the ***advancing front***. Node generation starts from the seeds and proceeds inwards by defining nodes on uniformly

displaced horizontal lines. In this way a generation front is created that propagates internally to the component until the full mesh is obtained.

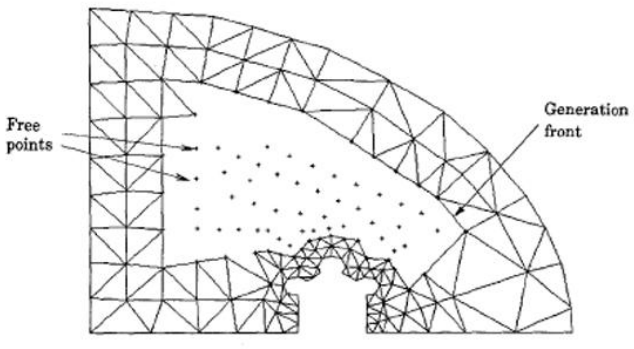

Figure 6.28: advancing front meshing technique.

- ***Mapped meshes***: the idea is to create meshes on simple and extremely regular geometries, always starting from seeds, that are then mapped onto the real component, providing the real elements (Figure 6.29). This is one of the few algorithm that allows to create very regular meshes of hexahedral elements. Such meshes are called ***structured meshes***. Despite this being an extremely powerful technique, it presents some important limitations. Namely, the geometry to be meshed must be very simple to obtain a mapped mesh. If the geometry to be meshed presents holes, isolated nodes or surfaces, ***partitions*** are required to divide it into simpler geometries (Figure 6.30). Then on these geometries, mapped meshing will be applied.

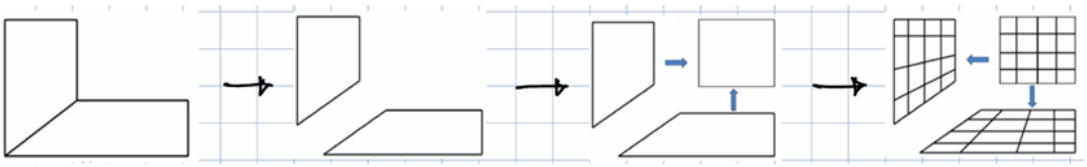

Figure 6.29: mapped meshing example.

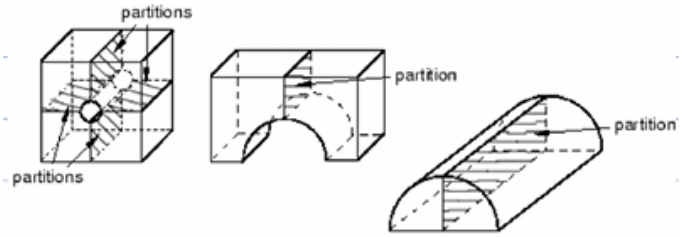

Figure 6.30: partitions needed to map mesh common irregular geometries.

- ***Medial axis***: the component's geometry is automatically broken down into simpler ones by means of medial objects, as shown in Figure 6.31, which are then meshed separately with structured meshes.

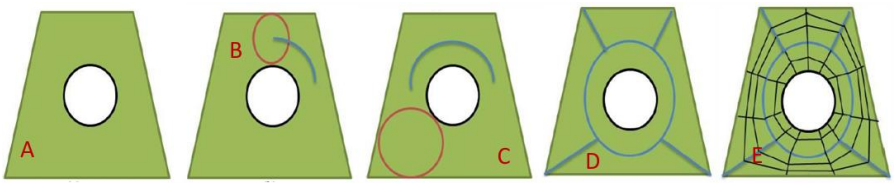

Figure 6.31: medial axis process.

6.6. Convergence

6.6.1. Definition of convergence

Since FEM is a numerical procedure, important considerations must be made regarding accuracy and convergence of results [2]. In considering the approximate FE solution, we need to recognize that different sources of error exist. In this section we'll discuss only about the FE ***discretization errors***, which are due to interpolation of the solution variables. Thus, in essence, we consider in this section the errors related to linear-elastic static problems with the geometry represented exactly with the exact calculation of the element matrices and solution of equations.

For the purpose of this section, i.e. the study of convergence, the PVW equation

$$\int_V \delta\underline{\underline{\varepsilon}}^T : \underline{\underline{\sigma}} dV = \int_V \delta\underline{u}^{\mathrm{T}} \underline{\mathrm{f}}^B dV + \int_{S_F} \delta\underline{u}^T \underline{\mathrm{f}}^S \, dS_F \quad \forall \delta\underline{u} : \delta\underline{u} = \underline{0} \text{ on } S_u$$

can be expressed using the following short notation:

$$\begin{cases} a(\underline{u}, \underline{v}) = (\underline{\mathrm{f}}, \underline{v}) & \forall \underline{v} \in V \\ a(\underline{u}_h, \underline{v}_h) = (\underline{\mathrm{f}}, \underline{v}_h) & \forall \underline{v}_h \in V_h \end{cases} \tag{6.41}$$

Here $\boldsymbol{u}$ is the real and $\boldsymbol{v}$ is the virtual displacement field of the analytical model, while $\boldsymbol{u}_h$ and $\boldsymbol{v}_h$ are the real and virtual displacement fields of the FE solution. Moreover, $\mathbf{f}$ represents the body and surface forces, while V and V_h are spaces that ensures that $\boldsymbol{v}$ and $\boldsymbol{v}_h$ are sufficiently smooth and that they satisfy the essential boundary condition on S_u. The operator $a(\cdot,\cdot)$ is a symmetric bilinear function and $(\mathbf{f},\cdot)$ is a linear function. The properties of these operators imply that, for any constants γ_1 and γ_2, the following relations hold true:

$$\begin{cases} a(\underline{u}, \underline{v}) = a(\underline{v}, \underline{u}) \\ a(\gamma_1 \underline{u}_1 + \gamma_2 \underline{u}_2, \underline{v}) = \gamma_1 a(\underline{u}_1, \underline{v}) + \gamma_2 a(\underline{u}_2, \underline{v}) \\ a(\underline{u}, \gamma_1 \underline{v}_1 + \gamma_2 \underline{v}_2) = \gamma_1 a(\underline{u}, \underline{v}_1) + \gamma_2 a(\underline{u}, \underline{v}_2) \\ (\underline{\mathrm{f}}, \gamma_1 \underline{v}_1 + \gamma_2 \underline{v}_2) = \gamma_1 (\underline{\mathrm{f}}, \underline{v}_1) + \gamma_2 (\underline{\mathrm{f}}, \underline{v}_2) \end{cases}$$

We can ***define convergence*** as the convergence of the strain energy of the FE solution to the strain energy of the mathematical model as the mesh is refined. Mathematically:

$$\begin{cases} a(\underline{u} - \underline{u}_h, \underline{u} - \underline{u}_h) \to 0 \\ a(\underline{u}_h, \underline{u}_h) \to a(\underline{u}, \underline{u}) \end{cases} \quad \text{as} \quad h \to 0 \tag{6.42}$$

Observation. This definition of convergence of the FE solution implies that convergence in energy requires convergence in displacement.

6.6.2. Criteria for monotonic convergence

Depending on the specific type of FEs used in a static analysis, convergence can be monotonic or nonmonotonic as element size decreases $h \to 0$ (or equivalently as the number of FEs increases). For monotonic convergence, two ***requirements*** must be fulfilled:

- Elements must be complete: this means that the elements must be able to represent rigid body motions without stress being developed in it. As mentioned in section 6.2, this condition is fulfilled simply by ensuring that constant terms appear in the shape functions.
- Elements must be compatible: this means that the displacement in the elements across the element boundaries must be continuous. In other words, compatibility ensures that no gaps form between elements. Again, this requirement is fulfilled by an adequate choice of the shape functions.

Observation. Note that compatibility is difficult to satisfy for plate bending analysis if rotations are derived from transverse displacements. For this reason, much effort has been directed toward the development of plate and shell elements, in which displacements and rotations are variables.

6.6.3. Properties of FE solution

In order to measure the error of the FE solution, two norms of interest can be defined. The first one is the ***energy norm***, which corresponds to twice of the strain energy stored in the body when it is subject to $\boldsymbol{v}$:

$$\|\underline{v}\|_E^2 = a(\underline{v},\underline{v})$$

The second one is the ***Sobolev norm***, for FE convergence we're interested in the order 1 Sobolev norm, which takes the form:

$$\|\underline{v}\|_1^{\ 2} = \int_V \sum_{i,j=1}^{3} \left(v_i^2 + \left(\frac{\partial v_i}{\partial x_j}\right)^2 \right) dV$$

In mathematical analysis, Sobolev norms are usually used to evaluate rate of convergence, but in practice the energy norm is frequently more easily evaluated. A link between the two can be found, if c_1 and c_2 are constant:

$$c_1\|\underline{v}\|_1 \leq \sqrt{a(\underline{v},\underline{v})} \leq c_2\|\underline{v}\|_2$$

Using this result, we can give an ***equivalent definition of convergence*** in terms of an order 1 Sobolev norm.

$$\|\underline{u} - \underline{u}_h\|_1 \to 0 \quad \text{as} \quad h \to 0 \tag{6.43}$$

The ***properties of a FE solution*** are the following:

- Orthogonality of the error in bilinear form: let the discretization error between the exact solution $\boldsymbol{u}$ and the FE solution $\boldsymbol{u}_h$ be defined as:

$$\underline{e}_h = \underline{u} - \underline{u}_h$$

Since the PVW must hold true for any $\boldsymbol{v}$ such as $\boldsymbol{u}_h \in V_h$, we can write:

$$\begin{matrix} a(\underline{u},\underline{v}_h) = (\underline{f},\underline{v}_h) \\ a(\underline{u}_h,\underline{v}_h) = (\underline{f},\underline{v}_h) \end{matrix} \quad \rightarrow \quad a(\underline{u}-\underline{u}_h,\underline{v}_h) = a(\underline{e}_h,\underline{v}_h) = 0 \qquad \forall \underline{u}_h \in V_h$$

- Convergence occurs from below: we can write:

$$a(\underline{u},\underline{u}) = a(\underline{u}_h+\underline{e}_h,\underline{u}_h+\underline{e}_h) = a(\underline{u}_h,\underline{u}_h) + 2a(\underline{u}_h,\underline{e}_h) + a(\underline{e}_h,\underline{e}_h)$$
$$= a(\underline{u}_h,\underline{u}_h) + a(\underline{e}_h,\underline{e}_h)$$

It follows that:

$$a(\underline{u},\underline{u}) \geq a(\underline{u}_h,\underline{u}_h) \tag{6.44}$$

- Minimization of difference in strain energy: for any generic $\boldsymbol{w}_h \in V_h$ we have that:

$$a(\underline{e}_h+\underline{w}_h,\underline{e}_h+\underline{w}_h) = a(\underline{e}_h,\underline{e}_h) + a(\underline{w}_h,\underline{w}_h)$$

$$a(\underline{e}_h,\underline{e}_h) \leq a(\underline{e}_h+\underline{w}_h,\underline{e}_h+\underline{w}_h)$$

By choosing

$$\underline{w}_h = \underline{u}_h - \underline{v}_h$$

we obtain:

$$a(\underline{e}_h,\underline{e}_h) \leq a(\underline{e}_h+\underline{u}_h-\underline{v}_h,\underline{e}_h+\underline{u}_h-\underline{v}_h) = a(\underline{u}-\underline{v}_h,\underline{u}-\underline{v}_h)$$

As a result of these properties, ***Cea's lemma*** can be considered, which states: the distance (1st Sobolev norm) between the FE solution $\boldsymbol{u}_h$ and the exact solution $\boldsymbol{u}$ is always lower than the minimum distance d between the exact solution $\boldsymbol{u}$ and any function in V_h, multiplied by a constant c dependent on material properties.

$$\|\underline{u}-\underline{u}_h\|_1 \leq c \min\|\underline{u}-\underline{v}_h\|_1 = cd(\underline{u},V_h) \tag{6.45}$$

6.6.4. Rate of convergence

In the previous sections we defined the requirements needed for monotonic convergence and the general properties of a FE solution, but we did not discuss the rate at which convergence is reached. If elements interpolate the displacement field with a complete polynomial (recall Pascal's triangle in section 6.2) of order k and if the exact solution is sufficiently smooth, from Cea's lemma we obtain that the ***order of convergence of the strains*** of the FE solution is k itself:

$$\|\underline{u}-\underline{u}_h\|_1 \leq ch^k\|\underline{u}\|_{k+1} \quad \rightarrow \quad O(h^k) \tag{6.46}$$

Similarly, the ***order of convergence for the displacements***, given by the zero order Sobolev norm, of the FE solution is ***one order higher than for strains***, i.e. $k+1$:

$$\left\|\underline{u}-\underline{u}_h\right\|_0 \leq ch^{k+1}\left\|\underline{u}\right\|_{k+1} \quad \rightarrow \quad O\left(h^{k+1}\right) \tag{6.47}$$

The ***error magnitude*** $\|\ldots\|_i$ depends on the following factors:

- Order of the complete polynomial k.
- Size of the element in the uniform mesh h.
- Constant c: it depends on material properties and type of element; thus this terms contains the effect of mesh distortion, which generally slows down convergence. Most of these distortions can be controlled by limiting the ratio of the largest dimension and the radius of the largest inscribed circle inside the m-th element:

$$\sigma_m = h_m/\rho_m$$

It is clear from (6.47) that the higher the order k of the complete polynomial, the smoother the exact solution $\boldsymbol{u}$. However, at local level, solution can be non-smooth due to sudden changes in geometry, loads or material properties. These local effects, among other things, lower the rate of convergence of the FE solution. In order to limit this phenomena, two solutions can be adopted:

- ***h-method***: it consists in mesh refinement in those regions where gradients are higher. Note that, because local effects are typical of zones with sharp geometric curves, where FE are typically quite distorted, the h-method has the additional advantage of providing less distorted mesh elements as well. Good graded meshes are obtained when error density is about the same in each element. For such cases the expression of the rate of convergence is the following:

$$\left\|\underline{u}-\underline{u}_h\right\|_1^2 \leq c\sum_m h_m^{2k}\left\|\underline{u}\right\|_{k+1,m}^2 \tag{6.48}$$

- ***p-method***: it consists in increasing the order of the polynomial rather than locally reducing element size. However, this approach presents poor performance when the FE are even slightly distorted, which is impossible to avoid in real cases. Of course h and p methods can be used together, however increasing the polynomial order *and* increasing the number of elements would increase the overall computational effort, even is convergence rate is higher.

6.7. Constraints and interactions

6.7.1. Transformation matrices

A formalism to apply constraints in global coordinates has been shown in sections 6.1.1 and 6.1.2. A more general case could involve the ***application of a constraint in an arbitrary direction***. Such case could be addressed by means of a transformation of coordinate applied at the global matrix or at the local element level. In the following example a model of beam elements is considered. Node 3 is constrained to move in a direction inclined at an angle β with respect to the horizontal axis. A transformation matrix can be defined for the DOF of node 3:

For rod elements

$$\begin{Bmatrix} U_3 \\ V_3 \end{Bmatrix} = \begin{bmatrix} c & s \\ -s & c \end{bmatrix} \begin{Bmatrix} U_3' \\ V_3' \end{Bmatrix}$$

For beam elements

$$\begin{Bmatrix} U_3 \\ V_3 \\ \vartheta_{z3} \end{Bmatrix} = \begin{bmatrix} c & s & 0 \\ -s & c & 0 \\ 0 & 0 & 1 \end{bmatrix} \begin{Bmatrix} U_3' \\ V_3' \\ \vartheta_{z3} \end{Bmatrix}$$

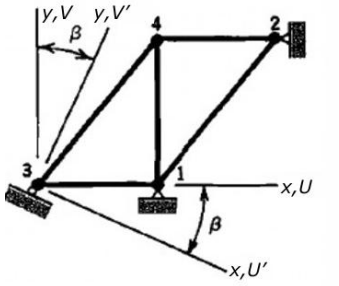

Figure 6.32: beam system.

6.7.2. Multi-point constraints and rigid bodies

In many complex cases complex models are developed by assembling different meshes, made with different elements, resulting in dissimilar meshes. A ***multi-point constraint is a solution used to connect the non-coincident DOFs of dissimilar meshes by creating a rigid link between them***. This approach is valid when part of the structure is much stiffer than the rest.

An example is provided below, where a beam element is connected to a Q4 element. The original and connected DOFs of the beam nodes can be written as follows:

Original	$\underline{\hat{u}} = \{u_5 \ v_5 \ \theta_{z5} \ u_6 \ v_6 \ \theta_{z6}\}^T$
Connected	$\underline{\hat{u}}' = \{u_2 \ v_2 \ u_3 \ v_3 \ u_6 \ v_6 \ \theta_{z6}\}^T$

$$\underline{\hat{u}} = [T]\underline{\hat{u}}' \quad \rightarrow \quad [T] = \begin{bmatrix} [T]_5 & [0] \\ [0] & [I] \end{bmatrix} \quad \rightarrow \quad [T]_5 = \begin{bmatrix} a & 0 & b & 0 \\ 0 & a & 0 & b \\ -\cos\beta & \sin\beta & \cos\beta & -\sin\beta \end{bmatrix}$$

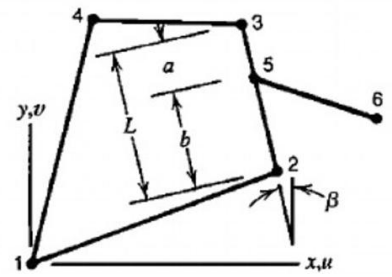

Figure 6.33: beam and Q4 element connection.

A generalization of a linear multi-point constraint are ***linear equations***. They can be used in Abaqus CAE and require a linear combination of nodal values to be equal to zero. If u_i^P is the i-th DOF at node P and A_N are the coefficients, the linear equation must be written as:

$$A_1 u_i^P + A_2 u_j^Q + \cdots + A_N u_k^R = 0$$

The implementation in Abaqus is shown with the following example:

$$u_3^5 = u_1^6 - u_3^{1000} \quad \rightarrow \quad u_3^5 - u_1^6 + u_3^{1000} = 0$$

term	node	DOF	coefficient
1	5	3	1
2	6	1	-1
3	1000	3	1

Table 6.3: linear equation constraint table.

In the input file: *EQUATION $N, P, i, A_i, Q, j, A_j, \ldots$ → *EQUATION 3, 5, 1, 6, 1, -1, 1000, 3, 1

6.7.3. Lagrange multiplier method

The Lagrange multiplier method LMM has the opposite approach to transformation matrices: ***we increase the DOFs, but we do not require any transformation***, which can be computationally costly.

Consider initially a simple constraint $U_j = \bar{U}_j$, according to LMM the condition of stationary Π with the imposed constraint is equivalent to the stationary condition for amended potential:

$$\Pi = \frac{1}{2}\underline{\hat{U}}^T \underline{\underline{K}}\,\underline{\hat{U}} - \underline{\hat{U}}^T \underline{R} + \lambda\left(U_j - \bar{U}_j\right) \quad \rightarrow \quad \delta\Pi = \frac{1}{2}\delta\underline{\hat{U}}^T \underline{\underline{K}}\,\underline{\hat{U}} - \delta\underline{\hat{U}}^T \underline{R} + \delta\lambda\left(U_j - \bar{U}_j\right) + \lambda\delta U_j$$
$$= 0$$

A new set of DOFs can be defined as $\left\{\underline{U}, \lambda\right\}^T$, thus a new matrix system can be defined as follows:

$$\begin{bmatrix} \underline{\underline{K}} & \underline{e}_j^T \\ \underline{e}_j & 0 \end{bmatrix} \begin{Bmatrix} \underline{U} \\ \lambda \end{Bmatrix} = \begin{Bmatrix} \underline{R} \\ \bar{U}_j \end{Bmatrix} \qquad 6.49$$

Where $\underline{e_j}$ is a vector of null values besides the j-th entry. LMM leaves unchanged the original matrix and is useful in non-linear analyses, where constraints can change. The ***method can be generalized*** to represent a specific set of constraints:

- $\underline{\underline{C}}$ is a rectangular matrix of zeros and ones of N = DOF columns and N_c = constrained DOFs rows.
- $\underline{\underline{C}}\underline{\widehat{U}}$ represents the set of DOF we want to constrain.
- $\underline{Q}$ represents the values we want to impose to $\underline{\underline{C}}\underline{\widehat{U}}$.

$$\underline{\underline{C}}\underline{\widehat{U}} = \underline{Q}$$

The amended potential is the following, where $\underline{\lambda}^T$ is a vector of N_c Lagrange multipliers:

$$\Pi^* = \frac{1}{2}\underline{\widehat{U}}^T\underline{\underline{K}}\underline{\widehat{U}} - \underline{\widehat{U}}^T\underline{R} + \underline{\lambda}^T\left(\underline{\underline{C}}\underline{\widehat{U}} - \underline{Q}\right) \tag{6.50}$$

The solving system consists of $N + N_c$ equations in the same number of unknowns:

$$\begin{bmatrix}\underline{\underline{K}} & \underline{\underline{C}}^T \\ \underline{\underline{C}} & \underline{\underline{0}}\end{bmatrix}\begin{Bmatrix}\underline{U} \\ \underline{\lambda}\end{Bmatrix} = \begin{Bmatrix}\underline{R} \\ \underline{Q}\end{Bmatrix} \tag{6.51}$$

6.7.4. Penalty method

This method is equivalent to the introduction of a pre-loaded spring of very high stiffness in correspondence of the constrained DOF. The constraint equation is:

$$\alpha\widehat{U}_j = \alpha q \tag{6.52}$$

Such equation is summed to the i-th finite element equation. The stiffness α in the constraint is much higher than that of the element K_{ij} of the problem stiffness matrix. The addition of such a large term at both sides of the i-th FE equation leads directly to:

$$\widehat{U}_j = q$$

Note that α needs to not be excessively large to avoid problems related to ill conditioning of $[K]$.

6.7.5. Overview of constraints in Abaqus

The main types of constraint methods in Abaqus are:

- Rigid bodies: the motion of a collection of nodes/elements/surfaces is governed by the motion of a reference node RF. Thus, loads and BCs can be applied to the RF and be automatically transferred to the linked nodes. When a rigid body is defined through a connection of nodes there are two options: PIN (1) links only the translational DOFs, while TIE (2) links also the rotational ones.

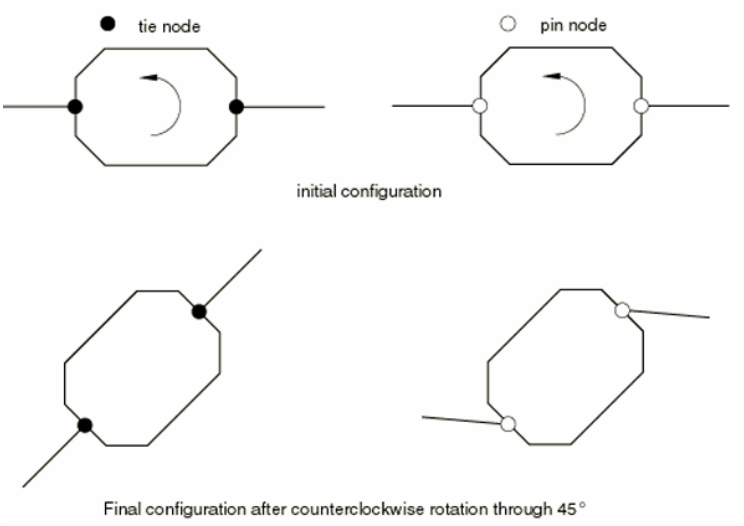

Figure 6.34: PIN and TIE RB.

- Kinematic coupling: these allow us to link only specific DOFs between RF and slave nodes.
- Surface-based tie constraints: they are used to join dissimilar meshes in large zones with low effort. They tie two surfaces together without creating a rigid body since constraints are created locally and they guarantee the possibility of deformation of connected parts.
- Distributed coupling: not really a constraint, it's used to distribute a force or a moment on a set of nodes without constraining them in a rigid body.
- Shell to solid coupling: a constraint type that can connect the DOFs of a surface defined on a solid to the edge of a shell mesh. It's used to introduce local mesh refinement where shell elements are not appropriate.

7. Strength based criteria

The ***idea*** of strength based criteria is to obtain an equivalent stress σ^* and a material allowable σ_0, a parameter that represents material strength. Then, comparing these parameters trough one or more inequalities (depending on if the material is isotropic or orthotropic), we can assess if the structure is safe or not. All the criteria that assess structures in this way are called strength-based criteria. Criteria for isotropic materials are discussed in this section, strength criteria for composite materials are discussed in section 9.3. The overall process of assessment through strength criteria of aerostructures is depicted in Figure 7.1. We can identify two main branches: analytical and experimental.

Isotropic:	$\frac{f(\sigma_I, \sigma_{II}, \sigma_{III})}{\sigma_0} \leq 1$
Orthotropic:	$f(\sigma_{xx}, \sigma_{yy}, \sigma_{zz}, \tau_{xy}, \tau_{yz}, \tau_{xz}, parameters) \leq 1$
In general:	$f(\underline{\sigma}, parameters) \leq 1$

7.1

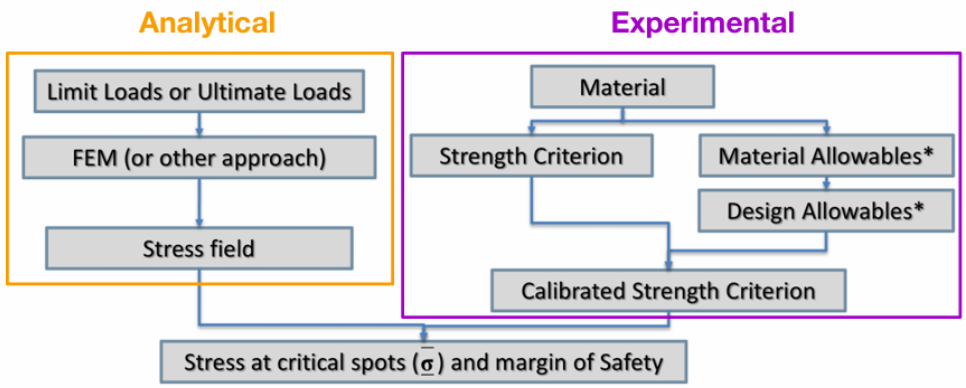

Figure 7.1: σ-based assessment.

Analytical branch. The goal of this branch is to identify the hotspots, i.e. the parts of the structure where the highest stresses manifest upon load application. This branch starts with the choice of the relevant loads to be considered during design, which, according to regulation CS 25.305, are the following:

- Limit loads (LL): maximum operational loads, at full scale tests no plasticization is allowed, even in the presence of damage.
- Ultimate loads (UL): 1.5 times the LL, at full scale tests, if UL are applied for 3 seconds, they must not produce any catastrophic damage.

Applying these loads to the structure we compute the stress field using analytical or numerical models. Then we are able to identify the hot spots.

Experimental branch. The goal of this branch is to experimentally obtain the allowables used to implement the strength criteria. It must be pointed out that two types of allowables exist, material and design allowables.

Material allowables are obtained by performing characterization tests and filtering the data via a statistical process. The number of tests can be greatly reduced depending on the mathematical model used and material tested. For example, strength based criteria for isotropic materials only require the yielding stress σ_Y for static assessment. The statistical process divides the material allowables in two types:

- A-basis: a value that is expected to be exceeded by 99% of the population with confidence of 95%[3]. By regulation, these allowables need to be used when the failure of a component made of this material would cause loss of structural integrity.
- B-basis: a value that is expected to be exceeded by 90% of the population with confidence of 95%. By regulation, these allowables need to be used when the failure of a component made of this material would imply safe redistribution of the load to adjacent components. Thus, the discriminant between A and B basis is redundancy of load paths.

As the name suggests, material allowables only characterize the material properties. However, in many structures the stress field in some critical parts may be too complex to predict analytically. Numerical analyses may help, but they might require too much computational power or time to set up the analysis, only to obtain approximated results, making the process not worth the effort. Moreover, these hotspots may be difficult to produce, making them subject to defects that cannot be modelled numerically. In these cases, some additional experimental tests are required to characterize such parts of the structure (see Building block approach – section 9.4). The output of these characterization tests are ***design allowables***, i.e. correction of the material allowables via engineering considerations. Design allowables are the actual parameters used in the strength

[3] 99 components out of 100 would exceed this value 95 times out of 100 we do the same experiment.

criteria, what we previously indicated with σ_0. Once the design allowables are defined, and the strength criterion is chosen, we can ***calibrate the strength criterion***. Meaning, we can safely adapt the *parameter* to the specific case we're studying, in order to obtain a reliable design.

Finally, once we identified the hotspots and we obtained a calibrated criterion, we compute the ***safety margin*** for the hotspots. Assuming $\bar{\boldsymbol{\sigma}}$ is a reference stress state, corresponding to a reference load configuration, the general expression of the safety margin is the following:

$$SM = \frac{\underline{\sigma}(\text{load at failure})}{\underline{\bar{\sigma}}(\text{load})} - 1 \tag{7.2}$$

Given that stress components are linear with applied load, we may define the load at failure as the reference load $\bar{\boldsymbol{\sigma}}$ multiplied by an amplification factor α. By doing so, the safety margin can be computed as follows:

$$SM = \frac{\alpha\underline{\bar{\sigma}}(\text{load})}{\underline{\bar{\sigma}}(\text{load})} - 1 = \alpha - 1 \tag{7.3}$$

Stress tensor decomposition. Strength criteria are usually based on principal stresses. Such quantities can be obtained by solving the following problem:

$$\det([\sigma] - \lambda[I]) = \lambda^3 - I_1\lambda^2 + I_2\lambda - I_3 = 0$$

In the previous equation we can identify the following terms:

- Principal stresses $(\sigma_I, \sigma_{II}, \sigma_{III})$: they are the eigenvalues of the equation and represent the values of normal stress acting on the planes oriented so that shear stresses are zero.

$$[\sigma] = \begin{bmatrix} \sigma_I & 0 & 0 \\ 0 & \sigma_{II} & 0 \\ 0 & 0 & \sigma_{III} \end{bmatrix} \quad \text{where} \quad \sigma_I > \sigma_{II} > \sigma_{III}$$

- Stress invariants (I_1, I_2, I_3): they are scalar combination of stress components, they are the coefficients of the eigenvalue problem.

$$\begin{aligned} I_1 &= \sigma_{xx} + \sigma_{yy} + \sigma_{zz} = \mathrm{tr}(\boldsymbol{\sigma}) \\ I_2 &= \sigma_{xx}\sigma_{yy} + \sigma_{yy}\sigma_{zz} + \sigma_{zz}\sigma_{xx} - \tau_{xy}^2 - \tau_{yz}^2 - \tau_{zx}^2 \\ I_3 &= \det(\boldsymbol{\sigma}) \end{aligned} \quad \longleftrightarrow \quad \begin{aligned} I_1 &= \sigma_1 + \sigma_2 + \sigma_3 \\ I_2 &= \sigma_1\sigma_2 + \sigma_2\sigma_3 + \sigma_3\sigma_1 \\ I_3 &= \sigma_1\sigma_2\sigma_3 \end{aligned}$$

- Principal directions: the eigenvalues of the problem, they are the normals of the planes on which the principal stresses act.

A second important $\boldsymbol{\sigma}$ decomposition is the following:

- Hydrostatic tensor $(p\boldsymbol{I})$: related to changes in volume of the material. It's related to the first invariant of the stress tensor. Due to the fact that most isotropic materials do not fail in pure compression or tension, this term is often neglected in strength based criteria.
- Deviatoric tensor $\boldsymbol{S}$: related to changes in shape of the material, which is the primary cause of isotropic materials failure.

$$\underline{\underline{\boldsymbol{\sigma}}} = \begin{bmatrix} p & 0 & 0 \\ 0 & p & 0 \\ o & 0 & p \end{bmatrix} + \begin{bmatrix} \sigma_{xx} - p & \tau_{xy} & \tau_{xz} \\ \tau_{xy} & \sigma_{yy} - p & \tau_{yz} \\ \tau_{xz} & \tau_{yz} & \sigma_{zz} - p \end{bmatrix}$$

[pl] [s]

7.1. Static criteria

7.1.1. Galileo-Rankine

Used for ***brittle materials***, which fail for separation perpendicular with respect to direction of the highest principal stress. The equivalent stress is simply the highest between $|\sigma_I|$ and $|\sigma_{III}|$, and according to which is higher we need to consider the respective allowable. Thus, the assessment is simply:

$$\begin{cases} \sigma_I \leq \dfrac{\sigma_U}{\eta} & \text{for traction} \\ |\sigma_{III}| \leq \dfrac{\sigma_C}{\eta} & \text{for compression} \end{cases} \qquad 7.4$$

The graphical representation for a 2D stress state of the safe zone will be:

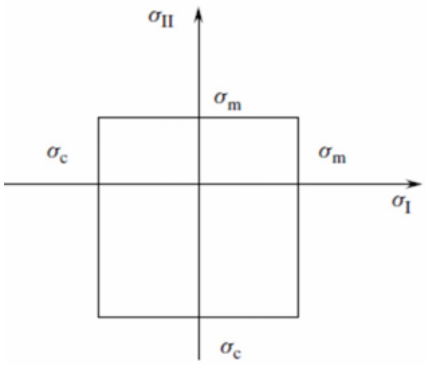

Figure 7.2: Galileo-Rankine graphical representation.

7.1.2. Guest-Tresca and Von Mises

Used for ***ductile isotropic materials***; thus they are based on the deviatoric component of $\boldsymbol{\sigma}$. For Guest-Tresca (GT) the equivalent stress σ_{GT}^* is the maximum shear stress τ_{max} which develops on 45° oriented planes with respect to the principal directions. This shear stress can be easily expressed as a function of principal stress, thus it's independent of the coordinate system. This stress is then compared to the yielding stress of the material σ_Y.

$$\tau_{max} = \max\left(\frac{\sigma_I - \sigma_{II}}{2}, \frac{\sigma_{II} - \sigma_{III}}{2}, \frac{\sigma_{III} - \sigma_I}{2}\right) \qquad 7.5$$

For Von Mises (VM) the equivalent stress σ_{VM}^* is the square root of the second invariant I_2 of the stress tensor $\boldsymbol{\sigma}$. Alternatively, the second invariant J_2 of the deviatoric stress tensor $\boldsymbol{S}$ can be used. The second invariant is related to the maximum deformation energy that the material is able to store before failure.

$$\sigma_{VM}^{*} = \sqrt{3J_2} = \sqrt{\frac{3}{2}(S_I^2 + S_{II}^2 + S_{III}^2)} = \sqrt{3(\sigma_I^2 + \sigma_{II}^2 + \sigma_{III}^2 - \sigma_I\sigma_{II} - \sigma_{II}\sigma_{III} - \sigma_{III}\sigma_I)} \quad 7.6$$

By comparing the plane stress state graphical representation of the two criteria, we can see that GT is a bit more conservative than VM. Moreover, in a plane stress state and in pure torsion we can derive the following simplified formulas.

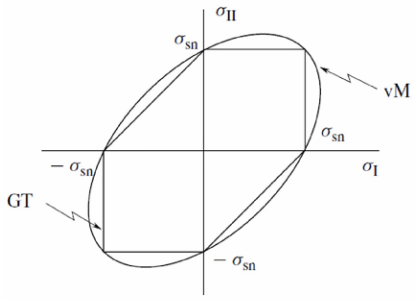

	torsion	2D [σ]
Guest-Tresca	$\tau_{sn} = \frac{\sigma_{sn}}{2}$	$\sigma_{GT}^{*} = \sqrt{\sigma^2 + 4\tau^2}$
Von Mises	$\tau_{sn} = \frac{\sigma_{sn}}{\sqrt{3}}$	$\sigma_{vM}^{*} = \sqrt{\sigma^2 + 3\tau^2}$

Figure 7.3: left) GT and VM 2D representation. right) simplified equation for GT and VM criteria.

7.1.3. Drucker-Prager

Used for ***isotropic material that exhibit asymmetry of yielding stress in tension/compression*** $|\sigma_{YT}| \neq |\sigma_{YC}|$. The asymmetry is caused by the hydrostatic component of the stress tensor $p\boldsymbol{I}$. Thus, this criterion accounts for this component as well. Materials that exhibit such behaviors are concrete, rocks, some types of polymers and short fiber reinforced ceramics.

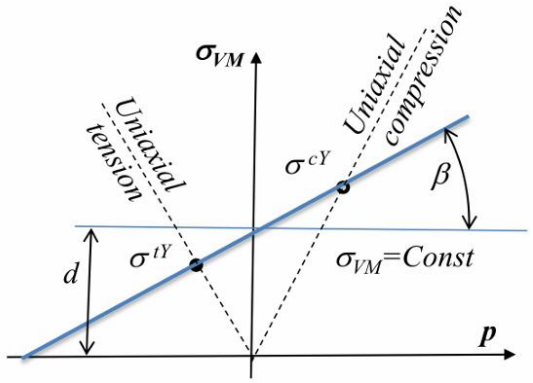

Figure 7.4: Drucker-Prager meridional plane.

This criteria is plotted on the meridional plane (Figure 7.4), on which we can identify the hydrostatic pressure p on the x-axis (positive if compressive) and the Von Mises stress σ_{VM}^{*} on the y-axis. Notice that, if $p = 0$, we revert back to the Von Mises criterion. The limit line for the DP criteria is inclined by an angle β and cuts the y-axis at the value of the Von Mises stress for the material at $\sigma_{VM}^{*}(p = 0) = d$. The limit line then intersects the uniaxial compression and tension lines, which stem out of the origin, respectively at σ_{YC} and σ_{YT}. The expression of the limit line is the following:

$$\sigma_{VM}^{*} < d + p\tan\beta \quad \text{where} \quad d = \frac{\sigma_{YT}\sigma_{YC}}{\sigma_{YT} + \sigma_{YC}} \quad \beta = \frac{\sigma_{YT} - \sigma_{YC}}{\sigma_{YT} + \sigma_{YC}} \quad 7.7$$

7.1.4. Statistical approach for brittle materials

The fracture strength of brittle material exhibits scatter related to the presence of microscopic flaws inside them. Thus, to characterize their fracture strength we must assess the distribution of the weakest links via a ***statistical approach***. The strength criteria will provide a ***probability of failure***, which must be below a certain threshold.

Assuming the flaws have a normal distribution, the biggest flaws will have a Weibull distribution instead. By adopting such distribution, we can define the probability of safety P_s, of failure P_f and of strength $F(\sigma)$ as in Equations 7.8. These indices depend on two factors:

- Shape factor (m): determines the scatter of fracture strength, higher m means less scatter.
- Scale parameter (σ_0): strength at which 63.2% of the specimen fail.

$$P_s = \exp\left(-\frac{\sigma}{\sigma_0}\right)^m$$
$$P_f = 1 - P_s = 1 - \exp\left(-\frac{\sigma}{\sigma_0}\right)^m \qquad 7.8$$
$$F(\sigma) = \frac{dP_f}{d\sigma} = \frac{m}{\sigma_0}\left(\frac{\sigma}{\sigma_0}\right)^{m-1} \exp\left(-\frac{\sigma}{\sigma_0}\right)^m$$

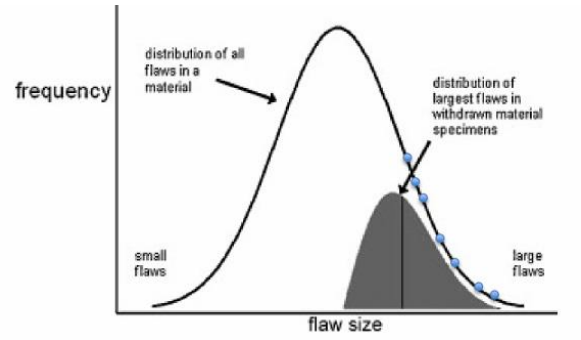

Figure 7.5: Weibull distribution.

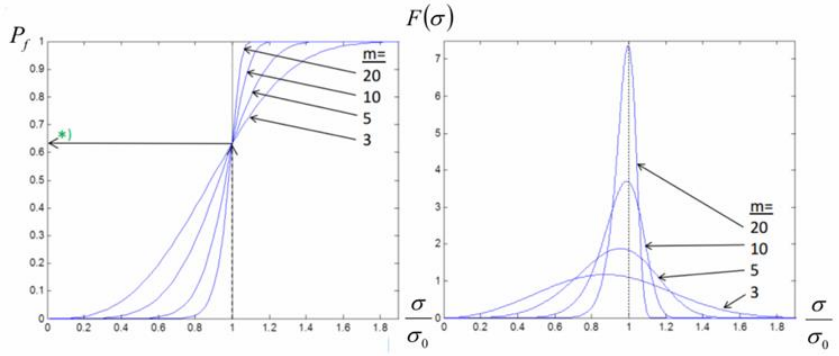

Figure 7.6: probability of fracture and of strength.

To apply a probabilistic approach to a structural component we need a failure criterion (1), the actual stress distribution in the material (2) and the component size (3). Size accounts for the probability of flaws: the bigger the component the more likely the bigger defects are. Consider an example in which the component is divided in n sub-volumes of volume ΔV all uniformly loaded by a stress σ_i. For each volume the probability of survivability is:

$$P_{si} = \exp\left(-\frac{\sigma_i}{\sigma_{0\Delta V}}\right)^m$$

Then, the probability of survivability for the whole component will be the product of all P_{si}.

$$P_s(V) = \prod_i^n \exp\left(-\frac{\sigma_i}{\sigma_{0\Delta V}}\right)^m = \exp\left(-\sum_i^n \left(\frac{\sigma_i}{\sigma_{0\Delta V}}\right)^m\right)$$

Now, if the sub-volumes become infinitesimal in value, we can write:

$$\lim_{n\to\infty} \sum_i^n \left(\frac{\sigma_i}{\sigma_{0\Delta V}}\right)^m = \lim_{\Delta V\to dV} \sum_i^{V/\Delta V} \left(\frac{\sigma_i}{\sigma_{0\Delta V}}\right)^m \frac{\Delta V}{\Delta V} = \frac{1}{\Delta V}\int_V \left(\frac{\sigma_i(\underline{x})}{\sigma_{0\Delta V}}\right)^m dV$$

Since the component is loaded by a uniform σ_i, we obtain:

$$\frac{1}{\Delta V}\int_V \left(\frac{\sigma_i(\underline{x})}{\sigma_{0\Delta V}}\right)^m dV = \left(\frac{\sigma_i}{\sigma_{0dV}}\right)^m \frac{V_0}{dV}$$

Thus, the probability of failure will be:

$$P_f(V) = 1 - \exp\left(-\left(\frac{\sigma_i}{\sigma_{0dV}}\right)^m \frac{V_0}{dV}\right) = 1 - \exp\left(-\left(\frac{\sigma_i}{\sigma_0}\right)^m\right) \quad \text{where} \quad \sigma_0 = \sigma_{0dV}\left(\frac{dV}{V_0}\right)^{\frac{1}{m}}$$

If another uniformly loaded element of volume $V_1 \neq V_0$ is considered, then we can write:

$$P_f(V_1) = 1 - \exp\left(-\left(\frac{\sigma_i}{\sigma_{0dV}}\right)^m \frac{V_1}{dV}\frac{V_0}{V_0}\right) = 1 - \exp\left(-\left(\frac{\sigma_i}{\sigma_0}\right)^m \frac{V_1}{V_0}\right) = 1 - \exp\left(-\left(\frac{\sigma_i}{\sigma_{0V1}}\right)^m\right)$$

$$\sigma_{0V1} = \sigma_0\left(\frac{V_0}{V_1}\right)^{\frac{1}{m}}$$

This approach can be integrated into FEA to evaluate the probability of failure of a component. In particular, if the probability of failure of a specimen of volume V_0 is known, then we can compute the probability of survivability of each FE as:

$$P_{si} = \exp\left(-\frac{\sigma_i}{\sigma_{0FEi}}\right)^m \quad \text{where} \quad \sigma_{0FEi} = \sigma_0\left(\frac{V_0}{V_{FEi}}\right)^{\frac{1}{m}} \qquad 7.9$$

7.2. Fatigue criteria

All structural parts of an aircraft are subject to cycling loads. Thus, fatigue assessment plays a critical role in the design process. Time dependent stress could be caused by:

- Rotating loads: then the modulus of the load is a function of time $|F| = f(t)$.
- Rotating components: then the modulus of the loads is constant, but the grains of the component still experience varying values of mean stress.

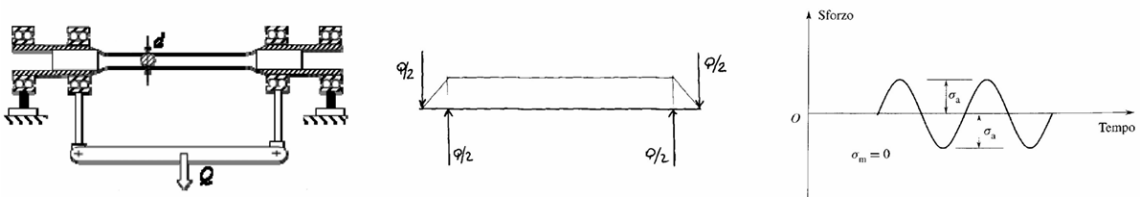

Figure 7.7: example of a rotating element - train shaft.

This distinction underlies an ***important aspect of fatigue***: the difference between static and fatigue strength lies in the inhomogeneity of the micro-structure of the material. More precisely, the driving force of fatigue failure is the average stress acting on the grains of the microstructure. Thus, to properly address fatigue, we must take into consideration the grain dimension, presence of micro-defects, inclusion etc. Intuitively, a statistical approach is necessary, and component dimension will play a role as it did for the statistical approach to brittle materials.

Failure mode due to fatigue follows three steps: first is nucleation of the crack in the most stressed point. Then, due to cyclic loading, the crack propagates leaving very distinctive marks on the cross section, called beach marks. Finally, when the effective cross section is reduced enough, the component fails in a brittle way.

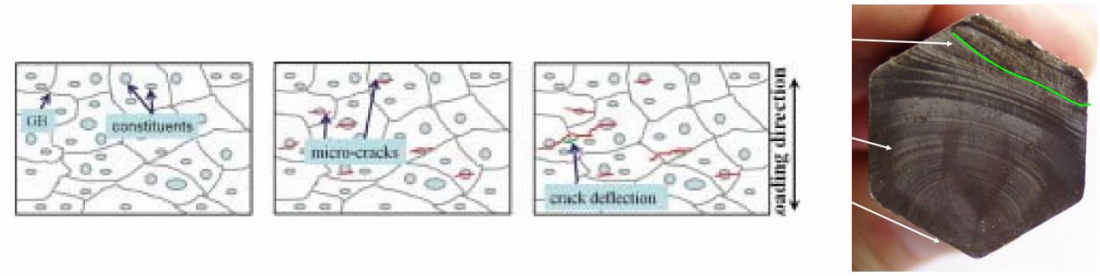

Figure 7.8: left) process of crack nucleation and propagation; right) fatigue failure on specimen.

To characterize fatigue we introduce the following parameters.

$$\sigma_a = \frac{\sigma_{max} - \sigma_{min}}{2} \qquad \sigma_m = \frac{\sigma_{max} + \sigma_{min}}{2} \qquad R = \frac{\sigma_{min}}{\sigma_{max}} \tag{7.10}$$

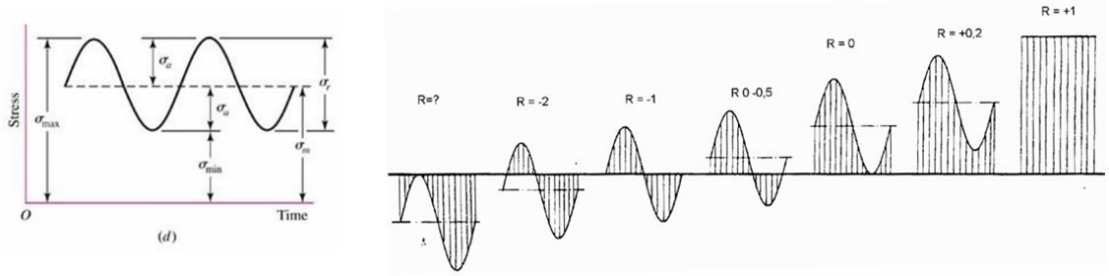

Figure 7.9: left) fatigue parameters; right) fatigue loading as a function of R.

7.2.1. Uniaxial fatigue

7.2.1.1. Whooler curve

The Whooler curve is the result of an experimental campaign in which uniaxial fatigue tests were performed on standard specimen with null mean stress $\sigma_m = 0$. The Whooler curve has the following characteristics:

- It plots the values of the ***fatigue strength*** $\boldsymbol{\sigma_a}$, or the alternate stress, as a function of the number of cycles N_f. The number of cycles is plotted in a logarithmic scale, making the plot semi-logarithmic.
- The curve represents a 50% probability of failure. This choice is due to the huge scatter of data.
- Plot is related to the specific material tested, not real components: this is due to the fact that these tests have been carried out on standard specimen.
- Two parts of the curve can be identified: finite fatigue life and infinite fatigue life. The two occur at *roughly* $N_f < 10^7$ and $N_f > 10^7$ for steel. Finite and infinite fatigue life can also be identified based on the ***fatigue limit of the material*** $\boldsymbol{\sigma_e = \sigma_F = \sigma_{FA}}$. In short, if the load level is lower than a threshold value, i.e. the fatigue limit σ_e, the life of the material can be considered infinite, otherwise it will resist up until a certain number of cycle before reaching failure.

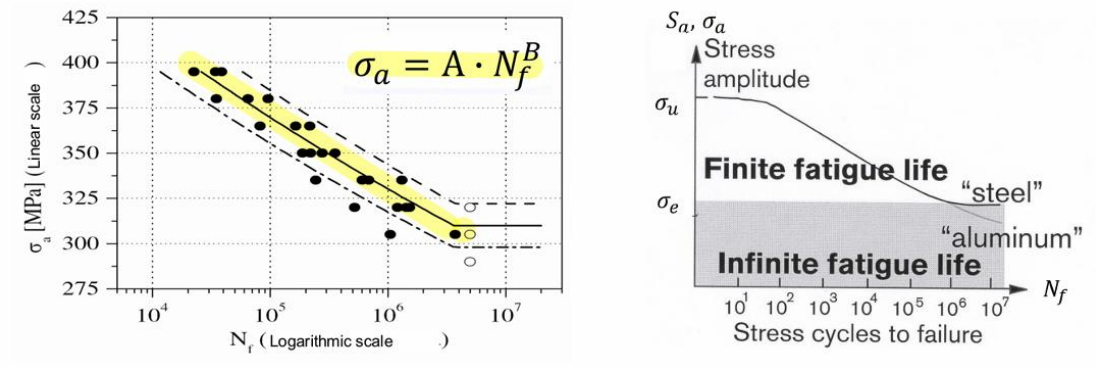

Figure 7.10: Whooler curve.

Finite fatigue life. As the name suggests, if $\sigma_a > \sigma_e$ the material can survive a limited amount of cycles N_f, which for steel is roughly $N_f < 10^7$. In the semi logarithmic plot, this part of the Whooler curve is linear, and it's described by Basquin's equation (the equation of a line in log form):

$$\sigma_a = A \cdot N_f^B = \sigma_f'(2N_f)^b \quad \xrightarrow{\text{in log form}} \quad \log(\sigma_a) = \log(\sigma_f') + b\log(2N_f) \tag{7.11}$$

In Basquin equation:

- Coefficients b, B: represent the slope of the linear curve, thus they must be negative.
- Fitting coefficient σ_f': the term $\log(\sigma_f')$ represents the stress value at which the linear part intersects the y-axis. We distinguish between two scenarios:
  - Linear part goes up to the y-axis: then σ_f' is the fatigue strength σ_a for one cycle $N = 1$, often approximated as $\sigma_f' = \sigma_{UTS}$, or some percentage of σ_{UTS}.
  - Linear part starts after the y-axis: in this case we usually assume the linear part to start from $N = 10^3$ and progress up to $N = 10^7$. In this case, the σ_f' term is much different from σ_{UTS}, and it can be computed along with b by setting up the following system of equations, where we considered $\sigma_a(N = 10^3) = 0{,}9 \cdot \sigma_{UTS}$:

$$\begin{cases} 0{,}9 \cdot \sigma_{UTS} = \sigma_f'(2 \cdot 10^3)^b \\ \sigma_e' = \sigma_f'(2 \cdot 10^7)^b \end{cases} \quad \rightarrow \quad \{b, \sigma_f'\} \text{ known}$$

Assuming to have a material subject to $\hat{\sigma}_a$ for $\hat{N}$ cycles, Basquin equation allows us to compute the safety coefficients in terms of cycles η_N and of stresses η_σ:

$$\hat{\sigma}_a = \sigma_f'(2N_f)^b \quad \rightarrow \quad N_f = \frac{1}{2}\left(\frac{\hat{\sigma}_a}{\sigma_f'}\right)^{\frac{1}{b}} \quad \rightarrow \quad \eta_N = \frac{N_f}{\hat{N}}$$

Assuming $\sigma_{a,f}$ is the fatigue strength corresponding to $\hat{N}$ cycles:

$$\eta_\sigma = \frac{\sigma_{a,f}}{\hat{\sigma}_a} = \frac{\sigma_f'(2\hat{N})^b}{\sigma_f'(2N_f)^b} = \left(\frac{\hat{N}}{N_f}\right)^b = \eta_N^{-b} \quad \rightarrow \quad \eta_\sigma = \eta_N^{-b}$$

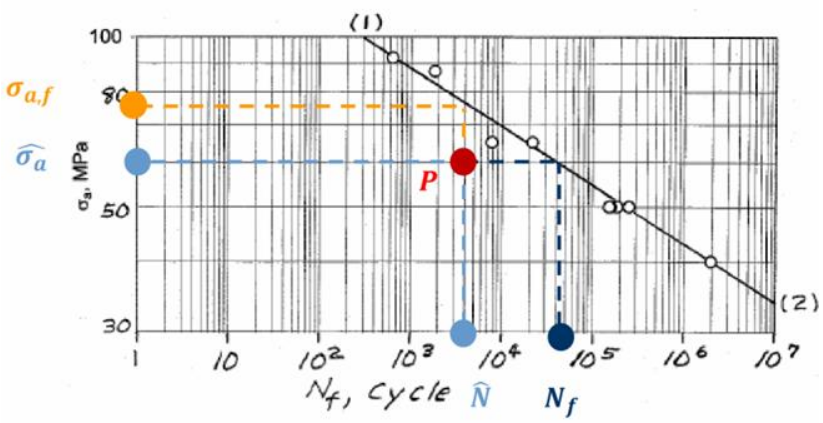

Figure 7.11: example of application of the Basquin equation.

In order to determine the remain life of a material we can use the Miner rule. Note that this rule is *extremely* approximative since it does not consider may important aspects, such as the order in which the loads are applied. The rule reads:

$$D = \sum_i \frac{N_i}{N_{fi}} \quad \rightarrow \quad D = 1 \text{ means failure} \qquad 7.12$$

Where N_i is the number of cycles done at the i-th load level and N_{fi} is the number of cycles causing failure at the i-th load level. So, basically, we are summing up percentages of the "used life" due to different load levels, when the total percentage reaches 100%, the material breaks.

Infinite fatigue life. If the material is loaded with an alternate load σ_a below its fatigue limit σ_e, then its life can be assumed to be infinite. For steels this happens at roughly $N > 10^7$, thus the fatigue limit is simply $\sigma_e = \sigma_a(N \approx 10^7)$. The fatigue limit of a material can be estimated via the following relations:

$$\begin{cases} \sigma_{e,b} = (0.4 - 0.6)\sigma_{UTS} & \text{for bending} \\ \sigma_{e,a} = (0.3 - 0.45)\sigma_{UTS} & \text{for traction} \\ \sigma_{e.t} = (0.23 - 0.33)\sigma_{UTS} & \text{for torsion} \end{cases} \qquad 7.13$$

Observation. Aluminum does not exhibit a fatigue limit, for this reason fatigue is considered particularly insidious for this material.

Notice that we always referred to the previous properties as being of the material. This is only natural since the Whooler curve is obtained via testing of standardized specimen, thus they provide quantities that characterize the material. However, real components do not have the same mechanical properties of these specimen, they are rougher, bigger and notched. In order to account for these component-related characteristics we introduce the following ***component-related coefficients***:

- Surface finish coefficient m_s: to understand why this aspect needs to be considered, it's useful to think of surface crests as micro-notches. A rougher surface will have more pronounced crests, thus more pronounced notches. This coefficient is defined as follows:

$$m_s = \frac{\sigma_e'(R_a)}{\sigma_e} \leq 1 \tag{7.14}$$

- Dimensional coefficient m_d: this coefficient accounts for two phenomena, both related to the nature of fatigue failure (average stress acting on the grains of the microstructure):
  - Gradient effect: consider a beam subject to a bending moment causing a maximum stress $\bar{\sigma}$ according to the well-known butterfly stress distribution. Consider a second beam with the same cross section geometry of the first beam but wider. Assume the second beam to be subject to a bending moment that produces the same $\bar{\sigma}$ at the extremities of the butterfly stress-distribution. Since the second beam has a wider cross section, a bigger portion of it will be subject to higher stresses due to a lower stress gradient. This implies higher mean stress values on the grains of the outer portions of the cross section.
  - Defect distribution: defects must be considered to properly characterize fatigue because they affect the mean stress values acting on the grains. Intuitively, the amount of defects scales with the component dimension, i.e. the bigger the component the higher the probability of it having flaws.

$$m_d = \frac{\sigma_e'(D)}{\sigma_e} \leq 1 \tag{7.15}$$

- Notch effect K_f: clearly, since notches cause stress intensifications, they are detrimental in fatigue as well. The notch coefficient is defined with respect to the notch sensitivity q, a function of material properties (ρ, a) and the radius at the tip of the notch r. The ratios a/ρ and ρ/r define the capability of the material to redistribute/smooth out the stress gradients. More precisely:
  - $q = 0 \rightarrow K_f = 1$: notch has no effect.
  - $q = 1 \rightarrow K_f = K_t$: notch has maximum effect.

$$K_f = 1 + q(K_t - 1) \tag{7.16}$$

$$\begin{cases} q = \dfrac{1}{1 + a/\rho} \\ q = \dfrac{1}{1 + \sqrt{\rho/r}} \end{cases} \quad \text{where} \quad a \approx 0.025 \left(\frac{2070}{\sigma_U}\right)^2$$

Using these component-related coefficients, we can define the ***fatigue limit of the component*** $\boldsymbol{\sigma'_e}$ as follows:

$$\boxed{\sigma'_e = \frac{\sigma_e m_s m_d}{K_f} \leq \sigma_e} \qquad 7.17$$

7.2.1.2. Haigh diagram

The Haigh diagram builds on the Whooler curve by ***quantifying the effect of the mean stress*** $\boldsymbol{\sigma_m}$ ***on the fatigue limit*** $\boldsymbol{\sigma_e}$. The Haigh diagram plots the alternate stress σ_a as a function of the mean stress σ_m. Thus, the Whooler curve is collapsed in the y-axis of the Haigh diagram. There are several approximation for determining how the fatigue limit changes with the mean stress $\sigma_e = \sigma_e(\sigma_m)$ on the Haigh diagram. We're interested in the Goodman approximation, which reads:

$$\frac{\sigma_a}{\sigma_e} + \frac{\sigma_m}{\sigma_{UTS}} = 1 \qquad 7.18$$

Note that the Goodman rule assumes that the fatigue limit σ_e varies linearly with the mean stress σ_m. More precisely, for $\sigma_m = 0$ the fatigue limit remain the same as per the Whooler curve, naturally. Then, the mean stress can increase up to the ultimate tensile strength of the material σ_{UTS}, Intuitively, in this case the fatigue limit goes to zero $\sigma_e(\sigma_m = \sigma_{UTS}) = 0$. Naturally, if components rather than materials are considered, the fatigue limit and UTS values must be scaled by the coefficients introduced earlier.

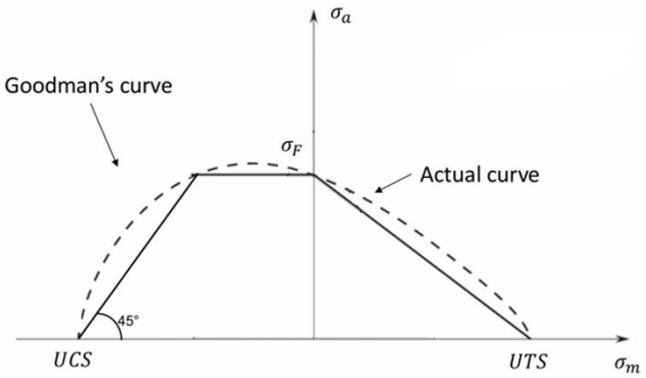

Figure 7.12: Haigh diagram with Goodman approximation (solid line).

Based on where the stress state of the material/component lands on the Haigh diagram, we can compute the safety coefficient with respect to the fatigue limit of the material. This depends on the loading scenario:

- Radial loading: if the load line can be express via a linear relation $\sigma_a = C\sigma_m$, the safety factor can be determined as follows:

$$\eta = \frac{\overline{OP}_{lim}}{\overline{OP}} = \frac{\sigma_a(R)}{\bar{\sigma}_a}$$

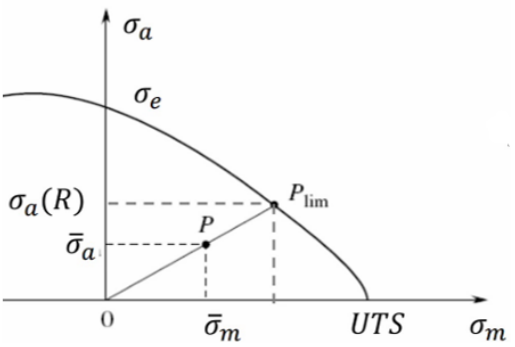

Figure 7.13: safety factor for radial loading on Haigh diagram.

- Non-radial loading: consider a system like the one in Figure 7.14 – left. If the angular velocity ω of the shaft increases, only the mean part of the stress increases, while the alternate remains constant. In this case, the safety coefficient will be:

$$\eta = \frac{P_{lim}}{\bar{\sigma}_{med}}$$

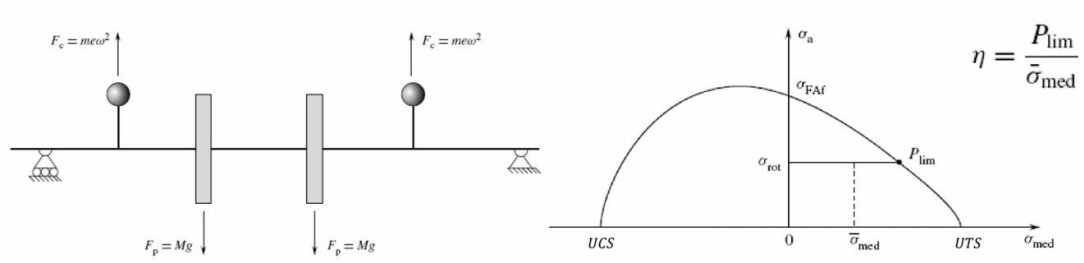

Figure 7.14: non-radial load line example.

7.2.2. Multiaxial fatigue

Multiaxial fatigue is a rather complex subject, and it is not simple to understand how damage accumulates under multiaxial loading conditions. The simplest way to deal with it is to refer to phenomenological methods based on the results of multiaxial fatigue tests. The two criteria we'll present make the following ***assumptions***, which are satisfied in many practical cases:

- Stress orientation does not change: stresses act over planes that may change orientation due to the fact that the alternate stress component σ_a changes orientation. We assume that this does not happen.
- Stress components have the same frequency: we talk about synchronous loading.
- Stress components have the same phase: we talk about in-phase loading.

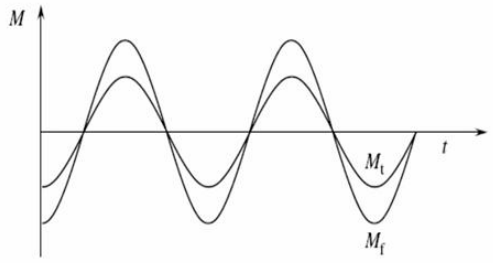

Figure 7.15: multiaxial fatigue load configuration.

7.2.2.1. Gough-Poullard criterion

As previously mentioned, this criteria was developed starting from a large experimental campaign on standard specimen subject to bending and torsion cyclic loads. Because tests were run on standardized specimen, they characterize the material and not real components. Such experimental campaign resulted in the definition of the following ***elliptic limit curve in the $\sigma_a - \tau_a$ plane***:

$$\left(\frac{\sigma_a}{\sigma_{e,b}}\right)^2 + \left(\frac{\tau_a}{\tau_{e,t}}\right)^2 = 1 \qquad 7.19$$

Where $\sigma_{e,b}$ and $\sigma_{e,t}$ are the material fatigue limits according to equations (7.13). If a component rather than the material is considered, the alternate stresses σ_a, τ_a must be scaled by the component-related coefficients of equation (7.17), yielding σ'_a, τ'_a. Figure 7.15 shows the graphical representation of the Gough-Poullard limit curve, along with the effects of the mean stress and notches.

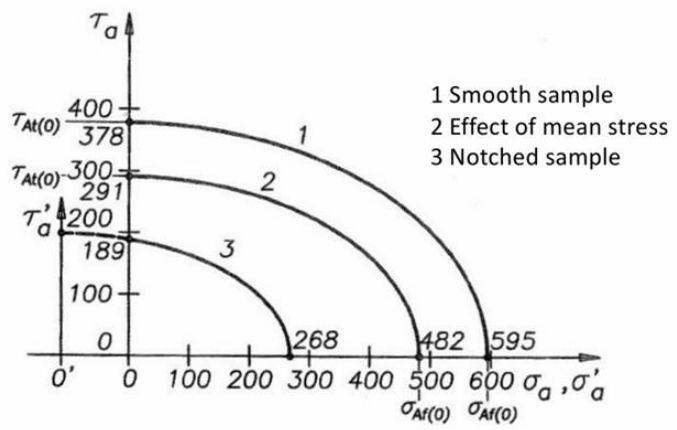

Figure 7.16: elliptic limit curves according to the Gough-Poullard criterion.

Pure alternate load. Consider the case with null mean stress first, i.e. $\sigma_m = 0$. Then, using equation (7.19), we can compute the ***equivalent bending stress according to the Gough-Poullard criterion σ^*_{GP}***. This stress is equivalent in the sense that, starting from the generic point in the $\bar{\sigma}'_a - \bar{\tau}'_a$ plane corresponding to the current stress state, we move along the ellipse of equation (7.19) to obtain an equivalent stress state that is purely axial, or purely related to bending. This equivalent stress will then be compared to the allowable $\sigma_0 = \sigma_{e,b}$.

$$\left(\frac{\sigma_a}{\sigma_{e,b}}\right)^2 + \left(\frac{\tau_a}{\tau_{e,t}}\right)^2 = 1 \quad \rightarrow \quad \sigma_{e,b}^2\left(\frac{\sigma_a}{\sigma_{e,b}}\right)^2 + \sigma_{e,b}^2\left(\frac{\tau_a}{\tau_{e,t}}\right)^2 = \sigma_{e,b}^2 \quad \xrightarrow{H=\frac{\sigma_{e,b}}{\tau_{e,t}}} \quad \sigma_a^2 + H^2\tau_a^2 = \sigma_{e,b}^2$$
$$= (\sigma^*_{GP})^2$$

Considering the component rather than the material, the Gough-Poullard criterion for a safe life design (infinite fatigue life of the component) reads:

$$\boxed{\sigma^*_{GP} = \sqrt{\sigma_a^2 + H'^2\tau_a^2} \leq \frac{\sigma_{lim}}{\eta} \qquad \text{where} \quad H' = \frac{\sigma_{lim}}{\tau_{lim}} = \frac{\sigma'_{e,b}}{\tau'_{e,t}}} \qquad 7.20$$

In many engineering applications is common to have an alternate bending moment coupled with a constant torsional moment. This is the case of rotating shafts with constant angular velocity.

Indicating the shear stress due to the constant torsional moment with $\tau_m = \tau_0$, the previous expression simplifies to:

$$\sigma_{GP}^* = \sqrt{\sigma_a^2 + H'^2\tau_0^2} \leq \frac{\sigma_{lim}}{\eta} \quad \text{where} \quad H' = \frac{\sigma_{lim}}{\tau_{lim}} = \frac{\sigma'_{e,b}}{0{,}8 \cdot \sigma_{UTS}} \tag{7.21}$$

Effect of the mean loads. If a mean component is present, we must correct the limit values, i.e. the fatigue limits, according to the Haigh diagram. More precisely, only the axial fatigue limit load must be corrected since Sines proved that $\tau'_a \neq \tau'_a(\tau_m)$. Using Goodman relation (7.18), we obtain the general expression of the fatigue limit corrected for the presence of the mean stress $\sigma'_{e,b}(R)$ to be:

$$\frac{\sigma_a}{\sigma'_{e,b}} + \frac{\sigma_m}{\sigma_{UTS}} = 1 \quad \rightarrow \quad \sigma_a\left(\frac{1}{\sigma'_{e,b}} + \frac{\sigma_m}{\sigma_a}\frac{1}{\sigma_{UTS}}\right) = 1 \quad \rightarrow \quad \sigma_a = \sigma_{lim} = \frac{1}{\frac{1}{\sigma'_{e,b}} + \frac{\sigma_m}{\sigma_a}\frac{1}{\sigma_{UTS}}}$$

Thus, the general formulation of the Gough-Poullard criterion accounting for the effect of the mean stresses is the following:

$$\sigma_{GP}^* = \sqrt{\sigma_a^2 + H'^2\tau_a^2} \leq \frac{\sigma_{lim}}{\eta}$$

where

$$H' = \frac{\sigma_{lim}}{\tau_{lim}} \begin{cases} \sigma_{lim} = \sigma'_{e,b}(R) = \dfrac{1}{\frac{1}{\sigma'_{e,b}} + \frac{\sigma_m}{\sigma_a}\frac{1}{\sigma_{UTS}}} \\ \tau_{lim} = 0.8 \cdot \sigma_{lim} \end{cases} \tag{7.22}$$

Some common cases may be identified here:

- Alternate and mean components are the same ($R = 0$): meaning $(\sigma, \tau)_a = (\sigma, \tau)_m$, then the previous equation simplifies to:

$$\sigma_{lim} = \frac{1}{\frac{1}{\sigma'_{e,b}} + \frac{1}{\sigma_{UTS}}} = \frac{\sigma'_{e,b}}{1 + \frac{\sigma'_{e,b}}{\sigma_{UTS}}}$$

  Moreover, even if the alternate shear stress is not a function of the mean shear stress, i.e. $\tau_a \neq \tau_a(\tau_m)$, we still take a reference value based on the effect of mean stress on the alternating normal stress. Such approximation is simply:

$$\tau_{lim} = 0.8 \cdot \sigma_{lim} \quad \text{or} \quad \tau_{lim} = 0.8 \cdot \sigma_{UTS}$$

  Thus, in this case we obtain the following limit values:

$$\begin{cases} \sigma_{lim} = \sigma'_{e,b}(R) = \dfrac{1}{\frac{1}{\sigma'_{e,b}} + \frac{1}{\sigma_{UTS}}} \\ \tau_{lim} = 0.8 \cdot \sigma_{lim} \end{cases} \tag{7.23}$$

- $\underline{R = 0 \text{ with constant torsion}}$: since $\tau_a = 0$, in the Gough-Poullard equivalent stress σ_{GP}^* we must use the mean value $\tau_m = \tau_0$. The limit values are the those of equation (7.23).

$$\sigma_{GP}^* = \sqrt{\sigma_a^2 + H'^2\tau_0^2} \leq \frac{\sigma_{lim}}{\eta} \qquad 7.24$$

7.2.2.2. Sines criterion

As for the Gough-Poullard criterion, the Sines criterion is the product of a large experimental campaign. It should be noted that, aside from defining the criterion, the experimental campaign ***proved two things***:

- The fatigue limit due to traction $\sigma_{e,a}$ is a function of the mean stress σ_m, i.e. $\sigma_{e,a} = \sigma_{e,a}(\sigma_m)$.
- The shear fatigue limit due to torsion $\tau_{e,t}$ is not a function of the mean shear stress τ_m, i.e. $\tau_{e,t} \neq \tau_{e,t}(\tau_m)$.

The Sines criterion is based on the variable stresses acting on the octahedral plan. An equivalent stress related to the alternate part σ_a^* is obtained and compared to the fatigue limit of the material $\sigma_{e,a}$. The fatigue limit is reduced according to the mean principal stresses $I_{1,m}$ scaled by a coefficient k, which is the slope of the Goodman line on the Haigh diagram.

$$\begin{cases} \sigma_S^* \approx \sigma_{VM}^* = \sqrt{\sigma_{I,a}^2 + \sigma_{II,a}^2 + \sigma_{III,a}^2 - \sigma_{I,a}\sigma_{II,a} - \sigma_{II,a}\sigma_{III,a} - \sigma_{III,a}\sigma_{I,a}} \\ \sigma_{lim} = \sigma'_{e,b} - kI_{1,m} = \sigma'_{e,b} - \dfrac{\sigma'_{e,b}}{\sigma_{UTS}}\left(\sigma_{I,m} + \sigma_{II,m} + \sigma_{III,m}\right) = \sigma'_{e,b}\left(1 - \dfrac{I_{1,m}}{\sigma_{UTS}}\right) \end{cases} \qquad 7.25$$

$$\sigma_a^* \leq \sigma_{lim} \quad \rightarrow \quad \sigma_a^* \leq \sigma'_{e,b}\left(1 - \frac{I_{1,m}}{\sigma_{UTS}}\right)$$

The ***Sines equivalent axial stress*** $\boldsymbol{\sigma_S^*}$ can be computed and the Sines criterion implemented as follows:

$$\boxed{\frac{\sigma_S^*}{1 - \dfrac{I_{1,m}}{\sigma_{UTS}}} \leq \frac{\sigma'_{e,b}}{\eta}} \qquad 7.26$$

8. Fracture mechanics

In aeronautical history it's been proven numerous times that static and fatigue assessment is not enough for a safe design. To guarantee structural integrity we must understand how structures behave in presence of defects. The effect of crack size on fatigue life is very well represented in Figure 8.1, in which three types of crack growth are illustrated:

- Type 1: defects nucleated by fatigue in virgin material.
- Type 2: defects caused by microstructural damage (corrosion, micro-impacts).
- Type 3: defects caused by low/medium energy impacts.

Type 3 cracks are the type of damage we're trying to account for by implementing damage tolerant design. Such design philosophy is divided into three areas:

- Prediction of residual crack strength: we need to understand if the current load level will cause failure of the component due to crack propagation under static loading.
- Crack propagation under cyclic loading: we want to understand how and if a crack grows due to cyclic loading, i.e. fatigue, and how many cycles remain until failure.
- Definition of methods to detect crack-damage: this is done via non-destructive evaluation (NDE).

An ***important consideration for aerostructures*** has to be made: crack growth is only allowed for metallic materials; composite structures must prove to be able to sustain LLs without detrimental crack growth.

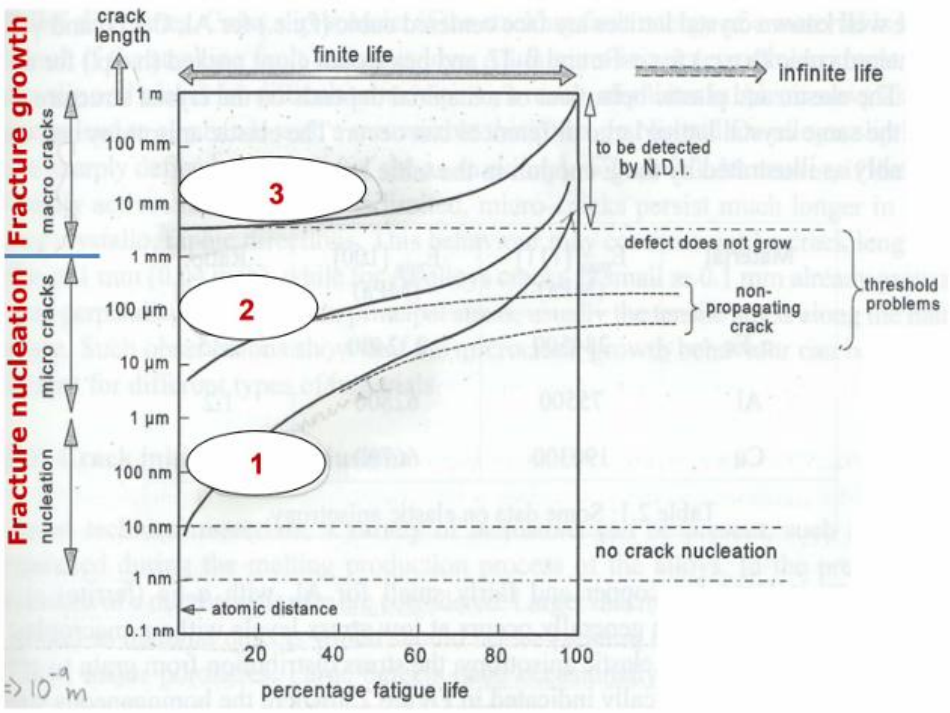

Figure 8.1: evolution of crack length during fatigue life.

8.1. Crack strength

Similar to static and fatigue assessment, we need to compute a quantity indicative of the stress state inside the material and compare it to a limit value.

8.1.1. Irwin empirical approach

Irwin's empirical approach allows us to understand ***if*** the crack grows via a linear approach, i.e. linear elastic fracture mechanics (LEFM). A linear approach is valid under the ***assumption*** that crack length is much higher than the characteristic length of the plasticization zone at the crack tip. In other words, this theory is valid for "big cracks". This assumption allows us to neglect the nonlinear phenomena due to plasticization and employ a linear approach.

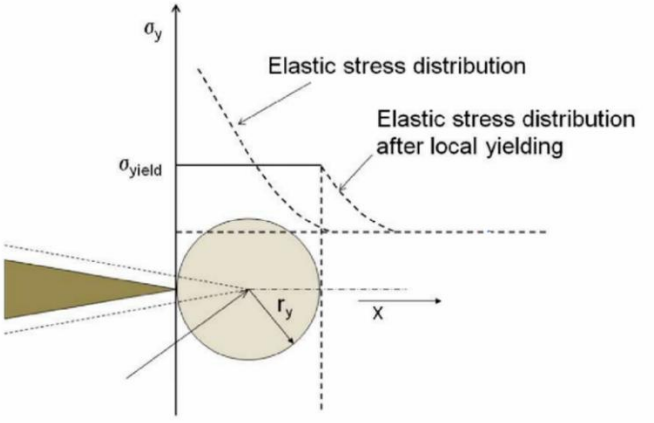

Figure 8.2: elastic stress and real stress in yielding zone.

The basic stress field around a notch can be used to present the basics of the stress field at a crack tip. If ρ is the radius of the circle inscribed in the crack tip, and a is the half width of the crack, we can write:

$$\sigma_{tip} = \sigma_\infty \left(1 + \sqrt{\frac{a}{\rho}}\right) \tag{8.1}$$

The case of a crack would mean $\rho \to 0$ but this causes a singularity since $\sigma_{tip} \to \infty$. We "solve" this problem by defining the ***stress intensity factor (SIF) K*** as a quantity that does not go to infinity for $\rho \to 0$.

$$K = \lim_{r\to 0} \sqrt{2\pi r}\,\sigma_{tip}(r) \qquad \left[\frac{MPa}{m^{1/2}}\right] \tag{8.2}$$

In general, three types of SIF have been defined, each pertaining to a mode of crack opening:

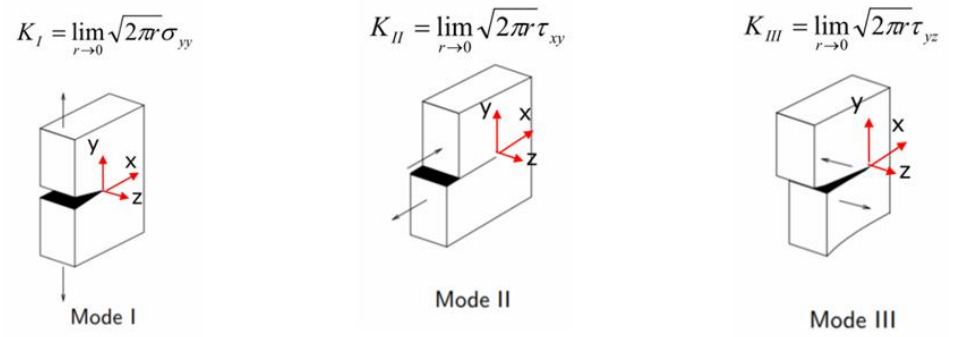

Figure 8.3: modes of crack propagation.

A crack grows under monotonic loading if K is higher than a certain critical value K_c, which is determined experimentally. The definition of K is only valuable from a theoretical point of view. In practical application, K is expressed in an equivalent form (8.3) and tabulated. In such equation, σ_∞ is the far stress field, a the crack length and β a geometry coefficient.

$$\boxed{K = \sigma_\infty \sqrt{a\pi}\beta} \tag{8.3}$$

Theory of critical distances. It has been stated that LEFM neglects plasticization near the crack tip, where plasticization occurs. The characteristic lengths of the plasticization zones are referred to as plastic zone r_p for ductile materials and process zone l_{pz} for brittle materials.

$$\sigma_Y = \sqrt{2\pi r_p} K_C \quad \to \quad r_p = \frac{1}{2\pi}\left(\frac{K_C}{\sigma_Y}\right)^2 \quad \xrightarrow{LEFM} \quad \begin{cases} a \gg r_p \propto \left(\dfrac{K_c}{\sigma_y}\right)^2 \\ a \gg l_{pz} \propto \left(\dfrac{K_c}{\sigma_R}\right)^2 \end{cases} \tag{8.4}$$

Observation. Note that the yielding zone is actually beneficial for crack propagation. Assuming to be in mode I, a traction load will be applied to the component. When such load is released, the adjacent not yielded material will tend to return to its original configuration, inducing a

compressive stress on the yielded zone. Such compressive stress is antagonistic to crack propagation, and thus beneficial.

In short, LEFM is valid for big cracks. For small cracks the stress intensification due to the crack presence can be considered null. In this case, yielding of the material is the limiting factor and $\sigma_\infty = \sigma_Y$. For medium sized cracks, experimental data shows a transition zone that can be studied via the ***theory of critical distances***. The point of such model is to suggest where or how to evaluate stress, three approaches exist:

- Point method PM: evaluation of σ at one point at a given distance from crack tip.
- Line method LM: average of stress acting along a line stemming from crack tip.
- Area method AM: average stress acting on an area close to crack tip.

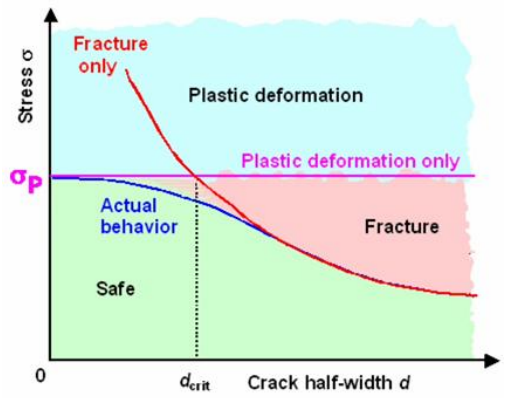

Figure 8.4: behavior of fracture limit as a function of crack half-length.

As an example, the line method will be presented. Consider the example presented in Figure 8.5. To understand if σ_Y is exceeded and thus crack propagation occurs, we need to evaluate σ at the *critical distance* $L/2$ from the crack tip on the focused path. The limit condition will be $\sigma(L/2) = \sigma_Y$, here we unite crack propagation and classic static approach:

$$K_c = \sqrt{2\pi \frac{L}{2}}\sigma_Y \quad \rightarrow \quad L = \frac{1}{\pi}\left(\frac{K_c}{\sigma_Y}\right)^2 = 2r_p \quad \rightarrow \quad \frac{L}{2} = r_p \qquad 8.5$$

Note how $L \propto r_p$ and how both are a function of the material since:

- K_c is very small: typical of brittle materials.
- σ_R/σ_Y are very high: very strong materials tend to be brittle.

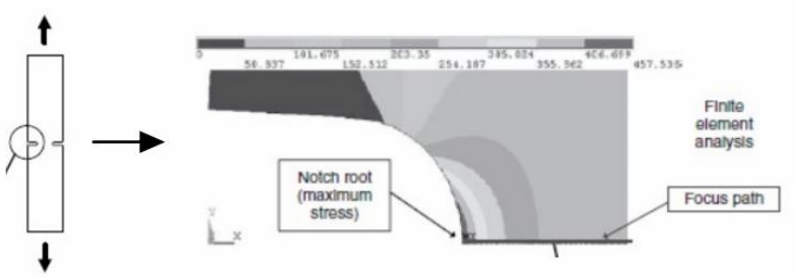

Figure 8.5: example for Pm application.

8.1.2. Griffith/energy approach

With the Irwin approach we are able to tell *if* a crack grows. With the energetic approach we want to be able to tell *how* a crack grows as well. This is possible with Griffith energy approach.

Consider the body in Figure 8.6, with width B, crack of length a, and a force P applied to induce a mode I crack propagation. If $K > K_c$, the point of application of such force will move a certain distance u, and the crack will grow of da. The energy balance in dt reads:

$$\dot{U}_e = \dot{U}_d + \dot{U}_s + \dot{U}_k + BR\dot{a} \tag{8.6}$$

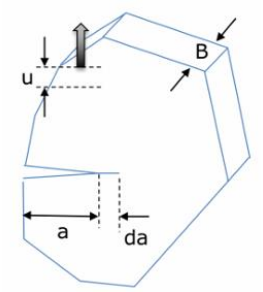

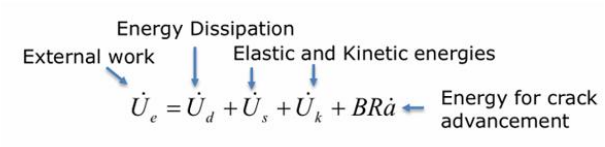
Energy Dissipation
External work
Elastic and Kinetic energies
$\dot{U}_e = \dot{U}_d + \dot{U}_s + \dot{U}_k + BR\dot{a}$
Energy for crack advancement

Figure 8.6: reference "Griffith" body.

Assuming to have an elastic material $\dot{U}_d = 0$ and static conditions $\dot{U}_k = 0$, we obtain the following equation. Such equation says that the difference between the rate of external energy and that of elastic energy equals the energy available to have a possible crack propagation.

$$\dot{U}_e - \dot{U}_s = BR\dot{a} \tag{8.7}$$

We can define the *energy release rate* G as follows:

$$\frac{dU_e}{dt} - \frac{dU_s}{dt} = BR\frac{da}{dt} \quad \rightarrow \quad dU_e - dU_s = BRda \quad \rightarrow \quad G = \frac{1}{B}\left(\frac{dU_e}{da} - \frac{dU_s}{da}\right) \tag{8.8}$$

Using R and G we can define the same typer of criterion we introduced for the empiric approach ($K > K_c$): we have crack propagation if:

$$\frac{1}{B}\left(\frac{dU_e}{da} - \frac{dU_s}{da}\right) = G \geq R \tag{8.9}$$

Irwin-Kies equation. Such equation provides a useful expression of G. With respect to Figure 8.7, we can identify OA as the loading phase, material is elastic but not necessarily linear. Segment AA' defines crack propagation, Δu is produced. A'O is the unloading phase, material still behaves as elastic. The energy balance reads:

$$dU_e - dU_s = BGda \tag{8.10}$$

The energy components can be expressed as follows:

- $BGda = OAA' =$ energy required to propagate the crack.
- $dU_s = OA'B' - OAB$ is the difference between the elastic energy introduced by the loading phase and the elastic energy released by the unloading phase.
- $dU_e = BAA'B'$: the work performed by P due to du.

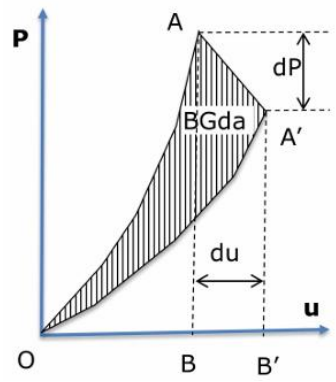

Figure 8.7: crack propagation on P-u curve.

By plugging these terms into the energy balance we obtain:

$$Pdu - dU_s = BGda \quad \rightarrow \quad P\frac{du}{da} - \frac{d}{da}\int Pdu = BG$$

Now we assume linear elasticity, and we define the compliance $C = \frac{u}{P} = \frac{1}{K}$, where K = stiffness, then:

$$\frac{u}{C}\frac{du}{da} - \frac{d}{da}\int \frac{u}{C}du \quad \rightarrow \quad \frac{u}{C}\frac{du}{da} - \frac{d}{da}\frac{u^2}{2C}$$

Since compliance is a function of crack length $C = f(a)$, we can write:

$$\frac{u}{C}\frac{du}{da} - \frac{d}{da}\frac{u^2}{2C} = \frac{u}{C}\frac{du}{da} - \frac{1}{C}\frac{d}{da}\left(\frac{u^2}{2}\right) - \frac{u^2}{2}\frac{d}{da}\left(\frac{1}{C}\right) = \frac{u}{C}\frac{du}{da} - \frac{u}{C}\frac{du}{da} - \frac{u^2}{2C^2}\frac{dC}{da} = \frac{P^2}{2}\frac{dC}{da}$$

In the end, the energy release rate G can be expressed using the ***Irwin-Kies equation***. It's clear that the ERR is a function of both the load applied and the crack length $G = G(P, a)$.

$$\boxed{G = \frac{P^2}{2B}\frac{dC}{da}} \qquad 8.11$$

So, ***assuming we know dC/da***, we can understand:

- If we have crack propagation: simply if $G \geq R$.
- The behavior of the crack propagation: if the energy available for the crack G is higher than that that resists its propagation R, then the crack propagation is unstable, otherwise it's stable.

R = const

If $\begin{cases} G = R \\ dG/da > 0 \end{cases}$

If $\begin{cases} G = R \\ dG/da \leq 0 \end{cases}$

R != const

If $\begin{cases} G = R \\ dG/da > dR/da \end{cases}$

if $\begin{cases} G = R \\ dG/da \leq dR/da \end{cases}$

8.1.3. Equivalence between K and energy approach

We introduced two ways of computing the same thing. If both are valid, some kind of equivalence must be found. Imagine we are applying to our specimen a quasi-static displacement u, so that crack propagation da happens at a fixed rate → $dU_e/da = 0$. It follows from Equation 8.10 that only variations in elastic energy can cause crack growth.

$$-\Delta U_s = BG\Delta a \tag{8.12}$$

We can evaluate ΔU_s as the energy required from σ_{yy} to restore the initial configuration.

$$-\Delta U_s = \Delta W \quad \rightarrow \quad \Delta W = \int_0^{\Delta a} \frac{1}{2}\sigma_{yy} \cdot 2v dx \quad \rightarrow \quad G = \lim_{\Delta a \to 0} \frac{\Delta W}{\Delta a}$$

With reference to Figure 8.8, we define two reference systems: one on the crack tip (x, y) and one on shifted by Δa along the x-axis (x', y'). Now we use the analytical solution of mode I crack propagation, provided by the empirical approach. To do so, we must choose the right coordinate system: $r = x$ and $\theta = 0$, and we can write:

$$\sigma_{yy} = \frac{K_I}{\sqrt{2\pi x}}$$

The for the vertical displacement v, with $r' = \Delta a - x$ and $\theta = \pi$ and we assume a plain strain condition:

$$v = \frac{2(1+\nu)}{E} K_I \sqrt{\frac{\Delta a - x}{2\pi}} 2(1-\nu) = 4K_I \frac{1-\nu^2}{E} \sqrt{\frac{\Delta a - x}{2\pi}}$$

By plugging this into G, we obtain the equation that links G and K_I, thus linking the empirical and energetic approaches.

$$G = \lim_{\Delta a \to 0} \frac{1}{\Delta a} \int_0^{\Delta a} \sigma_{yy} v dx = \lim_{\Delta a \to 0} \frac{1}{\Delta a} \int_0^{\Delta a} \left(\frac{K_I}{\sqrt{2\pi x}}\right)\left(4K_I \frac{1-\nu^2}{E} \sqrt{\frac{\Delta a - x}{2\pi}}\right) dx \tag{8.13}$$
$$= \frac{1-\nu^2}{E} K_I^2$$

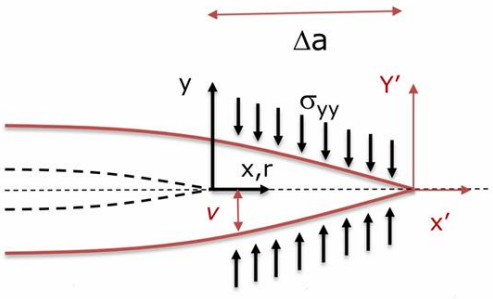

Figure 8.8: reference systems for crack growth.

8.2. Fatigue crack growth

The ***goal*** of fatigue crack growth is the evaluation of the number of cycles required for the crack to grow to a point where crack strength is exceeded. Intuitively, crack strength is lower in fatigue loading than monotonic. The study of crack growth under fatigue is mainly based on the work of Paris, who in the 60's proved that cyclic range of K controls crack growth rate $\Delta a/\Delta N$.

$$\frac{\Delta a}{\Delta N} = f\left(\Delta K = \Delta\sigma\sqrt{\pi a}\beta\right)$$

In Figure 8.9 are reported the results of Paris experimental campaign, which characterized the behavior of the materials, recall that ΔK is a function of the material. Even if significant scattering is present, there is a clear link between crack propagation and number of cycles. Three regions may be identified in these plots:

- Threshold region: ΔK is lower than a threshold value ΔK_{TH}, as a consequence it has no effect on crack growth (similar to the role of the fatigue limit σ_e).
- Linear region: da/dN is proportional to a power of ΔK, more precisely this region is described by Paris' law, where m and C are empirical constants $(2 < m < 9)$:

$$\frac{da}{dN} = C(\Delta K)^m \qquad 8.14$$

- Fracture region: as $K_{max} \to K_c$ we see that $da/dN \to \infty$.

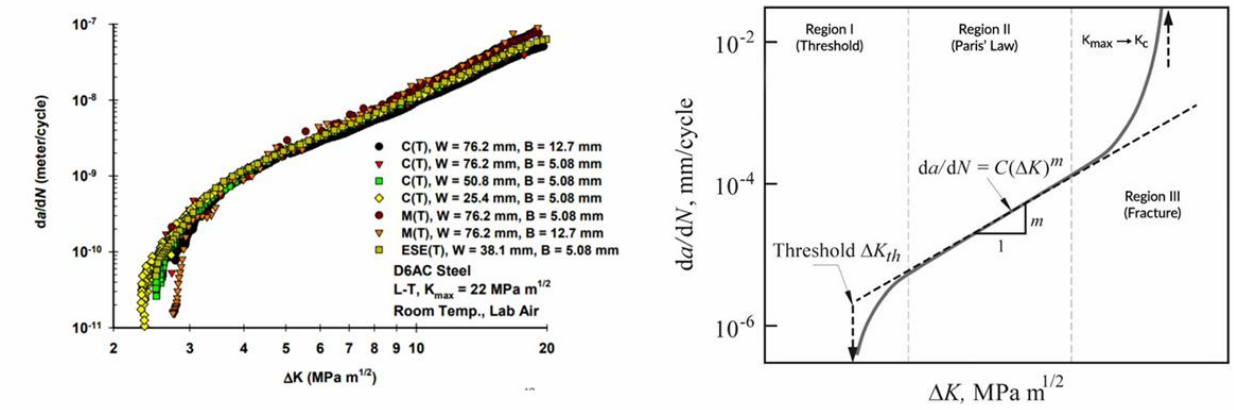
da/dN (meter/cycle)
ΔK (MPa m^1/2)
C(T), W = 76.2 mm, B = 12.7 mm
C(T), W = 76.2 mm, B = 5.08 mm
C(T), W = 50.8 mm, B = 5.08 mm
C(T), W = 25.4 mm, B = 5.08 mm
M(T), W = 76.2 mm, B = 5.08 mm
M(T), W = 76.2 mm, B = 12.7 mm
ESE(T), W = 38.1 mm, B = 5.08 mm
D6AC Steel
L-T, Kmax = 22 MPa m^1/2
Room Temp., Lab Air
Region I (Threshold)
Region II (Paris' Law)
Kmax → Kc
da/dN = C(ΔK)^m
Region III (Fracture)
Threshold ΔKth
m
1
da/dN, mm/cycle
ΔK, MPa m^1/2

Figure 8.9: left) experimental data; right) interpolation of data.

The effect of mean stress is accounted for by the NASGRO model. This model computes fracture growth speed for every cycle, and it's valid only for metallic materials.

Forman law:

$$\frac{da}{dN} = \frac{C(\Delta K)^m}{(1-R)K_c - \Delta K}$$

NASGRO model:

$$\frac{da}{dN} = C\left[\left(\frac{1-f}{1-R}\right)\Delta K\right]^n \frac{(1-\Delta K_{th}/\Delta K)^p}{(1-K_{max}/K_c)^q}$$

fracture growth speed is computed **cycle-by-cycle for metallic structure**

8.3. Non-destructive evaluation (NDE)

The key application of NDE is to use NDI to detect damage to monitor structural health and for maintenance purposes. These aspects are crucial for the tolerance design structures since the size of detectable damage influences the design process.

NDE is implemented in two ways. First, NDI must be able to provide information about the defect size a so that if a critical length a^* is exceeded, the component does not pass the inspection. In the ideal case, given a^*, we would be able to tell with a net yes/no if a component is flight worthy or not. The real case is different, some acceptable defects can be rejected, and some that are not acceptable can pass the evaluation. In the first case we talk about type I (economic) error, in the second of type II (safety) error.

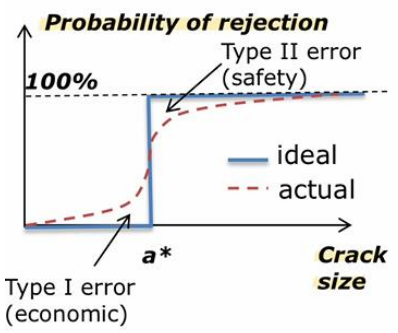

Figure 8.10: real and ideal probability of rejection curve.

The second way we implement NDE is to define proper maintenance schedule. This is done by monitoring all defects that surpass the detectable crack length a^* again. Once a crack has $a > a^*$ and thus is detected, we establish $t^* =$ time it will take for the crack to grow to a point where crack strength will be exceeded. Based on t^* we define the maintenance schedule. An appropriate safety factor must be considered to prevent unforeseen failure due to anomalies.

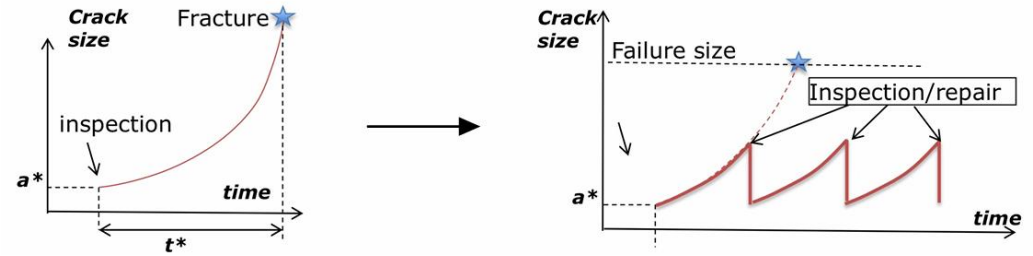

Figure 8.11: effect of inspections and repair on crack size.

9. Composite materials

Composite materials are widely used in aeronautical structures due to three main reasons:

1. High strength-to-weight and stiffness-to-weight ratios.
2. Superior performance in fatigue conditions when compared to metals.
3. Possibility to produce large monolithic components, reducing cost of assembly and need for junctions.

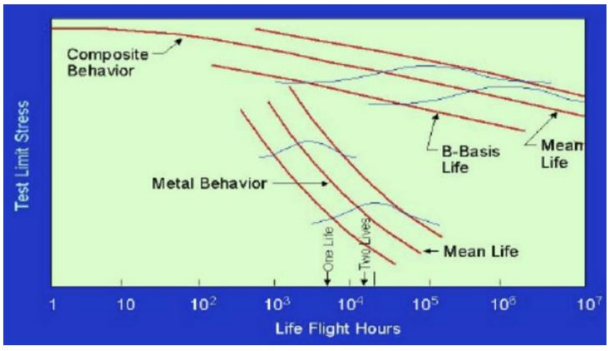

Figure 9.1: left) fatigue comparison between composites and metals; right) example of a large monolithic part.

However, composite design presents many problems related to the nature of this material, such as:

- Lack of standardization of base materials: due to the infinite combinations of materials, lamination sequences, thickness etc.
- Behavior of composites: high temperature, humidity and internal damage greatly reduce composite strength.
- Designs approaches: they are not standardized and the solutions adopted by the different companies are not shared in the industry.

These problems related to composites have a great impact on certification requirements. More specifically, we need to prove that a certain level of damage can be sustained for the entire life of the component. By regulation 25.305 of the FEA:

- composite materials must not allow crack growth.
- composite structures must guarantee no detrimental deformation al limit loads in presence of permanent damage.

For metallic material the requirements accept crack propagation, but we need to prove that any damage will be detected before it reaches a critical length a^* (see section 8.3).

Finally, the analytical model used to describe the behavior of composite materials is described in section 0.

9.1. Composite damage

9.1.1. Intralaminar damage

9.1.1.1. Transverse matrix cracking

Consider the example provided in Figure 9.2, laminated plate with only 0/90 UD plies. Assume the laminate to be symmetric and only loaded in-plane by N_x acting on the geometrical midplane (no bending). For such plate, the σ_{max} will be reached in the 90° plies well before than for the 0° plies. Thus, a series of cracks in transverse direction will appear in the 90° oriented plies. This can be proven with simple computations:

$$\varepsilon_{xx}^c = \frac{\sigma_{xx}^c}{E_x^c} \quad \rightarrow \quad \sigma_{xx}^{90} = E_x^{90}\varepsilon_{xx}^c = \sigma_{xx}^c \frac{E_x^{90}}{E_x^c} \gg \sigma_{UTS}^{90}$$

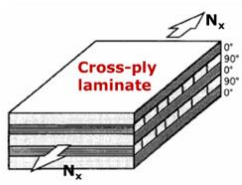

	E (Gpa)	σ^U (Mpa)	ε^U (%)
0	E_0 = 150	1800	1.2%
90	E_{90} =10	50	0.5%

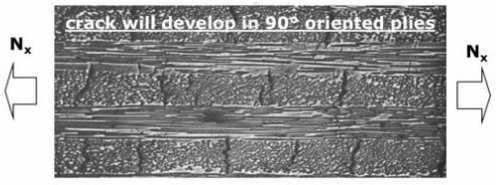

Figure 9.2: transverse matrix cracking.

So, ***in short***, for a composite laminate, due to the different orientation and orthotropy of each ply, when a load is applied in one direction, the plies oriented in a different direction experience cracking of the matrix. This phenomenon is called *transverse matrix cracking* TMC. Intuitively, in a composite plate there will always be a certain degree of TMC since there are always a certain number of off-axis plies. Furthermore, the weakest link approach can be applied to matrix strength.

The ***severity of TMC*** depends on:

- Crack density: as depicted in Figure 9.5 – left, the intralaminar τ needs a certain amount of space to develop and flow in and out of the 90° ply. This implies that if crack density is too high, τ will not flow back into the ply, it will remain in the intralaminar plane, which is a worst case scenario for delaminations.
- Thickness of 90° plies block: it's been shown experimentally that the higher the thickness of the 90° plies block in between two 0° plies, the lower is resistance to TMC. So in

general, if we consider the case of UD plies oriented in any arbitrary direction, like 45°, or fabric plies, the higher number of off-axis plies, the higher the number of cracks, the bigger the effect on the laminate stiffness.

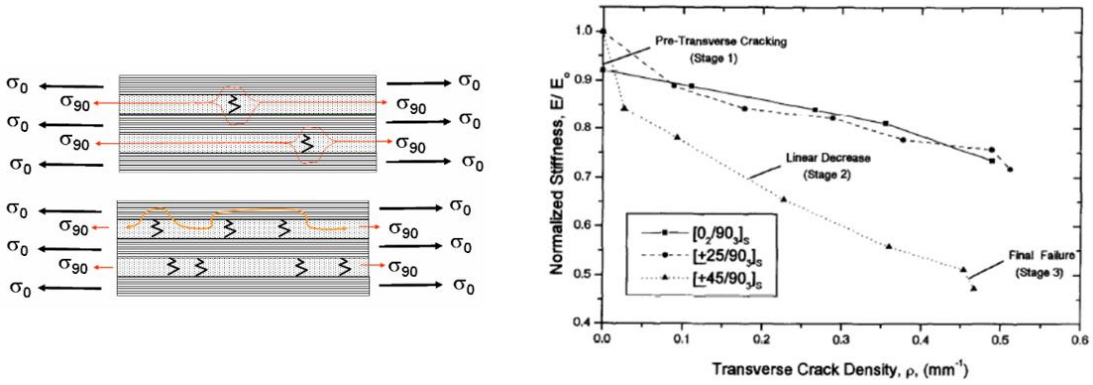

Figure 9.3: left) effect of crack density; right) effect of 90° block thickness.

Moreover, ***the real danger of TMC is that it induces delaminations***. This is because the cracks interrupt the stress path of σ_{90} which will be redistributed to the adjacent σ_0. Additional stress is no problem, but for the stress to flow in the adjacent plies, a shear flux must develop. This implies that a shear stress acting on the interlaminar layer, which is matrix dominated, develops. In other words, ***an interlaminar shear stress that favors delaminations is developed***, as depicted in Figure 9.5. Such shear stress can be roughly computed as follows:

$$\tau = t^{90} \frac{d\sigma_{xx}^{90}}{dx} \qquad 9.1$$

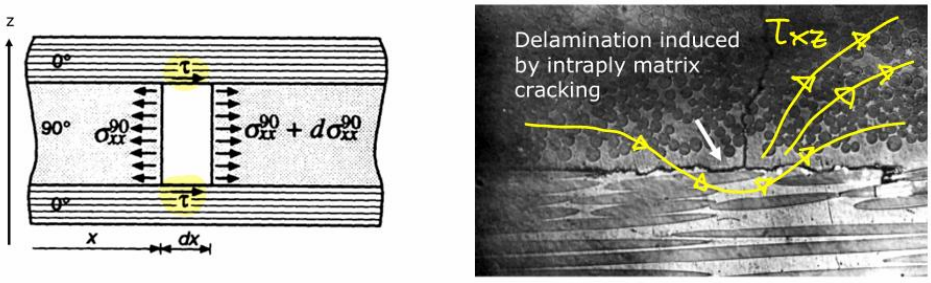

Figure 9.4: left) scheme of τ; right) delamination induced by TMC.

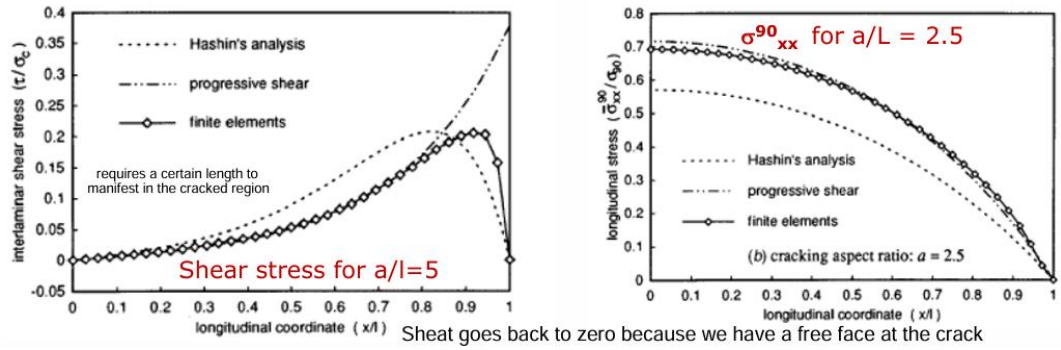
Hashin's analysis
progressive shear
finite elements
requires a certain length to
manifest in the cracked region
Shear stress for a/l=5
interlaminar shear stress (τ/σc)
longitudinal coordinate (x/l)
σ90xx for a/L = 2.5
Hashin's analysis
progressive shear
finite elements
(b) cracking aspect ratio: a = 2.5
longitudinal stress (σ90xx/σ90)
longitudinal coordinate (x/l)
Sheat goes back to zero because we have a free face at the crack

Figure 9.5: left) normalized shear stress; right) normalized axial stress in 90° plies.

For FB plies, or 45° plies, due to the fact that the in-plane stress state in dominated by shear, there is a high degree of non-linearity in the response of FB plies. Of course, all that's been said for UD plies about TMC applies to FB as well.

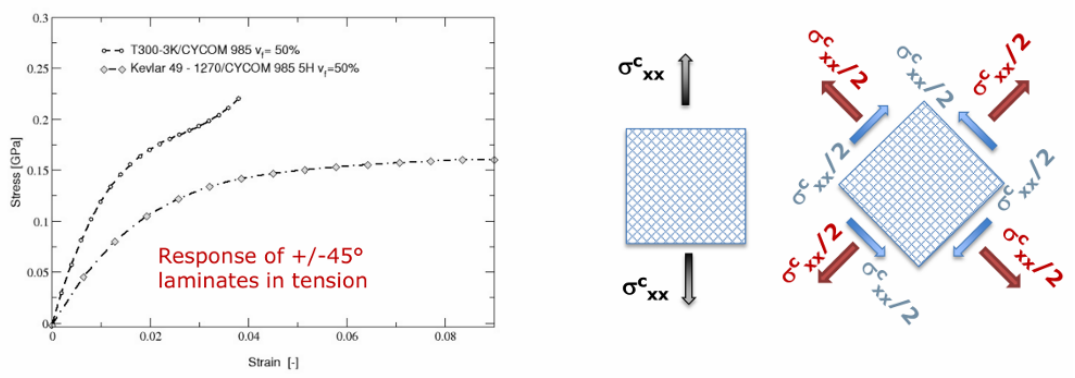

Figure 9.6: left) non-linear response of FB plies; right) stress acting on 45° ply.

9.1.1.2. Fiber tensile failure

When a ply is loaded in fiber direction, its response is dominated by the fibers' properties, both for strength and stiffness. A quick way to see this is:

$$\sigma_c = \sigma_f V_f + \sigma_m(1 - V_f) \approx \sigma_f V_f \quad \text{where } (V_f)_{max} \approx 60\%$$

In general, ***four stages of fiber response*** can be identified: (1) both fibers and matrix are elastic; (2) matrix experiences TMC; (3) fibers go into plastic deformation; (4) fibers break when ε_{max}.

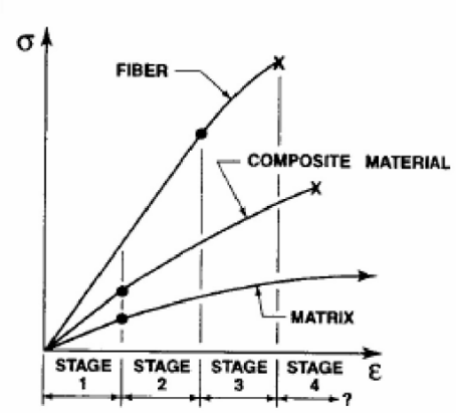

Figure 9.7: four stages of fiber response.

However, ***the weakest link approach cannot be applied to fibers embedded in composites***, because when one fiber breaks the adjacent one share part of it load. This is very similar to what happens with plies in MTC, and in the same way the flux is transferred to adjacent fibers via a TSS τ which acts on the fiber-matrix interface. As for MTC, for the stress to flow to the adjacent fibers, τ must develop along an *ineffective fiber length* δ_E. Such length can be defined as follows:

$$\delta_E = \left(\frac{E_f}{G_m}\right)^{\frac{1}{2}} \left(\frac{1 - V_f^{1/2}}{2V_f^{1/2}}\right)^{\frac{1}{2}} d_f$$

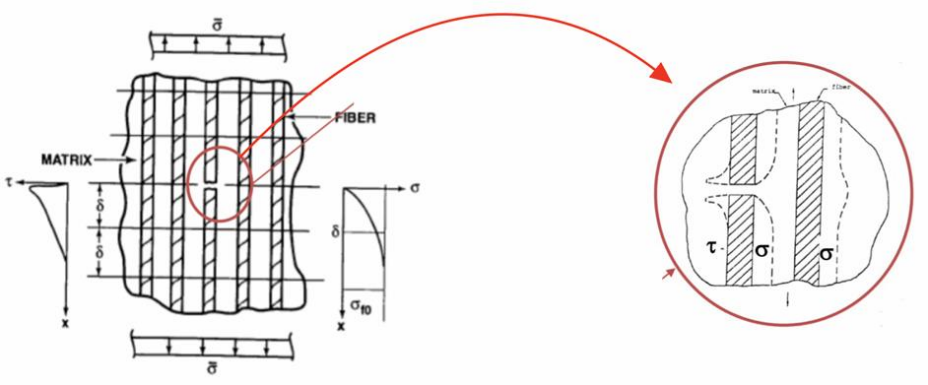

Figure 9.8: behavior of σ and τ in fiber tensile failure.

9.1.1.3. Fiber compressive failure

In general, composites fail in compression when the surrounding matrix loses its capability to prevent instability of the compressed fibers. Thus, compressive failure, or ***micro-buckling***, ***is a matrix dominated property and anything that damages the matrix*** (via TMC for example) ***also greatly reduces the compressive strength of a laminate***.

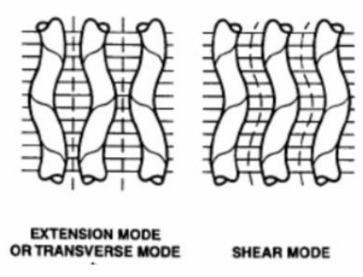

Figure 9.9: micro-buckling.

Micro-buckling in shear mode involves the shear deformation of the matrix in between two adjacent fibers. Initial studies on this subject led to the following *maximum sustainable compressive strength* MSCS:

$$\sigma_{MSCS} = \frac{G_m}{1 - V_f} \qquad 9.2$$

However, a ***more accurate model*** was developed which makes the following ***assumptions***:

- Fibers are only subject to compression and their flexural stiffness can be neglected.
- Misalignment ϕ_0 is accounted for.
- The local shear response $\tau_0(\gamma_0)$, necessary to sustain the inclined fibers, is identical to the average macroscopic shear response of the composite $\tau(\gamma)$.

The equilibrium equation, obtained from the configuration in Figure 9.10, is reported below. From such equation σ_F is derived, which has an upper limit representing the capability of the matrix to resist micro-buckling. This maximum can be found graphically.

$$\tau_{\phi 0}(\gamma_{\phi 0}) = \sigma_F(\phi_0 + \gamma_{\phi 0}) \quad \rightarrow \quad \sigma_F = \frac{\tau_{\phi 0}(\gamma_{\phi 0})}{\phi_0 + \gamma_{\phi 0}} \approx \frac{\tau(\gamma)}{\phi_0 + \gamma} \quad \rightarrow \quad \sigma_{MSCS} = \max\left(\frac{\tau(\gamma)}{\phi_0 + \gamma}\right) \tag{9.3}$$

Note that this model has no practical applications but highlights the fact that micro-buckling is matrix related.

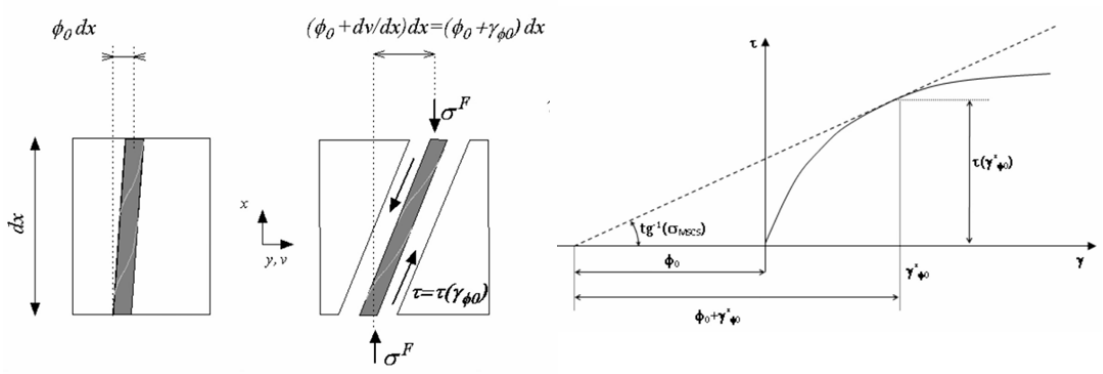

Figure 9.10: left) initial configuration; center) loaded configuration; right) graphical interpretation.

9.1.2. Delaminations

A delamination is the ***partial separation of two adjacent plies in a composite plate***. This situation is critical since (1) it cuts off stress transfer between adjacent plies. Moreover, delaminations are caused by 3D stress states, as we've seen for TMC, thus CLT cannot predict this phenomenon (2). Such out-of-plane stress components act on interlaminar planes rich in resin bypassing the fibers, thus fibers oriented in different direction cannot help mitigate delaminations (3). Lastly, delaminations are generally invisible from outside (4) aside from particular cases such as those caused by barely visible impact damage (BVID).

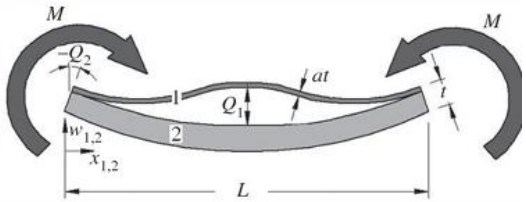

Figure 9.11: example of bending-induced delamination.

9.1.2.1. Causes of delaminations

Manufacturing. Typical and main cause of delaminations. Some common mistakes that lead to delamination are leaving air pockets in the plies during the lamination process, insufficient pressure during curing, mismatch of CTE of adjacent plies.

Layup drop-off. Consider the scheme in Figure 9.12, as for TMC, the problem is that the σ_{zz} of the terminated ply must flow in the adjacent one. This occur via an out of plane shear stress τ_{xz} that develops near the drop-off. Furthermore, the drop-off generates matrix pockets at the end of the terminated ply. These are weak spots from which cracks nucleate and propagate. Note that ply drop-offs are inevitable in aeronautical structures since they are needed to taper the laminates.

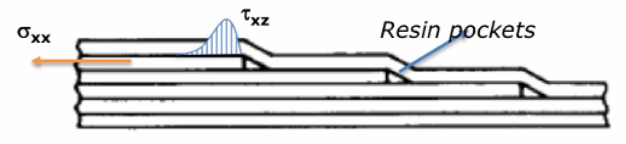

Figure 9.12: drop-off on laminated plate.

Laminate curvature. Consider the component of Figure 9.13 - left, curved and subject to bending. For such component an axial σ_{xx} will develop. The vertical component of σ_x has to be equilibrated by an out-of-plane σ_{zz}. As a consequence, components that work in similar conditions usually fail in mode I, with a response like the one in Figure 9.13 – right.

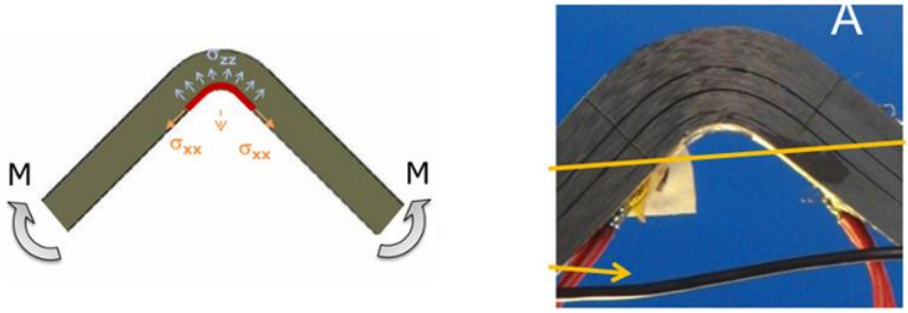

Figure 9.13: left) curved laminate subject to bending scheme; right) FEM analysis.

Free edge effects. At the edge of a composite ply, the solution of CLT is not able to capture the correct state of stress. More specifically, in CLT the interaction of adjacent plies enforce compatibility via the development of in plane shear stresses τ_{xy}. However, this solution is acceptable only inside the laminate, τ_{xy} cannot exist on the laminate edges. Thus, at the edges of the laminate, equilibrium must be restored by development of interlaminar shear stresses τ_{xz}, which favor delaminations.

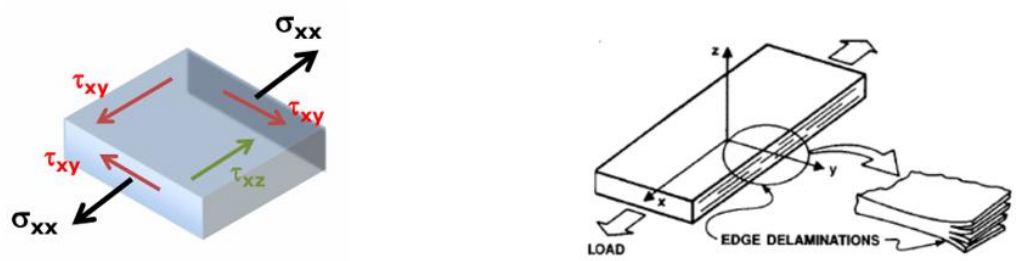

Figure 9.14: left) equilibrium state at the edge; right) edge effect delamination.

To suppress free edge delaminations there are multiple solutions: edge caps, interlaminar adhesive layers, tapering, notching or even stitching (very rare and of debatable effect).

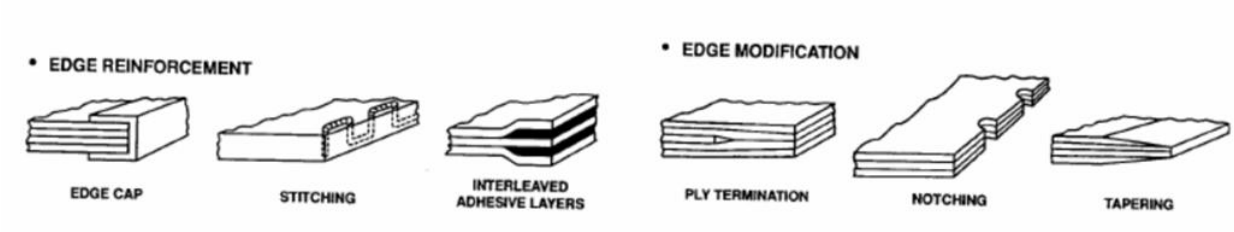

Figure 9.15: solution to free edge delaminations.

Such 3D stress state could be described by the Pipes-Pagano equations, which correctly predicts that σ_{xx} and τ_{xy} go to zero as we approach the edge. The model also predicts $\tau_{xz} \neq 0$ as we approach the edge, but this value goes to infinity, which is wrong and can be accounted for by other more refined models.

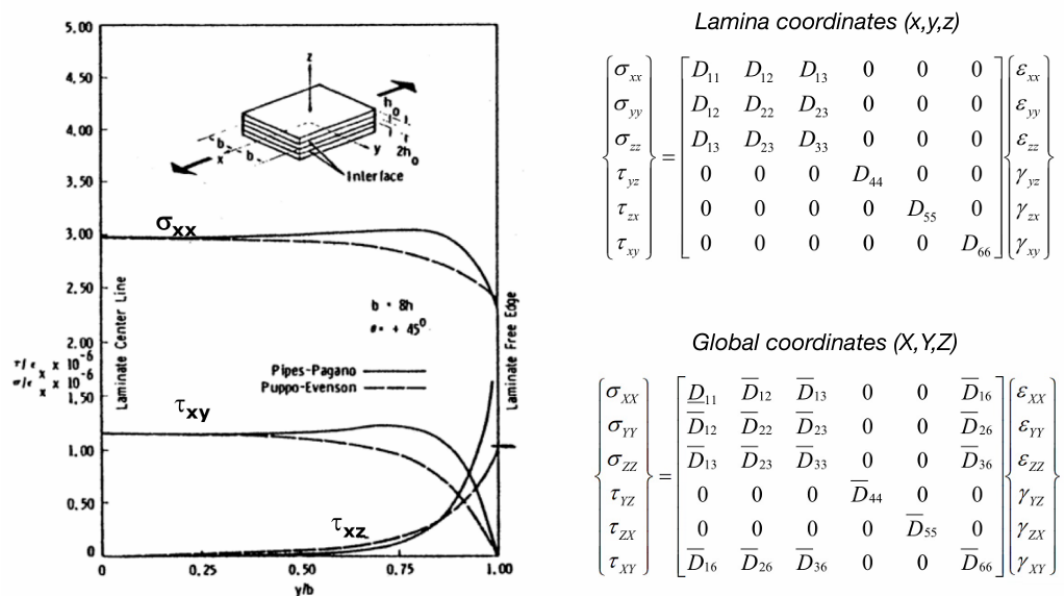

Figure 9.16: left) Pipes-Pagano solution.

Low-energy impacts. Even if low-energy impacts usually don't cause perforation in composites, they can cause internal damage. Such damage occurs in the form of delaminations and matrix cracking, usually in a pine-tree configuration, as shown in Figure 9.17Figure 9.20. Intuitively, the higher the energy, the wider the area damaged.

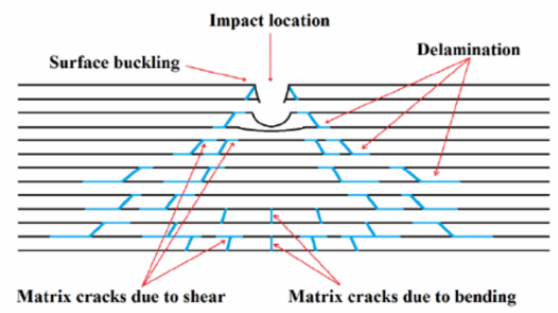

Figure 9.17: pine-tree damage due to BVID.

Recall that matrix cracking reduces the resistance to micro-buckling. Compressive strength is also reduced due to the behavior of delaminated plies in compressive loading conditions. Generally speaking, ***BVID greatly reduce the compressive strength of laminates, this delayed composite use in aerostructures by decades***. Such behavior is illustrated in Figure 9.18, although no general rule exists, the initial part of the curve can be very steep.

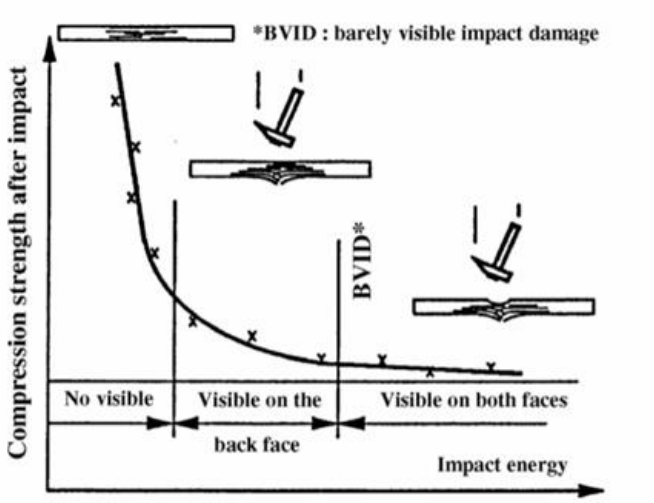

Figure 9.18: effect of BVID on composite mechanical properties.

It's clear at this point that it's ***crucial to identify the*** minimum energy level that causes internal delaminations, ***BVID threshold***, ***and estimate the residual strength in this state***. This can be done analytically, an *estimation* of the BVID threshold is provided by Davies-Robinson:

$$P_{cr} = \sqrt{\frac{8\pi^2 E t^3}{9(1-\nu^2)} G_{IIc}} \qquad 9.4$$

However, in practical applications, the ***BVID threshold and the residual strength are found experimentally***. Tests are discussed in the next section.

9.1.2.2. Characterization tests

Due to the influence of delaminations on structural integrity, characterization of interlaminar properties assumes crucial importance. Crack propagation tests will be discussed; for more information see section 0.

Test for delaminations induced by BVID. As mentioned in the previous section, two tests are needed:

- Impact test (BVID threshold): ***characterizes BVID threshold***. Impacts at increasing energy are simulated with falling weights of increasing mass to obtain plots like the ones in Figure 9.20. The composite specimen, 100mm in width, is fixed at the base of the setup, and the weight falls on its center. This is a laminate level test/allowable (see section 9.2.1).

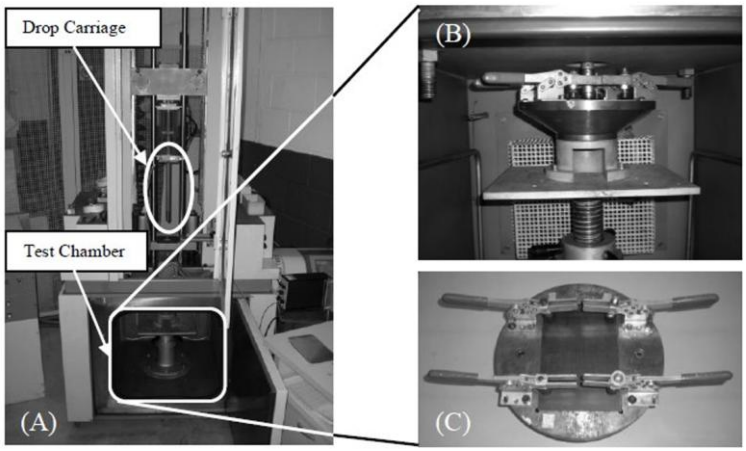

Figure 9.19: impact test setup.

The typical response of a laminate is shown in Figure 9.20. We can clearly distinguish a loading phase, a plateau corresponding to the delamination, and an unloading phase. Note that if impact energy is high enough (purple line), the unloading phase does not return to the starting configuration.

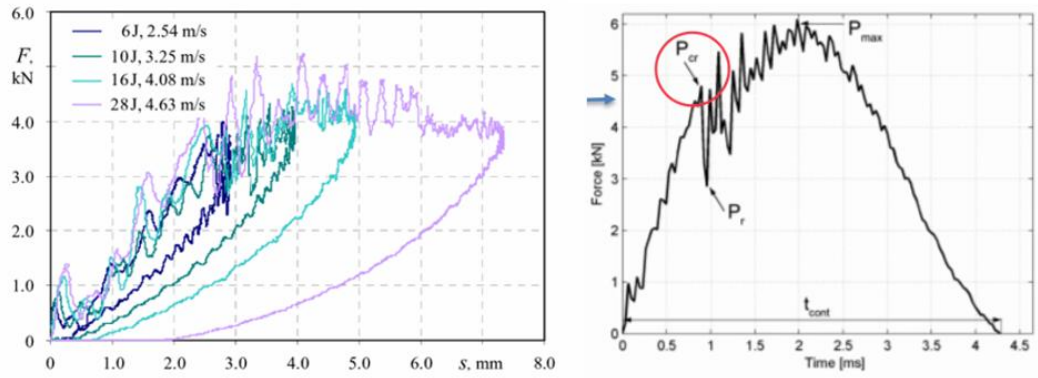

Figure 9.20: left) $F - s$ response; right) $F - t$ response.

- Compression after impact test CAI: ***characterizes residual compressive strength.*** The impacted laminate is inserted into anti-buckling guides and then compressed. Instability starts at the center and then propagates.

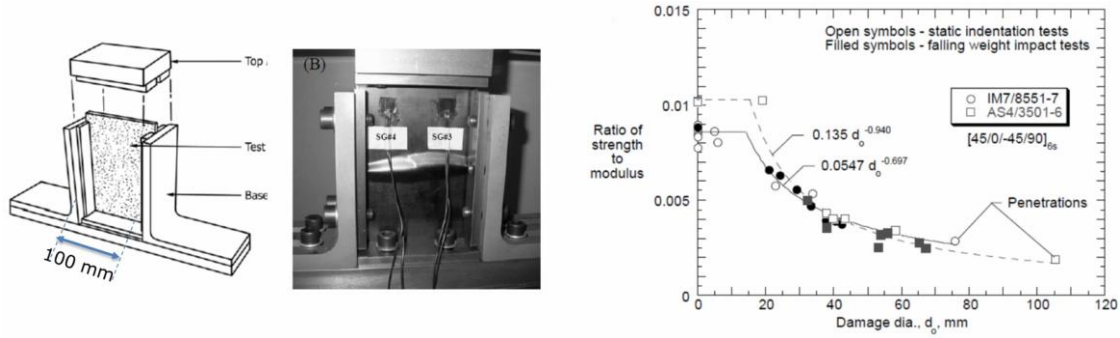

Figure 9.21: left) compression test setup; right) compressive strength with increasing damage diameter.

Double cantilever beam test (DCBT). This test ***characterizes mode I interlaminar toughness***. It follows the ASTM D5528 regulation. Note that this regulation is valid for UD laminates, but it's widely used to also characterize fabric laminates. Specimens have a thickness $2h \approx 3 - 10mm$, width $b = 25mm$ and length of $150 - 200mm$. The specimens are manufactured by inserting a

pre-crack at one side, to emulate delamination, typically done via a sheet of Teflon. Then, two *hinges* are bonded to the external surface of the beams, at a distance a_0 from the cracked tip. The test is carried out by applying a vertical force to the hinges that tends to open the crack in mode I. The hinges are chosen to enforce a purely vertical load (no bending) at all times during the test. Note that specimens must be appropriately designed in order to avoid any inelastic mechanism aside from crack propagation.

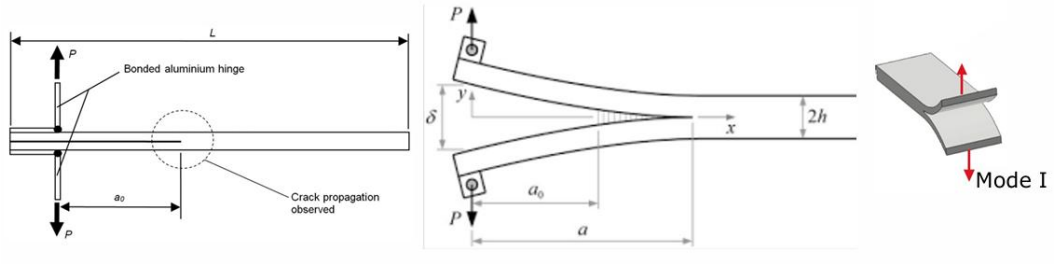

Figure 9.22: double cantilever beam test – specimen.

The typical response of laminates subject to this test is illustrated in Figure 9.23, assuming a linear $P-u$ response. After the loading phase, the critical energy release rate R is reached and stable crack propagation starts. Note that generally $(K, C) = f(a)$, thus, if at any point of the test the load is removed and reapplied, the reloading curve has variable slope.

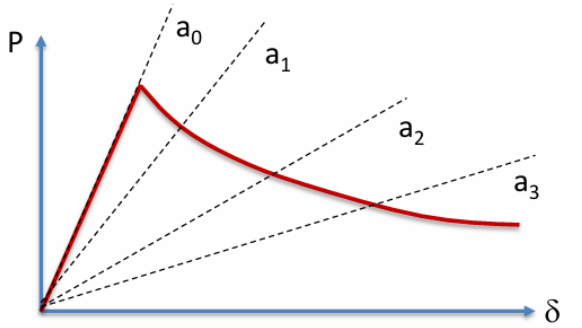

Figure 9.23: double cantilever beam test response.

A simple formula for the evaluation of the critical energy release rate $R_I = G_{Ic}$ can be obtained by applying the Euler-Bernoulli beam model. Such model provides a way to compute the displacement of the cracked end. The compliance is then immediately found to be $C \propto a^3$:

$$\frac{\delta}{2} = \frac{Pa^3}{3E_{11}I_{11}} = \frac{Pa^3}{3E_{11}\frac{1}{12}Bh^3} = \frac{4Pa^3}{E_{11}Bh^3} \quad \rightarrow \quad C(a) = \frac{2\cdot\frac{\delta}{2}}{P} = \frac{\delta}{P} = \frac{8Pa^3}{E_{11}Bh^3}\cdot\frac{1}{P} = \frac{8a^3}{E_{11}Bh^3}$$

At this point we simply plug this into the Irwin-Kies equation (8.11) and we obtain:

$$G_{Ic} = R_I = \frac{P^2}{2B}\frac{dC}{da} = \frac{P^2}{2B}\frac{24a^2}{E_{11}Bh^3} = \frac{12P^2a^2}{E_{11}B^2h^3} = \frac{3}{2}\frac{P\delta}{Ba} \qquad 9.5$$

Note that this result provided by beam theory is significantly approximated and overestimates R. Nonetheless, ASTM standard suggests computing R using compliance calibration methods, which

require the computation of dC/da from linear regression of experimental data. This can also be done numerically.

End notched flexure test (ENF). This test ***characterizes mode II interlaminar toughness***. This is done via a 3 point bending test of pre-cracked specimens with dimensions similar to those of DCBT ($2h \leq 10mm, b \approx 25mm, l \approx 150 - 200mm$). In this loading condition, interlaminar stresses develop at crack tip. Such stress value is infinite according to the elastic solution, so the response is totally driven by the energy available to propagate the crack.

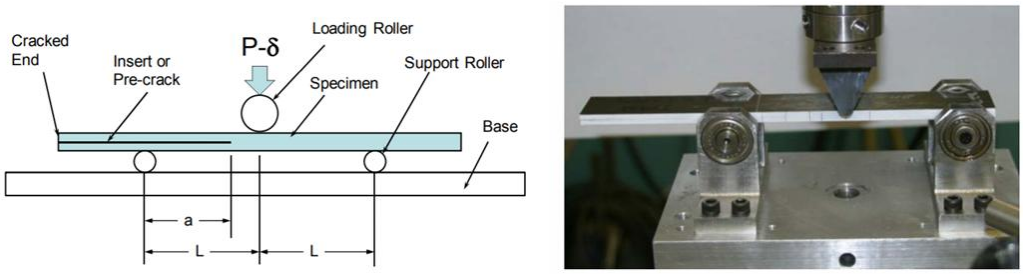

Figure 9.24: three point bending test.

In this case the crack propagation is unstable, the typical response is the one reported in Figure 9.25. Because of this unstable mode, the value of G_{cII} is computed only for the load corresponding to the sudden drop shown in Figure 9.25. As for DCBT, by applying beam theory we're able to compute mode II critical energy release rate $G_{cII} = R_{II}$ for such load:

$$G_{cII} = \frac{9P^2a^2}{16E_{11}B^2h^3}\left(1 + 0.2\frac{E_{11}}{G_{13}}\left(\frac{h}{a}\right)^2\right) \qquad 9.6$$

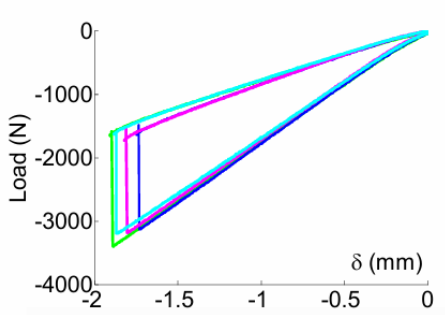

Figure 9.25: response of mode II test.

Note that stable crack propagation can be achieved in this mode with a 4 point ENF test, but it's more difficult to accomplish and significantly affected by friction. As a general rule $R_{II} > R_I$, and $R_{II}^{UD} < R_{II}^{FB}$.

Short beam test (SBT). This test ***characterizes interlaminar shear strength ILSS***. The specimen has thickness of $6 - 12mm$ and short length of $40mm$ to minimize bending effects. The specimen is tested in 3 point bending. If the specimen has a homogeneous $[0]_n$ layup, the TSS distribution is parabolic, as shown in the picture below. Failure occurs at a critical load value P_{cr} and the failure mode is the one presented below. This test provides an estimation of ILSS, which can be computed as follows, where h is the thickness and b the width.

$$\tau_{xz} = \frac{3}{4}\frac{P_{cr}}{bh} \qquad 9.7$$

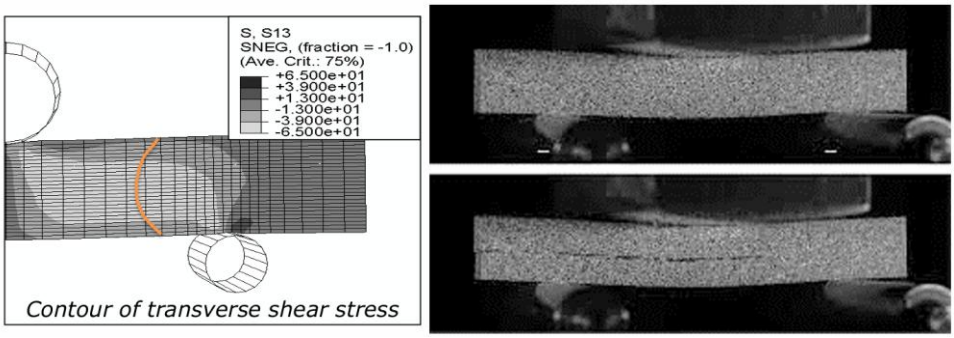

Figure 9.26: left) FEM simulation of SBT; right) failure mode of ST specimen.

Curved beam test (CBT). This test wants to evaluate the minimum out-of-plane normal stress σ_{zz} that induces delamination in the curved beam. The test is a 4 point bending test performed on a curved beam specimen of $t \approx 10mm$, $w \approx 25mm$ and inner radius of the curvature of $\approx 6mm$. With respect to the geometrical quantities reported in Figure 9.27, the maximum load P is determined experimentally, and then the maximum σ_{cbt} is determined as:

$$\sigma_{zz} = \frac{M}{w} = \frac{P}{2w\cos\phi}\left(\frac{d_x}{\cos\phi} + (D+t)\tan\phi\right) \qquad 9.8$$

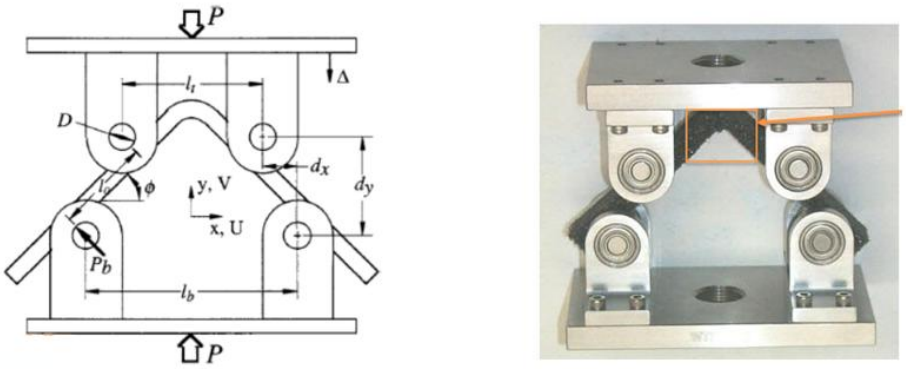

Figure 9.27: setup of a curved beam test.

9.2. Strength based criteria (orthotropy)

Strength analysis for composites follows the same scheme introduced for isotropic materials and reported here. However, important differences exist between the application of this procedure to isotropic and orthotropic materials. More specifically, the experimental branch is more complex because of the numerous factors we need to consider when obtaining the allowables. The analytical branch must be revised carefully to use appropriate numerical models that can correctly describe a 3D stress state when needed.

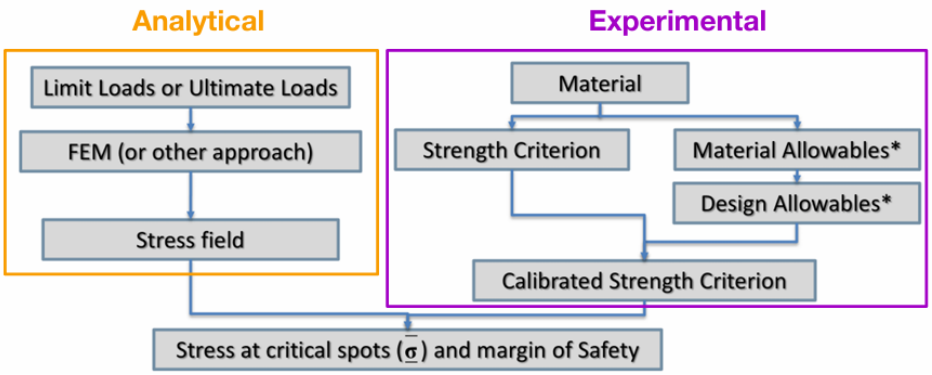

Figure 9.28: tree-scheme of strength based criteria.

An important concept in composite structure design is the building block approach. Although this will be studied in a dedicated section (9.4). The core idea is to use the allowables of the smaller components to analyze the behavior of bigger components. This allows us to not rely on excessively conservative or critical results due to the uncertainty of the stress field.

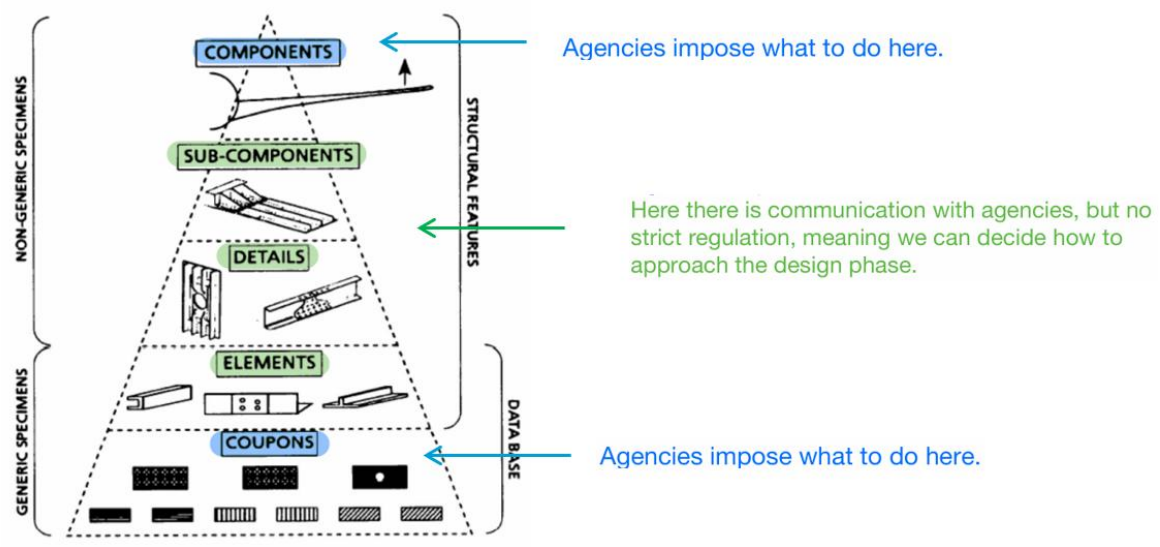

Figure 9.29: building block approach scheme.

9.2.1. Allowables

The definition of material allowables for orthotropic is not as straightforward as for metals. A crucial distinction must be made with respect to the how the allowables is obtained: lamina or laminate level? Based on this choice, different strength based criteria can be used to assess composite structures.

For both set of allowables, in order to properly characterize the material, the tests must be repeated at different combinations of temperature and humidity. More precisely:

	$[°F]$	$[°C]$
Cold temperature dry (CTD)	-65	-53
Room temperature dry (RTD)	70	21
Elevated temperature dry (ETD)	250	121
Elevated temperature wet (ETW)	250	121

Table 9.1: temperature/humidity conditions for allowable tests.

9.2.1.1. Lamina level

Traditionally, characterization of lamina properties has been carried out via tests on homogeneous or quasi-homogeneous layups of UD plies [3] – Chapter 6.8. Lamina level allowables have two main advantages: it's easy to characterize intraply failure modes (1) with a small number of specimens (2).

However, some serious drawbacks need to be pointed out: such allowables do not consider adjacent ply interactions, residual thermal stress and edge effects. Thus, lamina level allowables are generally lower and exhibit more scatter than laminate level allowables. For this reason correction factors (1) and sophisticated laboratories are needed (2). Moreover, complex strength criteria must be used to actually employ these allowables (3). For example interactive criteria like Tsai-Wu or separate mode criteria like Hashin.

Tests performed at lamina level are:

- In plane allowables: homogeneous UD plies are used to determine $X_C. X_T, Y_C, Y_T, S_{xy}$. To consider the effect of TMC, the same tests can be performed on layups with a mix of [0/90]n plies.
- Out-of-plane allowables: short beam tests and curved beam tests are performed to obtain S_{xz}, Z_T (see section 9.1.2.2).

9.2.1.2. Laminate level

As we said in the previous paragraph, ply properties have been traditionally obtained from testing UD [0/90]n laminates. As material capabilities have increased, deficiencies associated with these specimen have been greatly amplified. As an example, fiber/load misalignment of 1° with respect to 0° direction in UD plies, can cause up to a 30% reduction in strength in the tested material. Hence, experienced personnel and sophisticated instrumentation is needed for these tests.

As an alternative, testing of *crossply*[4] laminates has been increasingly used to indirectly determine lamina level allowables from CLT. Thus, ***laminate level allowables are still applied at lamina level***.

The most compelling reason to use laminate level allowables is because they are more representative of the actual component behavior. This is due to different factors, first of all, laminate level allowables intrinsically consider the interaction of adjacent plies, residual thermal stress and edge effects (1). Due to these aspects being accounted for by tests, allowables are generally higher and exhibit less scatter when compared to the lamina level allowables (2). Moreover, we can also test the laminate with a certain degree of induced damage, to characterize also residual strength after impact (3). Lastly, because allowables are more accurate, we can use simpler criteria, like maximum strain (4).

The biggest drawback is that laminate level allowables are valid only for the specific layup tested (1). Moreover, more tests are needed than in the case of lamina level allowables (2). Because of this, specimens of laminate level allowables have only been standardized crossply laminates, such as:

- Quasi-isotropic laminates → [25/50/25]n.
- Matrix-dominated laminates → [10/80/10]n.
- Fiber-dominated laminates → [50/40/10]n.

Note how in all three configurations, at least 10% of fibers are in transverse direction. Remember: we always need to support the matrix in transverse direction to limit TMC (see section 9.1.1.1). Tests performed at laminate level are:

- Open hole tension/compression (OHT/OHC): they characterize notch sensitivity.
- Filled hole tension/compression (FHT/FHC): they characterize riveted zones.
- Impact tests: to characterize BVID threshold.
- Compression after impact (CAI): characterizes residual compressive strength after impact, performed on quasi-isotropic laminates.

While there are a number of standards for in-plane properties (ASTM) of laminated materials, this is not the case for out-of-plane properties. Out-of-plane related allowables must be determined with the tests introduced in section 9.1.2.2.

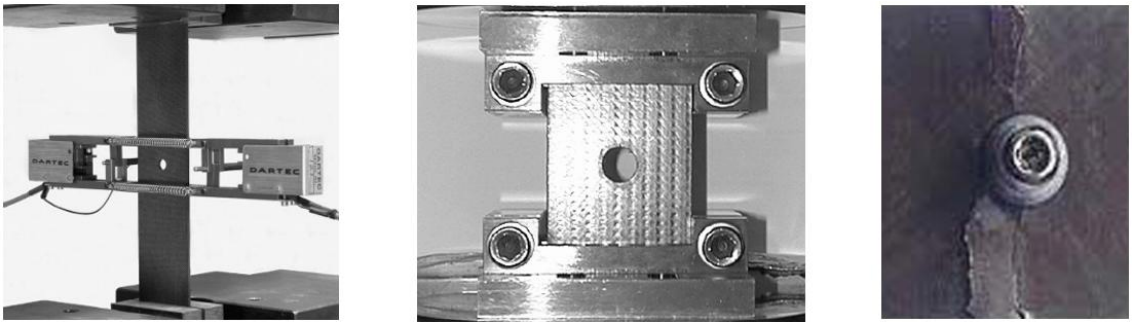

Figure 9.30: left) OHT test; center) OHC test; right) FOT test.

[4] A crossply laminate is a multidirectional laminate, that contains any combination of [0/45/90] plies.

9.2.2. Stress field

9.2.2.1. Out of plane stress components

The question here is ***how to accurately model the 3D stress fields***. First of all, recall that a 3D stress state cannot be accurately studied with shell elements. This is because shell elements are based on MPT, which does not include a TSS component in its CL. Thus, the values returned are a gross approximation based on cylindrical bending. Such correction assumes no gradient of any kind along the depth and more importantly no tapers in geometry. We now know that 3D stress states are a direct byproduct of tapering geometries, thus TSS values of shell elements are not reliable.

There are several ***solutions***:

- Solid/brick elements: modelling each homogeneous sequence of plies (with the same orientation) using bricks works, but the modelling time is huge. Thus, this approach cannot be applied to very large structures.

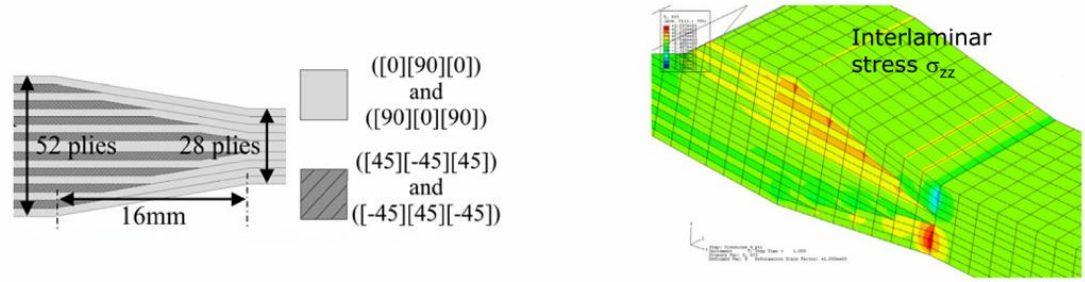

Figure 9.31: brick model of tapered laminate.

- Global-local approach: we can use a 2D mesh to identify critical spots, then use 3D elements to study those areas more accurately, but this could still take much modelling effort. Because of this, laminated brick elements were developed: they allow us to define a stack direction, layup, material law and number of IP through the thickness of each ply. Note that *to obtain good results for TSS we need a refined mesh*.

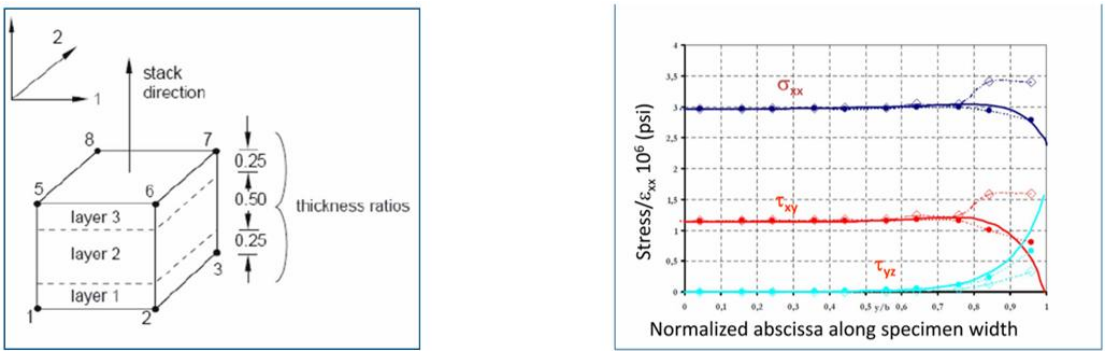

Figure 9.32: left) laminated brick element scheme; right) solution of laminated bricks.

9.2.2.2. Hygrothermal effects.

Hygrothermal effects can be analytically described by CLT (see section:
Classical lamination theory). Residual thermal stress is caused by the production process of laminates, more specifically by the cooling and the fact that thermal expansion of a laminate is intuitively highly orthotropic. Two things must be considered when assessing thermal stress:

1. Matrix cracking helps with releasing such stress.

2. At high temperatures, viscoelastic effects help to relax some thermal stress. Thus, residual thermal stress must be computed starting from the temperature at which the material can be considered elastic.

Moist absorption affects composites with polymeric matrix that are placed in humid environments. They will absorb moisture up until saturation, causing swelling and greatly reducing the laminates mechanical properties.

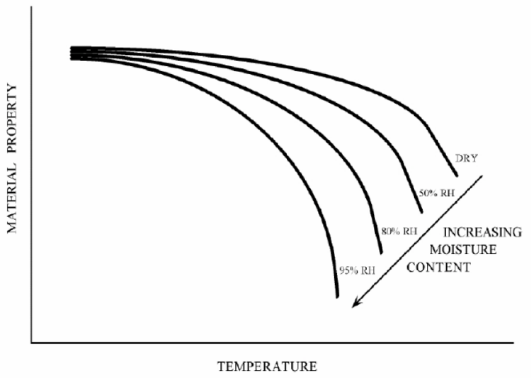

Figure 9.33: effect of moisture absorption of mechanical properties of composite laminates.

Moist absorption in composites shows close analogies with thermal expansion. In fact, the two phenomena are so similar that they have the same exact formulation for orthotropic materials (Equation 9.9). The big difference between the two phenomena is the time scale: heat transfer happens within minutes; moisture absorption is a matter of days.

Temperature Conductivities

$$K_x \frac{\partial^2 T}{\partial^2 x} + K_y \frac{\partial^2 T}{\partial^2 y} + K_z \frac{\partial^2 T}{\partial^2 z} = \frac{\partial T}{\partial t}$$

Moisture concentration Diffusivities

$$D_x \frac{\partial^2 c}{\partial^2 x} + D_y \frac{\partial^2 c}{\partial^2 y} + D_z \frac{\partial^2 c}{\partial^2 z} = \frac{\partial c}{\partial t} \qquad 9.9$$

9.3. Strength criteria

A somewhat empirical approach will be adopted to define strength criteria for composites. More precisely, the actual failure envelopes in stress space are compared with simplified failure envelopes [4] – chapter 2.9. The actual failure envelops are obtained experimentally, and they represent the stress levels at which macroscopic failure occurs. Thus, they mask all the phenomena that are occurring during the loading process up to failure, such as yielding for metals. The simplified failure envelopes are obtained by fitting the data obtained experimentally, i.e. the actual envelops. Thus, simplified envelops also do not consider the phenomena that manifest during the loading process. ***The mathematical relations defining the simplified envelop are the actual strength criteria***. We refer to these analytical equations as "criteria" and not "theories" because the latter implies a formal derivation process, while the models presented here are phenomenological, i.e. they fit data. Our ***goal*** is to define the analytical formulation of the simplified failure envelops that are simple enough to be used in design.

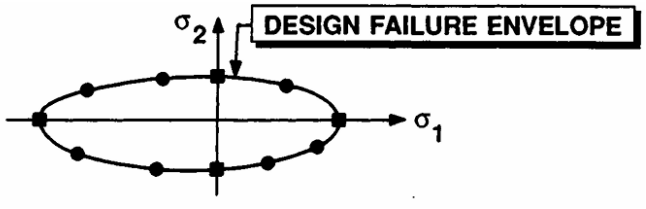

Figure 9.34: Hypothetical Two-Dimensional Failure Data and Design Curve.

It is important to point out that, if on one hand the analytical expression of the failure surface is somewhat easily obtained by curve-fitting experimental data, we also (in general) ***lose the ability to determine the failure mode***. John Hart-Smith stated:

"most failure criteria are meaningless curves passed through unrelated data points"

In fact, each of the principal material direction strengths X_T, X_C, Y_T, Y_C, corresponding to the solid squares in Figure 9.34, represents a totally different failure mode, so why should they be connected with a single curve? That is, as we will see later, X_T corresponds to fiber fracture, X_T to fiber buckling, Y_T to matrix failure, and Y_T to matrix compression failure. And the material behavior, or structural behavior in the case of X_C, corresponding to each failure is drastically different. Thus, there is no physical reason to justify connecting the various failure points with a single continuous curve. In fact, there is reason not to connect the principal material strength data points with a continuous curve. Nevertheless, designers need something simple enough to use every day, so we pursue the curve-fitting approach.

In all failure criteria presented here, the ***allowables*** X, Y, Z and S ***are all assumed to be positive***. Thus, for compressive loading and compression allowables, the signs of the relevant terms will be adjusted with respect to the source cited for this section [4] – chapter 2.9. Moreover, the ***material is assumed to be orthotropic but homogeneous***. Thus, we cannot account for some of the failure mechanisms at the microscopic level. At the same time, the failure criteria tend to be smoother than the actual behavior that often exhibits considerable data scatter because of testing technique, manufacturing nonuniformities, etc. For each of the failure criteria, we will generate biaxial stresses by off-axis loading of a unidirectionally reinforced lamina. That is, the uniaxial off-axis stress σ_x at θ to the fibers is transformed into biaxial stresses in the principal material coordinates as shown in Figure 9.35 and using the equations below. To produce a state of mixed tension and compression in principal material coordinates, some other loading state will be applied.

$$\begin{cases} \sigma_1 = \sigma_x \cos^2\theta \\ \sigma_2 = \sigma_x \sin^2\theta \\ \tau_{12} = -\sigma_x \cos\theta \sin\theta \end{cases} \tag{9.10}$$

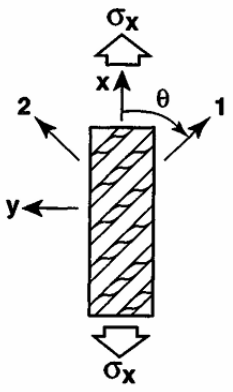

Figure 9.35: Biaxial Stresses from Off-Axis Uniaxial Loading.

Most comparisons of a failure criterion with failure data will be for the glass-epoxy data shown in Figure 9.36 and Table 9.2. The tension data are denoted by solid circles, and the compression data by solid squares. The tension data were obtained by use of dog-bone-shaped specimens, whereas the compression data were obtained by use of specimens with uniform rectangular cross sections. The shear strength for this glass-epoxy is 55 MPa instead of the 41 MPa.

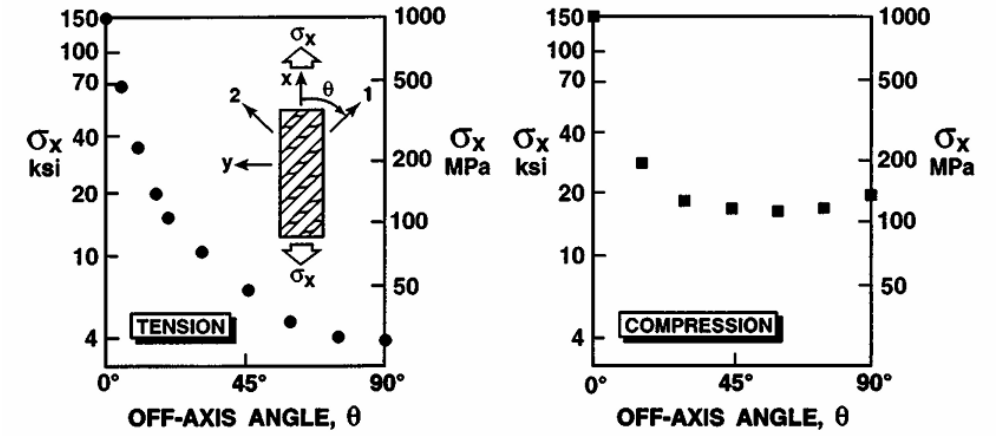

Figure 9.36: Measured Failure Data for Glass-Epoxy in tension (left) and compression (right).

	Glass-epoxy	Boron-epoxy	Graphite-epoxy	Kevlar-epoxy
E_1	54 GPa	207 GPa	207 GPa	76 GPa
E_2	18 GPa	21 GPa	5 GPa	5.5 GPa
ν_{12}	0.25	0.3	0.25	0.34
G_{12}	9 GPa	7 GPa	2.6 GPa	2.1 GPa
X_t	1035 MPa	1380 MPa	1035 MPa	1380 MPa
Y_t	28 MPa	83 MPa	41 MPa	28 MPa
S	55 MPa	124 MPa	69 MPa	44 MPa
X_c	1035 MPa	2760 MPa	689 MPa	276 MPa
Y_c	138 MPa	276 MPa	117 MPa	138 MPa

Table 9.2: Typical Mechanical Properties of Some Composite Materials.

9.3.1. Maximum stress and strain

This is a ***lamina-level criterion*** in which each and every one of the stresses in principal material coordinates must be less than the respective strengths; otherwise, fracture is said to have occurred. This criterion can be summarized with the following linear inequalities:

$$\begin{cases} -X_c < \sigma_1 < X_t \\ -Y_c < \sigma_2 < Y_t \\ |\tau_{12}| < S \end{cases} \tag{9.11}$$

If any of these inequalities is not verified, the assumption is that the material has failed by the failure mechanism associated with the inequality that is violated. The linear inequalities in the above equation are ***able to account for different strengths in tension and compression***. Being σ_1, σ_2 and τ_{12} the stress components in material frame, the above criterion can be expressed in global coordinates using the transformations provided by equations (9.12), yielding:

$$\begin{cases} -\dfrac{X_c}{\cos^2\theta} < \sigma_x < \dfrac{X_t}{\cos^2\theta} \\ -\dfrac{Y_c}{\sin^2\theta} < \sigma_x < \dfrac{Y_t}{\sin^2\theta} \\ |\sigma_x| < \dfrac{|S|}{\cos\theta\,\sin\theta} \end{cases} \tag{9.12}$$

Analogous inequalities can be derived if strains are considered instead of stresses. Two graphical representations of this criterion are provided in order to show the ***limitations of this criterion***. The first one is in Figure 9.37, presenting the theoretical compression and tension fail surfaces for the glass-epoxy in Table 9.2. The ***theoretical cusps in the strength variation*** are not seen in the experimental data. Moreover, the theoretical strength variation does not adequately represent the experimental strength variation, i.e. the strength should decrease smoothly as θ increases. Moreover, the plot in Figure 9.37 is in logarithmic scale, meaning that the maximum stress and strain criteria are incorrect by 100% at θ =30°!

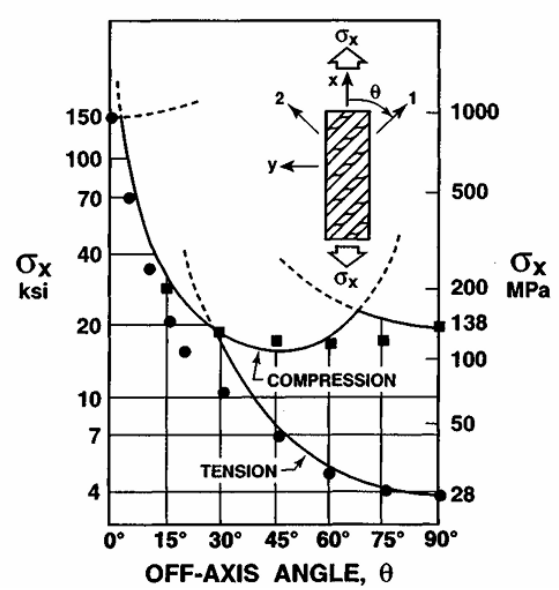

Figure 9.37: Maximum Stress Failure Criterion.

Figure 9.38 shows another crucial limitation of this criterion. Because stress components are compared to the respective allowable via linear inequalities, ***stress components interactions are not considered***. Thus, the highlighted zones in Figure 9.38 cannot be really considered safe, even if in accordance with this criterion, and thus the safe zone must be properly scaled in order to make the criterion usable.

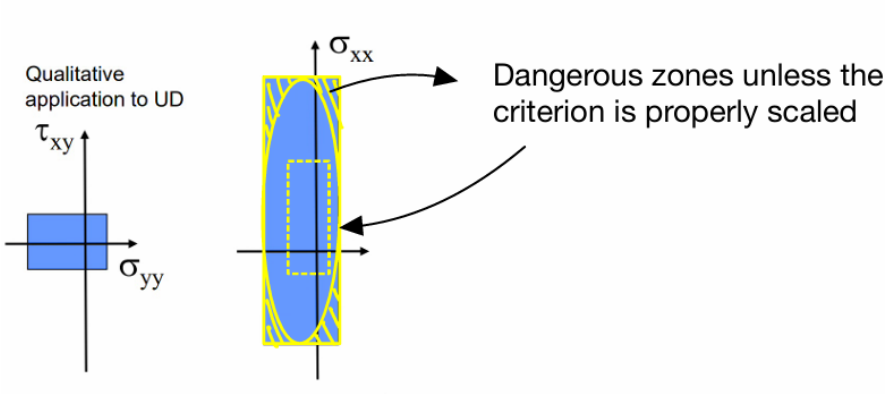

Figure 9.38: application and scaling of max stress/strain criteria.

9.3.2. Tsai-Hill criterion

The previous criterion is able to account for different strength in tension and compression thanks to linear terms. However, it is not able to account for interaction between stress components. In order to achieve this, Hill proposed the following ***lamina level*** criterion of the quadratic type:

$$(G+H)\sigma_1^2 + (F+H)\sigma_2^2 + (F+G)\sigma_3^2 - 2H\sigma_1\sigma_2 - 2G\sigma_1\sigma_3 - 2F\sigma_2\sigma_3 + 2L\tau_{23}^2 + 2M\tau_{13}^2 + 2N\tau_{12}^2 = 1 \tag{9.13}$$

The failure strength parameters F, G, H, L, M and N were related to the usual failure strengths X, Y and S for a lamina by Tsai:

$$\begin{cases} 2N = \dfrac{1}{S^2}, & \text{only } \tau_{12} \\ G+H = \dfrac{1}{X^2}, & \text{only } \sigma_1 \\ F+H = \dfrac{1}{Y^2}, & \text{only } \sigma_2 \\ F+G = \dfrac{1}{Z^2}, & \text{only } \sigma_3 \end{cases} \quad \text{and} \quad \begin{cases} 2F = -\dfrac{1}{X^2} + \dfrac{1}{Y^2} + \dfrac{1}{Z^2} \\ 2G = +\dfrac{1}{X^2} - \dfrac{1}{Y^2} + \dfrac{1}{Z^2} \\ 2H = +\dfrac{1}{X^2} + \dfrac{1}{Y^2} - \dfrac{1}{Z^2} \end{cases}$$

Where the allowables X, Y and Z are selected based on if the load is compressive or tensile. In the case of a ***plane stress state in the 1-2 plane of a UD lamina*** with fibers in the 1-axis, the null components are $\sigma_3 = \tau_{23} = \tau_{31} = 0$. Moreover, $Y = Z$ due to the transverse isotropy of such material (Figure 9.39). Thus, the Tsai-Hill criterion simplifies to:

$$\frac{\sigma_1^2}{X^2} - \frac{\sigma_1\sigma_2}{X^2} + \frac{\sigma_2^2}{Y^2} + \frac{\tau_{12}^2}{S^2} = 1 \tag{9.14}$$

Where the tension or compression ***allowables must be selected based on the signs of the stresses***. Considering the global reference frame of the laminate, the criterion can be expressed as follows:

$$\frac{\cos^4\theta}{X^2} + \left[\frac{1}{s^2} - \frac{1}{X^2}\right]\cos^2\theta\sin^2\theta + \frac{\sin^4\theta}{Y^2} = \frac{1}{\sigma_x^2} \tag{9.15}$$

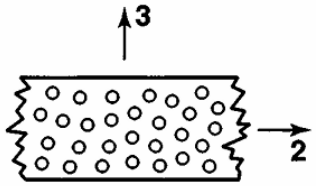

Figure 9.39: cross-section of a UD lamina.

Results for this criterion are plotted in Figure 9.40 along with the experimental data for E-glass-epoxy. It is easy to notice that there is ***good agreement*** between the Tsai-Hill failure criterion and ***experimental data*** at various orientations of the biaxial stress field. Moreover, the variation of strength with angle of lamina orientation is smooth and decreasing as θ grows from 0°, unlike the previous criteria. Thus, the Tsai-Hill failure criterion appears to be much more applicable to failure prediction for this E-glass-epoxy composite material than either the maximum stress criterion or the maximum strain failure criterion. A second advantage of the Tsai-Hill criterion is that it is a ***quadratic criterion***, which implies that it's able to account for interactions between

different stress components. In other words, interaction effects are accounted for by the terms $\sigma_1\sigma_2$ and $\sigma_2\sigma_3$ and $\sigma_1\sigma_3$.

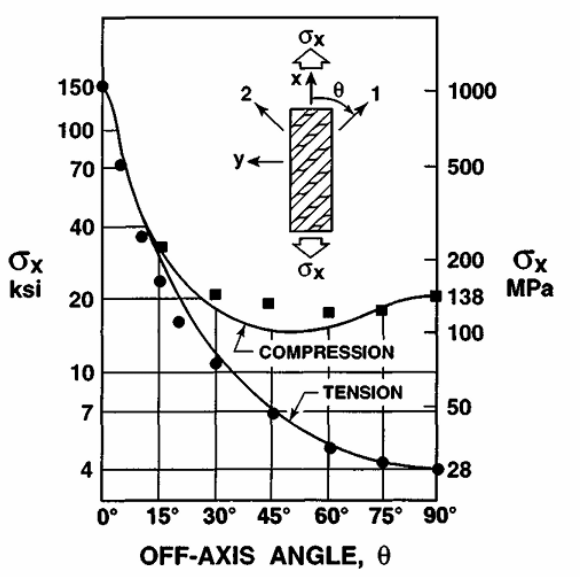

Figure 9.40: Tsai-Hill Failure Criterion for glass-epoxy.

9.3.2 Hoffmann criterion

Another ***lamina-level*** quadratic criterion, Hoffmann added linear terms to Hill's equation in order to account for different strengths in tension and compression. The general formulation of the criteria in 3D is the following:

$$H_1(\sigma_2-\sigma_3)^2 + H_2(\sigma_3-\sigma_1)^2 + H_3(\sigma_1-\sigma_2)^2 + H_4\sigma_1 + H_5\sigma_2 + H_6\sigma_3 + H_7\tau_{23}^2 + H_8\tau_{13}^2 + H_9\tau_{12}^2 = 1 \qquad (9.16)$$

Where the coefficients H_i are related to the material allowables in principal material coordinates as follows:

$$2H_1 = -\frac{1}{X_T^2X_C^2} + \frac{1}{Y_T^2Y_C^2} + \frac{1}{Z_T^2Z_C^2} \quad H_4 = \frac{1}{X_T} - \frac{1}{X_C} \quad H_7 = \frac{1}{S_{23}^2}$$
$$2H_2 = +\frac{1}{X_T^2X_C^2} - \frac{1}{Y_T^2Y_C^2} + \frac{1}{Z_T^2Z_C^2} \quad H_5 = \frac{1}{Y_T} - \frac{1}{Y_C} \quad H_8 = \frac{1}{S_{13}^2}$$
$$2H_3 = +\frac{1}{X_T^2X_C^2} + \frac{1}{Y_T^2Y_C^2} - \frac{1}{Z_T^2Z_C^2} \quad H_6 = \frac{1}{Z_T} - \frac{1}{Z_C} \quad H_9 = \frac{1}{S_{12}^2}$$

For composite design we usually deal with plates and shells, in which the stress state can be approximated as a ***plane stress state*** in the plane 1-2. In such simplified case an ***inconsistency*** can be spotted: even if the stress components related to axis 3 are put to zero, $\sigma_3 = \tau_{13} = \tau_{23} = 0$, the coefficients H_1, H_2 and H_3 survive. The inconsistency lies in the fact these terms are a function of the allowables in 3 direction, Z_T and Z_C, while the state of stress is assumed to be plane in 1-2. Such problem can be dealt with by assuming that allowables along 3 are the same as the ones along y, which is ***verified for transverse isotropic materials***, i.e. ***UD laminates***. In this case, the allowables are such that $Y = Z$ and the criterion simplifies to:

$$\frac{\sigma_1}{X_T X_C} - \frac{\sigma_1 \sigma_2}{X_T X_C} + \frac{\sigma_2^2}{Y_T Y_C} + \left(\frac{1}{X_T} - \frac{1}{X_C}\right)\sigma_1 + \left(\frac{1}{Y_T} - \frac{1}{Y_C}\right)\sigma_2 + \frac{\tau_{12}^2}{S_{12}^2} = 1 \tag{9.17}$$

The graphical representation of the 2D case is reported in Figure 9.41: the Hoffmann and the Tsai-Hill criterion are both ***ellipsoids*** in the stress planes. Contrarily to the maximum stress/strain criteria, the ellipsoidal shape is granted by the quadratic terms. That is, when interaction effects are accounted for between the various stress components (Hoffmann and Tsai-Hill), the safe zone is "rounded off" with respect to when they are not accounted for (max stress/strain). Figure 9.42 shows that a compressive normal stress σ_{yy} (in material coordinates σ_2), the matrix dominated direction, increases shear resistance of the matrix. Figure 9.43 shows that the Hoffmann criterion is in very good agreement with experimental data for both glass-epoxy and boron-epoxy laminates.

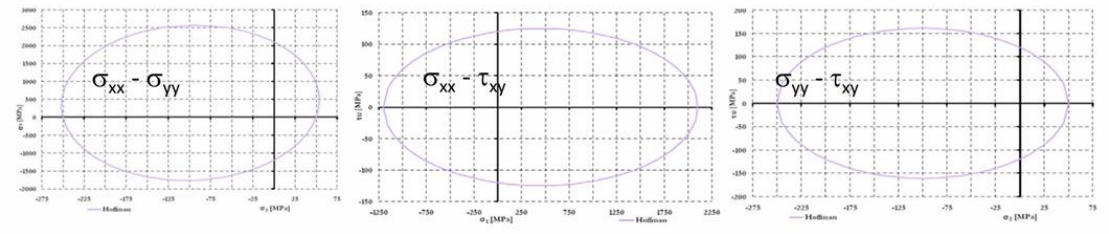

Figure 9.41: Hoffmann criteria in multiple planes.

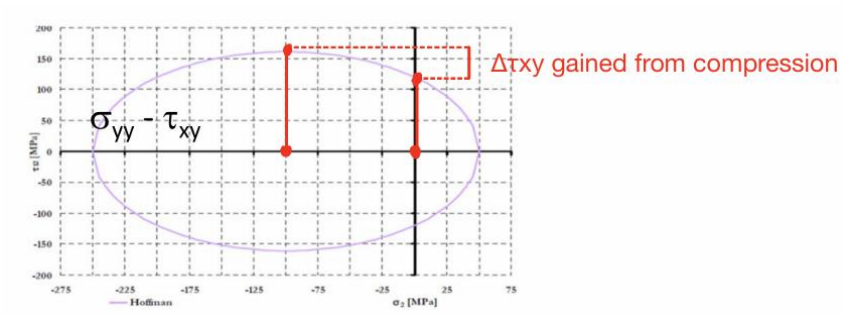

Figure 9.42: effect of compressive σ_{yy} on τ_{xy}.

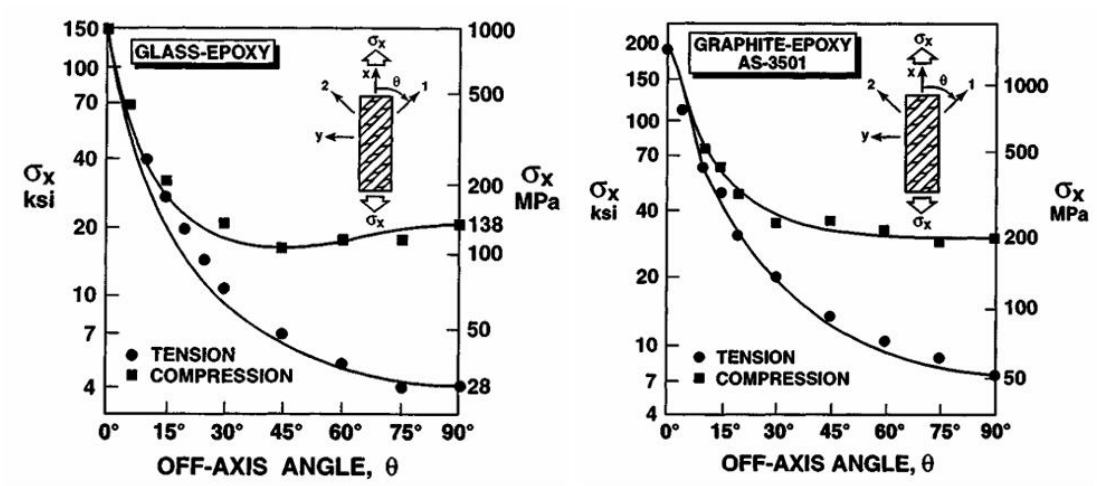

Figure 9.43: Hoffmann criterion for glass-epoxy (left) and graphite-epoxy (right).

9.3.3. Tsai-Wu criterion

Another ***lamina-level*** quadratic form that gets rid of the inconsistency of the Hoffmann criterion. An intuitive way to improve the correlation between a criterion and experimental data is to increase the umber of terms in the prediction equation. Tsai and Wu proposed a failure surface that exists in a six-dimensional space in the form of:

$$F_i\sigma_i + F_{ij}\sigma_i\sigma_j = 1 \tag{9.18}$$

Using Voight notation, so that $\sigma_4 = \tau_{32}, \sigma_5 = \tau_{31}$ and $\sigma_6 = \tau_{12}$, the complete form of the above equation would be:

$$\begin{aligned} F_1\sigma_1 + F_2\sigma_2 + F_3\sigma_3 + F_{11}\sigma_1^2 + F_{22}\sigma_2^2 + F_{33}\sigma_3^2 + F_{44}\tau_{32}^2 + F_{55}\tau_{31}^2 + F_{66}\tau_{12}^2 \\ + 2F_{12}\sigma_1\sigma_2 + 2F_{23}\sigma_2\sigma_3 + 2F_{31}\sigma_3\sigma_1 = 1 \end{aligned} \tag{9.19}$$

Where the coefficients F_i and F_{ij} are obtained as follows:

$$\begin{aligned} F_{11} &= \frac{1}{X_C X_T} \quad F_{44} = \frac{1}{S_{32}^2} \quad F_1 = \frac{1}{X_T} - \frac{1}{X_C} \\ F_{22} &= \frac{1}{Y_C Y_T} \quad F_{55} = \frac{1}{S_{31}^2} \quad F_2 = \frac{1}{Y_T} - \frac{1}{Y_C} \quad F_{12} = ? \\ F_{33} &= \frac{1}{Z_C Z_T} \quad F_{66} = \frac{1}{S_{12}^2} \quad F_3 = \frac{1}{Z_T} - \frac{1}{Z_C} \end{aligned}$$

In the case of a plane-stress state, only the components related to the 1-2 axes are retained, and equation (9.19) simplifies to:

$$F_1\sigma_1 + F_2\sigma_2 + F_{11}\sigma_1^2 + F_{22}\sigma_2^2 + F_{66}\tau_{12}^2 + 2F_{12}\sigma_1\sigma_2 = 1 \tag{9.20}$$

As usual, the terms that are linear in the stresses are able to account for different strengths in tension and compression, generating a rectangular failure surface in the stress space. The terms that are quadratic are able to account for stress interaction effects, rounding the rectangle in an ellipsoid. It is easy to notice that, for the 2D stress state in the 1-2 plane, the fallacy of the Hoffmann criteria is dealt with. Thus, ***this criterion can be reliably applied to fabric composites***. Moreover, in the plane stress case, the coefficient F_6 is null, reason why it does not appear in equation (9.20). Moreover, the coefficient F_{12} is new and quite different from the coefficient $H = 1/2X^2$ of the plane stress state Tsai-Hill criterion. Furthermore, the determination of the F_{12} coefficient requires a very complicated test. Thus, two choices are available:

$$F_{12} = \begin{cases} -\frac{1}{2}\sqrt{F_{11}F_{22}}, & \text{proposed by Tsai} \\ 0, & \text{in good agreement with experimental data} \end{cases} \tag{9.21}$$

It should be noted that F_{12} seems to have little impact on the final results. It can be proven that the Hoffmann and Tsai-Hill criteria are a special case of the Tsai-Wu criterion, which thus has more general validity, making this a ***more complete criterion***. The Tsai-Wu criterion also has a ***greater curve-fitting capability*** then the previous criteria due to an additional term in its formulation.

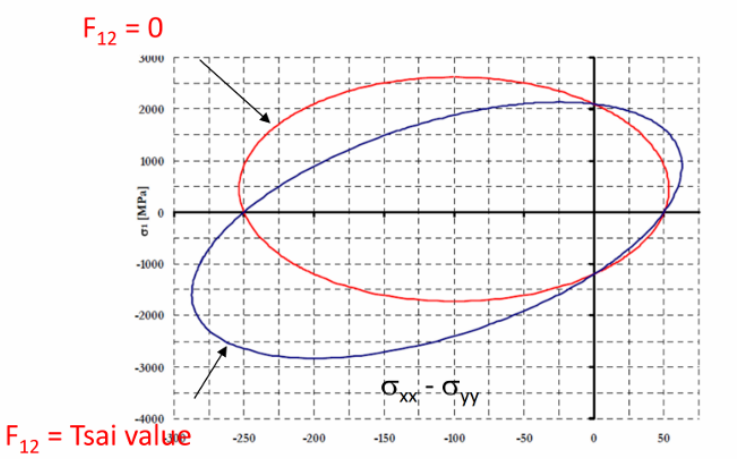

Figure 9.44: graphical representation of the Tsai-Wu criteria.

9.3.4. Hashin-Rotem criterion

A ***lamina-level*** criterion that aims to provide an information about not only *if* a ply fails but also about *how* it fails. To achieve this, the criterion uses ***separate sub-criteria*** for different failure modes. The ability to identify the failure mode is important to differentiate between progressive and critical failure, and to identify possible modification of the layup in order to reinforce the laminate. The criteria is derived from more complex criteria and is ***only applicable only to UD plies***. The failure criteria are maximum stress for fiber failure (1-axis) and quadratic form for matrix failure (2-axis).

$$\begin{cases} \dfrac{\sigma_1}{X_T} = 1, & \sigma_1 > 0 \\ -\dfrac{\sigma_1}{X_C} = 1, & \sigma_1 < 0 \\ \left(\dfrac{\sigma_2}{Y}\right)^2 + \left(\dfrac{\tau_{12}}{S_{12}}\right)^2 = 1 \end{cases} \tag{9.22}$$

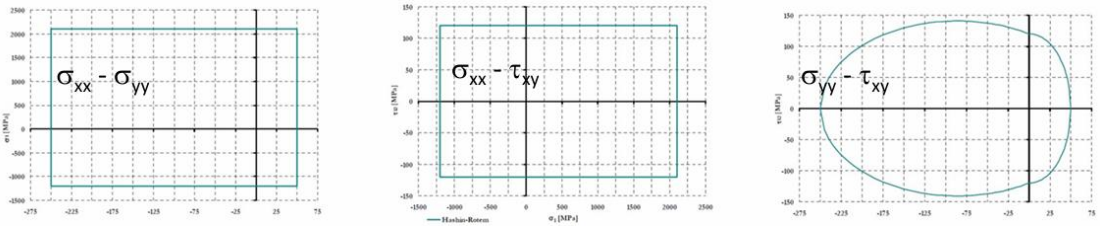

Figure 9.45: 2D stress failure surfaces according to Hashin criteria.

Note that this criterion uses a linear inequality for fiber failure, and thus it is not conservative in this failure mode because it does not consider stress interaction. This is clearly visible in all stress planes related to σ_1. Recall that more advanced versions of this criteria exists, this is a simplified 2D version for UD laminates. In fact, an ***improved version of the Hashin*** takes into consideration:

- Positive effect of compressive σ_2 on failure induced by τ_{12} via a parameter μ, that usually assumes values in the range $[0.4 - 0.8]$.
- Stress interaction in fiber failure, which becomes quadratic and includes τ_{xy}.

$$\begin{cases} \left(\frac{\sigma_1}{X}\right)^2 + \left(\frac{\tau_{12}}{S_{12}}\right)^2 = 1 \\ \left(\frac{\sigma_2}{Y_C}\right)^2 + \left(\frac{\tau_{12}}{S_{12} - \mu\sigma_2}\right)^2 = 1 \end{cases} \tag{9.23}$$

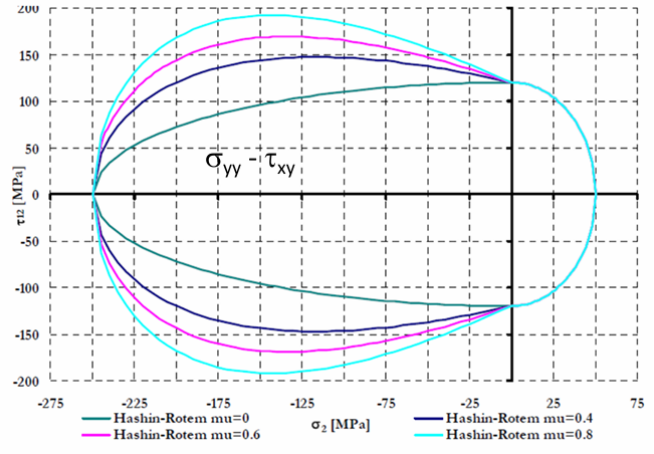

Figure 9.46: improved Hashin criteria.

9.3.5. Delamination onset criteria

A ***lamina-level*** criterion that necessitates of a complete 3D stress state to be available. The onset of delamination damage can be detected by using a simple quadratic criteria that only considers out-of-plane stress components:

$$\left(\frac{\sigma_3}{Z}\right)^2 + \left(\frac{\tau_{13}}{S_{13}}\right)^2 + \left(\frac{\tau_{23}}{S_{23}}\right)^2 = 1 \tag{9.24}$$

However, this criterion ***does not consider the interaction with in-plane stress components***, which is accounted for by interactive 3D criteria. However, the separation between in-plane and out-of-plane stress components is a typical choice, since these interactions are difficult to capture with strength criteria.

9.3.6. Comparison of lamina-level criteria

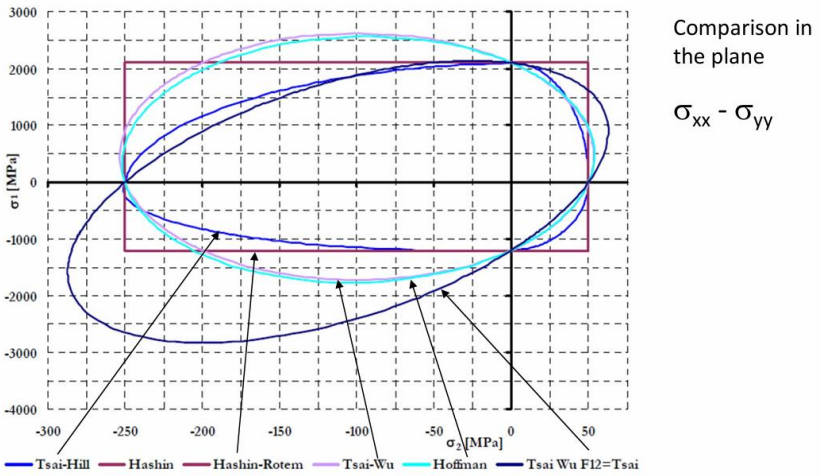

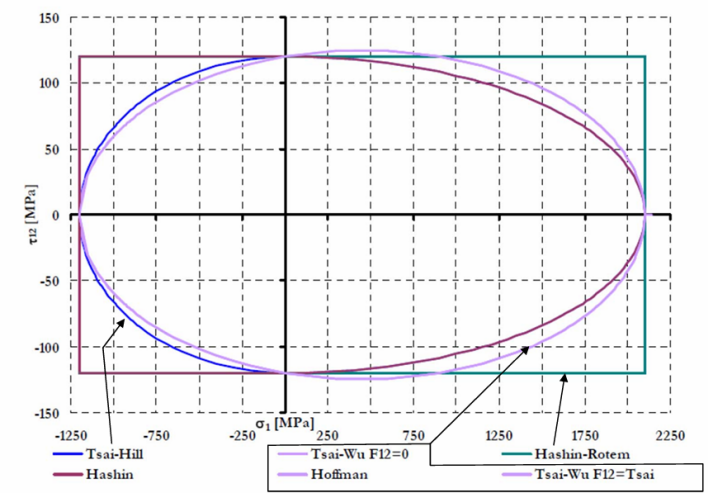

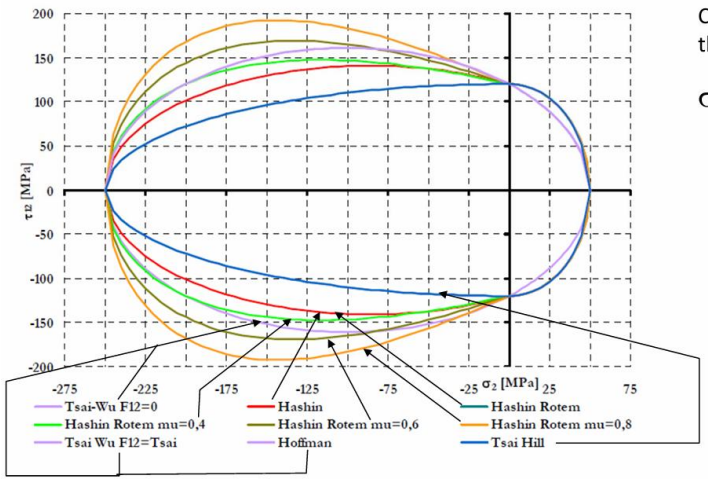

9.3.7. Laminate level

In this case ***strength analysis and allowables are related to strain rather than stress***. This is due to the fact that stress is subject to local amplification, and it can only be approximated, analytically or numerically. Moreover, strain can be accurately predicted even by means of analytical theories, such as CLT (section 0). Two strain levels are of interest: the one at which non-catastrophic first-ply failure occurs, and the other at which catastrophic failure occurs, identifying the ultimate strain ε_{max}. We present the ***fiber failure approach***, a criteria is valid for laminates with fiber-dominated behavior, meaning matrix cracking has negligible effects (it's accounted for anyway because allowables are laminate level). Thus, the criteria is based only on fibers strain allowables. Such laminates are called well-designed laminates.

$$\begin{matrix} X_{C\varepsilon} < \varepsilon_1 < X_{T\varepsilon} & |\varepsilon_1 - \varepsilon_2| < \left(1 + \nu_{12}^{ply}\right) X_{T\varepsilon} \\ Y_{C\varepsilon} < \varepsilon_2 < Y_{T\varepsilon} & |\varepsilon_1 - \varepsilon_2| < \left(1 + \nu_{12}^{ply}\right) X_{C\varepsilon} \end{matrix} \tag{9.25}$$

Of course, since allowables are laminate level, the ***criterion can be tuned*** to account for notches, open or filled holes, impact damage etc. by using the allowables derived from the tests (remember this is the point!). The graphical representation in the 1-2 strain plane of the failure boundary is the following:

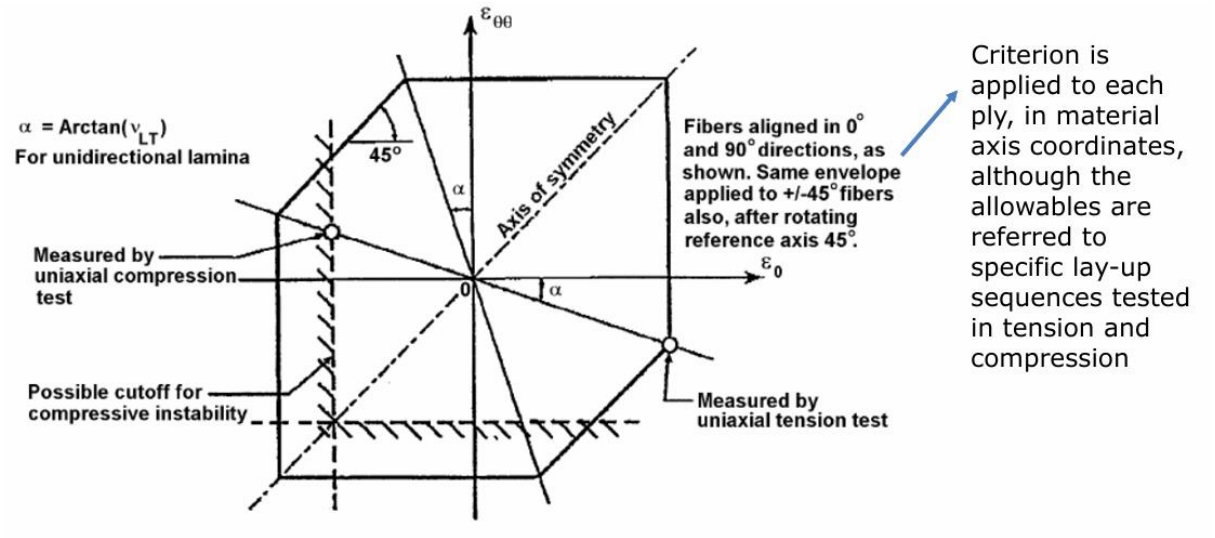
$\varepsilon_{\theta\theta}$
α = Arctan(ν_{LT})
For unidirectional lamina
45°
α
Axis of symmetry
Fibers aligned in 0° and 90° directions, as shown. Same envelope applied to +/-45° fibers also, after rotating reference axis 45°.
Measured by uniaxial compression test
0
ε_0
α
Possible cutoff for compressive instability
Measured by uniaxial tension test
Criterion is applied to each ply, in material axis coordinates, although the allowables are referred to specific lay-up sequences tested in tension and compression

Figure 9.47: safe zone of fiber failure approach.

9.4. Building block approach

The building block approach is a characterization process (design and testing) used for aerostructures [5] – chapter 4. Such approach has two fundamental characteristics, the first one being that ***analytical theory is combined with testing*** (1). Analytical theory alone is not sophisticated enough to accurately predict the behavior of complex structures, especially in the presence of defects. Testing alone can be extremely expensive due to the number of specimens and tests needed to verify geometry, loading, environment and failure mode. In the building block approach, analytical predictions are verified by tests, and testing is guided by analysis. The second fundamental aspect of the building block approach is that ***testing and analysis are carried out at different levels of the aerostructure*** (2), starting from specimen and progressing through structural elements until the full scale product. ***Each level builds on the knowledge gained from the previous, less complex, level***. This ensures that, in the characterization process, a greater number of smaller less expensive specimens are tested, while bigger full scale components are tested fewer times. Furthermore, the probability of significant surprises materializing at the end of the program is greatly reduced by testing at various levels.

In simple terms, the building block approach divides the design process in many levels, each building on the previous one, and combines testing and analytical theory in order to reduce the overall effort, in terms of time and costs, necessary to safely design and test aerostructures.

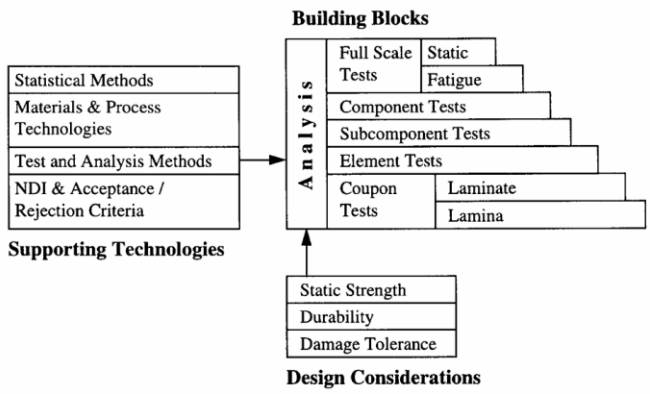

Figure 9.48: building block integration.

Note that the building block approach it's not standardized. Usually, different programs may have different requirements that impose program-specific criteria. Furthermore, different companies implement the building block approach at different levels of rigor. These aspects affect the specifics of how the building block approach is implemented. What is standardized are the first and last levels. On the first level, regulations impose how to conduct the experiments illustrated in section 9.2.1 and how material allowables should be obtained. On the last level, regulation impose how a structure should behave when loaded with LL and UL (see section 0).

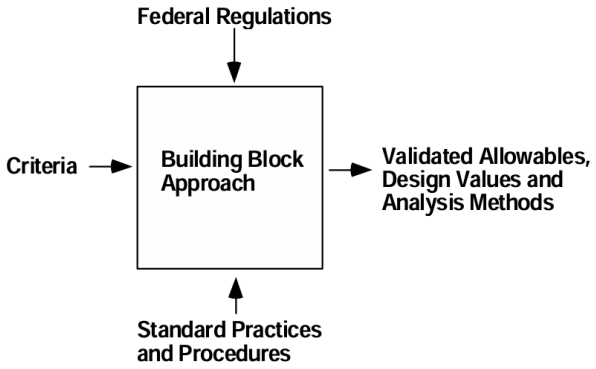

Figure 9.49: factors that influence building block approach implementation.

Each block of the program, besides the one at the bottom, has the general workflow idealized in Figure 9.50. In short, knowledge from the previous level is combined with requirements to be met and used to define the design and analysis step. If analysis is satisfactory, we proceed to testing, if not design and/or analysis must be changed. Verification testing now takes place. If satisfactory results are obtained, we progress to the next level; if not we have to review the test methodology or the design of the component at this level.

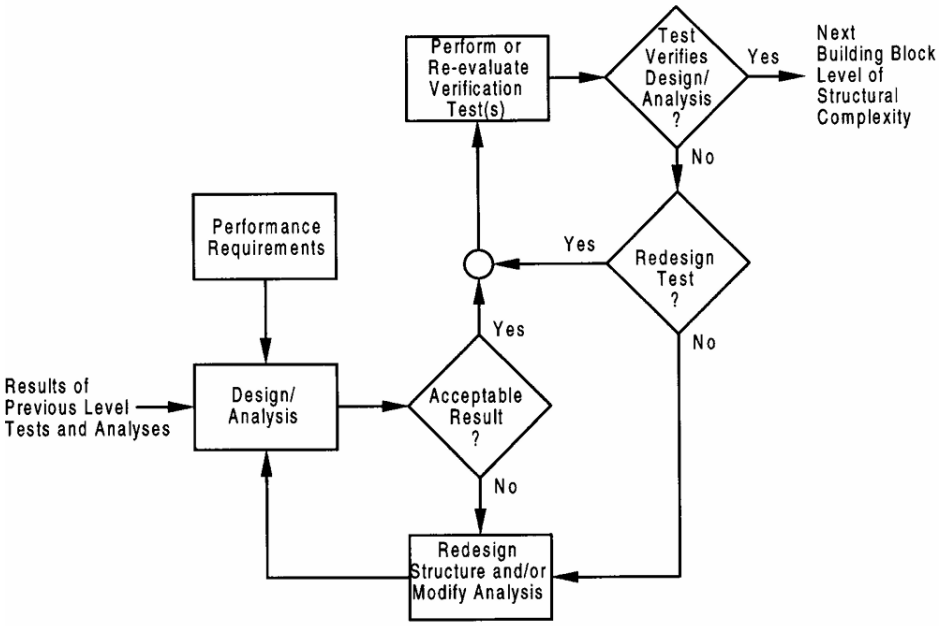

Figure 9.50: idealized general building block scheme (one level).

The workflow depicted in Figure 9.50 convey the idea that the BB approach is a sequence of steps that neatly progress in order from one block to the next. However, a typical building block workflow is not so linear. In reality, portions of different blocks overlap in time, due to schedule and availability of resources. An example of a typical building block approach is shown in Figure 9.51.

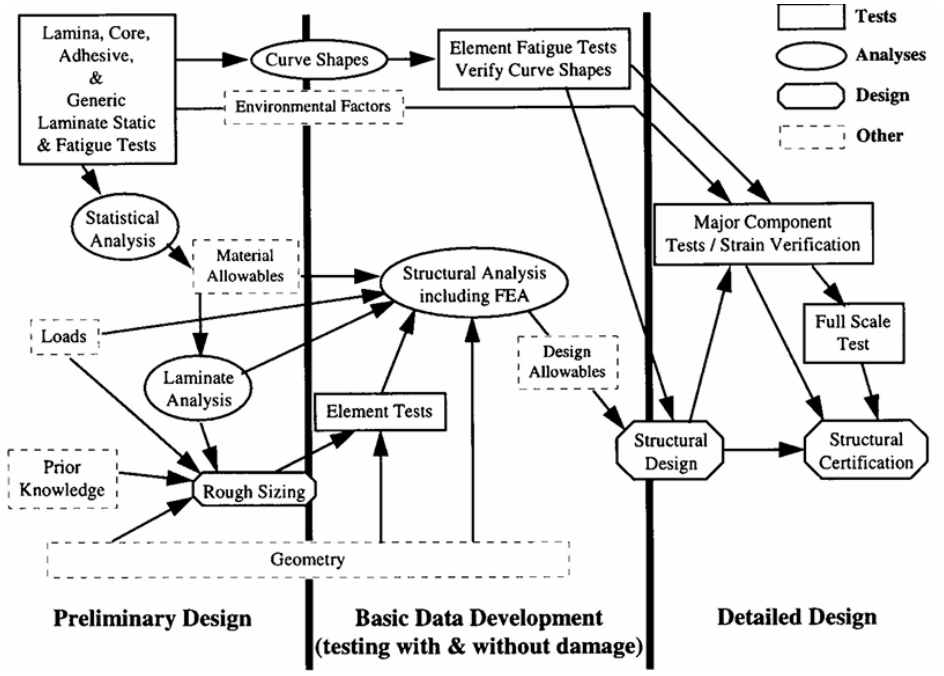

Figure 9.51: typical building block workflow.

Particular focus in Figure 9.51 should be given to the position of material allowables and design allowables, the central role of FEA and the stages at which design is carried out. Recall the crucial difference between material and design allowables (see section 0):

- Material allowable: material property statistically derived from test data.
- Design allowable: properly scaled material property based on engineering considerations, approved for design and analysis of structures.

9.4.3. Application of building block approach

The building block approach, when applied to commercial aircraft, can be divided in three main groups, and each composed by a number of blocks, for a total of 6 blocks, as illustrated in Figure 9.52.

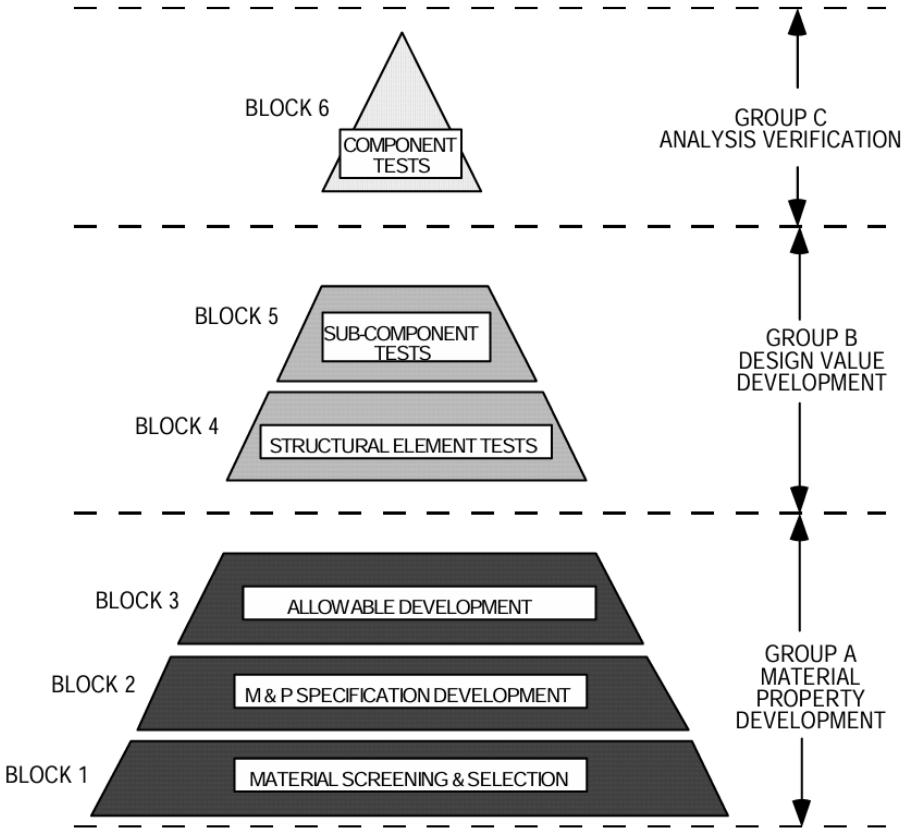

Figure 9.52: building block approach.

9.4.3.1. Group A - material property development

This group deals with those blocks that have the main purpose of defining the general behavior of the material. Here we do numerous tests to determine material allowables on less complex specimens. This group is made of three blocks:

- Block 1 – material screening and selection: gather data related to possible material candidates and actually make the decision on which to use in the program.
- Block 2 – material process and specification development: we need to qualify the material by testing for its key mechanical properties. Basically, we want to understand how the material is affected by process variables to then define the specification for the material.
- Block 3 – allowable development: we perform the tests needed to develop material allowables. The specific allowables to obtain depend on the type of aircraft (civil, military, business etc.).

9.4.3.2. Group B - design value development

The objective of this group is to define the design allowables that reflect the behavior of the actual structure. Clearly, a preliminary design of the structure to be tested is necessary. The design allowables obtained at this stage may become very specific and not applicable to any other programs. This group is made of two blocks:

- Block 4 – structural elements test: tests at this level are performed on recurring structural elements within the aircraft. The goal of these tests is to assess the sensitivity of the structural element to damages/defects caused by the fabrication process (1). A second objective of testing in block 4 is to characterize the local failure modes related to the structural elements (2). Of course, design allowables at this level start to become unique, and usually cannot be applied to other programs. The data obtained is used to support analytical or numerical models and develop appropriate safety margins, or in other words, design allowables.

  Examples of structural elements evaluated here are:
  - Junctions of composite elements.
  - Delaminations in curved and tapered elements, especially in non-conventional designs.
  - Crippling strengths of stiffeners: these may be co-bonded with another structural component; thus we need to obtain design allowables for local failure modes.
  - Sandwich panels.

  The number of tests at this stage of the building block approach can exceed several hundreds.

- Block 5 – sub-components tests: here we test sections of a component, like wing sections, empennage sections, fuselage sections etc. The design allowables obtained by this stage are more representative of the actual structure than the previous block.

  The objectives of this block are:
  - Design allowables derived from structural elements are able to predict structural behavior.
  - Effect of damage – static: residual strength is evaluated and appropriate design allowables are developed.
  - Effect of damage – fatigue: we need to prove no detrimental damage growth under operational fatigue loading.
  - Environmental effect testing may be meaningful at this level.

9.4.3.3. Group C - analysis verification

This group is made of only one block: component testing. These tests are one level below the final full scale test. At this level extensive verification of analysis and computer modelling is carried out with two objectives:

- Verification of internal load modelling and reliability of results.
- Large-scale verification of design and analysis methodology.

At this level we test for behavior of the components with BVID, crack (no) growth under fatigue loading.

10. Appendix

10.1. Data analysis

10.1.1. Statistical descriptive quantities

In this section we present some summarizing statistics, where a statistic is a numerical quantity, whose value is determined by the data [6] – pp 83 of the pdf.

10.1.1.1. Sample mean, median and mode

In this section we introduce some ***statistics that are used to describe the center of a data set***.

To begin, suppose we have a data set of n values $x_1, x_2, \dots, x_n$. The ***sample mean*** $\bar{x}$ is the arithmetic average of these values

$$\bar{x} = \sum_{i=1}^{n} \frac{x_i}{n} \qquad 10.1$$

Assume to have a data set $y_1, y_2, \dots, y_n$ such that $y = ax + b$, where a, b are constants. Then, to find the sample mean of the Y population we'll write:

$$\bar{y} = \sum_{i=1}^{n} \frac{y_i}{n} = \sum_{i=1}^{n} \frac{ax_i + b}{n} = a \sum_{i=1}^{n} \frac{x_i}{n} + b = a\bar{x} + b$$

Sometimes we want to determine the mean value of a dataset presented in a frequency table listing k distinct values $v_1, \dots, v_k$ and the corresponding frequencies $f_1, \dots f_k$. The mean value of such data set can be computed as the *weighted average* of the distinct values, where the weight is the relative frequency f_k/n, where $k = \sum f_k$:

$$\bar{x} = \sum_{i=1}^{k} v_i \frac{f_i}{n}$$

The ***sample median*** is the middle value of the data set when the data values are arranged in increasing value. To find the sample median, first arrange the n data values from smallest to largest then:

- If n is odd, the median is the value in position $(n + 1)/2$.
- If n is even, the median is the average of the values in position $n/2$ and $n/2 + 1$.

It's clear that while the sample mean is affected by extreme values that are much larger/smaller than the others, the sample median is not, since this value makes use only of one or two middle values.

The ***sample mode*** is the value that occurs with the highest frequency. If no single value occurs most frequently, than the values with the highest frequency are called *modal values*.

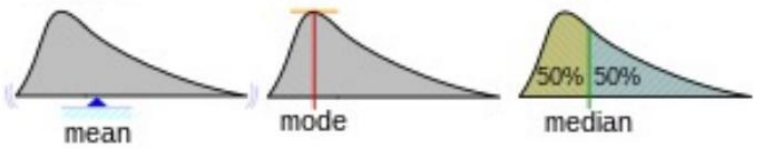

Figure 10.1: comparison of sample mean, median and mode.

10.1.1.2. Sample variance and standard deviation

Aside from the statistics that represent the central tendencies of a dataset, the ***statistics representing the spread or variability of data sets*** must also be introduced.

The ***sample variance*** $\boldsymbol{s^2}$ is the statistic that measure the average value of the square distance between the data values and the sample mean. In other words:

$$\boxed{s^2 = \sum_{i=1}^{n} \frac{(x_i - \bar{x})^2}{n-1}} \qquad 10.2$$

Moreover, the square of the distance $x_i - \bar{x}$ can be rewritten as follows:

$$\sum_{i=1}^{n}(x_i - \bar{x})^2 = \sum_{i=1}^{n}\left(x_i^2 - 2x_i\bar{x} + \bar{x}^2\right) = \sum_{i=1}^{n} x_i^2 - 2\bar{x}\sum_{i=1}^{n} x_i + \sum_{i=1}^{n}\bar{x}^2 = \sum_{i=1}^{n} x_i^2 - 2n\bar{x}^2 + n\bar{x}^2$$

$$\sum_{i=1}^{n}(x_i - \bar{x})^2 = \sum_{i=1}^{n} x_i^2 - n\bar{x}^2 \qquad 10.3$$

Where we used $n\bar{x} = \sum x_i$. Such relation is useful when considering the case $y_i = a + bx_i$ for $i = 1, \dots, n$, being $\bar{y} = a + b\bar{x}$ we can write:

$$\sum_{i=1}^{n}(y_i - \bar{y})^2 = \sum_{i=1}^{n}(a + bx_i - a - b\bar{x})^2 = b^2\sum_{i=1}^{n}(x_i - \bar{x})^2$$

In other words, *adding a constant* a *to each data value does not change the sample variance, while multiplying each data value by constant* b *results in a new sample variance of* $(bs)^2$.

The sample ***standard deviation*** $\boldsymbol{s}$ is the square root of the variance, it is measured in the same unit as the data.

$$\boxed{s = \sqrt{\sum_{i=1}^{n} \frac{(x_i - \bar{x})^2}{n-1}}} \qquad 10.4$$

10.1.1.3. Sample percentiles

Simply stated, the sample $100p$ percentile of a data set is that data value such that at least $100p$ percent of data values are less than or equal to it and at least $100(1-p)$ percent are greater than or equal to it. Note that $0 \leq p \leq 1$. To determine the sample $100p$ percentile of a data set of size n, we need to determine the data values that:

- At least np are of the values are less than or equal to it.

- At least $(1-p)n$ are greater than or equal to it.

To accomplish this, first arrange the data in increasing order. Then, note that if np is not an integer, say it is 17.6, the only data value that satisfied the percentile conditions is the smallest integer exceeding np, 18 in this case.

Another way to determine the $100p$ percentile is to determine the value x_p such that the cumulative probability that $X < x_p$ is p:

$$\Pr(X \leq x_p) = p \tag{10.5}$$

Some important percentiles can be introduced:

- First quartile $p = 0.25$: the sample 25 percentile, the value x_{25} that is greater than or equal to 25% of the population.
- Second quartile $p = 0.5$: the sample 50 percentile, the value x_{50} that is greater than or equal to 50% of the population. This value is also known as the ***sample median***.
- Third quartile $p = 0.75$: the sample 75 percentile, the value x_{75} that is greater than or equal to 75% of the population.

10.1.2. Chebyshev's inequality

Let $\bar{x}$ and s be the sample mean and standard deviation of a data set. Assuming that $s > 0$, Chebyshev's inequality states that for any value $k \geq 1$, more than $100(1 - 1/k^2)$ percent of the data lies between $\bar{x} - ks$ and $\bar{x} + ks$. In other words, *by deciding k we decide the distance from the mean value $\bar{x}$ in both directions, and Chebyshev inequality tells us the percentage of data points contained in this distance*. Some notable values of k are the following:

- $k = 3/2$: we get that 55.6% of the data points lie within $1.5s$ from $\bar{x}$.
- $k = 2$: we obtain that 75% of data points lie within $2s$ of $\bar{x}$.
- $k = 3$: we obtain that 88.9% of data points lie within $3s$ of $\bar{x}$.

Chebyshev inequality. Let $\bar{x}$ and s be the sample mean and standard deviation of the data set consisting of the data $x_1, \ldots, x_n$, where $s > 0$. Let S_k be the set of data points that lie within k standard deviations of $\bar{x}$:

$$S_k = \{i : |x_i - \bar{x}| < ks\}$$

And let $|S_k|$ be the number of elements of S_k. Then, for any $k > 1$:

$$\frac{|S_k|}{n} \geq 1 - \frac{n-1}{nk^2} \tag{10.6}$$

One sided Chebyshev inequality. Suppose now that we ae interested in the fraction of data values $N(k)$ that exceed the sample mean by $k > 0$ standard deviations. It can be proven that:

$$\frac{N(k)}{n} \leq \frac{1}{1+k^2} \tag{10.7}$$

10.1.3. Elements of probability

We define an *event/outcome* A as the result of an experiment, and the process of obtaining such result is called *sampling*. There are two possible interpretations of the *probability of an event* [6] – pp. 53 (118 of pdf):

1. Frequency interpretation: probability of an event/outcome is the proportion of the samples that result in that outcome/event. Thus, based on this definition, two observations can be made: (1) probability is a property of the event/outcome and (2) the underlying assumption is that the event/outcome can be repeated.
2. Subjective interpretation: does not consider probability as a property of the event/outcome but rather as a belief of the person who is quoting the probability, concerning the change that the event will occur.

Regardless of which interpretation one gives to probability, however, there is a consensus that the mathematics of probability are the same in either case. For the scope of this document, the ***frequency interpretation will be adopted***. Thus, probability of the event A is the ratio of the number n of occurrences of A over the total number of trials N:

$$0 \leq \Pr(A) = \lim_{N\to\infty} \frac{n}{N} \leq 1 \tag{10.8}$$

So, intuitively, as you repeat the experiment more and more $N \to \infty$ the relative frequency n/N converges to the true probability of A. Such finite number is bounded by a 0 as lower limit, impossible event, and 1 as upper limit, certain event.

If the probability is intended as probability of failure, as it will be in this document, then we can define the ***reliability R*** of an event as the complementary quantity to the probability, such that $R(A) + \Pr(A) = 1$. Naturally, the reliability is also bounded by 0 and 1.

$$0 \leq R(A) = 1 - \Pr(A) \leq 1 \tag{10.9}$$

Some important cases can be examined immediately, consider two possible events A and B, then:

- *Mutually exclusive*: A and B cannot happen at the same time (example: rolling a die, event A is rolling a 2, event B is rolling a 5). The probability that the outcome of the experiment is *either* A or B is the sum of the probabilities.

$$\Pr(A + B) = \Pr(A) + \Pr(B)$$

- *Indipendent*: A and B do not influence each other, the probability that the two events occur *together* is the product of the two probabilities.

$$\Pr(AB) = \Pr(A) \cdot \Pr(B)$$

- *Not mutually exclusive and independent*: A and B can happen at the same time (example: rolling a die, event A is rolling an even number, event B is rolling a number greater than 3). So the probability that either A or B happen is the sum of the probability that they occur independently, minus the probability that they occur at the same time (sometimes when A happens so does B, and vice versa, so we must not count this twice in the probability).

$$\Pr(A + B) = \Pr(A) + \Pr(B) - \Pr(A) \cdot \Pr(B)$$

10.1.3.1. Random variables

When an experiment is performed, we are often not interested in all of the details of the experiment result but only in the value of some numerical quantity determined by the result of the experiment [6] – pp. 89 (153 pdf). These quantities of interest are known as ***random variables X***. There are two types of random variables:

- Discrete*:* number of defects, life of a component, number of bits in a file etc.
- Continuous*:* pressure, temperature, time and so on.

The random variable X represents all of the possible outcomes of an experiment, meaning all of the possible events. So considering the event A, mathematically $A \subset X$. So if $\boldsymbol{x}$ is the ***observed variable***, the actual outcome of the experiment, then if the event A occurs it must be $x \in A$.

The ***cumulative (probability) distribution function F*** of the random variable X is defined for any real number x as:

$$F(a) = \Pr\{X \leq x\} \tag{10.10}$$

Meaning, $F(X)$ is the probability that X takes on a value that is less than or equal to x. The cumulative function F is a tool we can use to describe the probability characteristic of the random variable X. For example, suppose we want to compute $\Pr\{a < X \leq b\}$, then we could write:

$$\Pr\{a < X \leq b\} = \Pr\{X \leq b\} - \Pr\{X \leq a\} = F(b) - F(a)$$

Discrete random variables. Discrete random variables are variables whose set of possible values is a sequence, either finite or infinite. For a discrete random variable X, we define the ***probability mass function*** $\boldsymbol{p(a)}$ of X as:

$$0 \leq p(a) = \Pr\{X = a\} \leq 1 \tag{10.11}$$

The cumulative distribution function $F(x)$ can be expressed as a function of $p(x)$ as follows:

$$F(a) = \sum_{all\ x \leq a} p(x) \tag{10.12}$$

Since X is a discrete random variable, the cumulative function $F(a)$ will be a step function (Figure 10.2).

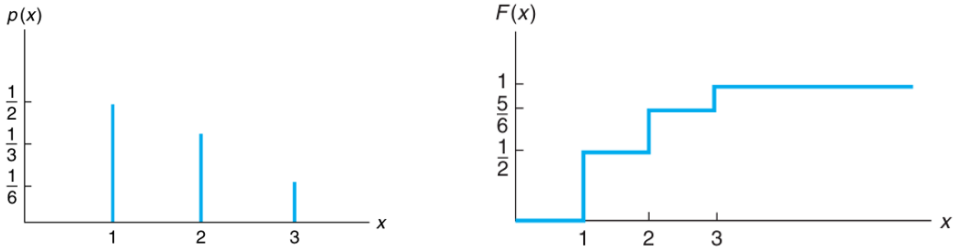

Figure 10.2: $p(x)$ for $x = 1,2,3$; left) corresponding cumulative function.

Continuous random variables. We say that X is a continuous random variable if there exists a nonnegative function $f(x)$, defined for all real $x \in (-\infty, \infty)$, such that for any set B of real numbers:

$$\Pr\{X \in B\} = \int_B f(x)dx \qquad 10.13$$

Where $\boldsymbol{f(x)}$ is the ***probability density function*** of the random variable X. A more intuitive interpretation of the density function $f(x)$ is the following: the probability that X will be contained in an interval of length dx around point a is $f(a)dx$. Thus, $f(a)$ is a measure of how likely it is that X will be near a. Equation 10.13 states that the probability that X will be in B may be obtained by integrating the probability density function over the set B.

All probability statements about X can be answered in terms of $f(x)$. For example the probability that $X \in B = (-\infty, +\infty)$ results to be 1, which is coherent with our intuitive understanding of probability:

$$\Pr\{X \in (-\infty, +\infty)\} = \int_{-\infty}^{\infty} f(x)dx = 1$$

Another check would be the probability that X assumes any articular value, say a. Since X is a continuous random variable, this must be 0, which is confirmed by the integration:

$$\Pr\{X = a\} = \int_a^a f(x)dx = 0$$

The probability that $X \in B = [a, b]$ will then be:

$$\Pr\{a \leq X \leq b\} = \int_a^b f(x)dx$$

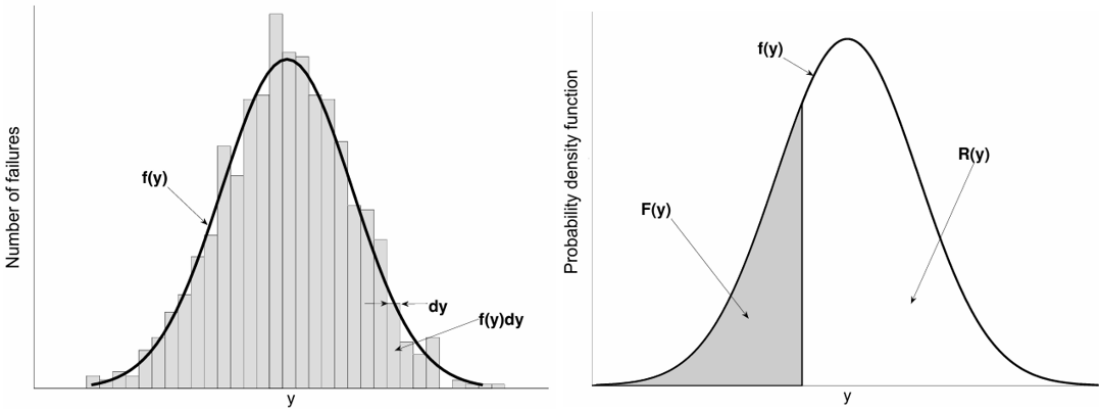

Figure 10.3: left) probability density function; right) cumulative probability and reliability.

10.1.3.2. Conditional reliability

The concept of conditional probability deals with the *computation of probability once some partial information about the outcome of the experiment is known*. In such conditions, the probabilities computed are known as conditional probabilities. Moreover, it often turns out that the easiest way to compute the probability of an event is to first "condition" on the occurrence or nonoccurrence of an event.

As an illustration of conditional probability, suppose that one rolls a pair of dice. The sample space S of this experiment will have 36 possible outcomes:

$$S = \begin{Bmatrix} (i,j) & i = 1,\dots,6 \\ & j = 1,\dots,6 \end{Bmatrix}$$

Suppose that each of the possible 36 outcomes is equally possible, and thus it has probability $1/36$ (in such situation we say that the dice are *fair*). Assume that the first dice rolls a 3, so $i = 3$ and ask yourself: what is the probability that the sum of the two dices will be 8? Since the first dice rolled a 3, we only have 6 more possible outcomes with equal probability $1/6$, of which only one satisfies $3 + x = 8$. Thus, the conditional probability of the second roll to give a total of 8 is $1/6$.

In the scope of fracture mechanics and structural reliability, conditional probability is almost always associated to the lifetime of components. Thus, we define ***conditional reliability*** $\boldsymbol{R(\Delta, t)}$ the probability of a component of surviving a mission of duration t when it has already survived a lifetime Δ. Thus, the probability of surviving up to $\Delta + t$ is the product of the probability to survive up to Δ, multiplied by the conditional reliability $R(\Delta, t)$:

$$R(\Delta + t) = R(\Delta) \cdot R(\Delta, t) \quad \rightarrow \quad \boxed{R(\Delta, t) = \frac{R(\Delta + t)}{R(\Delta)}} \qquad 10.14$$

As a consequence, the conditional reliability of the component will be the ratio between the component's reliability to survive $\Delta + t$ and the component's reliability of surviving up to $T = \Delta$.

10.1.3.3. Hazard rate

Consider the positive continuous random variable T to be the lifespan of a component, having a distribution function F and density f [6] – pp 649 of the pdf. The ***hazard rate function*** $\boldsymbol{\lambda(t)}$ ***of F*** is defined as:

$$\boxed{\lambda(t) = \frac{f(t)}{1 - F(t)} = \frac{f(t)}{R(t)}} \qquad 10.15$$

Thus, the hazard rate $\lambda(t)$ of F represents the probability that the component fails after reaching a life value of t. In other words, *the hazard rate* $\lambda(t)$ *represents the conditional probability that a component that survived up until* t *will fail in the next moment* dt.

Thus, the probability of failure of the component in the interval $(t, t + dt]$, so $f(t)dt$, is the product between the probability that the component survives beyond t, so $R(t)$, and the probability it will fail after reaching t, what we just defined as the hazard rate $\lambda(t)$.

$$f(t) = R(t) \cdot \lambda(t) \qquad 10.16$$

The average value of $\lambda(t)$ calculated over a life corresponding to the 10% percentile is called ***failure rate***. Note that it's not uncommon for $\lambda(t)$ itself to be called failure rate. If a mechanical system has many parts working in series, the failure rate of the system is the sum of the failure rates of each component.

10.1.4. Normal distributions

Many large data sets have histograms with peaks around the sample median and then decreasing values on both sides. Such data sets are thus *bell* shaped and called *normal distributions*. [6] – pp 97 pdf

A random variable X is said to be normally distributed if its density function $f(x)$ is [6] – pp 234 of the pdf:

$$f(x) = \frac{1}{\sqrt{2\pi}\sigma} e^{-\frac{(x-\mu)^2}{2\sigma^2}} \quad \text{for} \quad -\infty < x < \infty \tag{10.17}$$

Where μ *is the mean* and σ^2 *is the variance* of the normal distribution. Normally distributed random variables are symmetric bell-shaped curves about μ with maximum value of $1/\sqrt{2\pi}\sigma \approx 0.399/\sigma$ at $x = \mu$. For a normal distribution, the ***empirical rule*** tells us the approximate percentage of data that is contained within k standard deviations σ from the sample mean μ:

- $k = 1 \rightarrow 68\%$ of data lies within $\mu \pm \sigma$.
- $k = 2 \rightarrow 95\%$ of data lies within $\mu \pm 2\sigma$.
- $k = 3 \rightarrow 99.7\%$ of data lies within $\mu \pm 3\sigma$.

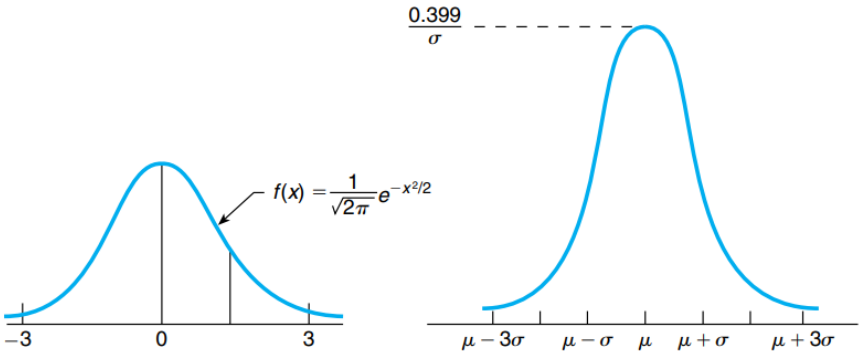

Figure 10.4: left) standard normal distribution; right) generic normal distribution.

A very important property of the generic normal random variables X with mean μ and variance σ^2 is that we can define the ***standard normal distribution Z***: a normal distribution with mean $\mu = 0$ and variance $\sigma^2 = 1$, depicted in Figure 10.4 – left.

$$Z = \frac{X - \mu}{\sigma} \tag{10.18}$$

The standard normal function Z is important because it allows us to express all statistical statements about X in terms of Z. In fact, if we know Z, μ and σ, we can express the generic normal random variable X as follows:

$$X = \mu + \sigma Z \tag{10.19}$$

The corresponding ***standard cumulative distribution function (CDF)*** $\boldsymbol{\Phi(z)}$ can be defined as follows:

$$\Phi(x) = \frac{1}{\sqrt{2\pi}} \int_{-\infty}^{x} e^{-\frac{y^2}{2}} dy \quad \text{for} \quad -\infty < x < \infty \tag{10.20}$$

The actual value of the standard distribution function $\Phi(z)$ has been determined by an approximation and the results have been presented in Table 10.1, which tabulates $\Phi(z)$ to a 4-digit level of accuracy for a wide range of nonnegative values of z. Note that despite Table 10.1 tabulates $\Phi(z)$ for nonnegative values of z, we also obtain $\Phi(-z)$ using the symmetry of about zero of the standard normal distribution.

$$\Phi(-z) = 1 - \Phi(z) \tag{10.21}$$

x	.00	.01	.02	.03	.04	.05	.06	.07	.08	.09
.0	.5000	.5040	.5080	.5120	.5160	.5199	.5239	.5279	.5319	.5359
.1	.5398	.5438	.5478	.5517	.5557	.5596	.5636	.5675	.5714	.5753
.2	.5793	.5832	.5871	.5910	.5948	.5987	.6026	.6064	.6103	.6141
.3	.6179	.6217	.6255	.6293	.6331	.6368	.6406	.6443	.6480	.6517
.4	.6554	.6591	.6628	.6664	.6700	.6736	.6772	.6808	.6844	.6879
.5	.6915	.6950	.6985	.7019	.7054	.7088	.7123	.7157	.7190	.7224
.6	.7257	.7291	.7324	.7357	.7389	.7422	.7454	.7486	.7517	.7549
.7	.7580	.7611	.7642	.7673	.7704	.7734	.7764	.7794	.7823	.7852
.8	.7881	.7910	.7939	.7967	.7995	.8023	.8051	.8078	.8106	.8133
.9	.8159	.8186	.8212	.8238	.8264	.8289	.8315	.8340	.8365	.8389
1.0	.8413	.8438	.8461	.8485	.8508	.8531	.8554	.8577	.8599	.8621
1.1	.8643	.8665	.8686	.8708	.8729	.8749	.8770	.8790	.8810	.8830
1.2	.8849	.8869	.8888	.8907	.8925	.8944	.8962	.8980	.8997	.9015
1.3	.9032	.9049	.9066	.9082	.9099	.9115	.9131	.9147	.9162	.9177
1.4	.9192	.9207	.9222	.9236	.9251	.9265	.9279	.9292	.9306	.9319
1.5	.9332	.9345	.9357	.9370	.9382	.9394	.9406	.9418	.9429	.9441
1.6	.9452	.9463	.9474	.9484	.9495	.9505	.9515	.9525	.9535	.9545
1.7	.9554	.9564	.9573	.9582	.9591	.9599	.9608	.9616	.9625	.9633
1.8	.9641	.9649	.9656	.9664	.9671	.9678	.9686	.9693	.9699	.9706
1.9	.9713	.9719	.9726	.9732	.9738	.9744	.9750	.9756	.9761	.9767
2.0	.9772	.9778	.9783	.9788	.9793	.9798	.9803	.9808	.9812	.9817
2.1	.9821	.9826	.9830	.9834	.9838	.9842	.9846	.9850	.9854	.9857
2.2	.9861	.9864	.9868	.9871	.9875	.9878	.9881	.9884	.9887	.9890
2.3	.9893	.9896	.9898	.9901	.9904	.9906	.9909	.9911	.9913	.9916
2.4	.9918	.9920	.9922	.9925	.9927	.9929	.9931	.9932	.9934	.9936
2.5	.9938	.9940	.9941	.9943	.9945	.9946	.9948	.9949	.9951	.9952
2.6	.9953	.9955	.9956	.9957	.9959	.9960	.9961	.9962	.9963	.9964
2.7	.9965	.9966	.9967	.9968	.9969	.9970	.9971	.9972	.9973	.9974
2.8	.9974	.9975	.9976	.9977	.9977	.9978	.9979	.9979	.9980	.9981
2.9	.9981	.9982	.9982	.9983	.9984	.9984	.9985	.9985	.9986	.9986
3.0	.9987	.9987	.9987	.9988	.9988	.9989	.9989	.9989	.9990	.9990
3.1	.9990	.9991	.9991	.9991	.9992	.9992	.9992	.9992	.9993	.9993
3.2	.9993	.9993	.9994	.9994	.9994	.9994	.9994	.9995	.9995	.9995
3.3	.9995	.9995	.9995	.9996	.9996	.9996	.9996	.9996	.9996	.9997
3.4	.9997	.9997	.9997	.9997	.9997	.9997	.9997	.9997	.9997	.9998

Table 10.1: Standard normal distribution function values.

Experimental dataset. Given a dataset with n entries, we assign to each *ordered* data point x_i of the random variable X an empirical cumulative probability:

$$F(x_i) = \frac{i}{n+1} \tag{10.22}$$

If the data set is approximately normally distributed, these empirical probabilities are a good approximation of the actual CDF of the standard normal distribution:

$$F(x_i) \approx \Phi(z_i)$$

Where z_i are the corresponding quantiles of the standard normally distributed random variable Z. The values z_i can be obtained either from statistical tables (Table 10.1) or computationally with MALAB's "*norminv*(·)", which takes as input the CDF and gives as output the corresponding percentile z_i.

The ***percentiles z_i can be used to check if the data x_i of X is approximately normally distributed***. What we do is plot the percentiles z_i as a function of the actual value x_i and compare this with the plot of the percentiles z_i as a function of the values of initial data x_i^{ID} required for X to be exactly normally distributed. The values x_i^{ID} are determined via equation 10.19:

$$x_i^{ID} = \mu + \sigma z_i$$

To compute the $100p$ percentile of the X dataset, we simply compute the 5% percentile of the standard distribution Z using *norminv*. Then, we translate this value to the 5% percentile of X using the linear relation 10.19:

$$p5 = \mu + \sigma \cdot norminv(0.05)$$

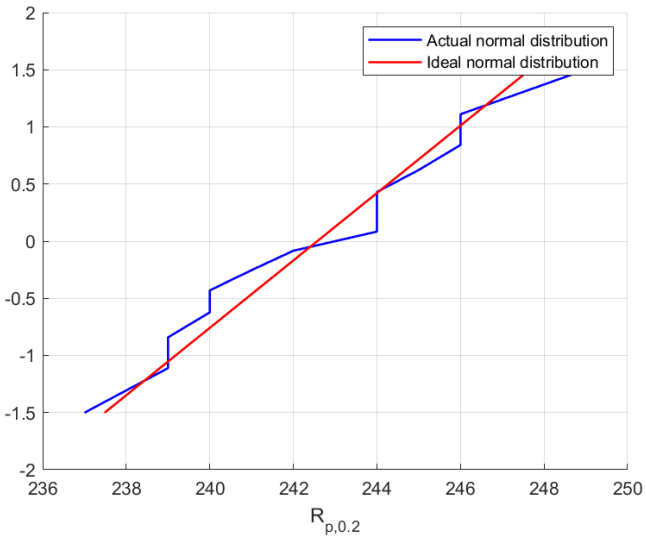

Figure 10.5: ideal versus real percentiles.

10.1.5. Weibull distribution

10.1.6. Estimators

Let $x_1, \dots, x_n$ be n realizations of a sample extracted from a given distribution with a density function $f(x, \theta)$, where θ is unknown. Then, θ can be estimated with an estimator $\hat{X}$

$$\hat{X} = f(x_1, x_2, \dots, x_n)$$

The idea is to try to estimate the distribution to which the estimators belong.

Estimators have the following important properties:

- Correct:
- To be efficient:
- To be consistent:

10.1.7. Other statistical distributions

10.1.7.1. Histogram

The histogram is a *useful tool for studying data distribution*. Let us consider an experiment described by a continuous random variable X, suppose we have N observations with observed values $x_1, \dots, x_N$. First, the field of existence is discretized in *classes*. This can be done in multiple ways, for example choosing class intervals of equal length, where the number of classes can be obtained as:

$$k = 1 + 3.3 \log N \tag{10.23}$$

The number of observations in a given class is called *frequency* n_i, while the *relative frequency* f_i is defined as:

$$f_i = \frac{n_i}{\sum n_i} = \frac{n_i}{N} \tag{10.24}$$

The *density* δ_i of the i-th class is defined as its relative frequency over its width:

$$\delta_i = \frac{f_i}{d_i} \tag{10.25}$$

The histogram is then obtained by plotting a chart of the frequencies, represented as a set of boxes (Figure 10.6). Note that it could also be plotted in terms of density δ_i, in such case a curve is drawn rather than the boxes.

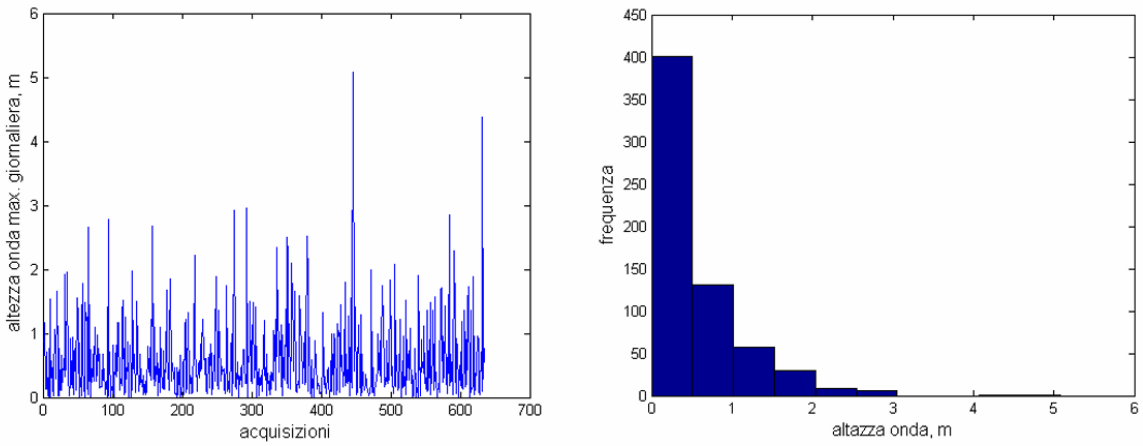

Figure 10.6: left: raw data points/observed values; right) frequency histogram.

10.1.7.2. Scatter diagrams

A scatter diagram is an *useful way to plot pairs of data sets that may be correlated to each other*. If the data set of paired values are x_i and y_i, the scatter diagram plots x_i on the x-axis and y_i on the y-axis (Figure 10.7). It must be immediately pointed out that ***correlation does not imply causation***. Meaning that if we find that x_i and y_i are strongly correlated, it will not justify us to say that x causes y, we can only say that the two are correlated. Usually, the explanation for such an association lies in an unexpressed factor related to both quantities considered.

To determine if the two sets of paired data are actually correlated, we introduce the ***sample correlation coefficient*** $\boldsymbol{r}$, defined as follows:

$$-1 \leq r = \frac{\sum_i^n (x_i - \bar{x})(y_i - \bar{y})}{(n-1)s_x s_y} = \frac{\sum_{i=1}^n (x_i - \bar{x})(y_i - \bar{y})}{\sqrt{\sum_{i=1}^n (x_i - \bar{x})^2 \sum_{i=1}^n (y_i - \bar{y})^2}} \leq 1 \qquad 10.26$$

The sample correlation coefficient has the following ***properties***:

- The coefficient is bounded by -1 and 1 with:
  - $|r|$ gives the strength of the linear correlation between x and y values of the data pair. $|r| = 0.9$ suggest a strong linear correlation, $|r| = 0.3$ a weak one.
  - $sign(r)$ gives the direction of the correlation:
  - If $r > 0$ we say that the data pair is *positively correlated*, meaning that the line has positive inclination.
  - If $r < 0$ we say that the data pair is *negatively correlated* (small $x \rightarrow$ large y).
- If there is a linear relationship between x_i and y_i such that for constants a, b we have that $y_i = a + bx_i$ then we can say that:
  - If a, b are both positive or both negative, then $r = 1$ (large x values are paired with large y values).
  - If $b < 0$ then $r = -1$ (large y values are paired to small x values).
  - If b, d are both positive or both negative and r is the sample correlation coefficient for the data pairs $x_i, y_i, i = 1, \dots, n$ then it's also the coefficient of the pairs $a + x_i b$ and $c + y_i d$.

The last property implies that r *does not change for two data pairs obtained by adding and multiplying for a constant the* r *of an original data pair*. This, in turn implies that r does not depend on the units used to describe the data sets.

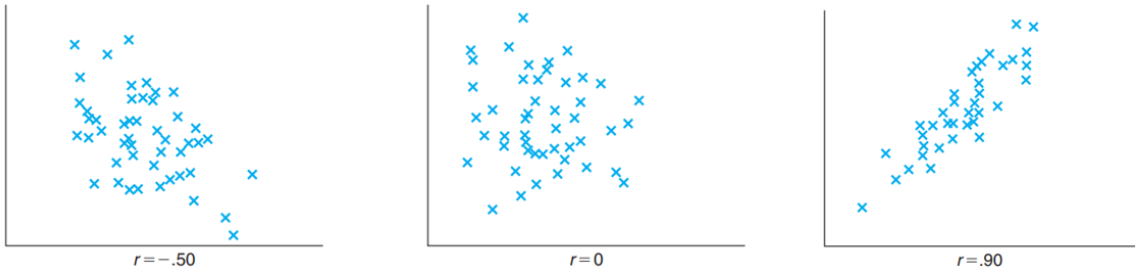

Figure 10.7: scatter diagrams with different r.

10.2. DSV solution for shear – examples

10.2.1. Open sections

Recall from section 0 that any open cross section can be modelled as an assembly of strips. For each strip we can identify the axis normal to shear flow direction n and the one tangent to shear flow direction s. The axis normal to the cross section is the z-axis, along which acts the internal action M_z or M_t. The following relations have also been found in the aforementioned section, and they will be used in the following examples:

$$\begin{cases} \tau_{nz} = 0 \\ \tau_{sz} = -\dfrac{2M_t}{J} n \end{cases} \quad \text{and} \quad J = \begin{cases} \displaystyle\int_{-b/2}^{+b/2} \frac{b^3(x)}{3} dx, & b = b(x) \\ \dfrac{1}{3} a b^3, & b = \text{const} \end{cases}$$

10.2.1.1. Example 1

Consider the beam in Figure 10.8 – left and assume that we want to evaluate (1) the maximum stress over the section, and (2) the relative rotation between the beam root and its tip.

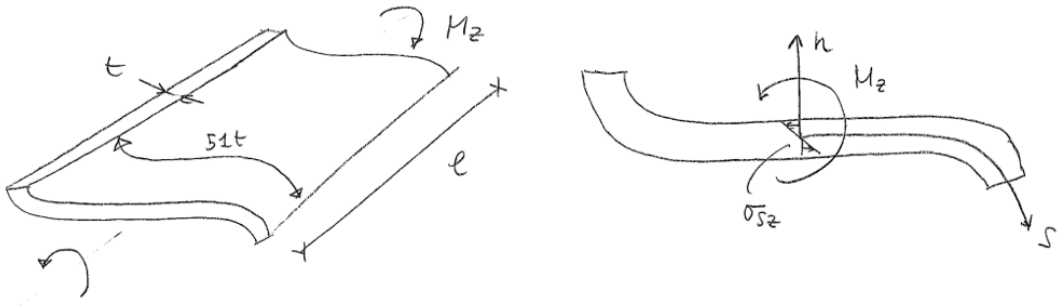

Figure 10.8: left) beam with open cross section subject to a torsional moment M_z; right) shear stresses on such beam.

We know that, according to the approximate solution found in section 0, the shear stress acting along s is linear with n. Thus, we expect $(\tau_{zs})_{\max}$ to develop at the extremities of the beam, i.e. $\pm n/2$. We know that, according to the approximate solution found in section 0, the shear stress acting along s is linear with n. Thus, we expect $(\tau_{zs})_{\max}$ to develop at the extremities of the beam, i.e. $\pm n/2$. For the case at hand, the shear stress acting along s can be computed as follows:

$$\tau_{sz} = -\frac{2M_z}{J} n = -\frac{2M_z}{\frac{1}{3} a b^3} n = -\frac{2M_z}{\frac{1}{3} 51t \cdot t^3} n = -\frac{2M_z}{17t^4} n \quad \rightarrow \quad (\tau_{zs})_{\max} = \pm \frac{M_z}{17t^3}$$

The relative rotation can be computed via the torsion θ' which is assumed to be constant along the z-axis. Thus, θ is linear with z and we simply write:

$$\theta' = \frac{M_t}{GJ} = \frac{M_t}{17Gt^4} \quad \rightarrow \quad \theta = \theta' l = \frac{M_t l}{17Gt^4}$$

10.2.1.2. Example 2

Consider the approximation of a wing profile presented in Figure 10.9, the thickness of which can be assumed to be:

$$b(x) = b_0\left[1 - \left(\frac{2x}{a}\right)^2\right]$$

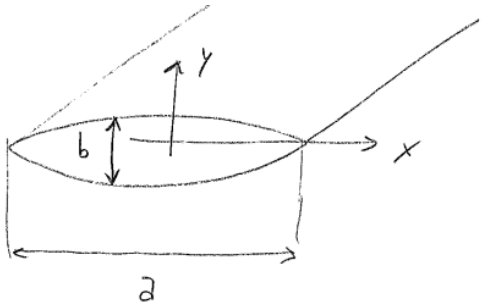

Figure 10.9: wing profile.

We want to determine the maximum shear stress due to a torsional moment M_z. The shear stress can be computed as follows:

$$\tau_{sz} = \tau_{xz} = -\frac{2M_t}{J}y$$

The parameter J can be computed as follows:

$$J = \int_A 4y^2 dA = \int_{-a/2}^{+a/2}\int_{-b(x)/2}^{+b(x)/2} 4y^2 dy dx = \int_{-a/2}^{+a/2} 4\frac{b(x)^3}{12}dx = \frac{1}{3}\int_{-a/2}^{+a/2} b_0^3\left[1 - \left(\frac{2x}{a}\right)^2\right]^3 dx$$
$$= \frac{16}{105}ab_0^3$$

The maximum stress is again found at $\pm y_{\max} = \pm b_0/2$, which yields:

$$(\tau_{xz})_{\max} = \pm\frac{2M_t}{J}\frac{b_0}{2} = \pm\frac{M_t}{16}\frac{105}{ab_0^2}$$

10.2.1.3. Example 3

We now want to evaluate the torsional stiffness of the beam in the figure below. The parameter J can be computed by modelling the "C" beam as an assembly of strips:

$$J = \frac{1}{3}\sum_i a_i b_i^3 = \frac{1}{3}db^3 + \frac{1}{3}db^3 + \frac{1}{3}2db^3 = \frac{4}{3}db^3$$

The maximum stress will be the same for every strip since the maximum shear flow arm is $b/2$ in all of them. Thus, we'll write:

$$(\tau_{sz})_{\max} = -\frac{2M_t}{J}\frac{b}{2} = \frac{3M_t}{4db^2}$$

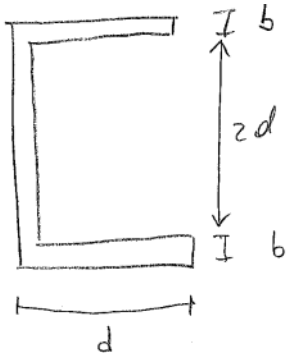

Figure 10.10: "C" beam.

10.2.2. Closed sections

For a beam with a closed cross section the torsional internal action can be expressed via Bredt formula, which reads:

$$M_z = 2\Omega q$$

The torsional inertia can be evaluated as follows:

$$J = \frac{4\Omega^2}{\oint_\Gamma \frac{1}{t(s)} d\Gamma}$$

10.2.2.1. Example 4

Consider the two tubes presented in Figure 10.11, completely equivalent but for the small cut in the one on the right. The tubes have small thickness as $D = 16t$. The purpose of the exercise is to apply the theories developed in section 2.1.6 and compare the results. Naturally, we expect to find that the closed cross section will develop lower shear stresses and have higher torsional stiffness.

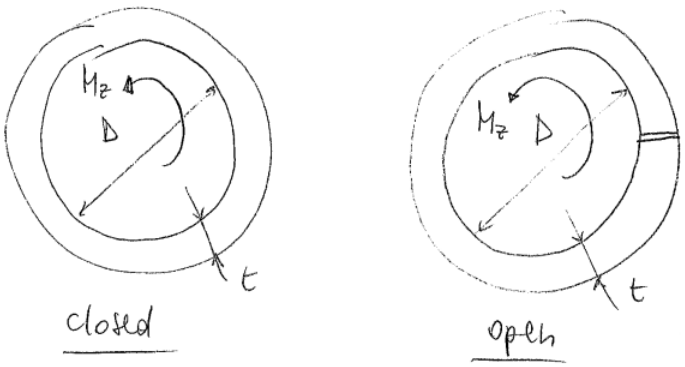

Figure 10.11: circular tubes with closed (left) and open (right) sections.

For the open tube the torsional inertia is provided by:

$$J = \frac{1}{3} ab^3 = \frac{1}{3} \pi D t^3$$

Thus, we can compute the maximum shear stress as follows:

$$(\tau_{sz})_{\max} = -\frac{2M_z}{J}\frac{t}{2} = \frac{3}{\pi}\frac{M_z}{Dt^2}$$

For the closed tube the inertia is provided by:

$$J = \frac{4\Omega^2}{\oint_\Gamma \frac{1}{t} d\Gamma} = \frac{4\left(\frac{\pi D^2}{4}\right)^2}{\frac{\pi D}{t}} = \frac{\pi}{4} D^3 t$$

The stress is provided by:

$$\sigma_{sz} = \frac{q}{t} = \frac{M_z/2\Omega}{t} = \frac{2M_z}{\pi D^2 t}$$

By comparing the stress and the inertia, it's clear that the closed section provides superior performance.

$$\frac{J_{closed}}{J_{open}} = \frac{\frac{\pi}{4} D^3 t}{\frac{\pi}{3} D t^3} = \frac{3D^2}{4t^2} = 192$$

$$\frac{\sigma_{open}}{\sigma_{closed}} = \frac{\frac{3}{\pi}\frac{M_z}{Dt^2}}{\frac{2M_z}{\pi D^2 t}} = \frac{3}{2}\frac{D}{t} = 24$$

10.3. Symmetry in beams - examples

10.3.1. Example 1

Consider the beam in Figure 10.12 – left, it is easy to notice that such beam has symmetric load, geometry and BCs. Thus, symmetry considerations can be applied to simplify the problem. It is also easy to see that the rotation about the x-axis and displacement along the z-axis of such beam are both null, i.e. $\theta_x = w = 0$. Assuming for convenience to temporarily place the origin of the reference system at the midpoint of the beam, the displacements components related to symmetry considerations are:

$$\begin{cases} v(z) = v(-z) & \rightarrow \quad v(z) \neq 0 \\ \theta_x(z) = -\theta_x(-z) & \rightarrow \quad \theta_x(0) = 0 \\ w(z) = -w(-z) & \rightarrow \quad w(0) = 0 \end{cases}$$

Considering now the reference system in Figure 10.12 – left, the internal actions of the beam are simply determined as:

$$T_y(z) = -qz + \frac{ql}{2} \quad \rightarrow \quad M_x(z) = \int_z T_y(z)dz = -\frac{qz^2}{2} + \frac{qzl}{2}$$

The internal action diagrams are reported in Figure 10.12 – right. It is interesting to notice the relationship between the symmetries of the displacements/rotations and the ones of the internal forces/moments. More precisely:

- v is symmetric while T_y is anti-symmetric.
- θ_x is anti-symmetric while M_x is symmetric.

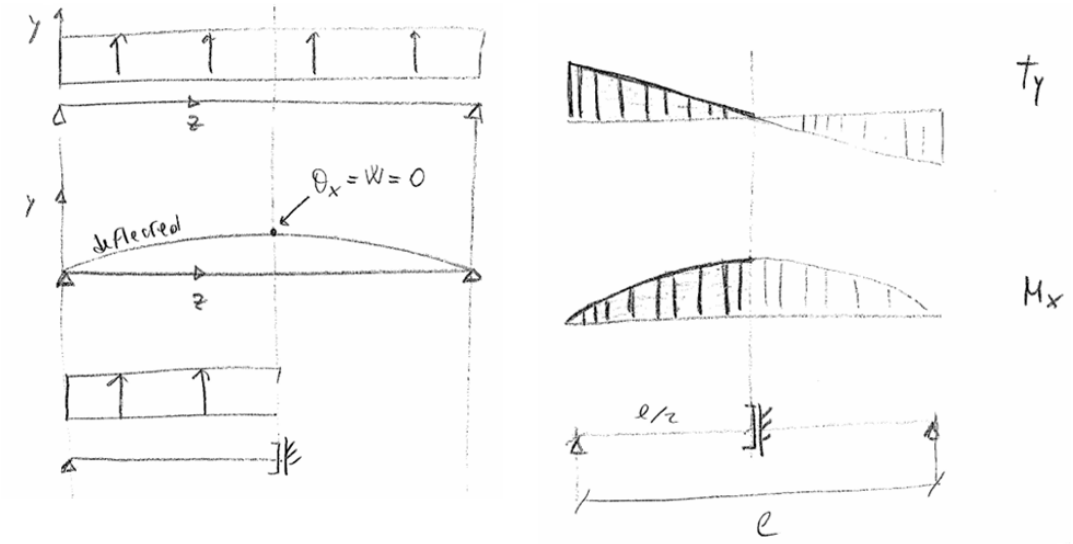

Figure 10.12: left) symmetric beam with symmetric distributed shear load; right) internal actions diagrams.

10.3.2. Example 2

Consider now the symmetric structure with anti-symmetric loading in Figure 10.13 – left. The displacement/rotations related to symmetries considerations are the following:

$$\begin{cases} v(z) = -v(-z) & \rightarrow & v(0) = 0 \\ \theta_x(z) = \theta_x(-z) & \rightarrow & \theta_x(0) \neq 0 \\ w(z) = w(-z) & \rightarrow & w(0) \neq 0 \end{cases}$$

The distributed load can be expressed as $q(z) = \bar{q}z/l$, where $\bar{q}$ is the maximum value. Then, the internal actions are determined as follows:

$$T_y(z) = \frac{\bar{q}z^2}{2l} - \frac{\bar{q}l}{10} \quad \rightarrow \quad M_x(z) = \frac{\bar{q}z^3}{6l} - \frac{\bar{q}lz}{10}$$

The internal action diagrams are reported in Figure 10.13 – right. Again ,the relationship of the symmetries of displacements/rotations and internal forces/moments is:

- T_y is symmetric while v is anti-symmetric.
- M_x is anti-symmetric while θ_x is symmetric.

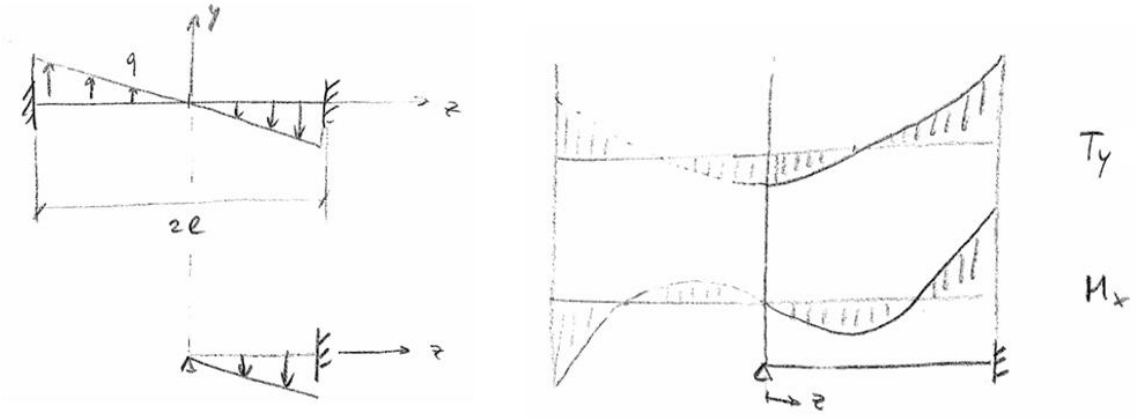

Figure 10.13: left) symmetric structure with anti-symmetric distributed shear load; right) internal actions.

10.4. Ritz method

10.4.1. Example 1

Consider the bar in Figure 10.14, characterized by a varying axial stiffness $EA = EA(x)$ and subject to a distributed axial load and a concentrated force at its tip. We examine the approximated solution with the methods previously introduced.

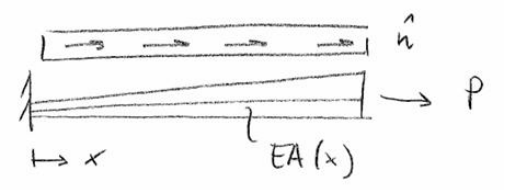

Figure 10.14: bar with varying cross section.

Ritz. We apply this method to the weak form of equilibrium, which for this problem is simply:

$$\Pi = \frac{1}{2}\int_l u_{\backslash x} EA(x) u_{\backslash x} dx - \int_l u\hat{n} dx - u(l)P$$

The Ritz trial functions ϕ_i must satisfy the essential BCs, i.e. $u(0) = 0$. Thus, we set $\phi_0 = 0$ and the approximation of the axial displacement reads:

$$u \approx \sum_i^N c_i \phi_i(x)$$

By substitution in the total potential energy:

$$\Pi = \frac{1}{2}\sum_{i,j}^{N,N} \int_l c_i \phi_{i\backslash x} EA(x) c_j \phi_{j\backslash x} dx - \sum_i^N \int_l c_i \phi_i \hat{n} dx - \sum_i^N c_i \phi_i(l) P$$

Imposing the equilibrium condition $\delta\Pi = \partial\Pi / \partial c_i = 0$ leads to:

$$\delta\Pi = \sum_{i,j}^{N,N} \int_l \delta c_i \phi_{i\backslash x} EA(x) c_j \phi_{j\backslash x} dx - \sum_i^N \int_l \delta c_i \phi_i \hat{n} dx - \sum_i^N \delta c_i \phi_i(l) P = 0$$

Rearranging the terms:

$$\sum_{i,j}^{N,N} \int_l \phi_{i\backslash x} EA(x) \phi_{j\backslash x} dx \, c_j = \sum_i^N \int_l \phi_i \hat{n} dx + \sum_i^N \phi_i(l) P$$

Thus, we obtain a formulation that is analogous to that of equation (5.7), i.e.

$$\underline{\underline{K}}\underline{c} = \underline{f} \quad \text{where} \quad \begin{cases} K_{ij} = \int_l \phi_{i\backslash x} EA(x) \phi_{j\backslash x} dx \\ f_i = \sum_i^N \int_l \phi_i \hat{n} dx + \sum_i^N \phi_i(l) P \end{cases}$$

Galerkin formulation. The differential problem reads:

$$\begin{cases} \left(EAu_{\backslash x}\right)_{\backslash x} + \hat{n} = (EA)_{\backslash x} u_{\backslash x} + EAu_{\backslash xx} + \hat{n} = 0 \\ EAu_{\backslash x} = P \quad \text{in } x = l \\ u = 0 \quad \text{in } x = 0 \end{cases}$$

The displacement is approximated identically to Ritz:

$$\tilde{u} = \sum_i^N c_i \phi_i(x)$$

However, the functions ϕ_i must now be chosen so that the BCs are respected. The residual R is obtained by substituting the approximation of u into the differential equation:

$$R = (EA)_{\backslash x} \tilde{u}_{\backslash x} + EA\tilde{u}_{\backslash xx} + \hat{n} = (EA)_{\backslash x} \sum_i^N c_i \phi_{i\backslash x} + EA \sum_i^N c_i \phi_{i\backslash xx} + \hat{n}$$

We now minimize the residual over the domain by weighting the residual with functions that are equal to the trial functions, yielding:

$$\int_\Omega \phi_i R d\Omega = \int_0^l \phi_i \left[(EA)_{\backslash x} \sum_j^N c_j \phi_{j\backslash x} + EA \sum_j^N c_j \phi_{j\backslash xx} + \hat{n} \right] dx = 0$$

The above equation can be written in the form:

$$K_{ij} c_j = f_i \quad \text{where} \quad \begin{cases} K_{ij} = \int_0^l \phi_i \left[(EA)_{\backslash x} \sum_j^N \phi_{j\backslash x} + EA \sum_j^N \phi_{j\backslash xx} \right] dx \\ f_i = -\int_0^l \phi_i \hat{n} dx \end{cases}$$

Note that the expression of K_{ij} for the Galerkin method contains the second derivative of the trial functions $\phi_{j\backslash xx}$, while in the Ritz method approach only the first derivative appears. For this reason, the smoothness of the trial functions must be higher in the Galerkin method. This is a typical feature of these methods, and it can be reconducted to the fact that, in the Ritz method, the natural BCs are already accounted for in the formulation of the weak form, while in the strong form this is not true.

Modified Galerkin. The effect due to the natural BCs it is now considered, and a second residual associated to such conditions is introduced:

$$\begin{cases} R_\Omega = (EA)_{\backslash x}\tilde{u}_{\backslash x} + EA\tilde{u}_{\backslash xx} + \hat{n} = (EA)_{\backslash x}\sum_i^N c_i\phi_{i\backslash x} + EA\sum_i^N c_i\phi_{i\backslash xx} + \hat{n} \\ R_F = EA\tilde{u}_{\backslash x} - P = EA\sum_i^N c_i\phi_{i\backslash x}(l) - P \end{cases}$$

The weighted residual minimization then reads:

$$\int_\Omega \phi_i R_\Omega d\Omega + \int_{S_F} \phi_i R_F dS_F = \int_0^l \phi_i R_\Omega dx + \phi_i(l)R_F = 0$$

Expanding the above equation leads to:

$$\int_0^l \phi_i \left[(EA)_{\backslash x}\sum_j^N c_j\phi_{j\backslash x} + EA\sum_j^N c_j\phi_{j\backslash xx} + \hat{n} \right] dx + \phi_i(l)\left[EA\sum_j^N c_j\phi_{j\backslash x}(l) - P \right] = 0$$

Expressing this equation in the form of a linear system of equations yields:

$$K_{ij}c_j = f_i$$

$$\text{where} \quad \begin{cases} K_{ij} = \int_0^l \phi_i \left[(EA)_{\backslash x}\sum_j^N \phi_{j\backslash x} + EA\sum_j^N \phi_{j\backslash xx} \right] dx + \phi_i(l)EA\sum_j^N \phi_{j\backslash x}(l) \\ f_i = -\int_0^l \phi_i \hat{n} dx + \phi_i(l)P \end{cases}$$

10.4.2. Example 2

Consider the simply supported beam depicted in Figure 10.15, loaded with a uniformly distributed shear load q. We now want to determine the deflected configuration of such beam using a Ritz approximation with 1, 2 and 3 polynomial terms.

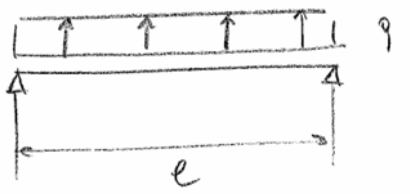

Figure 10.15: simply supported beam with uniformly distributed shear load.

First we derive the general form of the solution. The Ritz method relies on the weak form of equilibrium, thus we write the total potential energy and the BCs as follows:

$$\begin{cases} \Pi = \frac{1}{2}\int_0^l w_{\backslash xx} EI w_{\backslash xx} dx - \int_0^l wq dx\,, & \text{weak form} \\ \begin{cases} w(0) = 0 \\ w(l) = 0 \end{cases}, & \text{essential BCs} \\ \begin{cases} w_{\backslash xx}(0) = 0 \\ w_{\backslash xx}(l) = 0 \end{cases}, & \text{natural BCs} \end{cases}$$

Where the natural BCs are already accounted by the weak form, and so the trial functions ϕ_i must be chosen to satisfy only the essential BCs. The Ritz approximation is takes as:

$$w = \sum_i^N c_i \phi_i(x)$$

The total potential energy then reads:

$$\Pi = \frac{1}{2}\int_0^l \sum_{i,j}^{N,N} \left(c_i \phi_{i\backslash xx} EI c_j \phi_{j\backslash xx}\right) dx - \int_0^l \sum_i^N c_i \phi_i \, q dx$$

Imposing the equilibrium condition $\delta\Pi = (\partial\Pi/\partial c_i)\delta c_i = 0$ leads to:

$$\delta\Pi = \sum_j^N \left(\int_0^l \left(\delta c_i \phi_{i\backslash xx} EI c_j \phi_{j\backslash xx}\right) dx \right) - \int_0^l \delta c_i \phi_i q dx = 0$$

Given the arbitrariness of δc_i, the equilibrium condition is simplified to:

$$\delta\Pi = \sum_j^N \left(\int_0^l \left(\phi_{i\backslash xx} EI c_j \phi_{j\backslash xx}\right) dx \right) - \int_0^l \phi_i q dx = 0$$

In matrix notation:

$$K_{ij} c_j - f_i = 0 \quad \rightarrow \quad \begin{cases} K_{ij} = \int_0^l \left(\phi_{i\backslash xx} EI \phi_{j\backslash xx}\right) dx = EI \int_0^l \left(\phi_{i\backslash xx} \phi_{j\backslash xx}\right) dx \\ f_i = \int_0^l \phi_i q dx = q \int_0^l \phi_i dx \end{cases} \tag{10.27}$$

The trial functions are chosen to be polynomials in this example. More precisely, we consider polynomials up to the fourth, and then solve the problem multiple times, each considering a different amount of terms. The general expression is then:

$$w = a_0 + a_1 x + a_2 x^2 + a_3 x^3 + a_4 x^4$$

We ***immediately reformulate this expression by imposing the essential BCs***, i.e.

$$\begin{cases} w(0) = 0 \\ w(l) = 0 \end{cases} \rightarrow \begin{cases} a_0 = 0 \\ a_1 l + a_2 l^2 + a_3 l^3 + a_4 l^4 = 0 \end{cases}$$

From the second relation we obtain:

$$a_1 = -a_2 l - a_3 l^2 - a_4 l^3$$

Thus, the displacement reads:

$$w = (-a_2 l - a_3 l^2 - a_4 l^3) + a_1 x + a_2 x^2 + a_3 x^3 + a_4 x^4$$

Rearranging and renaming the coefficients for convenience, from a_{i+1} to b_i, we obtain the final expression of the approximation of the transverse displacement:

$$\begin{aligned} w &= a_2(x^2 - xl) + a_3(x^3 - xl^2) + a_4(x^4 - xl^3) \\ &= b_1(x^2 - xl) + b_2(x^3 - xl^2) + b_3(x^4 - xl^3) \end{aligned} \tag{10.28}$$

10.4.2.1. Solution with one polynomial term

In this case, the transverse displacement is approximated as follows:

$$w = c_1 \phi_1 = b_1(x^2 - xl)$$

According to (10.27) the stiffness matrix, actually a scalar since we only have one trial function, and the vector (again a scalar) of the external loads are obtained as follows:

$$\begin{cases} K = \int_0^l \phi_{1\backslash xx} EI \phi_{1\backslash xx} dx = 4lEI \\ f = q \int_0^l \phi_1 dx = -\frac{1}{6} q l^3 \end{cases}$$

Thus, the coefficient $b_1 = f/K$ is obtained as:

$$b_1 = -\frac{q l^2}{24EI}$$

10.4.2.2. Solution using two polynomial terms

In this case the approximation of the displacement of equation (10.28) reads:

$$w = c_1 \phi_1 + c_2 \phi_2 = b_1(x^2 - xl) + b_2(x^3 - xl^2)$$

Having used two terms in the displacement approximation, the stiffness matrix $\boldsymbol{K}$ will be a $\mathbb{R}^{2\times2}$ matrix, while the vector of external loads $\boldsymbol{f}$ will be of dimension $\mathbb{R}^{2\times1}$. The components of such entities are determined as follows:

$$\begin{cases} k_{11} = \int_0^l \phi_{1\backslash xx} EI \phi_{1\backslash xx} dx = 4lEI \\ k_{12} = k_{21} = \int_0^l \phi_{1\backslash xx} EI \phi_{2\backslash xx} dx = 6l^2 EI \\ k_{22} = \int_0^l \phi_{2\backslash xx} EI \phi_{2\backslash xx} dx = 12l^3 EI \end{cases} \qquad \begin{cases} f_1 = q\int_0^l \phi_1 = -\frac{1}{6} ql^3 \\ f_2 = q\int_0^l \phi_2 = -\frac{1}{4} ql^4 \end{cases}$$

Thus, the equilibrium condition $\delta\Pi = 0$ approximated via the Ritz method yields a system of algebraic equations in the form:

$$\begin{bmatrix} 4lEI & 6l^2EI \\ 6l^2EI & 12l^3EI \end{bmatrix} \begin{Bmatrix} b_1 \\ b_2 \end{Bmatrix} = \begin{Bmatrix} -ql^3/6 \\ -ql^4/4 \end{Bmatrix} \quad \rightarrow \quad \begin{Bmatrix} b_1 = -ql^2/24EI \\ b_2 = 0 \end{Bmatrix}$$

The result is then identical to the one with only one approximating term. This is easy to accept by noticing that the function ϕ_2 is not symmetric, while the deflection of the beam is expected to be. Thus, the contribution of ϕ_2 is null.

10.4.2.3. Solution using three polynomial terms

We now consider the full expression of the displacement in equation (10.28), i.e.

$$w = b_1(x^2 - xl) + b_2(x^3 - xl^2) + b_3(x^4 - xl^3)$$

We only compute the additional terms of the stiffness matrix $\boldsymbol{K}$, which now will be a $\mathbb{R}^{3\times3}$ matrix, and of the vector of external loads $\boldsymbol{f}$, which now is of dimensions $\mathbb{R}^{3\times1}$.

$$\begin{cases} K_{31} = \int_0^l \phi_{3\backslash xx} EI \phi_{1\backslash xx} dx = 8l^3 EI \\ K_{32} = \int_0^l \phi_{3\backslash xx} EI \phi_{2\backslash xx} dx = 18l^4 EI \\ K_{33} = \int_0^l \phi_{3\backslash xx} EI \phi_{3\backslash xx} dx = \frac{144}{5} l^5 EI \end{cases} \qquad f_3 = q\int_0^l \phi_3 dx = -\frac{3}{10} ql^5$$

Thus, the matrix form of the problem and the solution is the following:

$$\begin{bmatrix} 4lEI & 6l^2EI & 8l^3EI \\ 6l^2EI & 12l^3EI & 18l^4EI \\ 8l^3EI & 18l^4EI & 144l^5EI/5 \end{bmatrix} \begin{Bmatrix} b_1 \\ b_2 \\ b_3 \end{Bmatrix} = \begin{Bmatrix} -ql^3/6 \\ -ql^4/4 \\ -3ql^5/10 \end{Bmatrix} \quad \rightarrow \quad \begin{Bmatrix} b_1 = 0 \\ b_2 = -ql/12EI \\ b_3 = q/24EI \end{Bmatrix}$$

Thus, the displacement results to be following, which is also the exact one:

$$w = b_1(x^2 - xl) + b_2(x^3 - xl^2) + b_3(x^4 - xl^3) = \frac{ql^4}{24EI}\left(\frac{x}{l} - 2\frac{x^3}{l^3} + \frac{x^4}{l^4}\right)$$

Some important ***considerations***:

- Exact solution: in this case, the exact solution is the Ritz solution with three polynomial components. However, it is not a general rule to obtain the exact solution. In this case, the exact solution is a polynomial one, so a polynomial approximation is able to capture it. When this happens, increasing the order of the Ritz polynomial above the one providing the exact solution would not increase the accuracy of the solution, as we would obtain $b_4 = b_5 = \cdots = b_n = 0$.
- Trial functions: other choice of polynomial shape functions are available. For example, we could have taken:

$$w = a_1 x(x-l) + a_2 x^2(x-l) + a_3 x^3(x-l)$$

It is easy to see that this choice of trial functions still satisfies the essential BCs. Naturally, the expression of the entries of the stiffness matrix and of the vector of external loads would be different.

- Comparison of results: more insight can be gained on the Ritz method by comparing results in terms of displacements and energies. Consider $l = 100mm$, $EI = 10^8/24$ and $q = 1$. Table 10.2 shows the values of displacement and bending moment at the midpoint of the beam, as well as the total potential energy absorbed for polynomial Ritz approximations with 1,2 and 3 terms. Table 10.3 shows the percentage error at the midpoint and the global error of both displacement and bending moment. It is clear that the solution with 1 and 2 terms is rather poor, as the errors on displacement and bending moment are of 20% and 33.33% respectively. However, the convergence of the method is very fast, as the expansion up to the third order can represent the exact solution.

	w_{mid}	$M_{x,mid} \cdot 10^7$	Π
$N = 1,2$	0.2500	0.8333	-8.3333
$N = 3$	0.3125	1.2500	-10.000

Table 10.2: displacement and bending moment at mid-point of the beam, and total potential energy for different number of polynomial terms.

	$w_{mid}[\%]$	$\|e^w\|_{L^2} \cdot 10^2$	$M_{x,mid}[\%]$	$\|e^{M_x}\|_{L^2} \cdot 10^2$
$N = 1,2$	-20	17.96	-33.33	40.8250
$N = 3$	0.00	0.00	0.00	0.00

Table 10.3: errors for displacement and bending moment with respect to exact solution.

10.4.3. Example 3

We now consider the same problem presented in the previous example, but this time we aim at solving it with trigonometric trial functions. The displacement field is then approximated as follows:

$$w = \sum_{m=1,3,5}^{N} c_m \sin\left(\frac{m\pi x}{l}\right)$$

This choice of trial functions clearly satisfies the essential BCs, and they also satisfy the natural ones. Note also that the even contributions are neglected, as they are anti-symmetric and therefore the work associated to the external loads is zero. In this case, the stiffness matrix and the forcing term entries are obtained as follows:

$$\begin{cases} K_{ij} = \delta_{ij} EI \left(\frac{i\pi}{l}\right)^4 \frac{l}{2} \\ f_i = \frac{2l}{i\pi} \end{cases}$$

Where δ_{ij} is the Kronecker delta, such that $\delta = 1$ when $i = j$, otherwise $\delta = 0$. We discuss the results obtained with different numbers of trial functions.

	w_{mid}	$M_{x,mid} \cdot 10^3$	Π
$N = 1$	0.3137	1.2901	-9.9856
$N = 3$	0.3124	1.2423	-9.9992
$N = 5$	0.3125	1.2526	-9.9999
⋮	⋮	⋮	⋮
$N = 23$	0.3125	1.2500	-10.0000

Table 10.4: displacement and bending moment at mid-point of the beam, and total potential energy for different number of polynomial terms.

	$w_{mid}[\%]$	$\|e^w\|_{L^2} \cdot 10^2$	$M_{x,mid}[\%]$	$\|e^{M_x}\|_{L^2} \cdot 10^2$
$N = 1$	0.3857	0.4128	3.2049	3.8013
$N = 3$	-0.0274	0.0326	-0.6175	0.8673
$N = 5$	0.0047	0.0062	0.2081	0.3364
⋮	⋮	⋮	⋮	⋮
$N = 23$	0.0000	0.0000	-0.0037	0.0112

Table 10.5: errors for displacement and bending moment with respect to exact solution.

The following ***considerations*** can be made:

- Local and global stiffness: the displacement in the midpoint with $N = 1$ is higher than those for $N > 1$. One could be tempted to conclude that the models associated with $N > 1$ are stiffer than the model with $N = 1$. This conclusion would be wrong. Indeed the stiffness of the model, as a whole, has to be intended in a global sense: the correct metric is the total potential energy. With this regard it can be seen that the value of Π gets smaller as the number of trial functions considered N increases, thus the model becomes more and more compliant as the number of DOFs increases.
- Convergence of w: the percentage error of the displacement of the beam midpoint displays some oscillations in terms of sign, however the module keeps decreasing with each added term N. The convergence of w is better represented by $\|e^w\|_{L^2}$.

- Convergence of M_x: it is important to notice that it is slower than the convergence of the displacement w. In fact, the bending moment is associated to the second derivative of the displacement $M_x = Eiw_{\backslash xx}$. This slows down the convergence of M_x, as previously discussed.
- Comparison of $N = 1$ with polynomials: comparing the accuracy of the $N = 1$ term with that of the polynomial trial function (Table 10.2), it is clear that the trigonometric function is a better choice. The sine-type function is in fact a good representation of the exact pattern.

References

[1] T. Megson, Aircraft structures sixth edition, Butterworth-Heinemann, 2017.

[2] K.-J. Bathe, Finite element procedures, PRENTICE HALL, 1996.

[3] DoD, "MIL-HDBK-17-1F - Composite materials handbook," Departement of Defense USA, 2002.

[4] R. M. Jones, Mechanics of composite materials, 1999.

[5] DoD, "MIL-HDBK-17-3F - Composite materials handbook," Department of Defence USA, 2002.

[6] S. Ross, "Introduction to statistics".

[7] R. D. Cook, Concepts Applications of FEM.